

ELG 6369

NONLINEAR MICROWAVE DEVICES AND EFFECTS

CHAPTER VIII

MICROWAVE FILTERS

The appropriate type of technology and its impact on system costing will vary greatly depending upon the application. Planar lines (like microstrips) can be economically implemented in many low-to-medium power circuits and systems (Figure VIII-1).

They are widely used in hybrid and monolithic microwave integrated circuits (MICs and MMICs). The evolution of MIC technologies does not mean that coaxial line and waveguide-based design are abandoned.

On the contrary, such propagating structures assume continuing and significant roles especially in high power transmission and in circuits where a high-Q component is deemed necessary.

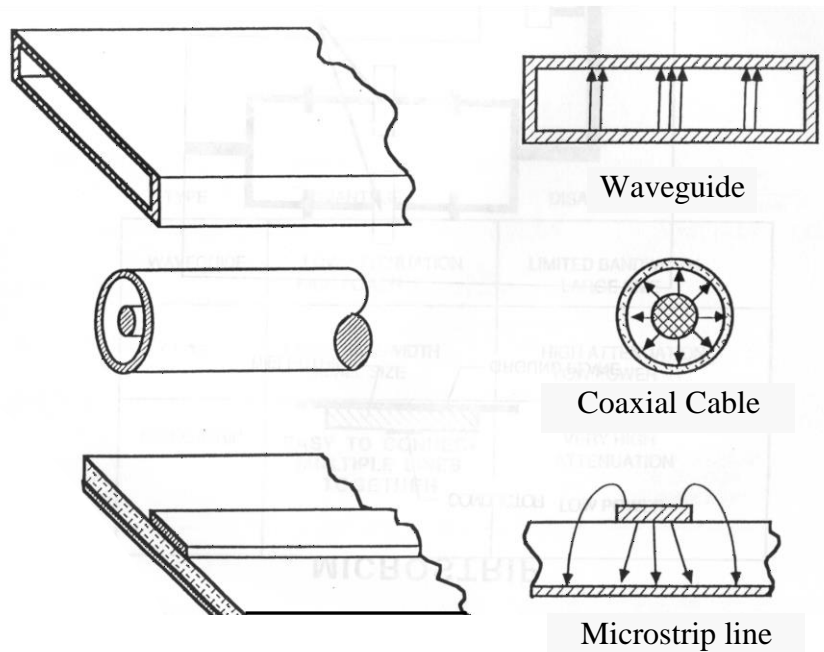


Fig. VIII-1: Different supports of transmission.

The materials you receive for this course are protected by copyright and to be used for this course only. You do not have permission to upload the course materials, including any lecture recordings you may have, to any website. If you require clarification, please consult your professor.

B – MIC TRANSMISSION LINE STRUCTURES

I – Distributed components

In the low microwave frequency range, lumped elements are replaced by distributed components in the form of transmission lines with different lengths, widths and shapes.

Some of the most used distributed inductances and capacitances are shown on Figure VIII-2 and Figure VIII-3 respectively.

II – Transmission planar lines

The above distributed components were used for both integrated and hybrid circuits. In the last decades, many planar structures for MIC design have been conceived (Figure VIII-4).

The materials you receive for this course are protected by copyright and to be used for this course only. You do not have permission to upload the course materials, including any lecture recordings you may have, to any website. If you require clarification, please consult your professor.

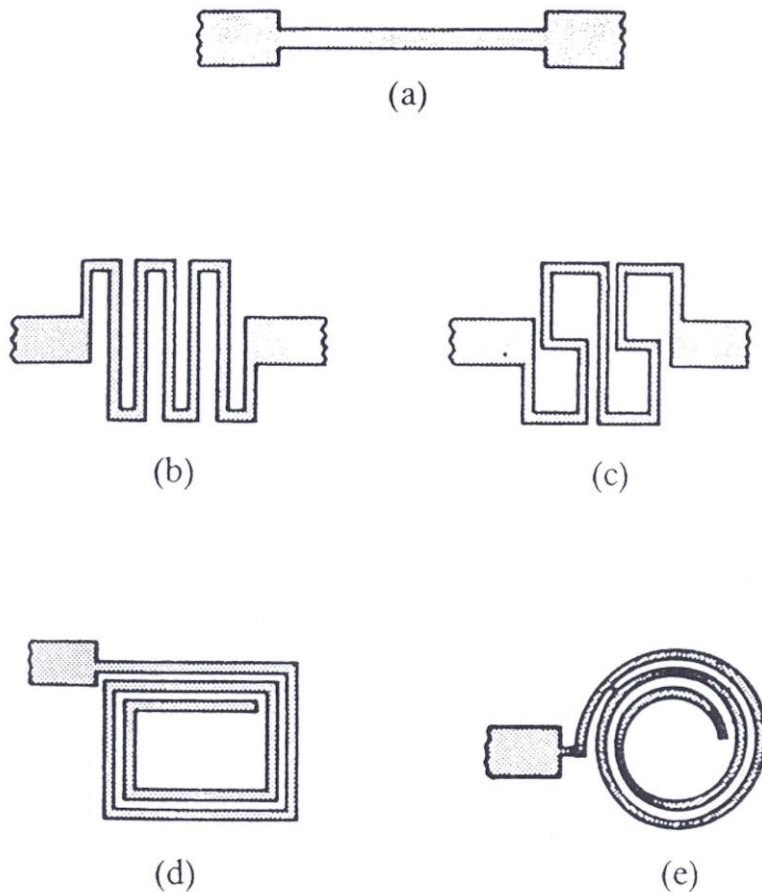


Fig. VIII-2: Some planar inductor configurations

- (a) High impedance section line
- (b) Meander line
- (c) S-line
- (d) Square spiral
- (e) Circular spiral

The materials you receive for this course are protected by copyright and to be used for this course only. You do not have permission to upload the course materials, including any lecture recordings you may have, to any website. If you require clarification, please consult your professor.

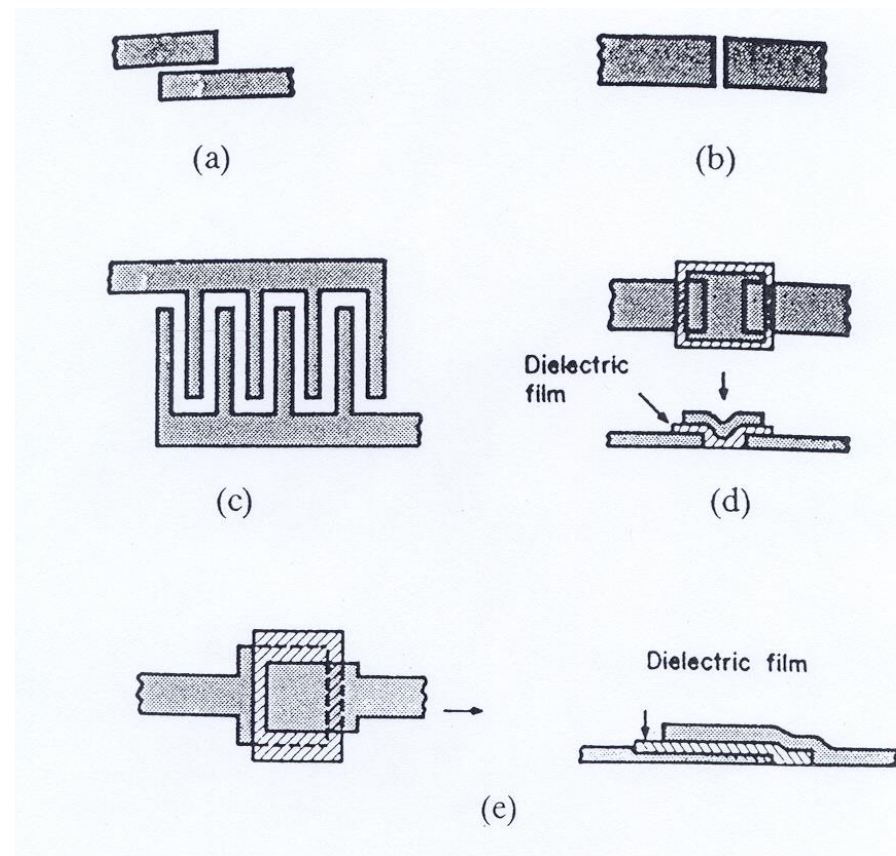


Fig. VIII-3: Some planar capacitor configurations

- (a) Broadside coupled
- (b) End coupled
- (c) Interdigitated
- (d) End coupled overlay
- (e) Overlay

The materials you receive for this course are protected by copyright and to be used for this course only. You do not have permission to upload the course materials, including any lecture recordings you may have, to any website. If you require clarification, please consult your professor.

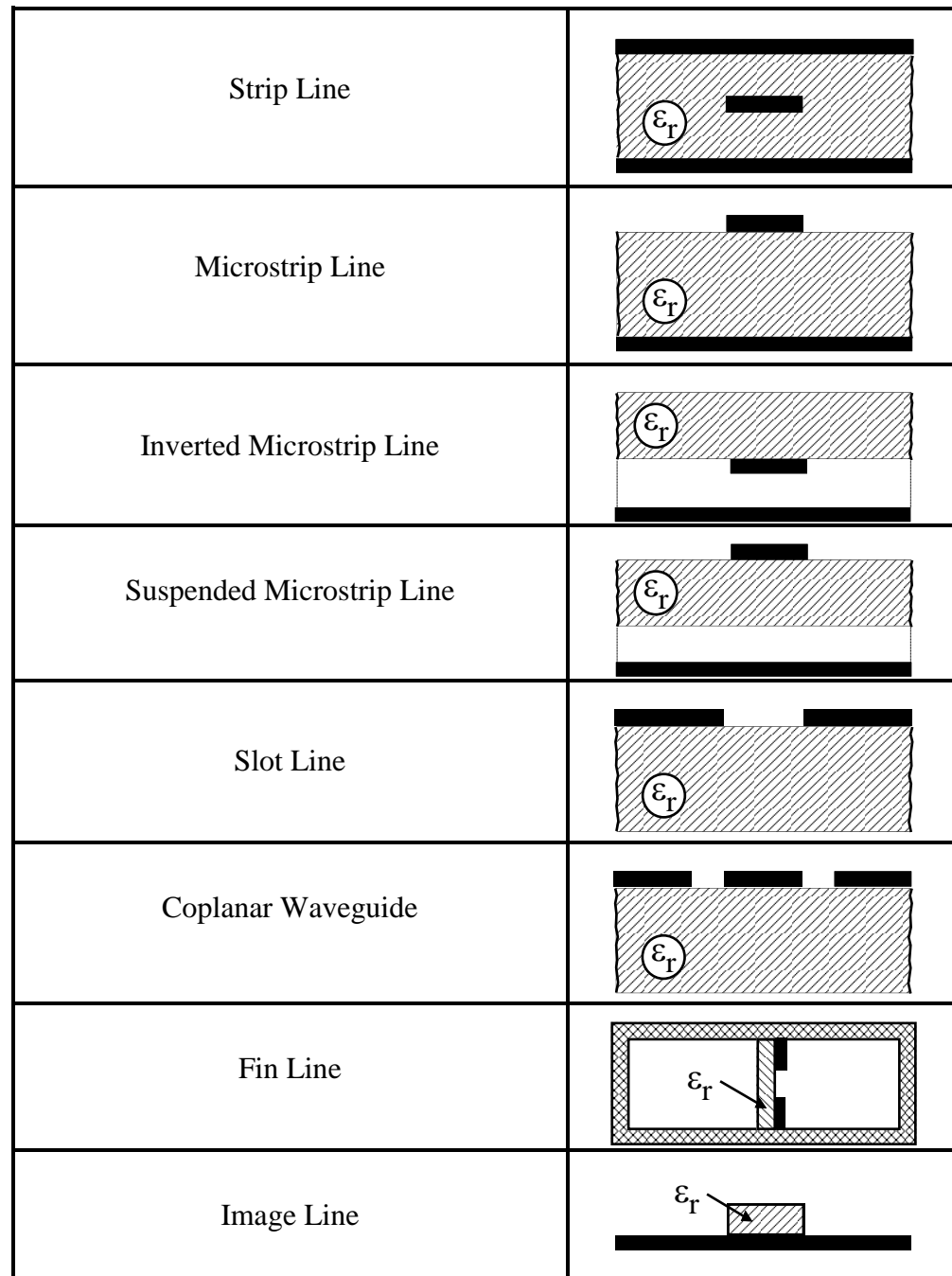


Fig. VIII-4: Transmission planar lines used in microwave circuits

The materials you receive for this course are protected by copyright and to be used for this course only. You do not have permission to upload the course materials, including any lecture recordings you may have, to any website. If you require clarification, please consult your professor.

Every structure comprises a combination of metal and dielectric. As microstrip lines are the most widely used planar lines in the centimeter range, the entire project will be built using this type of transmission lines.

B – MICROSTRIP LINES

I- Definition of a microstrip transmission line

Microstrip transmission line is a kind of "high grade" printed circuit construction, consisting of a track of copper or other conductor on an insulating substrate. There is a "ground plane" on the other side of the insulating substrate, formed from similar conductor (Figure VIII-5).

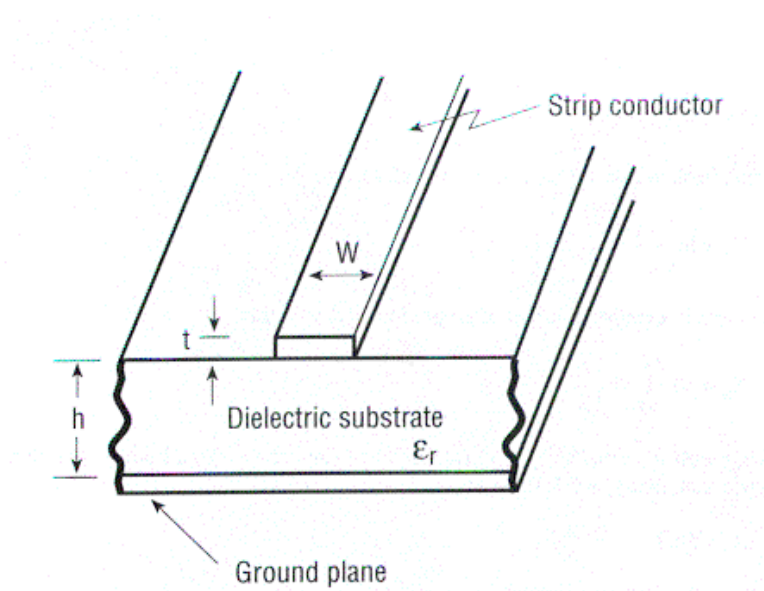


Fig. VIII-5: Microstrip parameters

The materials you receive for this course are protected by copyright and to be used for this course only. You do not have permission to upload the course materials, including any lecture recordings you may have, to any website. If you require clarification, please consult your professor.

Looked at end on, there is a "hot" conductor that is the track on the top, and a "return" conductor that is the plane on the bottom. Microstrip is therefore a variant of 2-wire transmission line.

If one solves the electromagnetic equations to find the field distributions, one finds very nearly a completely TEM (transverse electromagnetic) pattern. This means that there are only a few regions in which there is a component of electric or magnetic field in the direction of wave propagation.

The field pattern is commonly referred to as a Quasi TEM pattern. Under some conditions one has to take account of the effects due to longitudinal fields. An example is geometrical dispersion, where different wave frequencies travel at different phase velocities, and the group and phase velocities are different.

The quasi TEM pattern arises because of the interface between the dielectric substrate and the surrounding air. The electric field lines have a discontinuity in direction at the interface.

The boundary conditions for electric field are that the normal component (i.e. the component at right angles to the surface) of the electric field times the dielectric constant is continuous across the boundary; thus in the dielectric which may have dielectric constant 10, the electric field suddenly drops to 1/10 of its value in air.

On the other hand, the tangential component (parallel to the interface) of the electric field is continuous across the boundary. In general then we observe a sudden change of direction of electric field lines at the interface, which gives rise to a longitudinal magnetic field component from the second Maxwell's equation,

$$\text{curl } E = - \frac{dB}{dt} \quad (\text{VIII-1})$$

The materials you receive for this course are protected by copyright and to be used for this course only. You do not have permission to upload the course materials, including any lecture recordings you may have, to any website. If you require clarification, please consult your professor.

Since some of the electric energy is stored in the air and some in the dielectric, the effective dielectric constant for the waves on the transmission line will lie somewhere between that of the air and that of the dielectric. Typically the effective dielectric constant will be 50-85% of the substrate dielectric constant. As an example, in air spaced microstrip the velocity of waves would be $3 * 10^8$ meters per second. We have to divide this value by the square root of the effective dielectric constant to find the actual wave velocity for the real microstrip line.

At 10 GHz the wavelength on air spaced microstrip is therefore 3 cm; however on a substrate with effective dielectric constant of 7 the wavelength is

$$\lambda_{guided} = \frac{\lambda_0}{\sqrt{\epsilon_r}} = \frac{3}{\sqrt{7}} = 1.13\text{cm} \quad (\text{VIII-2})$$

Thus the maximum length for a stub to be used in stub matching, which is no more than half a wavelength, is about 5.6 mm. There is a rough and ready monogram for calculating the impedance of microstrip from the dielectric properties and the geometry. (Figure VIII-6).

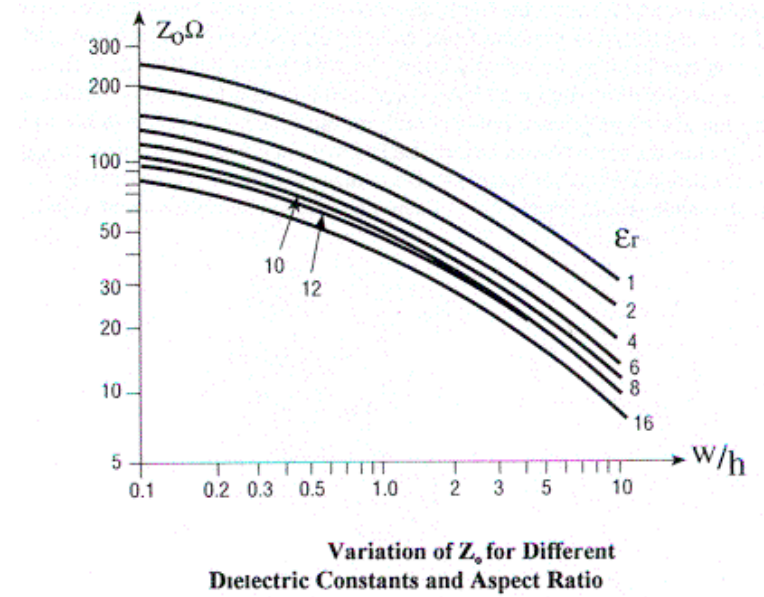


Fig. VIII-6: monogram for calculating the impedance of microstrip
II - substrate material choice

Many facets, mechanical and thermal as well as electronic and economic, influence the decision process leading to the correct choice of a particular substrate for a specific type of MIC and application.

Important qualities of the dielectric substrate include

- The microwave dielectric constant
- The frequency dependence of this dielectric constant which gives rise to "material dispersion" in which the wave velocity is frequency-dependent
- The surface finish and flatness
- The dielectric loss tangent, or imaginary part of the dielectric constant, which sets the dielectric loss
- The cost

The materials you receive for this course are protected by copyright and to be used for this course only. You do not have permission to upload the course materials, including any lecture recordings you may have, to any website. If you require clarification, please consult your professor.

Chapter VIII: Microwave Filters

- The thermal expansion and conductivity
- The dimensional stability with time
- The surface adhesion properties for the conductor coatings
- The manufacturability (ease of cutting, shaping, and drilling)
- The porosity (for high vacuum applications we don't want a substrate which continually "outgasses" when pumped)

Types of substrate include plastics, sintered ceramics, glasses, and single crystal substrates (single crystals may have anisotropic dielectric constants; "anisotropic" means they are different along the different crystal directions with respect to the crystalline axes.)

The materials you receive for this course are protected by copyright and to be used for this course only. You do not have permission to upload the course materials, including any lecture recordings you may have, to any website. If you require clarification, please consult your professor.

III – Common substrate materials

- Plastics are cheap, easily manufacturable, have good surface adhesion, but have poor microwave dielectric properties when compared with other choices. They have poor dimensional stability, large thermal expansion coefficients, and poor thermal conductivity.
 - Dielectric constant: 2.2 (fast substrate) or 10.4 (slow substrate)
 - Loss tangent 1/1000 (fast substrate) 3/1000 (slow substrate)
 - Surface roughness about 6 microns (electroplated)
 - Low thermal conductivity, 3/1000 watts per cm sq per degree
- Ceramics are rigid and hard; they are difficult to shape, cut, and drill; they come in various purity grades and prices each having domains of application; they have low microwave loss and are reasonably non-dispersive; they have excellent thermal properties, including good dimensional stability and high thermal conductivity; they also have very high dielectric strength. They cost more than plastics. In principle the size is not limited.
 - Dielectric constant 8-10 (depending on purity) so slow substrate
 - Loss tangent 1/10,000 to 1/1,000 depending on purity
 - Surface roughness at best 1/20 micron
 - High thermal conductivity, 0.3 watts per sq cm per degree K
- Single crystal sapphire is used for demanding applications; it is very hard, needs orientation for the desired dielectric properties which are anisotropic; is very expensive, can only be made in small sheets; has high dielectric constant so is used for very compact circuits at high frequencies; has low dielectric loss; has excellent thermal properties and surface polish.

The materials you receive for this course are protected by copyright and to be used for this course only. You do not have permission to upload the course materials, including any lecture recordings you may have, to any website. If you require clarification, please consult your professor.

- Dielectric constant 9.4 to 11.6 depending on crystal orientation (slow substrate)
 - Loss tangent 5/100,000
 - Surface roughness 1/100 micron
 - High thermal conductivity 0.4 watts per sq cm per degree K
-
- Single crystal Gallium Arsenide (GaAs) and Silicon (Si) are both used for monolithic microwave integrated circuits (MMICs).
 - GaAs is expensive and piezoelectric; acoustic modes can propagate in the substrate and can couple to the electromagnetic waves on the conductors. So, dealing with GaAs first we have
 - Dielectric constant 13 (slow substrate)
 - Loss tangent 6/10,000 (high resistivity GaAs)
 - Surface roughness 1/40 micron
 - Thermal conductivity 0.3 watts per sq cm per degree K (high)
 - Now dealing with Silicon we have
 - Dielectric constant 12 (slow substrate)
 - Loss tangent 5/1000 (high resistivity)
 - Surface roughness 1/40 micron
 - Thermal conductivity 0.9 watts per sq cm per degree K (high)

The dielectric strength of ceramics and of single crystals far exceeds the strength of plastics, and so the power handling abilities are correspondingly higher, and the breakdown of high Q filter structures correspondingly less of a problem.

The materials you receive for this course are protected by copyright and to be used for this course only. You do not have permission to upload the course materials, including any lecture recordings you may have, to any website. If you require clarification, please consult your professor.

It is also a good idea to have a high dielectric constant substrate and a slow wave propagation velocity; this reduces the radiation loss from the circuits. However at the higher frequencies the circuits get impossible small, which restricts the power handling capability. For these applications one often chooses fused quartz (dielectric constant 3.8).

C – LC ELEMENTS IN MICROSTRIP LINES

I – Basic relations in microstrip

The effective permittivity of a microstrip is given by:

$$\epsilon_{eff} = \frac{C}{C_1} \quad (\text{VIII-3})$$

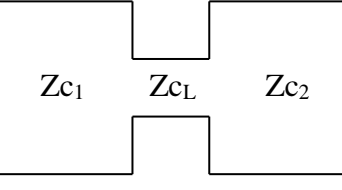
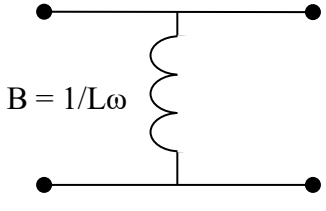
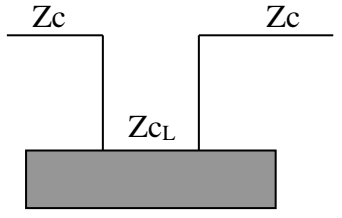
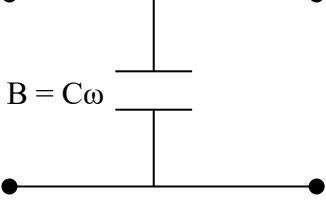
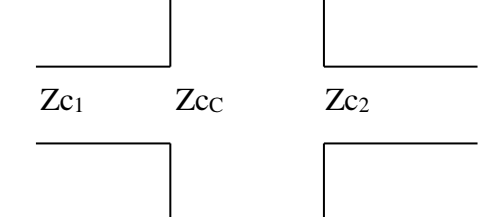
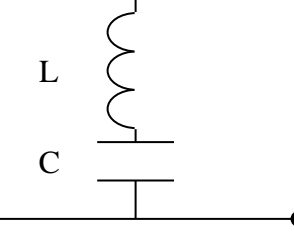
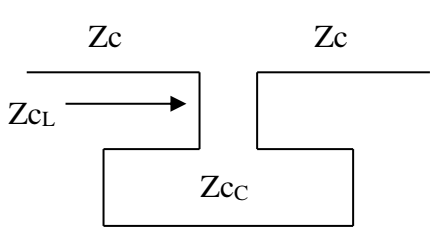
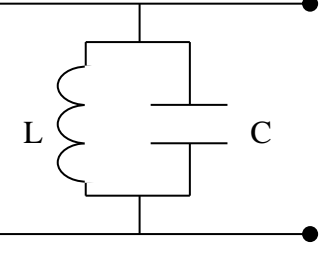
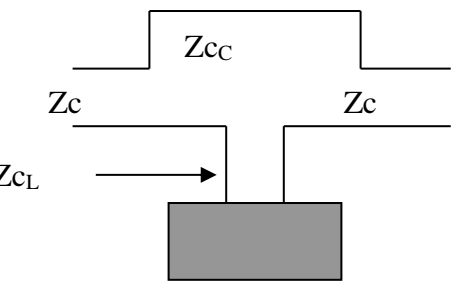
where C and C_1 are the microstrip capacitance per strip with the substrate present and absent respectively. Then, the velocity of propagation is related to the effective permittivity and to the characteristic impedance by:

$$v_p = \frac{c}{\sqrt{\epsilon_{eff}}} \quad (\text{VIII-4-a})$$

$$Z_0 = \frac{1}{v_p C} = \frac{1}{c C_1 \sqrt{\epsilon_{eff}}} \quad (\text{VIII-4-b})$$

The materials you receive for this course are protected by copyright and to be used for this course only. You do not have permission to upload the course materials, including any lecture recordings you may have, to any website. If you require clarification, please consult your professor.

II – Ideal equivalent L or C transmission line in microstrip

Circuit	Model
 $X = L\omega$	 Z_{c1} Z_{cL} Z_{c2} $Z_{cL} \gg Z_{c1,2}$
 $B = 1/L\omega$	 Z_c Z_c Z_{cL} $Z_{cL} \gg Z_c$
 $B = C\omega$	 Z_{c1} Z_{cc} Z_{c2} $Z_{cc} \ll Z_{c1,2}$
 L C	 Z_c $Z_{cL} \rightarrow$ Z_{cc} $Z_{cc} \ll Z_c \ll Z_{cL}$
 L C	 Z_c $Z_{cL} \rightarrow$ Z_{cc} Z_c $Z_{cc} \ll Z_c \ll Z_{cL}$

The materials you receive for this course are protected by copyright and to be used for this course only. You do not have permission to upload the course materials, including any lecture recordings you may have, to any website. If you require clarification, please consult your professor.

The above table shows the equivalent L/C distributed elements in microstrip lines. These representations are ideal. In fact, due to the discontinuity effects, inductive or capacitive microstrip lines are much more complicated to model.

III – Synthesis formulae for the $\{w/h\}$ ratio and $\epsilon_{\text{effective}}$

Z_o (characteristic impedance of the line) and permittivity ϵ_r are given

W/h RATIO

for narrow strips : { $Z_o > (44 - 2 \epsilon_r)$ },

$$\left(\frac{w}{h}\right) = \frac{1}{\left(\frac{\exp(H')}{8} - \frac{1}{4\exp(H')}\right)}$$

$$H' = \frac{Z_o \sqrt{2(\epsilon_r + 1)}}{119.9} + \frac{1}{2} \left(\frac{\epsilon_r - 1}{\epsilon_r + 1} \right) \left(\ln\left(\frac{\pi}{2}\right) + \frac{1}{\epsilon_r} \ln\left(\frac{4}{\pi}\right) \right)$$

for wide strips : { $Z_o < (44 - 2 \epsilon_r)$ },

$$\left(\frac{w}{h}\right) = \frac{2}{\pi} \left((d - 1) - \ln(2d - 1) \right) + \frac{\epsilon_r - 1}{\pi \epsilon_r} \left(\ln(d - 1) + 0.293 - \frac{0.517}{\epsilon_r} \right)$$

$$d = \frac{59.95 \pi^2}{Z_o \sqrt{\epsilon_r}}$$

ϵ_{eff}

for narrow strips : { $Z_o > (63 - 2 \epsilon_r)$ },

$$\epsilon_{eff} = \frac{\epsilon_r + 1}{2} \left(1 - \frac{1}{2H'} \left(\frac{\epsilon_r - 1}{\epsilon_r + 1} \right) \left(\ln \left(\frac{\pi}{2} \right) + \frac{1}{\epsilon_r} \ln \left(\frac{4}{\pi} \right) \right) \right)^{-2}$$

$$H' = \frac{Z_o \sqrt{2(\epsilon_r + 1)}}{119.9} + \frac{1}{2} \left(\frac{\epsilon_r - 1}{\epsilon_r + 1} \right) \left(\ln \left(\frac{\pi}{2} \right) + \frac{1}{\epsilon_r} \ln \left(\frac{4}{\pi} \right) \right)$$

if we have Z_o or if we have w/h

$$H' = \ln \left(4 \frac{h}{w} + \sqrt{16 \left(\frac{h}{w} \right)^2 + 2} \right)$$

IV – Analysis formulae for Z_o (w/h and permittivity ϵ_r are given)

for narrow strips : { $w/h < 3.3$ },

$$Z_o = \frac{119.9}{\sqrt{2(\epsilon_r + 1)}} \left[\ln \left(4 \frac{h}{w} + \sqrt{16 \left(\frac{h}{w} \right)^2 + 2} \right) \right]$$

for wide strips : { $w/h \geq 3.3$ },

$$Z_o = \frac{119.9 \pi}{2 \sqrt{\epsilon_r}} \frac{1}{\frac{1}{2} \frac{w}{h} + \frac{\ln(4)}{\pi} + \left(\frac{\ln(e \pi^2 / 16)}{2 \pi} \right) \left(\frac{\epsilon_r - 1}{\epsilon_r^2} \right) + \left(\frac{\epsilon_r + 1}{2 \pi \epsilon_r} \right) \left(\frac{\ln(e \pi)}{2} + \ln \left(\frac{1}{2} \frac{w}{h} + 0.94 \right) \right)}$$

“e” is the exponential base : $e = 2.71828$.

V – Real equivalent L or C transmission line in microstrip

For short ($< \lambda_g/4$) loss-free lines, basic transmission line theory gives the input reactance X_L of a predominantly inductive line of length l_L as

$$X_L = Z_{oL} \tan\left(\frac{2\pi l_L}{\lambda_{gL}}\right) \quad (\text{VIII-5})$$

where Z_{oL} is the characteristic impedance of the inductive line and λ_{gL} the guided wavelength. Then, the length is

$$l_L = \frac{\lambda_{gL}}{2\pi} \tan^{-1}\left(\frac{2\pi f L}{Z_{oL}}\right) \quad (\text{VIII-6})$$

But equation (VIII-5) implies that the inductive effect can exist only if the high impedance inductive line is presented with adjacent lengths of low impedance, and therefore, wide lines (Fig. VIII-7). This step discontinuity presents a step capacitance of susceptance:

$$B_{CL} = \frac{1}{Z_{oL}} \tan\left(\frac{2\pi l_{CL}}{\lambda_{gL}}\right) \quad (\text{VIII-7})$$

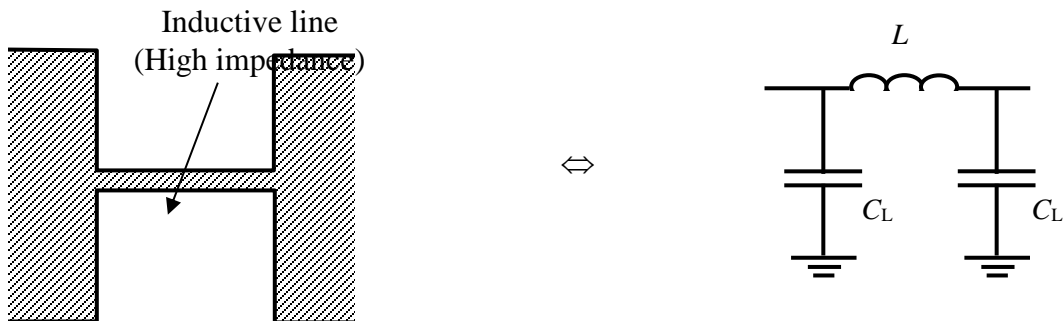


Fig. VIII-7: Inductive microstrip line.

The materials you receive for this course are protected by copyright and to be used for this course only. You do not have permission to upload the course materials, including any lecture recordings you may have, to any website. If you require clarification, please consult your professor.

so that

$$l_{CL} = \frac{\lambda_{gL}}{2\pi} \tan^{-1}(2\pi f CZ_{oL}) \quad (\text{VIII-8})$$

$$C_L = \frac{1}{2\pi f Z_{oL}} \tan\left(\frac{2\pi l_{CL}}{\lambda_{gL}}\right) \quad (\text{VIII-9})$$

Similarly, the input susceptance B_C of a predominantly capacitive line of length l_C is given by

$$B_C = \frac{1}{Z_{oC}} \tan\left(\frac{2\pi l_C}{\lambda_{gC}}\right) \quad (\text{VIII-10})$$

where Z_{oC} is the characteristic impedance of the capacitive line and λ_{gC} the guided wavelength. Then, the length is

$$l_C = \frac{\lambda_{gC}}{2\pi} \tan^{-1}(2\pi f CZ_{oC}) \quad (\text{VIII-11})$$

As for the inductive line, the capacitive effect will be predominant only if the low impedance capacitive line is presented with adjacent lengths of high impedance, and therefore, narrow lines (Fig. VIII-8). Thus, the end inductance is

$$X_{LC} = Z_{oC} \tan\left(\frac{2\pi l_{LC}}{\lambda_{gC}}\right) \quad (\text{VIII-12})$$

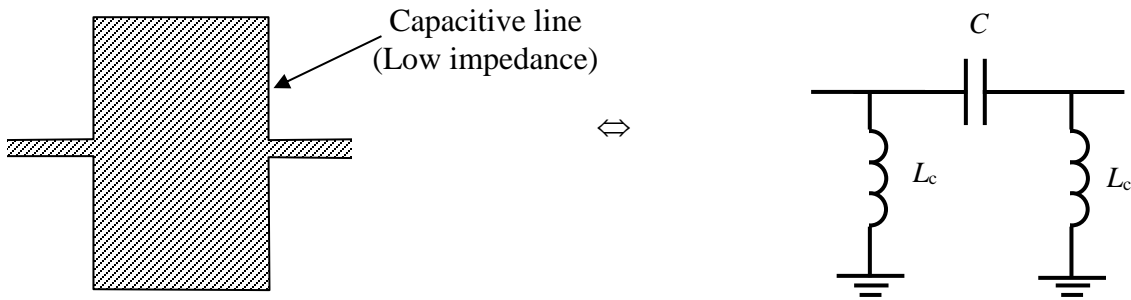


Fig. VIII-8: Capacitive microstrip line.

so that

$$l_{LC} = \frac{\lambda_{gC}}{2\pi} \tan^{-1} \left(\frac{2\pi f L_C}{Z_{oC}} \right) \quad (\text{VIII-13})$$

and

$$L_C = \frac{Z_{oC}}{2\pi f} \tan \left(\frac{2\pi l_{LC}}{\lambda_{gC}} \right) \quad (\text{VIII-14})$$

In conclusion,

- * The step discontinuity from narrow to wide width is equivalent to a parallel capacitance that should be subtracted from the circuit
- * The step discontinuity from wide to narrow width is equivalent to a series inductance that should be subtracted from the circuit

Other discontinuities are present in a microstrip circuit as the end-effect line (line loaded by an infinite resistance) or the series gap (interruption in the conducting strip). The exact formulas can be easily found in the technical literature.

The materials you receive for this course are protected by copyright and to be used for this course only. You do not have permission to upload the course materials, including any lecture recordings you may have, to any website. If you require clarification, please consult your professor.

VI – Parallel-coupled microstrip lines

Any pair of parallel lines in microstrip technology (or coupled lines) exhibits a dual mode behavior (Fig. VIII-9). The consistent field patterns correspond to two waves traveling in opposite directions along the respective line. At any instant, the relative polarities of the potentials, taken at any specific plane along the structure, will either be **alike or opposite**. We refer to the different field configurations set up by such polarities as the **even mode** and the **odd mode** respectively.

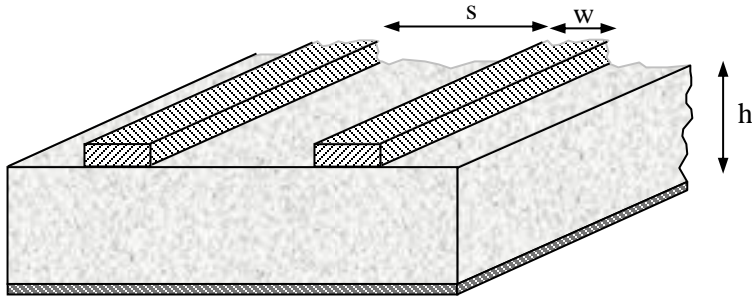


Fig. VIII-9: Parallel microstrip lines.

For odd and even modes, we therefore have respectively

$$Z_{0o} = \frac{1}{cC_{1o}\sqrt{\epsilon_{effo}}} \quad (\text{VIII-15})$$

and

$$Z_{0e} = \frac{1}{cC_{1e}\sqrt{\epsilon_{effe}}} \quad (\text{VIII-16})$$

The materials you receive for this course are protected by copyright and to be used for this course only. You do not have permission to upload the course materials, including any lecture recordings you may have, to any website. If you require clarification, please consult your professor.

As an illustration, some numerical data obtained using the even- and odd-mode characteristic impedances of parallel-coupled microstrip lines above equations are presented graphically ((a) for air spaced lines and (b) with a substrate having relative permittivity ϵ_r).

In these graphs (Fig. VIII-10), Z_{0e} and Z_{0o} are marked on the vertical axis for the appropriate substrate material (ϵ_r). It is then necessary to read these values across horizontally until two points are found lying vertically above one another, and at identical values of s/h . Dropping a vertical ordinate through these points then also yields the required values of w/h . Interpolation and other difficulties with the graphs makes this an approximate and rather clumsy design technique. However, it may be useful for a first turn design. From the characteristic impedances, we can obtain a relation relating the coupling factor of a parallel-coupled microstrip with the characteristic impedances of the even and odd modes:

$$C' = 20 \log \left(\frac{Z_{0e} - Z_{0o}}{Z_{0e} + Z_{0o}} \right) \quad (\text{VIII-17})$$

Using the impedance relationship

$$Z_0^2 \approx \sqrt{Z_{0e} Z_{0o}} \quad (\text{VIII-18})$$

From these expressions, the impedances required are

$$Z_{0e} \approx Z_0 \sqrt{\frac{1+10^{C'/20}}{1-10^{C'/20}}} \quad (\text{VIII-19})$$

$$Z_{0o} \approx Z_0 \sqrt{\frac{1-10^{C'/20}}{1+10^{C'/20}}} \quad (\text{VIII-20})$$

The materials you receive for this course are protected by copyright and to be used for this course only. You do not have permission to upload the course materials, including any lecture recordings you may have, to any website. If you require clarification, please consult your professor.

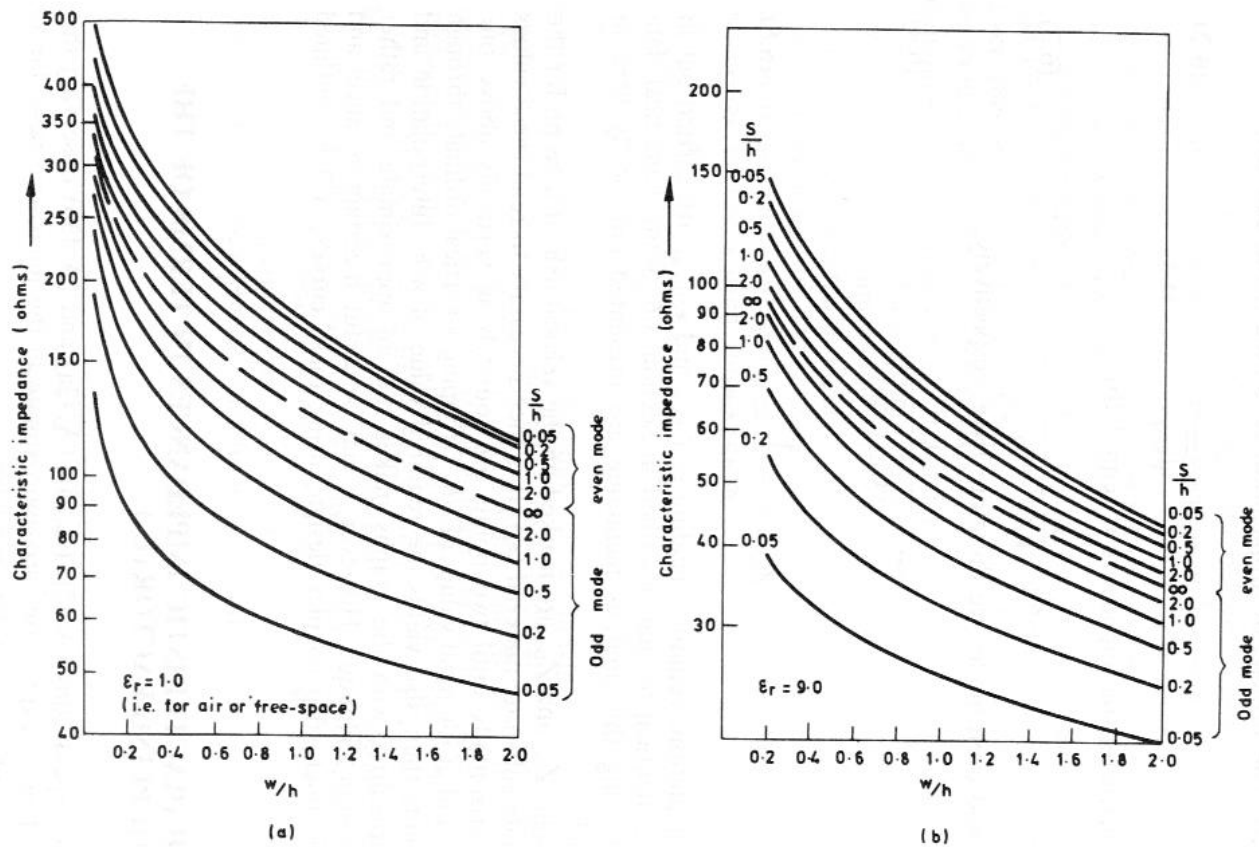


Fig. VIII-10: Even- and odd-mode characteristic impedances of parallel-coupled microstrip lines

(a) For air spaced lines (b) With a substrate having relative permittivity ϵ_r .

V – Analysis formulae for parallel-coupled microstrip

For the parallel-coupled microstrip design, we must define the total capacitances for each mode (Fig. VIII-11). We have:

$$C_e = C_p + C_f + C'_f \quad (\text{VIII-21})$$

The materials you receive for this course are protected by copyright and to be used for this course only. You do not have permission to upload the course materials, including any lecture recordings you may have, to any website. If you require clarification, please consult your professor.

and

$$C_o = C_p + C_f + C_{ga} + C_{gd} \quad (\text{VIII-22})$$

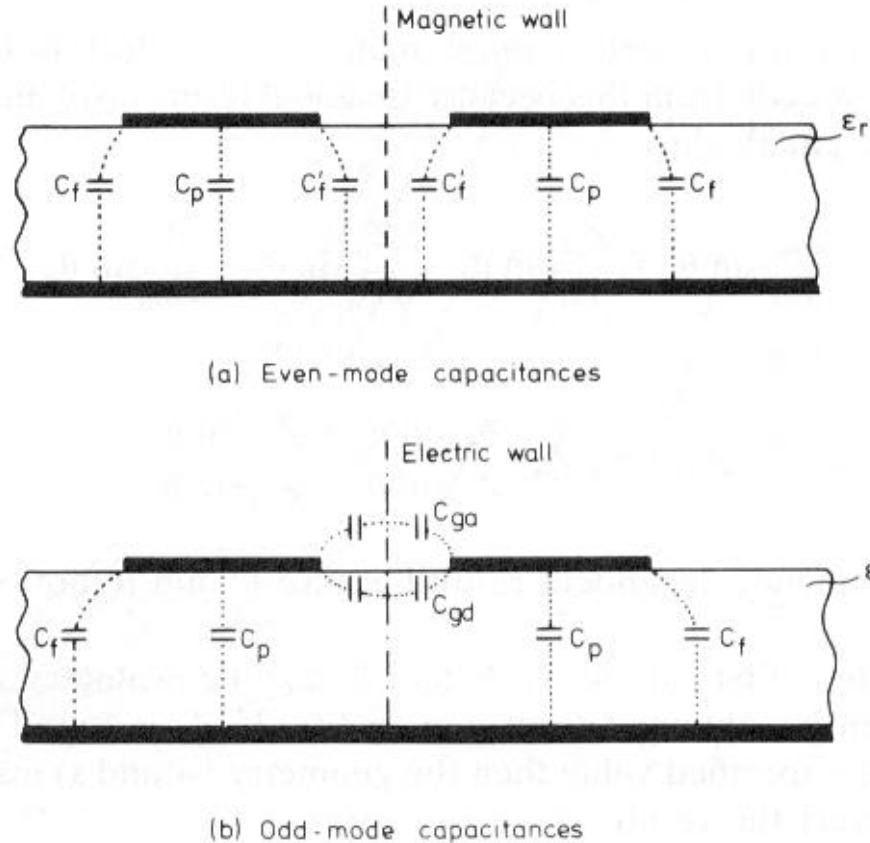


Fig. VIII-11: Total capacitances for the even- and odd-modes of parallel-coupled microstrip lines.

The capacitance C_p simply relates the parallel-plate line value given by

$$C_p = \epsilon_0 \epsilon_r \frac{w}{h} \quad (\text{VIII-23})$$

and C_f is the fringing capacitance due to each microstrip taken alone, as if for the single strip.

The materials you receive for this course are protected by copyright and to be used for this course only. You do not have permission to upload the course materials, including any lecture recordings you may have, to any website. If you require clarification, please consult your professor.

Then, we have

$$C_f = \frac{1}{2} \left(\frac{\sqrt{\epsilon_{eff}}}{cZ_o} - C_p \right) \quad (\text{VIII-24})$$

An empirical expression for C'_f is given as:

$$C'_f = \frac{C_f}{1 + \left(A \frac{h}{s} \right) \tanh \left(\frac{8s}{h} \right)} \sqrt{\frac{\epsilon_r}{\epsilon_{eff}}} \quad (\text{VIII-25})$$

where

$$A = \exp \left(-0.1 e^{2.33 - 2.53 \frac{w}{h}} \right) \quad (\text{VIII-26})$$

As can be seen from the above figure that C_{ga} and C_{gd} are respectively the odd-mode fringing field capacitances for the air and dielectric regions across the coupling gap. C_{ga} is obtained using the elliptic functions K

$$C_{ga} = \epsilon_o \frac{K(k)}{K(\bar{k})} \quad (\text{VIII-27})$$

$$k = \frac{s}{\frac{s}{h} + \frac{2w}{h}} \quad (\text{VIII-28})$$

The materials you receive for this course are protected by copyright and to be used for this course only. You do not have permission to upload the course materials, including any lecture recordings you may have, to any website. If you require clarification, please consult your professor.

and

$$k' = \sqrt{1 - k^2} \quad (\text{VIII-29})$$

where the ratio of the elliptic functions is

for $0 \leq k^2 \leq 0.5$

$$\frac{K(k')}{K(k)} = \frac{1}{\pi} \ln \left(2 \frac{1 + \sqrt{k'}}{1 - \sqrt{k'}} \right) \quad (\text{VIII-30})$$

for $0.5 \leq k^2 \leq 1$

$$\frac{K(k')}{K(k)} = \frac{\pi}{\ln \left\{ 2 \frac{1 + \sqrt{k}}{1 - \sqrt{k}} \right\}} \quad (\text{VIII-31})$$

The capacitance C_{gd} was determined differently

$$C_{gd} = \frac{\epsilon_o \epsilon_r}{\pi} \ln \left\{ \coth \left(\frac{\pi}{4} \frac{s}{h} \right) \right\} + 0.65 C_f \left\{ \frac{0.02}{s/h} \sqrt{\epsilon_r} + 1 - \epsilon_r^{-2} \right\} \quad (\text{VIII-32})$$

The even-mode and odd-mode characteristic impedances are then

$$Z_{0e} = \frac{1}{c \sqrt{C_e C_{e1}}} \quad (\text{VIII-33})$$

The materials you receive for this course are protected by copyright and to be used for this course only. You do not have permission to upload the course materials, including any lecture recordings you may have, to any website. If you require clarification, please consult your professor.

and

$$Z_{0o} = \frac{1}{c\sqrt{C_o C_{o1}}} \quad (\text{VIII-34})$$

VIII – Synthesis technique for the $\{w/h\}$ and $\{s/h\}$ ratios

For the parallel-coupled microstrip design, the goal is to determine the $\{w/h\}$ and $\{s/h\}$ ratios. We can use universal graphs or a relatively simple computer routine. The process necessitates two steps:

- The first one is the determination of equivalent single microstrip shape ratios $\{w/h\}_{se}$.
- The second step relates the required $\{w/h\}$ and $\{s/h\}$ ratios for the coupled structure to the equivalent single microstrip shape ratios.

A summary of the design stages is thus:

- 1- Determine the shape ratios for equivalent single microstrip lines. We use the following relationships:

$$Z_{0se} = \frac{Z_{0e}}{2} \quad (\text{VIII-35})$$

for single microstrip shape ratio $\{w/h\}_{se}$, and

$$Z_{0so} = \frac{Z_{0o}}{2} \quad (\text{VIII-36})$$

for single microstrip shape ratio $\{w/h\}_{so}$. These relations can be also derived from the coupling factor:

$$Z_{0se} \approx \frac{Z_0}{2} \sqrt{\frac{1+10^{C'/20}}{1-10^{C'/20}}} \quad (\text{VIII-37})$$

$$Z_{0so} \approx \frac{Z_0}{2} \sqrt{\frac{1-10^{C'/20}}{1+10^{C'/20}}} \quad (\text{VIII-38})$$

Akhtarzad *et al.* have given a family of useful expressions to obtain the shape ratio $\{w/h\}_{se}$:

$$\left(\frac{w}{h}\right)_{se} = \frac{2}{\pi} \cosh^{-1} \left(\frac{2d-g+1}{g+1} \right) \quad (\text{VIII-39})$$

For $\{w/h\}_{so}$ we use one of the two following expressions:

For $\varepsilon_r \leq 6$

$$\left(\frac{w}{h}\right)_{so} = \frac{2}{\pi} \cosh^{-1} \left(\frac{2d-g-1}{g-1} \right) + \frac{4}{\pi \left(1 + \frac{\varepsilon_r}{2} \right)} \cosh^{-1} \left(1 + 2 \frac{w/h}{s/h} \right) \quad (\text{VIII-40})$$

For $\varepsilon_r > 6$

$$\left(\frac{w}{h}\right)_{so} = \frac{2}{\pi} \cosh^{-1} \left(\frac{2d-g-1}{g-1} \right) + \frac{1}{\pi} \cosh^{-1} \left(1 + 2 \frac{w/h}{s/h} \right) \quad (\text{VIII-41})$$

where

$$g = \cosh\left(\frac{\pi s}{2h}\right) \quad (\text{VIII-42})$$

and

$$d = \cosh\left(\pi \frac{w}{h} + \frac{\pi s}{2h}\right) \quad (\text{VIII-43})$$

Equation (VIII-39) has to be solved with either (VIII-40) or (VIII-41) as appropriate for the particular permittivity range.

- 2- **Unfortunately, the problem is exactly the inverse.** From Z_{ose} and Z_{oso} we obtain $\{w/h\}_{se}$ and $\{w/h\}_{so}$ and then, we **have to deduce** the $\{w/h\}$ and $\{s/h\}$ ratios. So equations (VIII-35)-(VIII-36) should be used as two nonlinear equations with two unknown variables namely $\{w/h\}$ and $\{s/h\}$. The resolution of this nonlinear system is relatively difficult, so it is more convenient to use the following explicit formula for $\{s/h\}$:

$$\frac{s}{h} = \frac{2}{\pi} \cosh^{-1} \left(\frac{\cosh\left(\frac{\pi}{2} \left(\frac{w}{h} \right)_{se}\right) + \cosh\left(\frac{\pi}{2} \left(\frac{w}{h} \right)_{so}\right) - 2}{\cosh\left(\frac{\pi}{2} \left(\frac{w}{h} \right)_{so}\right) - \cosh\left(\frac{\pi}{2} \left(\frac{w}{h} \right)_{se}\right)} \right) \quad (\text{VIII-44})$$

and then to deduce the $\{w/h\}$ ratio. But compared to the results of Bryant and Weiss, an error of the order of 10% has been quoted for this synthesis technique. So, this technique may still be used to obtain an initial design, after which the more accurate analysis of Garg and Bahl could be employed to correct the design dimensions.

The sequence is:

- With the required Z_{0e} and Z_{0o} determine the first values $\{w/h\}_1$ and $\{s/h\}_1$ by the approximate synthesis.
- Using these values, recalculate Z_{0e} and Z_{0o} by means of the semi-empirical analysis formulae given by equations (VIII-35) and (VIII-36).
- Compare the new values thus calculated Z_{0e} and Z_{0o} with those originally required. A suitable program will then enable iterations to be made incrementing $\{w/h\}$ and $\{s/h\}$ until the impedances agree within a specified tolerance.

As an illustration, we want to design a coupler in a microstrip technology (input/output impedances of 50Ω), with a coupling factor of 10 dB (in fact -10dB), using a substrate of permittivity $\epsilon_r = 9.0$ and $h = 1\text{mm}$ at 5GHz. The above relations give

$$Z_{0e} = 69.5\Omega \quad Z_{0o} = 36\Omega$$

We can verify that the following relation is a good approximation:

$$Z_0^2 = \sqrt{69.5 * 36} = 50.02\Omega$$

From these values, we obtain:

$$Z_{0se} = \frac{Z_{0e}}{2} = 35\Omega$$

$$Z_{0so} = \frac{Z_{0o}}{2} = 18\Omega$$

and then:

$$\left(\frac{w}{h}\right)_{se} \approx 2.0$$

$$\left(\frac{w}{h}\right)_{so} \approx 5.0$$

Now, the final $\{w/h\}$ and $\{s/h\}$ ratios can be deduced:

$$\left(\frac{w}{h}\right) \approx 0.85 \quad \left(\frac{s}{h}\right) \approx 0.25$$

IX – Synthesis technique for the lengths

We can show that the maximum degree of coupling occurs when the length of the coupled region is made $\lambda_g/4$ where λ_g is the mid-band wavelength.

In the case of parallel-coupled lines, the odd- and even-mode wavelengths can be deduced from the flowing equations where the frequency f is in GHz:

$$\lambda_{ge} \approx \frac{300}{f} \frac{Z_{0e}}{Z_{0le}} \quad (\text{VIII-45})$$

The materials you receive for this course are protected by copyright and to be used for this course only. You do not have permission to upload the course materials, including any lecture recordings you may have, to any website. If you require clarification, please consult your professor.

and

$$\lambda_{go} \approx \frac{300}{f} \frac{Z_{0o}}{Z_{0le}} \quad (\text{VIII-46})$$

where the impedances Z_{0le} and Z_{0lo} are the even and odd impedances when the substrate is removed (i.e., when $\epsilon_r = 1$). They can be obtained using the above synthesis formulae of Z_{0e} and Z_{0o} with $\epsilon_r = 1$. If we return to the coupler designed in the above section, we obtain:

$$\lambda_{ge} = 22.54 \text{ mm} \qquad \lambda_{goe} = 28.8 \text{ mm}$$

X – Impedance and admittance inverters

The simplest form of an impedance inverter is the quarter-wave transformer. Such circuit transforms any load impedance by the quantity Z_o^2 where Z_o is the characteristic impedance of the quarter-wave transforming section of line.

Moreover, we can show that a network consisting of admittance inverters, or J-inverters, and uniform-type resonant circuits is to be made equivalent to the original network consisting of two types of resonant circuit-series and parallel.

XI – End effects: the foreshortened open circuit (end open line effect)

End effects of open lines in pass-band filters are not negligible. So I advice you to take it into account.

When a physical line is abruptly terminated, it will be equivalent to an open circuit (Fig. 12). Then, the main phenomena associated with this open circuit are the fringing fields (extended *beyond* the abrupt physical end of the metallic strip) and the radiated energy from the open end. These effects can be modeled by a capacitance C_f equal to

$$\frac{C_f}{w} = \exp \left(2.2036 \sum_{i=1}^5 K_\varepsilon \left(\log \frac{w}{h} \right)^{i-1} \right) \quad \text{in pF/m}$$

where the coefficients K_ε and are given in Table I as function of ε_r . In practice, this capacitance is equivalent to an equivalent extra length of microstrip line l_{eo} (Fig. 13).

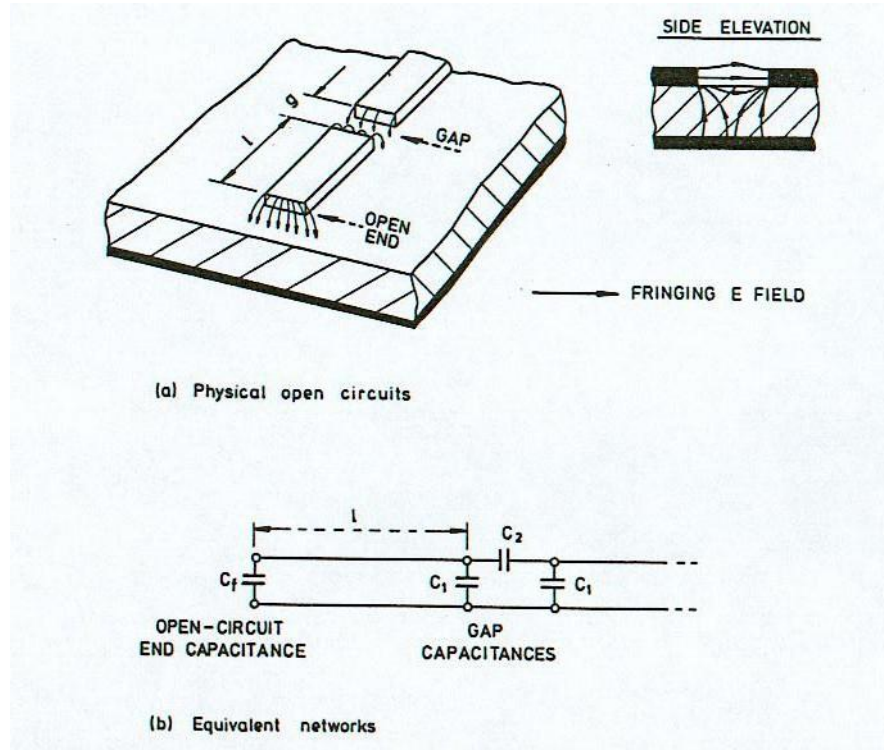


Fig. 12. Microstrip open circuit (a) and its equivalent lumped capacitive network (b).

The materials you receive for this course are protected by copyright and to be used for this course only. You do not have permission to upload the course materials, including any lecture recordings you may have, to any website. If you require clarification, please consult your professor.

Table I: Coefficients K_ε for C_f .

ϵ_r	1.0	2.5	4.2	9.6	16.0	51.0
i						
1	1.110	1.295	1.443	1.738	1.938	2.403
2	-0.2892	-0.2817	-0.2535	-0.2538	-0.2233	-0.2220
3	0.1815	0.1367	0.1062	0.1308	0.1317	0.2170
4	-0.0033	-0.0133	-0.0260	-0.0087	-0.0267	-0.0240
5	-0.0540	-0.0267	-0.0073	-0.0113	-0.0147	-0.0840

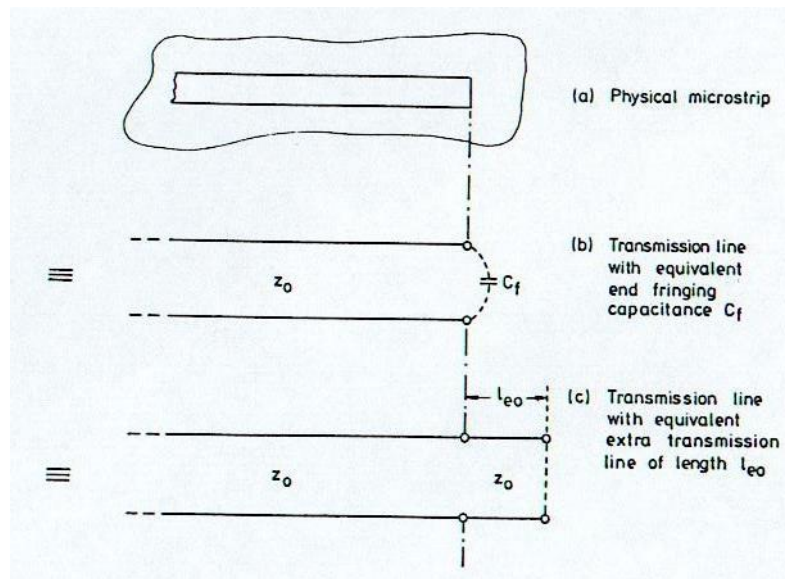


Fig. 13. Development of the equivalent end-effect length concept.

The materials you receive for this course are protected by copyright and to be used for this course only. You do not have permission to upload the course materials, including any lecture recordings you may have, to any website. If you require clarification, please consult your professor.

The input reactance to the extra length l_{eo} is given by the standard open-circuit terminated line equation

$$X_{eo} = \frac{Z_o}{j \tan(\beta l_{eo})}$$

On the other hand, the capacitive reactance due to C_f is

$$X_f = \frac{1}{j \omega C_f}$$

So, for equivalence, we must equate the two equations

$$\frac{1}{j \omega C_f} = \frac{Z_o}{j \tan(\beta l_{eo})}$$

Then

$$l_{eo} = \frac{1}{\beta} \tan^{-1} (\omega C_f Z_o)$$

$$l_{eo} = \frac{\lambda_g}{2\pi} \tan^{-1} (\omega C_f Z_o) = \frac{\lambda_o}{2\pi \sqrt{\epsilon_{eff}}} \tan^{-1} (\omega C_f Z_o) = \frac{c}{\omega \sqrt{\epsilon_{eff}}} \tan^{-1} (\omega C_f Z_o)$$

where c is the free-space velocity. Since the length is very small, then $\{ l_{eo} \ll \lambda_g \}$ and the above equation can be simplified to

$$l_{eo} \approx \frac{\lambda_g}{2\pi} \omega C_f Z_o \approx \frac{c \omega C_f Z_o}{\omega \sqrt{\epsilon_{eff}}} \approx \frac{c C_f Z_o}{\sqrt{\epsilon_{eff}}}$$

D – MICROSTRIP LOW-PASS FILTERS

I – Lumped equivalent circuit

As a low-pass filter unit cell is equivalent to an inductance with a parallel capacitance, The low-pass filter design using microstrip line technology implies the utilization of a cascade of L-series and C-parallel components. The series inductors, which exhibit high impedance, are implemented with high impedance (narrow) microstrip lines. The low impedance shunt capacitors are implemented with sections of low impedance (wide) microstrip lines. The resulting design is a cascade of wide and narrow microstrip sections. Determining the microstrip lengths for the circuit is algorithmic process that must be iterated a number of times. First we will assume that the characteristic impedance of the microstrip sections are known or calculated using the synthesis formulae.

We have shown on Figure VIII-7 and VIII-8 that adjacent capacitive lines bound the inductive line (and similarly, adjacent inductive lines bound the capacitive line as shown on Figure VIII-14).

The materials you receive for this course are protected by copyright and to be used for this course only. You do not have permission to upload the course materials, including any lecture recordings you may have, to any website. If you require clarification, please consult your professor.

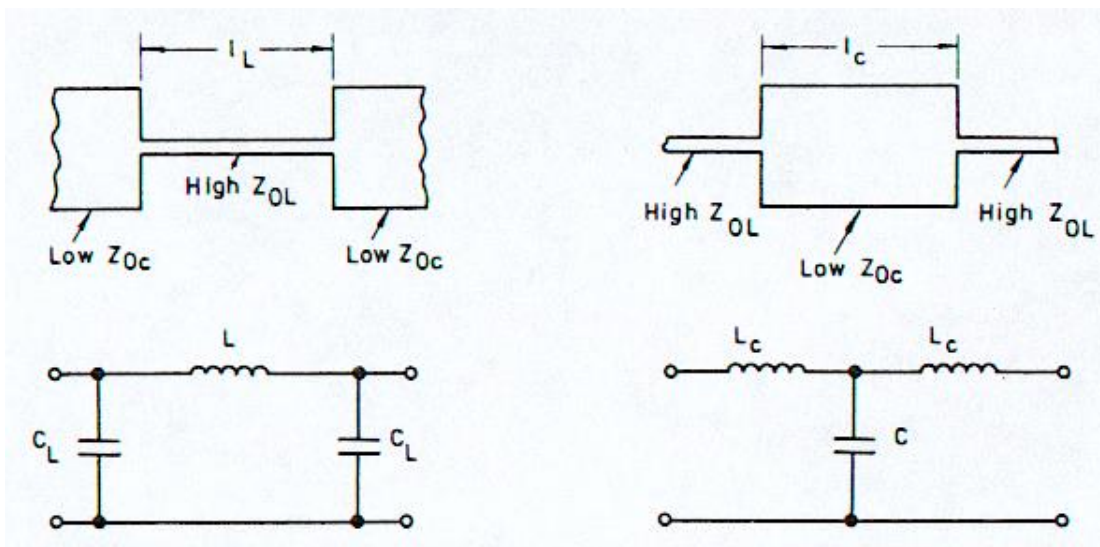


Fig. VIII-14: Inductive length of line with adjacent capacitive lines
and capacitive length of line with adjacent inductive lines

Then, if we add the contributions of all different discontinuities (steps), the complete lumped equivalent circuit of the low-pass filter will be equivalent to the one shown on Figure VIII-15. As an initial calculation, the reactance of a high-impedance microstrip section of length l_L is given by

$$X_L = Z_{0L} \tan\left(\frac{2\pi l_L}{\lambda_{gL}}\right) \quad (\text{VIII-47})$$

where λ_{gL} is the wavelength in the inductive microstrip section. This equation implies that the length should be

$$l_L = \frac{\lambda_{gL}}{2\pi} \tan^{-1}\left(\frac{\omega L}{Z_{0L}}\right) \quad (\text{VIII-48})$$

The materials you receive for this course are protected by copyright and to be used for this course only. You do not have permission to upload the course materials, including any lecture recordings you may have, to any website. If you require clarification, please consult your professor.

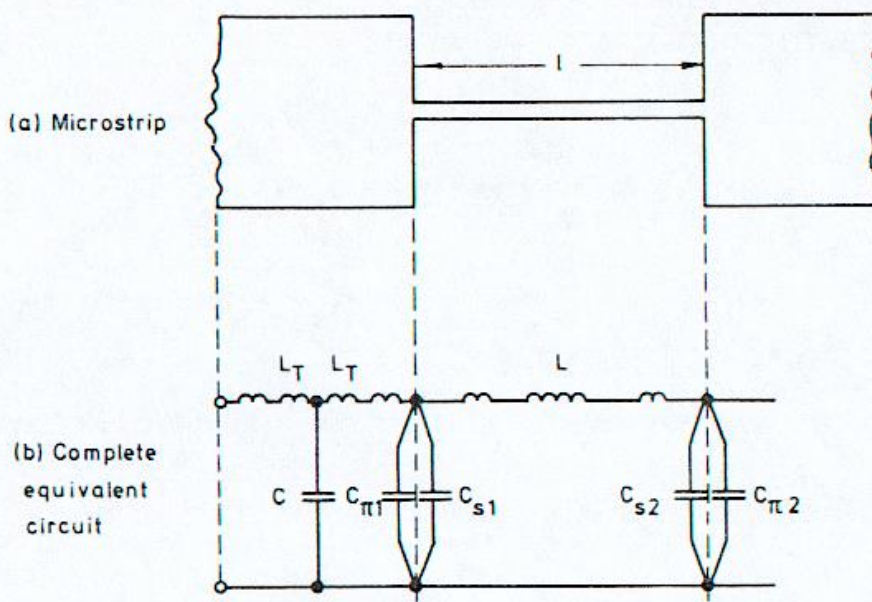


Fig. VIII-15: Low-pass filter in microstrip line

(a) LC cell, (b) Lumped equivalent circuit including discontinuities.

The capacitance of a low-impedance microstrip section of length l_C is given by

$$B_C = \frac{1}{Z_{0C}} \tan\left(\frac{2\pi l_C}{\lambda_{gC}}\right) \quad (\text{VIII-49})$$

which implies that the length should be

$$l_C = \frac{\lambda_{gC}}{2\pi} \tan^{-1}(\omega C Z_{0C}) \quad (\text{VIII-50})$$

The materials you receive for this course are protected by copyright and to be used for this course only. You do not have permission to upload the course materials, including any lecture recordings you may have, to any website. If you require clarification, please consult your professor.

but a closer analysis reveals that the inductive sections contribute end susceptances and the step discontinuities between inductive and capacitive sections create capacitances as well. The end inductances of the capacitive section are calculated as

$$L_C = \frac{l_C Z_0}{2f\lambda_{gC}} \quad (\text{VIII-51})$$

while the end capacitances of the inductive section are given as

$$C_L = \frac{l_L}{2fZ_L\lambda_{gL}} \quad (\text{VIII-52})$$

As well, the capacitance of a step discontinuity is given by

$$C_S = \sqrt{w_1 w_2} \left\{ (10.1 \log \varepsilon_r + 2.33) \frac{w_2}{w_1} - 12.6 \log \varepsilon_r - 3.17 \right\} \quad (\text{VIII-53})$$

for

$$\varepsilon_r \leq 10 ; 1.5 \leq \frac{\omega_2}{\omega_1} \leq 3.5$$

and

$$C_S = \sqrt{w_1 w_2} \left\{ 130 \log \left(\frac{w_2}{w_1} \right) - 44 \right\} \quad (\text{VIII-54})$$

for

$$\varepsilon_r \leq 10 ; 3.5 \leq \frac{\omega_2}{\omega_1} \leq 10$$

The contributions of the induced inductances and capacitances are significant and must be accounted for in the microstrip circuit design. Therefore the capacitance of the initially calculated length l_C plus the end capacitances and step capacitances will overshoot the required value, and the length l_C must be reduced accordingly so that the total capacitance due to all contributions will be the proper value.

Adjusting l_C also changes L_C and therefore the inductance length l_L will have to be adjusted to compensate for the change in L_C . This cycle must be re-iterated until the values of l_C and l_L are changing insignificantly from cycle to cycle.

II – Worked example of a low-pass filter design

We shall assume that an alumina substrate is to be used with permittivity 9.6 and thickness 0.635 mm. The filter specifications are

- $f_{cutt-off} = 2 \text{ GHz}$
- Insertion loss = 30 dB at 4 GHz
- Source and load impedances both 50Ω .

The materials you receive for this course are protected by copyright and to be used for this course only. You do not have permission to upload the course materials, including any lecture recordings you may have, to any website. If you require clarification, please consult your professor.

Let us further assume that the network topology (Figure VIII-16) is already obtained with the following lumped element values

- $C_1 = 2.55 \text{ pF}$ $C_3 = 2.1 \text{ pF}$ $C_5 = 0.49 \text{ pF}$
- $L_2 = 6.25 \text{ nH}$ $L_4 = 3.66 \text{ nH}$

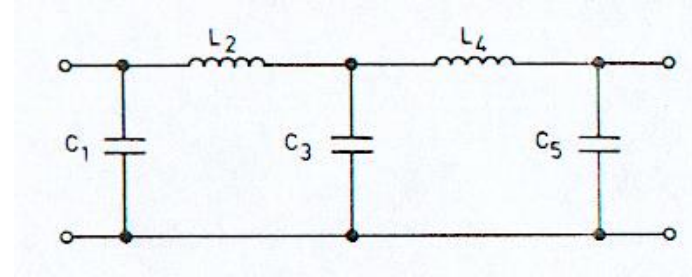


Fig. VIII.16: Network topology for the low-pass filter

The equivalent microstrip configuration is shown in Figure VIII-17.

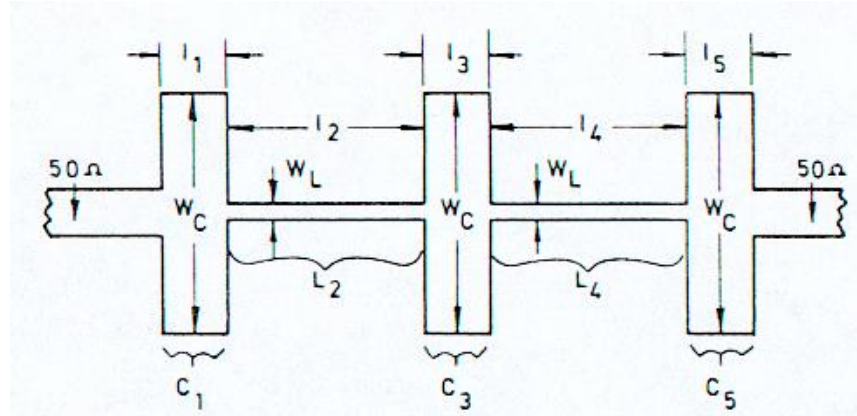


Fig. VIII.17: Microstrip configuration for the low-pass filter

Note: Due to the fairly low microwave frequency, we can neglect the dispersive effect of the microstrip lines.

As

$$Z_{0 \text{ capacitances}} < Z_o (50\Omega) < Z_{0 \text{ inductances}} \quad (\text{VIII-55})$$

it is reasonable to fix the characteristic impedance of the capacitive line in order to avoid the existence of any transverse resonance modes at the highest frequencies of operation. Similarly, the inductive line must be not so large that its manufacture becomes inordinately difficult (as a narrow line) or its current-carrying capability becomes a limitation.

In this case, based on the fixed characteristic impedances, microstrip lines widths as well as wavelengths can be calculated

Capacitive lines	$Z_{0c} = 25 \Omega$	Width = 2.00 mm	Wavelength (λ_{gC}) = 55.7 mm
Reference lines	$Z_0 = 50 \Omega$	Width = 0.632 mm	Wavelength (λ_{go}) = 64.7 mm
Inductive lines	$Z_{0L} = 90 \Omega$	Width = 0.132mm	Wavelength (λ_{gL}) = 65.0 mm

Because the parameters for the various lengths of line are interrelated we must perform initial calculations and then correct progressively via an iterative procedure as follows:

- Determine initial values for the lengths of microstrip lines l_L to replace inductances (equation VIII-48)
- Calculate the end capacitances associated with these lengths l_L (equation VIII-52)
- Calculate the step discontinuity capacitances (equation VIII-53 or VIII-54)

- (d) Reduce the originally specified lumped capacitance values by the appropriate amounts as calculated in (b) and (c), taking care to refer to the microstrip configuration so that the correct subtractions are carried out.
- (e) Calculate initial values for the lengths of microstrip lines l_C to replace these new capacitances
- (f) Determine the inductances of the T-sections associated with these capacitive lengths of line.
- (g) Reduce the originally specified lumped inductance values by the appropriate amounts as calculated in (f).
- (h) Repeat the entire procedure starting with the new values from step (g) in step (a) again.

For this example, the step discontinuity for $w_1/w_2 = 15.2$ gives an approximate value of 0.06pF. To show the procedure here, the new value required to be realized for C_3 is

$$C_3' = C_3 - C_{L2} - C_{L4} - C_{step} - C_{step} = 2.1 - 0.5182 - 0.2429 - 0.12 = 1.21 \text{ pF}$$

The complete 2-GHz microstrip low-pass filter is then shown on Figure VIII-18.

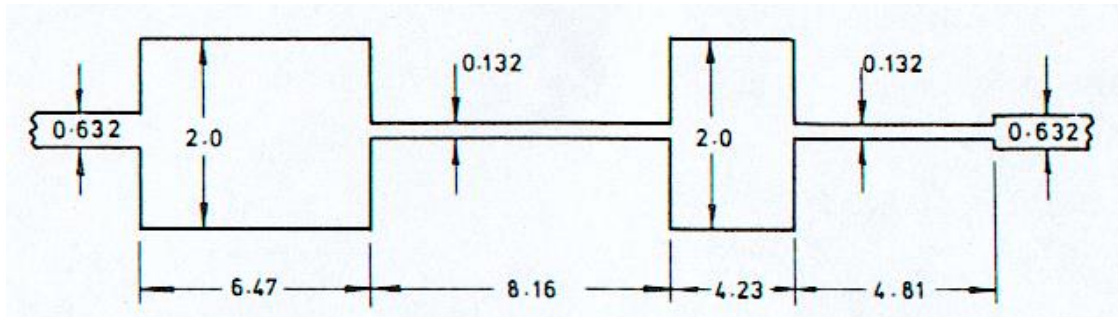


Fig. VIII-18: Complete low-pass filter with microstrip lines.

E – MICROSTRIP BAND-PASS FILTERS

The band-pass filter design using microstrip line technology implies the utilization of a cascade of half-wave resonators (each quarter-wave parallel coupled to its neighbors). This type of filters presents a narrow to moderate bandwidth.

Starting from the requirements, the designer should select the prototype for the desired response characteristic (i.e., the normalized values of the low-pass network) and then transform the low-pass prototype to the desired band-pass filter.

Once the equivalent lumped-element circuit established, the designer will convert the band-pass circuit to single-type resonators using parallel coupled half-wave resonator cascade structure.

A direct fabrication of this filter requires the design and interconnection of two distinctly different filters of resonant LC circuits (or resonators), then both series and parallel resonators would be required. However, in the microstrip technology, any microstrip resonator exhibits only one type of resonance – series or parallel – but not simultaneously from similar structures.

Then, there are two principal approaches to planar coupling between adjacent resonators: end coupling and edge coupling.

1- End-Coupled band-pass filters

The layout of an end-coupled microstrip filter is a series of coupling gaps between cascaded straight resonator elements (Figure VIII-19).

The materials you receive for this course are protected by copyright and to be used for this course only. You do not have permission to upload the course materials, including any lecture recordings you may have, to any website. If you require clarification, please consult your professor.



Fig. VIII-19: End-coupled microstrip lines filter

This type of filters is largely used in down converters and local oscillator rejection because it exhibits a relatively narrow-band. In these circuits based upon transmission line resonators the coupling gaps between resonators are of prime importance.

In fact, the coupling needs to be as tight as possible, implying gaps to be much smaller than the substrate height. Moreover, the resonator lengths depend not only upon the microstrip wavelength, but also on coupling reactances and the effect of shunt capacitances due to the gaps.

Cunningham shows that this length, excluding the effective gap lengths, is given by the following expression

$$l_h = \frac{\lambda_g}{2\pi} (\pi - X_{j-1,j} - X_{j,j+1}) - b_{j-1,j} - b_{j,j+1} \quad (\text{VIII-55})$$

where $b_{k,k+1}$ are lengths due to gap shunt capacitances and

$$X_{j-1,j} = 0.5 \left(\tan^{-1} \left(4\pi f \frac{C_{j-1,j}}{Y_o} \right) \right) \quad (\text{VIII-56})$$

2- Parallel-coupled (or edge-coupled) band-pass filters

As the length of each resonator element has to be $\lambda_g/4$, the total length could be too large to match the usual microwave circuit requirements. So, using the parallel-coupled line concept, we can design an edge-coupled band-pass filter (Figure VIII-20).

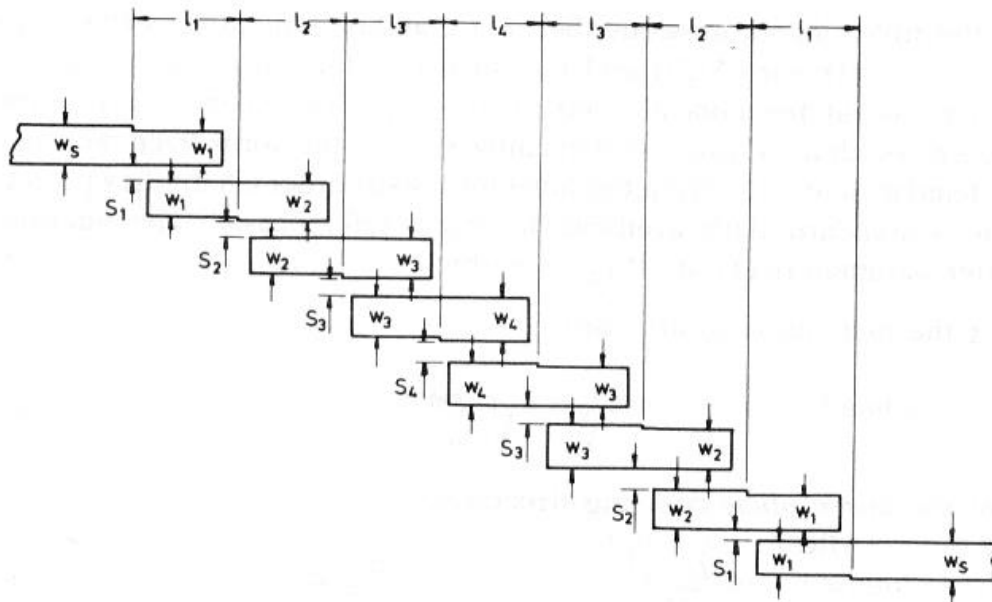


Fig. VIII-20: Edge-coupled microstrip lines filter

The cascade of parallel-coupled microstrip resonators can be designed on a basis of all-parallel resonator networks with intervening inverters. The process design has four steps:

- 1- Determine the one-type resonator network from the original prototype.
- 2- From the network parameters, determine the even- and odd-ordered characteristic impedance, Z_{0e} and Z_{0o} .
- 3- Relate the values of Z_{0e} and Z_{0o} to microstrip widths and separations (as described previously).

The materials you receive for this course are protected by copyright and to be used for this course only. You do not have permission to upload the course materials, including any lecture recordings you may have, to any website. If you require clarification, please consult your professor.

- 4- Calculate the whole resonator length $2l'$ slightly less than $\lambda_g/2$ and therefore the coupled-section length l' , which is slightly less than $\lambda_g/4$.

As the band-pass filter should be symmetric, the *first coupling structure* is that formed by $\{w_1, s_1, w_1\}$ and the *final coupling structure* is also $\{w_1, s_1, w_1\}$ at the opposite end of the filter.

If the quantities g_i refer to the prototype element values (Butterworth or Chebyshev), then the inverter parameter J are given by:

First coupling structure:

$$\frac{J_{01}}{Y_o} = \sqrt{\frac{\pi\delta}{2g_o g_1}} \quad (\text{VIII-56})$$

Jth coupling structure:

$$\left. \frac{J_{j,j+1}}{Y_o} \right|_{j=1 \text{ to } (n-1)} = \frac{\pi\delta}{2\omega_c \sqrt{g_j g_{j+1}}} \quad (\text{VIII-57})$$

Final coupling structure:

$$\frac{J_{n,n+1}}{Y_o} = \sqrt{\frac{\pi\delta}{2g_n g_{n+1}}} \quad (\text{VIII-58})$$

where δ is the fractional bandwidth

$$\delta = \frac{f_2 - f_1}{f_o} \quad (\text{VIII-59})$$

The frequency transformation from the low pass prototype filter to the band-pass microwave filter is then:

$$\frac{\omega_i'}{\omega_c'} = \frac{2}{\delta} \left(\frac{f_i - f_o}{f_o} \right) \quad (\text{VIII-60})$$

where ω_c' is the prototype cutoff angular frequency and ω_i' has to be defined accordingly to the required filter.

To proceed with the microstrip design, we require the even- and odd-ordered characteristic impedance, Z_{0e} and Z_{0o} . For this type of filter, they are given by:

$$(Z_{0e})_{j,j+1} = Z_0 (1 + aZ_0 + a^2 Z_0^2) \quad (\text{VIII-61})$$

and

$$(Z_{0o})_{j,j+1} = Z_0 (1 - aZ_0 + a^2 Z_0^2) \quad (\text{VIII-62})$$

where

$$a = J_{j,j+1} \quad (\text{VIII-63})$$

The materials you receive for this course are protected by copyright and to be used for this course only. You do not have permission to upload the course materials, including any lecture recordings you may have, to any website. If you require clarification, please consult your professor.

and Z_o is the characteristic impedance of the input/output lines.

⇒ The final stage is to obtain the $\{w/h\}$ and $\{s/h\}$ ratios for all the coupling structures.

3- Example of a parallel-coupled band-pass filter

If we consider the following insertion-loss characteristic of a band-pass filter where the pass-band insertion loss L_{AR} is taken as 0.01dB (Figure VIII-21).

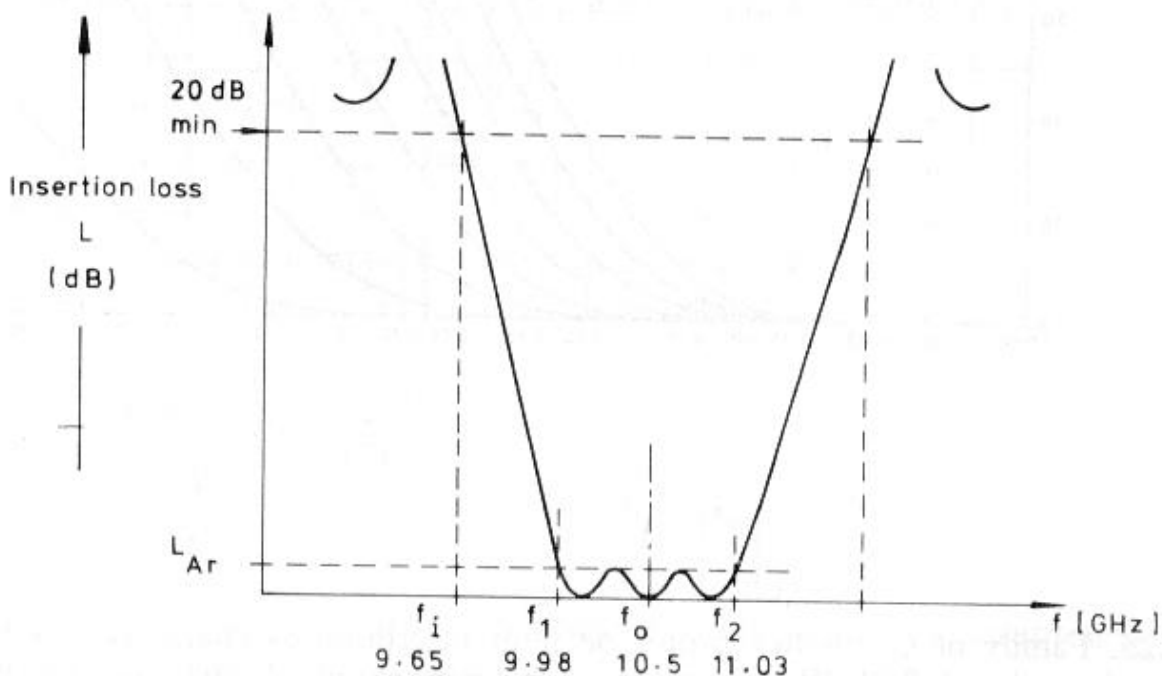


Fig. VIII-21: Pass-band insertion-loss characteristics

The materials you receive for this course are protected by copyright and to be used for this course only. You do not have permission to upload the course materials, including any lecture recordings you may have, to any website. If you require clarification, please consult your professor.

In the above figure we have:

$$\delta = \frac{f_2 - f_1}{f_o} = \frac{11.03 - 9.98}{10.5} = 0.1$$

and

$$\frac{\omega_i}{\omega_c} = \frac{2}{\delta} \left(\frac{f_i - f_o}{f_o} \right) = \frac{2}{0.1} \left(\frac{9.65 - 10.5}{10.5} \right) = -1.619$$

Then, with a pass-band ripple of 0.01dB, we use the family of Chebyshev prototype filter insertion-loss for a pass-band ripple of 0.01dB to obtain the filter order n (Figure VIII-22).

We can see that a sixth order ($n = 6$) design therefore gives an insertion loss of 23dB at ω_i (greater than the minimum insertion loss of 20 dB).

With $\{n = 6\}$, the element values for a Chebyshev filter are:

$$g_0 = 1.0$$

$$g_1 = 0.781$$

$$g_2 = 1.360$$

$$g_3 = 1.690$$

$$g_4 = 1.535$$

$$g_5 = 1.497$$

$$g_6 = 0.710$$

$$g_7 = 1.101$$

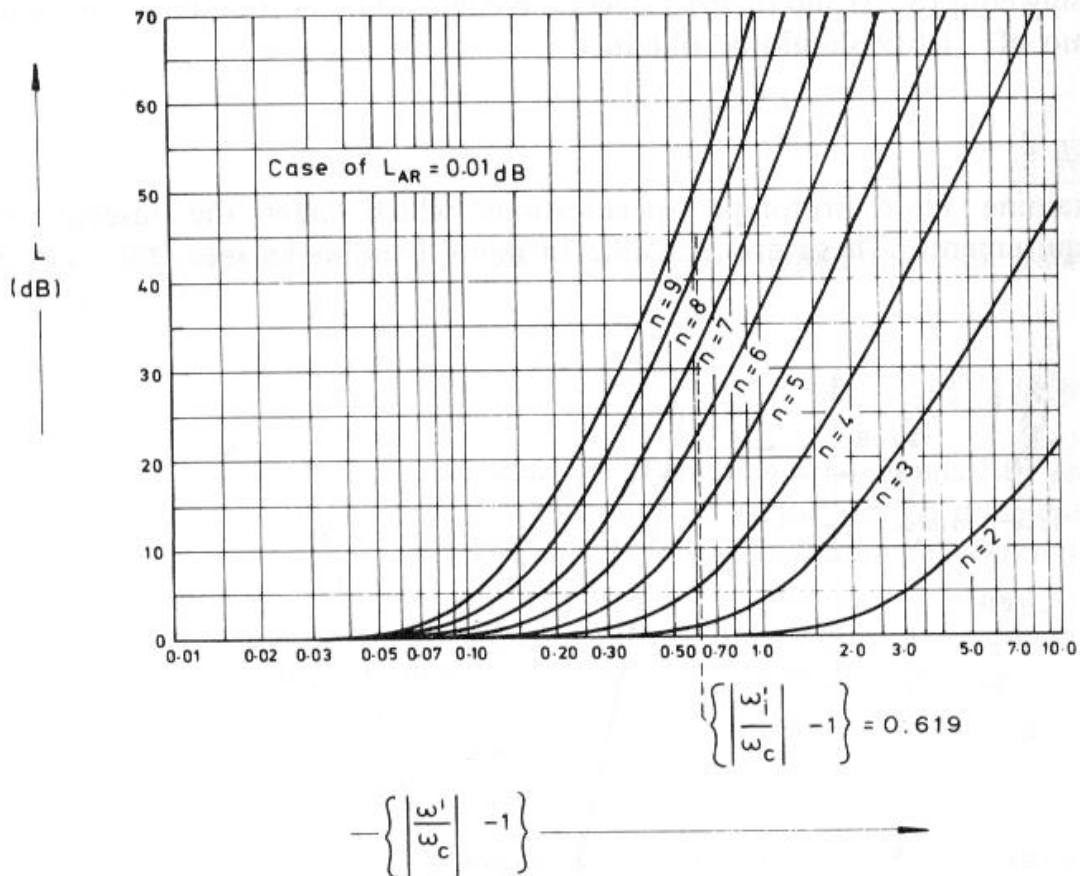


Fig. VIII-22: Family of Chebyshev prototype filter insertion-loss
for a pass-band ripple of 0.01dB

The materials you receive for this course are protected by copyright and to be used for this course only. You do not have permission to upload the course materials, including any lecture recordings you may have, to any website. If you require clarification, please consult your professor.

and then the calculated values of the inverter admittances are:

$$j = 0 \quad J_{j,j+1} / Y_o = 0.449$$

$$(Z_{0e})_{j,j+1} (\Omega) = 82.5$$

$$(Z_{0e})_{j,j+1} (\Omega) = 37.6$$

$$j = 1 \quad J_{j,j+1} / Y_o = 0.1529$$

$$(Z_{0e})_{j,j+1} (\Omega) = 58.8$$

$$(Z_{0e})_{j,j+1} (\Omega) = 43.5$$

$$j = 2 \quad J_{j,j+1} / Y_o = 0.1038$$

$$(Z_{0e})_{j,j+1} (\Omega) = 55.7$$

$$(Z_{0e})_{j,j+1} (\Omega) = 45.3$$

$$j = 3 \quad J_{j,j+1} / Y_o = 0.0976$$

$$(Z_{0e})_{j,j+1} (\Omega) = 55.4$$

$$(Z_{0e})_{j,j+1} (\Omega) = 45.6$$

The materials you receive for this course are protected by copyright and to be used for this course only. You do not have permission to upload the course materials, including any lecture recordings you may have, to any website. If you require clarification, please consult your professor.

The microstrip line dimensions are finally obtained as follows for a substrate permittivity of 10:

$$j=0 \left\{ \begin{array}{l} Z_{0se} = \frac{1}{2}Z_{0e} = 41.25\Omega \\ Z_{0so} = \frac{1}{2}Z_{0o} = 18.8\Omega \\ \left(\frac{w}{h}\right)_{se} = 1.5 \\ \left(\frac{w}{h}\right)_{so} = 4.8 \end{array} \right. \Rightarrow \left\{ \begin{array}{l} \frac{w}{h} = 0.65 \\ \frac{s}{h} = 0.2 \end{array} \right.$$

$$j=1 \left\{ \begin{array}{l} Z_{0se} = \frac{1}{2}Z_{0e} = 29.4\Omega \\ Z_{0so} = \frac{1}{2}Z_{0o} = 21.75\Omega \\ \left(\frac{w}{h}\right)_{se} = 2.5 \\ \left(\frac{w}{h}\right)_{so} = 4.0 \end{array} \right. \Rightarrow \left\{ \begin{array}{l} \frac{w}{h} = 1.0 \\ \frac{s}{h} = 0.68 \end{array} \right.$$

$$j=2 \left\{ \begin{array}{l} Z_{0se} = \frac{1}{2}Z_{0e} = 27.85\Omega \\ Z_{0so} = \frac{1}{2}Z_{0o} = 22.65\Omega \\ \left(\frac{w}{h}\right)_{se} = 2.7 \\ \left(\frac{w}{h}\right)_{so} = 3.7 \end{array} \right. \Rightarrow \left\{ \begin{array}{l} \frac{w}{h} = 1.0 \\ \frac{s}{h} = 1.0 \end{array} \right.$$

The materials you receive for this course are protected by copyright and to be used for this course only. You do not have permission to upload the course materials, including any lecture recordings you may have, to any website. If you require clarification, please consult your professor.

Since impedances are only 0.3Ω different from the $\{j = 2\}$ case, the same results are used for the $\{j = 3\}$ case:

$$j=3 \left\{ \begin{array}{l} \left(\frac{w}{h}\right)_{se} = 2.7 \\ \left(\frac{w}{h}\right)_{so} = 3.7 \end{array} \right. \Rightarrow \left\{ \begin{array}{l} \frac{w}{h} = 1.0 \\ \frac{s}{h} = 1.0 \end{array} \right.$$

If we assume that the substrate has a height of 0.635 mm, the final design dimensions of the pass-band filter are shown on Figure VIII-23.

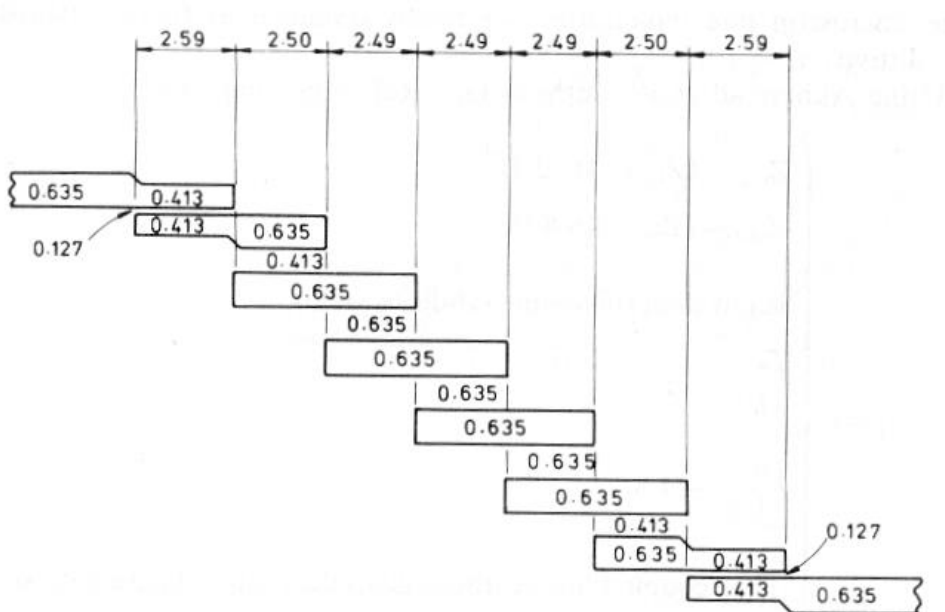


Fig. VIII-23: Final dimensions of the pass-band filter

Note: These dimensions are not the final optimized dimensions. We need to adjust the physical dimensions accordingly to the open-end and step discontinuity effects.

4- CAD of a parallel-coupled band-pass filter

A computer-aided design procedure can be developed for parallel-coupled band-pass filters. A designer needs the following input requirements (Figure VIII-24):

- Center frequency f_o (GHz)
- Ripple or band-edge insertion loss L_R (dB)
- Insertion loss at the attenuation points L_A (dB)
- Ripple bandwidth B_R (GHz)
- Attenuation bandwidth B_A (GHz)

and then the substrate specifications namely: the characteristic impedance of input/output lines Z_o (Ω), the substrate relative permittivity ϵ_r and the substrate height h (mm).

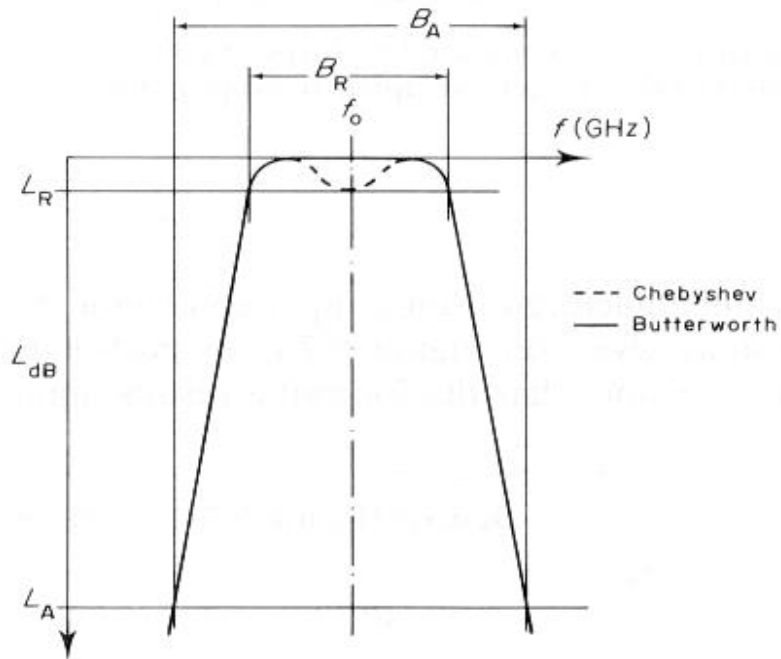


Fig. VIII-24: Characteristic of a pass-band filter.

CAD process stages should be then:

1. Calculate the required number of sections.
2. Determine the corresponding even and odd characteristic impedances Z_{0e} and Z_{0o} for each section. These impedances are noted (A).
3. Compute the $\{w/h\}$ and $\{s/h\}$ ratios using the Akhtarzad *et al.* synthesis technique described in the above sections.
4. Find new values of Z_{0e} and Z_{0o} for each section. These impedances are noted (B).
5. Compare the impedances (A) and (B). The latest $\{w/h\}$ and $\{s/h\}$ quantities are only outputs when the impedance differences $(A - B)$ are acceptable small **for each structure**.

The materials you receive for this course are protected by copyright and to be used for this course only. You do not have permission to upload the course materials, including any lecture recordings you may have, to any website. If you require clarification, please consult your professor.

6. Microstrip lengths are then required. Modified dispersion formulae can be used to calculate the even-and-odd mode phase velocities v_e and v_o at the center frequency f_o and the weighted-mean phase velocity v_n is then evaluated using

$$v_n = \frac{Z_{0e} + Z_{0o}}{\frac{Z_{0e}}{v_e} + \frac{Z_{0o}}{v_o}} \quad (\text{VIII-64})$$

7. Determine the microstrip wavelength

$$\lambda_{gn} = \frac{v_n}{f_o} \quad (\text{VIII-65})$$

8. Open-end and step discontinuity effects must be calculated.
9. Each corrected, physical quarter-wave length is then

$$l_n = \frac{\lambda_{gn}}{4} - l_{\text{effects}} \quad (\text{VIII-66})$$

The flow chart applicable to the CAD of pass-band filter is then summarized on Figure VIII-25.

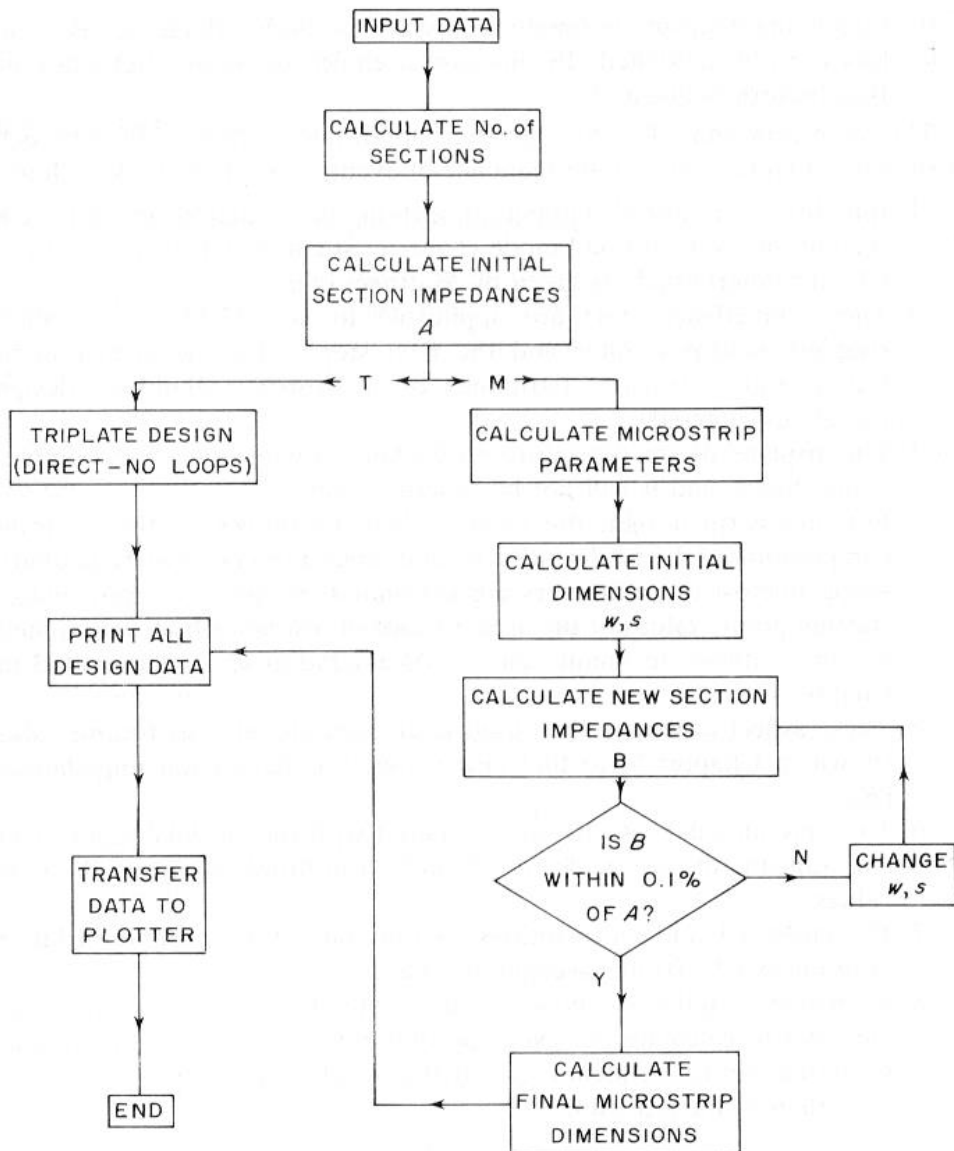


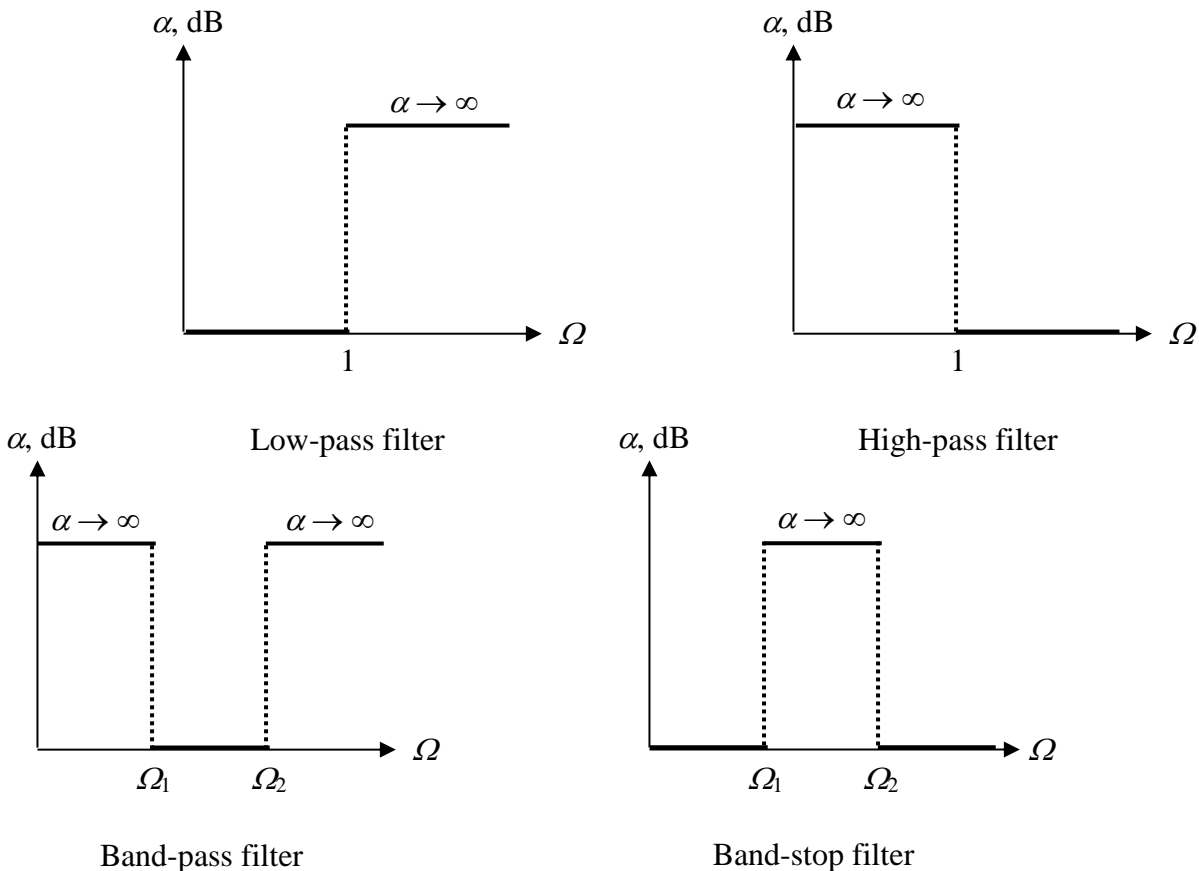
Fig. VIII-25: flow chart applicable to the CAD of pass-band filters

The materials you receive for this course are protected by copyright and to be used for this course only. You do not have permission to upload the course materials, including any lecture recordings you may have, to any website. If you require clarification, please consult your professor.

APPENDIX I

BASIC FILTER CONFIGURATIONS

It is convenient to introduce first the ideal behavior of the four basic filter types: low-pass, high-pass, band-pass and band-stop. The following figures summarize their attenuation α versus normalized angular frequency behavior.

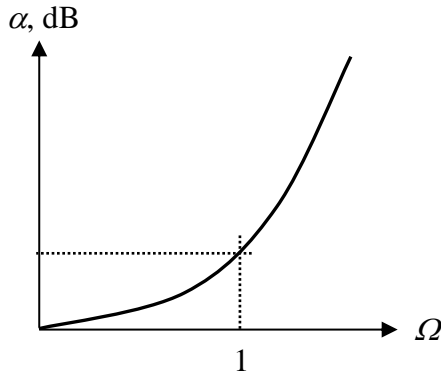


The materials you receive for this course are protected by copyright and to be used for this course only. You do not have permission to upload the course materials, including any lecture recordings you may have, to any website. If you require clarification, please consult your professor.

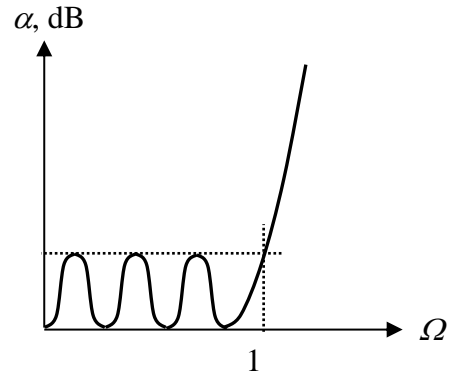
We have chosen the parameter $\Omega = \omega/\omega_c$ as a normalized frequency with respect to the angular frequency ω_c , which denotes **cut-off frequency** for low-pass and high-pass filters and **center frequency** for band-pass and band-stop filters:

$$\Omega = \frac{\Omega_2 + \Omega_1}{2} \quad (\text{AI-1})$$

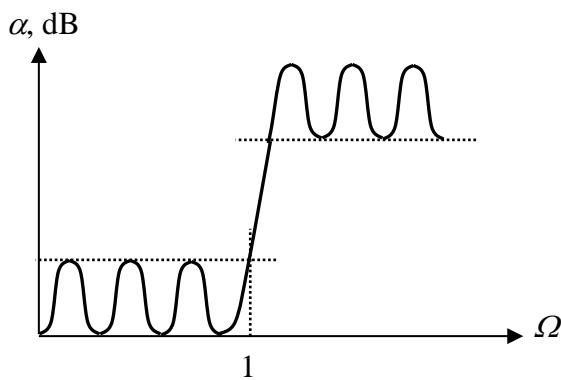
As we will see, the normalization will greatly simplify our task of developing standard filter approaches.



Binomial filter



Chebyshev filter



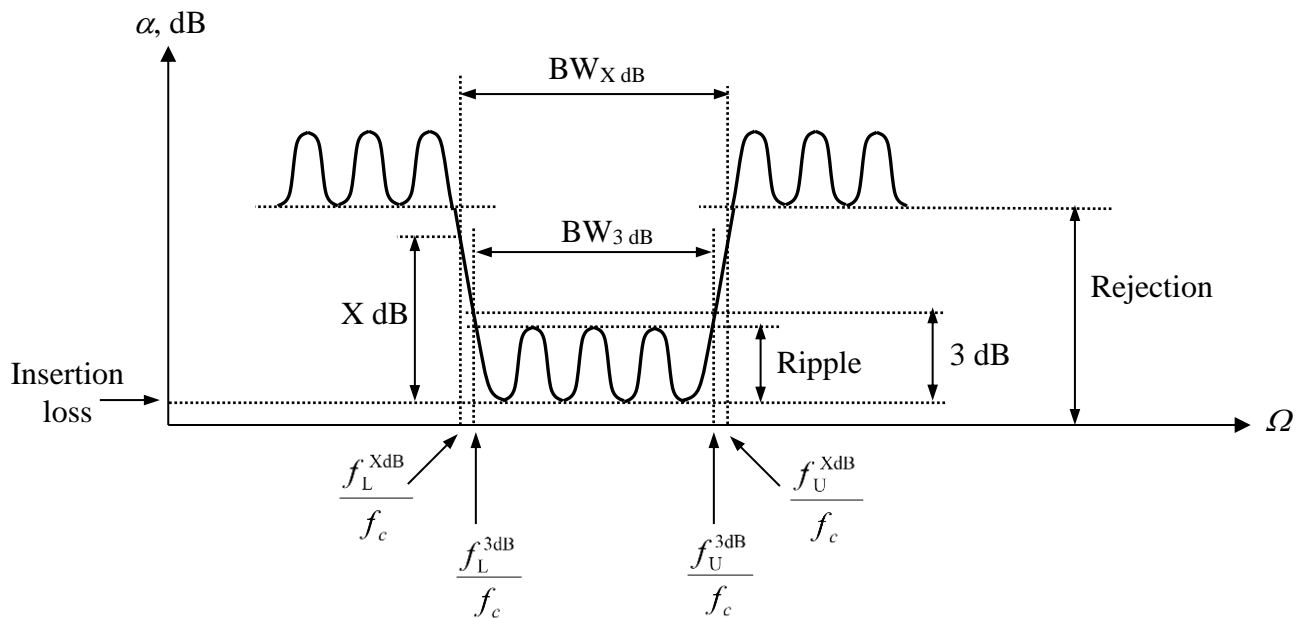
Elliptic filter

The materials you receive for this course are protected by copyright and to be used for this course only. You do not have permission to upload the course materials, including any lecture recordings you may have, to any website. If you require clarification, please consult your professor.

The binomial filter exhibits a monotonic attenuation profile that is generally easy to implement. Unfortunately, to achieve a steep attenuation transition from pass- to stop-band, a large number of components is needed. A better, steeper slope can be implemented if one permits a certain degree of variations, or **ripples**, in the pass band attenuation profile.

If these ripples maintain equal amplitude, either in the stop band or pass band, we speak of a Chebyshev filter since the design relies on the so-called Chebyshev polynomials. For both the binomial and the Chebyshev filter we observe that the attenuation approaches infinity as $\Omega \rightarrow \infty$.

This is in contrast to the elliptic filters, which allow the steepest transitions from pass band to stop band at the expense of ripples in both bands. Because of their mathematical complexity in designing elliptic filters, they are not investigated in details in almost technical literature. Using the following figure:



The materials you receive for this course are protected by copyright and to be used for this course only. You do not have permission to upload the course materials, including any lecture recordings you may have, to any website. If you require clarification, please consult your professor.

We can see that the following parameters play key roles in filter design:

- **Insertion loss.** Ideally a perfect filter inserted into the RF circuit path would introduce no power loss in the pass band. In other words, it would have zero insertion loss. In reality, however, we have to expect a certain amount of power loss associated with the filter. The insertion loss quantifies how much below the 0 dB line the power amplitude response drops. In mathematical terms, it states

$$IL = 10 \log \left(\frac{P_{in}}{P_L} \right) = -10 \log \left(1 - |\Gamma_{in}|^2 \right) = 10 \log (LF) \quad (\text{AI-2})$$

where P_L is the power delivered to the load, P_{in} is the input power from the source, and $|\Gamma_{in}|$ is the reflection coefficient looking into the filter. LF is the **loss factor**.

- **Ripple.** The flatness of the signal in the pass band can be quantified by specifying the ripple or difference between maximum and minimum amplitude response in either dB or Nepers. Usually, the Chebyshev filter design allows us to precisely control the magnitude of the ripple.
- **Bandwidth.** For a band-pass filter, bandwidth defines the difference between upper and lower frequencies typically recorded at the 3 dB attenuation points above the pass band:

$$BW^{3\text{dB}} = f_U^{3\text{dB}} - f_L^{3\text{dB}} \quad (\text{AI-3})$$

- **Shape factor.** This factor describes the sharpness of the filter response by taking the ratio between a desired X dB and the 3 dB bandwidths:

$$SF = \frac{BW^{X\text{dB}}}{BW^{3\text{dB}}} = \frac{f_U^{X\text{dB}} - f_L^{X\text{dB}}}{f_U^{3\text{dB}} - f_L^{3\text{dB}}} \quad (\text{AI-4})$$

The materials you receive for this course are protected by copyright and to be used for this course only. You do not have permission to upload the course materials, including any lecture recordings you may have, to any website. If you require clarification, please consult your professor.

- **Rejection.** For an ideal filter, we would obtain infinite attenuation level for the undesirable signal frequencies. However, in reality we expect an upper bound due to the deployment of a finite number of filter components.
-
- **Central frequency.** The central frequency f_c is normalized to $\Omega = 1$. The 3 dB lower and upper cut-off frequencies are symmetric with respect to this center frequency.

An additional parameter describes the selectivity of the filter. This parameter, known as the **Quality factor Q** , defines the ratio of the average stored energy to the energy loss per cycle at the resonant frequency:

$$Q = \omega \frac{\text{average stored energy}}{\text{energy loss per cycle}} \Big|_{\omega=\omega_c} = \omega \frac{\text{average stored energy}}{\text{power loss}} \Big|_{\omega=\omega_c} = \omega \frac{W_{\text{stored}}}{P_{\text{loss}}} \Big|_{\omega=\omega_c} \quad (\text{AI-5})$$

Here P_{loss} is the energy loss per unit time. Using this definition we should distinguish between loaded and unloaded filters.

As it is customary to consider the power loss as consisting of the power loss associate with the external load Z_L and the filter itself, the resulting quality factor is named loaded Q or Q_{LD} . This parameter can be also expressed in the following form:

$$Q_{LD} = \frac{f_c}{f_U^{\text{3dB}} - f_L^{\text{3dB}}} = \frac{f_c}{BW^{\text{3dB}}} \quad (\text{AI-6})$$

Interestingly, if we take the inverse of the loaded Q , we have:

$$\frac{1}{Q_{LD}} = \frac{1}{\omega} \left(\frac{\text{power loss in filter}}{\text{average stored energy}} \right) \Big|_{\omega=\omega_c} + \frac{1}{\omega} \left(\frac{\text{power loss in load}}{\text{average stored energy}} \right) \Big|_{\omega=\omega_c} \quad (\text{AI-7})$$

then:

$$\frac{1}{Q_{LD}} = \frac{1}{Q_F} + \frac{1}{Q_E} \quad (\text{AI-8})$$

I – Attenuation and phase vs. transfer function

We defined the response of a filter accordingly to the attenuation. In fact besides specifying the transfer function $H(\omega)$, it is more common to compute the attenuation factor such as:

$$\alpha(\omega) = -\ln |H(\omega)| = -\frac{1}{2} \ln |H(\omega)|^2 \quad (\text{AI-9})$$

or in dB as

$$\alpha_{dB} = -20 \log |H(\omega)| = -10 \log |H(\omega)|^2 \quad (\text{AI-10})$$

The corresponding phase is

$$\phi(\omega) = \tan^{-1} \left(\frac{\text{Im}\{H(\omega)\}}{\text{Re}\{H(\omega)\}} \right) \quad (\text{AI-11})$$

Directly related to phase is the group delay t_g , which is defined as the frequency derivative of the phase

$$t_g = \frac{d\phi(\omega)}{d\omega} \quad (\text{AI-12})$$

Note : It is often desirable to design a filter with nearly linear phase, i.e.,

$$\phi \approx \omega A \quad (\text{AI-13})$$

with A is an arbitrary constant factor.

II – Chebyshev filters

The design of an equi-ripple filter type is based on an insertion loss whose functional behavior is described by the Chebyshev polynomials $T_N(\Omega)$ in the following form:

$$IL = 10 \log \{LF\} = 10 \log \{1 + a^2 T_N^2(\Omega)\} \quad (\text{AI-14})$$

where N is the order of the filter and a is a constant. the Chebyshev polynomials $T_N(\Omega)$ are defined as

$$T_N(\Omega) = \begin{cases} \cos \{N[\cos^{-1}(\Omega)]\} & \text{for } |\Omega| \leq 1 \\ \cosh \{N[\cosh^{-1}(\Omega)]\} & \text{for } |\Omega| > 1 \end{cases} \quad (\text{AI-15})$$

It can be observed that all polynomials oscillate within a ± 1 interval, a fact that is exploited in the equi-ripple design. The magnitude of the transfer function $|H(j\Omega)|$ is obtained from the Chebyshev polynomial as follows:

$$|H(\Omega)| = \sqrt{H(\Omega)H(\Omega)^*} = \frac{1}{\sqrt{1 + a^2 T_N^2(\Omega)}} \quad (\text{AI-16})$$

The constant factor a allows to control the height of the pass band ripples. For instance, if we choose $a = 1$, then at $\Omega = 1$ we have

$$|H(0)| = \frac{1}{\sqrt{2}} \quad (\text{AI-17})$$

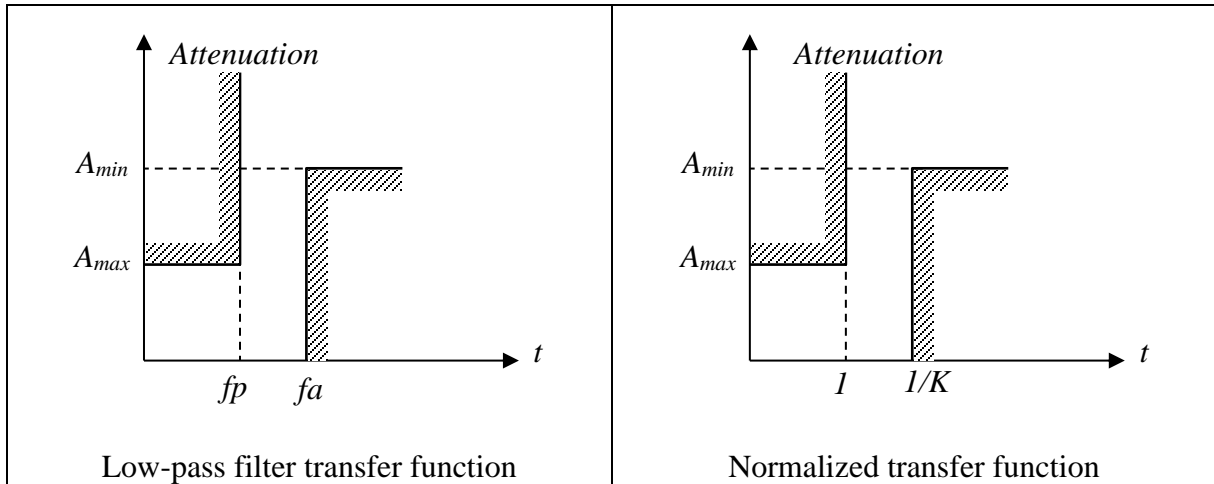
We can show that if the desired magnitude of the ripples is denoted as R_{dB} , then a should be chosen as

$$a = \sqrt{10^{R_{\text{dB}}/10} - 1} \quad (\text{AI-18})$$

The materials you receive for this course are protected by copyright and to be used for this course only. You do not have permission to upload the course materials, including any lecture recordings you may have, to any website. If you require clarification, please consult your professor.

III – Low pass filter (prototype)

We will focus on the low pass filter prototype.



$$K = \frac{fp}{fa} : \quad \text{Selectivity.}$$

A_{\max} : maximal Attenuation in the pass band.

A_{\min} : minimal Attenuation in the rejected band.

Let n be the filter order; the poles are defined as

$$\begin{aligned} P_k &= \alpha_k + j.B_k \\ P_k^* &= \alpha_k - j.B_k \end{aligned}$$

Chebycheff

$$a_k = \sin \left[\frac{(2k-1)\pi}{2n} \right] \quad b_k = \gamma^2 + \sin^2 \left[\frac{(k)\pi}{n} \right] \quad k = 1, 2, 3, \dots, n.$$

$$\gamma = \sin k \left(\frac{\beta_k}{2n} \right) \quad \beta = \operatorname{In} \left[\coth \left(\frac{A \max}{17,37} \right) \right]$$

$$\rightarrow \quad g_n = \frac{4a_k \cdot a_{k-1}}{b_{k-1} \cdot g_{k-1}} \quad g_a = \frac{2a_1}{\gamma}$$

P-configuration

$$\begin{aligned} C_k &= g_k & k &= 1, 3, 5, \dots, n. \\ L_k &= g_k & k &= 2, 4, 6, \dots, n. \end{aligned}$$

T-configuration

$$\begin{aligned} C_k &= g_k & k &= 2, 4, 6, \dots, n. \\ L_k &= g_k & k &= 1, 3, 5, \dots, n. \end{aligned}$$

Butterworth

$$\rightarrow \quad g_k = \sin \left[\frac{(2k-1)\pi}{2n} \right]$$

P-configuration

$$\begin{aligned} C_k &= g_n & k &= 1, 3, 5, \dots, n \\ L_k &= g_n & k &= 2, 4, 6, \dots, n \end{aligned}$$

T-configuration

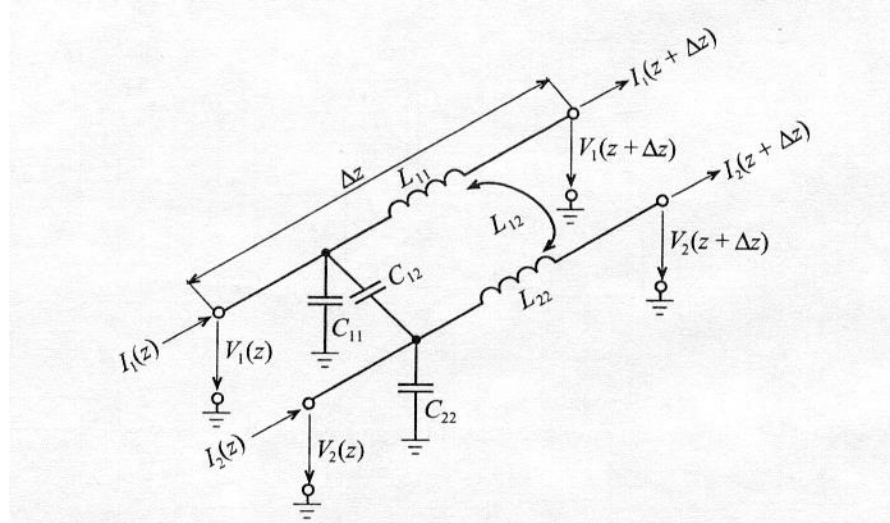
$$\begin{aligned} C_k &= g_n & k &= 2, 4, 6, \dots, n \\ L_k &= g_n & k &= 1, 3, 5, \dots, n \end{aligned}$$

IV – Coupled filters

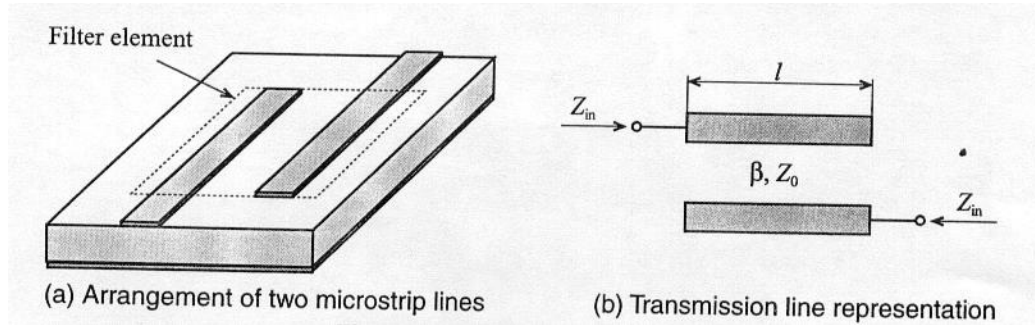
Coupled filter design is related to the odd and even wave coupling of transmission lines through a common ground plane, which results in odd and even characteristic line impedances.

The materials you receive for this course are protected by copyright and to be used for this course only. You do not have permission to upload the course materials, including any lecture recordings you may have, to any website. If you require clarification, please consult your professor.

A simple modeling approach of coupled microstrip line interaction is established when considering the geometry depicted in the following figure:



The configuration consists of two lines separated over a distance S and attached to a dielectric medium of thickness h and dielectric constant ϵ_r . The trip lines are W wide. The capacitive and inductive coupling phenomena between the lines and ground is schematically given on this figure



We can define now an even mode voltage V_e and current I_e and an odd voltage V_o and current I_o in terms of the total voltages and currents at terminals 1 and 2 such that

$$V_e = \frac{1}{2}(V_1 + V_2) \quad (\text{AI-19-a})$$

$$V_o = \frac{1}{2}(V_1 - V_2) \quad (\text{AI-19-b})$$

and

$$I_e = \frac{1}{2}(I_1 + I_2) \quad (\text{AI-20-a})$$

$$I_o = \frac{1}{2}(I_1 - I_2) \quad (\text{AI-20-b})$$

The benefit of introducing odd and even modes of operation is seen when establishing the fundamental equations.

It can be shown that for two lines we get a set of first-order, coupled ordinary differential equations similar in form to the transmission line equations in Chapter 2

$$-\frac{dV_e}{dz} = j\omega(L_{11} + L_{12})I_e \quad (\text{AI-21-a})$$

$$-\frac{dI_e}{dz} = j\omega(C_{11} + C_{12})V_e \quad (\text{AI-21-b})$$

and

$$-\frac{dV_o}{dz} = j\omega(L_{11} - L_{12})I_o \quad (\text{AI-22-a})$$

$$-\frac{dI_o}{dz} = j\omega(C_{11} - C_{12})V_o \quad (\text{AI-22-b})$$

It is important to notice that even and odd modes allow us to decouple the governing equations. The characteristic line impedances Z_{0e} and Z_{0o} for the even and odd modes respectively can be defined in terms of even and odd mode capacitances C_e , C_o , and the respective phase velocities as follows:

$$Z_{0e} = \frac{1}{v_{pe}C_e} \quad (\text{AI-23-a})$$

and

$$Z_{0o} = \frac{1}{v_{po}C_o} \quad (\text{AI-23-b})$$

If both conductors are equal in size and location, we have for the even mode

$$C_e = C_{11} = C_{22} \quad (\text{AI-24})$$

and for the odd mode

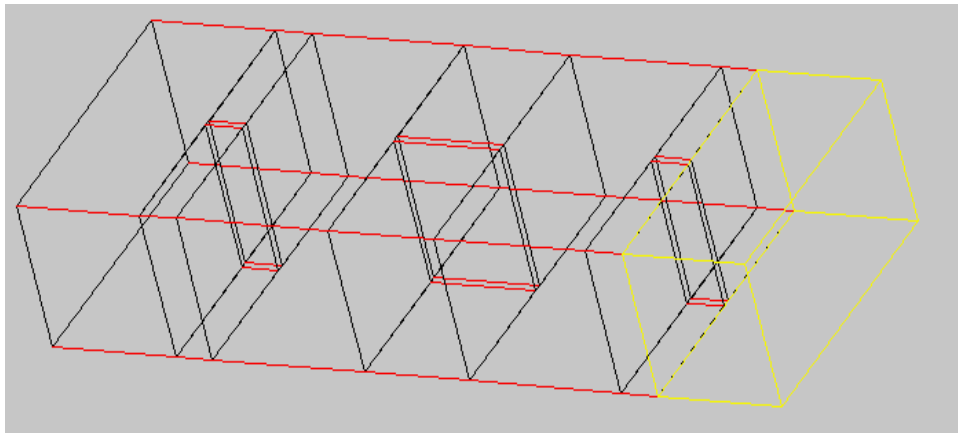
$$C_o = C_{11} + 2C_{12} = C_{22} + 2C_{12} \quad (\text{AI-25})$$

APPENDIX II

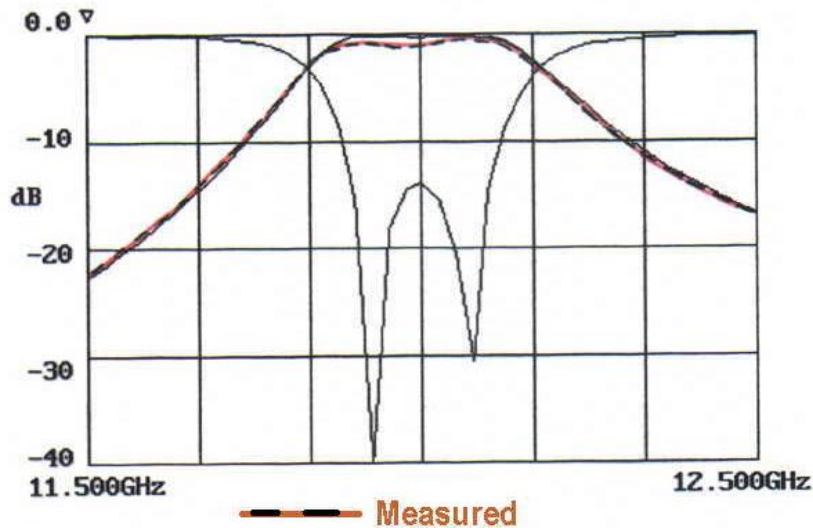
SOME EXAMPLES OF MICROWAVE FILTERS

I - Waveguide filters

This E Plane metal insert filter is based on the paper of Tajima, Y. et al., "Design and analysis of a waveguide sandwich microwave filter", IEEE MTT Vol 22, pp.839-841, 1974.

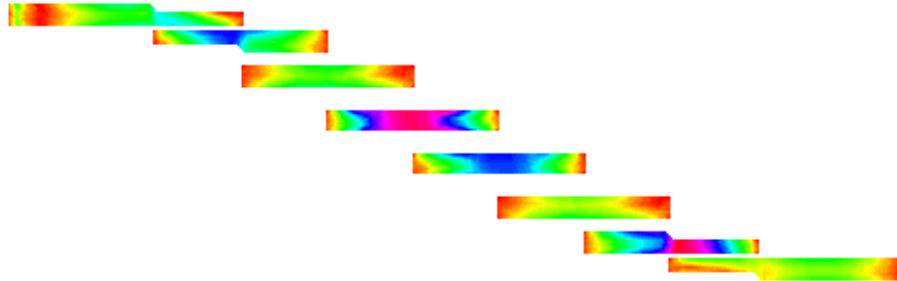


The materials you receive for this course are protected by copyright and to be used for this course only. You do not have permission to upload the course materials, including any lecture recordings you may have, to any website. If you require clarification, please consult your professor.



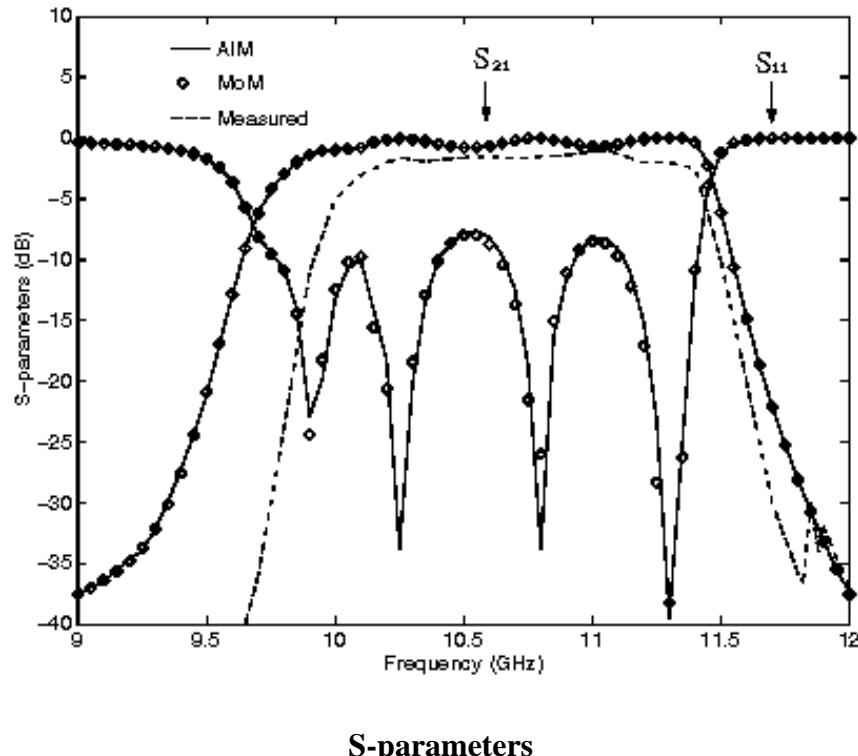
II – Microstrip parallel-coupled band-pass filter

The following Figures show the module of the electric field and the S parameters on a microstrip of the following type: substrate $\epsilon_r = 10.0$, thickness $h = 0.635$ mm (for more information refer to *Foundation for Microstrip Circuit Design* , T. Edwards, Chichester, UK: Wiley, 1991).



Module of the electric field at $f = 11.0$ GHz

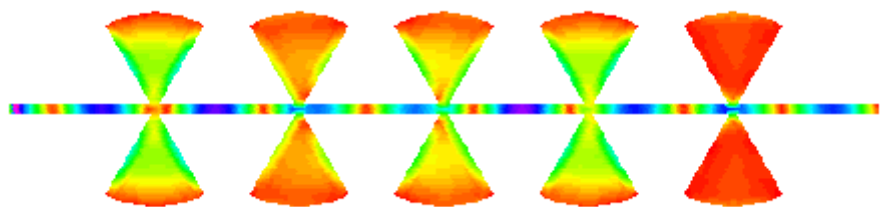
The materials you receive for this course are protected by copyright and to be used for this course only. You do not have permission to upload the course materials, including any lecture recordings you may have, to any website. If you require clarification, please consult your professor.



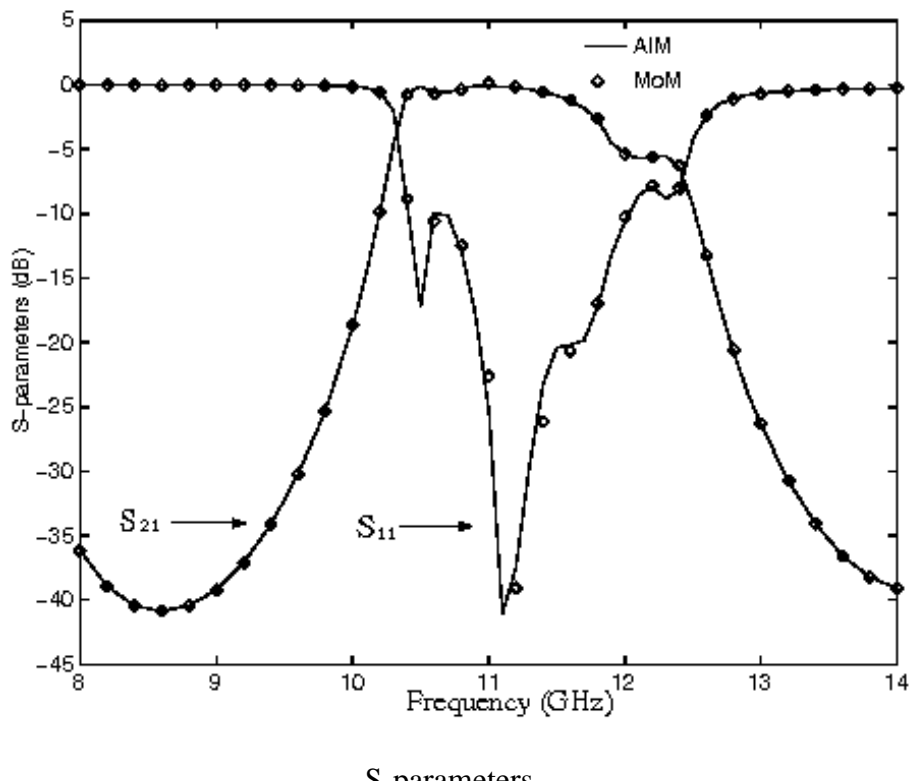
III - Cascaded radial stub

The following Figures show the module of the electric field and the S parameters on a cascaded radial stub of the following dimensions: radius = 5.0 mm, line width w = 0.6 mm, substrate ϵ_r = 10.0, and thickness h = 0.635 mm.

The materials you receive for this course are protected by copyright and to be used for this course only. You do not have permission to upload the course materials, including any lecture recordings you may have, to any website. If you require clarification, please consult your professor.



Module of the electric field at $f = 11.0$ GHz



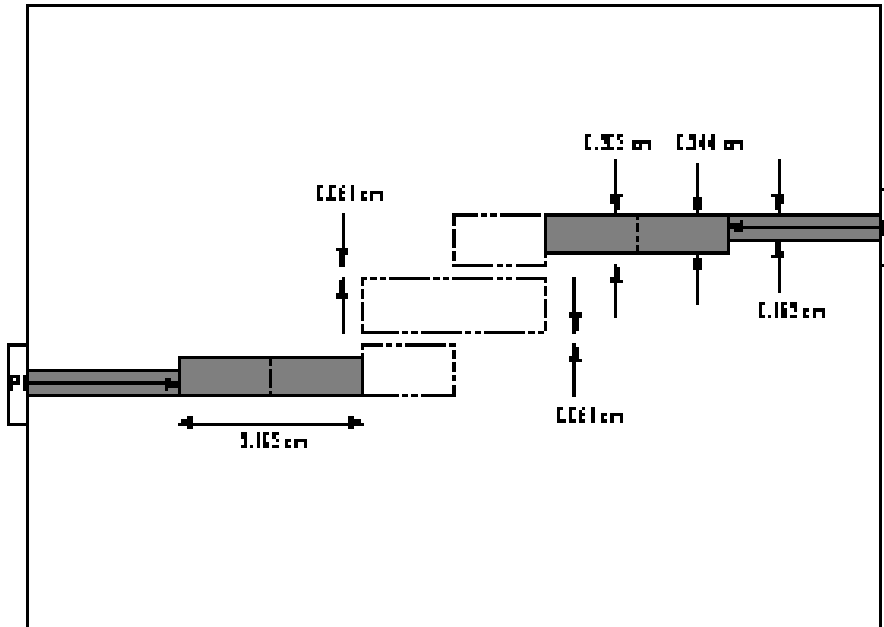
S-parameters

The materials you receive for this course are protected by copyright and to be used for this course only. You do not have permission to upload the course materials, including any lecture recordings you may have, to any website. If you require clarification, please consult your professor.

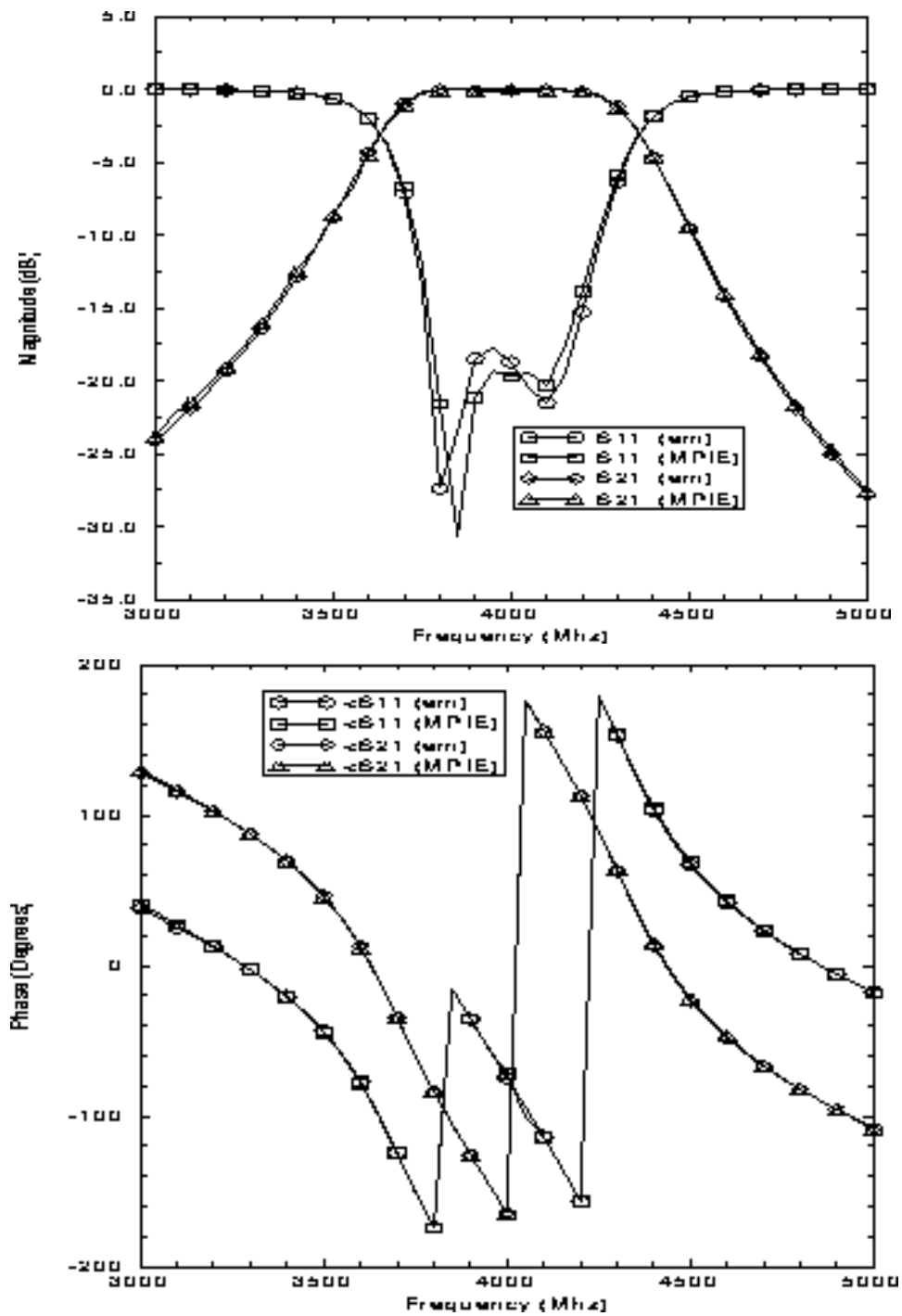
IV - Stripline coupled-line band-pass filter

In designing edge-coupled filters, it might be necessary to have small spacings, in other words large couplings, between the resonant elements, which would make the production of such filters very difficult. This difficulty can be circumvented by implementing such coupled lines in a stripline geometry with broad-side coupling. Here, by using this concept, a third-order band-pass filter is designed by following the design procedure based on the even- and odd-mode impedances of the coupled lines, which are available in literature.

Source: <http://www.ee.bilkent.edu.tr/research/em/emap/node13.html#FilterGeom>



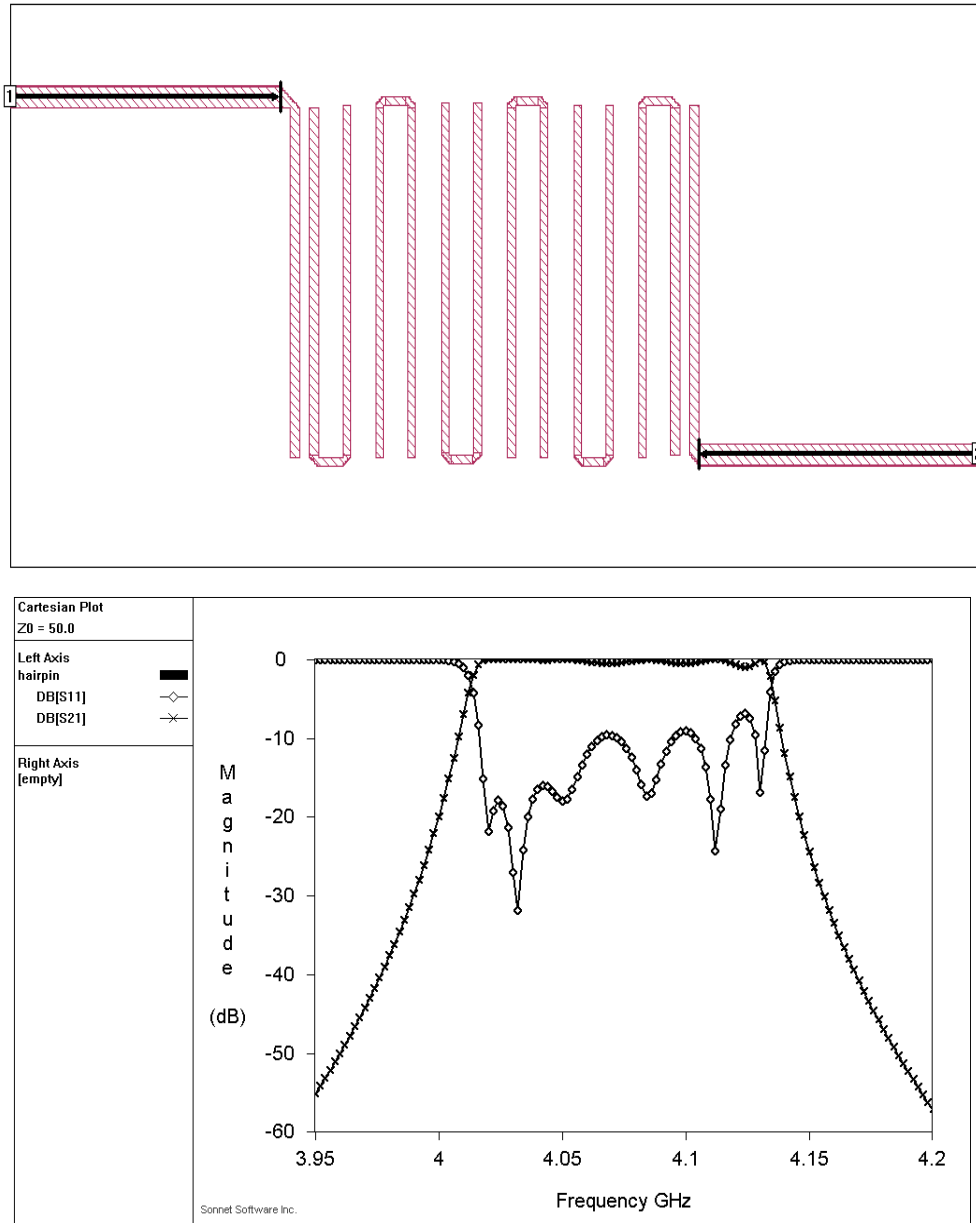
The materials you receive for this course are protected by copyright and to be used for this course only. You do not have permission to upload the course materials, including any lecture recordings you may have, to any website. If you require clarification, please consult your professor.



The materials you receive for this course are protected by copyright and to be used for this course only. You do not have permission to upload the course materials, including any lecture recordings you may have, to any website. If you require clarification, please consult your professor.

V - Hairpin filter

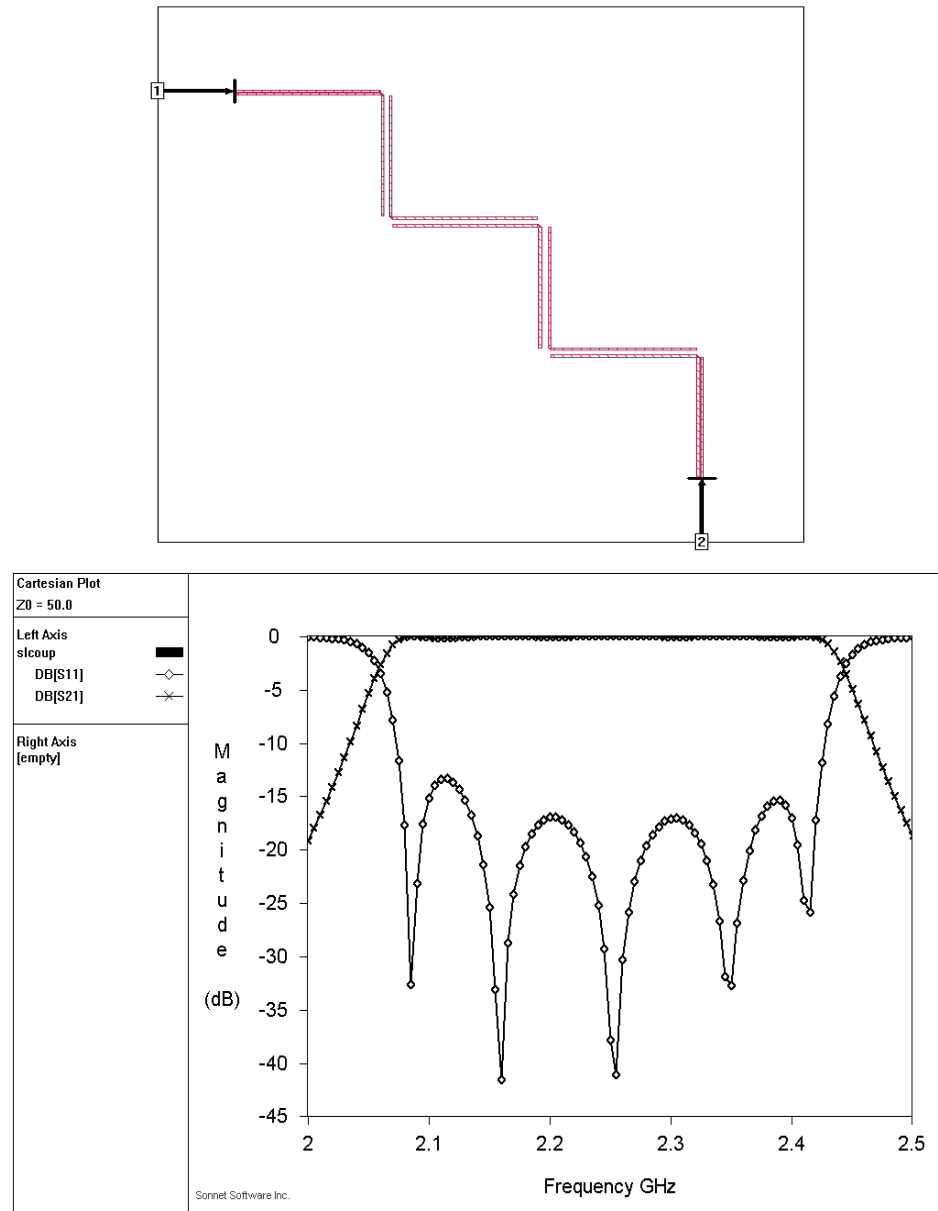
This is an example of a hairpin filter with a pass band of approximately 4.0 to 4.15 GHz (diagonal fill are used to improve the diagonal edges of the bends).



The materials you receive for this course are protected by copyright and to be used for this course only. You do not have permission to upload the course materials, including any lecture recordings you may have, to any website. If you require clarification, please consult your professor.

VI - Stripline filter

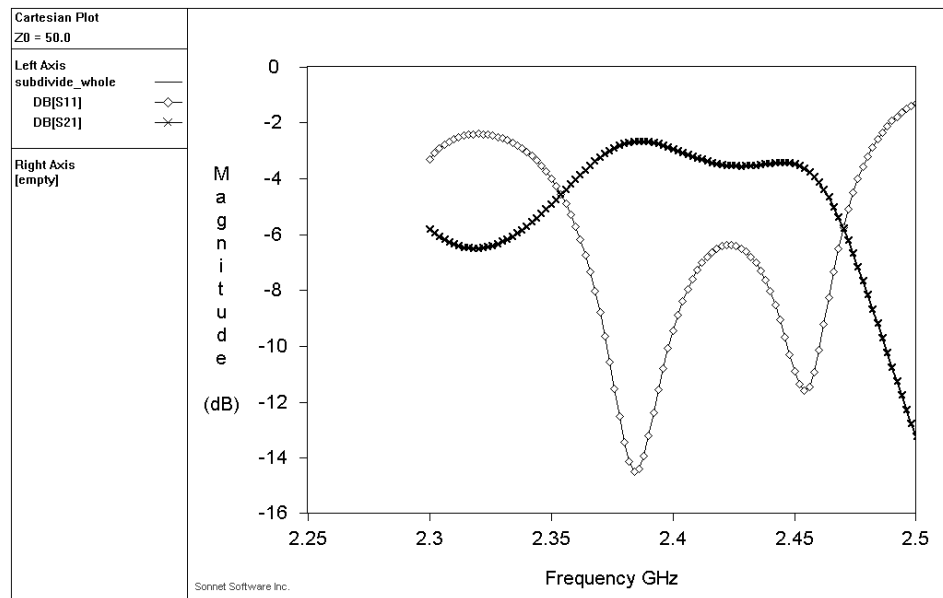
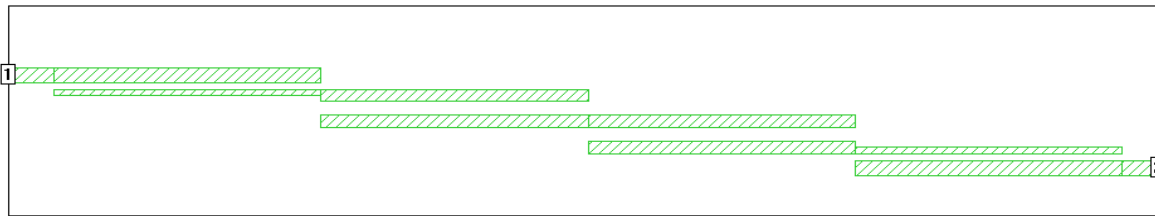
This example is a stripline coupled line filter. The stripline is composed of two 25 mil RT/duroid 6010 dielectric layers. The filter is composed of six-coupled line sections.



The materials you receive for this course are protected by copyright and to be used for this course only. You do not have permission to upload the course materials, including any lecture recordings you may have, to any website. If you require clarification, please consult your professor.

VIII - Band pass filter

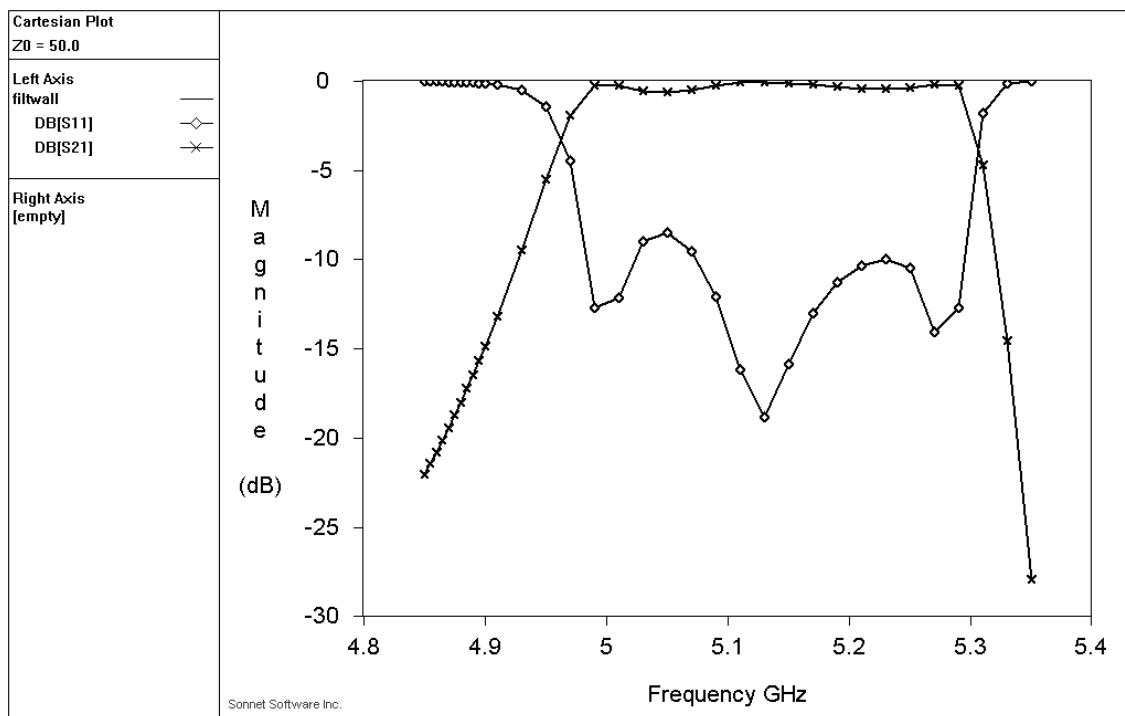
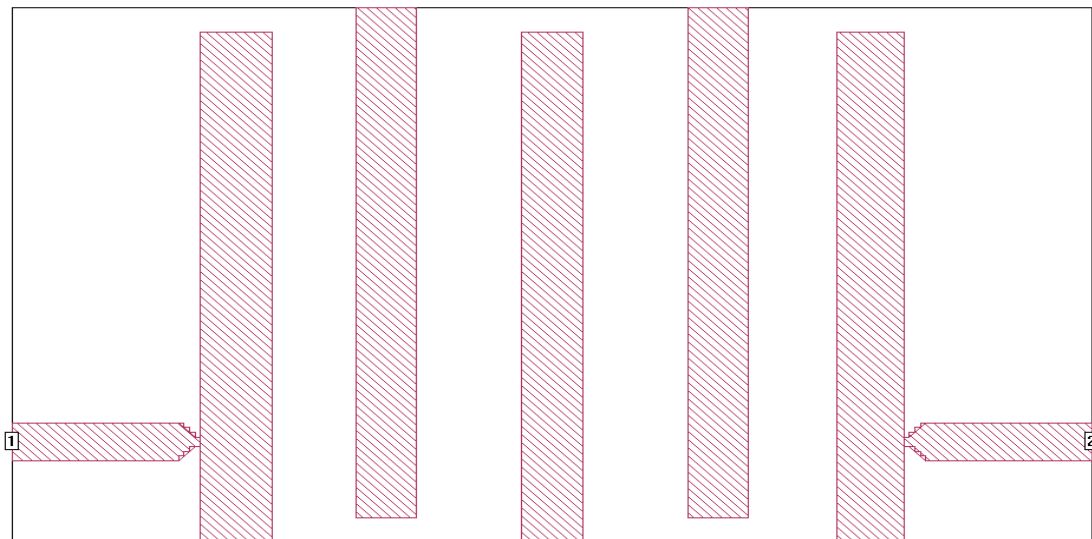
This is an example of a band-pass filter.



VIII - Interdigital bandpass filter using wall short-circuits

This is an example of a microstrip with a center frequency of 5.1 GHZ and a bandwidth of 340 MHZ. The filter consists of two impedance-transforming sections on the left and right sides and 3 resonator elements in between. Each resonator element is a quarter-wavelength long at the mid-band frequency and is short-circuited at one end and open-circuited at the other end. Note that the short-circuiting of the resonator elements is achieved in this example by attaching the ends of the elements to the top and bottom box walls. All box walls in are perfect grounds.

The materials you receive for this course are protected by copyright and to be used for this course only. You do not have permission to upload the course materials, including any lecture recordings you may have, to any website. If you require clarification, please consult your professor.



The materials you receive for this course are protected by copyright and to be used for this course only. You do not have permission to upload the course materials, including any lecture recordings you may have, to any website. If you require clarification, please consult your professor.

APPENDIX III

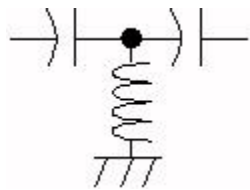
DC CONSIDERATIONS

The following section is from

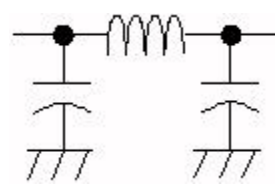
<http://www.microwaves101.com/encyclopedia/filters.cfm>

Tee versus pi networks

The terms "tee" and "pi" are used to describe lumped element filters, as well as attenuators and other networks. A tee element starts with a series element, while a pi network starts with a shunt element as shown below. The "tee" resembles a letter T while the "pi" resembles a Greek letter pi. The figures below are for three-pole networks. Odd numbers of poles still resemble the tee and pi letters somewhat, but for even numbers the distinction is nearly lost since a tee network would start with a series element and end with a shunt element.



Tee network high-pass filter



Pi network low-pass filter

The materials you receive for this course are protected by copyright and to be used for this course only. You do not have permission to upload the course materials, including any lecture recordings you may have, to any website. If you require clarification, please consult your professor.

We recommend that you use odd numbers of poles in your lumped element filters because the elements are symmetrical, that is, for a five-pole network, $C_1=C_5$, $C_2=C_4$, $L_1=L_5$ and $L_2=L_4$. This will cut down on your bill of materials and there will be fewer possibilities of assembly mistakes.

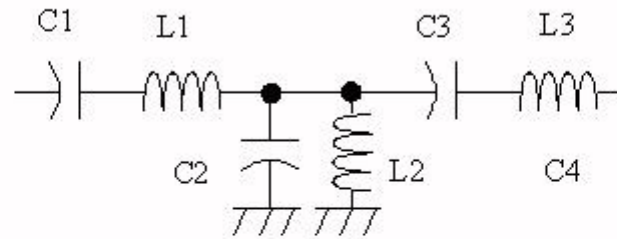
Below are pictures of $N=3$, $N=4$ and $N=5$ filters, pi and tee, BPF, LPF and HPF. Some things to note when selecting pi or tee, which will be apparent when you look over the figures.

- All LPFs will pass DC from input to output
- All HPFs block DC from input to output.
- In certain cases, filters will present a short circuit to ground on one or both inputs. In other cases the filter will look like an open circuit to DC. For $N=\text{even}$, the two ends of the filter are different.

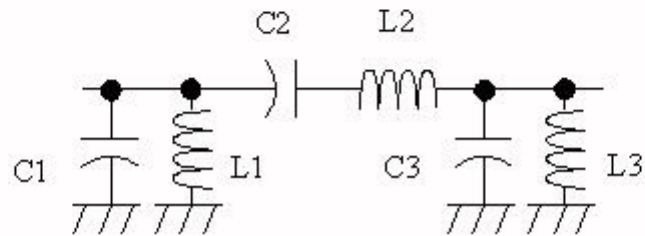
The DC properties of a filter are important to understand. Quite often in microwave design, transmission lines are used to provide DC bias voltages and currents to active devices.

The materials you receive for this course are protected by copyright and to be used for this course only. You do not have permission to upload the course materials, including any lecture recordings you may have, to any website. If you require clarification, please consult your professor.

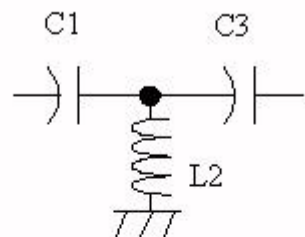
Bandpass Tee, N=3



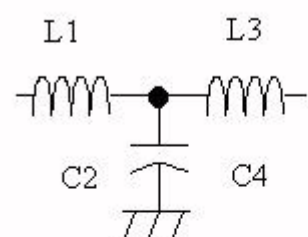
Bandpass Pi, N=3



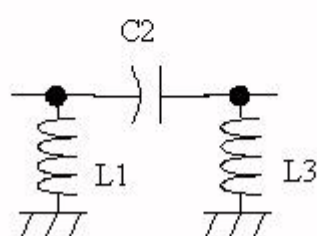
Highpass Tee, N=3



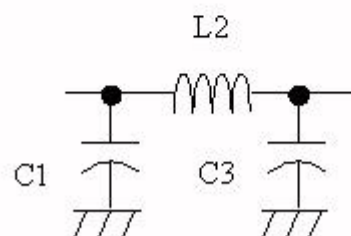
Lowpass Tee, N=3



Highpass Pi, N=3

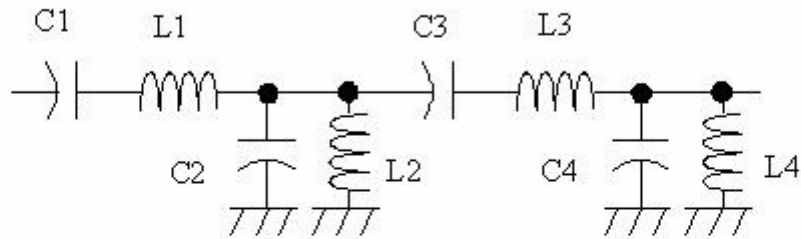


Lowpass Pi, N=3

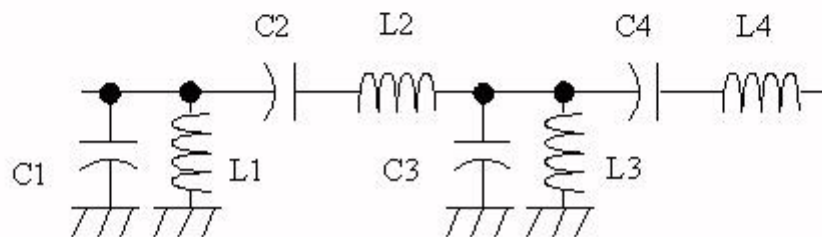


The materials you receive for this course are protected by copyright and to be used for this course only. You do not have permission to upload the course materials, including any lecture recordings you may have, to any website. If you require clarification, please consult your professor.

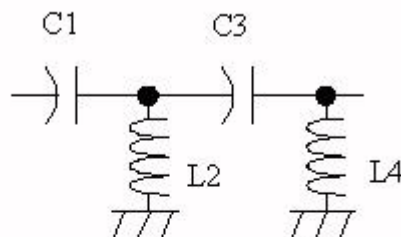
Bandpass Tee, N=4



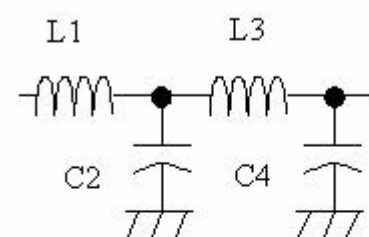
Bandpass Pi, N=4



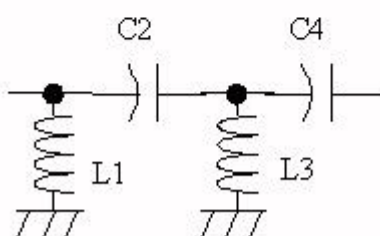
Highpass Tee, N=4



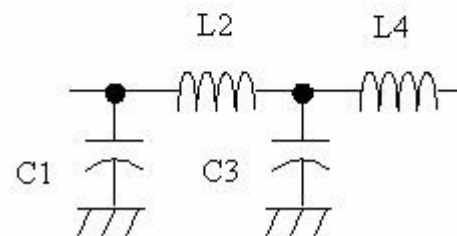
Lowpass Tee, N=4



Highpass Pi, N=4

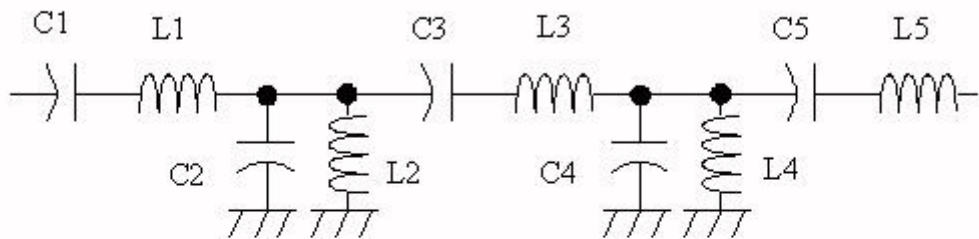


Lowpass Pi, N=4

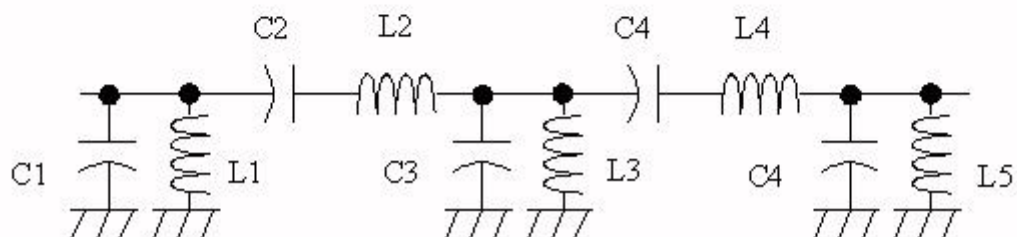


The materials you receive for this course are protected by copyright and to be used for this course only. You do not have permission to upload the course materials, including any lecture recordings you may have, to any website. If you require clarification, please consult your professor.

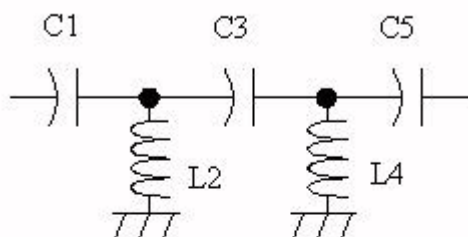
Bandpass Tee, N=5



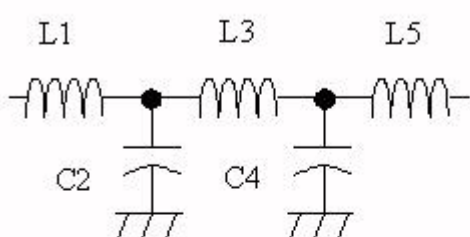
Bandpass Pi, N=5



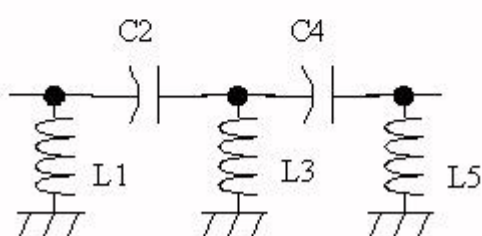
Highpass Tee, N=5



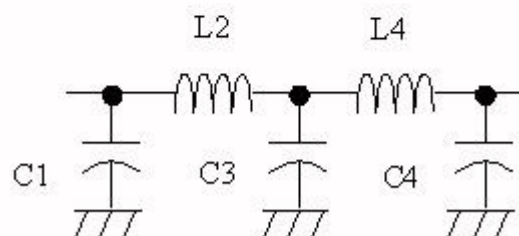
Lowpass Tee, N=5



Highpass Pi, N=5



Lowpass Pi, N=5



The materials you receive for this course are protected by copyright and to be used for this course only. You do not have permission to upload the course materials, including any lecture recordings you may have, to any website. If you require clarification, please consult your professor.

APPENDIX IV

SOME LINKS

1 - <http://www.microwaves101.com/encyclopedia/filters.cfm>

2 - <http://www.appwave.com/products/txline.html>

Transmission line calculator (calculate w and λ_g for most planar lines)

3 - <http://www.nuhertz.com/filter/>

4 - <http://www.aade.com/download.htm>

5 - Design on line : <http://www-users.cs.york.ac.uk/~fisher/lcfILTER/>

6 – Demo program : <http://www.gigasim.com/>

The materials you receive for this course are protected by copyright and to be used for this course only. You do not have permission to upload the course materials, including any lecture recordings you may have, to any website. If you require clarification, please consult your professor.

REFERENCES

- [1] T.C. Edwards, *Foundations for microstrip circuit design*, 2nd Ed., Chichester, England: Wiley, 1992.
- [2] R.M. Barrett, "Microwave printed circuits - A historical survey," *IRE Trans. Microwave Theory Tech.*, Vol 3 (2), 19, 1955.
- [3] G.L. Matthaei, L. Young, E.M.T. Jones, *Microwave filters, impedance matching networks and coupling structures*, London: Artech House, 1980.
- [4] K.C. Gupta, R. Garg, R. Chadha, *Computer aided design of microwave circuits*, Dedham MA : Artech House, 1981.
- [5] G.D. Vendelin, A.M. Pavio, U.L. Rohde, *Microwave circuit design using linear and nonlinear techniques*, New York : Wiley & Sons, 1990.
- [6] R.A. Pucel, *Monolithic microwave integrated circuits*, New-York: IEEE Press, 1985.
- [7] F. Gardiol, "Conception et réalisation de circuits microrubans," *Ann. Télécommun.*, Vol 43 (5-6), 220-236, 1988.
- [8] B.L. Smith, M.H. Carpentier, *The microwave engineering handbook*, Microwave Technology Series, Vol I and II, London: Chapman & Hall, 1993.

The materials you receive for this course are protected by copyright and to be used for this course only. You do not have permission to upload the course materials, including any lecture recordings you may have, to any website. If you require clarification, please consult your professor.

CHAPTER 8 ANALOG FILTERS

SECTION 8.1: INTRODUCTION	8.1
SECTION 8.2: THE TRANSFER FUNCTION	8.5
THE S-PLANE	8.5
F_o and Q	8.7
HIGH-PASS FILTER	8.8
BAND-PASS FILTER	8.9
BAND-REJECT (NOTCH) FILTER	8.10
ALL-PASS FILTER	8.12
PHASE RESPONSE	8.14
THE EFFECT OF NONLINEAR PHASE	8.16
SECTION 8.3: TIME DOMAIN RESPONSE	8.19
IMPULSE RESPONSE	8.19
STEP RESPONSE	8.20
SECTION 8.4: STANDARD RESPONSES	8.21
BUTTERWORTH	8.21
CHEBYSHEV	8.21
BESSEL	8.23
LINEAR PHASE with EQUIRIPPLE ERROR	8.24
TRANSITIONAL FILTERS	8.24
COMPARISON OF ALL-POLE RESPONSES	8.25
ELLIPTICAL	8.26
MAXIMALLY FLAT DELAY with CHEBYSHEV STOP BAND	8.27
INVERSE CHEBYSHEV	8.27
USING THE PROTOTYPE RESPONSE CURVES	8.29
RESPONSE CURVES	
BUTTERWORTH RESPONSE	8.31
0.01 dB CHEBYSHEV RESPONSE	8.32
0.1 dB CHEBYSHEV RESPONSE	8.33
0.25 dB CHEBYSHEV RESPONSE	8.34
0.5 dB CHEBYSHEV RESPONSE	8.35
1 dB CHEBYSHEV RESPONSE	8.36
BESSEL RESPONSE	8.27
LINEAR PHASE with EQUIRIPPLE ERROR of 0.05° RESPONSE	8.38
LINEAR PHASE with EQUIRIPPLE ERROR of 0.5° RESPONSE	8.39
GAUSSIAN TO 12 dB RESPONSE	8.40
GAUSSIAN TO 6 dB RESPONSE	8.41

■ BASIC LINEAR DESIGN

SECTION 8.4: STANDARD RESPONSES (cont.)

DESIGN TABLES

BUTTERWORTH DESIGN TABLE	8.42
0.01 dB CHEBYSHEV DESIGN TABLE	8.43
0.1 dB CHEBYSHEV DESIGN TABLE	8.44
0.25 dB CHEBYSHEV DESIGN TABLE	8.45
0.5 dB CHEBYSHEV DESIGN TABLE	8.46
1 dB CHEBYSHEV DESIGN TABLE	8.47
BESSEL DESIGN TABLE	8.48
LINEAR PHASE with EQUIRIPPLE ERROR of 0.05° DESIGN TABLE	8.49
LINEAR PHASE with EQUIRIPPLE ERROR of 0.5° DESIGN TABLE	8.50
GAUSSIAN TO 12 dB DESIGN TABLE	8.51
GAUSSIAN TO 6 dB DESIGN TABLE	8.52

SECTION 8.5: FREQUENCY TRANSFORMATION

LOW-PASS TO HIGH-PASS	8.55
LOW-PASS TO BAND-PASS	8.56
LOW-PASS TO BAND-REJECT (NOTCH)	8.59
LOW-PASS TO ALL-PASS	8.61

SECTION 8.6: FILTER REALIZATIONS

SINGLE POLE RC	8.64
PASSIVE LC SECTION	8.65
INTEGRATOR	8.67
GENERAL IMPEDANCE CONVERTER	8.68
ACTIVE INDUCTOR	8.69
FREQUENCY DEPENDENT NEGATIVE RESISTOR (FDNR)	8.70
SALLEN-KEY	8.72
MULTIPLE FEEDBACK	8.75
STATE VARIABLE	8.77
BIQUADRATIC (BIQUAD)	8.79
DUAL AMPLIFIER BAND-PASS (DABP)	8.80
TWIN T NOTCH	8.81
BAINTER NOTCH	8.82
BOCTOR NOTCH	8.83
1 BAND-PASS NOTCH	8.85
FIRST ORDER ALL-PASS	8.86
SECOND ORDER ALL-PASS	8.87

SECTION 8.6: FILTER REALIZATIONS (cont.)**DESIGN PAGES**

SINGLE-POLE	8.88
SALLEN-KEY LOW-PASS	8.89
SALLEN-KEY HIGH-PASS	8.90
SALLEN-KEY BAND-PASS	8.91
MULTIPLE FEEDBACK LOW-PASS	8.92
MULTIPLE FEEDBACK HIGH-PASS	8.93
MULTIPLE FEEDBACK BAND-PASS	8.94
STATE VARIABLE	8.95
BIQUAD	8.98
DUAL AMPLIFIER BAND-PASS	8.100
TWIN T NOTCH	8.101
BANTER NOTCH	8.102
BOCTOR NOTCH (LOW-PASS)	8.103
BOCTOR NOTCH (HIGH-PASS)	8.104
FIRST ORDER ALL-PASS	8.106
SECOND ORDER ALL-PASS	8.107

SECTION 8.7: PRACTICAL PROBLEMS IN FILTER**IMPLEMENTATION** 8.109

PASSIVE COMPONENTS	8.109
--------------------	-------

LIMITATIONS OF ACTIVE ELEMENTS (OP AMPS) IN FILTERS	8.114
---	-------

DISTORTION RESULTING FROM INPUT CAPACITANCE	
---	--

MODULATION	8.115
------------	-------

Q PEAKING AND Q ENHANCEMENT	8.117
-----------------------------	-------

SECTION 8.8: DESIGN EXAMPLES 8.121

ANTIALIASING FILTER	8.121
---------------------	-------

TRANSFORMATIONS	8.128
-----------------	-------

CD RECONSTRUCTION FILTER	8.134
--------------------------	-------

DIGITALLY PROGRAMMABLE STATE VARIABLE FILTER	8.137
--	-------

60 HZ. NOTCH FILTER	8.141
---------------------	-------

REFERENCES 8.143

▣ BASIC LINEAR DESIGN

CHAPTER 8: ANALOG FILTERS

SECTION 8.1: INTRODUCTION

Filters are networks that process signals in a frequency-dependent manner. The basic concept of a filter can be explained by examining the frequency dependent nature of the impedance of capacitors and inductors. Consider a voltage divider where the shunt leg is a reactive impedance. As the frequency is changed, the value of the reactive impedance changes, and the voltage divider ratio changes. This mechanism yields the frequency dependent change in the input/output transfer function that is defined as the frequency response.

Filters have many practical applications. A simple, single-pole, low-pass filter (the integrator) is often used to stabilize amplifiers by rolling off the gain at higher frequencies where excessive phase shift may cause oscillations.

A simple, single-pole, high-pass filter can be used to block dc offset in high gain amplifiers or single supply circuits. Filters can be used to separate signals, passing those of interest, and attenuating the unwanted frequencies.

An example of this is a radio receiver, where the signal you wish to process is passed through, typically with gain, while attenuating the rest of the signals. In data conversion, filters are also used to eliminate the effects of aliases in A/D systems. They are used in reconstruction of the signal at the output of a D/A as well, eliminating the higher frequency components, such as the sampling frequency and its harmonics, thus smoothing the waveform.

There are a large number of texts dedicated to filter theory. No attempt will be made to go heavily into much of the underlying math: Laplace transforms, complex conjugate poles and the like, although they will be mentioned.

While they are appropriate for describing the effects of filters and examining stability, in most cases examination of the function in the frequency domain is more illuminating.

An ideal filter will have an amplitude response that is unity (or at a fixed gain) for the frequencies of interest (called the *pass band*) and zero everywhere else (called the *stop band*). The frequency at which the response changes from passband to stopband is referred to as the *cutoff frequency*.

Figure 8.1(A) shows an idealized low-pass filter. In this filter the low frequencies are in the pass band and the higher frequencies are in the stop band.

■ BASIC LINEAR DESIGN

The functional complement to the low-pass filter is the high-pass filter. Here, the low frequencies are in the stop-band, and the high frequencies are in the pass band. Figure 8.1(B) shows the idealized high-pass filter.

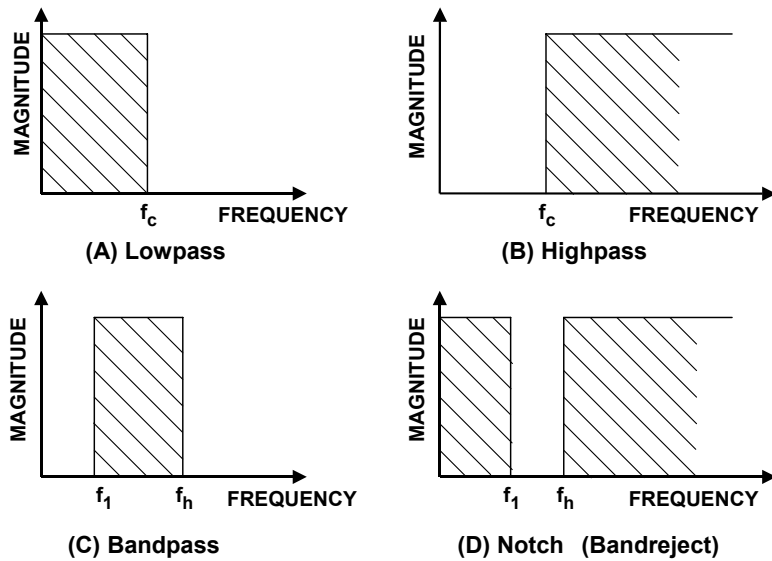


Figure 8.1: Idealized Filter Responses

If a high-pass filter and a low-pass filter are cascaded, a *band pass* filter is created. The band pass filter passes a band of frequencies between a lower cutoff frequency, f_1 , and an upper cutoff frequency, f_h . Frequencies below f_1 and above f_h are in the stop band. An idealized band pass filter is shown in Figure 8.1(C).

A complement to the band pass filter is the *band-reject*, or *notch* filter. Here, the pass bands include frequencies below f_1 and above f_h . The band from f_1 to f_h is in the stop band. Figure 8.1(D) shows a notch response.

The idealized filters defined above, unfortunately, cannot be easily built. The transition from pass band to stop band will not be instantaneous, but instead there will be a transition region. Stop band attenuation will not be infinite.

The five parameters of a practical filter are defined in Figure 8.2, opposite.

The *cutoff frequency* (F_C) is the frequency at which the filter response leaves the error band (or the -3 dB point for a Butterworth response filter). The *stop band frequency* (F_S) is the frequency at which the minimum attenuation in the stopband is reached. The *pass band ripple* (A_{\max}) is the variation (error band) in the pass band response. The *minimum pass band attenuation* (A_{\min}) defines the minimum signal attenuation within the stop band. The steepness of the filter is defined as the *order* (M) of the filter. M is also the number of poles in the transfer function. A pole is a root of the denominator of the transfer function. Conversely, a zero is a root of the numerator of the transfer function.

Each pole gives a -6 dB/octave or -20 dB/decade response. Each zero gives a $+6$ dB/octave, or $+20$ dB/decade response.

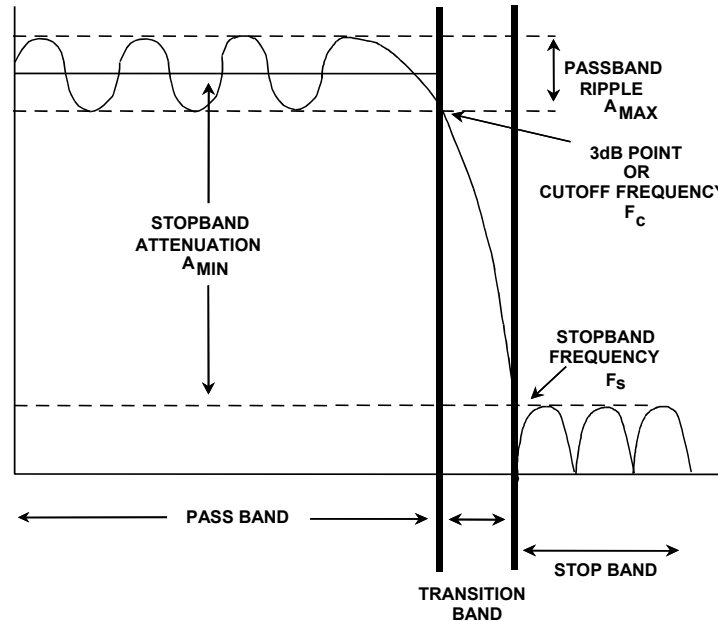


Figure 8.2: Key Filter Parameters

Note that not all filters will have all these features. For instance, all-pole configurations (i.e. no zeros in the transfer function) will not have ripple in the stop band. Butterworth and Bessel filters are examples of all-pole filters with no ripple in the pass band.

Typically, one or more of the above parameters will be variable. For instance, if you were to design an antialiasing filter for an ADC, you will know the cutoff frequency (the maximum frequency that you want to pass), the stop band frequency, (which will generally be the Nyquist frequency ($= \frac{1}{2}$ the sample rate)) and the minimum attenuation required (which will be set by the resolution or dynamic range of the system). You can then go to a chart or computer program to determine the other parameters, such as filter order, F_0 , and Q , which determines the peaking of the section, for the various sections and/or component values.

It should also be pointed out that the filter will affect the phase of a signal, as well as the amplitude. For example, a single-pole section will have a 90° phase shift at the crossover frequency. A pole pair will have a 180° phase shift at the crossover frequency. The Q of the filter will determine the rate of change of the phase. This will be covered more in depth in the next section.

▣ BASIC LINEAR DESIGN

Notes:

SECTION 8.2: THE TRANSFER FUNCTION

The S-Plane

Filters have a frequency dependent response because the impedance of a capacitor or an inductor changes with frequency. Therefore the complex impedances:

$$Z_L = s L \quad \text{Eq. 8-1}$$

and

$$Z_C = \frac{1}{s C} \quad \text{Eq. 8-2}$$

are used to describe the impedance of an inductor and a capacitor, respectively,

$$s = \sigma + j\omega \quad \text{Eq. 8-3}$$

where σ is the Neper frequency in nepers per second (NP/s) and ω is the angular frequency in radians per sec (rad/s).

By using standard circuit analysis techniques, the transfer equation of the filter can be developed. These techniques include Ohm's law, Kirchoff's voltage and current laws, and superposition, remembering that the impedances are complex. The transfer equation is then:

$$H(s) = \frac{a_m s^m + a_{m-1} s^{m-1} + \dots + a_1 s + a_0}{b_n s^n + b_{n-1} s^{n-1} + \dots + b_1 s + b_0} \quad \text{Eq. 8-4}$$

Therefore, $H(s)$ is a rational function of s with real coefficients with the degree of m for the numerator and n for the denominator. The degree of the denominator is the order of the filter. Solving for the roots of the equation determines the poles (denominator) and zeros (numerator) of the circuit. Each pole will provide a -6 dB/octave or -20 dB/decade response. Each zero will provide a $+6$ dB/octave or $+20$ dB/decade response. These roots can be real or complex. When they are complex, they occur in conjugate pairs. These roots are plotted on the s plane (complex plane) where the horizontal axis is σ (real axis) and the vertical axis is ω (imaginary axis). How these roots are distributed on the s plane can tell us many things about the circuit. In order to have stability, all poles must be in the left side of the plane. If we have a zero at the origin, that is a zero in the numerator, the filter will have no response at dc (high-pass or band pass).

Assume an RLC circuit, as in Figure 8.3. Using the voltage divider concept it can be shown that the voltage across the resistor is:

$$H(s) = \frac{V_o}{V_{in}} = \frac{RCs}{LCs^2 + RCs + 1} \quad \text{Eq. 8-5}$$

■ BASIC LINEAR DESIGN

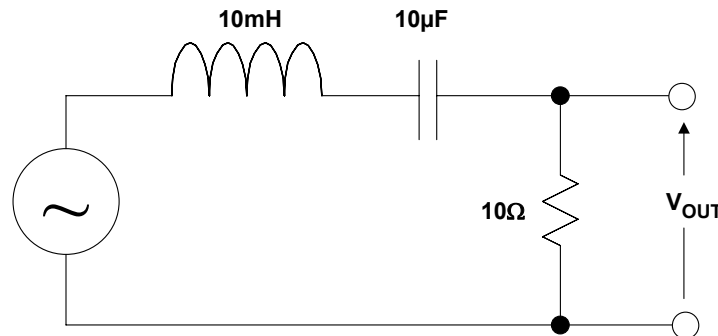


Figure 8.3: RLC Circuit

Substituting the component values into the equation yields:

$$H(s) = 10^3 \times \frac{s}{s^2 + 10^3 s + 10^7} \quad \text{Eq. 8-6}$$

Factoring the equation and normalizing gives:

$$H(s) = 10^3 \times \frac{s}{[s - (-0.5 + j 3.122) \times 10^3] \times [s - (-0.5 - j 3.122) \times 10^3]} \quad \text{Eq 8-7}$$

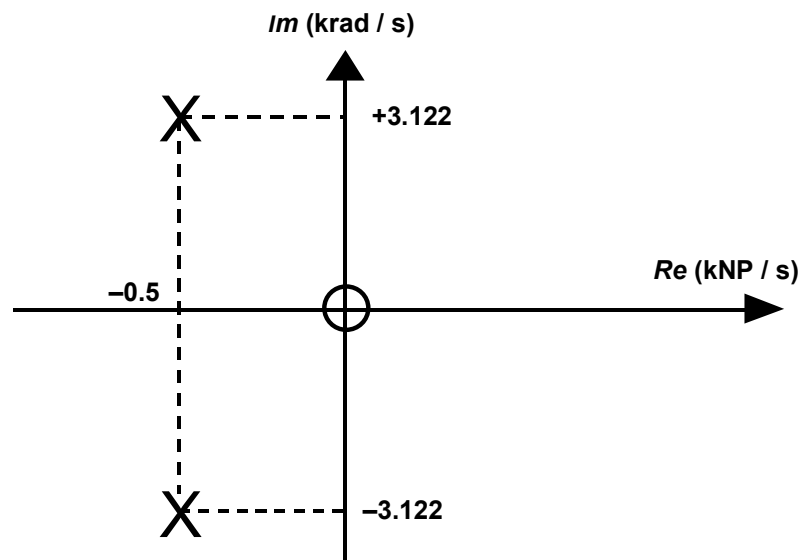


Figure 8.4: Pole and Zero Plotted on the s-Plane

This gives a zero at the origin and a pole pair at:

$$s = (-0.5 \pm j3.122) \times 10^3 \quad \text{Eq. 8-8}$$

Next, plot these points on the s plane as shown in Figure 8.4:

The above discussion has a definite mathematical flavor. In most cases we are more interested in the circuit's performance in real applications. While working in the s plane is completely valid, I'm sure that most of us don't think in terms of Nepers and imaginary frequencies.

F_o and Q

So if it is not convenient to work in the s plane, why go through the above discussion? The answer is that the groundwork has been set for two concepts that will be infinitely more useful in practice: F_o and Q.

F_o is the cutoff frequency of the filter. This is defined, in general, as the frequency where the response is down 3 dB from the pass band. It can sometimes be defined as the frequency at which it will fall out of the pass band. For example, a 0.1 dB Chebyshev filter can have its F_o at the frequency at which the response is down > 0.1 dB.

The shape of the attenuation curve (as well as the phase and delay curves, which define the time domain response of the filter) will be the same if the ratio of the actual frequency to the cutoff frequency is examined, rather than just the actual frequency itself. Normalizing the filter to 1 rad/s, a simple system for designing and comparing filters can be developed. The filter is then scaled by the cutoff frequency to determine the component values for the actual filter.

Q is the "quality factor" of the filter. It is also sometimes given as α where:

$$\alpha = \frac{1}{Q} \quad \text{Eq. 8-9}$$

This is commonly known as the *damping ratio*. ξ is sometimes used where:

$$\xi = 2\alpha \quad \text{Eq. 8-10}$$

If Q is > 0.707, there will be some peaking in the filter response. If the Q is < 0.707, rolloff at F_o will be greater; it will have a more gentle slope and will begin sooner. The amount of peaking for a 2 pole low-pass filter vs. Q is shown in Figure 8.5.

■ BASIC LINEAR DESIGN

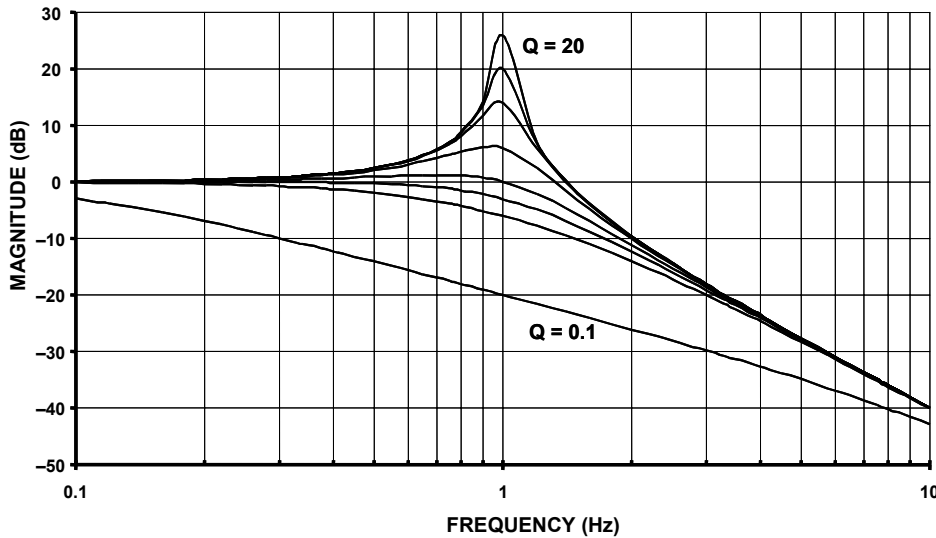


Figure 8.5: Low-Pass Filter Peaking vs. Q

Rewriting the transfer function $H(s)$ in terms of ω_0 and Q :

$$H(s) = \frac{H_0}{s^2 + \frac{\omega_0}{Q} s + \omega_0^2} \quad \text{Eq. 8-11}$$

where H_0 is the pass-band gain and $\omega_0 = 2\pi F_o$.

This is now the *low-pass prototype* that will be used to design the filters.

High-Pass Filter

Changing the numerator of the transfer equation, $H(s)$, of the low-pass prototype to H_0s^2 transforms the low-pass filter into a high-pass filter. The response of the high-pass filter is similar in shape to a low-pass, just inverted in frequency.

The transfer function of a high-pass filter is then:

$$H(s) = \frac{H_0 s^2}{s^2 + \frac{\omega_0}{Q} s + \omega_0^2} \quad \text{Eq. 8-12}$$

The response of a 2-pole high-pass filter is illustrated in Figure 8.6.

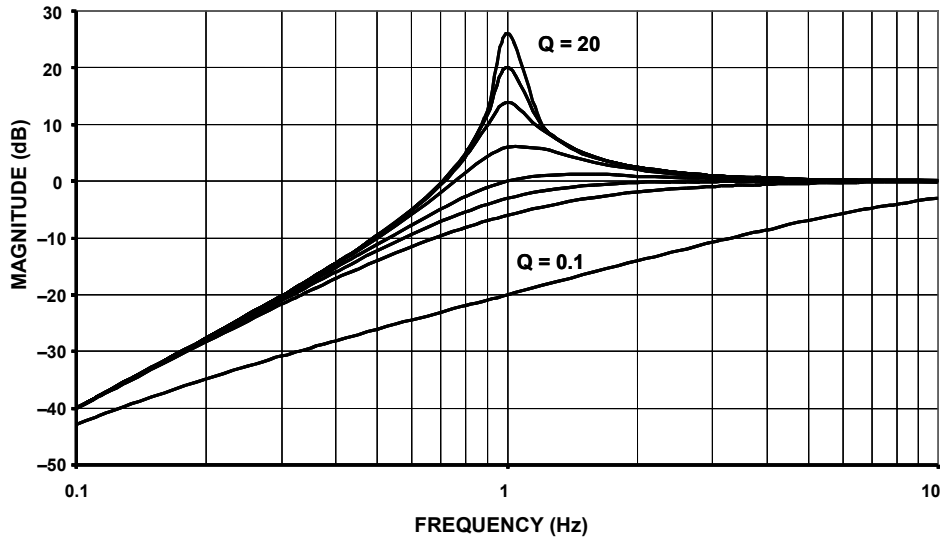


Figure 8.6: High- Pass Filter Peaking vs. Q

Band-Pass Filter

Changing the numerator of the lowpass prototype to $H_0\omega_0^2$ will convert the filter to a band-pass function.

The transfer function of a band-pass filter is then:

$$H(s) = \frac{H_0\omega_0^2}{s^2 + \frac{\omega_0}{Q} s + \omega_0^2} \quad \text{Eq. 8-13}$$

ω_0 here is the frequency ($F_0 = 2 \pi \omega_0$) at which the gain of the filter peaks.

H_0 is the circuit gain and is defined:

$$H_0 = H/Q. \quad \text{Eq. 8-14}$$

Q has a particular meaning for the band-pass response. It is the selectivity of the filter. It is defined as:

$$Q = \frac{F_0}{F_H - F_L} \quad \text{Eq. 8-15}$$

where F_L and F_H are the frequencies where the response is -3 dB from the maximum.

The bandwidth (BW) of the filter is described as:

It can be shown that the resonant frequency (F_0) is the geometric mean of F_L and F_H ,

$$\text{BW} = F_H - F_L \quad \text{Eq. 8-16}$$

■ BASIC LINEAR DESIGN

which means that F_0 will appear half way between F_L and F_H on a logarithmic scale.

$$F_0 = \sqrt{F_H F_L} \quad \text{Eq. 8-17}$$

Also, note that the skirts of the band-pass response will always be symmetrical around F_0 on a logarithmic scale.

The response of a band-pass filter to various values of Q are shown in Figure 8.7.

A word of caution is appropriate here. Band-pass filters can be defined two different ways. The narrow-band case is the classic definition that we have shown above.

In some cases, however, if the high and low cutoff frequencies are widely separated, the band-pass filter is constructed out of separate high-pass and low-pass sections. Widely separated in this context means separated by at least 2 octaves ($\times 4$ in frequency). This is the wideband case.

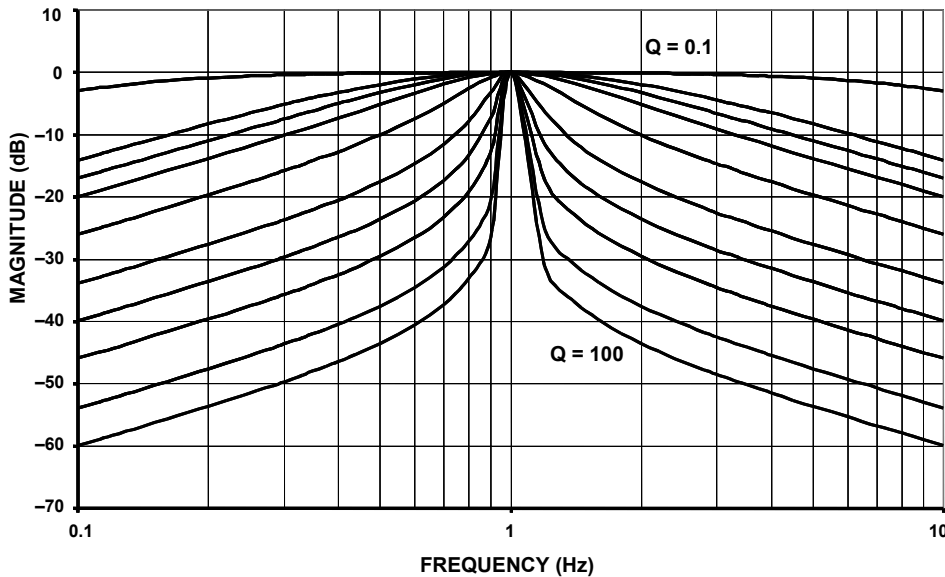


Figure 8.7: Band-Pass Filter Peaking vs. Q

Band-Reject (Notch) Filter

By changing the numerator to $s^2 + \omega_z^2$, we convert the filter to a band-reject or notch filter. As in the bandpass case, if the corner frequencies of the band-reject filter are separated by more than an octave (the wideband case), it can be built out of separate low-pass and high-pass sections. We will adopt the following convention: A narrow-band band-reject filter will be referred to as a *notch* filter and the wideband band-reject filter will be referred to as *band-reject* filter.

A notch (or band-reject) transfer function is:

$$H(s) = \frac{H_0(s^2 + \omega_z^2)}{s^2 + \frac{\omega_0}{Q}s + \omega_0^2} \quad \text{Eq. 8-18}$$

There are three cases of the notch filter characteristics. These are illustrated in Figure 8.8 (opposite). The relationship of the pole frequency, ω_0 , and the zero frequency, ω_z , determines if the filter is a standard notch, a lowpass notch or a highpass notch.

If the zero frequency is equal to the pole frequency a standard notch exists. In this instance the zero lies on the $j\omega$ plane where the curve that defines the pole frequency intersects the axis.

A lowpass notch occurs when the zero frequency is greater than the pole frequency. In this case ω_z lies outside the curve of the pole frequencies. What this means in a practical sense is that the filter's response below ω_z will be greater than the response above ω_z . This results in an elliptical low-pass filter.

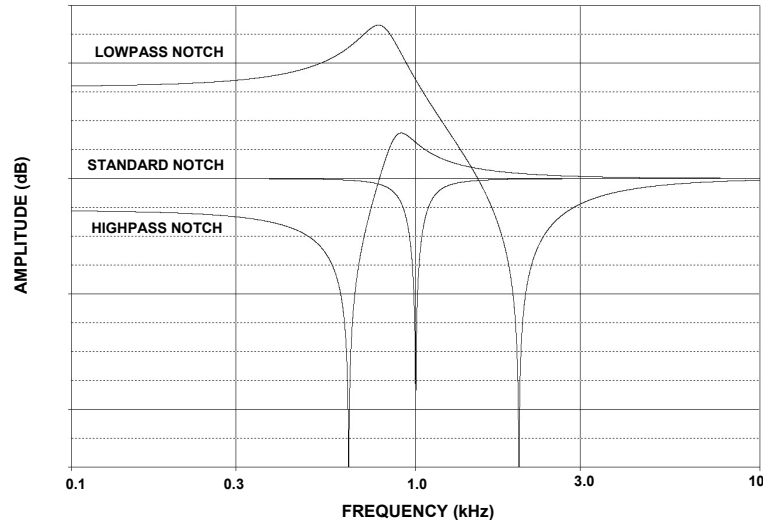


Figure 8.8: Standard, Lowpass, and Highpass Notches

A high-pass notch filter occurs when the zero frequency is less than the pole frequency. In this case ω_z lies inside the curve of the pole frequencies. What this means in a practical sense is that the filters response below ω_z will be less than the response above ω_z . This results in an elliptical high-pass filter.

■ BASIC LINEAR DESIGN

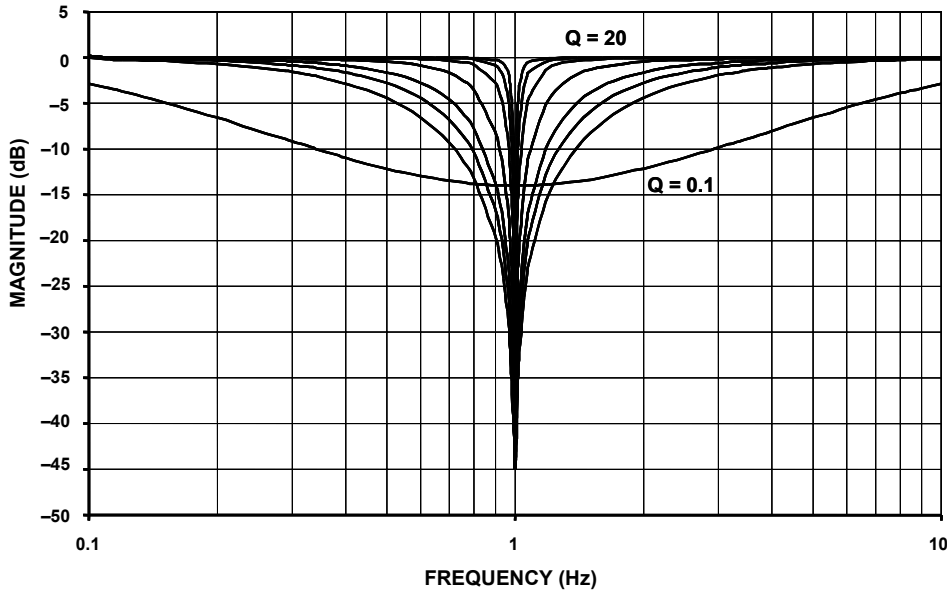


Figure 8.9: Notch Filter Width versus Frequency for Various Q Values

The variation of the notch width with Q is shown in Figure 8.9.

All-pass Filter

There is another type of filter that leaves the amplitude of the signal intact but introduces phase shift. This type of filter is called an *all-pass*. The purpose of this filter is to add phase shift (delay) to the response of the circuit. The amplitude of an all-pass is unity for all frequencies. The phase response, however, changes from 0° to 360° as the frequency is swept from 0 to infinity. The purpose of an all-pass filter is to provide phase equalization, typically in pulse circuits. It also has application in single side band, suppressed carrier (SSB-SC) modulation circuits.

The transfer function of an all-pass filter is:

$$H(s) = \frac{s^2 - \frac{\omega_0}{Q} s + \omega_0^2}{s^2 + \frac{\omega_0}{Q} s + \omega_0^2} \quad \text{Eq. 8-19}$$

Note that an all-pass transfer function can be synthesized as:

$$H_{AP} = H_{LP} - H_{BP} + H_{HP} = 1 - 2H_{BP}. \quad \text{Eq. 8-20}$$

Figure 8.10 (opposite) compares the various filter types.

FILTER TYPE	MAGNITUDE	POLE LOCATION	TRANSFER EQUATION
LOWPASS			$\frac{\omega_0^2}{s^2 + \frac{\omega_0}{Q}s + \omega_0^2}$
BANDPASS			$\frac{\frac{\omega_0}{Q}s}{s^2 + \frac{\omega_0}{Q}s + \omega_0^2}$
NOTCH (BANDREJECT)			$\frac{s^2 + \omega_z^2}{s^2 + \frac{\omega_0}{Q}s + \omega_0^2}$
HIGHPASS			$\frac{s^2}{s^2 + \frac{\omega_0}{Q}s + \omega_0^2}$
ALLPASS			$\frac{s^2 - \frac{\omega_0}{Q}s + \omega_0^2}{s^2 + \frac{\omega_0}{Q}s + \omega_0^2}$

Figure 8.10: Standard Second-order Filter Responses

■ BASIC LINEAR DESIGN

Phase Response

As mentioned earlier, a filter will change the phase of the signal as well as the amplitude. The question is, does this make a difference? Fourier analysis indicates a square wave is made up of a fundamental frequency and odd order harmonics. The magnitude and phase responses, of the various harmonics, are precisely defined. If the magnitude or phase relationships are changed, then the summation of the harmonics will not add back together properly to give a square wave. It will instead be distorted, typically showing overshoot and ringing or a slow rise time. This would also hold for any complex waveform.

Each pole of a filter will add 45° of phase shift at the corner frequency. The phase will vary from 0° (well below the corner frequency) to 90° (well beyond the corner frequency). The start of the change can be more than a decade away. In multipole filters, each of the poles will add phase shift, so that the total phase shift will be multiplied by the number of poles (180° total shift for a two pole system, 270° for a three pole system, etc.).

The phase response of a single-pole, low-pass filter is:

$$\phi(\omega) = -\arctan \frac{\omega}{\omega_0} \quad \text{Eq. 8-21}$$

The phase response of a low-pass pole pair is:

$$\begin{aligned} \phi(\omega) = & -\arctan \left[\frac{1}{\alpha} \left(2 \frac{\omega}{\omega_0} + \sqrt{4 - \alpha^2} \right) \right] \\ & -\arctan \left[\frac{1}{\alpha} \left(2 \frac{\omega}{\omega_0} - \sqrt{4 - \alpha^2} \right) \right] \end{aligned} \quad \text{Eq. 8-22}$$

For a single-pole, high-pass filter the phase response is:

$$\phi(\omega) = \frac{\pi}{2} - \arctan \frac{\omega}{\omega_0} \quad \text{Eq. 8-23}$$

The phase response of a high-pass pole pair is:

$$\begin{aligned} \phi(\omega) = & \pi - \arctan \left[\frac{1}{\alpha} \left(2 \frac{\omega}{\omega_0} + \sqrt{4 - \alpha^2} \right) \right] \\ & -\arctan \left[\frac{1}{\alpha} \left(2 \frac{\omega}{\omega_0} - \sqrt{4 - \alpha^2} \right) \right] \end{aligned} \quad \text{Eq. 8-24}$$

The phase response of a band-pass filter is:

$$\phi(\omega) = \frac{\pi}{2} - \arctan\left(\frac{2Q\omega}{\omega_0} + \sqrt{4Q^2 - 1}\right) - \arctan\left(\frac{2Q\omega}{\omega_0} - \sqrt{4Q^2 - 1}\right)$$
Eq. 8-25

The variation of the phase shift with frequency due to various values of Q is shown in Figure 8.11 (for low-pass, high-pass, band-pass, and all-pass) and in Figure 8.12 (for notch).

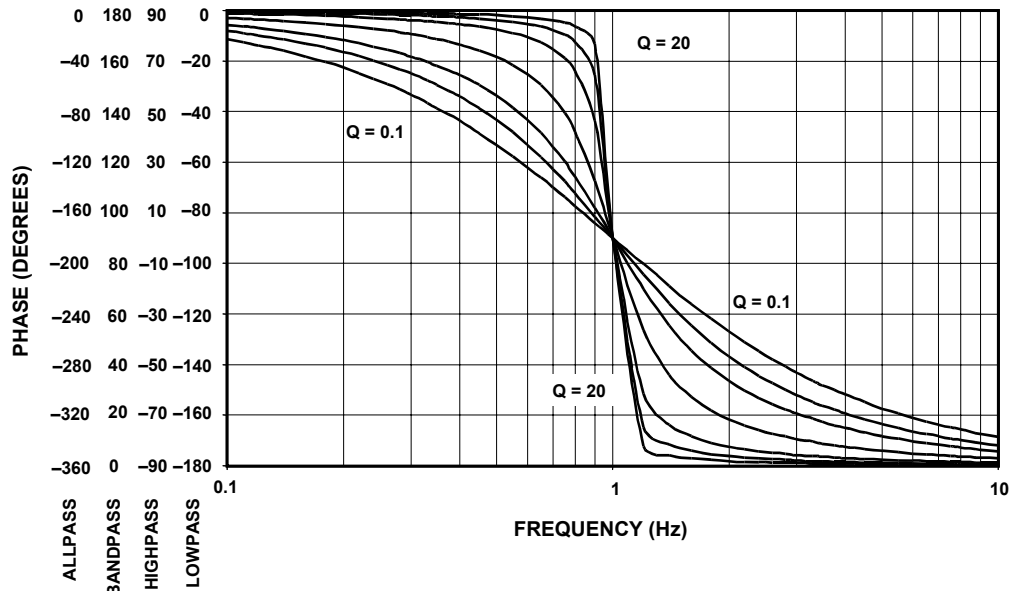


Figure 8.11: Phase Response vs. Frequency

■ BASIC LINEAR DESIGN

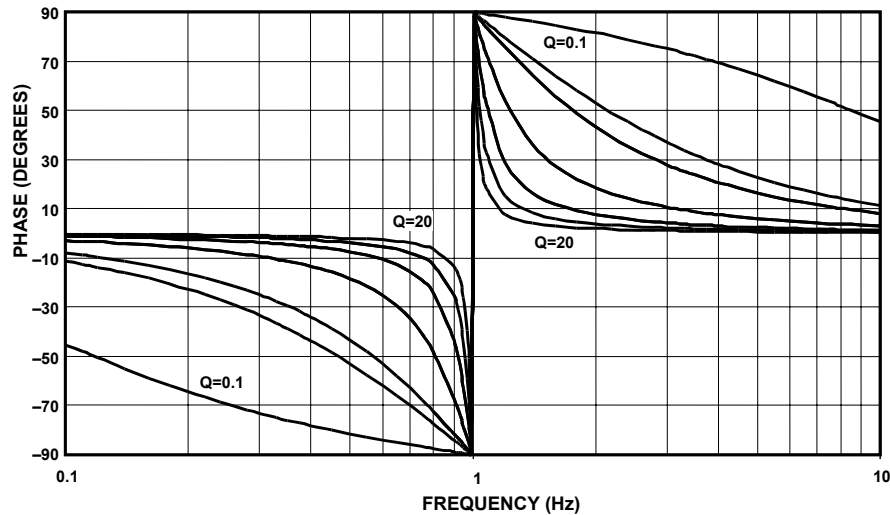


Figure 8.12: Notch Filter Phase Response

It is also useful to look at the change of phase with frequency. This is the group delay of the filter. A flat (constant) group delay gives best phase response, but, unfortunately, it also gives the least amplitude discrimination. The group delay of a single low-pass pole

$$\tau(\omega) = -\frac{d\phi(\omega)}{d\omega} = \frac{\cos^2 \phi}{\omega_0} \quad \text{Eq. 8-26}$$

is:

$$\tau(\omega) = \frac{2 \sin^2 \phi}{\alpha \omega_0} - \frac{\sin 2 \phi}{2 \omega} \quad \text{Eq. 8-27}$$

For the low-pass pole pair it is:

For the single high-pass pole it is:

For the high-pass pole pair it is:

$$\tau(\omega) = \frac{2 \sin^2 \phi}{\alpha \omega_0} - \frac{\sin 2 \phi}{2 \omega} \quad \text{Eq. 8-28}$$

$$\tau(\omega) = -\frac{d\phi(\omega)}{d\omega} = \frac{\sin^2 \phi}{\omega_0} \quad \text{Eq. 8-29}$$

And for the band-pass pole pair it is:

$$\tau(\omega) = \frac{2Q 2 \cos^2 \phi}{\alpha \omega_0} + \frac{\sin 2 \phi}{2 \omega} \quad \text{Eq. 8-30}$$

The Effect of Nonlinear Phase

A waveform can be represented by a series of frequencies of specific amplitude, frequency and phase relationships. For example, a square wave is:

$$F(t) = A \left(\frac{1}{2} + \frac{2}{\pi} \sin \omega t + \frac{2}{3\pi} \sin 3\omega t + \frac{2}{5\pi} \sin 5\omega t + \frac{2}{7\pi} \sin 7\omega t + \dots \right) \quad \text{Eq. 8-31}$$

If this waveform were passed through a filter, the amplitude and phase response of the filter to the various frequency components of the waveform could be different. If the phase delays were identical, the waveform would pass through the filter undistorted. If, however, the different components of the waveform were changed due to different amplitude and phase response of the filter to those frequencies, they would no longer add up in the same manner. This would change the shape of the waveform. These distortions would manifest themselves in what we typically call overshoot and ringing of the output.

Not all signals will be composed of harmonically related components. An amplitude modulated (AM) signal, for instance, will consist of a carrier and 2 sidebands at \pm the modulation frequency. If the filter does not have the same delay for the various waveform components, then “envelope delay” will occur and the output wave will be distorted.

Linear phase shift results in constant group delay since the derivative of a linear function is a constant.

▣ BASIC LINEAR DESIGN

Notes:

SECTION 8.3: TIME DOMAIN RESPONSE

Up until now the discussion has been primarily focused on the frequency domain response of filters. The time domain response can also be of concern, particularly under transient conditions. Moving between the time domain and the frequency domain is accomplished by the use of the Fourier and Laplace transforms. This yields a method of evaluating performance of the filter to a nonsinusoidal excitation.

The transfer function of a filter is the ratio of the output to input time functions. It can be shown that the impulse response of a filter defines its bandwidth. The time domain response is a practical consideration in many systems, particularly communications, where many modulation schemes use both amplitude and phase information.

Impulse Response

The impulse function is defined as an infinitely high, infinitely narrow pulse, with an area of unity. This is, of course, impossible to realize in a physical sense. If the impulse width is much less than the rise time of the filter, the resulting response of the filter will give a reasonable approximation actual impulse response of the filter response.

The impulse response of a filter, in the time domain, is proportional to the bandwidth of the filter in the frequency domain. The narrower the impulse, the wider the bandwidth of the filter. The pulse amplitude is equal to ω_c/π , which is also proportional to the filter bandwidth, the height being taller for wider bandwidths. The pulse width is equal to $2\pi/\omega_c$, which is inversely proportional to bandwidth. It turns out that the product of the amplitude and the bandwidth is a constant.

It would be a nontrivial task to calculate the response of a filter without the use of Laplace and Fourier transforms. The Laplace transform converts multiplication and division to addition and subtraction, respectively. This takes equations, which are typically loaded with integration and/or differentiation, and turns them into simple algebraic equations, which are much easier to deal with. The Fourier transform works in the opposite direction.

The details of these transform will not be discussed here. However, some general observations on the relationship of the impulse response to the filter characteristics will be made.

It can be shown, as stated, that the impulse response is related to the bandwidth. Therefore, amplitude discrimination (the ability to distinguish between the desired signal from other, out of band signals and noise) and time response are inversely proportional. That is to say that the filters with the best amplitude response are the ones with the worst time response. For all-pole filters, the Chebyshev filter gives the best amplitude discrimination, followed by the Butterworth and then the Bessel.

■ BASIC LINEAR DESIGN

If the time domain response were ranked, the Bessel would be best, followed by the Butterworth and then the Chebyshev. Details of the different filter responses will be discussed in the next section.

The impulse response also increases with increasing filter order. Higher filter order implies greater bandlimiting, therefore degraded time response. Each section of a multistage filter will have its own impulse response, and the total impulse response is the accumulation of the individual responses. The degradation in the time response can also be related to the fact that as frequency discrimination is increased, the Q of the individual sections tends to increase. The increase in Q increases the overshoot and ringing of the individual sections, which implies longer time response.

Step Response

The step response of a filter is the integral of the impulse response. Many of the generalities that apply to the impulse response also apply to the step response. The slope of the rise time of the step response is equal to the peak response of the impulse. The product of the bandwidth of the filter and the rise time is a constant. Just as the impulse has a function equal to unity, the step response has a function equal to $1/s$. Both of these expressions can be normalized, since they are dimensionless.

The step response of a filter is useful in determining the envelope distortion of a modulated signal. The two most important parameters of a filter's step response are the overshoot and ringing. Overshoot should be minimal for good pulse response. Ringing should decay as fast as possible, so as not to interfere with subsequent pulses.

Real life signals typically aren't made up of impulse pulses or steps, so the transient response curves don't give a completely accurate estimation of the output. They are, however, a convenient figure of merit so that the transient responses of the various filter types can be compared on an equal footing.

Since the calculations of the step and impulse response are mathematically intensive, they are most easily performed by computer. Many CAD (Computer Aided Design) software packages have the ability to calculate these responses. Several of these responses are also collected in the next section.

SECTION 8.4: STANDARD RESPONSES

There are many transfer functions that may satisfy the attenuation and/or phase requirements of a particular filter. The one that you choose will depend on the particular system. The importance of the frequency domain response versus the time domain response must be determined. Also, both of these considerations might be traded off against filter complexity, and thereby cost.

Butterworth

The Butterworth filter is the best compromise between attenuation and phase response. It has no ripple in the pass band or the stop band, and because of this is sometimes called a maximally flat filter. The Butterworth filter achieves its flatness at the expense of a relatively wide transition region from pass band to stop band, with average transient characteristics.

The normalized poles of the Butterworth filter fall on the unit circle (in the s plane). The pole positions are given by:

$$-\sin \frac{(2K-1)\pi}{2n} + j \cos \frac{(2K-1)\pi}{2n} \quad K=1,2,\dots,n \quad \text{Eq. 8-32}$$

where K is the pole pair number, and n is the number of poles.

The poles are spaced equidistant on the unit circle, which means the angles between the poles are equal.

Given the pole locations, ω_0 , and α (or Q) can be determined. These values can then be used to determine the component values of the filter. The design tables for passive filters use frequency and impedance normalized filters. They are normalized to a frequency of 1 rad/sec and impedance of 1Ω . These filters can be denormalized to determine actual component values. This allows the comparison of the frequency domain and/or time domain responses of the various filters on equal footing. The Butterworth filter is normalized for a -3 dB response at $\omega_0 = 1$.

The values of the elements of the Butterworth filter are more practical and less critical than many other filter types. The frequency response, group delay, impulse response, and step response are shown in Figure 8.15. The pole locations and corresponding ω_0 and α terms are tabulated in Figure 8.26.

Chebyshev

The Chebyshev (or Chevyshev, Tschebychev, Tschebyscheff or Tchevysheff, depending on how you translate from Russian) filter has a smaller transition region than the same-order Butterworth filter, at the expense of ripples in its pass band. This filter gets its name

■ BASIC LINEAR DESIGN

because the Chebyshev filter minimizes the height of the maximum ripple, which is the Chebyshev criterion.

Chebyshev filters have 0 dB relative attenuation at dc. Odd order filters have an attenuation band that extends from 0 dB to the ripple value. Even order filters have a gain equal to the pass band ripple. The number of cycles of ripple in the pass band is equal to the order of the filter.

The poles of the Chebyshev filter can be determined by moving the poles of the Butterworth filter to the right, forming an ellipse. This is accomplished by multiplying the real part of the pole by k_r and the imaginary part by k_I . The values k_r and k_I can be computed by:

$$K_r = \sinh A \quad \text{Eq. 8-33}$$

$$K_I = \cosh A \quad \text{Eq. 8-34}$$

where:

$$A = \frac{1}{n} \sinh^{-1} \frac{1}{\varepsilon} \quad \text{Eq. 8-35}$$

where n is the filter order and:

$$\varepsilon = \sqrt{10^R - 1} \quad \text{Eq. 8-36}$$

where:

$$R = \frac{R_{dB}}{10} \quad \text{Eq. 8-37}$$

where:

$$R_{dB} = \text{pass band ripple in dB} \quad \text{Eq. 8-38}$$

The Chebyshev filters are typically normalized so that the edge of the ripple band is at $\omega_0 = 1$. The 3 dB bandwidth is given by:

$$A_{3dB} = \frac{1}{n} \cosh^{-1} \left(\frac{1}{\varepsilon} \right) \quad \text{Eq. 8-39}$$

This is tabulated in Table 1.

The frequency response, group delay, impulse response and step response are cataloged in Figures 8.16 to 8.20 on following pages, for various values of pass band ripple (0 .01 dB, 0.1 dB, 0.25 dB, 0.5 dB, and 1 dB). The pole locations and corresponding ω_0 and α terms for these values of ripple are tabulated in Figures 8.27 to 8.31 on following pages.

ORDER	.01dB	.1dB	.25dB	.5dB	1dB
2	3.30362	1.93432	1.59814	1.38974	1.21763
3	1.87718	1.38899	1.25289	1.16749	1.09487
4	1.46690	1.21310	1.13977	1.09310	1.05300
5	1.29122	1.13472	1.08872	1.05926	1.03381
6	1.19941	1.09293	1.06134	1.04103	1.02344
7	1.14527	1.06800	1.04495	1.03009	1.01721
8	1.11061	1.05193	1.03435	1.02301	1.01316
9	1.08706	1.04095	1.02711	1.01817	1.01040
10	1.07033	1.03313	1.02194	1.01471	1.00842

Table 1: 3dB Bandwidth to Ripple Bandwidth for Chebyshev Filters

Bessel

Butterworth filters have fairly good amplitude and transient behavior. The Chebyshev filters improve on the amplitude response at the expense of transient behavior. The Bessel filter is optimized to obtain better transient response due to a linear phase (i.e. constant delay) in the passband. This means that there will be relatively poorer frequency response (less amplitude discrimination).

The poles of the Bessel filter can be determined by locating all of the poles on a circle and separating their imaginary parts by:

$$\frac{2}{n} \quad \text{Eq. 8-40}$$

where n is the number of poles. Note that the top and bottom poles are distanced by where the circle crosses the $j\omega$ axis by:

$$\frac{1}{n} \quad \text{Eq. 8-41}$$

or half the distance between the other poles.

The frequency response, group delay, impulse response and step response for the Bessel filters are cataloged in Figure 8.21. The pole locations and corresponding ω_o and α terms for the Bessel filter are tabulated in Figure 8.32.

■ BASIC LINEAR DESIGN

Linear Phase with Equiripple Error

The linear phase filter offers linear phase response in the pass band, over a wider range than the Bessel, and superior attenuation far from cutoff. This is accomplished by letting the phase response have ripples, similar to the amplitude ripples of the Chebyshev. As the ripple is increased, the region of constant delay extends further into the stopband. This will also cause the group delay to develop ripples, since it is the derivative of the phase response. The step response will show slightly more overshoot than the Bessel and the impulse response will show a bit more ringing.

It is difficult to compute the pole locations of a linear phase filter. Pole locations are taken from the Williams book (see Reference 2), which, in turn, comes from the Zverev book (see Reference 1).

The frequency response, group delay, impulse response and step response for linear phase filters of 0.05° ripple and 0.5° ripple are given in Figures 8.22 and 8.23. The pole locations and corresponding ω_0 and α terms are tabulated in Figures 8.33 and 8.34.

Transitional Filters

A transitional filter is a compromise between a Gaussian filter, which is similar to a Bessel, and the Chebyshev. A transitional filter has nearly linear phase shift and smooth, monotonic rolloff in the pass band. Above the pass band there is a break point beyond which the attenuation increases dramatically compared to the Bessel, and especially at higher values of n .

Two transition filters have been tabulated. These are the Gaussian to 6 dB and Gaussian to 12 dB.

The Gaussian to 6 dB filter has better transient response than the Butterworth in the pass band. Beyond the breakpoint, which occurs at $\omega = 1.5$, the rolloff is similar to the Butterworth.

The Gaussian to 12 dB filter's transient response is much better than Butterworth in the pass band. Beyond the 12dB breakpoint, which occurs at $\omega = 2$, the attenuation is less than the Butterworth.

As is the case with the linear phase filters, pole locations for transitional filters do not have a closed form method for computation. Again, pole locations are taken from Williams's book (see Reference 2). These were derived from iterative techniques.

The frequency response, group delay, impulse response and step response for Gaussian to 12 dB and 6 dB are shown in Figures 8.24 and 8.25. The pole locations and corresponding ω_0 and α terms are tabulated in Figures 8.35 and 8.36.

Comparison of All-Pole Responses

The responses of several all-pole filters, namely the Bessel, Butterworth, and Chebyshev (in this case of 0.5 dB ripple) will now be compared. An 8 pole filter is used as the basis for the comparison. The responses have been normalized for a cutoff of 1 Hz. Comparing Figures 8.13 and 8.14 below, it is easy to see the trade-offs in the response types. Moving from Bessel through Butterworth to Chebyshev, notice that the amplitude discrimination improves as the transient behavior gets progressively poorer.

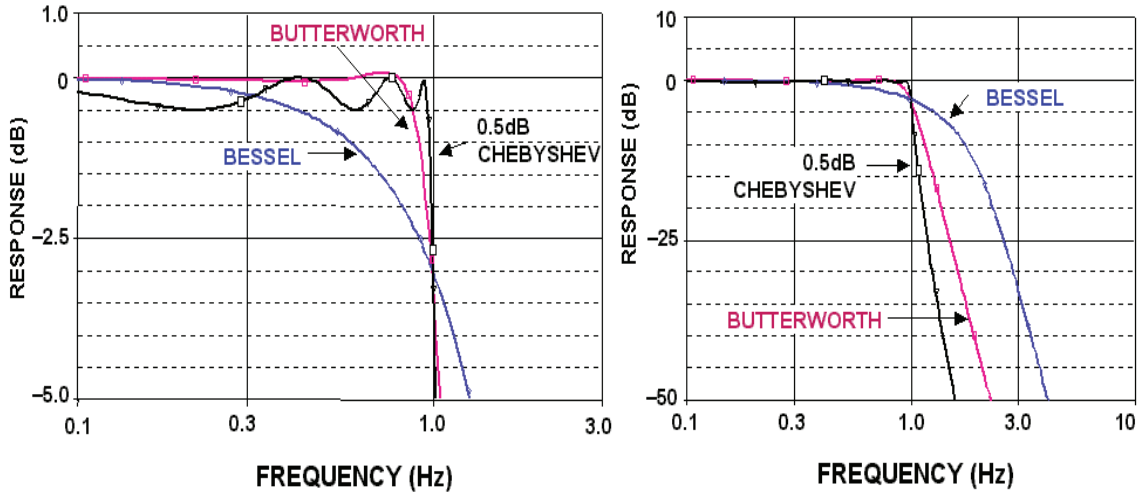


Figure 8.13: Comparison of Amplitude Response of Bessel, Butterworth, and Chebyshev Filters

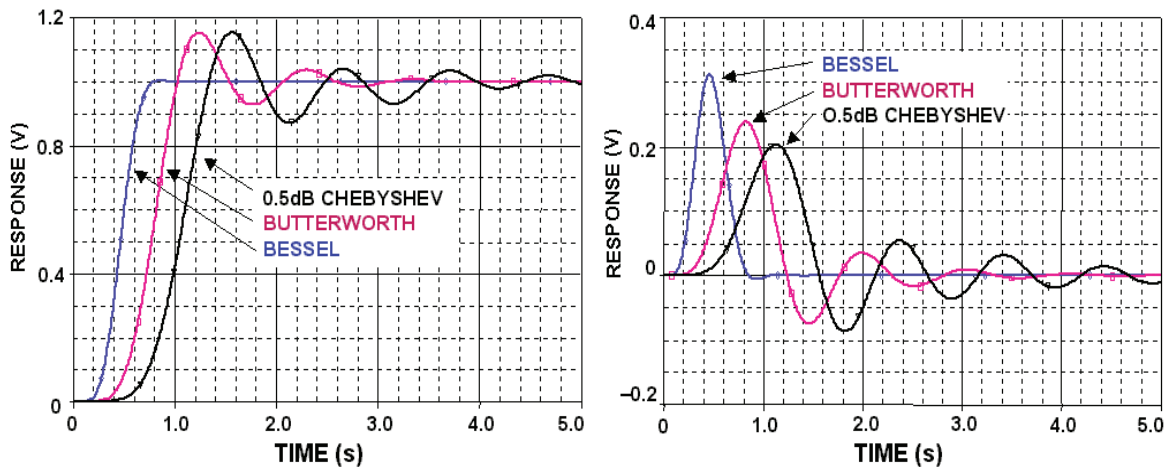


Figure 8.14: Comparison of Step and Impulse Responses of Bessel, Butterworth, and Chebyshev Filters

■ BASIC LINEAR DESIGN

Elliptical

The previously mentioned filters are all-pole designs, which mean that the zeros of the transfer function (roots of the numerator) are at one of the two extremes of the frequency range (0 or ∞). For a low-pass filter, the zeros are at $f = \infty$. If finite frequency transfer function zeros are added to poles an Elliptical filter (sometimes referred to as Cauer filters) is created. This filter has a shorter transition region than the Chebyshev filter because it allows ripple in both the stop band and pass band. It is the addition of zeros in the stop band that causes ripple in the stop band but gives a much higher rate of attenuation, the most possible for a given number of poles. There will be some “bounceback” of the stop band response between the zeros. This is the stop band ripple. The Elliptical filter also has degraded time domain response.

Since the poles of an elliptic filter are on an ellipse, the time response of the filter resembles that of the Chebyshev.

An Elliptic filter is defined by the parameters shown in Figure 8.2, those being A_{\max} , the maximum ripple in the passband, A_{\min} , the minimum attenuation in the stopband, F_c , the cutoff frequency, which is where the frequency response leaves the pass band ripple and F_s , the stopband frequency, where the value of A_{\max} is reached.

An alternate approach is to define a filter order n , the modulation angle, θ , which defines the rate of attenuation in the transition band, where:

$$\theta = \sin^{-1} \frac{1}{F_s} \quad \text{Eq. 8-42}$$

and ρ which determines the pass band ripple, where:

$$\rho = \sqrt{\frac{\epsilon^2}{1 + \epsilon^2}} \quad \text{Eq. 8-43}$$

where ϵ is the ripple factor developed for the Chebyshev response, and the pass band ripple is:

$$R_{dB} = -10 \log (1 - \rho^2) \quad \text{Eq. 8-44}$$

Some general observations can be made. For a given filter order n , and θ , A_{\min} increases as the ripple is made larger. Also, as θ approaches 90° , F_s approaches F_c . This results in extremely short transition region, which means sharp rolloff. This comes at the expense of lower A_{\min} .

As a side note, ρ determines the input resistance of a passive elliptical filter, which can then be related to the VSWR (Voltage Standing Wave Ratio).

Because of the number of variables in the design of an elliptic filter, it is difficult to provide the type of tables provided for the previous filter types. Several CAD (Computer Aided Design) packages can provide the design values. Alternatively several sources,

such as Williams's (see Reference 2), provide tabulated filter values. These tables classify the filter by

$$C \ n \ \rho \ \theta$$

where the C denotes Cauer. Elliptical filters are sometime referred to as Cauer filters after the network theorist Wilhelm Cauer.

Maximally Flat Delay with Chebyshev Stop Band

Bessel type (Bessel, linear phase with equiripple error and transitional) filters give excellent transient behavior, but less than ideal frequency discrimination. Elliptical filters give better frequency discrimination, but degraded transient response. A maximally flat delay with Chebyshev stop band filter takes a Bessel type function and adds transmission zeros. The constant delay properties of the Bessel type filter in the pass band are maintained, and the stop band attenuation is significantly improved. The step response exhibits no overshoot or ringing, and the impulse response is clean, with essentially no oscillatory behavior. Constant group delay properties extend well into the stop band for increasing n.

As with the elliptical filter, numeric evaluation is difficult. Williams's book (see Reference 2) tabulates passive prototypes normalized component values.

Inverse Chebyshev

The Chebyshev response has ripple in the pass band and a monotonic stop band. The inverse Chebyshev response can be defined that has a monotonic pass band and ripple in the stop band. The inverse Chebyshev has better pass band performance than even the Butterworth. It is also better than the Chebyshev, except very near the cutoff frequency. In the transition band, the inverse Chebyshev has the steepest rolloff. Therefore, the inverse Chebyshev will meet the A_{min} specification at the lowest frequency of the three. In the stop band there will, however, be response lobes which have a magnitude of:

$$\frac{\epsilon^2}{(1 - \epsilon)} \quad \text{Eq. 8-45}$$

where ϵ is the ripple factor defined for the Chebyshev case. This means that deep into the stop band, both the Butterworth and Chebyshev will have better attenuation, since they are monotonic in the stop band. In terms of transient performance, the inverse Chebyshev lies midway between the Butterworth and the Chebyshev.

■ BASIC LINEAR DESIGN

The inverse Chebyshev response can be generated in three steps. First take a Chebyshev low pass filter. Then subtract this response from 1. Finally, invert in frequency by replacing ω with $1/\omega$.

These are by no means all the possible transfer functions, but they do represent the most common.

Using the Prototype Response Curves

In the following pages, the response curves and the design tables for several of the low pass prototypes of the all-pole responses will be cataloged. All the curves are normalized to a -3 dB cutoff frequency of 1 Hz. This allows direct comparison of the various responses. In all cases the amplitude response for the 2 through 10 pole cases for the frequency range of 0.1 Hz. to 10 Hz. will be shown. Then a detail of the amplitude response in the 0.1 Hz to 2 Hz. pass band will be shown. The group delay from 0.1 Hz to 10 Hz and the impulse response and step response from 0 seconds to 5 seconds will also be shown.

To use these curves to determine the response of real life filters, they must be denormalized. In the case of the amplitude responses, this is simply accomplished by multiplying the frequency axis by the desired cutoff frequency F_C . To denormalize the group delay curves, we divide the delay axis by $2\pi F_C$, and multiply the frequency axis by F_C , as before. Denormalize the step response by dividing the time axis by $2\pi F_C$. Denormalize the impulse response by dividing the time axis by $2\pi F_C$ and multiplying the amplitude axis by the same amount.

For a high-pass filter, simply invert the frequency axis for the amplitude response. In transforming a low-pass filter into a high-pass (or band-reject) filter, the transient behavior is not preserved. Zverev (see Reference 1) provides a computational method for calculating these responses.

In transforming a lowpass into a narrowband bandpass, the 0Hz axis is moved to the center frequency F_0 . It stands to reason that the response of the bandpass case around the center frequency would then match the lowpass response around 0Hz . The frequency response curve of a lowpass filter actually mirrors itself around 0Hz , although we generally don't concern ourselves with negative frequency.

To denormalize the group delay curve for a bandpass filter, divide the delay axis by πBW , where BW is the 3dB bandwidth in Hz. Then multiply the frequency axis by $\text{BW}/2$. In general, the delay of the bandpass filter at F_0 will be twice the delay of the lowpass prototype with the same bandwidth at 0Hz . This is due to the fact that the lowpass to bandpass transformation results in a filter with order $2n$, even though it is typically referred to it as having the same order as the lowpass filter from which it is derived. This approximation holds for narrow-band filters. As the bandwidth of the filter is increased, some distortion of the curve occurs. The delay becomes less symmetrical, peaking below F_0 .

The envelope of the response of a band-pass filter resembles the step response of the lowpass prototype. More exactly, it is almost identical to the step response of a low-pass filter having half the bandwidth. To determine the envelope response of the band-pass filter, divide the time axis of the step response of the lowpass prototype by πBW , where BW is the 3dB bandwidth. The previous discussions of overshoot, ringing, etc. can now be applied to the carrier envelope.

■ BASIC LINEAR DESIGN

The envelope of the response of a narrow-band band-pass filter to a short burst of carrier (that is where the burst width is much less than the rise time of the denormalized step response of the band-pass filter) can be determined by denormalizing the impulse response of the low-pass prototype. To do this, multiply the amplitude axis and divide the time axis by πBW , where BW is the 3 dB bandwidth. It is assumed that the carrier frequency is high enough so that many cycles occur during the burst interval.

While the group delay, step and impulse curves cannot be used directly to predict the distortion to the waveform caused by the filter, they are a useful figure of merit when used to compare filters.

ANALOG FILTERS
STANDARD RESPONSES

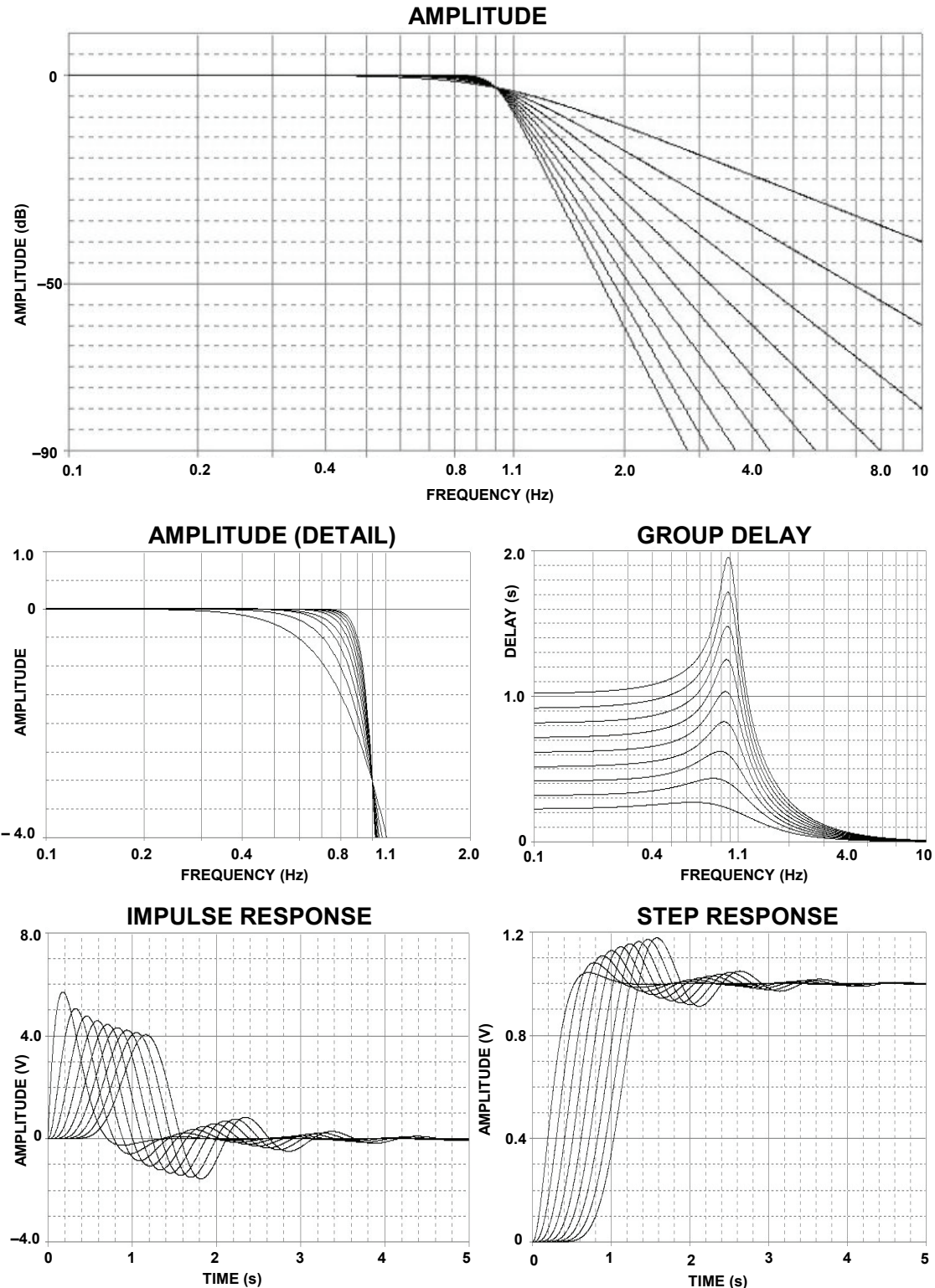


Figure 8.15: Butterworth Response

■ BASIC LINEAR DESIGN

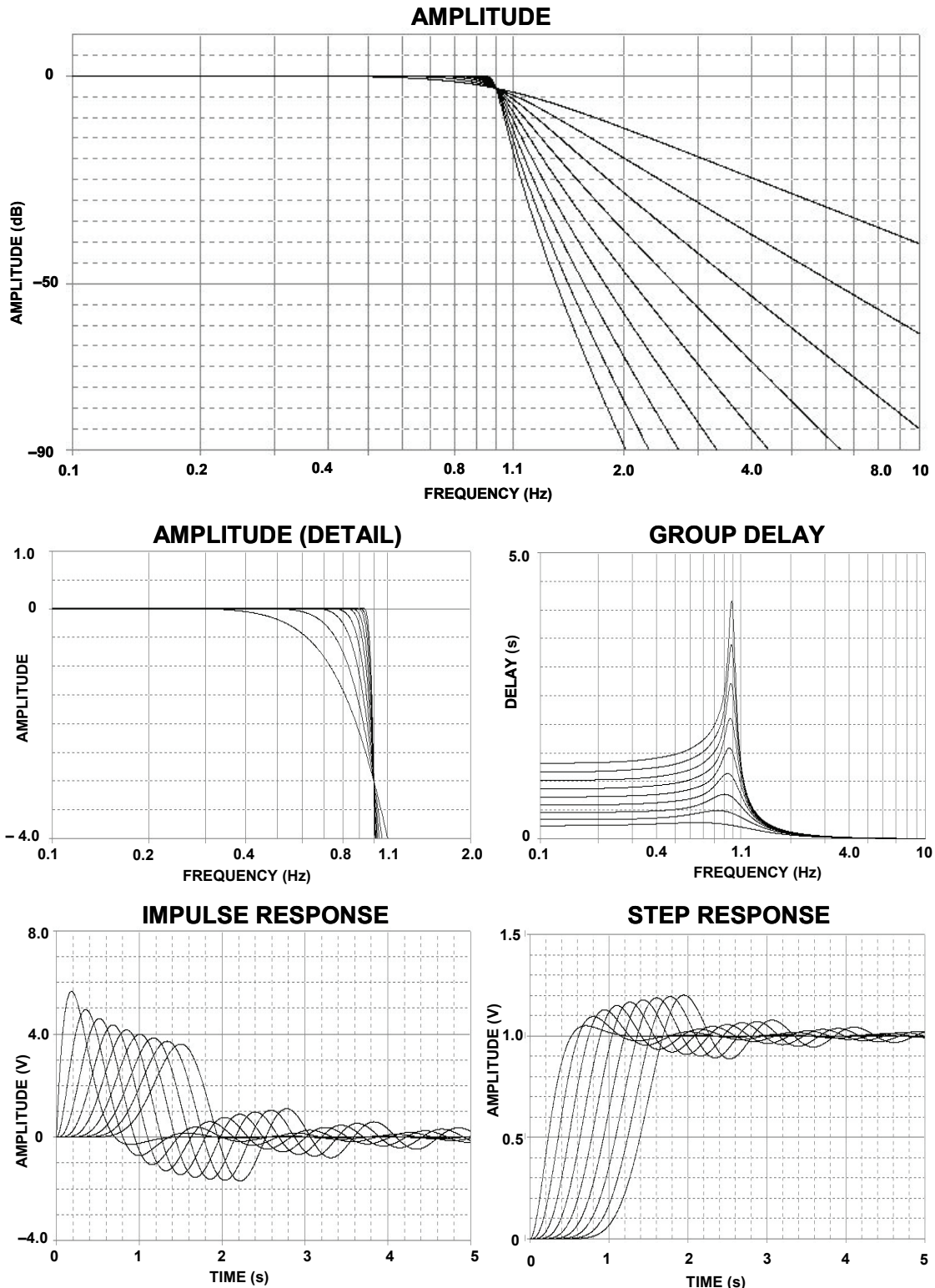


Figure 8.16: 0.01 dB Chebyshev Response

ANALOG FILTERS
STANDARD RESPONSES

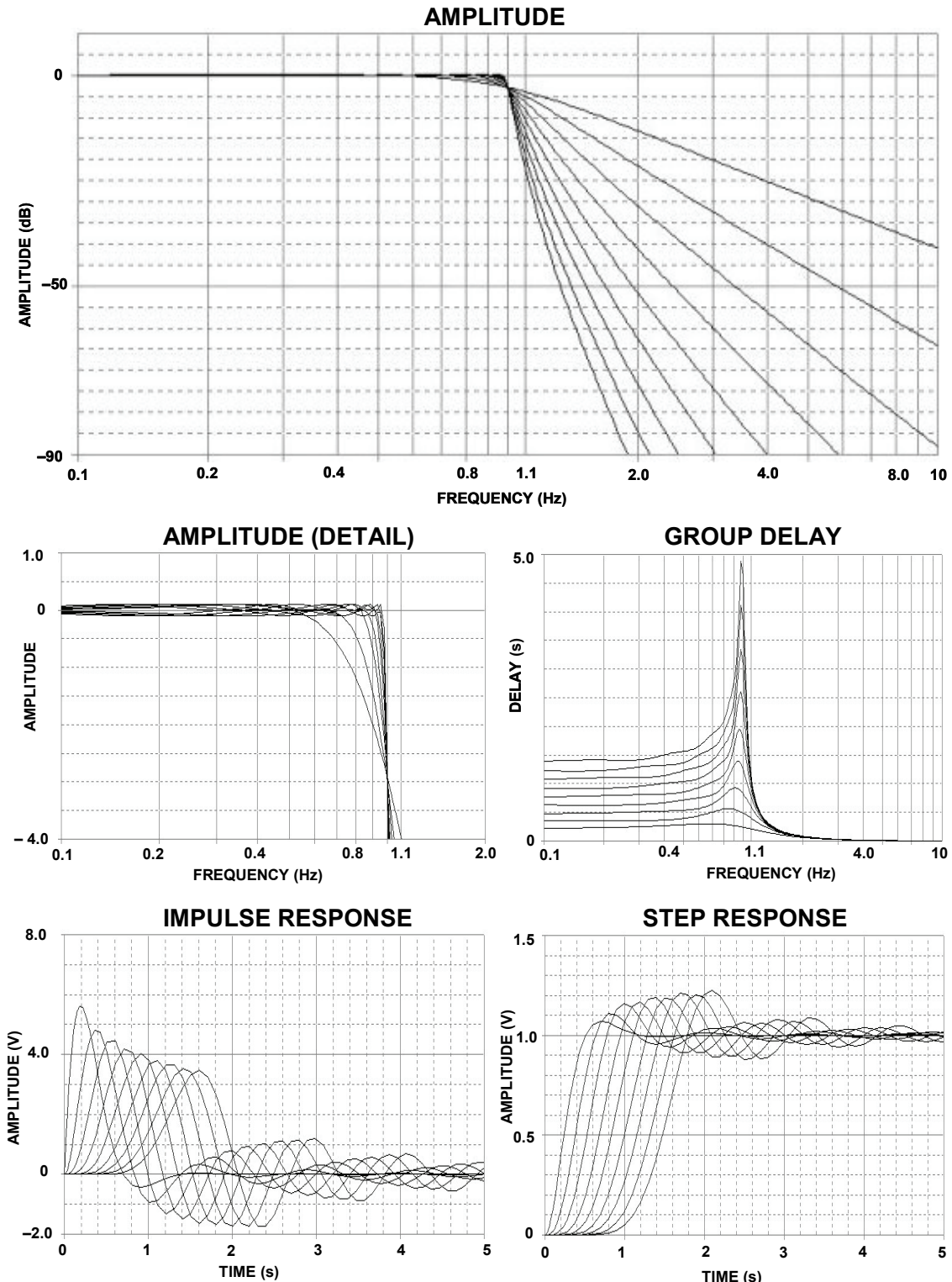


Figure 8.17: 0.1 dB Chebyshev Response

■ BASIC LINEAR DESIGN

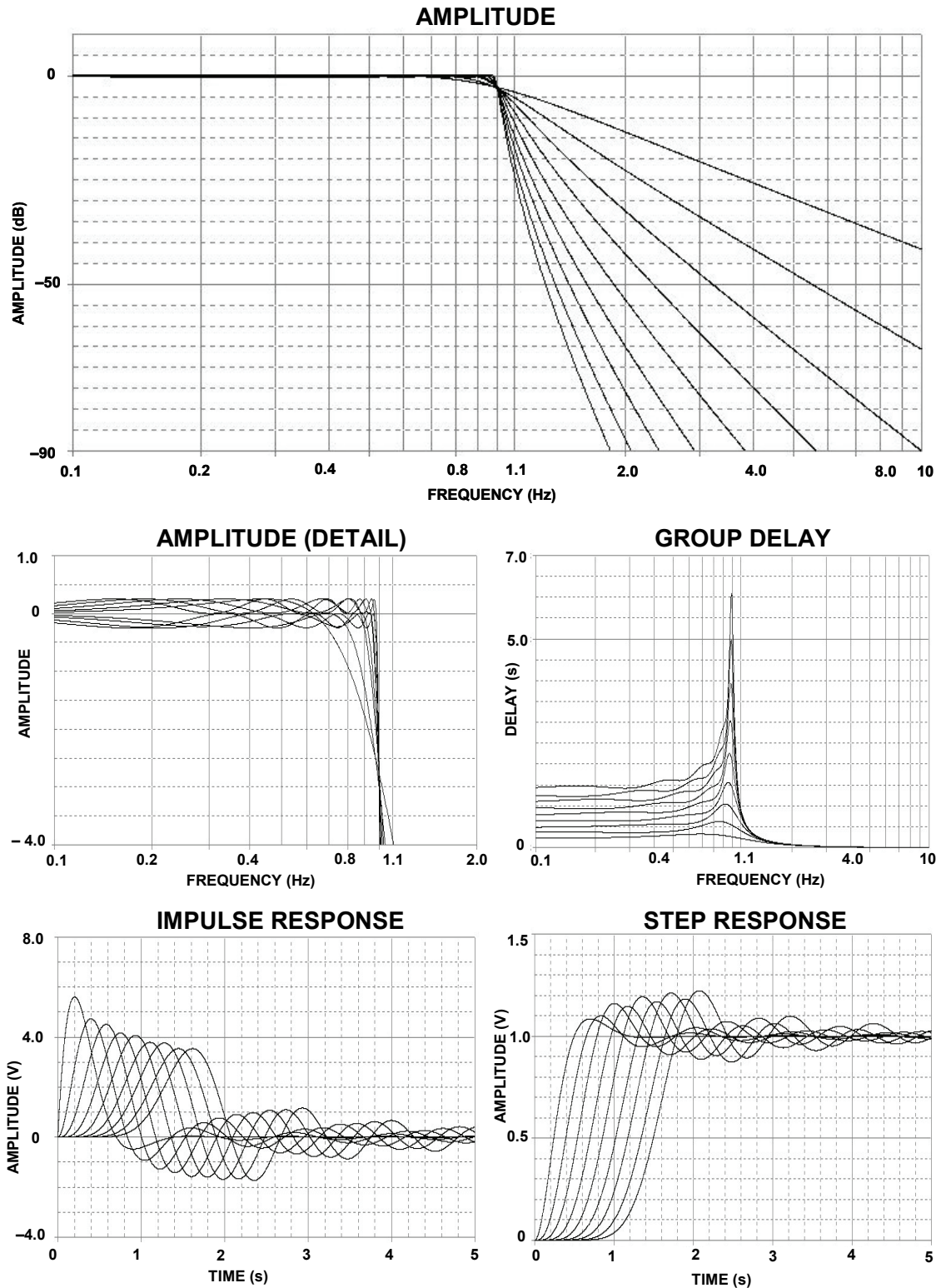


Figure 8.18: 0.25 dB Chebyshev Response

ANALOG FILTERS
STANDARD RESPONSES

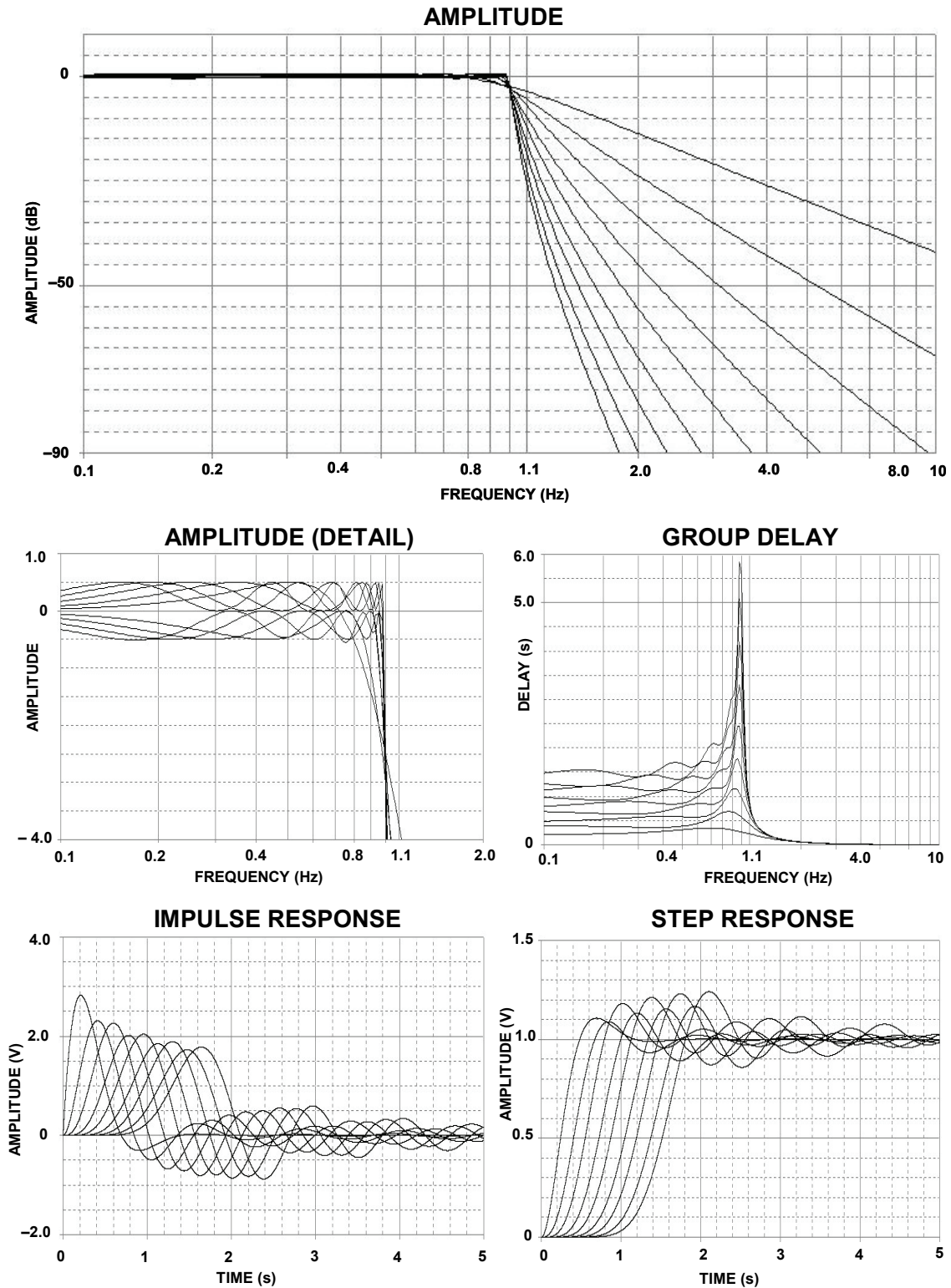


Figure 8.19: 0.5 dB Chebyshev Response

■ BASIC LINEAR DESIGN

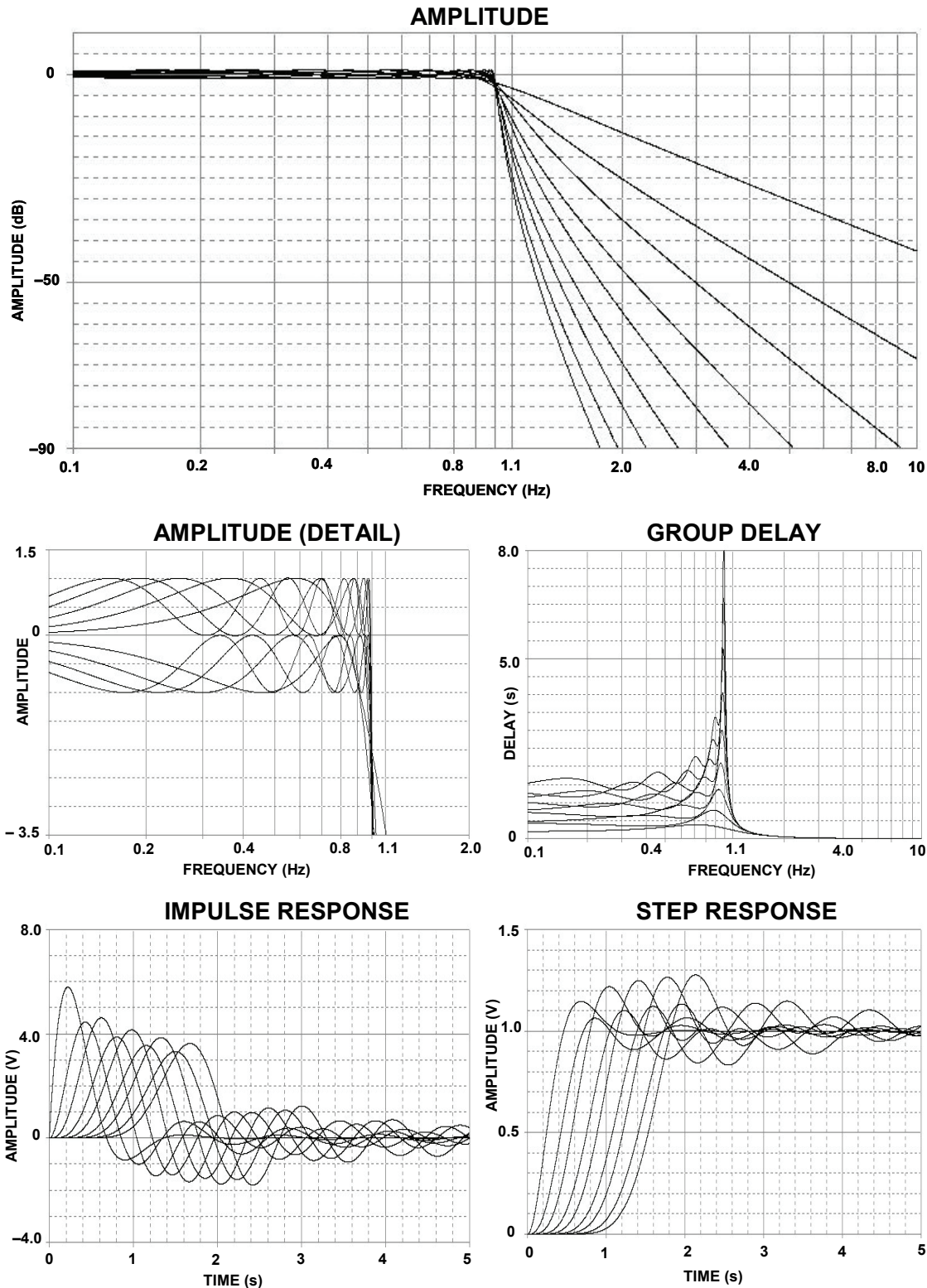


Figure 8.20: 1 dB Chebyshev Response

ANALOG FILTERS
STANDARD RESPONSES

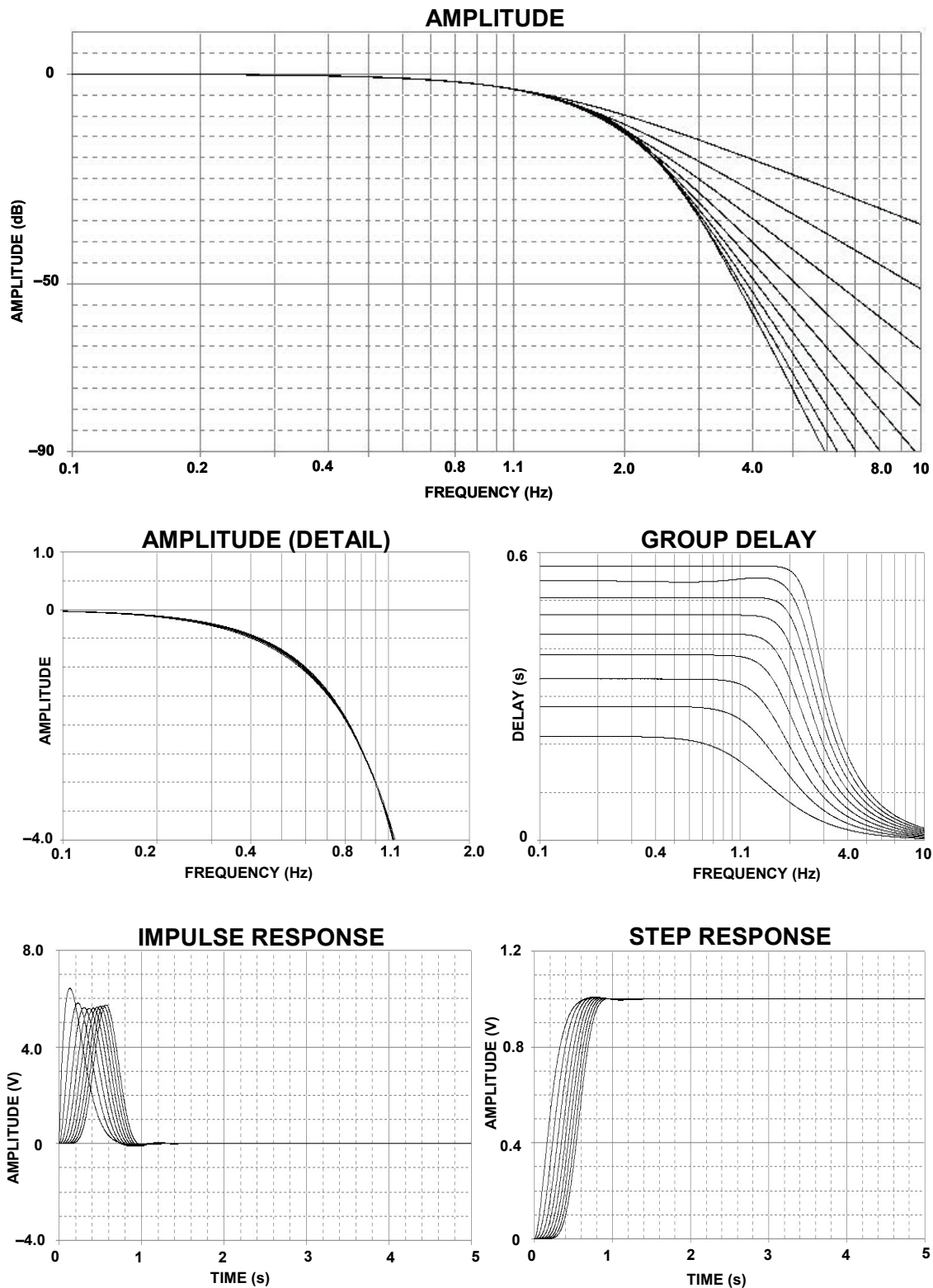


Figure 8.21: Bessel Response

■ BASIC LINEAR DESIGN

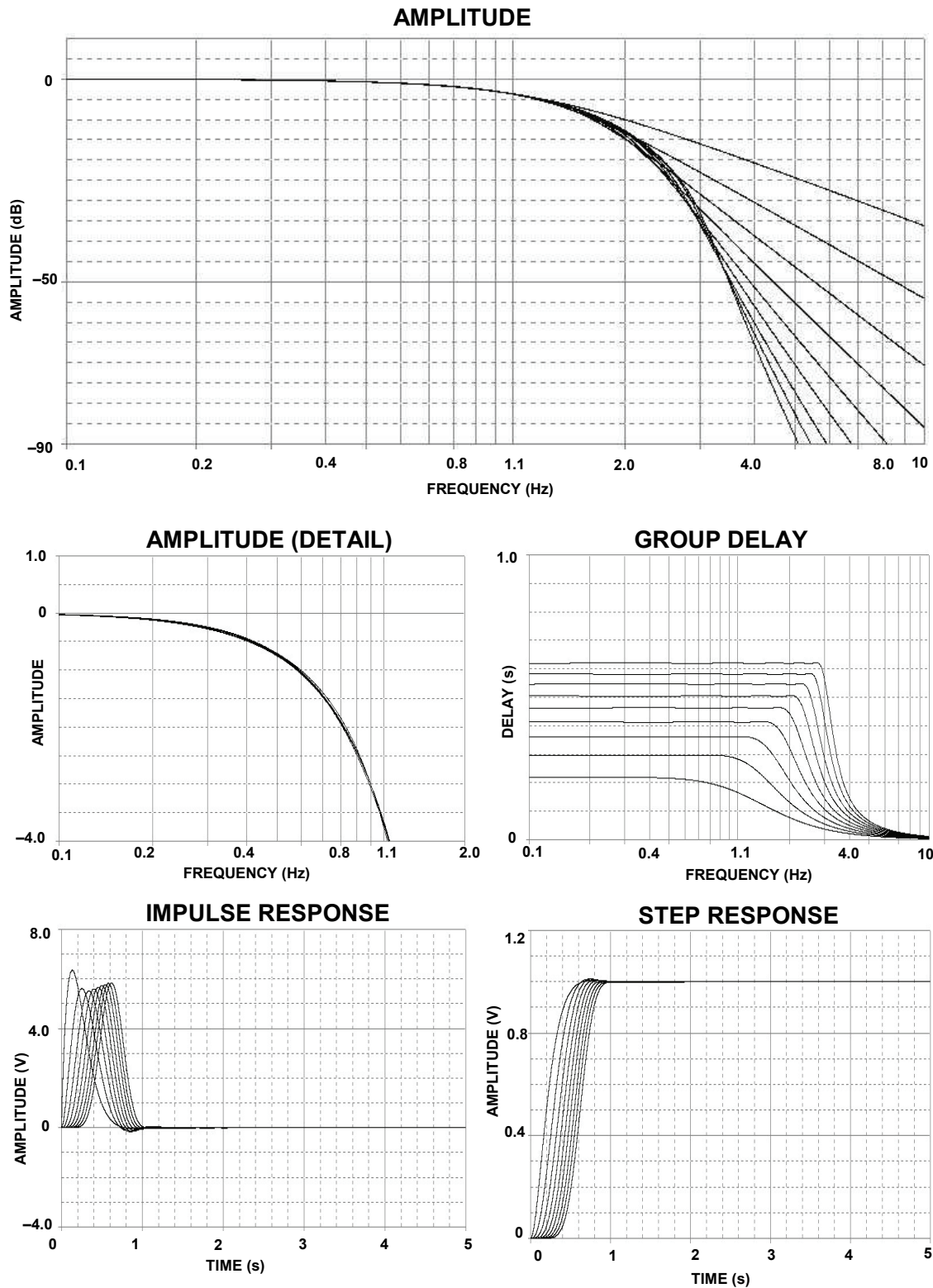


Figure 8.22: Linear Phase Response with Equiripple Error of 0.05°

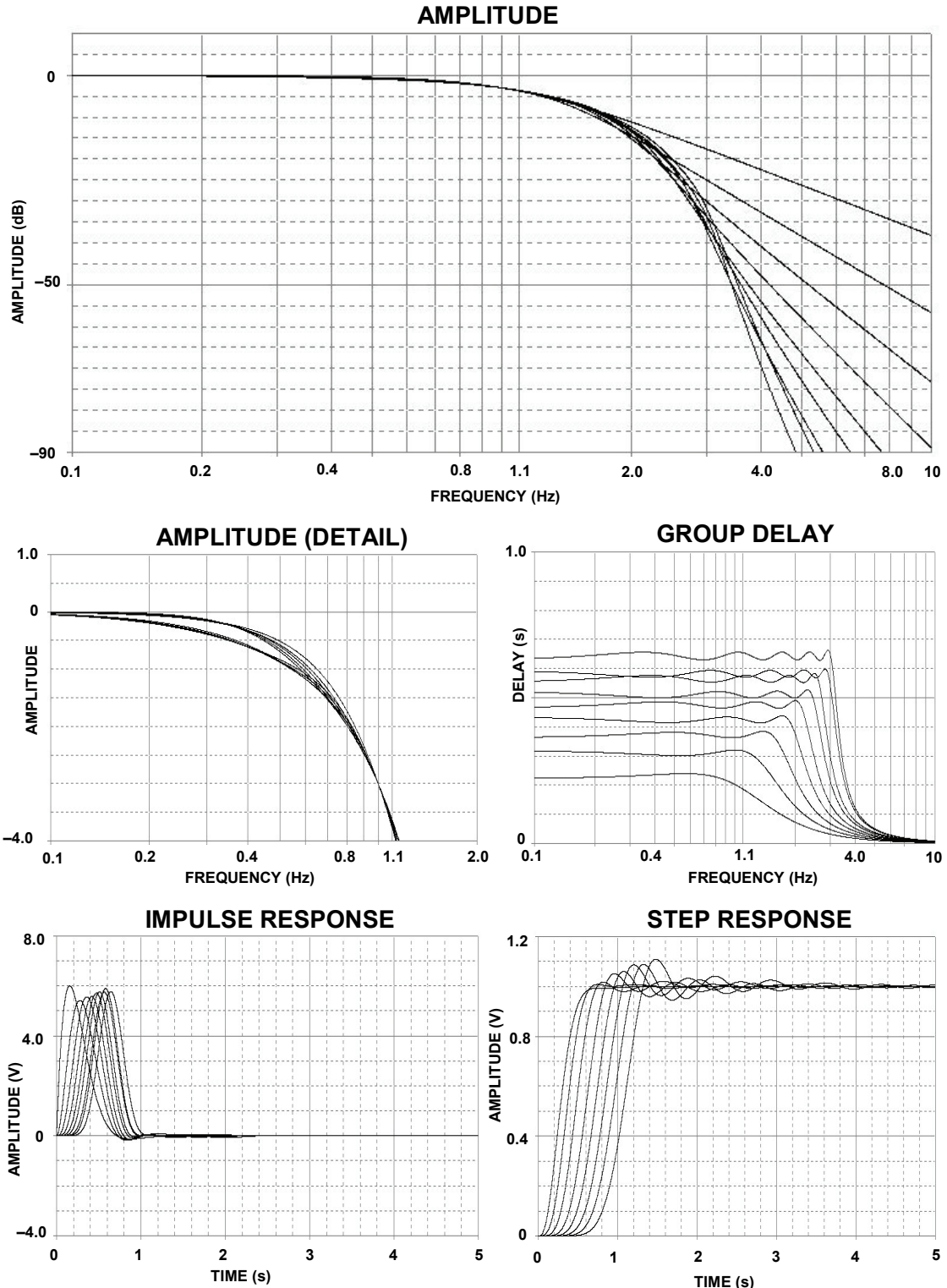


Figure 8.23: Linear Phase Response with Equiripple Error of 0.5°

■ BASIC LINEAR DESIGN

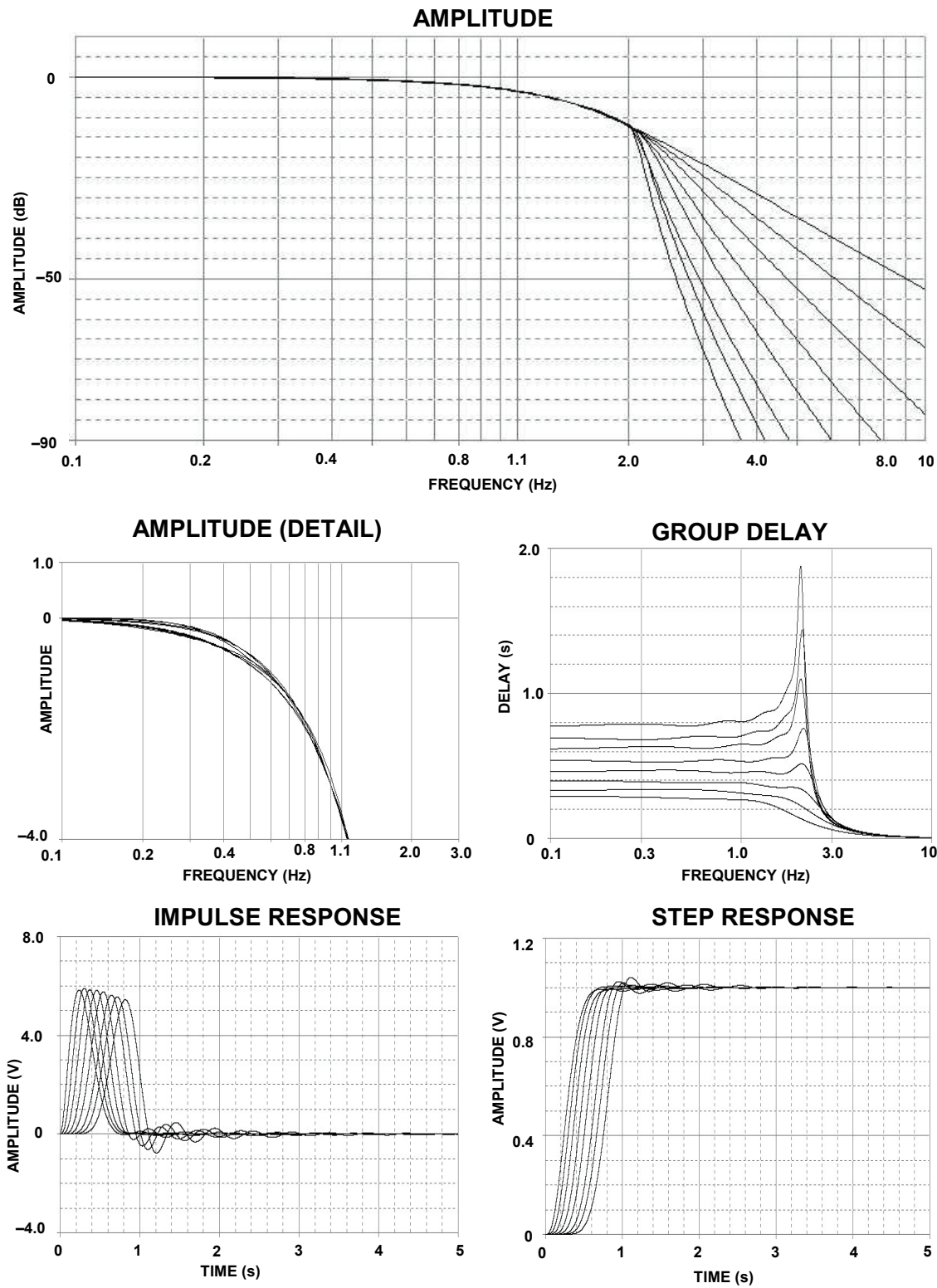


Figure 8.24: Gaussian to 12 dB Response

ANALOG FILTERS
STANDARD RESPONSES

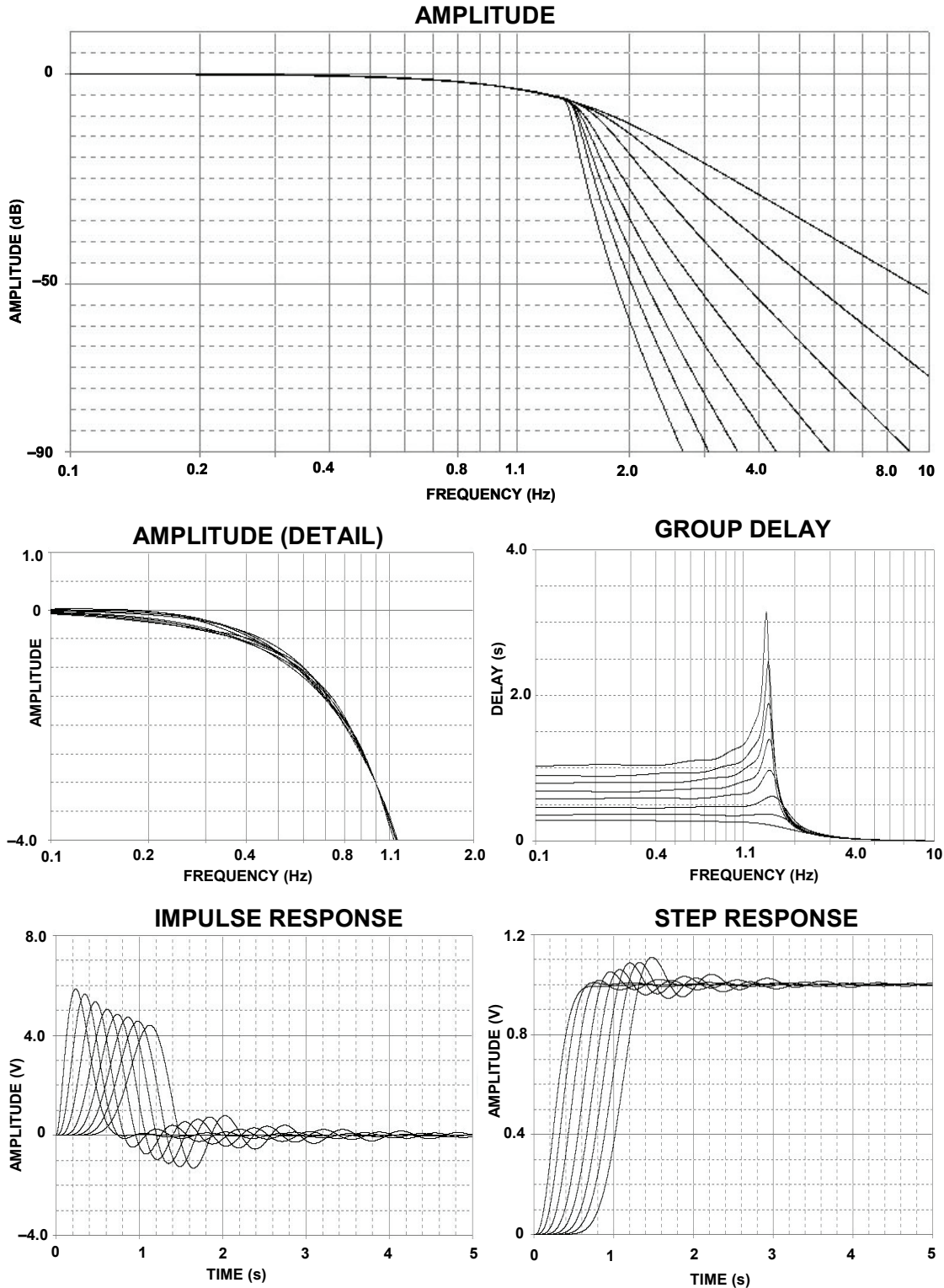


Figure 8.25: Gaussian to 6 dB Response

■ BASIC LINEAR DESIGN

ORDER	SECTION	REAL PART	IMAGINARY PART	F_o	α	Q	-3 dB FREQUENCY	PEAKING FREQUENCY	PEAKING LEVEL
2	1	0.7071	0.7071	1.0000	1.4142	0.7071	1.0000	0.7071	1.2493
3	1	0.5000	0.8660	1.0000	1.0000	1.0000	1.0000	1.0000	
	2	1.0000		1.0000					
4	1	0.9239	0.3827	1.0000	1.8478	0.5412	0.7195	0.8409	3.0102
	2	0.3827	0.9239	1.0000	0.7654	1.3065			
5	1	0.6090	0.5878	1.0000	1.6180	0.6180	0.8588	0.8995	4.6163
	2	0.3090	0.9511	1.0000	0.6180	1.6182			
	3	1.0000		1.0000			1.0000		
6	1	0.9659	0.2688	1.0000	1.9319	0.5176	0.6758		
	2	0.7071	0.7071	1.0000	1.4142	0.7071	1.0000		
	3	0.2588	0.9659	1.0000	0.5176	1.9319		0.9306	6.0210
7	1	0.9010	0.4339	1.0000	1.8019	0.5550	0.7449		
	2	0.6235	0.7818	1.0000	1.2470	0.8019		0.4717	0.2204
	3	0.2225	0.9749	1.0000	0.4450	2.2471		0.9492	7.2530
	4	1.0000		1.0000			1.0000		
8	1	0.9808	0.1951	1.0000	1.9616	0.5098	0.6615		
	2	0.8315	0.5556	1.0000	1.6629	0.6013	0.8295		
	3	0.5556	0.8315	1.0000	1.1112	0.9000		0.6186	0.6876
	4	0.1951	0.9808	1.0000	0.3902	2.5628		0.9612	8.3429
	5	1.0000		1.0000			1.0000		
9	1	0.9397	0.3420	1.0000	1.8794	0.5321	0.7026		
	2	0.7660	0.6428	1.0000	1.5320	0.6527	0.9172		
	3	0.5000	0.8660	1.0000	1.0000	1.0000		0.7071	1.2493
	4	0.1737	0.9848	1.0000	0.3474	2.8785		0.9694	9.3165
	5	1.0000		1.0000			1.0000		
10	1	0.9877	0.1564	1.0000	1.9754	0.5062	0.6549		
	2	0.6910	0.4540	1.0000	1.7820	0.5612	0.7564		
	3	0.7071	0.7071	1.0000	1.4142	0.7071	1.0000		
	4	0.4540	0.8910	1.0000	0.9080	1.1013		0.7667	1.8407
	5	0.1564	0.9877	1.0000	0.3128	3.1970		0.9752	10.2023

Figure 8.26: Butterworth Design Table

ANALOG FILTERS
STANDARD RESPONSES

ORDER	SECTION	REAL PART	IMAGINARY PART	F_0	α	Q	3 dB FREQUENCY	PEAKING FREQUENCY	PEAKING LEVEL
2	1	0.6743	0.7075	0.9774	1.3798	0.7247	0.2142	0.0100	
3	1	0.4233	0.8863	0.9642	0.8780	1.1389	0.7558	2.0595	
4	1	0.6762	0.3828	0.7770	1.7405	0.5746	0.6069	0.8806	5.1110
5	1	0.5120	0.5879	0.7796	1.3135	0.7613	0.2889	0.0827	
5	2	0.1956	0.9512	0.9711	0.4028	2.4824	0.9309	8.0772	
5	3	0.6328		0.6328			0.6328		
6	1	0.5335	0.2668	0.5930	1.7995	0.5557	0.4425	0.5895	1.4482
6	2	0.3906	0.7072	0.8079	0.9670	1.0342			10.7605
6	3	0.1430	0.9660	0.9766	0.2929	3.4144			
7	1	0.4393	0.4339	0.6175	1.4229	0.7028	0.6136	0.7204	3.4077
7	2	0.3040	0.7819	0.8389	0.7247	1.3798			13.1578
7	3	0.1085	0.9750	0.9810	0.2212	4.5208			
7	4	0.4876		0.4876			0.4876		
8	1	0.4268	0.1951	0.4693	1.8190	0.5498	0.3451	0.4564	1.3041
8	2	0.3168	0.5556	0.6396	0.9907	1.0094			5.4126
8	3	0.2418	0.8315	0.8659	0.55685	1.7906			
8	4	0.0849	0.9808	0.9845	0.1725	5.7978			
8	5	0.3923		0.3923			0.3923		
9	1	0.3686	0.3420	0.5028	1.4661	0.6821	0.4844	0.5682	2.3008
9	2	0.3005	0.6428	0.7096	0.8470	1.1807			7.3155
9	3	0.1961	0.8661	0.8880	0.4417	2.2642			
9	4	0.0681	0.9848	0.9872	0.1380	7.2478			
9	5	0.3923		0.3923			0.3923		
10	1	0.3522	0.1564	0.3854	1.8279	0.5471	0.2814	0.3242	0.5412
10	2	0.3178	0.454	0.5542	1.1469	0.8719			3.9742
10	3	0.2522	0.7071	0.7507	0.6719	1.4884			9.0742
10	4	0.1619	0.891	0.9056	0.3576	2.7968			
10	5	0.0558	0.9877	0.9893	0.1128	8.8645			18.9669

Figure 8.27: 0.01 dB Chebyshev Design Table

■ BASIC LINEAR DESIGN

ORDER	SECTION	REAL PART	IMAGINARY PART	F_0	α	Q	-3 dB FREQUENCY	PEAKING FREQUENCY	PEAKING LEVEL
2	1	0.6104	0.7106	0.9368	1.3032	0.7673	0.3638	0.0999	
3	1	0.3490	0.8684	0.9359	0.7458	1.3408	0.7952	3.1978	
	2	0.6970		0.6970			0.6970		
4	1	0.2177	0.9254	0.9507	0.4580	2.1834	0.8994	7.0167	
	2	0.5257	0.3833	0.6506	1.6160	0.6188	0.5596		
5	1	0.3842	0.5884	0.7027	1.0935	0.9145	0.4457	0.7662	
	2	0.1468	0.9521	0.9634	0.3048	3.2812	0.9407	10.4226	
	3	0.4749		0.4749			0.4749		
6	1	0.3916	0.2590	0.4695	1.6682	0.5995	0.3879		
	2	0.2867	0.7077	0.7636	0.7509	1.3316	0.6470	3.1478	
	3	0.1049	0.9667	0.9724	0.2158	4.6348	0.9610	13.3714	
7	1	0.3178	0.4341	0.5380	1.1814	0.8464	0.2957	0.4157	
	2	0.2200	0.7823	0.8126	0.5414	1.8469	0.7507	5.6595	
	3	0.0785	0.9755	0.9787	0.1604	6.2335	0.9723	15.9226	
	4	0.3528		0.3528			0.3528		
8	1	0.3058	0.1952	0.3628	1.6858	0.5932	0.2956		
	2	0.2529	0.5558	0.6106	0.8283	1.2073	0.4949	2.4532	
	3	0.1732	0.8319	0.8497	0.4077	2.4531	0.8137	7.9784	
	4	0.0608	0.9812	0.9831	0.1237	8.0819	0.9793	18.1669	
9	1	0.2622	0.3421	0.4310	1.2166	0.8219	0.2197	0.3037	
	2	0.2137	0.6430	0.6776	0.6308	1.5854	0.6064	4.4576	
	3	0.1395	0.8663	0.8775	0.3180	3.1450	0.8550	10.0636	
	4	0.0485	0.9852	0.9864	0.0982	10.1795	0.9840	20.1650	
	5	0.2790		0.2790			0.2790		
10	1	0.2493	0.1564	0.2943	1.6942	0.5902	0.2382		
	2	0.2249	0.4541	0.5067	0.8876	1.1266	0.3945	1.9880	
	3	0.1785	0.7073	0.7295	0.4894	2.0434	0.6844	6.4750	
	4	0.1146	0.8913	0.8986	0.2551	3.9208	0.8839	11.9386	
	5	0.0395	0.9880	0.9888	0.0799	12.5163	0.9872	21.9565	

Figure 8.28: 0.1 dB Chebyshev Design Table

ORDER	SECTION	REAL PART	IMAGINARY PART	F_0	α	Q	-3 dB FREQUENCY	PEAKING FREQUENCY	PEAKING LEVEL
2	1	0.5621	0.7154	0.9098	1.2356	0.8093	0.4425	0.2502	
3	1	0.3062	0.8712	0.9234	0.6632	1.5079	0.8156	4.0734	
	2	0.6124		0.6124					
4	1	0.4501	0.3840	0.5916	1.5215	0.6572	0.5470	8.2538	
	2	0.1865	0.9272	0.9458	0.3944	2.5556			
5	1	0.3247	0.5892	0.6727	0.9653	1.0359	0.4917	1.4585	
	2	0.1240	0.9533	0.9613	0.2580	3.8763			
	3	0.4013		0.4013					
6	1	0.3284	0.2593	0.4184	1.5697	0.6371	0.3730	4.3121	
	2	0.2404	0.7083	0.7480	0.6428	1.5557			
	3	0.0880	0.9675	0.9715	0.1811	5.5205			
7	1	0.2652	0.4344	0.5090	1.0421	0.9596	0.3441	1.0173	
	2	0.1835	0.7828	0.8040	0.4555	2.1908			
	3	0.0655	0.9761	0.9783	0.1339	7.4679			
	4	0.2944		0.2944					
8	1	0.2543	0.1953	0.3206	1.5862	0.6304	0.2822	3.4258	
	2	0.2156	0.5561	0.5964	0.7230	1.3332			
	3	0.1441	0.8323	0.8447	0.3412	2.9309			
	4	0.0506	0.9817	0.9830	0.1029	9.7713			
9	1	0.2116	0.3423	0.4056	1.0730	0.9520	0.2642	0.8624	
	2	0.1774	0.6433	0.6673	0.5317	1.8808			
	3	0.1158	0.8667	0.8744	0.2649	3.7755			
	4	0.0402	0.9856	0.9864	0.0815	12.2659			
	5	0.2315		0.2315					
10	1	0.2065	0.1565	0.2591	1.5940	0.6274	0.2267	3.0721	
	2	0.1863	0.4543	0.4910	0.7558	1.3178			
	3	0.1478	0.7075	0.7228	0.4090	2.4451			
	4	0.0949	0.8915	0.8965	0.2117	4.7236			
	5	0.0327	0.9883	0.9888	0.0661	15.1199			

Figure 8.29: 0.25 dB Chebyshev Design Table

■ BASIC LINEAR DESIGN

ORDER	SECTION	REAL PART	IMAGINARY PART	F_0	α	Q	-3 dB FREQUENCY	PEAKING FREQUENCY	PEAKING LEVEL
2	1	0.5129	0.7225	1.2314	1.1577	0.8638	0.7072	0.5002	
3	1	0.2683	0.8753	1.0688	0.5861	1.7061	0.9727	5.0301	
	2	0.5366	0.6265				0.6265		
4	1	0.3872	0.3850	0.5969	1.4182	0.7051	0.5951		
	2	0.1605	0.9297	1.0313	0.3402	2.9391	1.0010	9.4918	
5	1	0.2767	0.5902	0.6905	0.8490	1.1779	0.5522	2.2849	
	2	0.1057	0.9550	1.0178	0.2200	4.5451	1.0054	13.2037	
	3	0.3420	0.3623			0.3623			
6	1	0.2784	0.2596	0.3963	1.4627	0.6836	0.3827		
	2	0.2037	0.7091	0.7680	0.5522	1.8109	0.7071	5.5025	
	3	0.0746	0.9687	1.0114	0.1536	6.5119	1.0055	16.2998	
7	1	0.2241	0.4349	0.5040	0.9161	1.0916	0.3839	1.7838	
	2	0.1550	0.7836	0.8228	0.3881	2.5767	0.7912	8.3880	
	3	0.0553	0.9771	1.0081	0.1130	8.8487	1.0049	18.9515	
	4	0.2487	0.2562			0.2562			
8	1	0.2144	0.1955	0.2968	1.4779	0.6767	0.2835		
	2	0.1817	0.5565	0.5989	0.6208	1.6109	0.5381	4.5815	
	3	0.1214	0.8328	0.8610	0.2885	3.4662	0.8429	10.8885	
	4	0.0426	0.9824	1.0060	0.0867	11.5305	1.0044	21.2452	
	5	0.1949	0.1984			0.1984	0.1984		
9	1	0.1831	0.3425	0.3954	0.9429	1.0605	0.2947	1.6023	
	2	0.1493	0.6436	0.6727	0.4520	2.2126	0.6374	7.1258	
	3	0.0974	0.8671	0.8884	0.2233	4.4779	0.8773	13.0759	
	4	0.0338	0.9861	1.0046	0.0686	14.5829	1.0034	23.2820	
	5	0.1949	0.1984			0.1984	0.1984		
	10	1	0.1736	0.1566	0.2338	1.4851	0.6734	0.2221	
10	2	0.1566	0.4545	0.4807	0.6515	1.5349	0.4267	4.2087	
	3	0.1243	0.7078	0.7186	0.3459	2.8907	0.6968	9.3520	
	4	0.0798	0.8919	0.8955	0.1782	5.6107	0.8883	15.0149	
	5	0.0275	0.9887	0.9891	0.0556	17.9833	0.9883	25.1008	

Figure 8.30: 0.5 dB Chebyshev Design Table

ORDER	SECTION	REAL PART	IMAGINARY PART	F_0	α	Q	-3 dB FREQUENCY	PEAKING FREQUENCY	PEAKING LEVEL
2	1	0.4508	0.7351	0.8623	1.0456	0.9564	0.5806	0.9995	
3	1	0.2257	0.8822	0.9106	0.4957	2.0173	0.8538	6.3708	
	2	0.4513		0.4513			0.4513		
4	1	0.3199	0.3868	0.5019	1.2746	0.7845	0.2174	0.1557	
	2	0.1325	0.9339	0.9433	0.2809	3.5594	0.9245	11.1142	
5	1	0.2265	0.5918	0.6337	0.7149	1.3988	0.5467	3.5089	
	2	0.0865	0.9575	0.9614	0.1800	5.5559	0.9536	14.9305	
	3	0.2800		0.2800			0.2800		
6	1	0.2268	0.2601	0.3451	1.3144	0.7608	0.1273	0.0813	
	2	0.1550	0.7106	0.7273	0.4262	2.3462	0.6935	7.6090	
	3	0.0608	0.9707	0.9726	0.1249	8.0036	0.9688	18.0827	
7	1	0.1819	0.4354	0.4719	0.7710	1.2971	0.3956	2.9579	
	2	0.1259	0.7846	0.7946	0.3169	3.1558	0.7744	10.0927	
	3	0.0449	0.9785	0.9795	0.0918	10.8982	0.9775	20.7563	
	4	0.2019		0.2019			0.2019		
8	1	0.1737	0.1956	0.2616	1.3280	0.7530	0.0899	0.0611	
	2	0.1473	0.5571	0.5762	0.5112	1.9560	0.5373	6.1210	
	3	0.0984	0.8337	0.8395	0.2344	4.2657	0.8279	12.6599	
	4	0.0346	0.9836	0.9842	0.0702	14.2391	0.9830	23.0750	
	5	0.1577		0.1577			0.1577		
9	1	0.1482	0.3427	0.3734	0.7938	1.2597	0.3090	2.7498	
	2	0.1208	0.6442	0.6554	0.3686	2.7129	0.6328	8.8187	
	3	0.0788	0.8679	0.8715	0.1809	5.5268	0.8643	14.8852	
	4	0.0274	0.9869	0.9873	0.0555	18.0226	0.9885	25.1197	
	5	0.1577		0.1577			0.1577		
10	1	0.1403	0.1567	0.2103	1.3341	0.7496	0.0698	0.0530	
	2	0.1266	0.4548	0.4721	0.5363	1.8645	0.4368	5.7354	
	3	0.1005	0.7084	0.7155	0.2809	3.5597	0.7012	11.1147	
	4	0.0645	0.8926	0.8949	0.1441	6.9374	0.8903	16.8466	
	5	0.0222	0.9895	0.9897	0.0449	22.2916	0.9893	26.9650	

Figure 8.31: 1 dB Chebyshev Design Table

■ BASIC LINEAR DESIGN

ORDER	SECTION	REAL PART	IMAGINARY PART	F_0	α	Q	-3 dB FREQUENCY	PEAKING FREQUENCY	PEAKING LEVEL
2	1	1.1050	0.6368	1.2754	1.7328	0.5771	1.0020		
3	1	1.0509	1.0025	1.4524	1.4471	0.6910	1.4185		
	2	1.3270		1.3270			1.3270		
4	1	1.3596	0.4071	1.4192	1.9160	0.5219	0.9705		
	2	0.9877	1.2476	1.5912	1.2414	0.8055		0.7622	0.2349
5	1	1.3851	0.7201	1.5611	1.7745	0.5635	1.1876		
	2	0.9606	1.4756	1.7607	1.0911	0.9165		1.1201	0.7768
	3	1.5069		1.5069			1.5069		
6	1	1.5735	0.3213	1.6060	1.9596	0.5103	1.0638		
	2	1.3836	0.9727	1.6913	1.6361	0.6112		1.4323	
	3	0.9318	1.6640	1.9071	0.9772	1.0234			1.3786
7	1	1.6130	0.5896	1.7174	1.8784	0.5324	1.2074		
	2	1.3797	1.1923	1.8235	1.5132	0.6608		1.6964	
	3	0.9104	1.8375	2.0507	0.8879	1.1262			1.5961
	4	1.6853		1.6853			1.6853		1.3851
8	1	1.7627	0.2737	1.7838	1.9763	0.5060	1.1675		
	2	0.8955	2.0044	2.1953	0.8158	1.2258		1.7932	2.5585
	3	1.3780	1.3926	1.9591	1.4067	0.7109		0.2011	0.0005
	4	1.6419	0.8256	1.8378	1.7868	0.5597	1.3849		
9	1	1.8081	0.5126	1.8794	1.9242	0.5197	1.2774		
	2	1.6532	1.0319	1.9488	1.6966	0.5894		1.5747	
	3	1.3683	1.5685	2.0815	1.3148	0.7606			0.0807
	4	0.8788	2.1509	2.3235	0.7564	1.3220			1.9632
	5	1.8575		1.8575			1.8575		3.0949
10	1	1.9335	0.2451	1.9490	1.9841	0.5040	1.2685		
	2	1.8467	0.7335	1.9870	1.8587	0.5380		1.4177	
	3	1.6661	1.2246	2.0678	1.6115	0.6205		1.7848	
	4	1.3648	1.7395	2.2110	1.2346	0.8100			1.0785
	5	0.8686	2.2994	2.4580	0.7067	1.4150			2.1291
									3.5944

Figure 8.32: Bessel Design Table

ORDER	SECTION	REAL PART	IMAGINARY PART	F_o	α	Q	-3 dB FREQUENCY	PEAKING FREQUENCY	PEAKING LEVEL
2	1	1.0087	0.66680	1.2098	1.6675	0.5997	0.9999		
3	1	0.8541	1.0725	1.3710	1.2459	0.8026		0.6487	0.2232
	2	1.0459		1.0459			1.0459		
4	1	0.9648	0.4748	1.0753	1.7945	0.5573		0.8056	
	2	0.7448	1.4008	1.5885	0.9389	1.0650			1.1864
5	1	0.8915	0.8733	1.2480	1.4287	0.6999		1.2351	1.6286
	2	0.6731	1.7085	1.8363	0.7331	1.3641			1.5703
	3	0.9430		0.9430			0.9430		3.3234
6	1	0.8904	0.4111	0.9807	1.8158	0.5507		0.7229	
	2	0.8233	1.2179	1.4701	1.1201	0.8928		0.8975	0.6495
	3	0.6152	1.9810	2.0743	0.5932	1.6859		1.8831	4.9365
7	1	0.8425	0.7791	1.1475	1.4684	0.6810		1.1036	
	2	0.7708	1.5351	1.7177	0.8975	1.1143			1.3276
	3	0.5727	2.2456	2.3175	0.4942	2.0233			2.1713
	4	0.8615		0.8615			0.8615		6.3948
8	1	0.8195	0.3711	0.8996	1.8219	0.5489		0.6600	
	2	0.7030	1.1054	1.3604	1.1658	0.8578		0.7701	0.4705
	3	0.7213	1.8134	1.9516	0.7392	1.3528		1.6638	3.2627
	4	0.5341	2.4761	2.5330	0.4217	2.3713		2.4178	7.6973
	5	0.7983		0.7983			0.7983		
9	1	0.7853	0.7125	1.0604	1.4812	0.6751		1.0102	
	2	0.7555	1.4127	1.6020	0.9432	1.0602			1.1937
	3	0.6849	2.0854	2.1950	0.6241	1.6024		1.9697	4.5404
	4	0.5060	2.7133	2.7601	0.3667	2.7274		2.6657	8.8633
	5								
10	1	0.7592	0.3413	0.8324	1.8241	0.5482		0.6096	
	2	0.7467	1.0195	1.2637	1.1818	0.8462		0.6941	0.4145
	3	0.7159	1.6836	1.8295	0.7826	1.2778		1.5238	2.8507
	4	0.6415	2.3198	2.4085	0.5377	1.8598		2.2276	5.7152
	5	0.4777	2.9128	2.9517	0.3237	3.0895		2.8734	9.9130

Figure 8.33: Linear Phase with Equiripple Error of 0.05° Design Table

■ BASIC LINEAR DESIGN

ORDER	SECTION	REAL PART	IMAGINARY PART	F_0	α	Q	-3 dB FREQUENCY	PEAKING FREQUENCY	PEAKING LEVEL
2	1	0.8590	0.6981	1.1069	1.5521	0.6443	1.0000		
3	1	0.6969	1.1318	1.3292	1.0486	0.9536	0.8918	0.9836	
	2	0.8257		0.8257			0.8257		
4	1	0.7448	0.5133	0.9045	1.6468	0.6072	0.7597		
	2	0.6037	1.4983	1.6154	0.7475	1.3379	1.3713	3.1817	
5	1	0.6775	0.9401	1.1588	1.1693	0.8552	0.6518	0.4579	
	2	0.5412	1.8256	1.9041	0.5684	1.7592	1.7435	5.2120	
	3	0.7056		0.7056			0.7056		
6	1	0.6519	0.4374	0.7850	1.6608	0.6021	0.6522		
	2	0.6167	1.2963	1.4355	0.8592	1.1639	2.2016	1.1402	2.2042
	3	0.4893	2.0982	2.1545	0.4542		2.0404	7.0848	
7	1	0.6190	0.8338	1.0385	1.1922	0.8388	0.5586	0.3798	
	2	0.5816	1.6455	1.7453	0.6665	1.5004	1.5393	4.0353	
	3	0.4598	2.3994	2.4431	0.3764	2.6567	2.3549	8.6433	
	4	0.6283		0.6283			0.6283		
8	1	0.5791	0.3857	0.6958	1.6646	0.6007	0.5764		
	2	0.5665	1.1505	1.2824	0.8835	1.1319	1.0014	2.0187	
	3	0.5303	1.8914	1.9643	0.5399	1.8521	1.8155	5.6819	
	4	0.4148	2.5780	2.6112	0.3177	3.1475	2.5444	10.0703	
9	1	0.5688	0.7595	0.9489	1.1989	0.8341	0.5033	0.3581	
	2	0.5545	1.5099	1.6076	0.6899	1.4496	1.4033	3.7748	
	3	0.5179	2.2329	2.2922	0.4519	2.2130	2.1720	7.1270	
	4	0.4080	2.9028	2.9313	0.2784	3.5923	2.8740	11.1925	
	5	0.5728		0.5728			0.5728		
10	1	0.5249	0.3487	0.6302	1.6659	0.6003	0.5215		
	2	0.5193	1.0429	1.1650	0.8915	1.1217	0.9044	1.9598	
	3	0.5051	1.7264	1.7988	0.5616	1.7806	1.6509	5.3661	
	4	0.4711	2.3850	2.4311	0.3876	2.5802	2.3380	8.3994	
	5	0.3708	2.9940	3.0169	0.2458	4.0681	2.9709	12.2539	

Figure 8.34: Linear Phase with Equiripple Error of 0.5° Design Table

ORDER	SECTION	REAL PART	IMAGINARY PART	F_0	α	Q	-3 dB FREQUENCY	PEAKING FREQUENCY	PEAKING LEVEL
3	1	0.9360	1.2168	1.5352	1.2194	0.8201	0.9360	0.7775	0.2956
	2	0.9360		0.9360					
4	1	0.9278	1.6995	1.9363	0.9583	1.0435	1.4239	1.5025	
	2	0.9192	0.5560	1.0743	1.7113	0.5844			
5	1	0.8075	0.9973	1.2832	1.2585	0.7946	0.5853	0.4921	
	2	0.7153	0.2053	0.7442	1.9224	0.5202			
	3	0.8131		0.8131					
6	1	0.7019	0.4322	0.8243	1.7030	0.5872	0.6627	1.1080	1.7809
	2	0.6667	1.2931	1.4549	0.9165	1.0911			
	3	0.4479	2.1363	2.1827	0.4104	2.4366			
7	1	0.6155	0.7703	0.9860	1.2485	0.8010	0.4632	0.2168	
	2	0.5486	1.5154	1.6116	0.6808	1.4689			
	3	0.2905	2.1486	2.1681	0.2680	3.7318			
	4	0.6291		0.6291					
8	1	0.5441	0.3358	0.6394	1.7020	0.5876	0.5145	0.8512	1.7432
	2	0.5175	0.9962	1.1226	0.9220	1.0846			
	3	0.4328	1.6100	1.6672	0.5192	1.9260			
	4	0.1978	2.0703	2.0797	0.1902	5.2571			
9	1	0.4961	0.6192	0.7934	1.2505	0.7997	0.3705	0.2116	
	2	0.4568	1.2145	1.2976	0.7041	1.4203			
	3	0.3592	1.7429	1.7795	0.4037	2.4771			
	4	0.1489	2.1003	2.1056	0.1414	7.0704			
	5	0.5065		0.5065					
10	1	0.4535	0.2794	0.5327	1.7028	0.5873	0.4283	0.7055	1.6904
	2	0.4352	0.8289	0.9362	0.9297	1.0756			
	3	0.3886	1.3448	1.3998	0.5552	1.8011			
	4	0.2908	1.7837	1.8072	0.3218	3.1074			
	5	0.1136	2.0599	2.0630	0.1101	9.0802			

Figure 8.35: Gaussian to 12 dB Design Table

■ BASIC LINEAR DESIGN

ORDER	SECTION	REAL PART	IMAGINARY PART	F_0	α	Q	-3 dB FREQUENCY	PEAKING FREQUENCY	PEAKING LEVEL
3	1	0.9622	1.2214	1.5549	1.2377	0.8080	0.7523	0.2448	
	2	0.9776	0.5029	1.0994	1.7785	0.5623			
4	1	0.7940	0.5029	0.9399	1.6896	0.5919	0.7636	1.4058	3.0859
	2	0.6304	1.5407	1.6647	0.7574	1.3203			
5	1	0.6190	0.8254	1.0317	1.1999	0.8334	0.5460	0.3548	
	2	0.3559	1.5688	1.6087	0.4425	2.2600			
	3	0.6650		0.6650		0.6650			
6	1	0.5433	0.3431	0.6426	1.6910	0.5914	0.5215	0.8831	2.2992
	2	0.4672	0.9991	1.1029	0.8472	1.1804			
	3	0.2204	1.5067	1.5227	0.2895	3.4545			
7	1	0.4580	0.5932	0.7494	1.2223	0.8182	0.3770	0.2874	
	2	0.3649	1.1286	1.1861	0.6153	1.6253			
	3	0.1522	1.4938	1.5015	0.2027	4.9328			
	4	0.4828		0.4828		0.4828			
	5								
8	1	0.4222	0.2640	0.4979	1.6958	0.5897	0.4026	0.6697	1.9722
	2	0.3833	0.7716	0.8616	0.8898	1.1239			
	3	0.2678	1.2066	1.2360	0.4333	2.3076			
	4	0.1122	1.4798	1.4840	0.1512	6.6134			
	5								
9	1	0.3700	0.4704	0.5685	1.2365	0.8088	0.2905	0.8473	3.9831
	2	0.3230	0.9068	0.9626	0.6711	1.4901			
	3	0.2309	1.2634	1.2843	0.3596	2.7811			
	4	0.0860	1.4740	1.4765	0.1165	8.5804			
	5	0.3842		0.3842		0.3842			
10	1	0.3384	0.2101	0.3983	1.6991	0.5885	0.3212	0.5309	1.8164
	2	0.3164	0.6180	0.6943	0.9114	1.0972			
	3	0.2677	0.9852	1.0209	0.5244	1.9068			
	4	0.1849	1.2745	1.2878	0.2871	3.4825			
	5	0.0671	1.4389	1.4405	0.0931	10.7401			

Figure 8.36: Gaussian to 6 dB Design Table

**ANALOG FILTERS
STANDARD RESPONSES**

Notes:

▣ BASIC LINEAR DESIGN

Notes:

SECTION 8.5: FREQUENCY TRANSFORMATIONS

Until now, only filters using the low-pass configuration have been examined. In this section, transforming the low-pass prototype into the other configurations: high-pass, band-pass, band-reject (notch) and all-pass will be discussed.

Low-Pass to High-Pass

The low-pass prototype is converted to high-pass filter by scaling by 1/s in the transfer function. In practice, this amounts to capacitors becoming inductors with a value 1/C, and inductors becoming capacitors with a value of 1/L for passive designs. For active designs, resistors become capacitors with a value of 1/R, and capacitors become resistors with a value of 1/C. This applies only to frequency setting resistor, not those only used to set gain.

Another way to look at the transformation is to investigate the transformation in the s plane. The complex pole pairs of the low-pass prototype are made up of a real part, α , and an imaginary part, β . The normalized high-pass poles are given by:

$$\alpha_{HP} = \frac{\alpha}{\alpha^2 + \beta^2} \quad \text{Eq. 8-46}$$

and:

$$\beta_{HP} = \frac{\beta}{\alpha^2 + \beta^2} \quad \text{Eq. 8-47}$$

A simple pole, α_0 , is transformed to:

$$\alpha_{\omega,HP} = \frac{1}{\alpha_0} \quad \text{Eq. 8-48}$$

Low-pass zeros, $\omega_{Z,LP}$, are transformed by:

$$\omega_{Z,HP} = \frac{1}{\omega_{Z,LP}} \quad \text{Eq. 8-49}$$

In addition, a number of zeros equal to the number of poles are added at the origin.

After the normalized low-pass prototype poles and zeros are converted to high-pass, they are then denormalized in the same way as the low-pass, that is, by frequency and impedance.

As an example a 3 pole 1 dB Chebyshev low-pass filter will be converted to a high-pass filter.

■ BASIC LINEAR DESIGN

From the design tables of the last section:

$$\begin{aligned}\alpha_{LP1} &= .2257 \\ \beta_{LP1} &= .8822 \\ \alpha_{LP2} &= .4513\end{aligned}$$

This will transform to:

$$\begin{aligned}\alpha_{HP1} &= .2722 \\ \beta_{HP1} &= 1.0639 \\ \alpha_{HP2} &= 2.2158\end{aligned}$$

Which then becomes:

$$\begin{aligned}F_{01} &= 1.0982 \\ \alpha &= .4958 \\ Q &= 2.0173\end{aligned}$$

$$F_{02} = 2.2158$$

A worked out example of this transformation will appear in a latter section.

A high-pass filter can be considered to be a low-pass filter turned on its side. Instead of a flat response at dc, there is a rising response of $n \times (20 \text{ dB/decade})$, due to the zeros at the origin, where n is the number of poles. At the corner frequency a response of $n \times (-20 \text{ dB/decade})$ due to the poles is added to the above rising response. This results in a flat response beyond the corner frequency.

Low-Pass to Band-Pass

Transformation to the band-pass response is a little more complicated. Band-pass filters can be classified as either wideband or narrow-band, depending on the separation of the poles. If the corner frequencies of the band-pass are widely separated (by more than 2 octaves), the filter is wideband and is made up of separate low-pass and high-pass sections, which will be cascaded. The assumption made is that with the widely separated poles, interaction between them is minimal. This condition does not hold in the case of a narrowband band-pass filter, where the separation is less than 2 octaves. We will be covering the narrow-band case in this discussion.

As in the highpass transformation, start with the complex pole pairs of the low-pass prototype, α and β . The pole pairs are known to be complex conjugates. This implies symmetry around dc (0 Hz.). The process of transformation to the band-pass case is one of mirroring the response around dc of the low-pass prototype to the same response around the new center frequency F_0 .

This clearly implies that the number of poles and zeros is doubled when the band-pass transformation is done. As in the low-pass case, the poles and zeros below the real axis are ignored. So an n^{th} order low-pass prototype transforms into an n^{th} order band-pass,

ANALOG FILTERS
FREQUENCY TRANSFORMATIONS

even though the filter order will be $2n$. An n^{th} order band-pass filter will consist of n sections, versus $n/2$ sections for the low-pass prototype. It may be convenient to think of the response as n poles up and n poles down.

The value of Q_{BP} is determined by:

$$Q_{\text{BP}} = \frac{F_0}{\text{BW}} \quad \text{Eq. 8-50}$$

where BW is the bandwidth at some level, typically -3 dB.

A transformation algorithm was defined by Geffe (Reference 16) for converting low-pass poles into equivalent band-pass poles.

Given the pole locations of the low-pass prototype:

$$-\alpha \pm j\beta \quad \text{Eq. 8-51}$$

and the values of F_0 and Q_{BP} , the following calculations will result in two sets of values for Q and frequencies, F_H and F_L , which define a pair of band-pass filter sections.

$$C = \alpha^2 + \beta^2 \quad \text{Eq. 8-52}$$

$$D = \frac{2\alpha}{Q_{\text{BP}}} \quad \text{Eq. 8-53}$$

$$E = \frac{C}{Q_{\text{BP}}^2} + 4 \quad \text{Eq. 8-54}$$

$$G = \sqrt{E^2 - 4 D^2} \quad \text{Eq. 8-55}$$

$$Q = \sqrt{\frac{E + G}{2 D^2}} \quad \text{Eq. 8-56}$$

Observe that the Q of each section will be the same.

The pole frequencies are determined by:

$$M = \frac{\alpha Q}{Q_{\text{BP}}} \quad \text{Eq. 8-57}$$

$$W = M + \sqrt{M^2 - 1} \quad \text{Eq. 8-58}$$

$$F_{\text{BP}1} = \frac{F_0}{W} \quad \text{Eq. 8-59}$$

$$F_{\text{BP}2} = W F_0 \quad \text{Eq. 8-60}$$

Each pole pair transformation will also result in 2 zeros that will be located at the origin.

A normalized low-pass real pole with a magnitude of α_0 is transformed into a band-pass section where:

$$Q = \frac{Q_{\text{BP}}}{\alpha_0} \quad \text{Eq. 8-61}$$

■ BASIC LINEAR DESIGN

and the frequency is F_0 .

Each single pole transformation will also result in a zero at the origin.

Elliptical function low-pass prototypes contain zeros as well as poles. In transforming the filter the zeros must be transformed as well. Given the low-pass zeros at $\pm j\omega_z$, the band-pass zeros are obtained as follows:

$$M = \frac{\alpha Q}{Q_{BP}} \quad \text{Eq. 8-62}$$

$$W = M + \sqrt{M^2 - 1} \quad \text{Eq. 8-63}$$

$$F_{BP1} = \frac{F_0}{W} \quad \text{Eq. 8-64}$$

$$F_{BP2} = W F_0 \quad \text{Eq. 8-65}$$

Since the gain of a band-pass filter peaks at F_{BP} instead of F_0 , an adjustment in the amplitude function is required to normalize the response of the aggregate filter. The gain of the individual filter section is given by:

$$A_R = A_0 \sqrt{1 + Q^2 \left(\frac{F_0}{F_{BP}} - \frac{F_{BP}}{F_0} \right)^2} \quad \text{Eq. 8-66}$$

where:

A_0 = gain at filter center frequency

A_R = filter section gain at resonance

F_0 = filter center frequency

F_{BP} = filter section resonant frequency.

Again using a 3 pole 1 dB Chebychev as an example:

$$\alpha_{LP1} = .2257$$

$$\beta_{LP1} = .8822$$

$$\alpha_{LP2} = .4513$$

A 3 dB bandwidth of 0.5 Hz. with a center frequency of 1 Hz is arbitrarily assigned.

Then:

$$Q_{BP} = 2$$

Going through the calculations for the pole pair the intermediate results are:

$$\begin{array}{ll} C = 0.829217 & D = 0.2257 \\ E = 4.2073 & G = 4.18302 \\ M = 1.0247 & W = 1.245 \end{array}$$

and:

$$\begin{array}{ll} F_{BP1} = 0.80322 & F_{BP2} = 1.24499 \\ Q_{BP1} = Q_{BP2} = 9.0749 \end{array}$$

$$\text{Gain} = 4.1318$$

And for the single pole:

$$F_{BP3} = 1 \quad Q_{BP3} = 4.431642 \\ \text{Gain} = 1$$

Again a full example will be worked out in a latter section.

Low-Pass to Band-reject (Notch)

As in the band-pass case, a band-reject filter can be either wideband or narrow-band, depending on whether or not the poles are separated by 2 octaves or more. To avoid confusion, the following convention will be adopted. If the filter is wideband, it will be referred to as a band-reject filter. A narrow-band filter will be referred to as a notch filter.

One way to build a notch filter is to construct it as a band-pass filter whose output is subtracted from the input ($1 - BP$). Another way is with cascaded low-pass and high-pass sections, especially for the band-reject (wideband) case. In this case, the sections are in parallel, and the output is the difference.

Just as the band-pass case is a direct transformation of the low-pass prototype, where dc is transformed to F_0 , the notch filter can be first transformed to the high-pass case, and then dc, which is now a zero, is transformed to F_0 .

A more general approach would be to convert the poles directly. A notch transformation results in two pairs of complex poles and a pair of second order imaginary zeros from each low-pass pole pair.

First, the value of Q_{BR} is determined by:

$$Q_{BR} = \frac{F_0}{BW} \quad \text{Eq. 8-67}$$

where BW is the bandwidth at -3dB .

Given the pole locations of the low-pass prototype

$$-\alpha \pm j\beta \quad \text{Eq. 8-68}$$

and the values of F_0 and Q_{BR} , the following calculations will result in two sets of values for Q and frequencies, F_H and F_L , which define a pair of notch filter sections.

■ BASIC LINEAR DESIGN

$$C = \alpha^2 + \beta^2 \quad \text{Eq. 8-69}$$

$$D = \frac{\alpha}{Q_{BR}C} \quad \text{Eq. 8-70}$$

$$E = \frac{\beta}{Q_{BR}C} \quad \text{Eq. 8-71}$$

$$F = E^2 - D^2 + 4 \quad \text{Eq. 8-72}$$

$$G = \sqrt{\frac{F}{2}} + \sqrt{\frac{F^2}{4}} + D^2 E^2 \quad \text{Eq. 8-73}$$

$$H = \frac{DE}{G} \quad \text{Eq. 8-74}$$

$$K = \frac{1}{2} \sqrt{(D + H)^2 + (E + G)^2} \quad \text{Eq. 8-75}$$

$$Q = \frac{K}{D + H} \quad \text{Eq. 8-76}$$

the pole frequencies are given by:

$$F_{BR1} = \frac{F_0}{K} \quad \text{Eq. 8-77}$$

$$F_{BR2} = K F_0 \quad \text{Eq. 8-78}$$

$$F_Z = F_0 \quad \text{Eq. 8-79}$$

$$F_0 = \sqrt{F_{BR1} * F_{BR2}} \quad \text{Eq. 8-80}$$

where F_0 is the notch frequency and the geometric mean of F_{BR1} and F_{BR2} .

A simple real pole, α_0 , transforms to a single section having a Q given by:

$$Q = Q_{BR} \alpha_0 \quad \text{Eq. 8-81}$$

with a frequency $F_{BR} = F_0$. There will also be transmission zero at F_0 .

In some instances, such as the elimination of the power line frequency (hum) from low level sensor measurements, a notch filter for a specific frequency may be designed.

Assuming that an attenuation of A dB is required over a bandwidth of B, then the required Q for a single frequency notch is determined by:

$$Q = \frac{\omega_0}{B \sqrt{10^{0.1A} - 1}} \quad \text{Eq. 8-82}$$

For transforming a low-pass prototype, a 3 pole 1 dB Chebychev is again used as an example:

$$\begin{aligned}\alpha_{LP1} &= .2257 \\ \beta_{LP1} &= .8822 \\ \alpha_{LP2} &= .4513\end{aligned}$$

A 3 dB bandwidth of 0.1 Hz with a center frequency of 1 Hz is arbitrarily assigned. Then:

$$Q_{BR} = 10$$

Going through the calculations for the pole pair yields the intermediate results:

$$\begin{array}{ll} C = 0.829217 & D = 0.027218 \\ E = 0.106389 & F = 4.01058 \\ G = 2.002643 & H = 0.001446 \\ K = 1.054614 & \end{array}$$

and

$$\begin{array}{ll} F_{BR1} = 0.94821 & F_{BR2} = 1.0546 \\ Q_{BR1} = Q_{BR2} = 36.7918 & \end{array}$$

and for the single-pole

$$F_{BP3} = 1 \quad Q_{BP3} = 4.4513$$

Once again a full example will be worked out in a latter section.

Low-Pass to All-Pass

The transformation from low-pass to all-pass involves adding a zero in the right hand side of the s plane corresponding to each pole in the left hand side.

In general, however, the all-pass filter is usually not designed in this manner. The main purpose of the all-pass filter is to equalize the delay of another filter. Many modulation schemes in communications use some form or another of quadrature modulation, which processes both the amplitude and phase of the signal.

All-pass filters add delay to flatten the delay curve without changing the amplitude. In most cases a closed form of the equalizer is not available. Instead the amplitude filter is designed and the delay calculated or measured. Then graphical means or computer programs are used to figure out the required sections of equalization.

■ BASIC LINEAR DESIGN

Each section of the equalizer gives twice the delay of the low-pass prototype due to the interaction of the zeros. A rough estimate of the required number of sections is given by:

$$n = 2 \Delta_{BW} \Delta_T + 1 \quad \text{Eq. 8-83}$$

Where Δ_{BW} is the bandwidth of interest in hertz and Δ_T is the delay distortion over Δ_{BW} in seconds.

SECTION 8.6: FILTER REALIZATIONS

Now that it has been decided what to build, it now must be decided how to build it. That means that it is necessary to decide which of the filter topologies to use. Filter design is a two step process where it is determined what is to be built (the filter transfer function) and then how to build it (the topology used for the circuit).

In general, filters are built out of one-pole sections for real poles, and two-pole sections for pole pairs. While you can build a filter out of three-pole, or higher order sections, the interaction between the sections increases, and therefore, component sensitivities go up.

It is better to use buffers to isolate the various sections. In addition, it is assumed that all filter sections are driven from a low impedance source. Any source impedance can be modeled as being in series with the filter input.

In all of the design equation figures the following convention will be used:

H = circuit gain in the pass band or at resonance

F_0 = cutoff or resonant frequency in Hertz

ω_0 = cutoff or resonant frequency in radians/sec.

Q = circuit “quality factor”. Indicates circuit peaking.

$\alpha = 1/Q$ = damping ratio

It is unfortunate that the symbol α is used for damping ratio. It is not the same as the α that is used to denote pole locations ($\alpha \pm j\beta$). The same issue occurs for Q . It is used for the *circuit* quality factor and also the *component* quality factor, which are not the same thing.

The circuit Q is the amount of peaking in the circuit. This is a function of the angle of the pole to the origin in the s plane. The component Q is the amount of losses in what should be lossless reactances. These losses are the parasitics of the components; dissipation factor, leakage resistance, ESR (equivalent series resistance), etc. in capacitors and series resistance and parasitic capacitances in inductors.

■ BASIC LINEAR DESIGN

Single-Pole RC

The simplest filter building block is the passive RC section. The single-pole can be either low-pass or high-pass. Odd order filters will have a single-pole section.

The basic form of the low-pass RC section is shown in Figure 8.37(A). It is assumed that the load impedance is high ($> \times 10$), so that there is no loading of the circuit. The load will be in parallel with the shunt arm of the filter. If this is not the case, the section will have to be buffered with an op amp. A low-pass filter can be transformed to a high-pass filter by exchanging the resistor and the capacitor. The basic form of the high-pass filter is shown in Figure 8.37(B). Again it is assumed that load impedance is high.

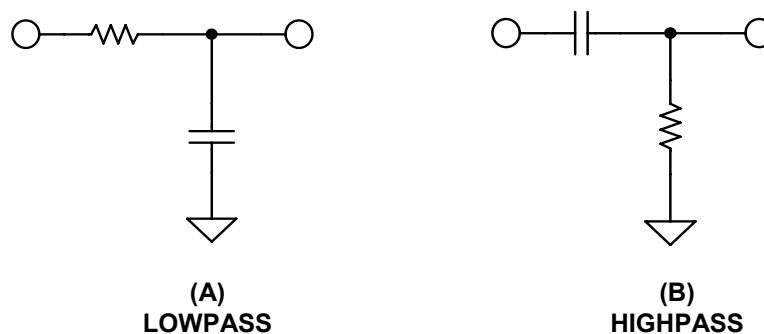


Figure 8.37: Single-Pole Sections

The pole can also be incorporated into an amplifier circuit. Figure 8.38(A) shows an amplifier circuit with a capacitor in the feedback loop. This forms a low-pass filter since as frequency is increased, the effective feedback impedance decreases, which causes the gain to decrease.

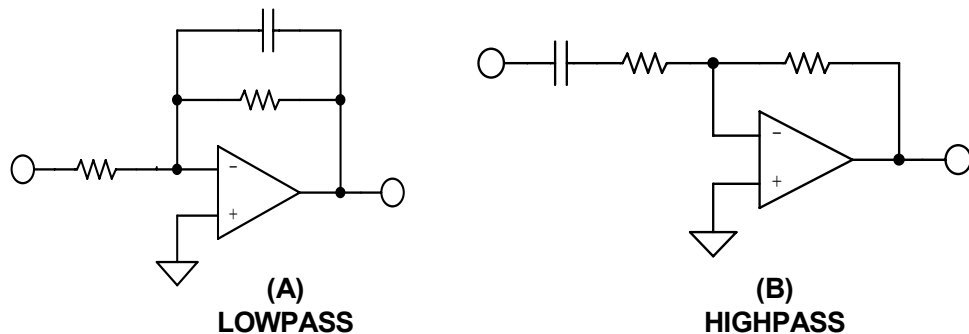


Figure 8.38: Single-Pole Active Filter Blocks

Figure 8.38(B) shows a capacitor in series with the input resistor. This causes the signal to be blocked at dc. As the frequency is increased from dc, the impedance of the capacitor decreases and the gain of the circuit increases. This is a high-pass filter.

The design equations for single-pole filters appear in Figure 8.66.

Passive LC Section

While not strictly a function that uses op amps, passive filters form the basis of several active filters topologies and are included here for completeness.

As in active filters, passive filters are built up of individual subsections. Figure 8.39 shows low-pass filter sections. The full section is the basic two pole section. Odd order filters use one half section which is a single-pole section. The m derived sections, shown in Figure 8.40, are used in designs requiring transmission zeros as well as poles.

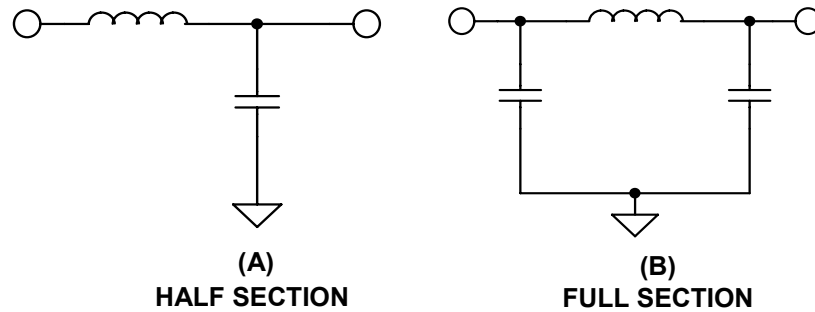


Figure 8.39: Passive Filter Blocks (Low-pass)

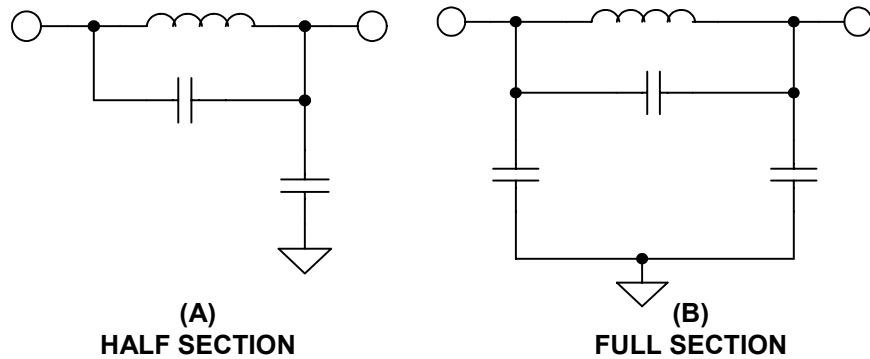


Figure 8.40: Passive Filter Blocks (Low-pass m-derived)

A low-pass filter can be transformed into a high-pass (see Figures 8.41 and 8.42) by simply replacing capacitors with inductors and vice versa so:

$$L_{HP} = \frac{1}{C_{LP}} \quad \text{Eq. 8-84}$$

and

$$C_{HP} = \frac{1}{L_{LP}} \quad \text{Eq. 8-85}$$

■ BASIC LINEAR DESIGN

Transmission zeros are also reciprocated in the transformation so:

$$\omega_{Z,HP} = \frac{1}{\omega_{Z,LP}} \quad \text{Eq. 8-86}$$

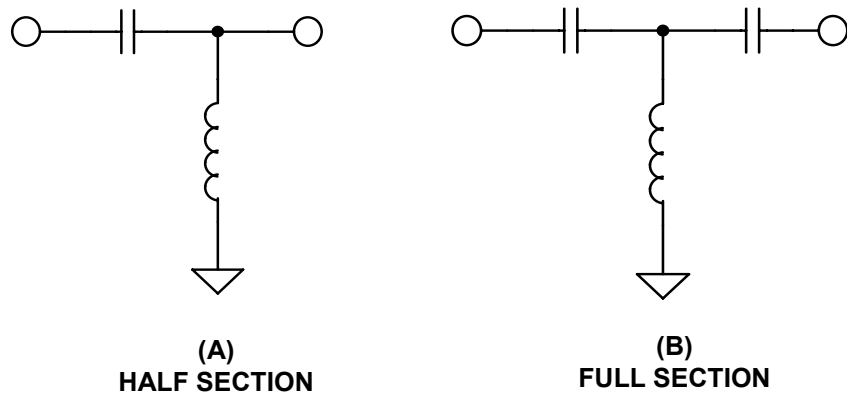


Figure 8.41: Passive Filter Blocks (High-pass)

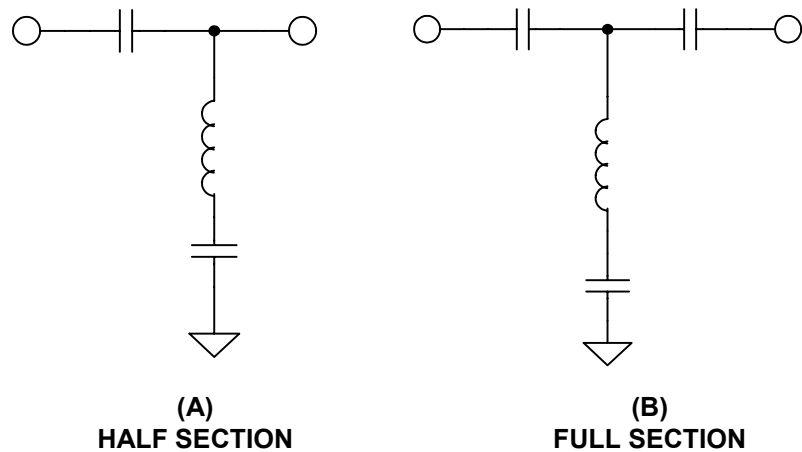


Figure 8.42: Passive Filter Blocks (High-pass m-derived)

The low-pass prototype is transformed to band-pass and band-reject filters as well by using the table in Figure 8.43.

For a passive filter to operate, the source and load impedances must be specified. One issue with designing passive filters is that in multipole filters each section is the load for the preceding sections and also the source impedance for subsequent sections, so

component interaction is a major concern. Because of this, designers typically make use of tables, such as in William's book (Reference 2).

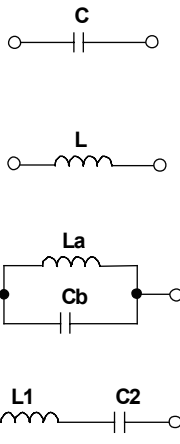
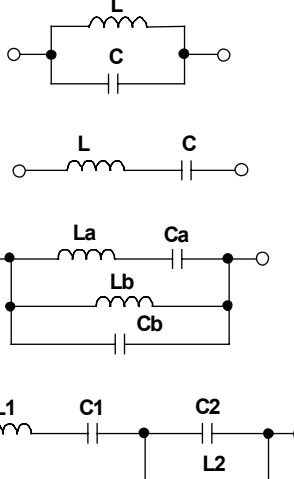
LOW-PASS BRANCH	BAND-PASS CONFIGURATION	CIRCUIT VALUES
		$C = \frac{1}{\omega_0^2 L}$ $L = \frac{1}{\omega_0^2 C}$ $C_a = \frac{1}{\omega_0^2 L_a}$ $L_b = \frac{1}{\omega_0^2 C_b}$ $C_1 = \frac{1}{\omega_0^2 L_1}$ $L_2 = \frac{1}{\omega_0^2 C_2}$
HIGH-PASS BRANCH	BAND-REJECT CONFIGURATION	CIRCUIT VALUES

Figure 8.43: Low-pass → Band-pass and High-pass → Band-reject Transformation

Integrator

Any time that you put a frequency-dependent impedance in a feedback network the inverse frequency response is obtained. For example, if a capacitor, which has a frequency dependent impedance that decreases with increasing frequency, is put in the feedback network of an op amp, an integrator is formed, as in Figure 8.44.

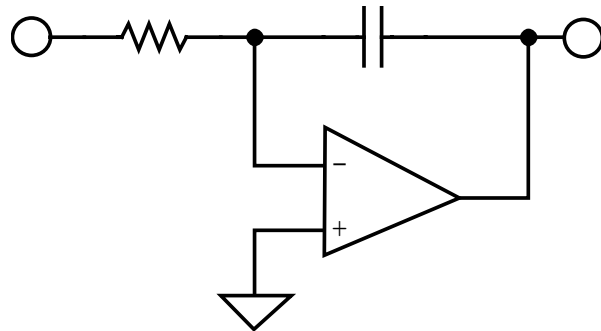


Figure 8.44: Integrator

The integrator has high gain (i.e., the open-loop gain of the op amp) at dc. An integrator can also be thought of as a low-pass filter with a cutoff frequency of 0 Hz.

■ BASIC LINEAR DESIGN

General Impedance Converter

Figure 8.45 is the block diagram of a general impedance converter. The impedance of this circuit is:

$$Z = \frac{Z_1 Z_3 Z_5}{Z_2 Z_4} \quad \text{Eq. 8-87}$$

By substituting one or two capacitors into appropriate locations (the other locations being resistors), several impedances can be synthesized (see Reference 25).

One limitation of this configuration is that the lower end of the structure must be grounded.

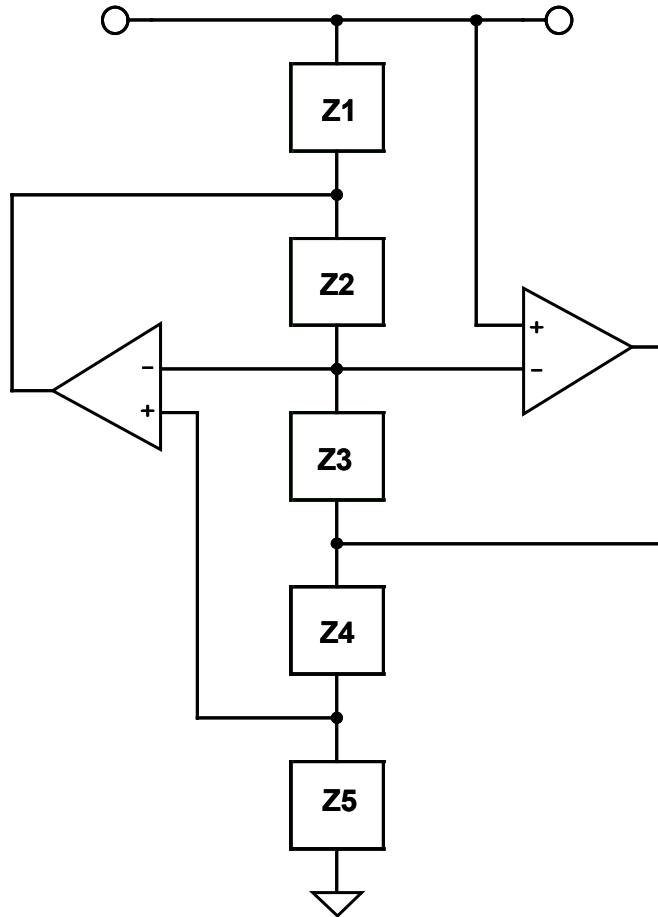


Figure 8.45: General Impedance Converter

Active Inductor

Substituting a capacitor for Z4 and resistors for Z1, Z2, Z3 & Z5 in the GIC results in an impedance given by:

$$Z_{11} = \frac{sC R_1 R_3 R_5}{R_2} \quad \text{Eq. 8-88}$$

By inspection it can be shown that this is an inductor with a value of:

$$L = \frac{C R_1 R_3 R_5}{R_2} \quad \text{Eq. 8-89}$$

This is just one way to simulate an inductor as shown in Figure 8.46.

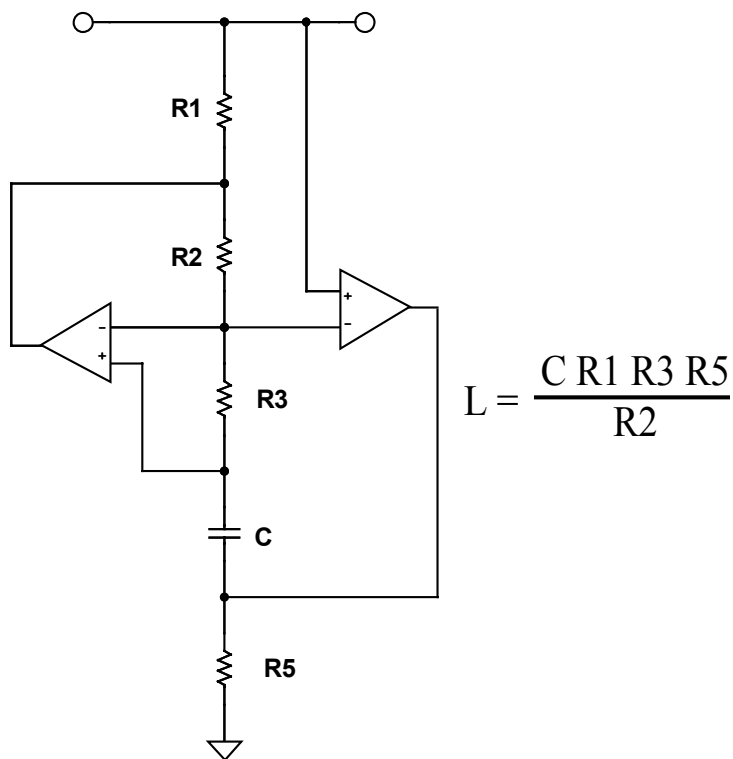


Figure 8.46: Active Inductor

► BASIC LINEAR DESIGN

Frequency Dependent Negative Resistor (FDNR)

By substituting capacitors for two of the Z1, Z3, or Z5 elements, a structure known as a frequency dependant negative resistance (FDNR) is generated. The impedance of this structure is:

$$Z_{11} = \frac{S C^2 R_2 R_4}{R_5} \quad \text{Eq. 8-90}$$

This impedance, which is called a D element, has the value:

$$D = C^2 R^4 \quad \text{Eq. 8-91}$$

assuming

$$C_1 = C_2 \text{ and } R_2 = R_5. \quad \text{Eq. 8-92}$$

The three possible versions of the FDNR are shown in Figure 8.47.

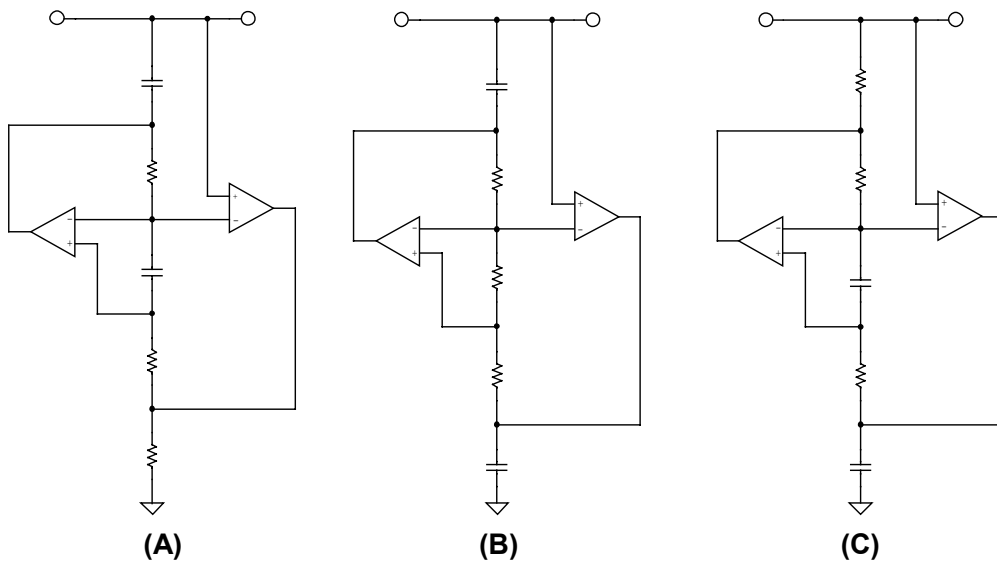


Figure 8.47: Frequency Dependent Negative Resistor Blocks

There is theoretically no difference in these three blocks, and so they should be interchangeable. In practice though there may be some differences. Circuit (a) is sometimes preferred because it is the only block to provide a return path for the amplifier bias currents.

For the FDNR filter (see Reference 24), the passive realization of the filter is used as the basis of the design. As in the passive filter, the FDNR filter must then be denormalized for frequency and impedance. This is typically done before the conversion by 1/s. First take the denormalized passive prototype filter and transform the elements by 1/s. This means that inductors, whose impedance is equal to sL , transform into a resistor with an

impedance of L. A resistor of value R becomes a capacitor with an impedance of R/s ; and a capacitor of impedance $1/sC$ transforms into a frequency dependent resistor, D, with an impedance of $1/s^2C$. The transformations involved with the FDNR configuration and the GIC implementation of the D element are shown in Figure 8.48. We can apply this transformation to low-pass, high-pass, band-pass or notch filters, remembering that the FDNR block must be restricted to shunt arms.

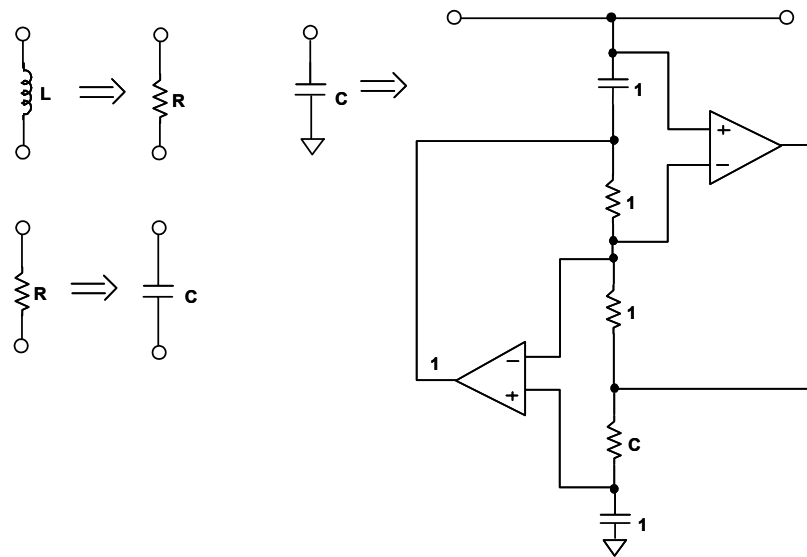


Figure 8.48: $1/s$ Transformation

A worked out example of the FDNR filter is included in the next section.

A perceived advantage of the FDNR filter in some circles is that there are no op amps in the direct signal path, which can add noise and/or distortion, however small, to the signal. It is also relatively insensitive to component variation. These advantages of the FDNR come at the expense of an increase in the number of components required.

■ BASIC LINEAR DESIGN

Sallen-Key

The Sallen-Key configuration, also known as a voltage control voltage source (VCVS), was first introduced in 1955 by R. P. Sallen and E. L. Key of MIT's Lincoln Labs (see Reference 14). It is one of the most widely used filter topologies and is shown in Figure 8.49. One reason for this popularity is that this configuration shows the least dependence of filter performance on the performance of the op amp. This is due to the fact that the op amp is configured as an amplifier, as opposed to an integrator, which minimizes the gain-bandwidth requirements of the op amp. This infers that for a given op amp, you will be able to design a higher frequency filter than with other topologies since the op amp gain bandwidth product will not limit the performance of the filter as it would if it were configured as an integrator. The signal phase through the filter is maintained (noninverting configuration).

Another advantage of this configuration is that the ratio of the largest resistor value to the smallest resistor value and the ratio of the largest capacitor value to the smallest capacitor value (component spread) are low, which is good for manufacturability. The frequency and Q terms are somewhat independent, but they are very sensitive to the gain parameter. The Sallen-Key is very Q-sensitive to element values, especially for high Q sections. The design equations for the Sallen-Key low pass are shown in Figure 8.67.

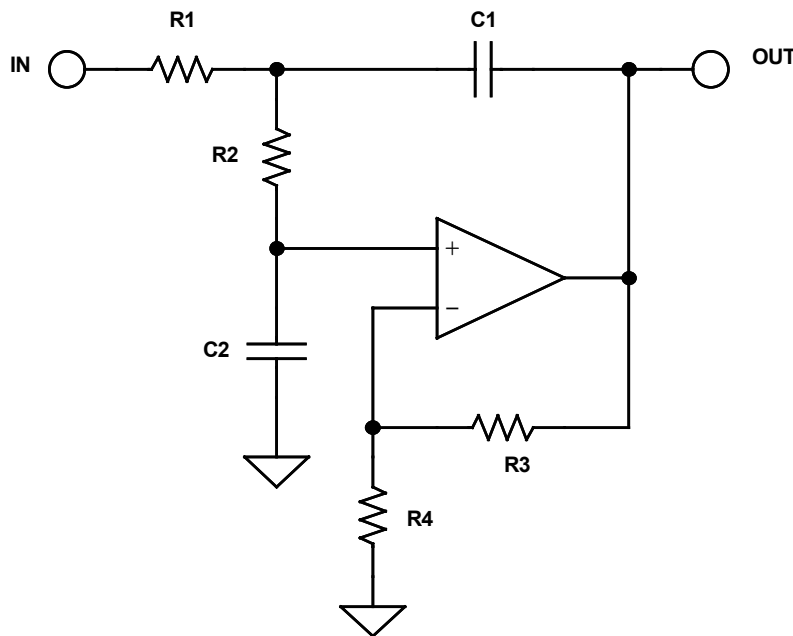


Figure 8.49: Sallen-Key Low-pass Filter

There is a special case of the Sallen-Key low-pass filter. If the gain is set to 2, the capacitor values, as well as the resistor values, will be the same.

While the Sallen-Key filter is widely used, a serious drawback is that the filter is not easily tuned, due to interaction of the component values on F_0 and Q.

To transform the low-pass into the high-pass we simply exchange the capacitors and the resistors in the frequency determining network (i.e. not the amp gain resistors). This is shown in Figure 8.50 (opposite). The comments regarding sensitivity of the filter given above for the low pass case apply to the high-pass case as well. The design equations for the Sallen-Key high-pass are shown in Figure 8.68.

The band-pass case of the Sallen-Key filter has a limitation (see Figure 8.51 below). The value of Q will determine the gain of the filter, i.e. it can not be set independent, as in the low-pass or high-pass cases. The design equations for the Sallen-Key band-pass are shown in Figure 8.69.

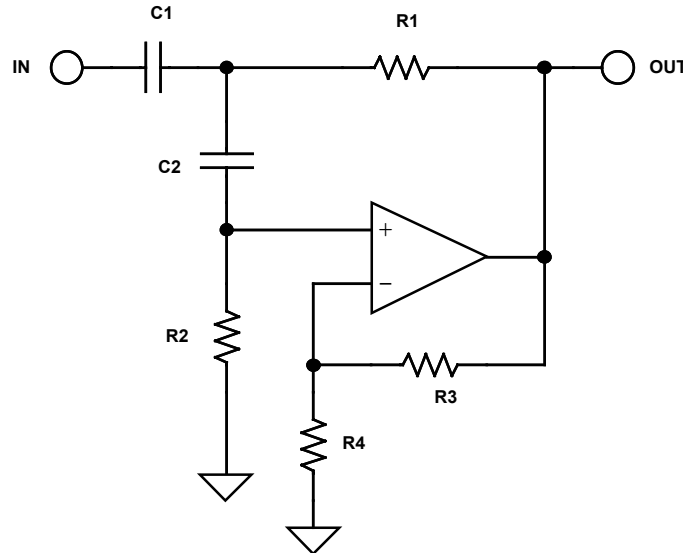


Figure 8.50: Sallen-Key High-pass Filter

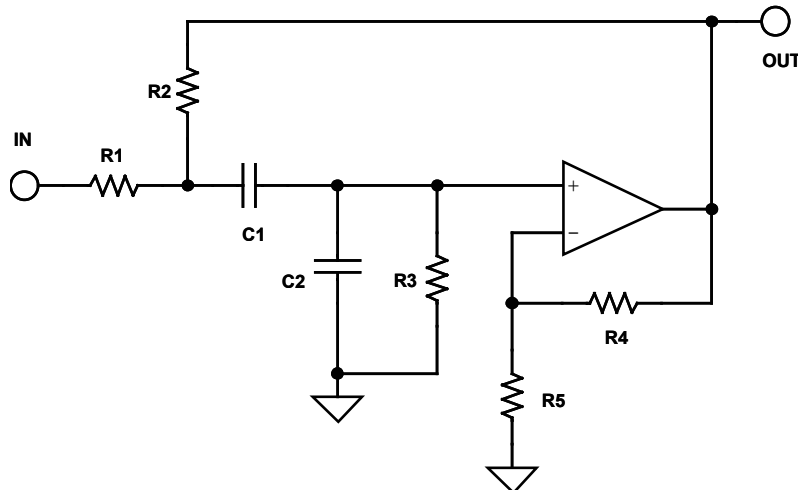


Figure 8.51: Sallen-Key Band-pass Filter

A Sallen-Key notch filter may also be constructed, but it has a large number of undesirable characteristics. The resonant frequency, or the notch frequency, can not be

■ BASIC LINEAR DESIGN

adjusted easily due to component interaction. As in the band-pass case, the section gain is fixed by the other design parameters, and there is a wide spread in component values, especially capacitors. Because of this and the availability of easier to use circuits, it is not covered here.

Multiple Feedback

The multiple feedback filter uses an op amp as an integrator as shown in Figure 8.52 below. Therefore, the dependence of the transfer function on the op amp parameters is greater than in the Sallen-Key realization. It is hard to generate high Q, high frequency sections due to the limitations of the open-loop gain of the op amp. A rule of thumb is that the open-loop gain of the op amp should be at least 20 dB ($\times 10$) above the amplitude response at the resonant (or cutoff) frequency, including the peaking caused by the Q of the filter. The peaking due to Q will cause an amplitude, A_0 :

$$A_0 = H Q \quad \text{Eq. 8-92}$$

where H is the gain of the circuit. The multiple feedback filter will invert the phase of the signal. This is equivalent to adding the resulting 180° phase shift to the phase shift of the filter itself.

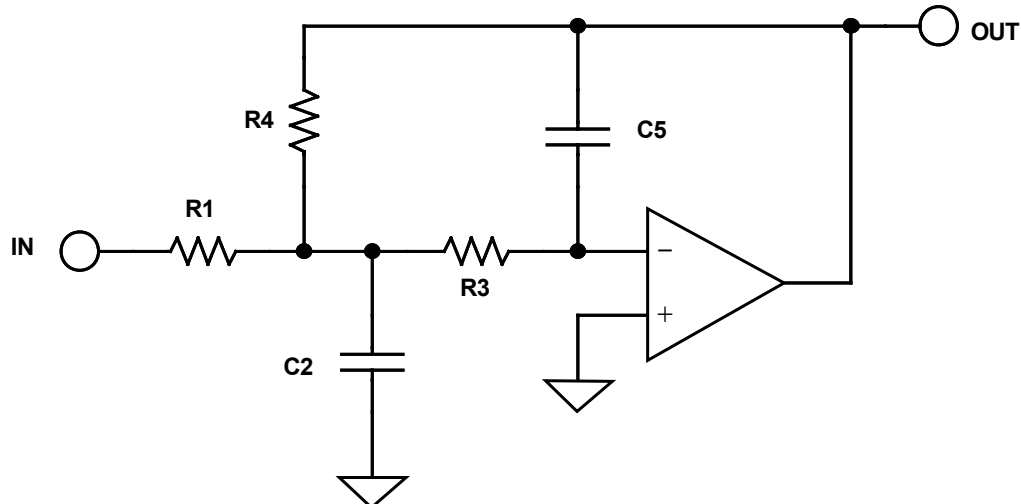


Figure 8.52: Multiple Feedback Low-pass

The maximum to minimum component value ratios is higher in the multiple feedback case than in the Sallen-Key realization. The design equations for the multiple feedback low-pass are given in Figure 8.70.

Comments made about the multiple feedback low-pass case apply to the high-pass case as

well (see Figure 8.53 opposite). Note that we again swap resistors and capacitors to convert the low-pass case to the high-pass case. The design equations for the multiple feedback high-pass are given in Figure 8.71.

The design equations for the multiple feedback band-pass case (see Figure 8.54 opposite) are given in Figure 8.72.

■ BASIC LINEAR DESIGN

This circuit is widely used in low Q (< 20) applications. It allows some tuning of the resonant frequency, F_0 , by making R2 variable. Q can be adjusted (with R5) as well, but this will also change F_0 .

Tuning of F_0 can be accomplished by monitoring the output of the filter with the horizontal channel of an oscilloscope, with the input to the filter connected to the vertical channel. The display will be a Lissajous pattern. This pattern will be an ellipse that will collapse to a straight line at resonance, since the phase shift will be 180° . You could also adjust the output for maximum output, which will also occur at resonance, but this is usually not as precise, especially at lower values of Q where there is a less pronounced peak.

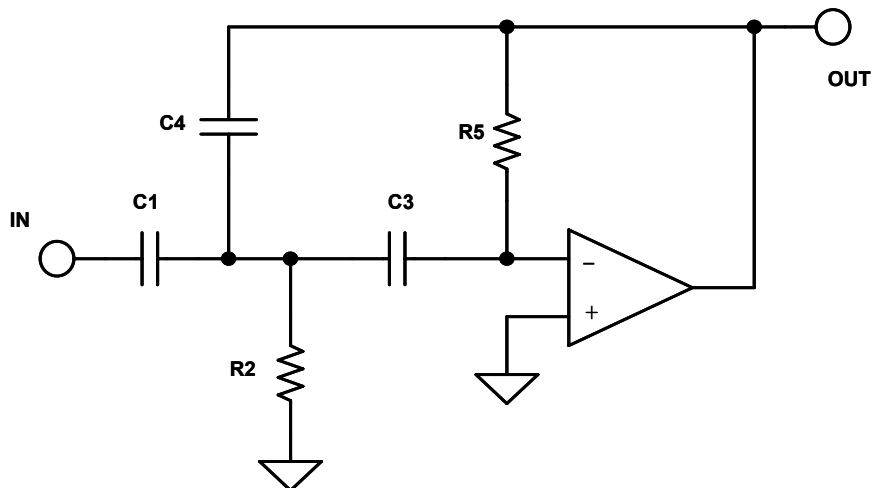


Figure 8.53: Multiple Feedback High-Pass

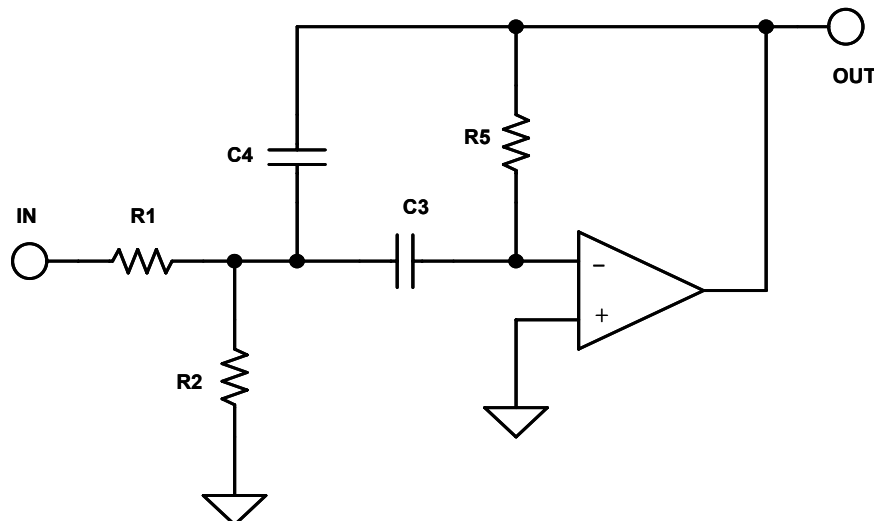


Figure 8.54: Multiple Feedback Band-Pass

State Variable

The state-variable realization (see Reference 11) is shown in Figure 8.55, along with the design equations in Figure 8.73. This configuration offers the most precise implementation, at the expense of many more circuit elements. All three major parameters (gain, Q & ω_0) can be adjusted independently, and low-pass, high-pass, and band-pass outputs are available simultaneously. Note that the low-pass and high-pass outputs are inverted in phase while the band-pass output maintains the phase. The gain of each of the outputs of the filter is also independently variable. With an added amplifier section summing the low-pass and high-pass sections the notch function can also be synthesized. By changing the ratio of the summed sections, low-pass notch, standard notch and high-pass notch functions can be realized. A standard notch may also be realized by subtracting the band-pass output from the input with the added op amp section. An all-pass filter may also be built with the four amplifier configuration by subtracting the band-pass output from the input. In this instance, the band-pass gain must equal 2.

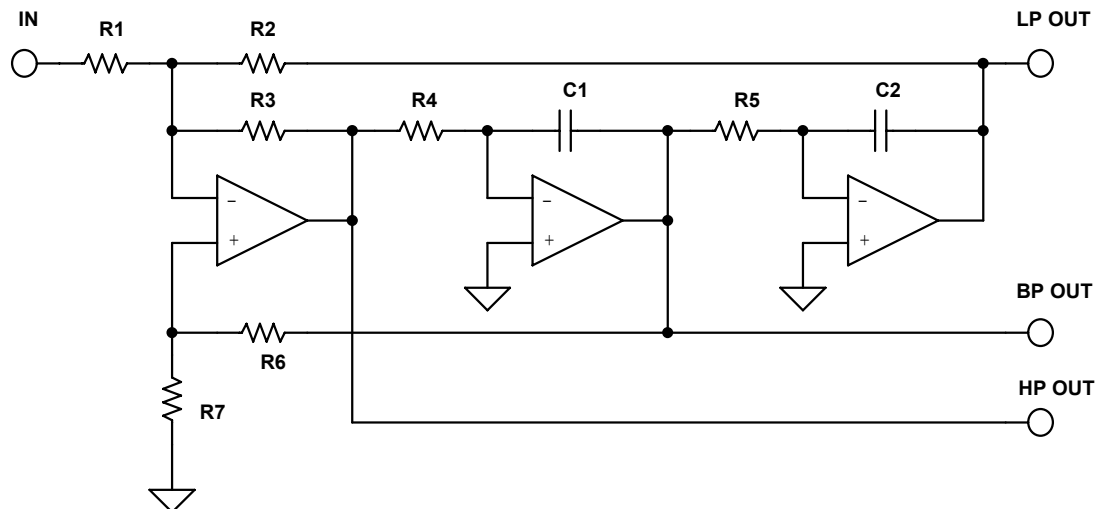


Figure 8.55: State Variable Filter

Since all parameters of the state variable filter can be adjusted independently, component spread can be minimized. Also, variations due to temperature and component tolerances are minimized. The op amps used in the integrator sections will have the same limitations on op amp gain-bandwidth as described in the multiple feedback section.

Tuning the resonant frequency of a state variable filter is accomplished by varying R4 and R5. While you don't have to tune both, if you are varying over a wide range it is generally preferable. Holding R1 constant, tuning R2 sets the low-pass gain and tuning R3 sets the high-pass gain. Band-pass gain and Q are set by the ratio of R6 & R7.

Since the parameters of a state variable filter are independent and tunable, it is easy to add electronic control of frequency, Q and ω_0 . This adjustment is accomplished by using

■ BASIC LINEAR DESIGN

an analog multiplier, multiplying DACs (MDACs) or digital pots, as shown in one of the examples in a later section. For the integrator sections adding the analog multiplier or MDAC effectively increases the time constant by dividing the voltage driving the resistor, which, in turn, provides the charging current for the integrator capacitor. This in effect raises the resistance and, in turn, the time constant. The Q and gain can be varied by changing the ratio of the various feedback paths. A digital pot will accomplish the same feat in a more direct manner, by directly changing the resistance value. The resultant tunable filter offers a great deal of utility in measurement and control circuitry. A worked out example is given in Section 8 of this chapter.

Biquadratic (Biquad)

A close cousin of the state variable filter is the biquad as shown in Figure 8.56. The name of this circuit was first used by J. Tow in 1968 (Reference 11) and later by L. C. Thomas in 1971 (see Reference 12). The name derives from the fact that the transfer function is a quadratic function in both the numerator and the denominator. Hence the transfer function is a biquadratic function. This circuit is a slight rearrangement of the state variable circuit. One significant difference is that there is not a separate high-pass output. The band-pass output inverts the phase. There are two low-pass outputs, one in phase and one out of phase. With the addition of a fourth amplifier section, high-pass, notch (low-pass, standard, and high-pass) and all-pass filters can be realized. The design equations for the biquad are given in Figure 8.74.

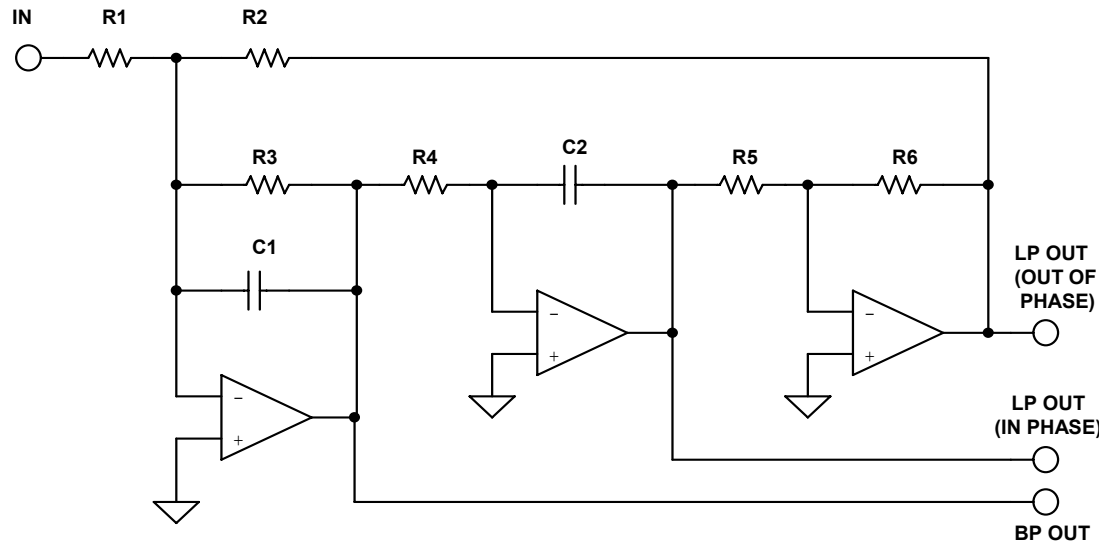


Figure 8.56: Biquad Filter

Referring to Figure 8.74, the all-pass case of the biquad, $R_8 = R_9/2$ and $R_7 = R_9$. This is required to make the terms in the transfer function line up correctly. For the high-pass output, the input, band-pass, and second low-pass outputs are summed. In this case the constraints are that $R_1 = R_2 = R_3$ and $R_7 = R_8 = R_9$.

Like the state variable, the biquad filter is tunable. Adjusting R_3 will adjust the Q. Adjusting R_4 will set the resonant frequency. Adjusting R_1 will set the gain. Frequency would generally be adjusted first followed by Q and then gain. Setting the parameters in this manner minimizes the effects of component value interaction.

■ BASIC LINEAR DESIGN

Dual Amplifier Band-Pass (DAPB)

The dual amplifier band-pass filter structure is useful in designs requiring high Qs and high frequencies. Its component sensitivity is small, and the element spread is low. A useful feature of this circuit is that the Q and resonant frequency can be adjusted more or less independently.

Referring to Figure 8.57 below, the resonant frequency can be adjusted by R2. R1 can then be adjusted for Q. In this topology it is useful to use dual op amps. The match of the two op amps will lower the sensitivity of Q to the amplifier parameters.

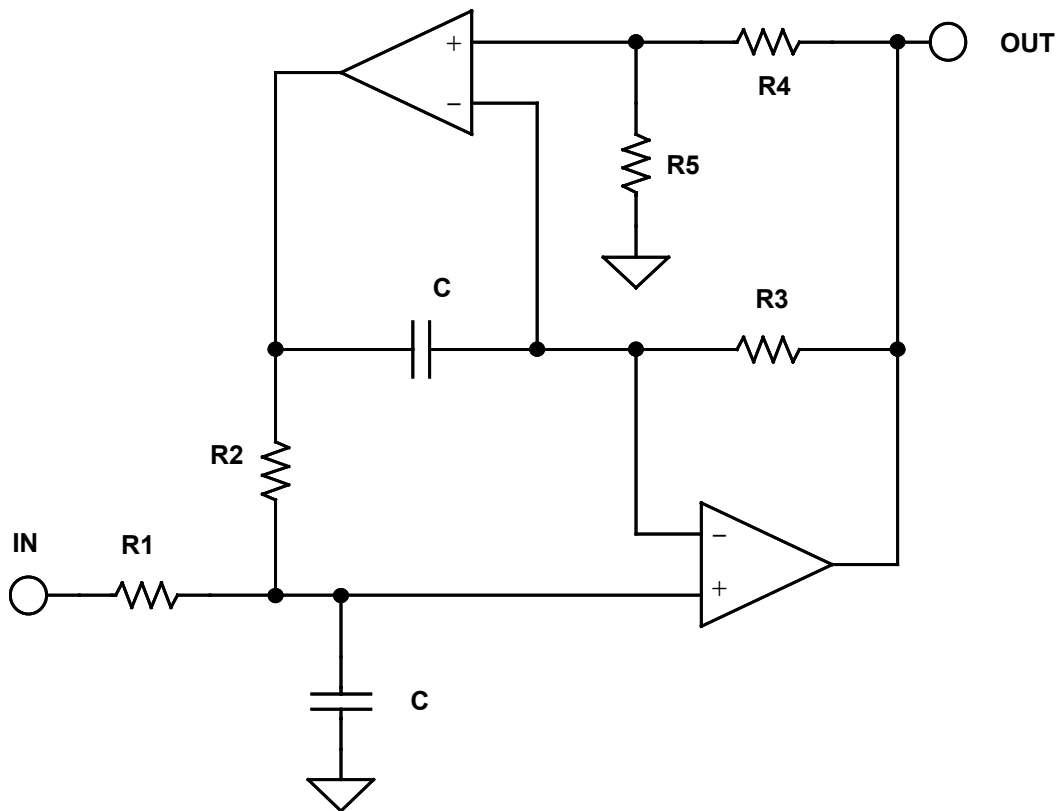


Figure 8.57: Dual Amplifier Band-Pass Filter

It should be noted that the DABP has a gain of 2 at resonance. If lower gain is required, resistor R1 may be split to form a voltage divider. This is reflected in the addendum to the design equations of the DABP, Figure 8.75.

Twin T Notch

The twin T is widely used as a general purpose notch circuit as shown in Figure 8.58. The passive implementation of the twin T (i.e. with no feedback) has a major shortcoming of having a Q that is fixed at 0.25. This issue can be rectified with the application of positive feedback to the reference node. The amount of the signal feedback, set by the R4/R5 ratio, will determine the value of Q of the circuit, which, in turn, determines the notch depth. For maximum notch depth, the resistors R4 and R5 and the associated op amp can be eliminated. In this case, the junction of C3 and R3 will be directly connected to the output.

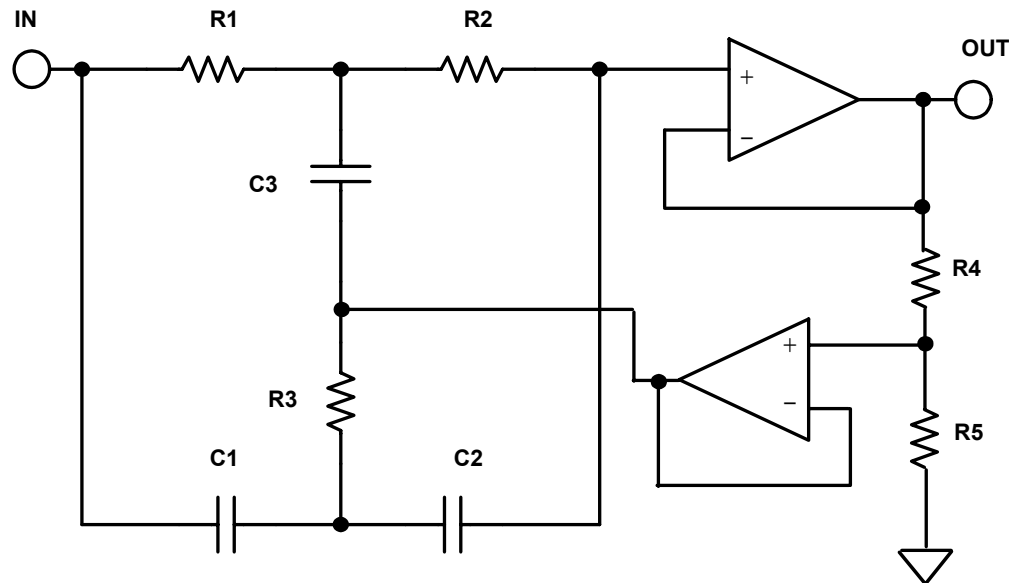


Figure 8.58: Twin-T Notch Filter

Tuning is not easily accomplished. Using standard 1% components a 60 dB notch is as good as can be expected, with 40 dB to 50 dB being more typical.

The design equations for the Twin T are given in Figure 8.76.

■ BASIC LINEAR DESIGN

Bainter Notch

A simple notch filter is the Bainter circuit (see Reference 21). It is composed of simple circuit blocks with two feedback loops as shown in Figure 8.59. Also, the component sensitivity is very low.

This circuit has several interesting properties. The Q of the notch is not based on component matching as it is in every other implementation, but is instead only dependant on the gain of the amplifiers. Therefore, the notch depth will not drift with temperature, aging and other environmental factors. The notch frequency may shift, but not the depth.

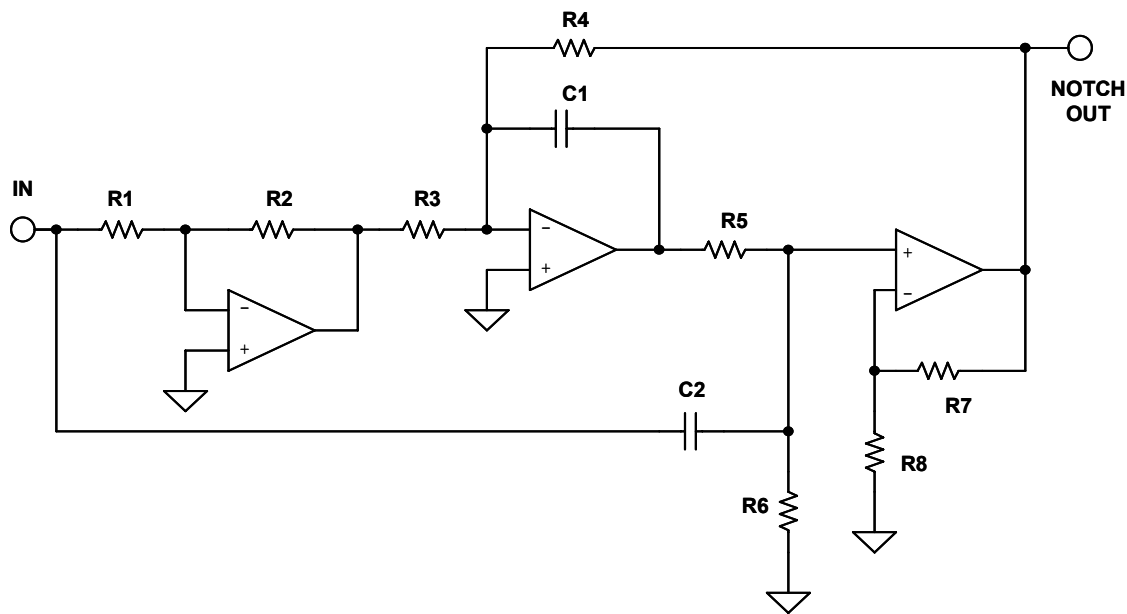


Figure 8.59: Bainter Notch Filter

Amplifier open loop gain of 10^4 will yield a Q_z of > 200 . It is capable of orthogonal tuning with minimal interaction. R6 tunes Q and R1 tunes ω_z . Varying R3 sets the ratio of ω_0/ω_z produces lowpass notch ($R4 > R3$), notch ($R4 = R3$) or highpass notch ($R4 < R3$).

The design equations of the Bainter circuit are given in Figure 8.77.

Boctor Notch

The Boctor circuits (see References 22, 23), while moderately complicated, uses only one op amp. Due to the number of components, there is a great deal of latitude in component selection. These circuits also offer low sensitivity and the ability to tune the various parameters more or less independently.

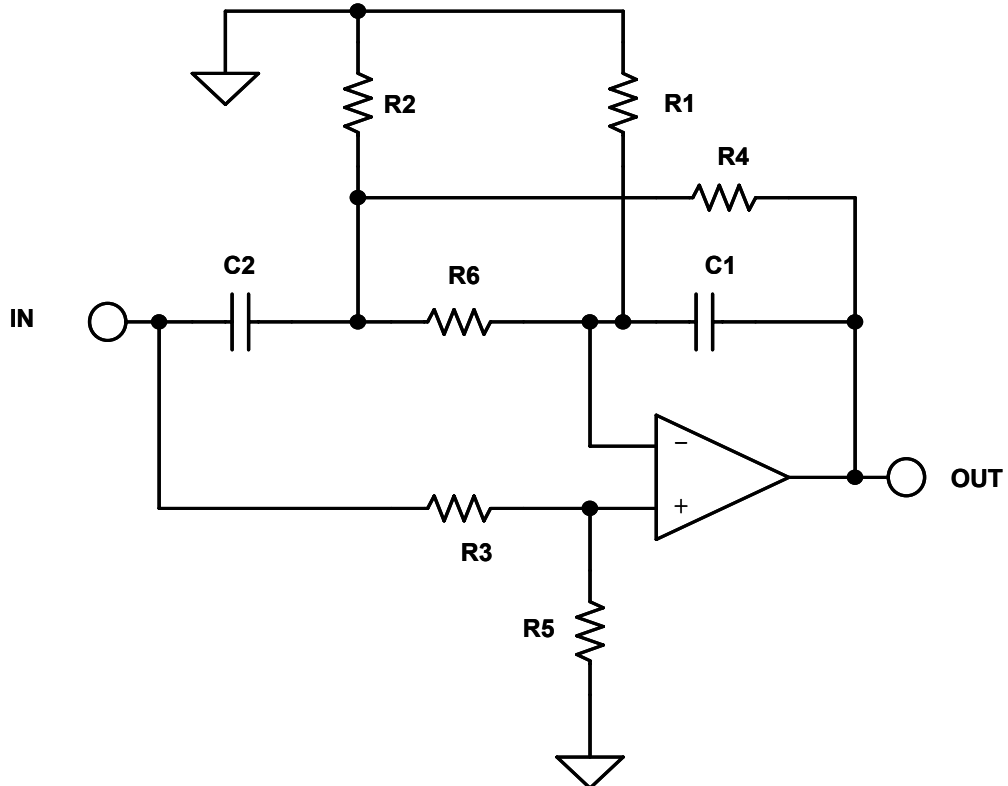


Figure 8.60: Boctor Low-Pass Notch Filter

There are two forms, a low-pass notch (Figure 8.60 above) and a high-pass notch (Figure 8.61 below). For the low-pass case, the preferred order of adjustment is to tune ω_0 with R4, then Q_0 with R2, next Q_z with R3 and finally ω_z with R1.

In order for the components to be realizable we must define a variable, $k1$, such that:

$$\frac{\omega_0^2}{\omega_z^2} < k1 < 1 \quad \text{Eq. 8-94}$$

The design equations are given in Figure 8.78 for the low-pass case and in Figure 8.79 for the high-pass case.

■ BASIC LINEAR DESIGN

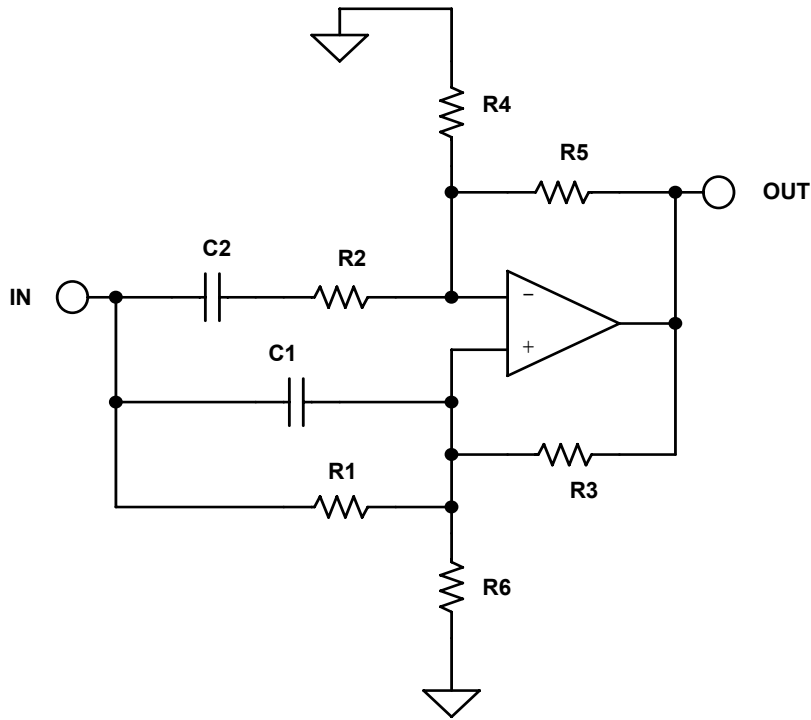


Figure 8.61: Boctor High-Pass Filter

In the high-pass case circuit gain is required and it applies only when

$$Q < \frac{1}{1 - \frac{\omega_z^2}{\omega_0^2}} \quad \text{Eq. 8-95}$$

but a high-pass notch can be realized with one amplifier and only two capacitors, which can be the same value. The pole and zero frequencies are completely independent of the amplifier gain. The resistors can be trimmed so that even 5% capacitors can be used.

"1 – Bandpass" Notch

As mentioned in the state variable and biquad sections, a notch filter can be built as 1 - BP. The band-pass section can be any of the all pole band-pass realizations discussed above, or any others. Keep in mind whether the band-pass section is inverting as shown in Figure 8.62 (such as the multiple feedback circuit) or noninverting as shown in Figure 8.63 (such as the Sallen-Key), since we want to subtract, not add, the band-pass output from the input.

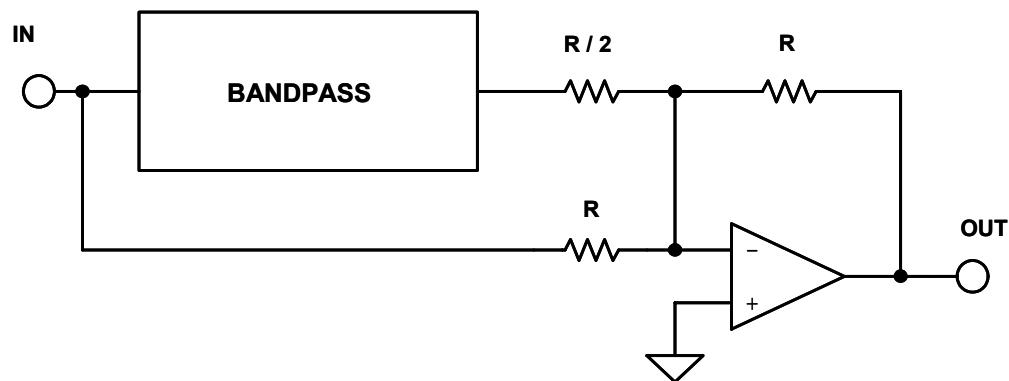


Figure 8.62: 1 – BP Filter for Inverting Band-Pass Configurations

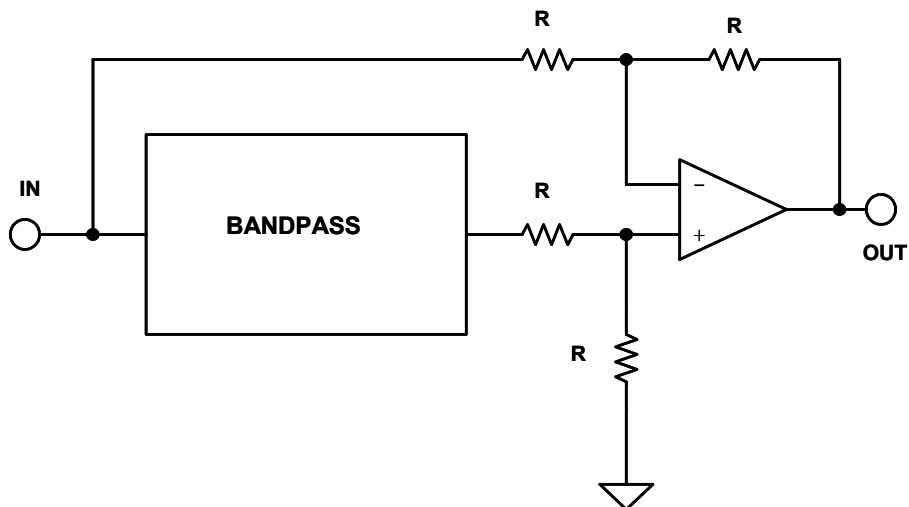


Figure 8.63: 1 – BP Filter for Noninverting Band-Pass Configurations

It should be noted that the gain of the band-pass amplifier must be taken into account in determining the resistor values. Unity gain band-pass would yield equal values.

■ BASIC LINEAR DESIGN

First Order All-Pass

The general form of a first order all-pass filter is shown in Figure 8.64. If the function is a simple RC high-pass (Figure 8.64A), the circuit will have a phase shift that goes from -180° at 0 Hz. and 0° at high frequency. It will be -90° at $\omega = 1/RC$. The resistor may be made variable to allow adjustment of the delay at a particular frequency.

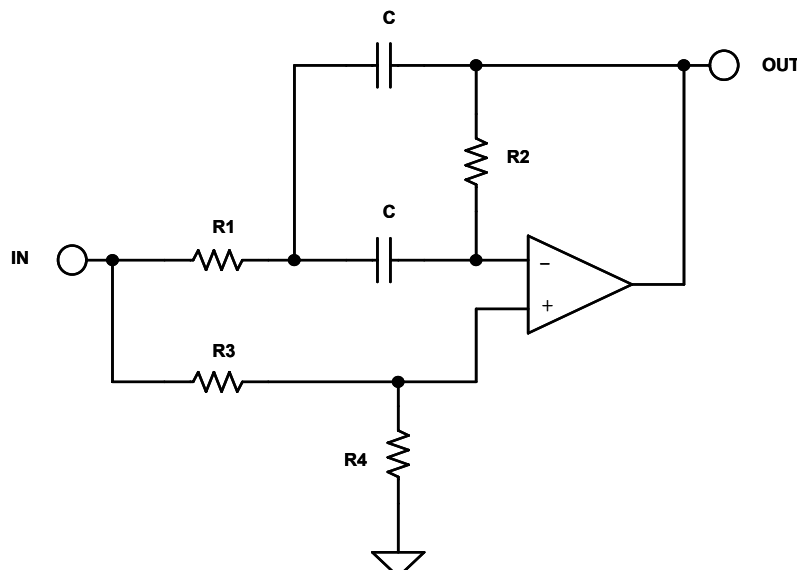


Figure 8.64: First Order All-Pass Filters

If the function is changed to a low-pass function (Figure 8.64B), the filter is still a first order all-pass and the delay equations still hold, but the signal is inverted, changing from 0° at dc to -180° at high frequency.

Second Order All-Pass

A second order all-pass circuit shown in Figure 8.65 was first described by Delyiannis (see Reference 17). The main attraction of this circuit is that it only requires one op amp. Remember also that an all-pass filter can also be realized as 1 – 2BP.

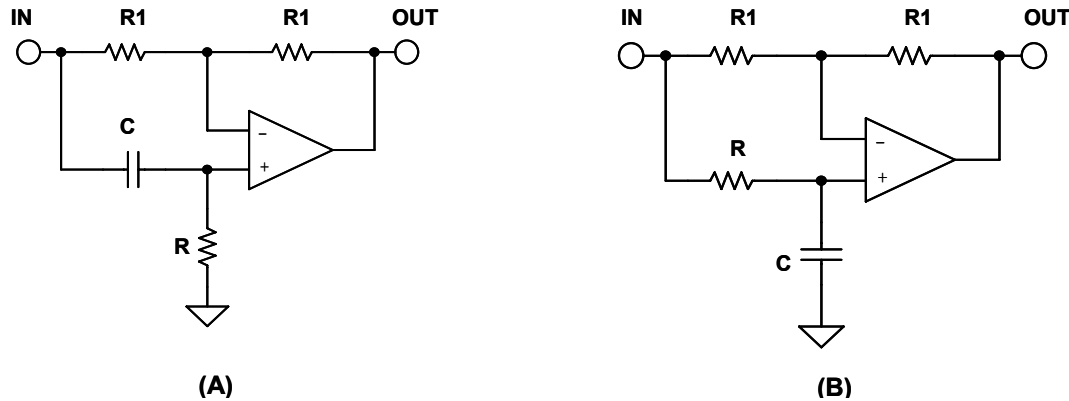


Figure 8.65: Second Order All-Pass Filter

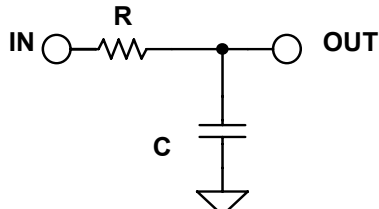
We may use any of the all pole realizations discussed above to build the filter, but you need to be aware of whether the BP inverts the phase or not. We must also be aware that the gain of the BP section must be 2. To this end, the DABP structure is particularly useful, since its gain is fixed at 2.

Figures 8.66 through 8.81 following summarize design equations for various active filter realizations. In all cases, H , ω_0 , Q , and α are given, being taken from the design tables.

■ BASIC LINEAR DESIGN

SINGLE POLE

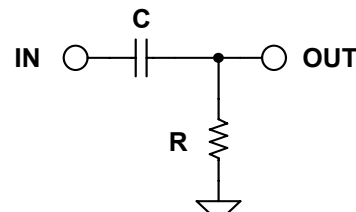
LOWPASS



$$\frac{V_o}{V_{IN}} = \frac{1}{sCR + 1}$$

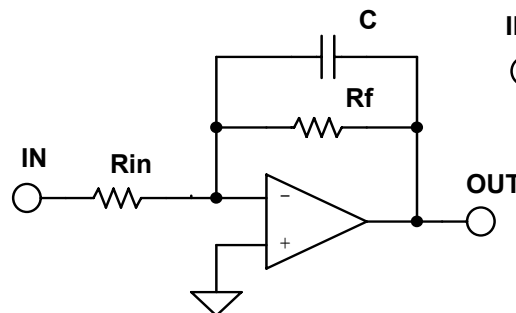
$$F_o = \frac{1}{2\pi RC}$$

HIGHPASS



$$\frac{V_o}{V_{IN}} = \frac{sCR}{sCR + 1}$$

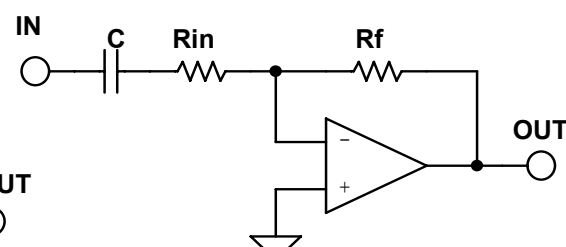
$$F_o = \frac{1}{2\pi RC}$$



$$\frac{V_o}{V_{IN}} = - \frac{Rf}{Rin} \frac{1}{sCR_2 + 1}$$

$$H_o = - \frac{Rf}{Rin}$$

$$F_o = \frac{1}{2\pi RfC}$$



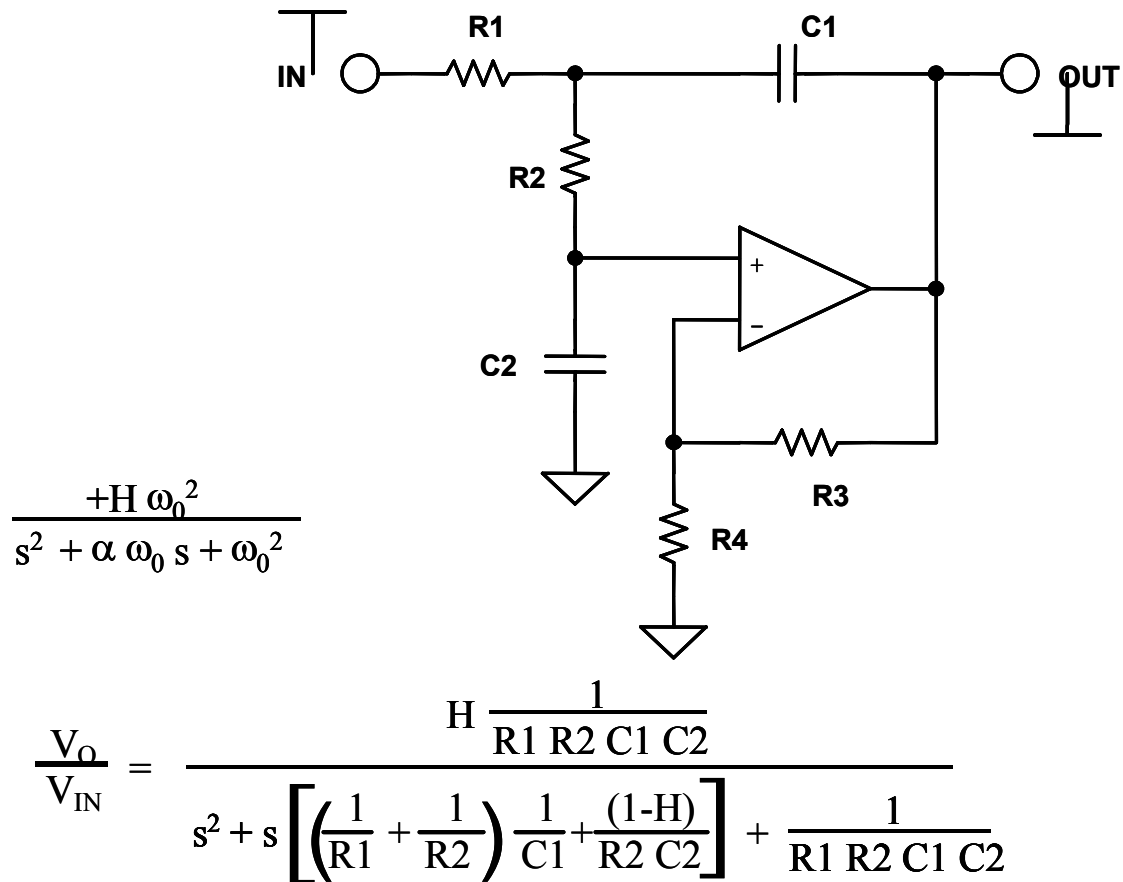
$$\frac{V_o}{V_{IN}} = - \frac{Rf}{Rin} \frac{sCR_1 + 1}{sCR_1 + 1}$$

$$H_o = - \frac{Rf}{Rin}$$

$$F_o = \frac{1}{2\pi Rin C}$$

Figure 8.66: Single-Pole Filter Design Equations

SALLEN-KEY LOWPASS



CHOOSE: C1 R3

THEN: $k = 2 \pi F_O C_1$ $R_4 = \frac{R_3}{(H-1)}$
 $m = \frac{\alpha^2}{4} + (H-1)$

$$C_2 = m C_1$$

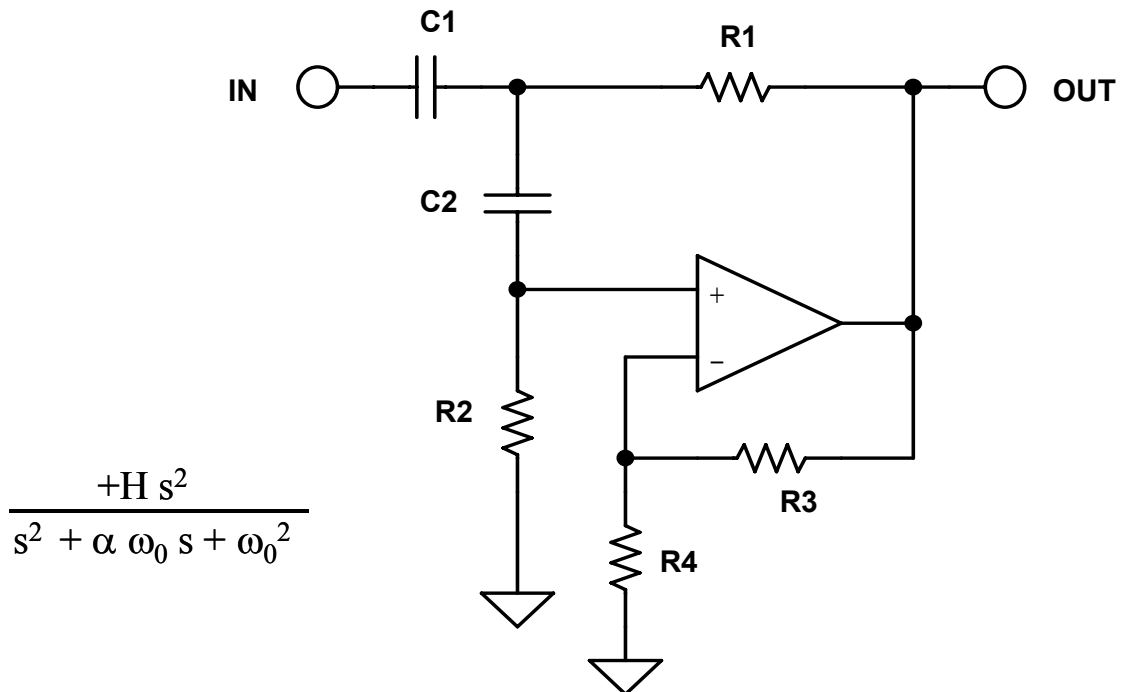
$$R_1 = \frac{2}{\alpha k}$$

$$R_2 = \frac{\alpha}{2mk}$$

Figure 8.67: Sallen-Key Low-Pass Design Equations

■ BASIC LINEAR DESIGN

SALLEN-KEY HIGHPASS



$$\frac{+H s^2}{s^2 + \alpha \omega_0 s + \omega_0^2}$$

$$\frac{V_O}{V_{IN}} = \frac{H s^2}{s^2 + s \left[\frac{C_2 + C_1}{R_2} + (1-H) \frac{C_2}{R_1} \right] + \frac{1}{R_1 R_2 C_1 C_2}}$$

CHOOSE: C1

R3

THEN: $k = 2 \pi F_O C_1$

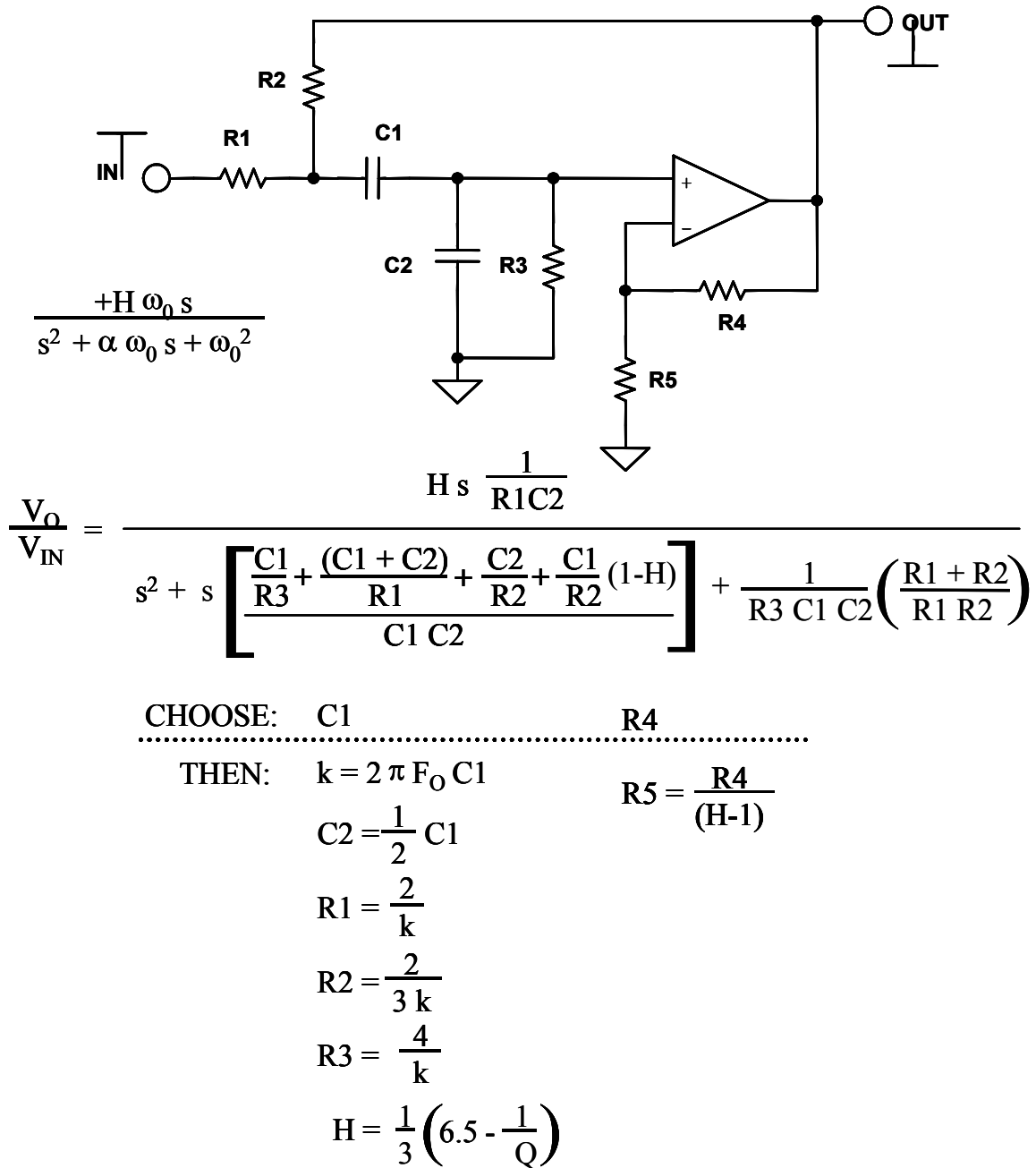
$$R_4 = \frac{R_3}{(H-1)}$$

$$C_2 = C_1$$

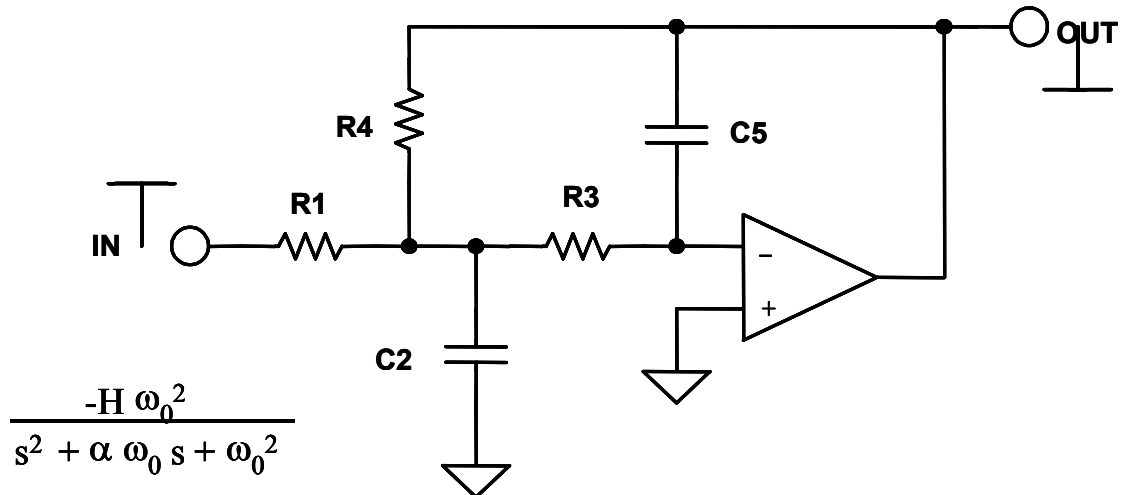
$$R_1 = \frac{\alpha + \sqrt{\alpha^2 + (H-1)}}{4k}$$

$$R_2 = \frac{4}{\alpha + \sqrt{\alpha^2 + (H-1)}} * \frac{1}{k}$$

Figure 8.68: Sallen-Key High-Pass Design Equations

SALLEN-KEY BANDPASS

Figure 8.69: Sallen-Key Band-Pass Design Equations

MULTIPLE FEEDBACK LOWPASS



$$\frac{V_O}{V_{IN}} = \frac{-H \frac{1}{R_1 R_3 C_2 C_5}}{s^2 + s \frac{1}{C_2} \left(\frac{1}{R_1} + \frac{1}{R_3} + \frac{1}{R_4} \right) + \frac{1}{R_3 R_4 C_2 C_5}}$$

CHOOSE: C_5

THEN: $k = 2 \pi F_O C_5$

$$C_2 = \frac{4}{\alpha^2} (H + 1) C_5$$

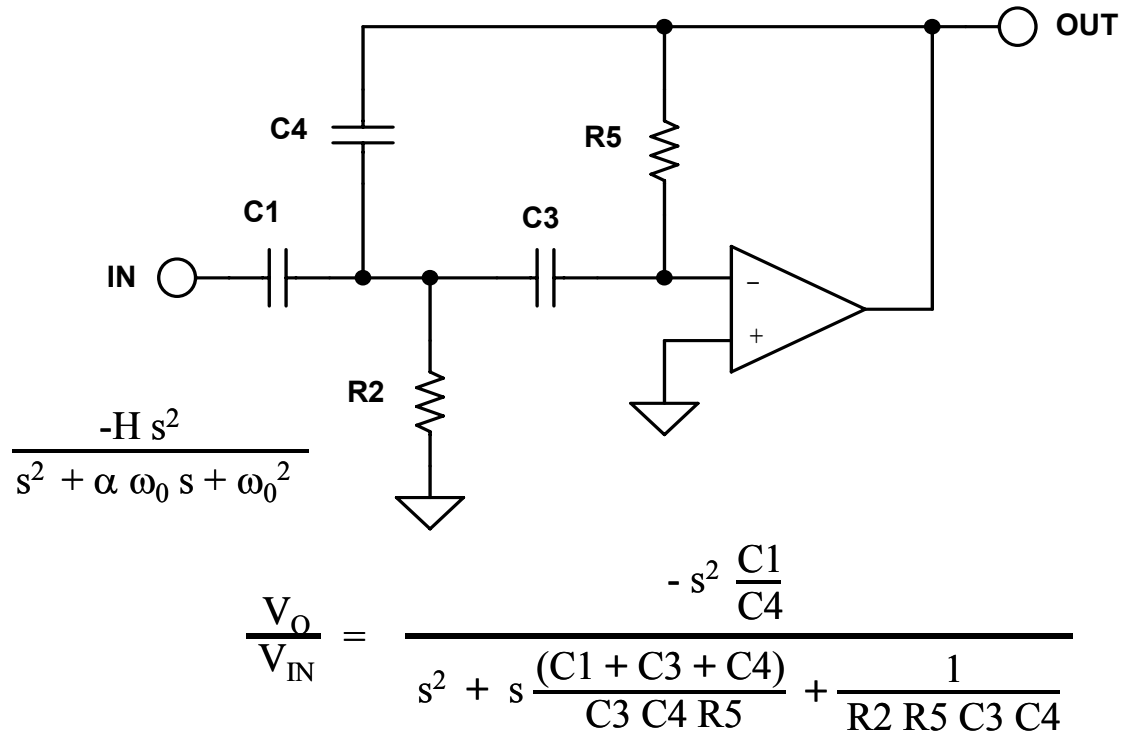
$$R_1 = \frac{\alpha}{2 H k}$$

$$R_3 = \frac{\alpha}{2 (H + 1) k}$$

$$R_4 = \frac{\alpha}{2 k}$$

Figure 8.70: Multiple Feedback Low-Pass Design Equations

MULTIPLE FEEDBACK HIGHPASS



CHOOSE: C_1

THEN: $k = 2 \pi F_0 C_1$

$$C_3 = C_1$$

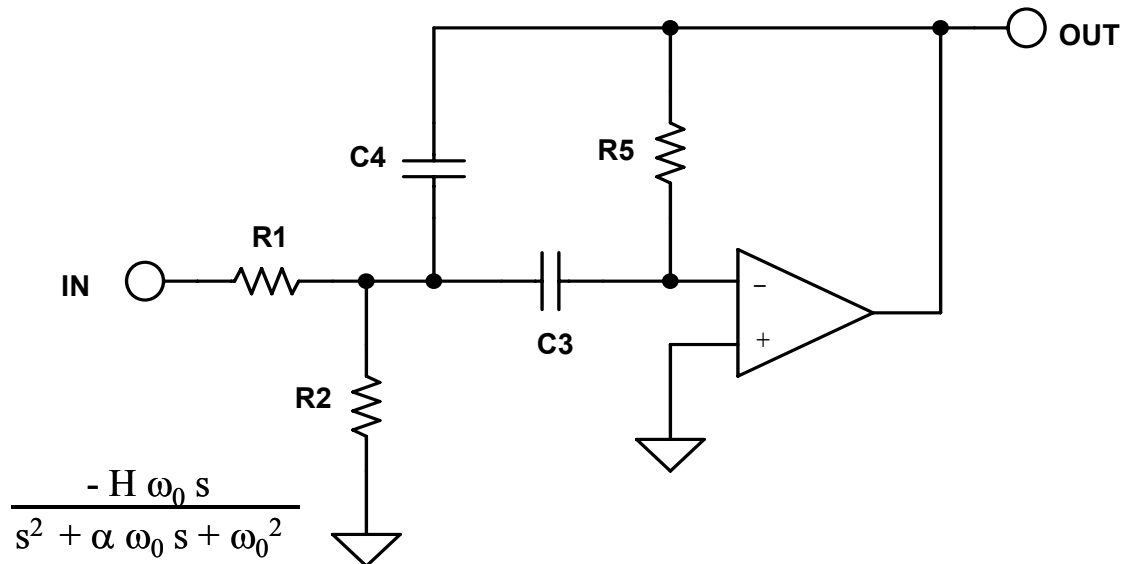
$$C_4 = \frac{C_1}{H}$$

$$R_2 = \frac{\alpha}{k \left(2 + \frac{1}{H} \right)}$$

$$R_5 = \frac{H \left(2 + \frac{1}{H} \right)}{\alpha k}$$

Figure 8.71: Multiple Feedback High-Pass Design Equations

MULTIPLE FEEDBACK BANDPASS



$$\frac{V_O}{V_{IN}} = \frac{-s \frac{1}{R_1 C_4}}{s^2 + s \frac{(C_3 + C_4)}{C_3 C_4 R_5} + \frac{1}{R_5 C_3 C_4} \left(\frac{1}{R_1} + \frac{1}{R_2} \right)}$$

CHOOSE: C_3

THEN: $k = 2\pi F_O C_3$

$$C_4 = C_3$$

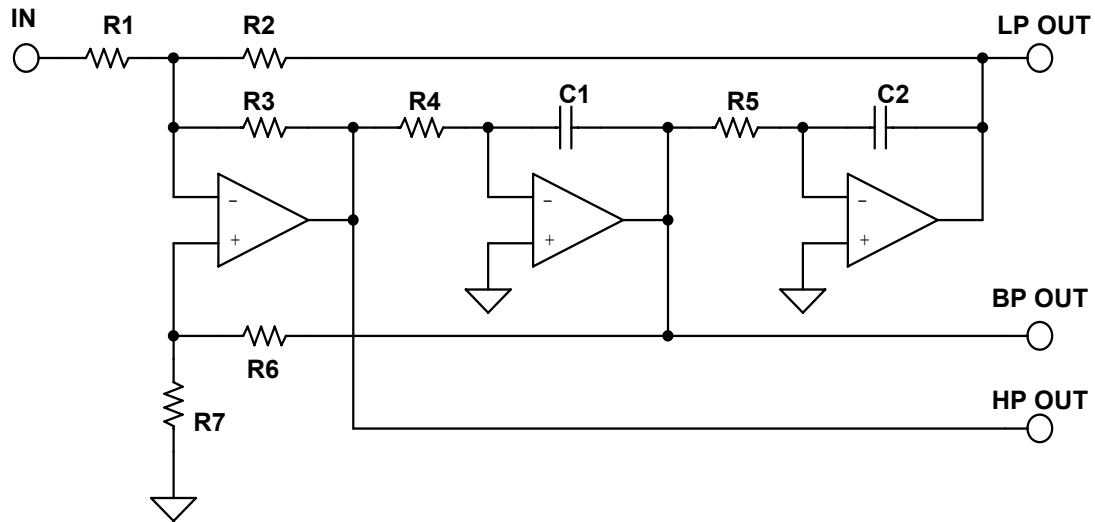
$$R_1 = \frac{1}{H k}$$

$$R_2 = \frac{1}{(2Q - H) k}$$

$$R_5 = \frac{2Q}{k}$$

Figure 8.72: Multiple Feedback Band-Pass Design Equations

STATE VARIABLE (A)



$$A_{LP} (s = 0) = - \frac{R_2}{R_1}$$

CHOOSE R1:

$$R_2 = A_{LP} R_1$$

$$A_{HP} (s = \infty) = - \frac{R_3}{R_1}$$

$$R_3 = A_{HP} R_1$$

$$\omega_0 = \sqrt{\frac{R_3}{R_2 R_4 R_5 C_1 C_2}}$$

CHOOSE C:

LET $R_4 = R_5 = R$, $C_1 = C_2 = C$

$$R = \frac{1}{2 \pi F_0 C} \sqrt{\frac{A_{HP}}{A_{LP}}}$$

$$A_{BP} (s = \omega_0) = \frac{\frac{R_6 + R_7}{R_7}}{R_1 \left(\frac{1}{R_1} + \frac{1}{R_2} + \frac{1}{R_3} \right)}$$

CHOOSE R7:

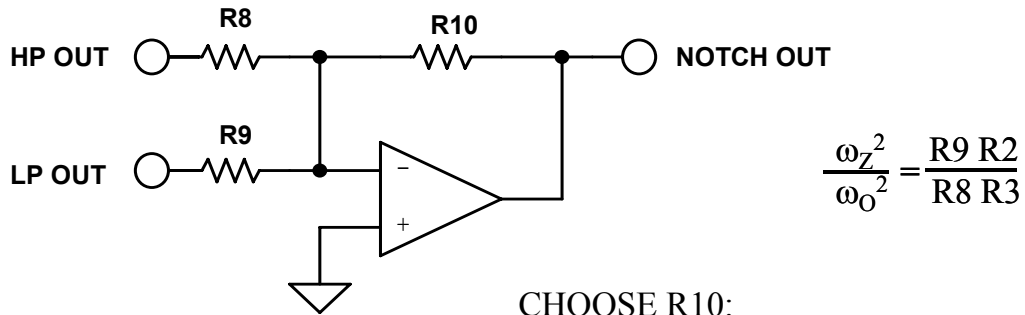
$$R_6 = \\ R_7 \sqrt{R_2 R_3} Q \left(\frac{1}{\frac{1}{R_1} + \frac{1}{R_2} + \frac{1}{R_3}} \right)$$

Figure 8.73A: State Variable Design Equations

■ BASIC LINEAR DESIGN

STATE VARIABLE (B)

FOR NOTCH:



CHOOSE A_{HP} , A_{LP} , $A_{NOTCH} = 1$:

$$\text{FOR } \omega_z = \omega_0: R8 = R9 = R10$$

$$\text{FOR } \omega_z < \omega_0: R9 = R10$$

$$R8 = \frac{\omega_0^2}{\omega_z^2} R10$$

$$\text{FOR } \omega_z > \omega_0: R8 = R10$$

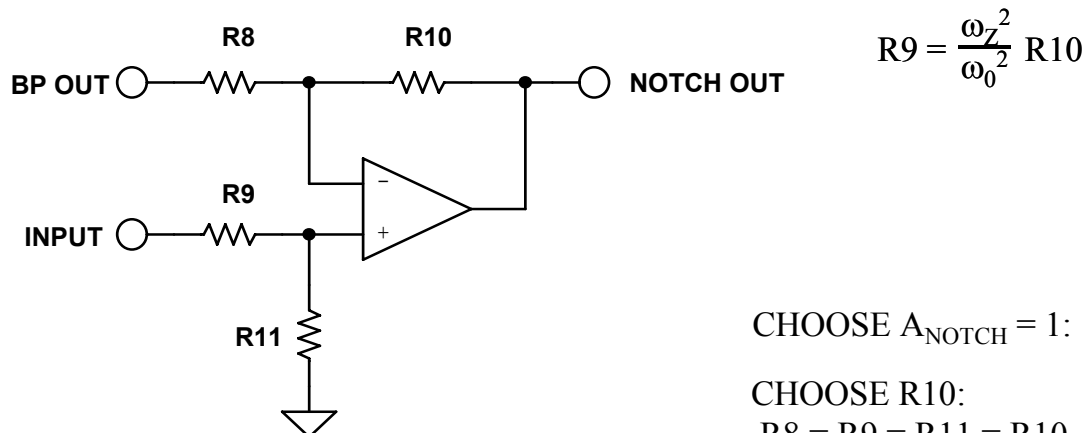
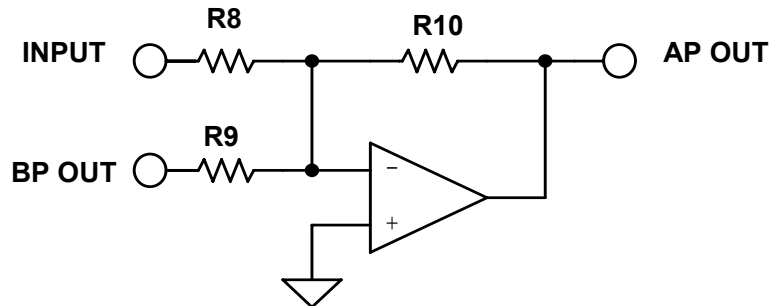


Figure 8.73B: State Variable Design Equations

STATE VARIABLE (C)

ALLPASS



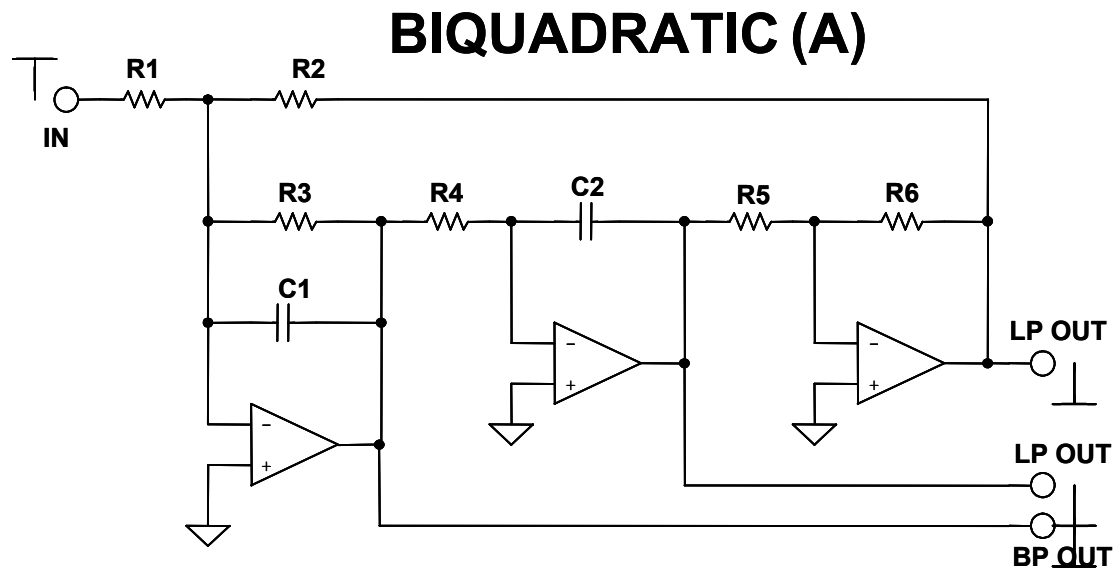
$$H = 1$$

$$R8 = R10$$

$$R9 = R8/2$$

Figure 7-73C: State Variable Design Equations

■ BASIC LINEAR DESIGN



CHOOSE C, R2, R5

$$K = 2 \pi f_0 C$$

$$C_1 = C_2 = C$$

$$R_1 = \frac{R_2}{H}$$

$$R_3 = \frac{1}{k \alpha}$$

$$R_4 = \frac{1}{k^2 R_2}$$

$$R_5 = R_6$$

HIGHPASS

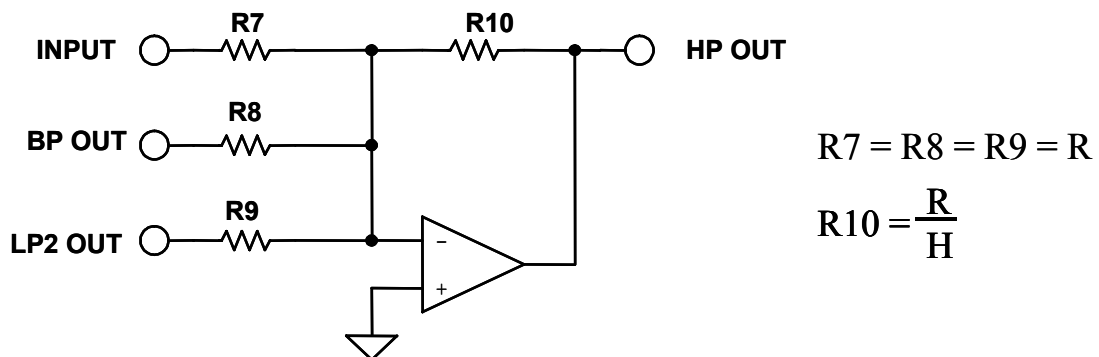


Figure 8.74A: Biquad Design Equations

BIBOQUADRATIC (B)

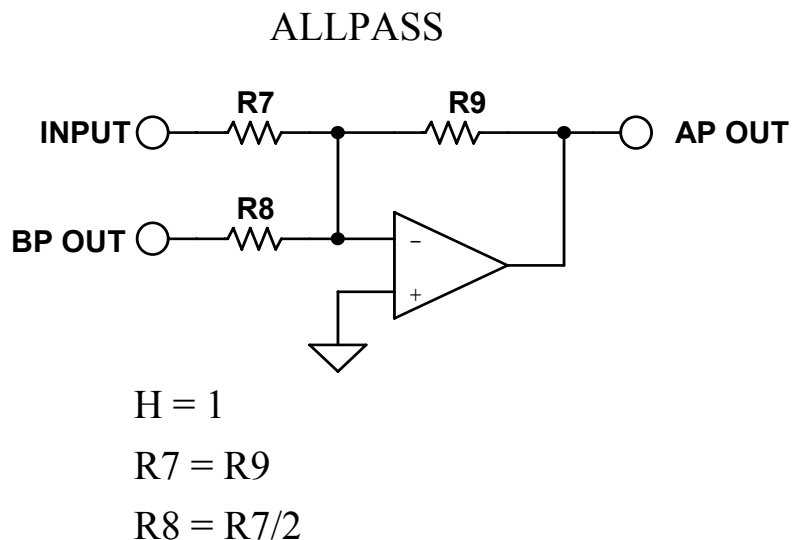
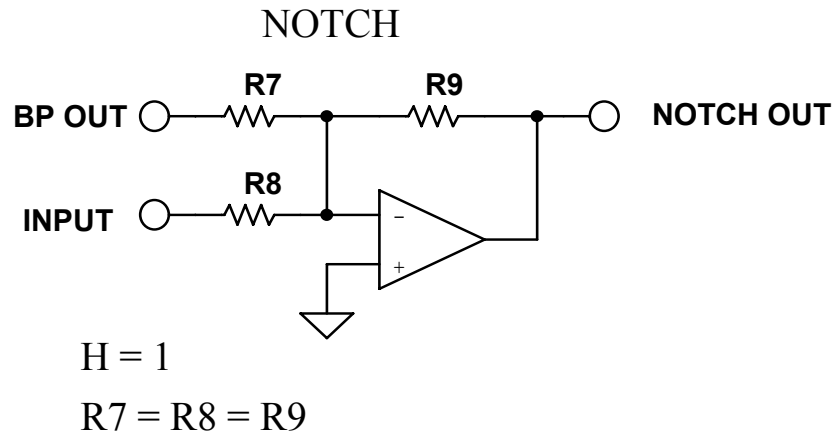
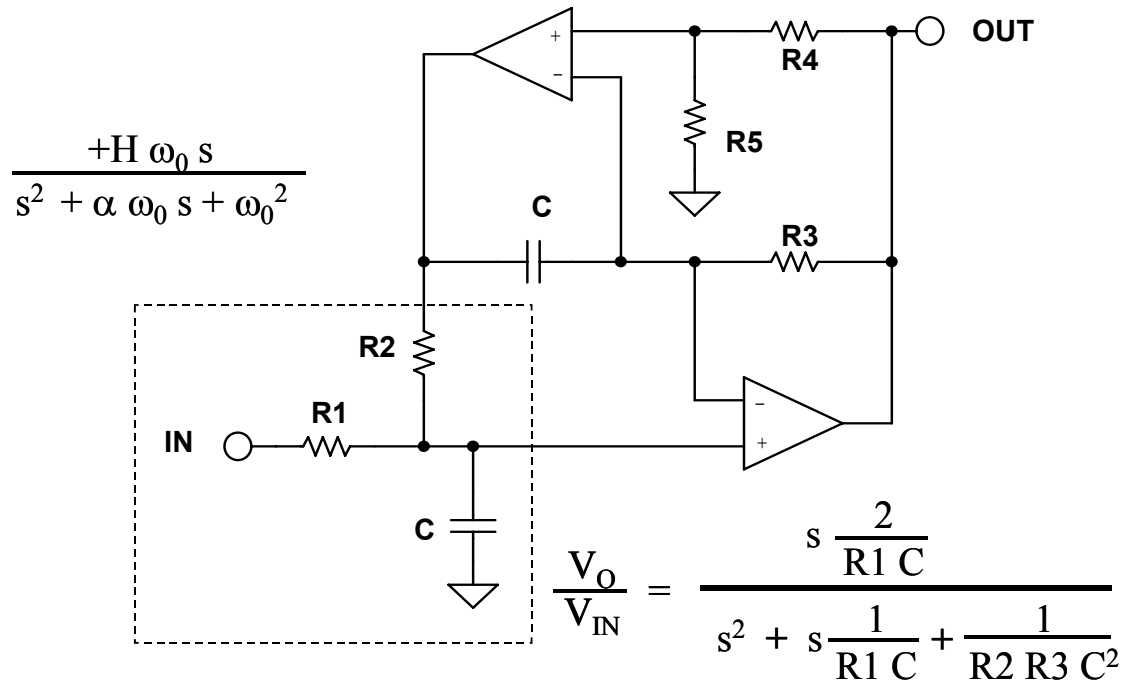


Figure 8.74B: Biquad Design Equations

DUAL AMPLIFIER BANDPASS



CHOOSE: C R4

THEN:

$$R = \frac{1}{2 \pi F_0 C}$$

$$R5 = R4$$

$$R1 = Q R$$

$$R2 = R3 = R$$

FOR GAINS LESS THAN 2 (GAIN = A_V):

$$R1A = \frac{2R1}{A_V}$$

$$R1B = \frac{R1A A_V}{2 - A_V}$$

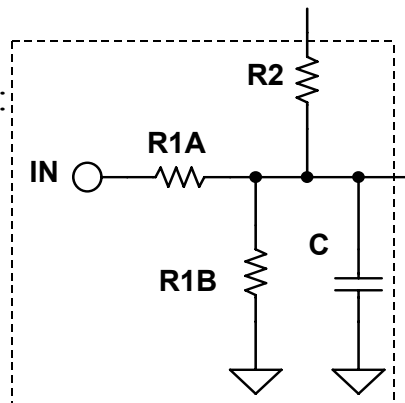
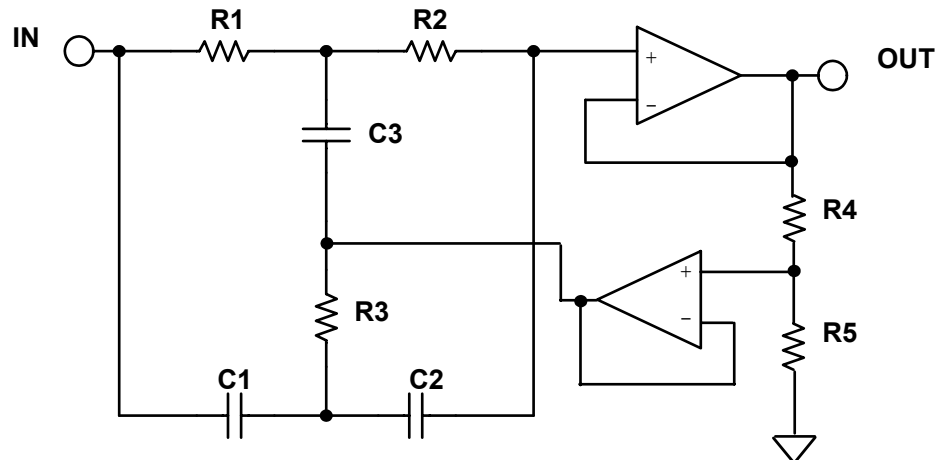


Figure 8.75: Dual Amplifier Band-Pass Design Equations

TWIN T NOTCH


$$\frac{V_0}{V_{IN}} = \frac{s^2 + \frac{1}{RC}}{s^2 + \frac{1}{RC} 4 \left(1 - \frac{R5}{R4+R5}\right)s + \frac{1}{RC}}$$

$$\frac{s^2 + \omega_0^2}{s^2 + 4\omega_0(1-K)s + \omega_0^2}$$

CHOOSE: C

R'

$$k = 2\pi F_0 C$$

$$R4 = (1 - K) R'$$

$$R = \frac{1}{k}$$

$$R5 = K R'$$

$$R = R1 = R2 = 2 R3$$

$$K = 1 - \frac{1}{4Q}$$

$$C = C1 = C2 = \frac{C3}{2}$$

$$F_0 = \frac{1}{2\pi RC}$$

for K = 1, eliminate R4 and R5

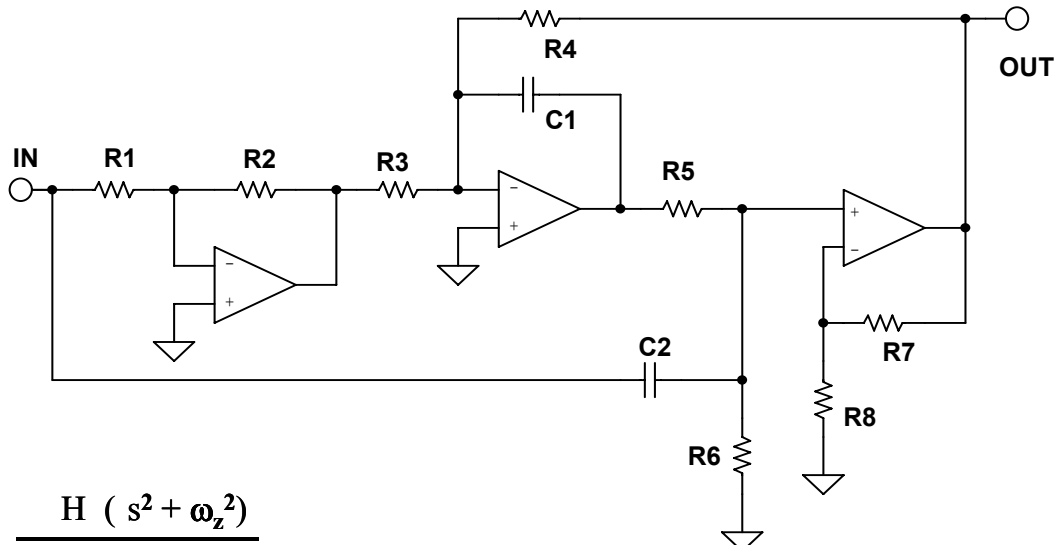
 (i.e R5 \rightarrow 0, Q $\rightarrow \infty$)

 for R \gg R4, eliminate buffer

Figure 8.76: Twin-T Notch Design Equations

■ BASIC LINEAR DESIGN

BAINTER NOTCH



$$\frac{H(s^2 + \omega_z^2)}{s^2 + \frac{\omega_0}{Q}s + \omega_0^2}$$

$$\frac{V_{\text{OUT}}}{V_{\text{IN}}} = \frac{K_2 * \left[s^2 + \frac{K_1}{R_3 R_5 C_1 C_2} \right]}{s^2 + \frac{(R_5 + R_6)}{R_5 R_6 C_2} s + \frac{K_2}{R_4 R_5 C_1 C_2}}$$

CHOOSE C1, R1, R7, K1, K2

$$C_2 = C_1 = C$$

$$k = 2 \pi F_0 C$$

$$R_2 = K_1 * R_1$$

$$Z = \left(\frac{\omega_z}{\omega_0} \right)^2$$

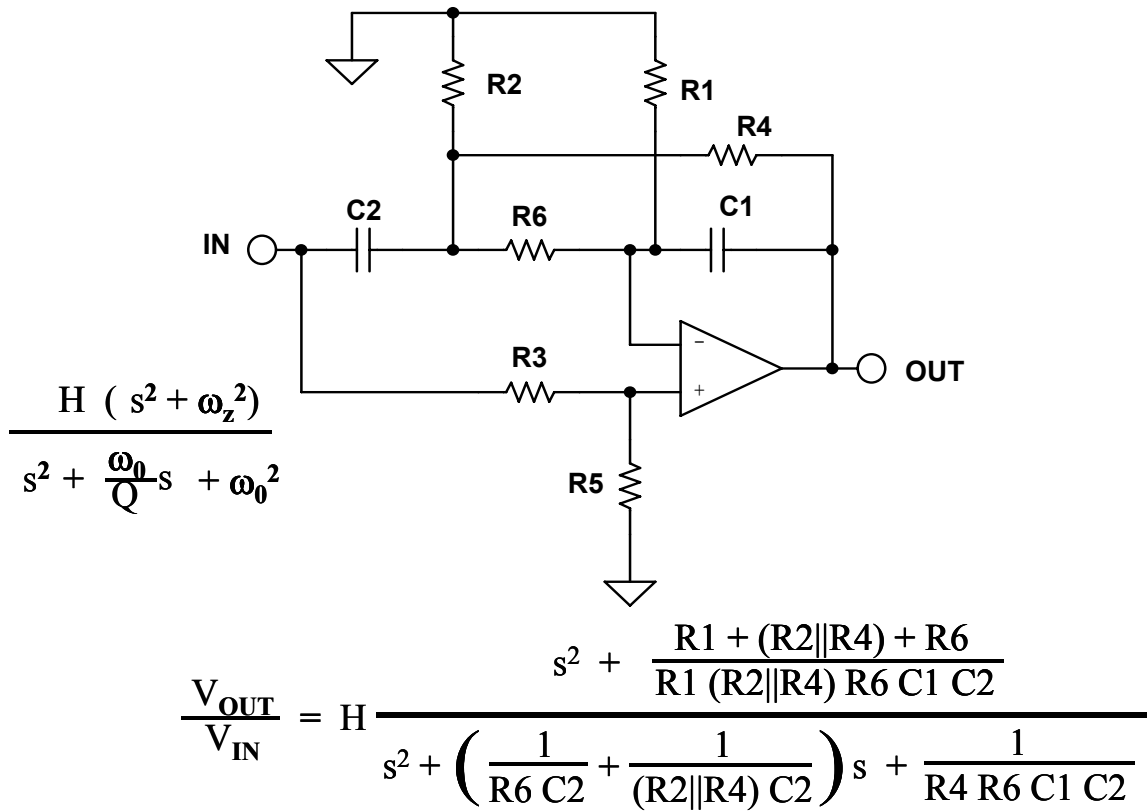
$$R_3 = \frac{K_1}{2 Z Q k}$$

$$R_4 = \frac{K_2}{2 Q k}$$

$$R_5 = R_6 = \frac{2 Q}{k}$$

$$R_8 = (K_2 - 1) R_7$$

Figure 8.77: Bainter Notch Design Equations

**BOCTOR NOTCH
LOWPASS**


GIVEN ω_0 , ω_z , Q_0

CHOOSE $R6$ $R5$ $C1$

$$R4 = \frac{1}{\omega_0 C1 2Q_0}$$

$$R3 = \left(\frac{R6}{R1} + 2 \frac{C1}{C2} \right) R5$$

$$R2 = \frac{R4 R6}{R4 = R6}$$

$$C2 = 4 Q_0^2 \frac{R4}{R6} C1$$

$$R1 = \frac{1}{2} \left(\frac{R6}{R4} \frac{\omega_z^2}{\omega_0^2} - 1 \right)$$

Figure 8.78: Boctor Notch, Low-Pass, Design Equations

■ BASIC LINEAR DESIGN

BOCTOR NOTCH

HIGHPASS (A)

$$\frac{H (s^2 + \omega_z^2)}{s^2 + \frac{\omega_0}{Q} s + \omega_0^2}$$

$$Q < \frac{1}{\frac{F_z^2}{1 - \frac{F_0^2}{F_z^2}}}$$

$$\frac{V_{OUT}}{V_{IN}} = \frac{\left(1 + \frac{R5}{R4}\right) \left(s^2 + \frac{1}{R1 R2 C1 C2}\right)}{s^2 + \left[\frac{1}{R_{EQ1} C1} \left(1 - \frac{R_{EQ1} R_{EQ2}}{R1 R2}\right)\right] s + \frac{1}{R_{EQ1} R_{EQ2} C1 C2}}$$

WHERE: $R_{EQ1} = R1 \parallel R3 \parallel R6$
 $R_{EQ2} = R2 + (R4 \parallel R5)$

GIVEN: $F_z \ F_0 \ H$

or

$F_z \ Q \ H$

$$Q = \frac{1}{\sqrt{2} \left(\frac{F_z^2}{F_0^2} - 1 \right)}$$

$$F_0 = F_z \sqrt{\frac{1}{1 - \frac{1}{2Q^2}}}$$

$$Y = \frac{1}{Q \left(1 - \frac{F_z^2}{F_0^2} \right)}$$

Figure 8.79A: Boctor Notch, High- Pass, Design Equations

BOCTOR NOTCH

HIGHPASS (B)

GIVEN: C, R₂, R₃

$$C_1 = C_2 = C$$

$$R_{EQ1} = \frac{1}{C Y 2\pi F_0}$$

$$R_{EQ2} = Y^2 R_{EQ1}$$

$$R_4 = R_{EQ2} - R_2 \left(\frac{H}{H-1} \right)$$

$$R_5 = (H-1) R_4$$

$$R_1 = \frac{1}{(2\pi F_0)^2 R_2 C^2}$$

$$R_6 = R_{EQ1}$$

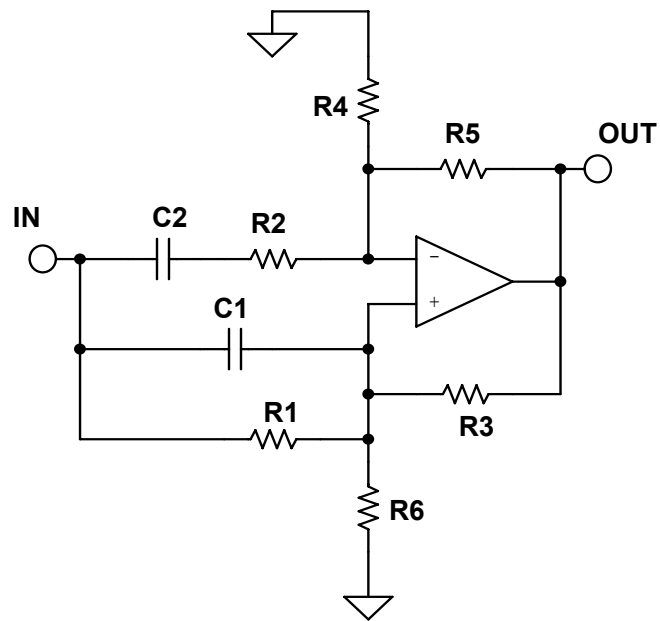
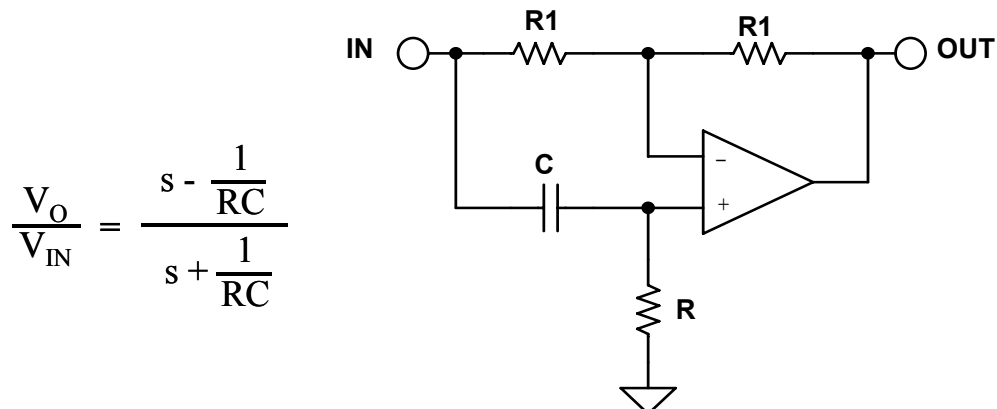


Figure 8.79-B: Boctor Notch, High-Pass, Design Equations (continued)

■ BASIC LINEAR DESIGN

FIRST ORDER ALLPASS



$$\frac{V_O}{V_{IN}} = \frac{s - \frac{1}{RC}}{s + \frac{1}{RC}}$$

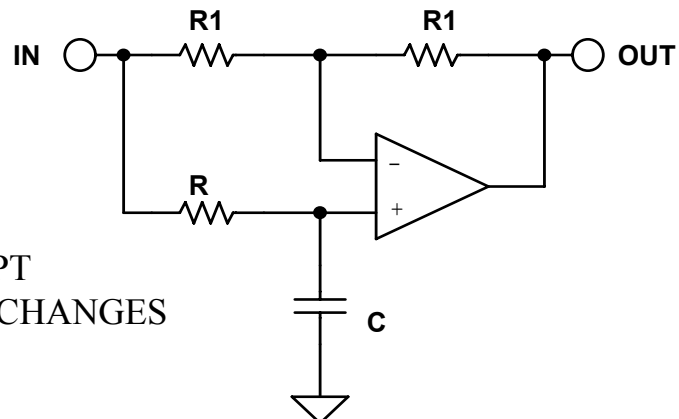
PHASE SHIFT (ϕ) = $-2 \tan^{-1}\left(\frac{RC}{2\pi F}\right)$

GROUP DELAY = $\frac{2RC}{(2\pi F RC)^2 + 1}$

DELAY AT DC = $2RC$

GIVEN A PHASE SHIFT OF ϕ AT A FREQUENCY = F

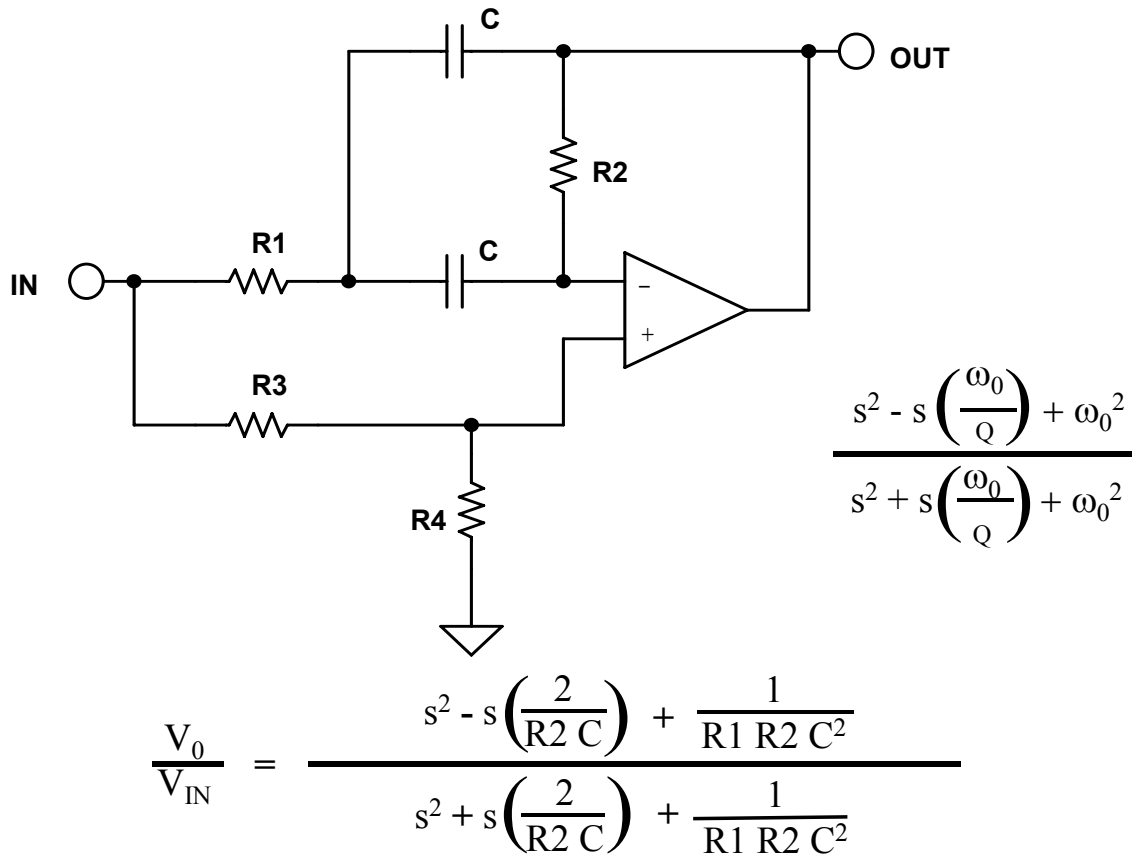
$$RC = 2\pi F \tan\left(-\frac{\phi}{2}\right)$$



DESIGN AS ABOVE EXCEPT
THE SIGN OF THE PHASE CHANGES

Figure 8.80: First Order All-Pass Design Equations

SECOND ORDER ALLPASS



CHOOSE: C

.....

$$k = 2 \pi F_0 C$$

$$R_2 = \frac{2 Q}{k}$$

$$R_1 = \frac{1}{2 k Q}$$

$$R_3 = R_1$$

$$R_4 = \frac{Q}{2}$$

Figure 8.81: Second Order All-Pass Design Equation

▣ BASIC LINEAR DESIGN

Notes:

SECTION 8.7: PRACTICAL PROBLEMS IN FILTER IMPLEMENTATION

In the previous sections filters were dealt with as mathematical functions. The filter designs were assumed to have been implemented with "perfect" components. When the filter is built with real-world components design tradeoffs must typically be made.

In building a filter with an order greater than two, multiple second and/or first order sections are used. The frequencies and Qs of these sections must align precisely or the overall response of the filter will be affected. For example, the antialiasing filter design example in the next section is a 5th-order Butterworth filter, made up of a second order section with a frequency (F_0) = 1 and a $Q = 1.618$, a second order section with a frequency (F_0) = 1 and a $Q = 0.618$, and a first order section with a frequency (F_0) = 1 (for a filter normalized to 1 rad/sec). If the Q or frequency response of any of the sections is off slightly, the overall response will deviate from the desired response. It may be close, but it won't be exact. As is typically the case with engineering, a decision must be made as to what tradeoffs should be made. For instance, do we really need a particular response exactly? Is there a problem if there is a little more ripple in the pass-band? Or if the cutoff frequency is at a slightly different frequency? These are the types of questions that face a designer, and will vary from design to design.

Passive Components (Resistors, Capacitors, Inductors)

Passive components are the first problem. When designing filters, the calculated values of components will most likely not be available commercially. Resistors, capacitors, and inductors come in standard values. While custom values can be ordered, the practical tolerance will probably still be $\pm 1\%$ at best. An alternative is to build the required value out of a series and/or parallel combination of standard values. This increases the cost and size of the filter. Not only is the cost of components increased, so are the manufacturing costs, both for loading and tuning the filter. Furthermore, success will be still limited by the number of parts that are used, their tolerance, and their tracking, both over temperature and time.

A more practical way is to use a circuit analysis program to determine the response using standard values. The program can also evaluate the effects of component drift over temperature. The values of the sensitive components are adjusted using parallel combinations where needed, until the response is within the desired limits. Many of the higher end filter CAD programs include this feature.

The resonant frequency and Q of a filter are typically determined by the component values. Obviously, if the component value is drifting, the frequency and the Q of the filter will drift which, in turn, will cause the frequency response to vary. This is especially true in higher order filters.

■ BASIC LINEAR DESIGN

Higher order implies higher Q sections. Higher Q sections means that component values are more critical, since the Q is typically set by the ratio of two or more components, typically capacitors.

In addition to the initial tolerance of the components, you must also evaluate effects of temperature/time drift. The temperature coefficients of the various components may be different in both magnitude and sign. Capacitors, especially, are difficult in that not only do they drift, but the temperature coefficient (TC) is also a function of temperature, as shown in Figure 8.82. This represents the temperature coefficient of a (relatively) poor film capacitor, which might be typical for a polyester or polycarbonate type. *Linear TC* in film capacitors can be found in the polystyrene, polypropylene, and Teflon dielectrics. In these types TC is on the order of 100 ppm/ $^{\circ}\text{C}$ to 200 ppm/ $^{\circ}\text{C}$, and if necessary, this can be compensated with a complementary TC elsewhere in the circuit.

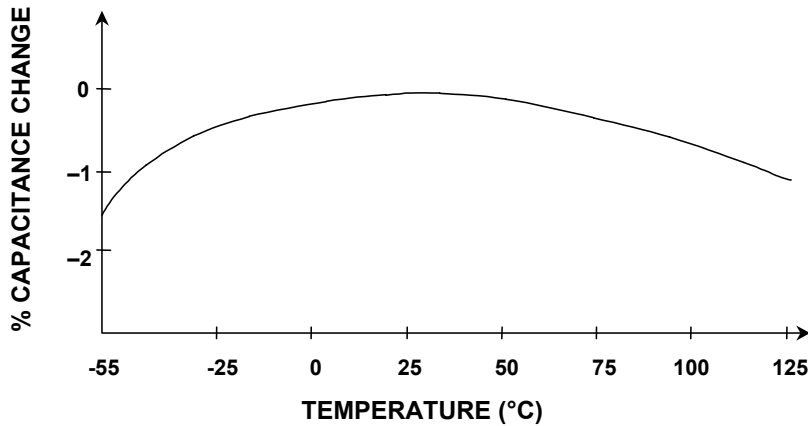


Figure 8.82: A Poor Film Capacitor Temperature Coefficient

The lowest TC dielectrics are NPO (or COG) ceramic ($\pm 30 \text{ ppm}/^{\circ}\text{C}$), and polystyrene ($-120 \text{ ppm}/^{\circ}\text{C}$). Some capacitors, mainly the plastic film types, such as polystyrene and polypropylene, also have a limited temperature range.

While there is infinite choice of the values of the passive components for building filters, in practice there are physical limits. Capacitor values below 10 pF and above 10 μF are not practical. Electrolytic capacitors should be avoided. Electrolytic capacitors are typically very leaky. A further potential problem is if they are operated without a polarizing voltage, they become nonlinear when the ac voltage reverse biases them. Even with a dc polarizing voltage, the ac signal can reduce the instantaneous voltage to 0 V or below. Large values of film capacitors are physically very large.

Resistor values of less than 100Ω should be avoided, as should values over $1 \text{ M}\Omega$. Very low resistance values (under 100Ω) can require a great deal of drive current and dissipate a great deal of power. Both of these should be avoided. And low values and very large values of resistors may not be as readily available. Very large values tend to be more prone to parasitics since smaller capacitances will couple more easily into larger impedance levels. Noise also increases with the square root of the resistor value. Larger

ANALOG FILTERS
PRACTICAL PROBLEMS IN FILTER IMPLEMENTATION

value resistors also will cause larger offsets due to the effects of the amplifier bias currents.

Parasitic capacitances due to circuit layout and other sources affect the performance of the circuit. They can form between two traces on a PC board (on the same side or opposite side of the board), between leads of adjacent components, and just about everything else you can (and in most cases can't) think of. These capacitances are usually small, so their effect is greater at high impedance nodes. Thus, they can be controlled most of the time by keeping the impedance of the circuits down. Remember that the effects of stray capacitance are frequency dependent, being worse at high frequencies because the impedance drops with increasing frequency.

Parasitics are not just associated with outside sources. They are also present in the components themselves.

A capacitor is more than just a capacitor in most instances. A real capacitor has inductance (from the leads and other sources) and resistance as shown in Figure 8.83. This resistance shows up in the specifications as leakage and poor power factor. Obviously, we would like capacitors with very low leakage and good power factor (see Figure 8.84).

In general, it is best to use plastic film (preferably Teflon or polystyrene) or mica capacitors and metal film resistors, both of moderate to low values in our filters.

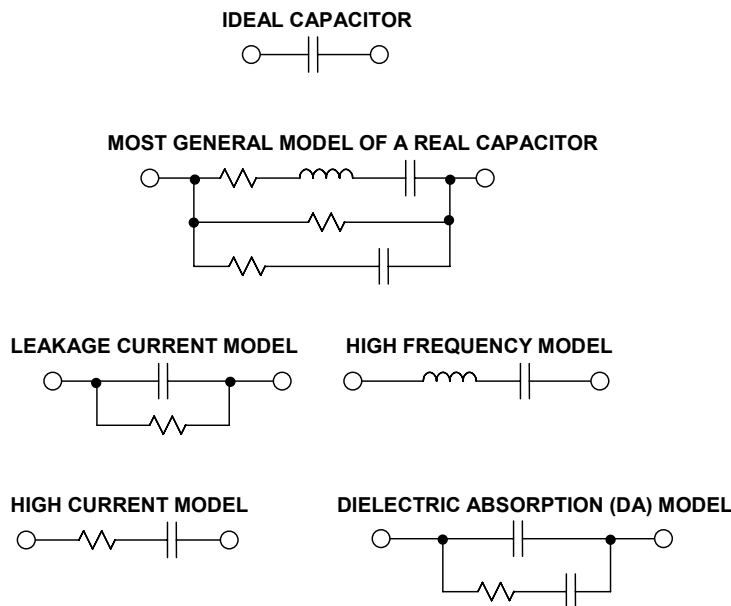


Figure 8.83: Capacitor Equivalent Circuit

One way to reduce component parasitics is to use surface mounted devices. Not having leads means that the lead inductance is reduced. Also, being physically smaller allows more optimal placement. A disadvantage is that not all types of capacitors are available in surface mount. Ceramic capacitors are popular surface mount types, and of these, the NPO family has the best characteristics for filtering. Ceramic capacitors may also be prone to microphonics. Microphonics occurs when the capacitor turns into a motion

■ BASIC LINEAR DESIGN

sensor, similar to a strain gauge, and turns vibration into an electrical signal, which is a form of noise.

Resistors also have parasitic inductances due to leads and parasitic capacitance. The various qualities of resistors are compared in Figure 8.85

RESISTOR COMPARISON CHART

	TYPE	ADVANTAGES	DISADVANTAGES
DISCRETE	Carbon Composition	Lowest Cost High Power/Small Case Size Wide Range of Values	Poor Tolerance (5%) Poor Temperature Coefficient (1500 ppm/°C)
	Wirewound	Excellent Tolerance (0.01%) Excellent TC (1 ppm/°C) High Power	Reactance is a Problem Large Case Size Most Expensive
	Metal Film	Good Tolerance (0.1%) Good TC (<1 to 100 ppm/°C) Moderate Cost Wide Range of Values Low Voltage Coefficient	Must be Stabilized with Burn-In Low Power
	Bulk Metal or Metal Foil	Excellent Tolerance (to 0.005%) Excellent TC (to <1 ppm/°C) Low Reactance Low Voltage Coefficient	Low Power Very Expensive
	High Mega Ohm	Very High Values ($10^8 \Omega$ to $10^{14} \Omega$) Only Choice for Some Circuits	High Voltage Coefficient (200 ppm/V) Fragile Glass Case (Needs Special Handling) Expensive
NETWORKS	Thick Film	Low Cost High Power Laser-Trimmable Readily Available	Fair Matching (0.1%) Poor TC (>100 ppm/°C) Poor Tracking TC (10 ppm/°C)
	Thin Film	Good Matching (<0.01%) Good TC (<100 ppm/°C) Good Tracking TC (2 ppm/°C) Moderate Cost Laser-Trimmable Low Capacitance Suitable for Hybrid IC Substrate	Often Large Geometry Limited Values and Configurations

Figure 8.84: Resistor Comparison Chart

CAPACITOR COMPARISON CHART

TYPE	TYPICAL DA	ADVANTAGES	DISADVANTAGES
Polystyrene	0.001% to 0.02%	Inexpensive Low DA Good stability (~120ppm/ $^{\circ}$ C)	Damaged by temperature > +85 $^{\circ}$ C Large High inductance Vendors limited
Polypropylene	0.001% to 0.02%	Inexpensive Low DA Stable (~200ppm/ $^{\circ}$ C) Wide range of values	Damaged by temperature > +105 $^{\circ}$ C Large High inductance
Teflon	0.003% to 0.02%	Low DA available Good stability Operational above +125 $^{\circ}$ C Wide range of values	Expensive Large High inductance
Polycarbonate	0.1%	Good stability Low cost Wide temperature range Wide range of values	Large DA limits to 8-bit applications High inductance
Polyester	0.3% to 0.5%	Moderate stability Low cost Wide temperature range Low inductance (stacked film)	Large DA limits to 8-bit applications High inductance (conventional)
NP0 Ceramic	<0.1%	Small case size Inexpensive, many vendors Good stability (30ppm/ $^{\circ}$ C) 1% values available Low inductance (chip)	DA generally low (may not be specified) Low maximum values (10nF)
Monolithic Ceramic (High K)	>0.2%	Low inductance (chip) Wide range of values	Poor stability Poor DA High voltage coefficient
Mica	>0.003%	Low loss at HF Low inductance Good stability 1% values available	Quite large Low maximum values (10nF) Expensive
Aluminum Electrolytic	Very high	Large values High currents High voltages Small size	High leakage Usually polarized Poor stability, accuracy Inductive
Tantalum Electrolytic	Very high	Small size Large values Medium inductance	High leakage Usually polarized Expensive Poor stability, accuracy

Figure 8.85: Capacitor Comparison Chart

■ BASIC LINEAR DESIGN

Limitations of Active Elements (Op Amps) in Filters

The active element of the filter will also have a pronounced effect on the response. In developing the various topologies (Multiple Feedback, Sallen-Key, State Variable, etc.), the active element was always modeled as a "perfect" operational amplifier. That is to say it has:

- 1) infinite gain
- 2) infinite input impedance
- 3) zero output impedance

none of which vary with frequency. While amplifiers have improved a great deal over the years, this model has not yet been realized.

The most important limitation of the amplifier has to do with its gain variation with frequency. All amplifiers are band limited. This is due mainly to the physical limitations of the devices with which the amplifier is constructed. Negative feedback theory tells us that the response of an amplifier must be first order (-6 dB per octave) when the gain falls to unity in order to be stable. To accomplish this, a real pole is usually introduced in the amplifier so the gain rolls off to <1 by the time the phase shift reaches 180° (plus some phase margin, hopefully). This roll off is equivalent to that of a single-pole filter. So in simplistic terms, the transfer function of the amplifier is added to the transfer function of the filter to give a composite function. How much the frequency dependent nature of the op amp affects the filter is dependent on which topology is used as well as the ratio of the filter frequency to the amplifier bandwidth.

The Sallen-Key configuration, for instance, is the least dependent on the frequency response of the amplifier. All that is required is for the amplifier response to be flat to just past the frequency where the attenuation of the filter is below the minimum attenuation required. This is because the amplifier is used as a gain block. Beyond cutoff, the attenuation of the filter is reduced by the rolloff of the gain of the op amp. This is because the output of the amplifier is phase shifted, which results in incomplete nulling when fed back to the input. There is also an issue with the output impedance of the amplifier rising with frequency as the open loop gain rolls off. This causes the filter to lose attenuation.

The state variable configuration uses the op amps in two modes, as amplifiers and as integrators. As amplifiers, the constraint on frequency response is basically the same as for the Sallen-Key, which is flat out to the minimum attenuation frequency. As an integrator, however, more is required. A good rule of thumb is that the open-loop gain of the amplifier must be greater than 10 times the closed-loop gain (including peaking from the Q of the circuit). This should be taken as the absolute minimum requirement. What this means is that there must be 20 dB loop gain, minimum. Therefore, an op amp with 10 MHz unity gain bandwidth is the minimum required to make a 1 MHz integrator. What happens is that the effective Q of the circuit increases as loop gain decreases. This phenomenon is called Q enhancement. The mechanism for Q enhancement is similar to that of slew rate limitation. Without sufficient loop gain, the op amp virtual ground is no

longer at ground. In other words, the op amp is no longer behaving as an op amp. Because of this, the integrator no longer behaves like an integrator.

The multiple feedback configuration also places heavy constraints on the active element. Q enhancement is a problem in this topology as well. As the loop gain falls, the Q of the circuit increases, and the parameters of the filter change. The same rule of thumb as used for the integrator also applies to the multiple feedback topology (loop gain should be at least 20 dB). The filter gain must also be factored into this equation.

In the FDNR realization, the requirements for the op amps are not as clear. To make the circuit work, we assume that the op amps will be able to force the input terminals to be the same voltage. This implies that the loop gain be a minimum of 20 dB at the resonant frequency.

Also it is generally considered to be advantageous to have the two op amps in each leg matched. This is easily accomplished using dual op amps. It is also a good idea to have low bias current devices for the op amps, so FET input op amps should be used, all other things being equal.

In addition to the frequency dependent limitations of the op amp, several others of its parameters may be important to the filter designer.

One is input impedance. We assume in the "perfect" model that the input impedance is infinite. This is required so that the input of the op amp does not load the network around it. This means that we probably want to use FET amplifiers with high impedance circuits.

There is also a small frequency dependent term to the input impedance, since the effective impedance is the real input impedance multiplied by the loop gain. This usually is not a major source of error, since the network impedance of a high frequency filter should be low.

Distortion Resulting from Input Capacitance Modulation

Another subtle effect can be noticed with FET input amps. The input capacitance of a FET changes with the applied voltage. When the amplifier is used in the inverting configuration, such as with the multiple feedback configuration, the applied voltage is held to 0 V. Therefore there is no capacitance modulation. However, when the amplifier is used in the noninverting configuration, such as in the Sallen-Key circuit, this form of distortion can exist.

There are two ways to address this issue. The first is to keep the equivalent impedance low. The second is to balance the impedance seen by the inputs. This is accomplished by adding a network into the feedback leg of the amplifier which is equal to the equivalent input impedance. Note that this will only work for a unity gain application.

■ BASIC LINEAR DESIGN

As an example, which is taken from the OP176 data sheet, a 1 kHz high-pass Sallen-Key filter is shown (Figure 8.86). Figure 8.87 shows the distortion for the uncompensated version (curve A1) as well as with the compensation (curve A2). Also shown is the same circuit with the impedances scaled up by a factor of 10 (B1 uncompensated, B2 compensated). Note that the compensation improves the distortion, but not as much as having low impedance to start with.

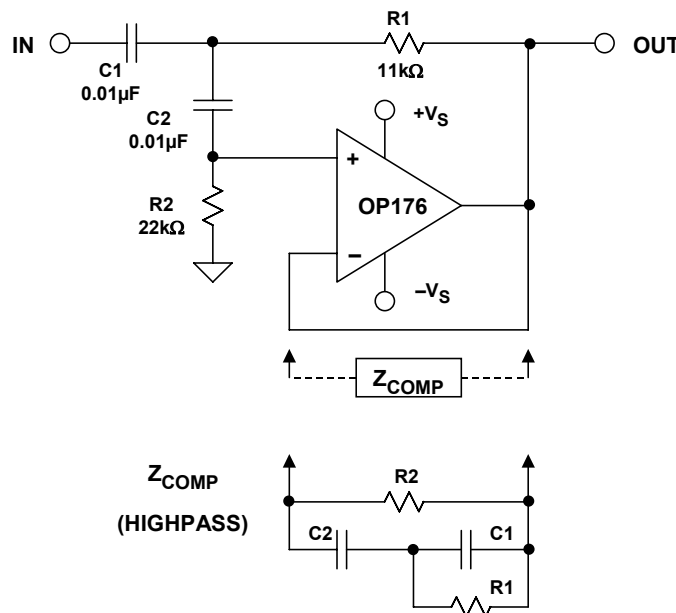


Figure 8.86: Compensation for Input Capacitance Voltage Modulation

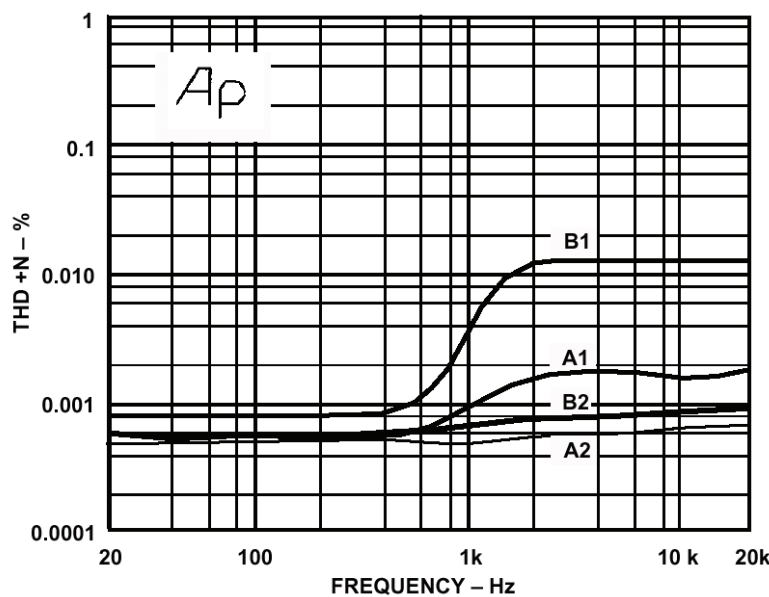


Figure 8.87: Distortion Due to Input Capacitance Modulation

Similarly, the op amp output impedance affects the response of the filter. The output impedance of the amplifier is divided by the loop gain, therefore the output impedance will rise with increasing frequency. This may have an effect with high frequency filters if the output impedance of the stage driving the filter becomes a significant portion of the network impedance.

The fall of loop gain with frequency can also affect the distortion of the op amp, since there is less loop gain available for correction. In the multiple feedback configuration the feedback loop is also frequency dependent, which may further reduce the feedback correction, resulting in increased distortion. This effect is counteracted somewhat by the reduction of distortion components in the filter network (assuming a low-pass or band-pass filter).

All of the discussion so far is based on using classical voltage feedback op amps. Current feedback, or transimpedance, op amps offer improved high frequency response, but are unusable in any topologies discussed except the Sallen-Key. The problem is that capacitance in the feedback loop of a current feedback amplifier usually causes it to become unstable. Also, most current feedback amplifiers will only drive a small capacitive load. Therefore, it is difficult to build classical integrators using current feedback amplifiers. Some current feedback op amps have an external pin that may be used to configure them as a very good integrator, but this configuration does not lend itself to classical active filter designs.

Current feedback integrators tend to be noninverting, which is not acceptable in the state variable configuration. Also, the bandwidth of a current feedback amplifier is set by its feedback resistor, which would make the Multiple Feedback topology difficult to implement. Another limitation of the current feedback amplifier in the Multiple Feedback configuration is the low input impedance of the inverting terminal. This would result in loading of the filter network. Sallen-Key filters are possible with current feedback amplifiers, since the amplifier is used as a noninverting gain block. New topologies that capitalize on the current feedback amplifiers superior high frequency performance and compensate for its limitations will have to be developed.

Q Peaking and Q Enhancement

The last thing that you need to be aware of is exceeding the dynamic range of the amplifier. Qs over 0.707 will cause peaking in the response of the filter (see Figures 8.5 through 8.7). For high Q's, this could cause overload of the input or output stages of the amplifier with a large input. Note that relatively small values of Q can cause significant peaking. The Q times the gain of the circuit must stay under the loop gain (plus some margin, again, 20 dB is a good starting point). This holds for multiple amplifier topologies as well. Be aware of internal node levels, as well as input and output levels. As an amplifier overloads, its effective Q decreases, so the transfer function will appear to change even if the output appears undistorted. This shows up as the transfer function changing with increasing input level.

■ BASIC LINEAR DESIGN

We have been dealing mostly with low-pass filters in our discussions, but the same principles are valid for high-pass, band-pass, and band-reject as well. In general, things like Q enhancement and limited gain/bandwidth will not affect high-pass filters, since the resonant frequency will hopefully be low in relation to the cutoff frequency of the op amp. Remember, though, that the high-pass filter will have a low-pass section, by default, at the cutoff frequency of the amplifier. Band-pass and band-reject (notch) filters will be affected, especially since both tend to have high values of Q.

The general effect of the op amp's frequency response on the filter Q is shown in Figure 8.88.

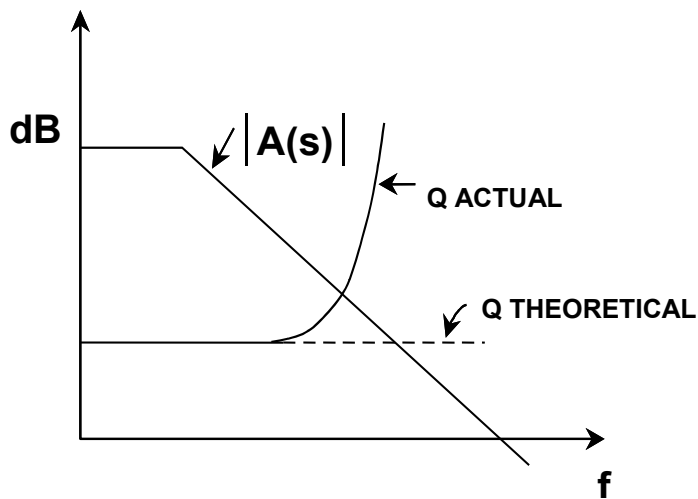


Figure 8.88: Q Enhancement

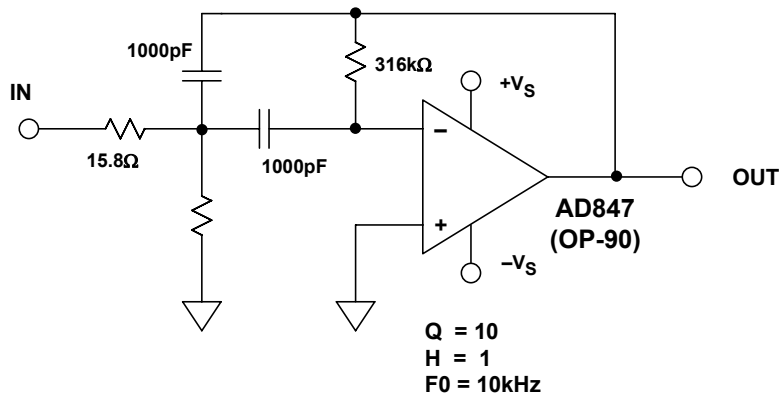


Figure 8.89: 1 kHz Multiple Feedback Band-Pass Filter

As an example of the Q enhancement phenomenon, consider the Spice simulation of a 10 kHz band-pass multiple feedback filter with $Q = 10$ and gain = 1, using a good high frequency amplifier (the AD847) as the active device. The circuit diagram is shown in Figure 8.89. The open-loop gain of the AD847 is greater than 70 dB at 10 kHz as shown

ANALOG FILTERS
PRACTICAL PROBLEMS IN FILTER IMPLEMENTATION

in Figure 8.91(A). This is well over the 20 dB minimum, so the filter works as designed as shown in Figure 8.90.

We now replace the AD847 with an OP-90. The OP-90 is a dc precision amplifier and so has a limited bandwidth. In fact, its open-loop gain is less than 10 dB at 10 kHz (see Figure 8.91(B)). This is not to imply that the AD847 is in all cases better than the OP-90. It is a case of misapplying the OP-90.

From the output for the OP-90, also shown in Figure 8.90, we see that the magnitude of the output has been reduced, and the center frequency has shifted downward.

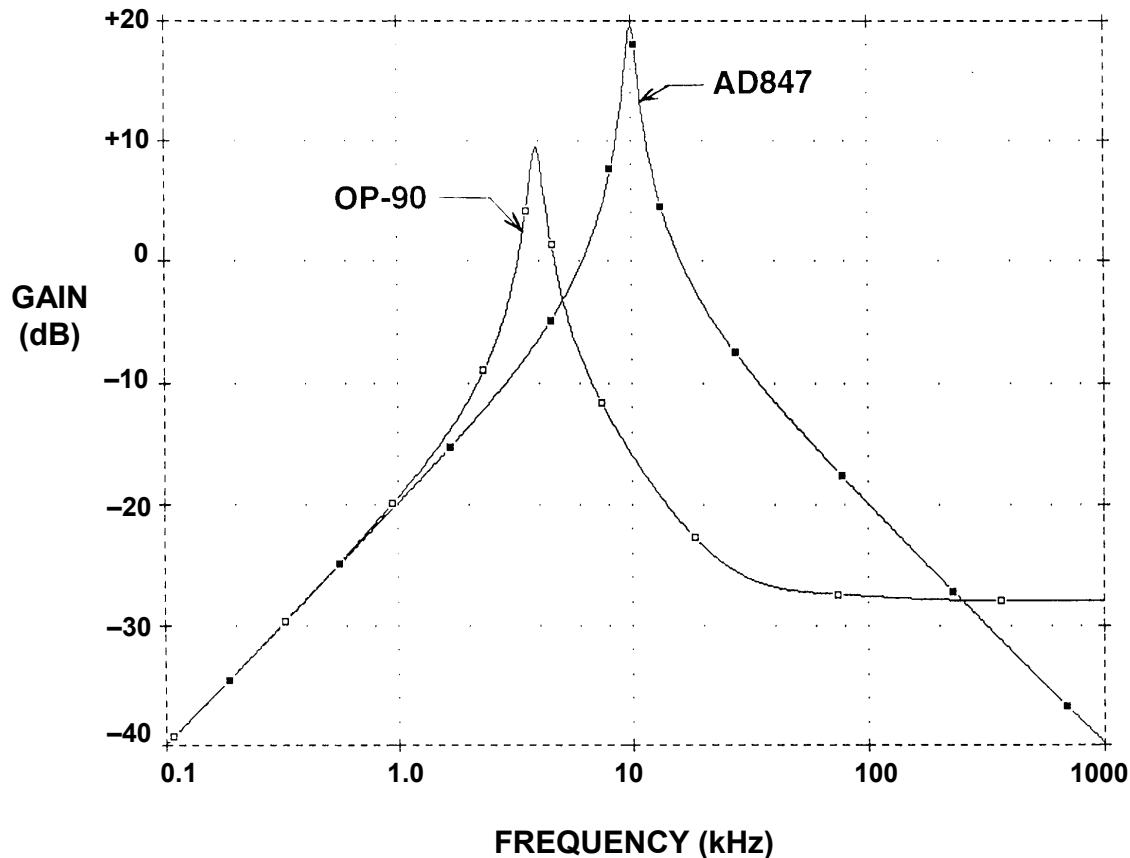


Figure 8.90: Effects of "Q Enhancement"

■ BASIC LINEAR DESIGN

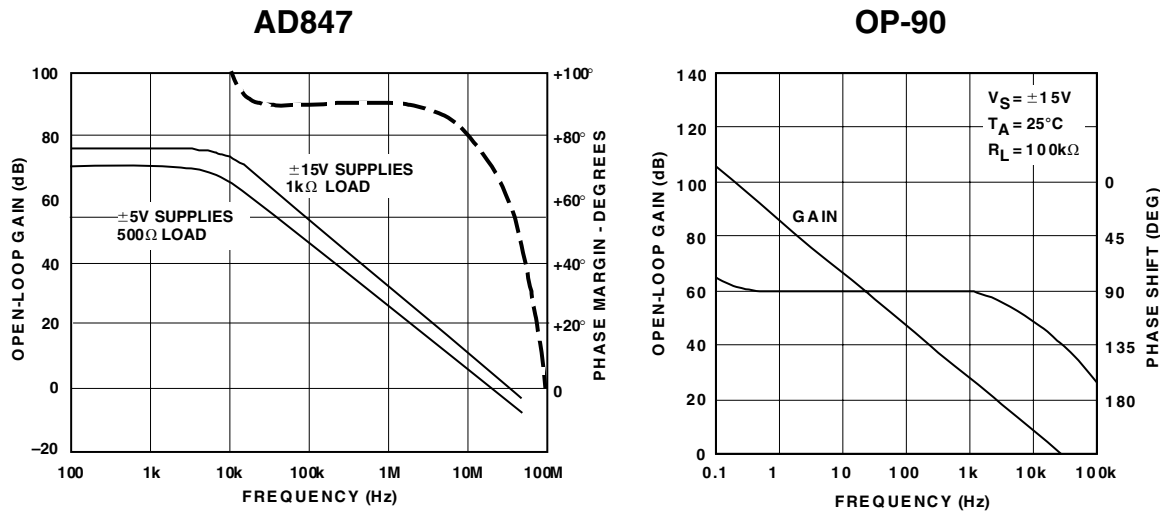


Figure 8.91: AD847 and OP-90 Bode Plots

SECTION 8.8: DESIGN EXAMPLES

Several examples will now be worked out to demonstrate the concepts previously discussed

Antialias Filter

As an example, passive and active antialias filters will now be designed based upon a common set of specifications. The active filter will be designed in four ways: Sallen-Key, Multiple Feedback, State Variable, and Frequency Dependent Negative Resistance (FDNR).

The specifications for the filter are given as follows:

- 1) The cutoff frequency will be 8 kHz.
- 2) The stopband attenuation will be 72 dB. This corresponds to a 12 bit system.
- 3) Nyquist frequency of 50 kSPS.
- 4) The Butterworth filter response is chosen in order to give the best compromise between attenuation and phase response.

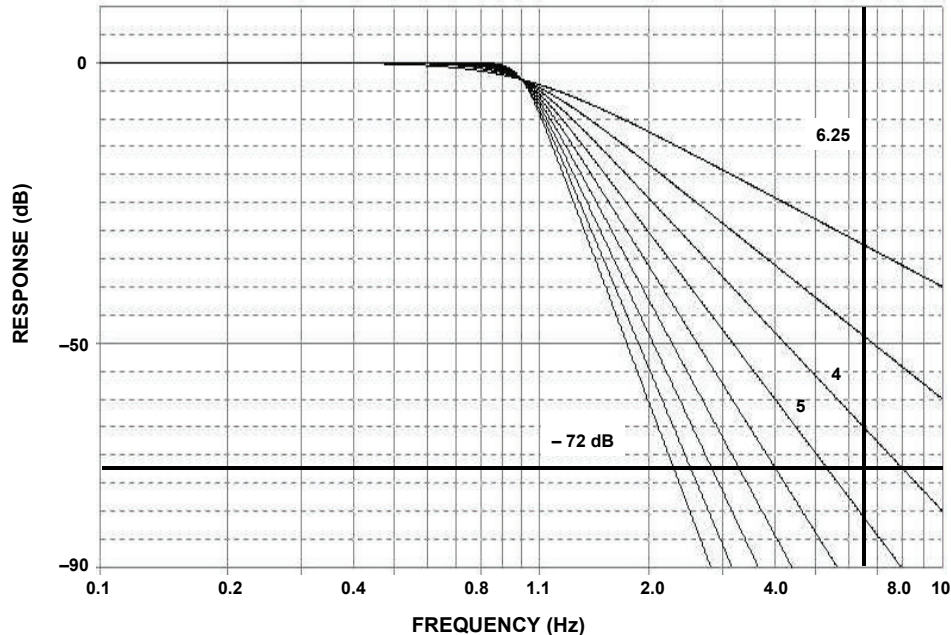


Figure 8.92: Determining Filter Order

■ BASIC LINEAR DESIGN

Consulting the Butterworth response curves (Figure 8.14, reproduced above in Figure 8.92), we see that for a frequency ratio of 6.25 (50 kSPS/8 kSPS), that a filter order of 5 is required.

Now consulting the Butterworth design table (Figure 8.25), the normalized poles of a 5th order Butterworth filter are:

STAGE	F_o	α
1	1.000	1.618
2	1.000	0.618
3	1.000	-----

The last stage is a real (single) pole, thus the lack of an alpha value. It should be noted that this is not necessarily the order of implementation in hardware. In general, you would typically put the real pole last and put the second order sections in order of decreasing alpha (increasing Q) as we have done here. This will avoid peaking due to high Q sections possibly overloading internal nodes. Another feature of putting the single-pole at the end is to bandlimit the noise of the op amps. This is especially true if the single-pole is implemented as a passive filter.

For the passive design, we will choose the zero input impedance configuration. While "classic" passive filters are typically double terminated, that is with termination on both source and load ends, we are concerned with voltage transfer not power transfer so the source termination will not be used. From the design table (see Reference 2, p. 313), we find the normalized values for the filter (see Figure 8.93).

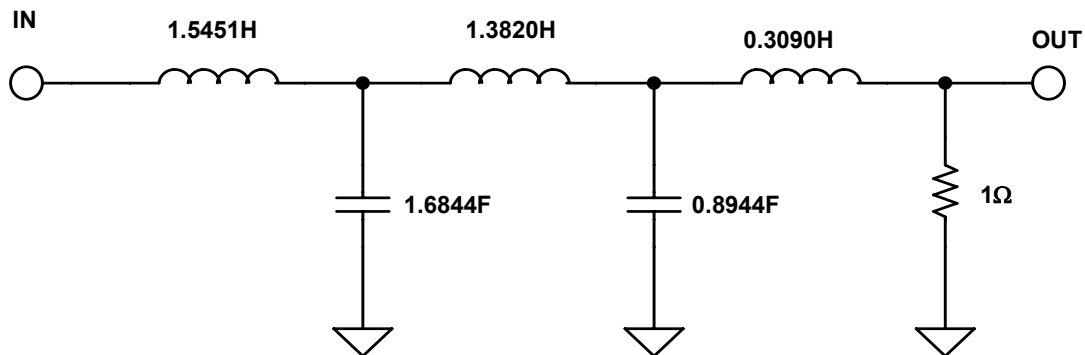


Figure 8.93: Normalized Passive Filter Implementation

These values are normalized for a 1 rad/s filter with a 1 Ω termination. To scale the filter we divide all reactive elements by the desired cutoff frequency, 8 kHz (= 50265 rad/sec, = $2\pi 8 \times 10^3$). This is commonly referred to as the frequency scale factor (FSF). We also need to scale the impedance.

For this example, an arbitrary value of 1000Ω is chosen. To scale the impedance, we multiply all resistor and inductor values and divide all capacitor values by this magnitude, which is commonly referred to as the impedance scaling factor (Z).

After scaling, the circuit looks like Figure 8.94.

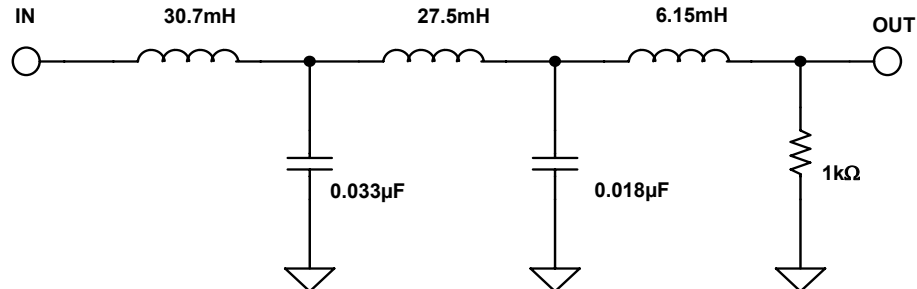


Figure 8.94: Passive Filter Implementation

For the Sallen-Key active filter, we use the design equations shown in Figure 8.49. The values for C_1 in each section are arbitrarily chosen to give reasonable resistor values. The implementation is shown in Figure 8.95.

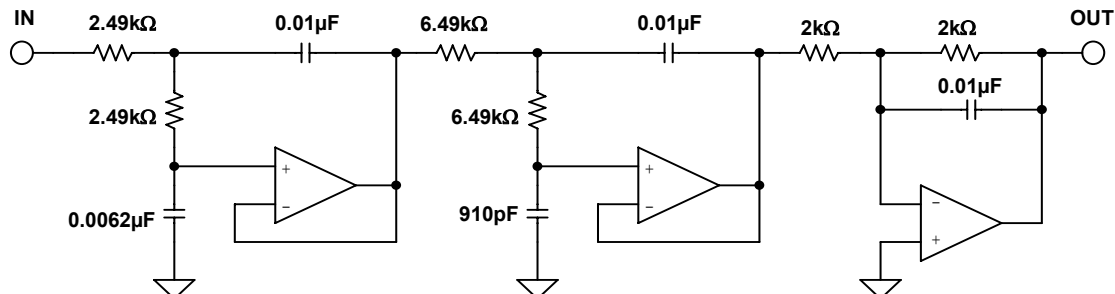


Figure 8.95: Sallen-Key Implementation

The exact values have been rounded to the nearest standard value. For most active realization to work correctly, it is required to have a zero-impedance driver, and a return path for dc due to the bias current of the op amp. Both of these criteria are approximately met when you use an op amp to drive the filter.

In the above example the single pole has been built as an active circuit. It would have been just as correct to configure it as a passive RC filter. The advantage to the active section is lower output impedance, which may be an advantage in some applications, notably driving an ADC input that uses a switched capacitor structure.

This type of input is common on sigma delta ADCs as well as many other CMOS type of converters. It also eliminates the loading effects of the input impedance of the following stage on the passive section.

■ BASIC LINEAR DESIGN

Figure 8.96 shows a multiple feedback realization of our filter. It was designed using the equations in Figure 8.52. In this case, the last section is a passive RC circuit.

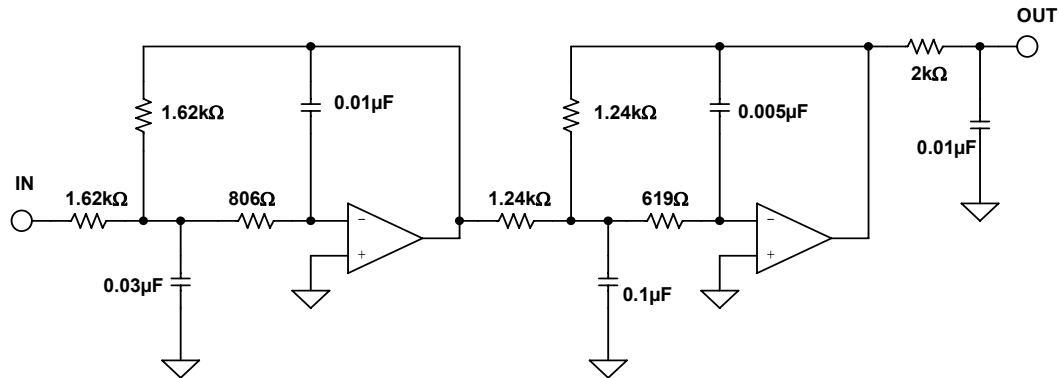


Figure 8.96: Multiple Feedback Implementation

An optional buffer could be added after the passive section, if desired. This would give many of the advantages outlined above, except for bandlimiting the noise of the output amp. By using one of the above two filter realizations, we have both an inverting and a noninverting design.

The state variable filter, shown in Figure 8.97, was designed with the equations in Figure 8.55. Again, we have rounded the resistor values to the nearest standard 1% value.

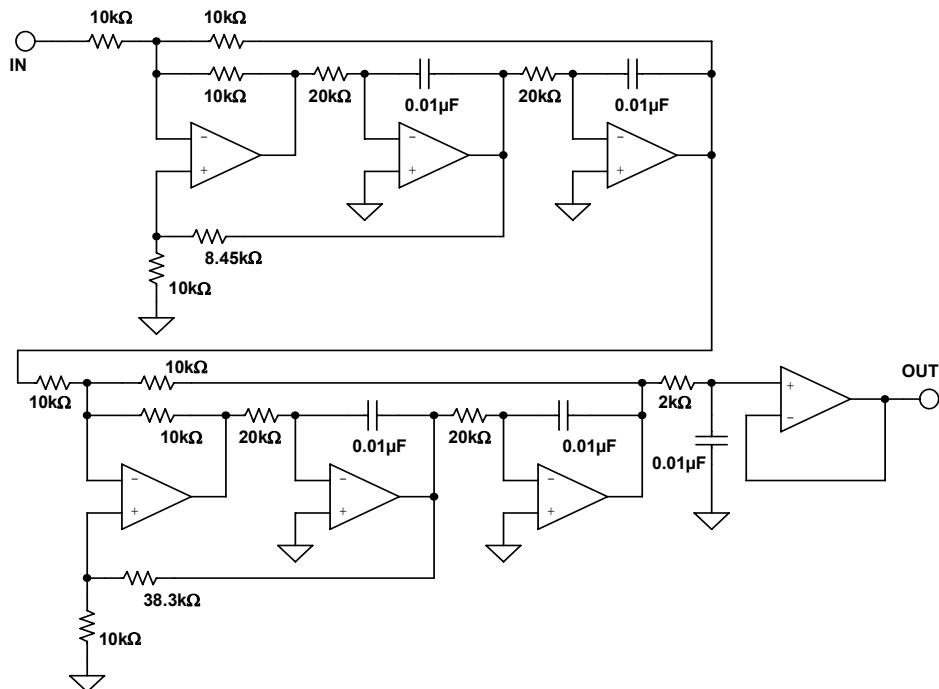


Figure 8.97: State Variable Implementation

Obviously this filter implementation has many more parts than either the Sallen-Key or the multiple feedback. The rational for using this circuit is that stability is improved and the individual parameters are independently adjustable.

The Frequency Dependent Negative Resistance (FDNR) realization of this filter is shown in Figure 8.98.

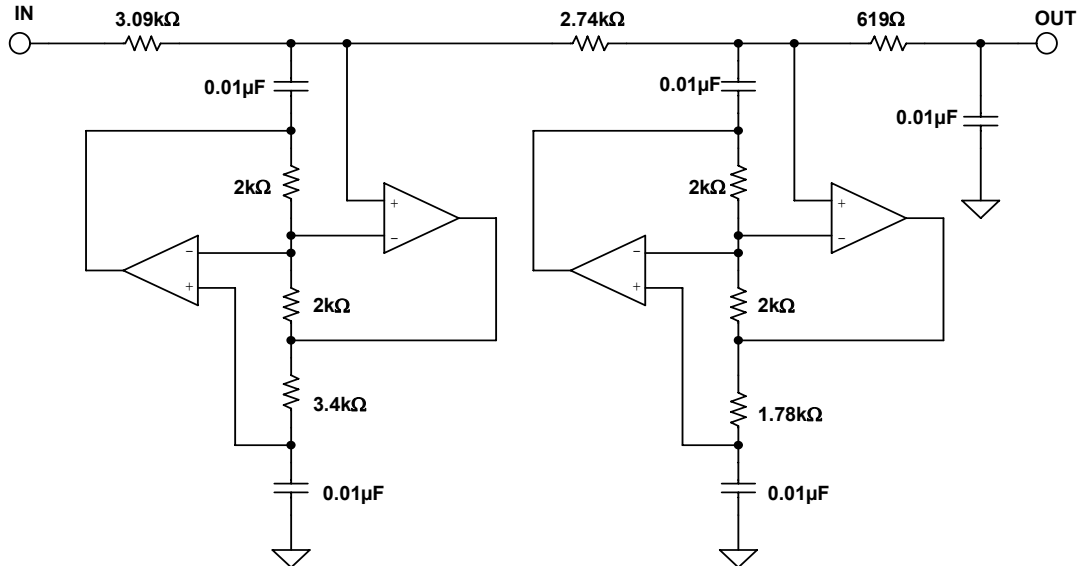


Figure 8.98: FDNR Implementation

In the conversion process from passive to FDNR, the D element is normalized for a capacitance of 1 F. We then scale the filter to a more reasonable value (0.01 μ F in this case).

In all of the above implementations standard values were used instead of the calculated values. Any variation from the ideal values will cause a shift in the filter response characteristic, but often the effects are minimal. The computer can be used to evaluate these variations on the overall performance and determine if they are acceptable.

To examine the effect of using standard values, take the Sallen-Key implementation. Figure 8.99 shows the response of each of the 3 sections of the filter. While the Sallen-Key was the filter used, the results from any of the other implementations will give similar results.

Figure 8.100 then shows the effect of using standard values instead of calculated values. Notice that the general shape of the filter remains the same, just slightly shifted in frequency. This investigation was done only for the standard value of the resistors. To understand the total effect of component tolerance the same type of calculations would have to be done for the tolerance of all the components and also for their temperature and aging effects.

■ BASIC LINEAR DESIGN

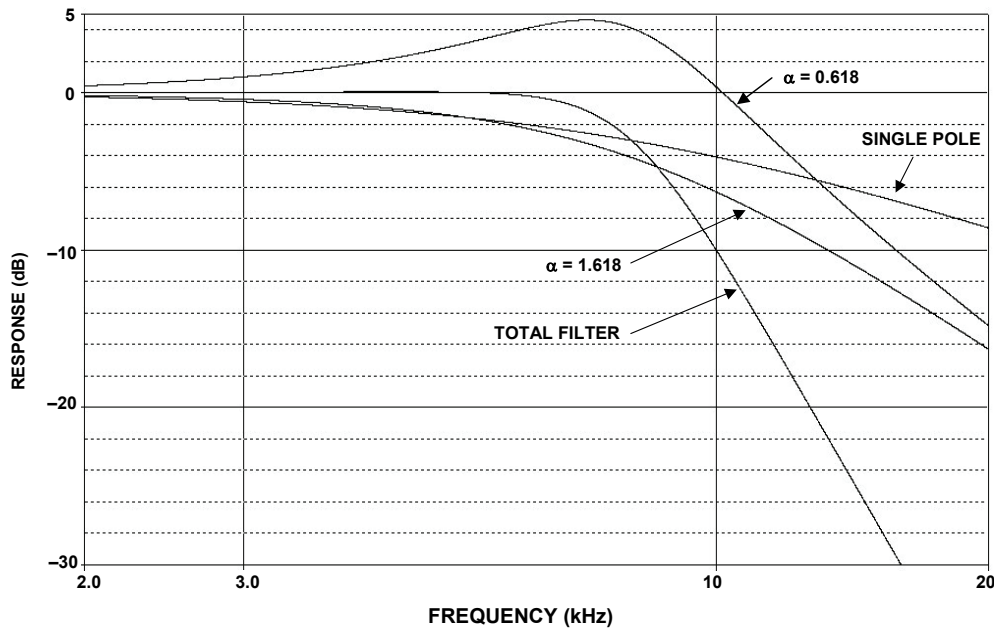


Figure 8.99: Individual Section Response

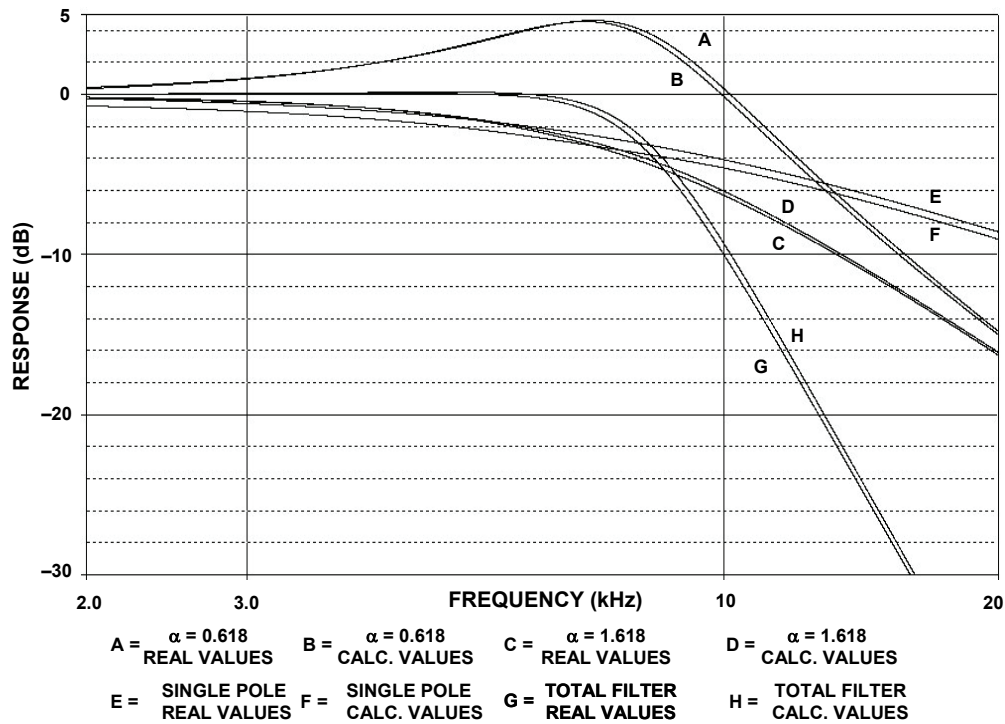


Figure 8.100: Effect of Using Standard Value Resistors

In active filter applications using op amps, the dc accuracy of the amplifier is often critical to optimal filter performance. The amplifier's offset voltage will be passed by the

ANALOG FILTERS DESIGN EXAMPLES

low-pass filter and may be amplified to produce excessive output offset. For low frequency applications requiring large value resistors, bias currents flowing through these resistors will also generate an output offset voltage.

In addition, at higher frequencies, an op amp's dynamics must be carefully considered. Here, slew rate, bandwidth, and open-loop gain play a major role in op amp selection. The slew rate must be fast as well as symmetrical to minimize distortion.

■ BASIC LINEAR DESIGN

Transformations

In the next example the transformation process will be investigated.

As mentioned earlier, filter theory is based on a low pass prototype, which is then manipulated into the other forms. In these examples the prototype that will be used is a 1 kHz, 3 pole, 0.5 dB Chebyshev filter. A Chebyshev was chosen because it would show more clearly if the responses were not correct, a Butterworth would probably be too forgiving in this instance. A 3 pole filter was chosen so that a pole pair and a single-pole would be transformed.

The pole locations for the LP prototype were taken from Figure 8.30. They are:

STAGE	α	β	F_O	α
1	0.2683	0.8753	1.0688	0.5861
2	0.5366			0.6265

The first stage is the pole pair and the second stage is the single-pole. Note the unfortunate convention of using α for 2 entirely separate parameters. The α and β on the left are the pole locations in the s-plane. These are the values that are used in the transformation algorithms. The α on the right is $1/Q$, which is what the design equations for the physical filters want to see.

The Sallen-Key topology will be used to build the filter. The design equations in Figure 8.67 (pole pair) and Figure 8.66 (single pole) where then used to design the filter. The schematic is shown in Figure 8.101.

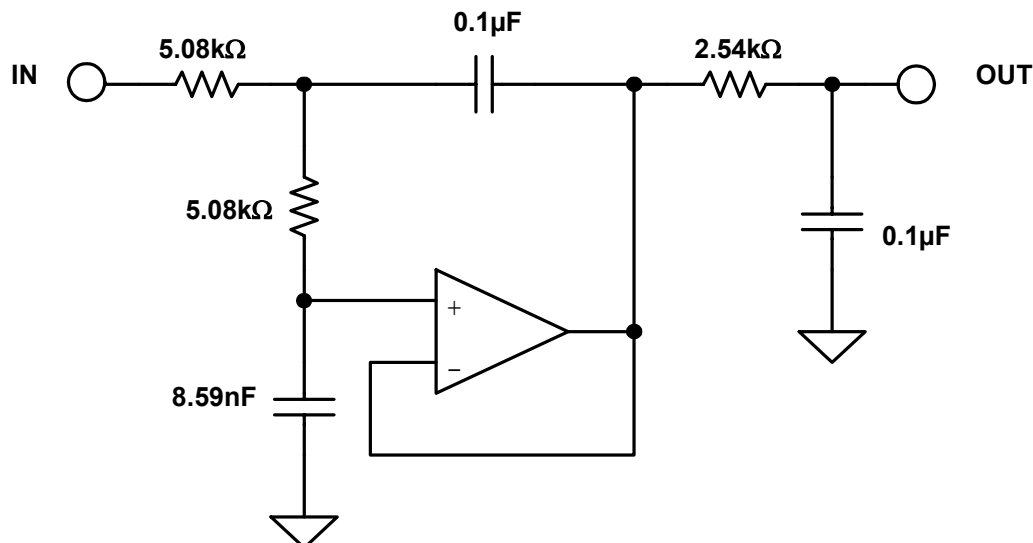


Figure 8.101: Low-Pass Prototype

Using the equation string described in Section 8, the filter is now transformed into a high-pass filter. The results of the transformation are:

STAGE	α	β	F_0	α
1	0.3201	1.0443	0.9356	0.5861
2	1.8636		1.596	

A word of caution is warranted here. Since the convention of describing a Chebyshev filter is to quote the end of the error band instead of the 3 dB frequency, the F_0 must be divided (for high-pass) by the ratio of ripple band to 3 dB bandwidth (Table 1, Section 4).

The Sallen-Key topology will again be used to build the filter. The design equations in Figure 8.68 (pole pair) and Figure 8.66 (single pole) where then used to design the filter. The schematic is shown in Figure 8.102.

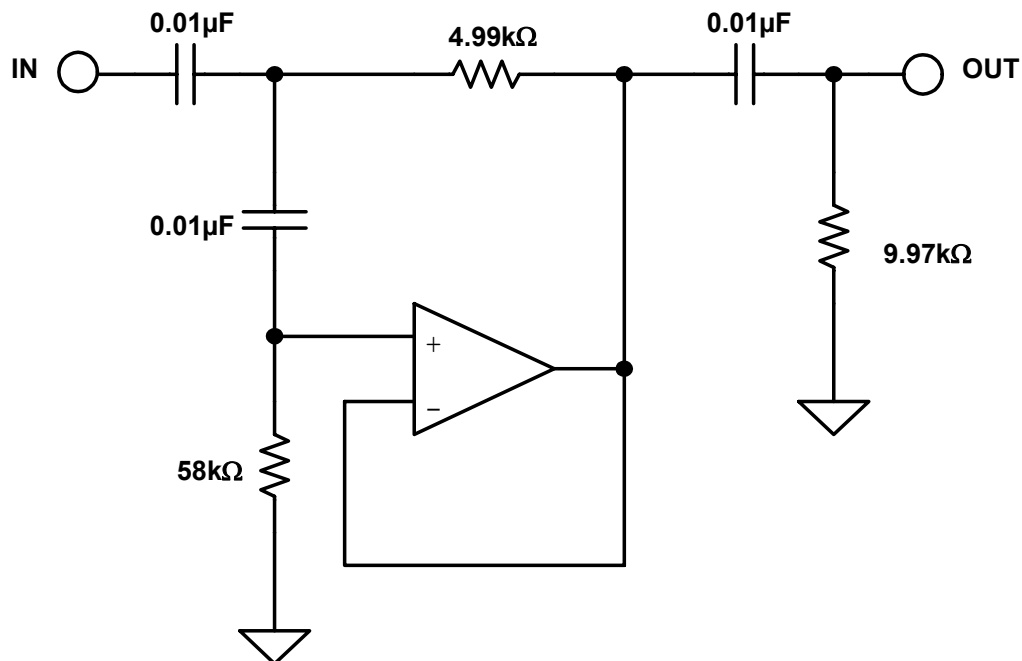


Figure 8.102: High-Pass Transformation

Figure 8.103 shows the response of the low-pass prototype and the high-pass transformation. Note that they are symmetric around the cutoff frequency of 1 kHz. Also note that the error band is at 1 kHz, not the -3 dB point, which is characteristic of Chebyshev filters.

■ BASIC LINEAR DESIGN

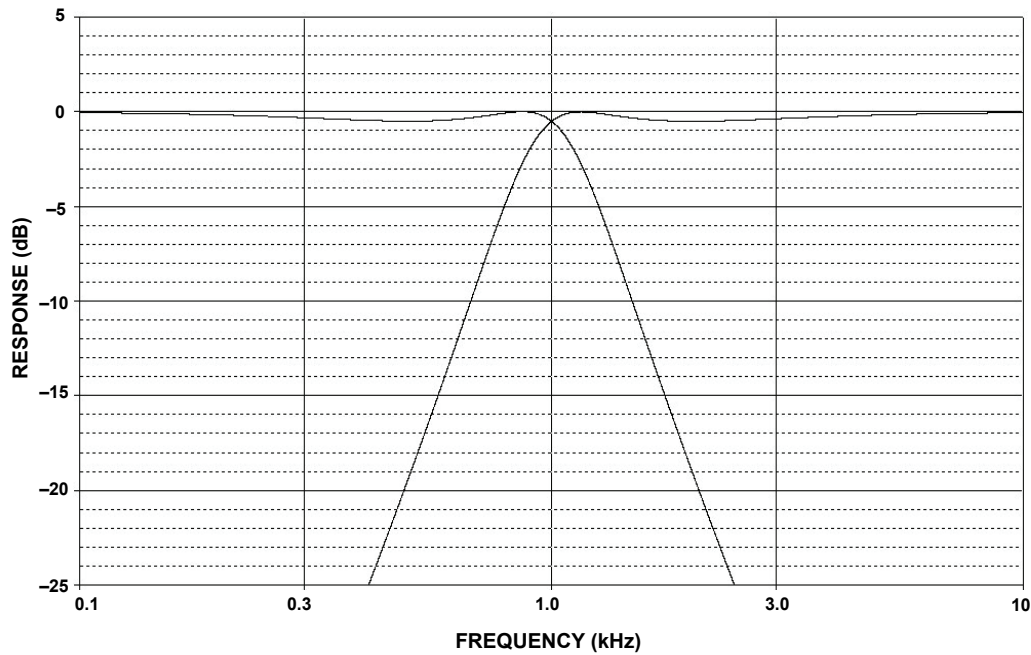


Figure 8.103: Low-Pass and High-Pass Response

The low-pass prototype is now converted to a band-pass filter. The equation string outlined in Section 8.5 is used for the transformation. Each pole of the prototype filter will transform into a pole pair. Therefore the 3 pole prototype, when transformed, will have 6 poles (3 pole pairs). In addition, there will be 6 zeros at the origin.

Part of the transformation process is to specify the 3 dB bandwidth of the resultant filter. In this case this bandwidth will be set to 500 Hz. The results of the transformation yield:

STAGE	F_0	Q	A_0
1	804.5	7.63	3.49
2	1243	7.63	3.49
3	1000	3.73	1

The reason for the gain requirement for the first 2 stages is that their center frequencies will be attenuated relative to the center frequency of the total filter. Since the resultant Q's are moderate (less than 20) the Multiple Feedback topology will be chosen. Figure 8.72 was then used to design the filter sections.

Figure 8.104 is the schematic of the filter and Figure 8.105 shows the filter response.

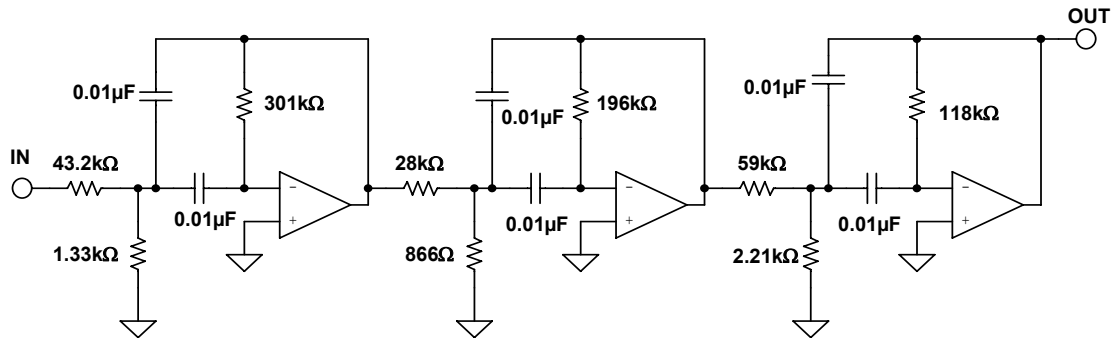


Figure 8.104: Band-Pass Transformation

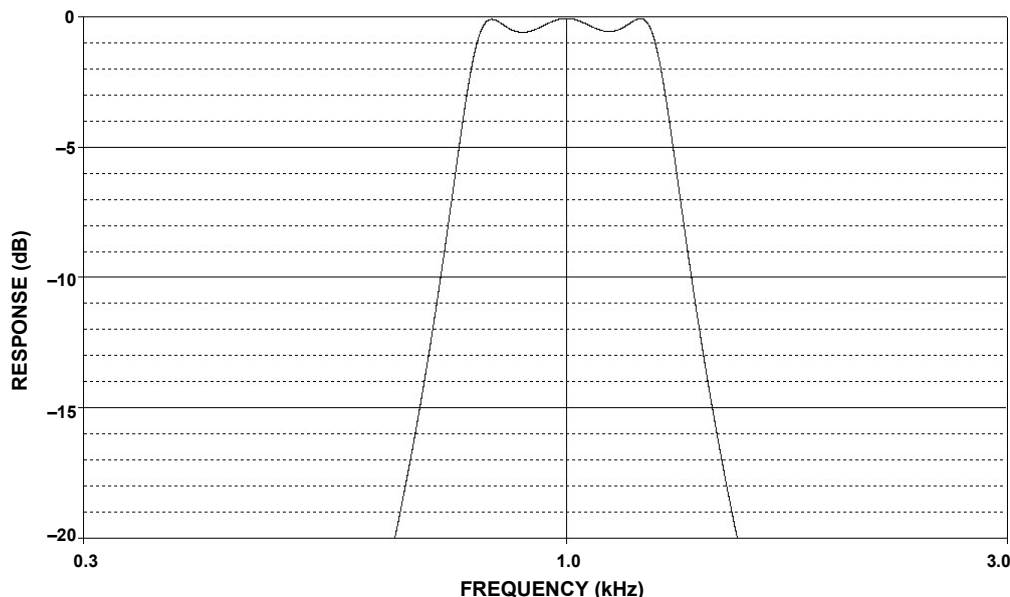


Figure 8.105: Band-Pass Filter Response

Note that again there is symmetry around the center frequency. Also the 800 Hz bandwidth is not 250 Hz either side of the center frequency (arithmetic symmetry). Instead the symmetry is geometric, which means that for any 2 frequencies (F_1 & F_2) of equal amplitude are related by:

$$F_0 = \sqrt{F_1 * F_2} \quad \text{Eq. 8-96}$$

Lastly the prototype will be transformed into a band-reject filter. For this the equation string in Section 8.5 is used. Again, each pole of the prototype filter will transform into a pole pair. Therefore, the 3 pole prototype, when transformed, will have 6 poles (3 pole pairs).

■ BASIC LINEAR DESIGN

As in the band-pass case, part of the transformation process is to specify the 3 dB bandwidth of the resultant filter. Again in this case this bandwidth will be set to 500 Hz. The results of the transformation yield:

STAGE	F_0	Q	F_{0Z}
1	763.7	6.54	1000
2	1309	6.54	1000
3	1000	1.07	1000

Note that there are three cases of notch filters required. There is a standard notch ($F_0 = F_Z$, section 3), a low-pass notch ($F_0 < F_Z$, section 1) and a high-pass notch ($F_0 > F_Z$, section 2). Since there is a requirement for all 3 types of notches, the Bainter Notch is used to build the filter. The filter is designed using Figure 8.77. The gain factors K_1 and K_2 are arbitrarily set to 1. Figure 8.106 is the schematic of the filter.

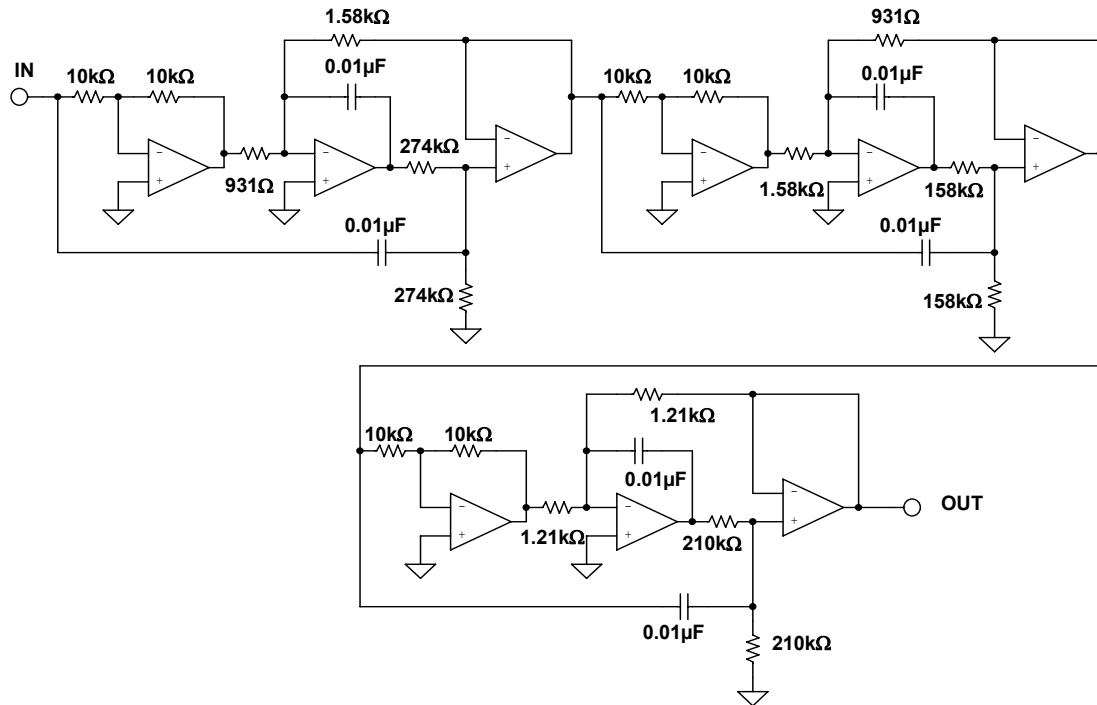


Figure 8.106: Band-reject Transformation

The response of the filter is shown in Figure 8.107 and in detail in Figure 8.108. Again, note the symmetry around the center frequency. Again the frequencies have geometric symmetry.

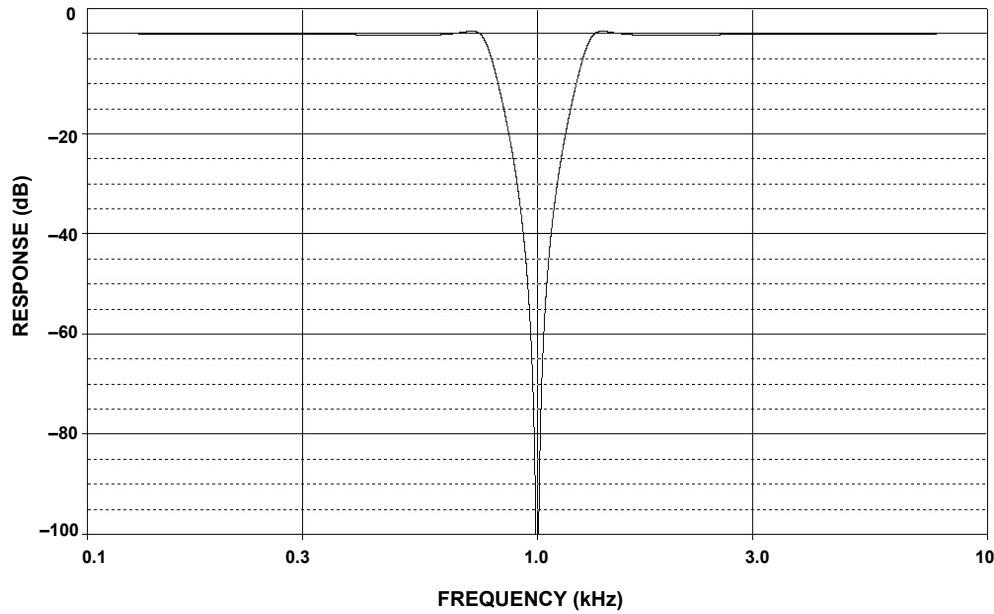


Figure 8.107: Band-reject Response

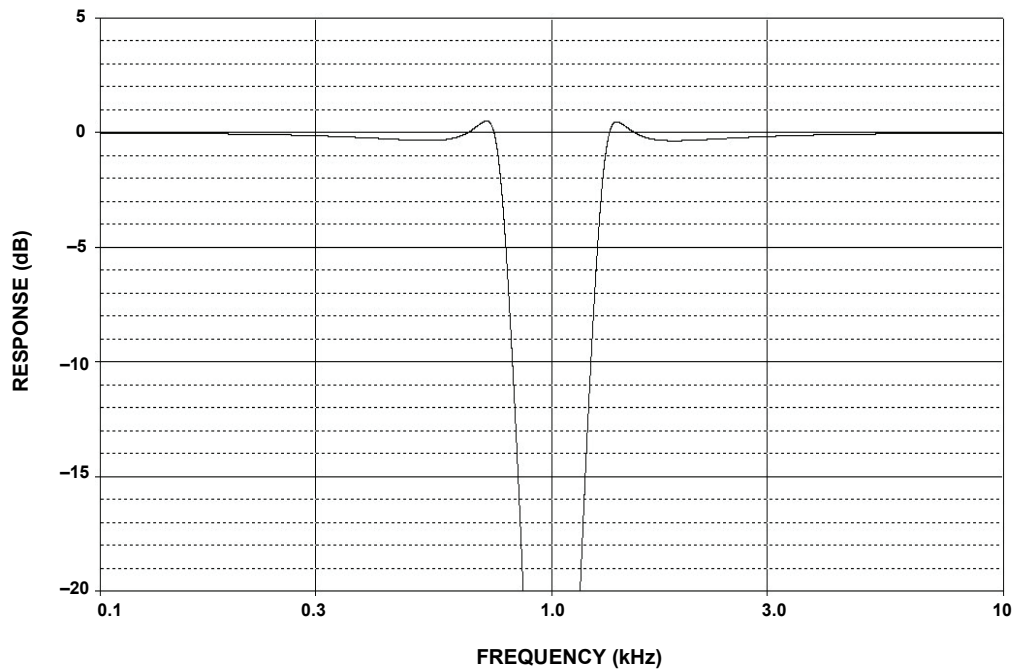


Figure 8.108: Band-reject Response (detail)

■ BASIC LINEAR DESIGN

CD Reconstruction Filter

This design was done for a magazine article describing a high quality outboard D/A converter for use with digital audio sources (see Reference 26).

A reconstruction filter is required on the output of a D/A converter because, despite the name, the output of a D/A converter is not really an analog voltage but instead a series of steps. The converter will put out a discrete voltage, which it will then hold until the next sample is asserted. The filter's job is to remove the high frequency components, smoothing out the waveform. This is why the filter is sometimes referred to as a smoothing filter. This also serves to eliminate the aliases of the conversion process. The "standard" in the audio industry is to use a 3rd-order Bessel function as the reconstruction filter. The reason to use a Bessel filter is that it has the best phase response. This helps to preserve the phase relationship of the individual tones in the music. The price for this phase "goodness" is that the amplitude discrimination is not as good as some other filter types. If we assume that we are using 8 \times oversampling of the 48 kSPS data stream in the D/A converter then the aliases will appear at 364 kHz ($8 \times 48\text{ k} - 20\text{ k}$). The digital filter that is used in the interpolation process will eliminate the frequencies between 20 kHz and 364 kHz. If we assume that the band-edge is 30 kHz, then we have a frequency ratio of approximately 12 ($364 \div 30$). We use 30 kHz as the band-edge, rather than 20 kHz to minimize the rolloff due to the filter in the pass-band. In fact, the complete design for this filter includes a shelving filter to compensate for the pass-band rolloff. Extrapolating from Figure 8.20, a 3rd-order Bessel will only provide on the order of 55 dB attenuation at $12 \times F_o$. This is only about 9 bit accuracy.

By designing the filter as 7th order, and by designing it as a linear phase with equiripple error of 0.05°, we can increase the stopband attenuation to about 120 dB at $12 \times F_o$. This is close to the 20 bit system that we are hoping for.

The filter will be designed as a FDNR type. This is an arbitrary decision. Reasons to choose this topology are its low sensitivities to component tolerances and the fact that the op amps are in the shunt arms rather than in the direct signal path.

The first step is to find the passive prototype. To do this, use the charts in Williams' book. We then get the circuit shown in Figure 8.109A. Next perform a translation in the s-plane. This gives the circuit shown in Figure 8.109B. This filter is scaled for a frequency of 1 Hz. and an impedance level of 1 Ω. The D structure of the converted filter is replaced by a GIC structure that can be physically realized. The filter is then denormalized by frequency (30 kHz) and impedance (arbitrarily chosen to be 1 kΩ). This gives a frequency-scaling factor (FS) of 1.884×10^5 ($= 2\pi (3 \times 10^4)$). Next arbitrarily choose a value of 1 nF for the capacitor. This gives an impedance-scaling factor (Z) of 5305 ($= (C_{OLD}/C_{NEW}) / FSF$).

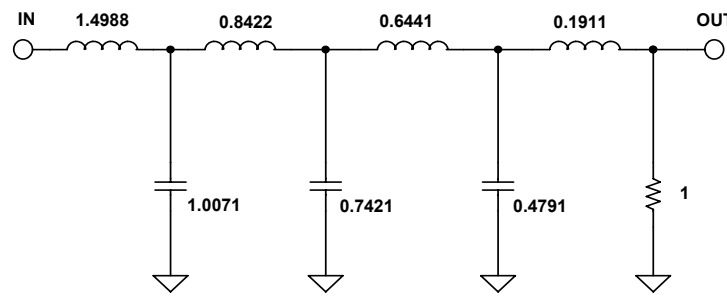


Figure 8.109A: CD Reconstruction Filter—Passive Prototype

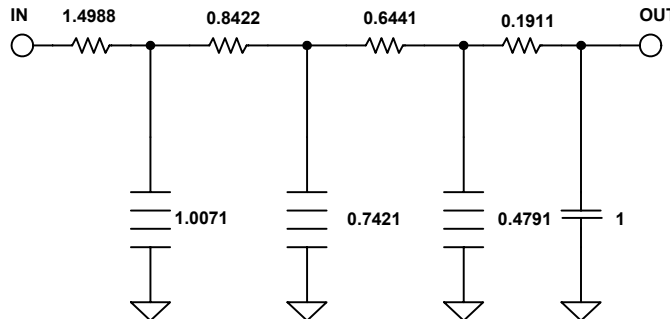


Figure 8.109B: CD Reconstruction Filter—Transformation in s-Plane

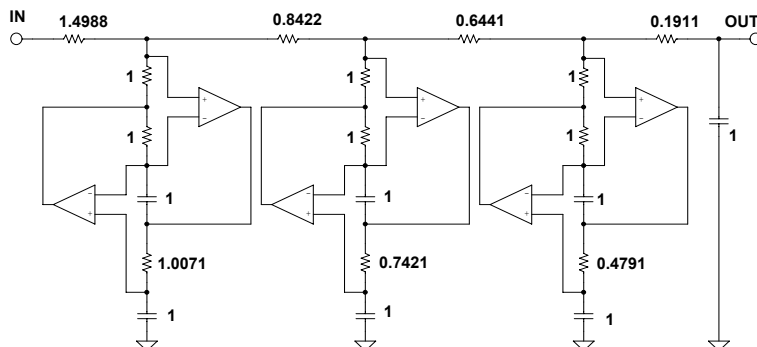


Figure 8.109C: CD Reconstruction Filter—Normalized FDNR

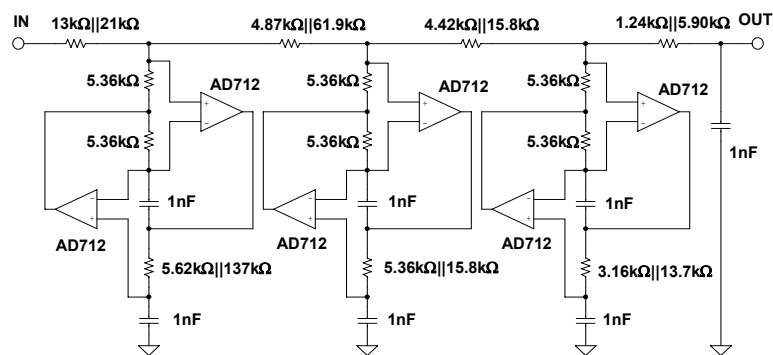


Figure 8.109D: CD Reconstruction Filter—Final Filter

■ BASIC LINEAR DESIGN

Then multiply the resistor values by Z. This results in the resistors that had the normalized value of 1Ω will now have a value of $5.305 \text{ k}\Omega$. For the sake of simplicity adopt the standard value of $5.36 \text{ k}\Omega$. Working backwards, this will cause the cutoff frequency to change to 29.693 kHz . This slight shift of the cutoff frequency will be acceptable.

The frequency scaling factor is then recalculated with the new center frequency and this value is used to denormalize the rest of the resistors. The design flow is illustrated in Figure 8.109. The final schematic is shown it Figure 8.109D.

The performance of the filter is shown in Figure 8.110(A-D).

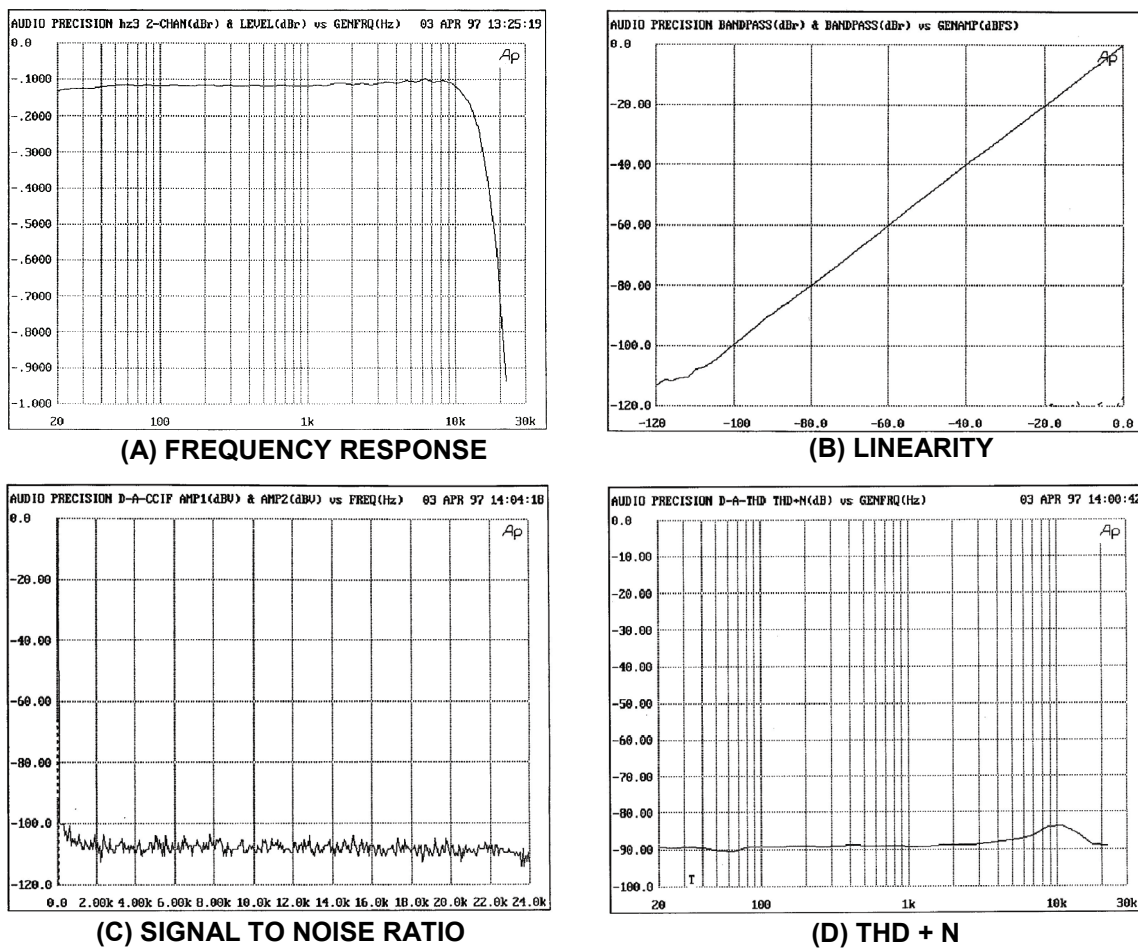


Figure 8.110: CD Filter Performance

Digitally Programmable State Variable Filter

One of the attractive features of the state variable filter is that the parameters (gain, cutoff frequency and "Q") can be individually adjusted. This attribute can be exploited to allow control of these parameters.

To start, the filter is reconfigured slightly. The resistor divider that determines Q (R6 & R7 of Figure 8.84) is changed to an inverting configuration. The new filter schematic is shown in Figure 8.111. Then the resistors R1, R2, R3 & R4 (of Figure 8.111) are replaced by CMOS multiplying DACs. Note that R5 is implemented as the feedback resistor implemented in the DAC. The schematic of this circuit is shown in Figure 8.112.

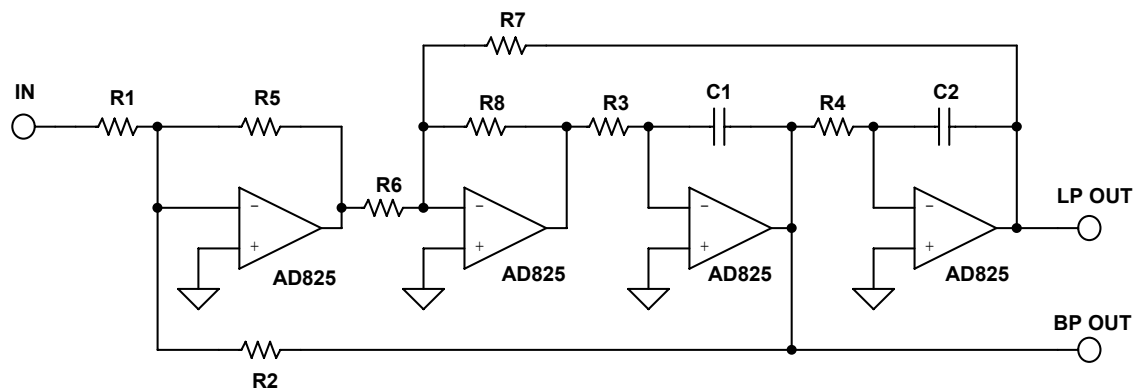


Figure 8.111: Redrawn State Variable Filter

The AD7528 is an 8 bit dual MDAC. The AD825 is a high speed FET input opamp. Using these components the frequency range can be varied from around 550 Hz to around 150 kHz (Figure 8.113). The Q can be varied from approximately 0.5 to over 12.5 (Figure 8.114). The gain of circuit can be varied from 0 dB to -48 dB (Figure 8.115).

The operation of the DACs in controlling the parameters can be best thought of as the DACs changing the effective resistance of the resistors. This relationship is:

$$\text{DAC EQUIVALENT RESISTANCE} = \frac{256 * \text{DAC RESISTANCE}}{\text{DAC CODE (DECIMAL)}} \quad \text{Eq. 8-97}$$

This, in effect, varies the resistance from 11 kΩ to 2.8 MΩ for the AD7528.

■ BASIC LINEAR DESIGN

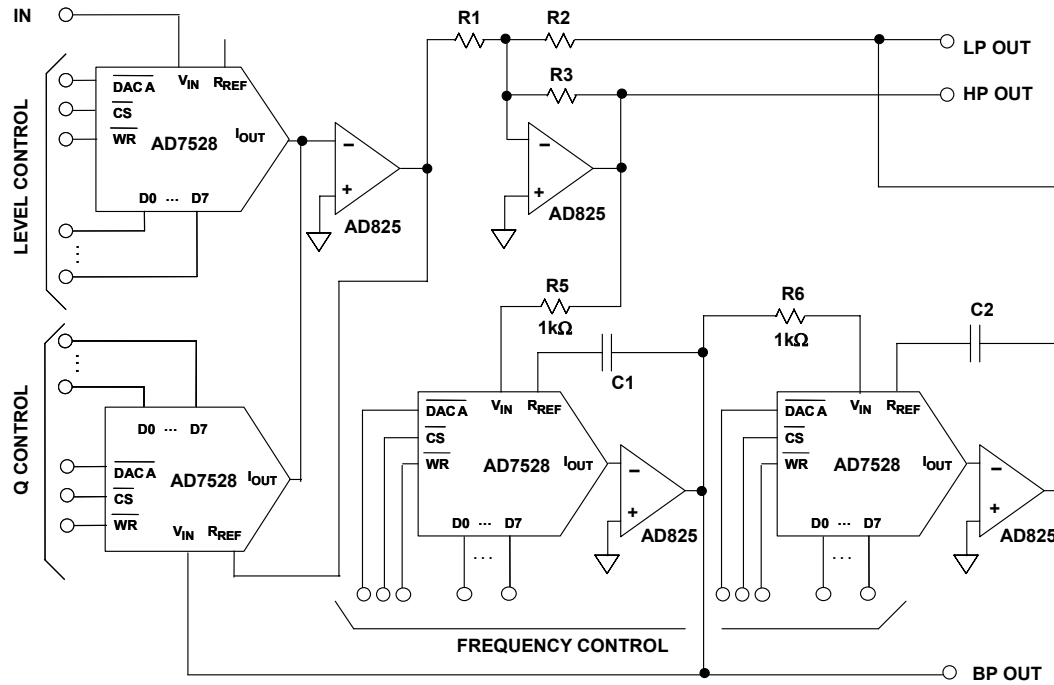


Figure 8.112: Digitally Controlled State Variable Filter

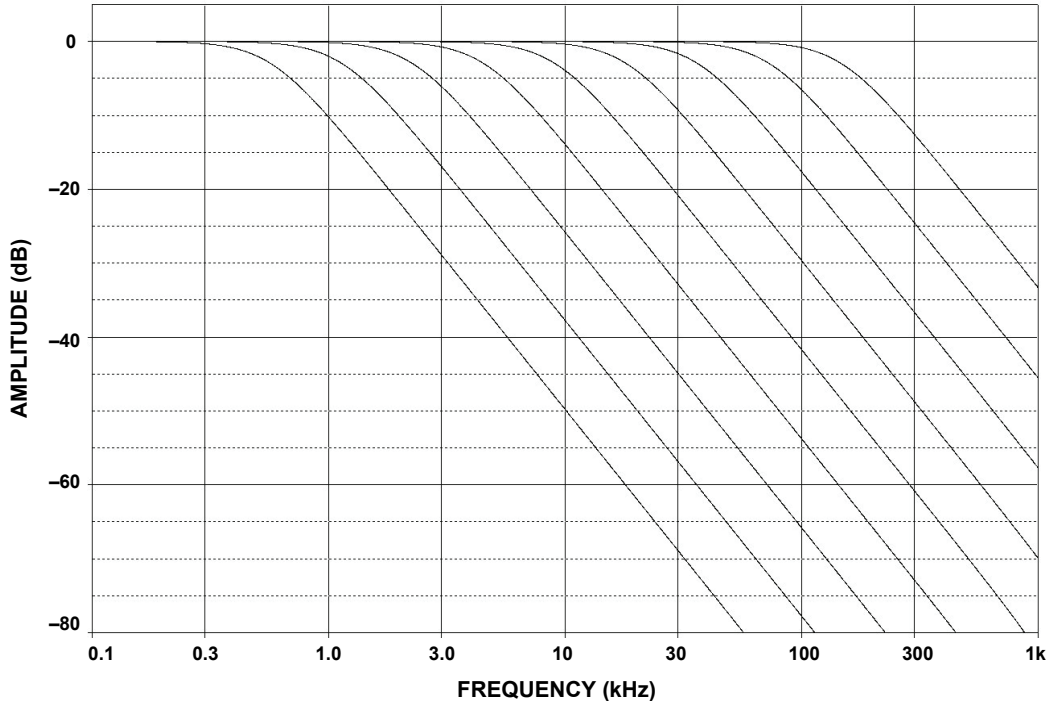


Figure 8.113: Frequency Response vs. DAC Control Word

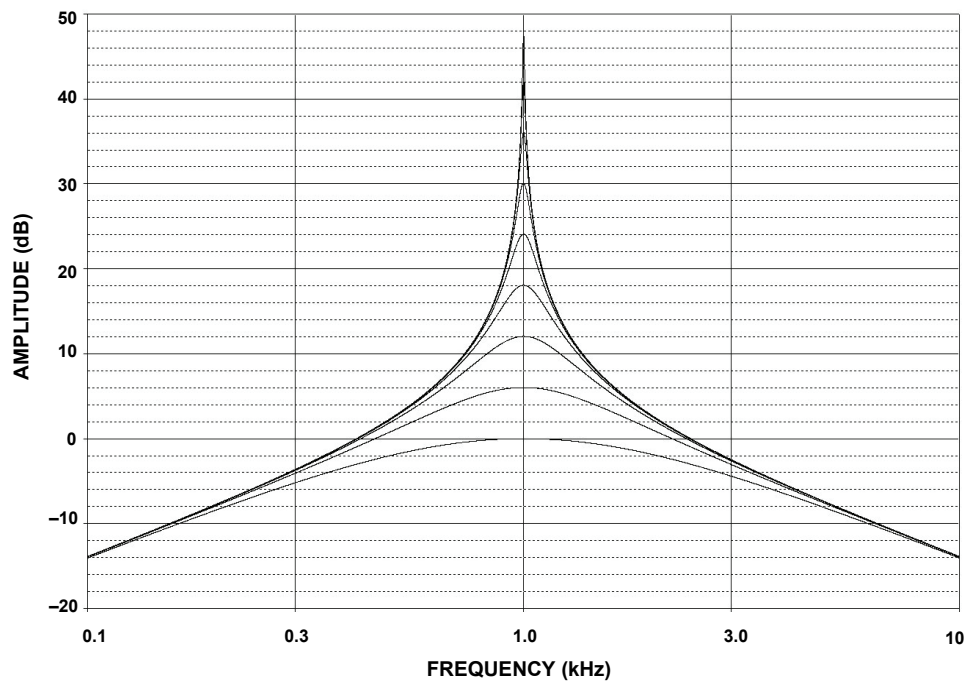


Figure 8.114: Q Variation vs. DAC Control Word

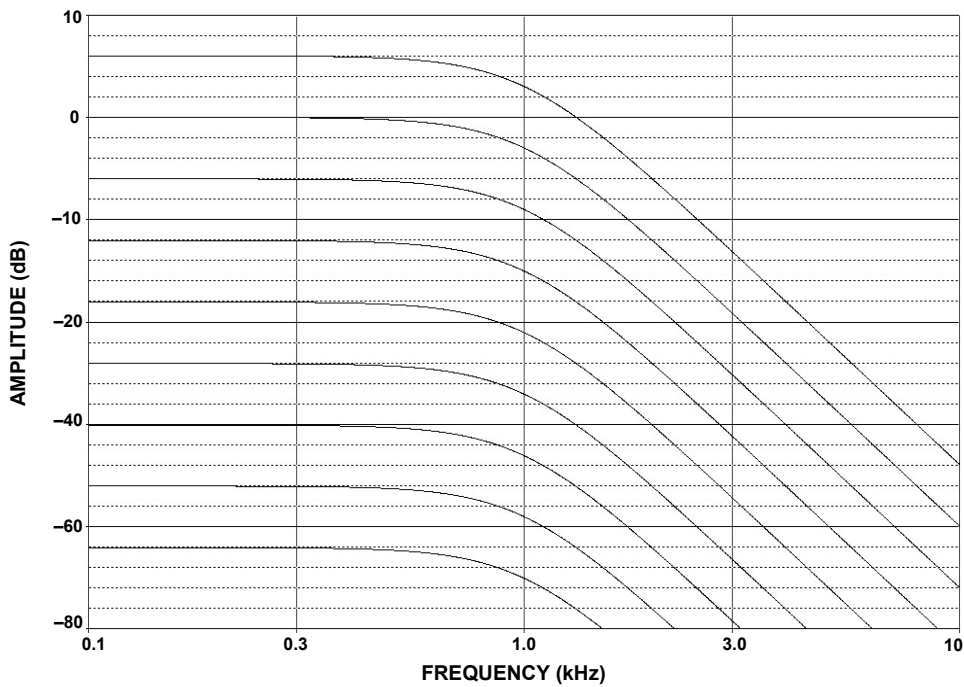


Figure 8.115: Gain Variation vs. DAC Control Word

■ BASIC LINEAR DESIGN

One limitation of this design is that the frequency is dependent on the ladder resistance of the DAC. This particular parameter is not controlled. DACs are trimmed so that the ratios of the resistors, not their absolute values, are controlled. In the case of the AD7528, the typical value is $11\text{ k}\Omega$. It is specified as $8\text{ k}\Omega$ min. and $15\text{ k}\Omega$ max. A simple modification of the circuit can eliminate this issue. The cost is 2 more op amps (Figure 8.116). In this case, the effective resistor value is set by the fixed resistors rather than the DAC's resistance. Since there are 2 integrators the extra inversions caused by the added op amps cancel.

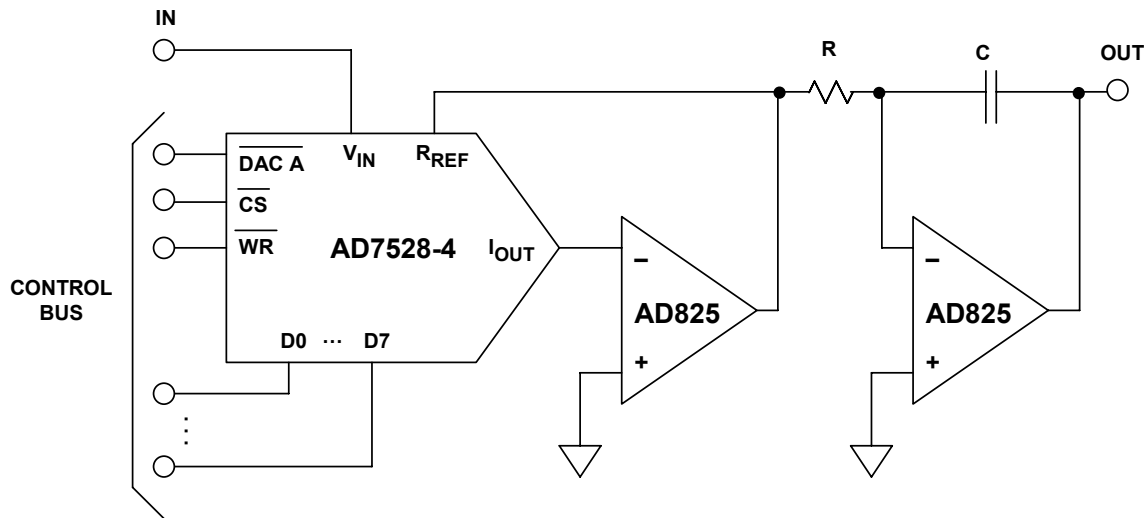


Figure 8.116: Improved Digitally Variable Integrator

As a side note, the multiplying DACs could be replaced by analog multipliers. In this case the control would obviously be an analog rather than a digital signal. We also could just as easily have used a digital pot in place of the MDACs. The difference is that instead of increasing the effective resistance, the value of the pot would be the maximum.

60 Hz Notch Filter

A very common problem in instrumentation is that of interference of the telemetry that is to be measured. One of the primary sources of this interference is the power line. This is particularly true of high impedance circuits. Another path for this noise is ground loops. One possible solution is to use a notch filter to remove the 60 Hz component. Since this is a single frequency interference, the Twin-T circuit will be used.

Since the maximum attenuation is desired and the minimum notch width is desired, the maximum Q of the circuit is desired. This means the maximum amount of positive feedback is used (R5 open and R4 shorted). Due to the high impedance of the network, a FET input op amp is used.

The filter is designed using Figure 8.78. The schematic is shown in Figure 8.117 and the response in Figure 8.118.

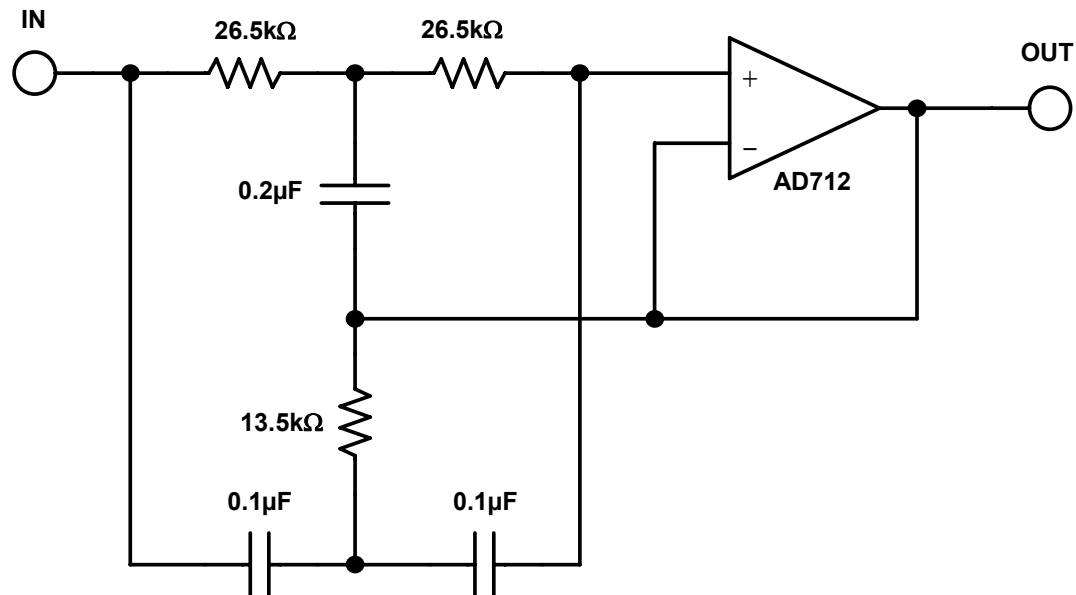


Figure 8.117: 60 Hz Twin-T Notch Filter

▣ BASIC LINEAR DESIGN

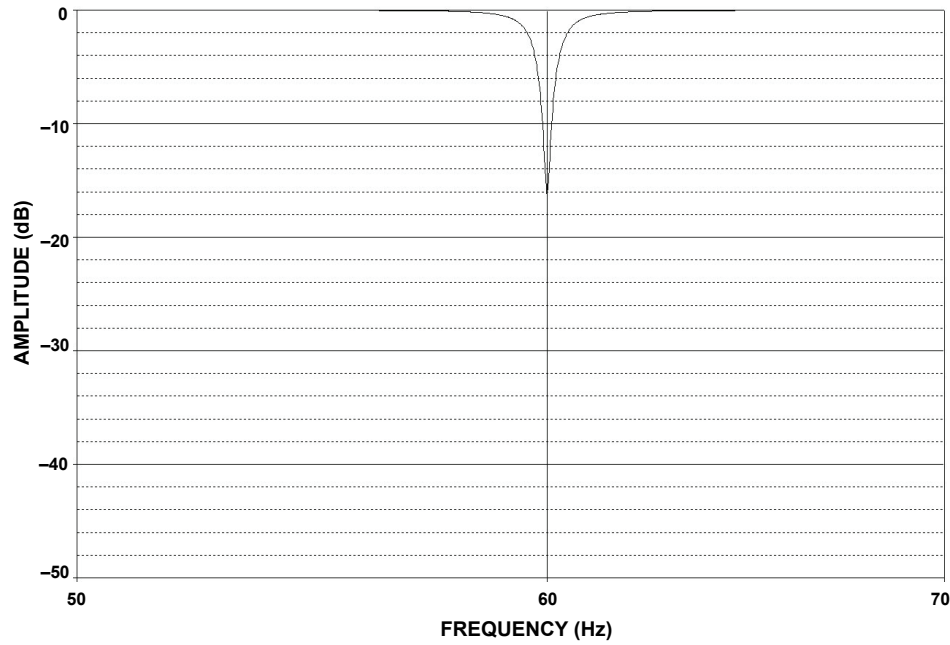


Figure 8.118: 60 Hz Notch Filter Response

REFERENCES:

1. A. I. Zverev, **Handbook of Filter Synthesis**, John Wiley, 1967.
2. A. B. Williams, **Electronic Filter Design Handbook**, McGraw-Hill, 1981, ISBN: 0-07-070430-9.
3. M. E. Van Valkenburg, **Analog Filter Design**, Holt, Rinehart & Winston, 1982
4. M. E. Van Valkenburg, **Introduction to Modern Network Synthesis**, John Wiley and Sons, 1960.
5. A. I. Zverev and H. J. Blinchikoff, **Filtering in the Time and Frequency Domain**, John Wiley and Sons, 1976.
6. S. Franco, **Design with Operational Amplifiers and Analog Integrated Circuits**, McGraw-Hill 1988, ISBN: 0-07-021799-8.
7. W. Cauer, **Synthesis of Linear Communications Networks**, McGraw-Hill, New York, 1958.
8. Aram Budak, **Passive and Active Network Analysis and Synthesis**, Houghton Mifflin Company, Boston, 1974.
9. L. P. Huelsman and P. E. Allen, **Introduction to the Theory and Design of Active Filters**, McGraw Hill, 1980, ISBN: 0-07-030854-3.
10. R. W. Daniels, **Approximation Methods for Electronic Filter Design**, McGraw-Hill, New York, 1974.
11. J. Tow, "Active RC Filters – a State-space Realization", **Proc. IEEE**, 1968, vol. 56, pp. 1137-1139.
12. L.C. Thomas, "The Biquad: Part I – Some Practical Design Considerations", **IEEE Trans. Circuits and Systems**, Vol. CAS-18, 1971, pp. 350-357.
13. L.C. Thomas, "The Biquad: Part I – A Multipurpose Active Filtering System," **IEEE Trans. Circuits and Systems**, Vol. CAS-18, 1971, pp. 358-361.
14. R. P. Sallen and E. L. Key, "A Practical Method of Designing RC Active Filters," **IRE Trans. Circuit Theory**, Vol. CT-2, 1955, pp. 74-85.
15. P. R. Geffe, "How to Build High-Quality Filters out of Low-Quality Parts," **Electronics**, Nov. 1976, pp. 111-113.
16. P. R. Geffe, "Designers Guide to Active Bandpass Filters," **EDN**, Apr. 5 1974, pp. 46-52.
17. T. Delyiannis, "High-Q Factor Circuit with Reduced Sensitivity," **Electronics Letters**, 4, Dec. 1968, p. 577.
18. J. J. Friend, "A Single Operational-Amplifier Biquadratic Filter Section," **1970 IEEE ISCT Digest Technical Papers**, 1970 p. 189.
19. L. Storch, "Synthesis of Constant-Time-Delay Ladder Networks Using Bessel Polynomials," **Proceedings of IRE**, Vol. 42, 1954, pp. 1666-1675.
20. K. W. Henderson and W. H. Kautz, "Transient Response of Conventional Filters," **IRE Trans. Circuit Theory**, Vol. CT-5, 1958, pp. 333-347.

■ BASIC LINEAR DESIGN

21. J. R. Bainter, "Active Filter Has Stable Notch and Response Can be Regulated," **Electronics**, Oct. 2 1975, pp.115-117.
22. S. A. Boctor, "Single Amplifier Functionally Tunable Low-Pass Notch Filter," **IEEE Trans. Circuits and Systems**, Vol. CAS-22, 1975, pp. 875-881.
23. S. A. Boctor, "A Novel second-order canonical RC-Active Realization of High-Pass-Notch Filter," **Proc. 1974 IEEE Int. Symp. Circuits and Systems**, pp. 640-644.
24. L. T. Burton, "Network Transfer Function Using the Concept of Frequency Dependant Negative Resistance," **IEEE Trans. Circuit Theory**, Vol. CT-16, 1969, pp. 406-408.
25. L. T. Burton and D. Trefleaven, "Active Filter Design Using General Impedance Converters," **EDN**, Feb. 1973, pp.68-75.
26. H. Zumbahlen, "A New Outboard DAC, Part 2," **Audio Electronics**, Jan. 1997, pp. 26-32, 42.
27. M. Williamsen, "Notch-Filter Design," **Audio Electronics**, Jan. 2000, pp. 10-17.
28. W. Jung, "Bootstrapped IC Substrate Lowers Distortion in JFET Op Amps," Analog Devices AN232.
29. H. Zumbahlen, "Passive and Active Filtering," Analog Devices AN281.
30. P. Toomey & W. Hunt, "AD7528 Dual 8-Bit CMOS DAC," Analog Devices AN318.
31. W. Slattery, "8th Order Programmable Lowpass Analog Filter Using 12-Bit DACs," Analog Devices AN209.
32. **CMOS DAC Application Guide**, Analog Devices.

Analog and IIR Filter Types

<http://www.nuhertz.com/filter/>

Basic Filters

Gaussian Filters

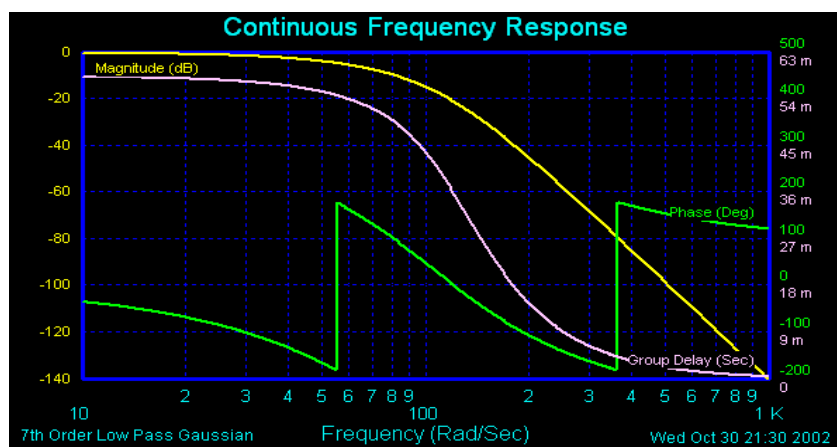
The Gaussian Filter is the filter type that results in the most gradual pass band roll-off and the lowest group delay. The step response of the Gaussian filter NEVER overshoots the steady state value. As the name states, the Gaussian Filter is derived from the same basic equations used to derive the Gaussian Distribution. The significant characteristic of the Gaussian Filter is that the step response contains no overshoot at all.

Filter Solutions normalizes the Gaussian filter such that the prototype high frequency attenuation matches the Butterworth filter. The pass band attenuation of the Gaussian filter increases with the order of the filter when this normalization is applied. However, Filter Solutions allows the user the option of selecting the desired pass band attenuation in dB's. 3dB attenuation is a popular choice for some.

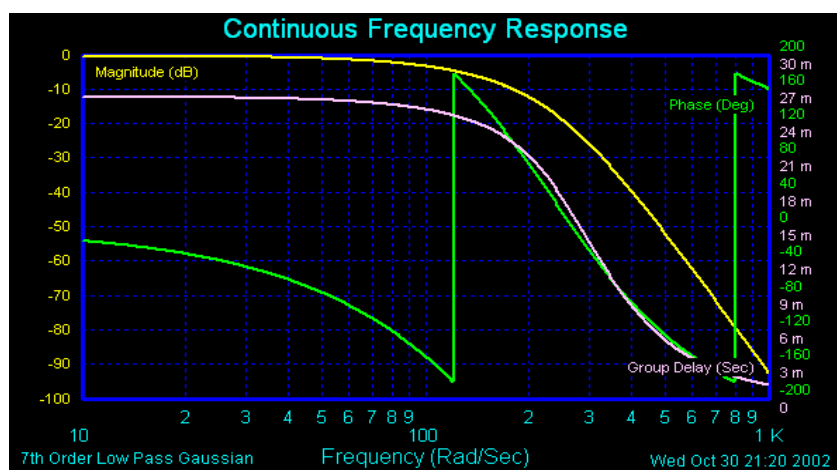
Gaussian Transitional Filters

It is occasionally desirable to transition from a Gaussian frequency response to a steeper roll off response at a user defined attenuation point. Filter Solutions provides 3, 6, 9, 12, and 15 dB Transitional Filters. Pass band attenuation is always set to 3.01 dB for Gaussian Transitional filters.

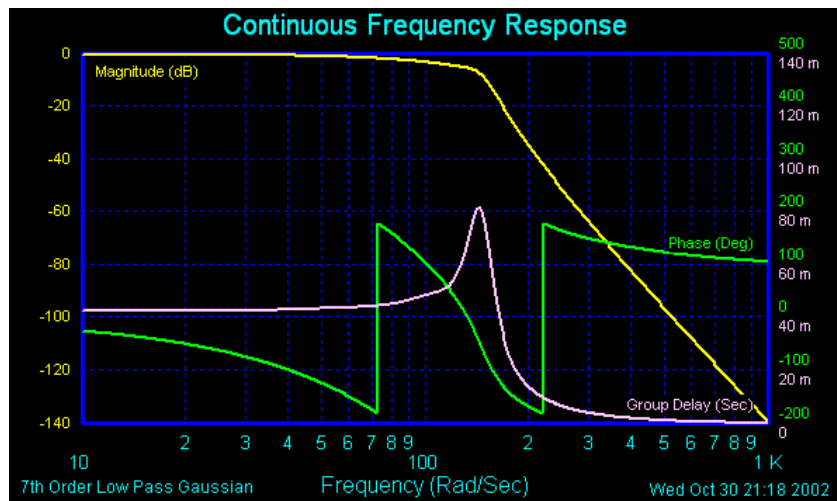
Gaussian Low Pass filter, 100Hz Pass Band Frequency



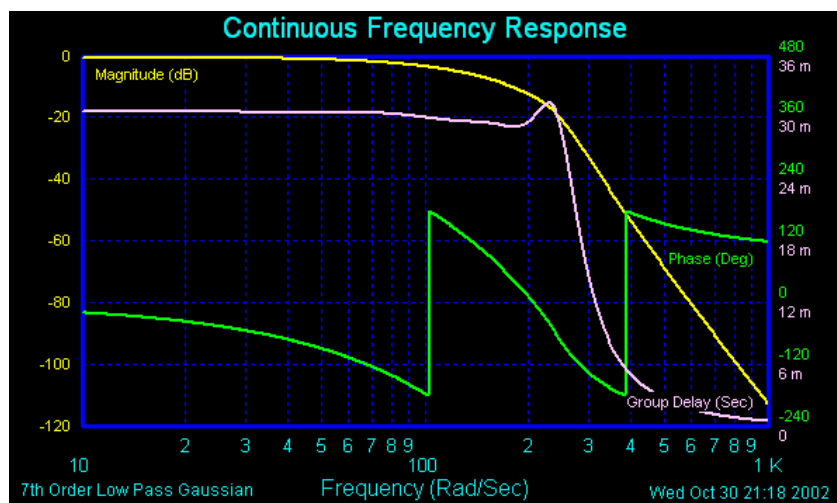
Gaussian With -3.01dB Pass Band Attenuation



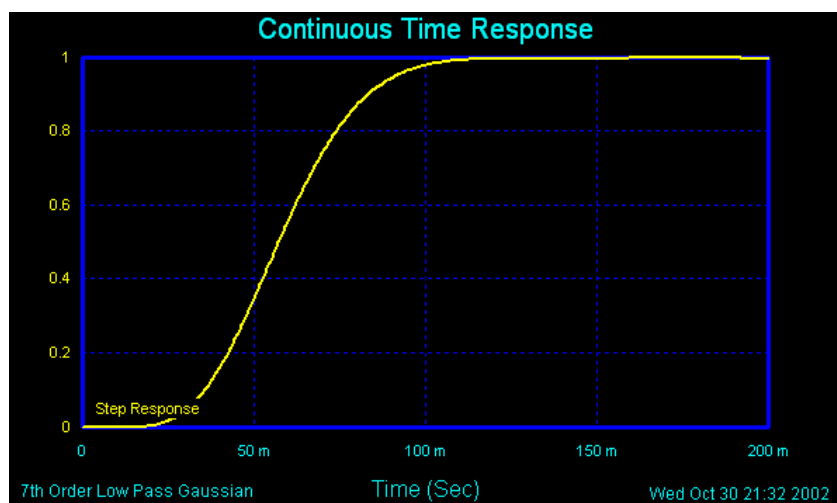
Gaussian With 6dB Transition



Gaussian With 15dB Transition



Gaussian Step Response



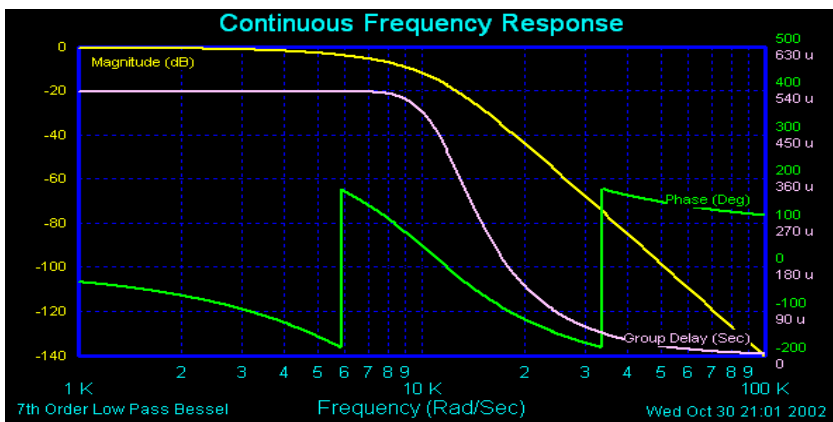
Bessel Filters

The Bessel Filter's distinguishing characteristic is the near constant group delay throughout the pass band of the low pass filter.

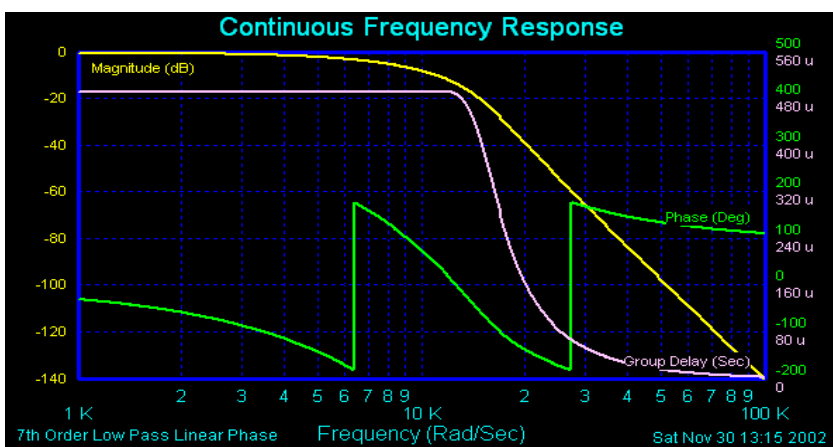
Filter Solutions normalizes the Bessel filter such that the prototype high frequency attenuation matches the Butterworth filter. The pass band attenuation of the Bessel filter increases with the order of the filter when this normalization is applied. However, Filter Solutions allows the user the option of selecting the desired pass band attenuation in dB's. 3dB attenuation is a popular choice for some.

Bessel filters may be modified for equiripple group delay, stop bands, or both. Filters with equiripple group delays are frequently referred to as Linear Phase filters, which is also the terminology used by Filter Solutions. The equiripple group delay had added efficiency in that the group delay remains flat farther into the stop band. See the description of Delay Filters for more on the equiripple group delay.

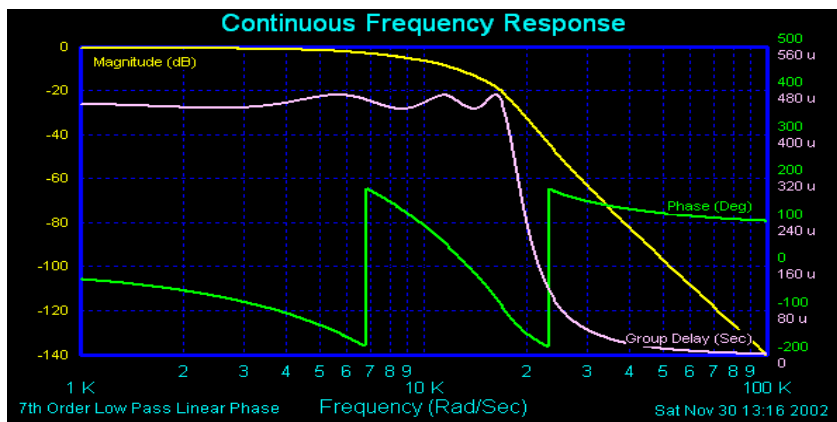
Bessel Low Pass filter, 10KHz Pass Band Frequency



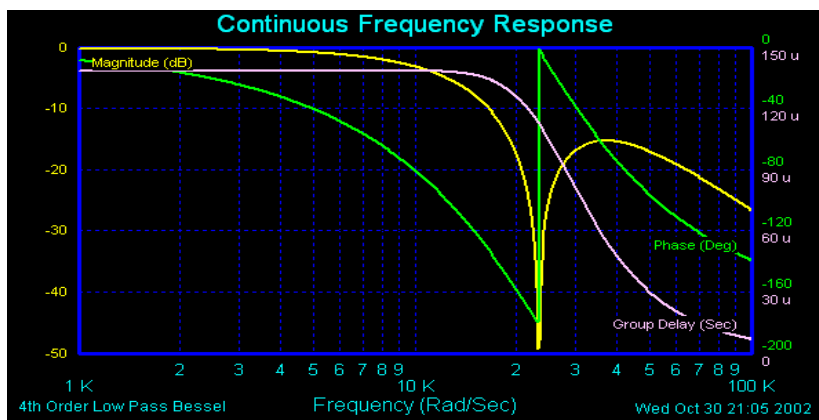
Linear Phase With Equiripple Group Delay, Period=2.0



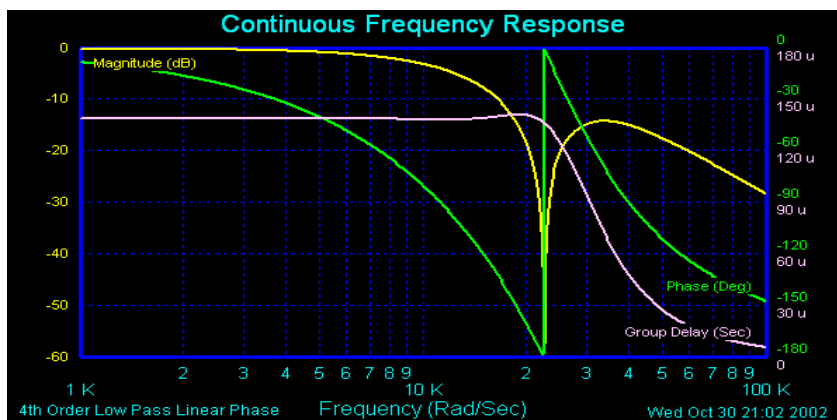
Linear Phase With Equiripple Group Delay, Period=2.6



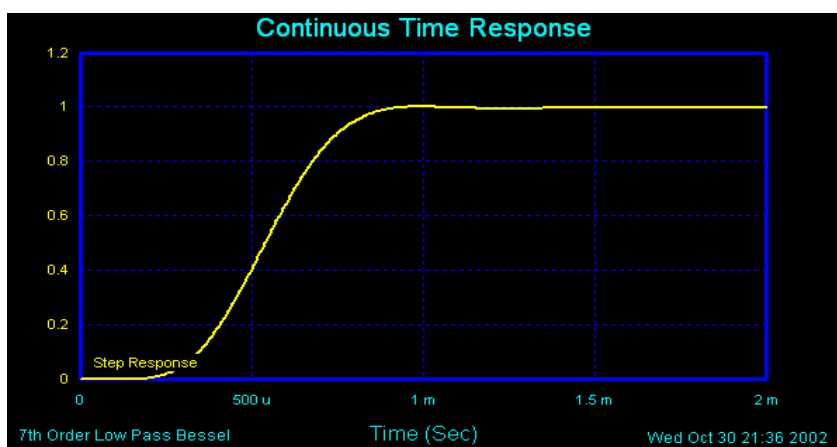
Bessel Modified With Stop Band



Linear Phase With Stop Band and Equiripple Group Delay



Bessel Low Pass Filter Step Response



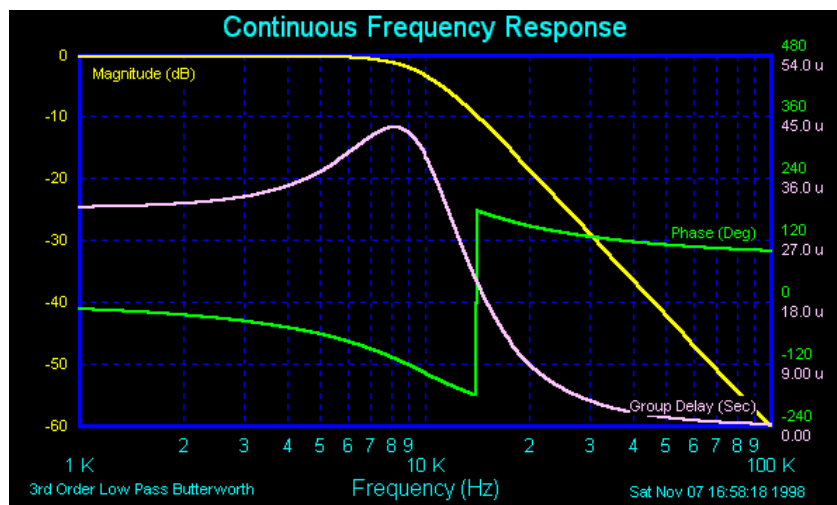
Butterworth Filters

The Butterworth Filter is the filter type that results in the flattest pass band and contains a moderate group delay.

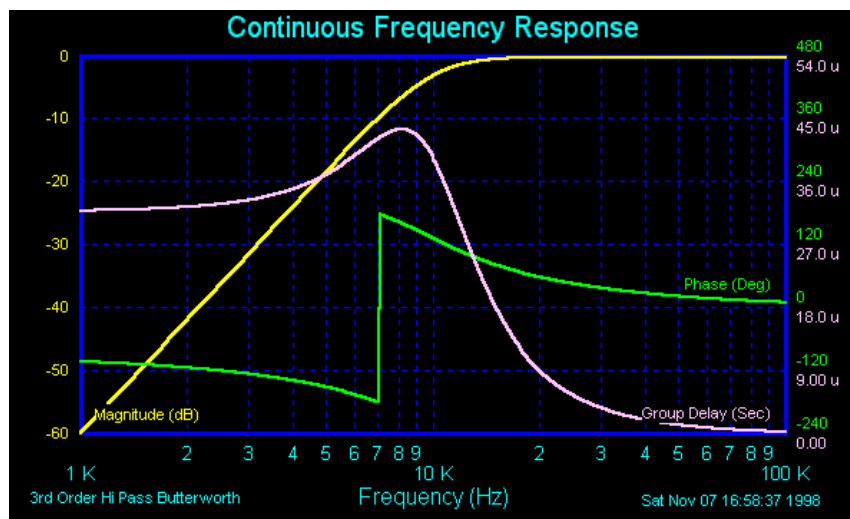
A standard Butterworth Filter's pass band attenuation is -3.01dB. However, Filter Solutions allows the user the option of selecting any pass band attenuation in dB's that will define the filters cut off frequency.

Filter Solutions also offers the user the option of placing user-defined zeros in the stop band. Such a filter with stop band zeros is no longer a true Butterworth Filter, but is still in the Maximally Flat filter family.

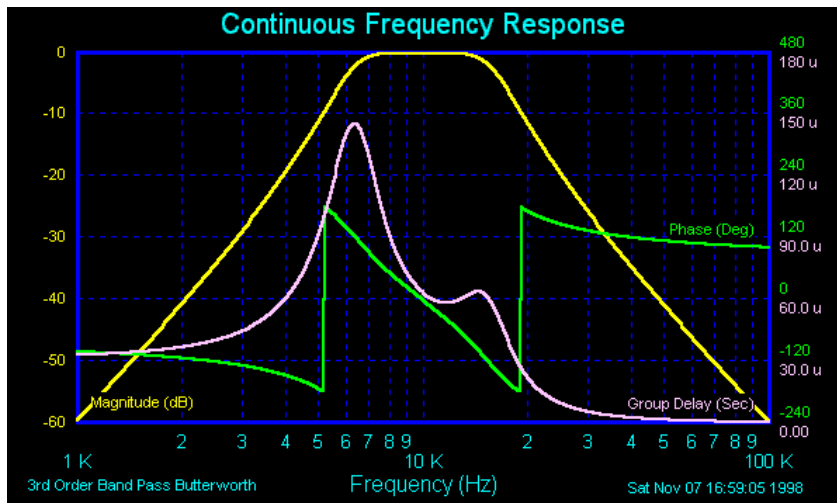
Butterworth Low Pass filter, 10KHz Pass Band Frequency



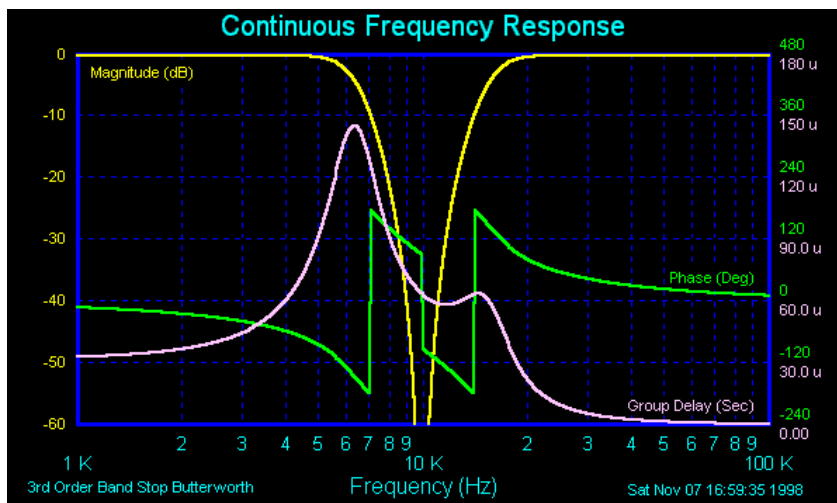
Butterworth High Pass filter, 10KHz Pass Band Frequency



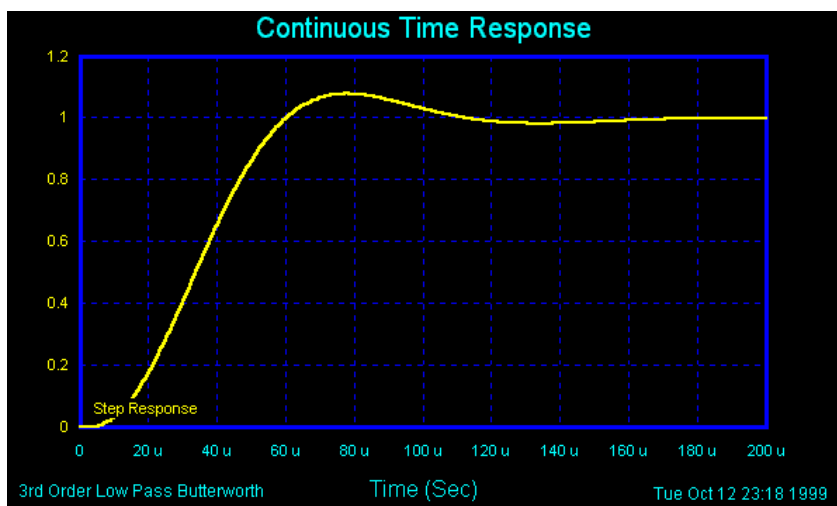
Butterworth Band Pass filter, 10KHz Center Frequency, 10KHz Pass Band Width



Butterworth Band Stop filter, 10KHz Center Frequency, 10Khz Pass Band Width



Butterworth Low Pass Step Response



Chebyshev Type I Filters

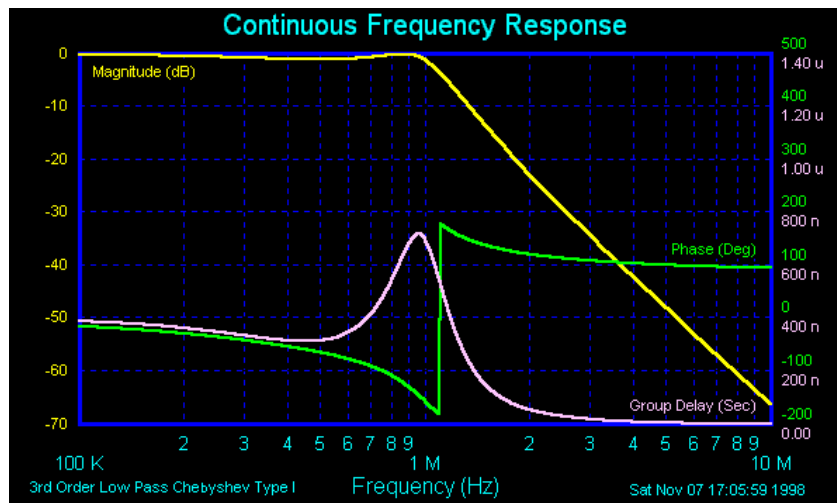
The Chebyshev Type I Filter is the filter type that results in the sharpest pass band cut off and

contains the largest group delay. The most notable feature of this filter is the ripple in the pass band magnitude.

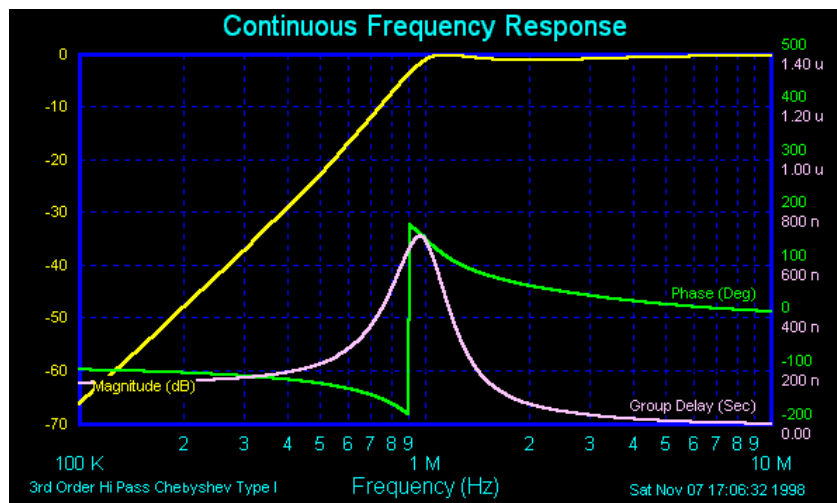
A standard Chebyshev Type I Filter's pass band attenuation is defined to be the same value as the pass band ripple amplitude. However, Filter Solutions allows the user the option of selecting any pass band attenuation in dB's that will define the filters cut off frequency.

Filter Solutions also offers the user the option of placing user-defined zeros in the stop band.

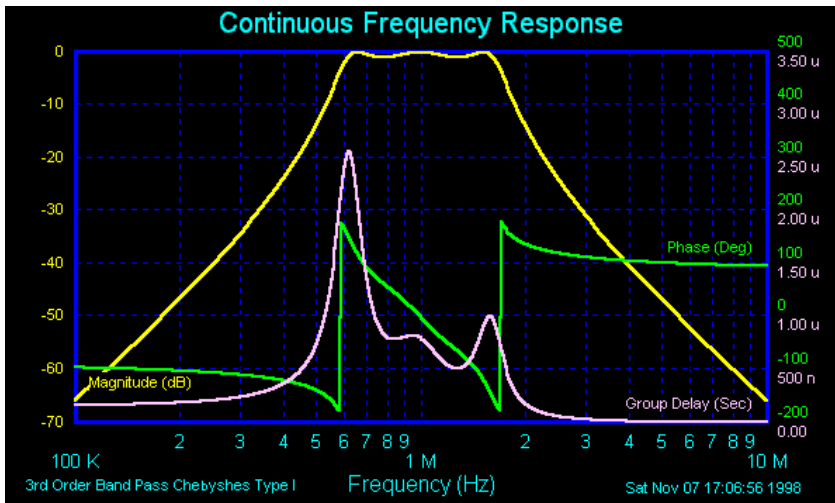
Chebyshev Type I Low Pass filter, 1MHz Pass Band Frequency



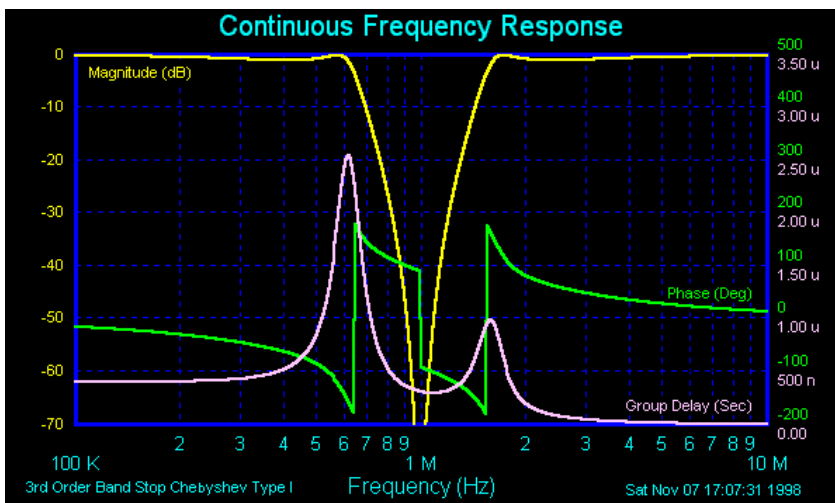
Chebyshev Type I High Pass filter, 1MHz Pass Band Frequency



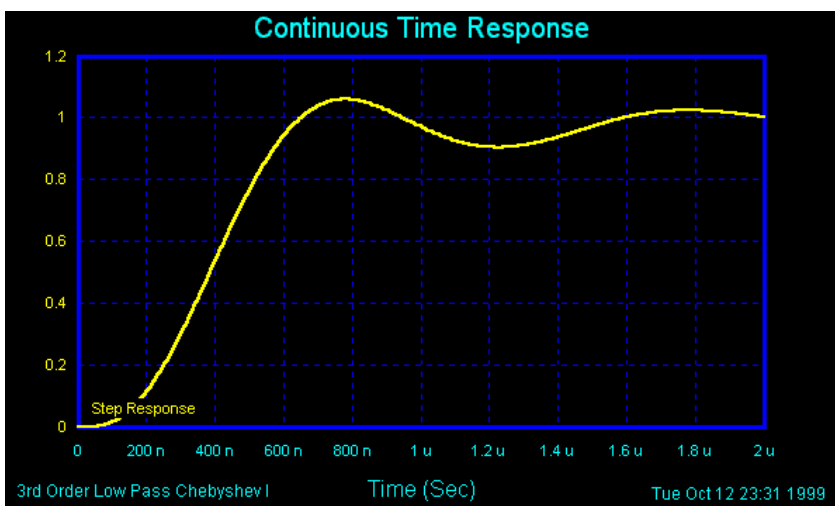
Chebyshev Type I Band Pass filter, 1MHz Center Frequency, 1MHz Pass Band Width



Chebyshev Type I Band Stop filter, 1MHz Center Frequency, 1MHz Pass Band Width



Chebyshev Type I Low Pass Step Response



Custom Filters

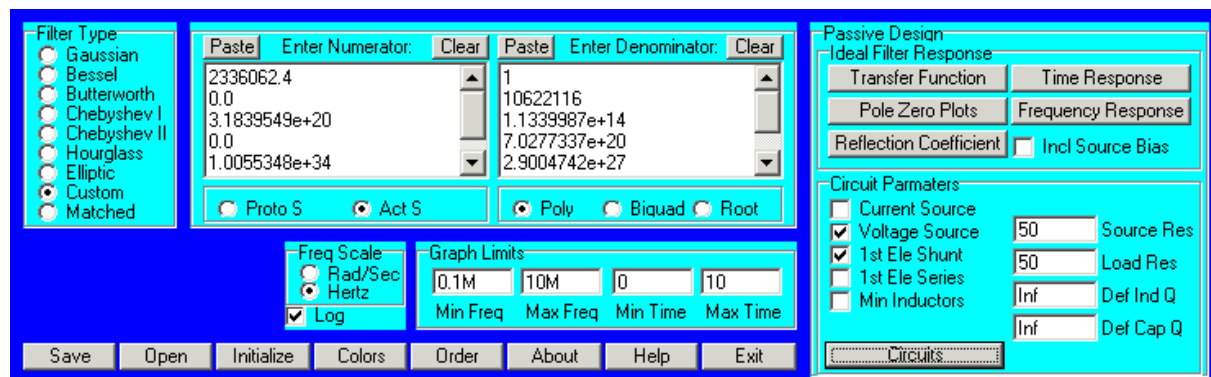
Filter Solutions supports filter design from user entered poles and zeros, biquads, or

polynomial with the use of the Custom windows. Transfer function pages in Filter Solutions may export transfer functions to the Custom windows where you may add, delete, or modify the filter transfer function. It is possible to create filters composed a combination of active and passive filters, or filters composed of Elliptic and Butterworth filters.

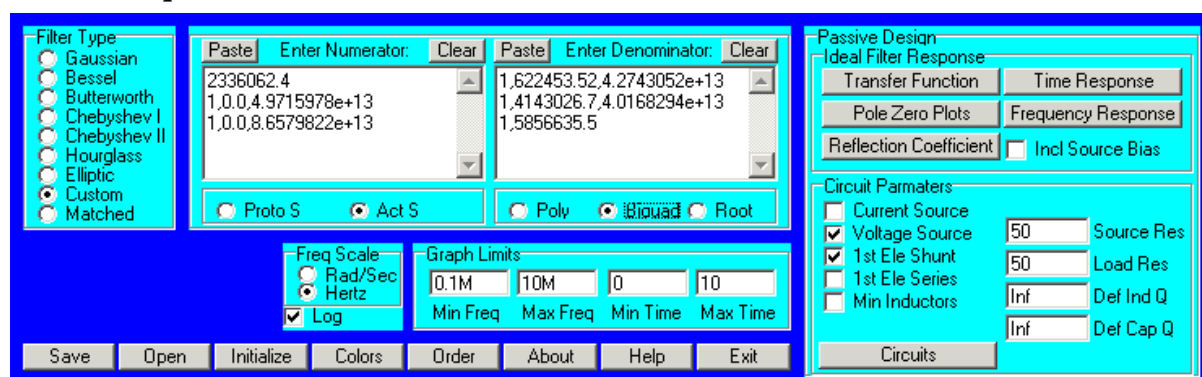
Each Transfer Function window contains a "Vec" button to display textual vectors. Each Vectors windows has a "Send to Custom" button to transfer all displayed vectors to the Custom window. The format of the vectors (Poly, Biquad, Root) will match the selected format of the Custom Window.

The pole/zero plot windows may also be used to add, delete, or modify pole or zero locations prior generating the transfer function.

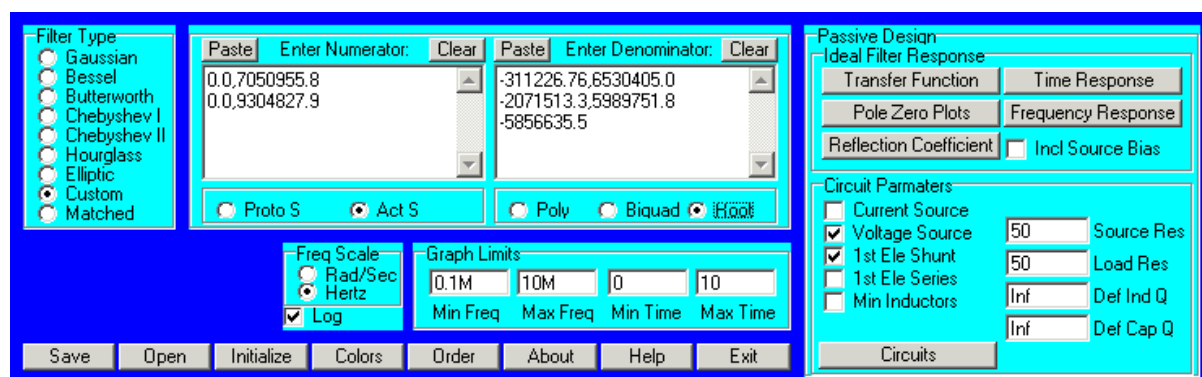
Custom Polynomials



Custom Biquads



Custom Roots



Advanced Filters

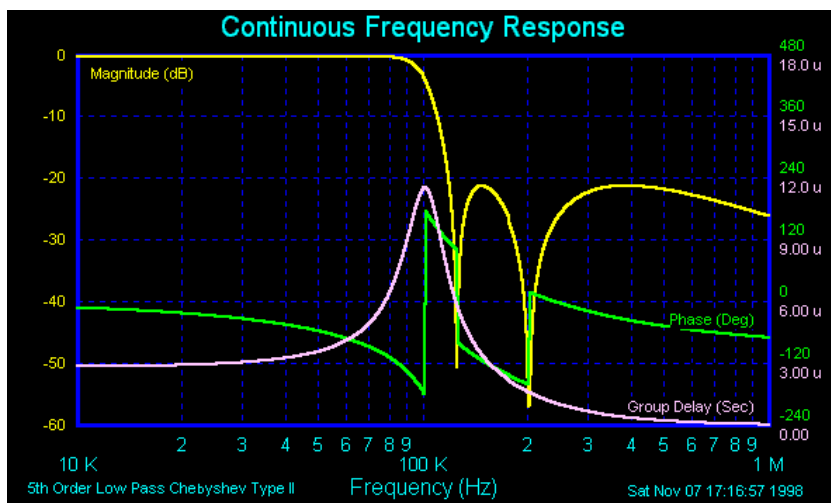
Chebyshev Type II Filters

The Chebyshev Type II Filter, also known as the Inverse Chebyshev Filter, contains a Butterworth style, or maximally flat, pass band, a moderate group delay, and an equiripple stop band.

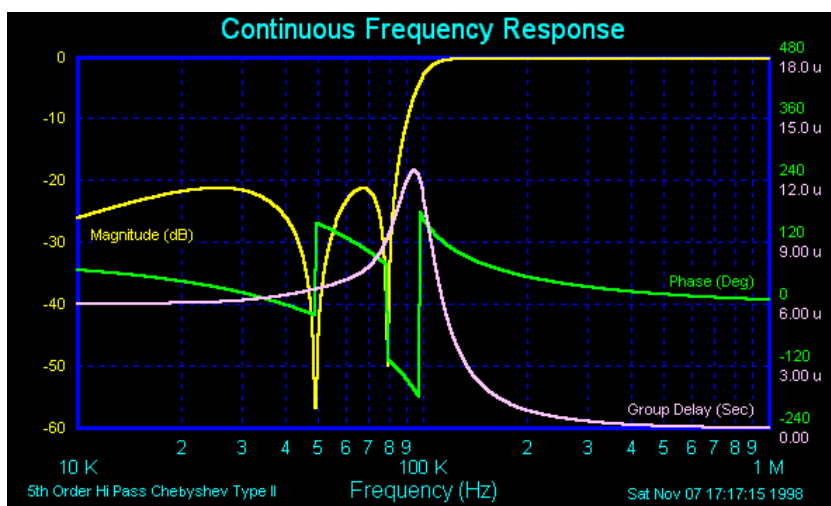
Like the Butterworth Filter, the pass band attenuation of the Chebyshev Type II Filter is defined to be -3.01 dB. However, Filter Solutions allows the user the option of selecting any pass band attenuation in dB's that will define the filters cut off frequency.

Below are examples of 5th order Chebyshev Type II low pass, high pass, band pass and band stop filters and the low pass step response. The stop band ratio is 1.2 in all cases shown. Compare the stop band attenuation and the group delay to that of the Hourglass and Elliptic Filters.

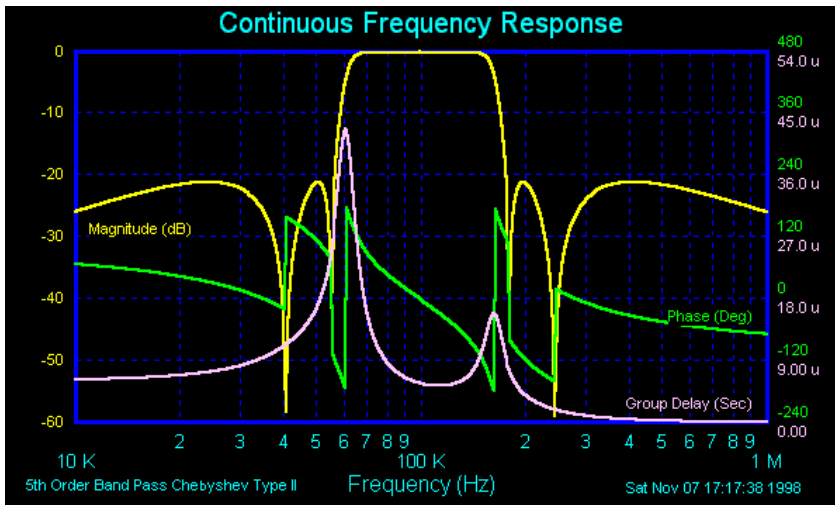
Chebyshev Type II Low Pass filter, 100KHz Pass Band Frequency



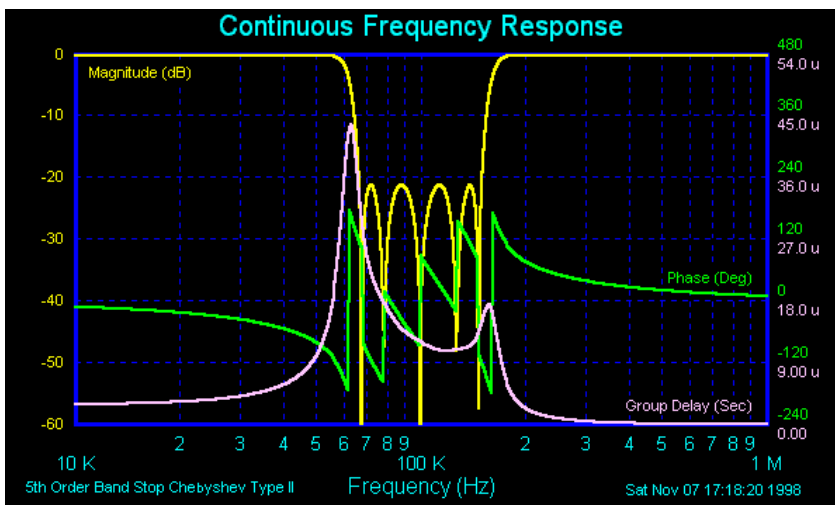
Chebyshev Type II High Pass filter, 100KHz Pass Band Frequency



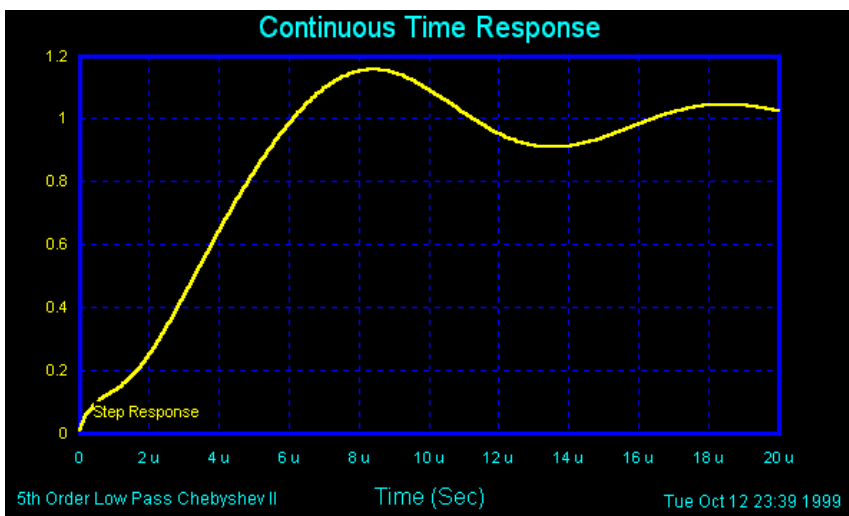
Chebyshev Type II Band Pass filter, 100KHz Center Frequency, 100KHz Pass Band Width



Chebyshev Type II Band Stop filter, 100KHz Center Frequency, 100KHz Pass Band Width



Chebyshev Type II Low Pass Step Response



Hourglass Filters

The Hourglass filter's distinguishing trait is that the reflection zero frequencies are exactly the

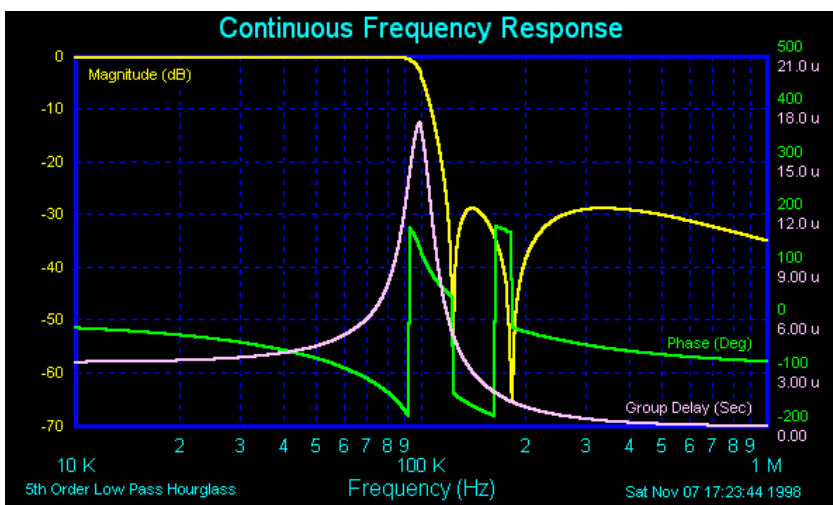
inverse of the transmission zero frequencies. The Hourglass Filter is similar to the Chebyshev Type II Filter, but has a sharper cut off, higher group delay, and greater stop band attenuation. The pass band also contains a slight equiripple characteristic, which makes it a special case of the Elliptic filter. The distinguishing feature of the Hourglass filter is that the reflection zeros are the reciprocal of the transmission zeros.

Like the Chebyshev Type II Filter, the pass band attenuation of the Chebyshev Type II Filter is defined to be -3.01 dB. However, Filter Solutions allows the user the option of selecting any pass band attenuation in dB's that will define the filters cut off frequency.

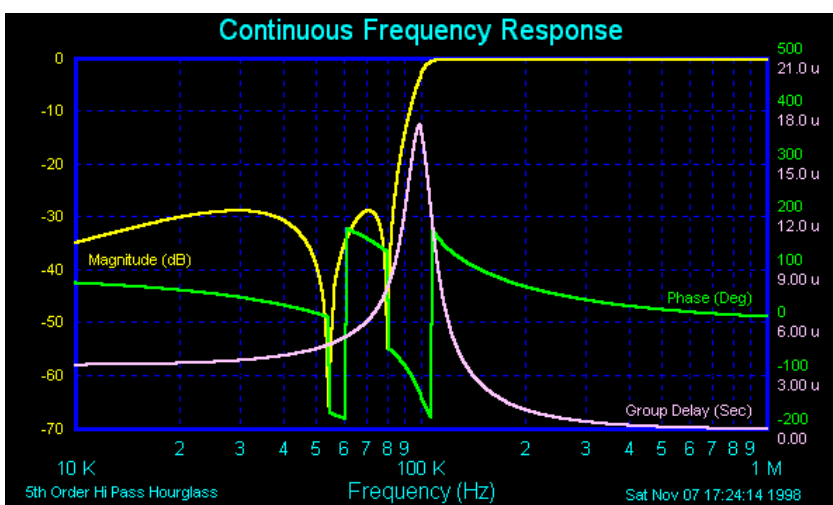
The Hourglass Filter was first derived by Dr. Byron Bennett of Montana State University, and is documented in IEEE Transactions on Circuits and Systems, December 1988, volume 12 page 1469.

Below are examples of 5th order Hourglass low pass, high pass, band pass and band stop filters and low pass step response. The stop band ratio is 1.2 in all cases shown. Compare the stop band attenuation and the group delay to that of the Chebyshev II and Elliptic Filters.

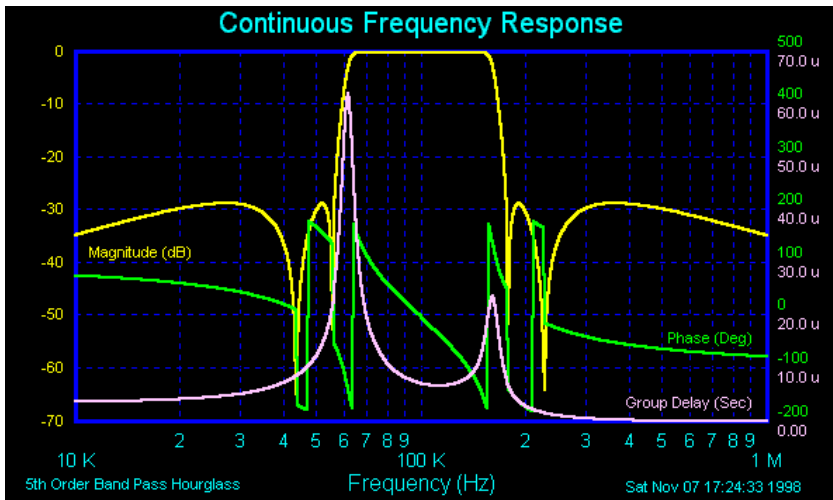
Hourglass Low Pass filter, 100KHz Pass Band Frequency



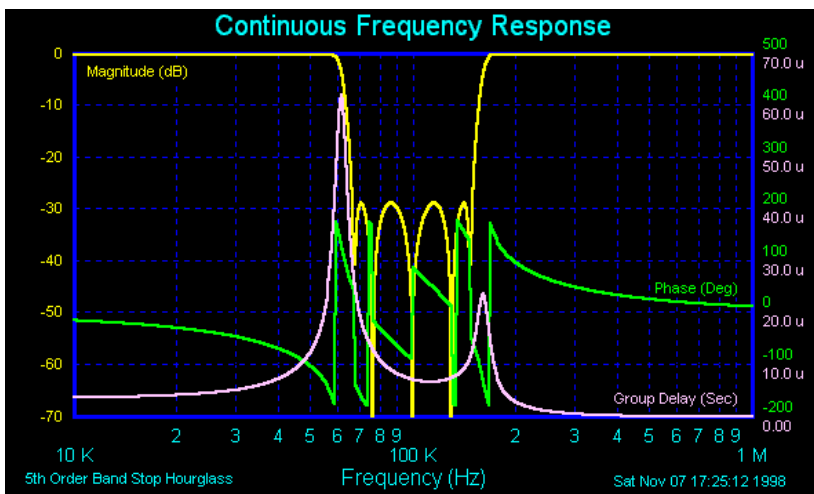
Hourglass High Pass filter, 100KHz Pass Band Frequency



Hourglass Band Pass filter, 100KHz Center Frequency, 100KHz Pass Band Width



Hourglass Band Stop filter, 100KHz Center Frequency, 100KHz Pass Band Width



Hourglass Band Stop Step Response

Elliptic Filters

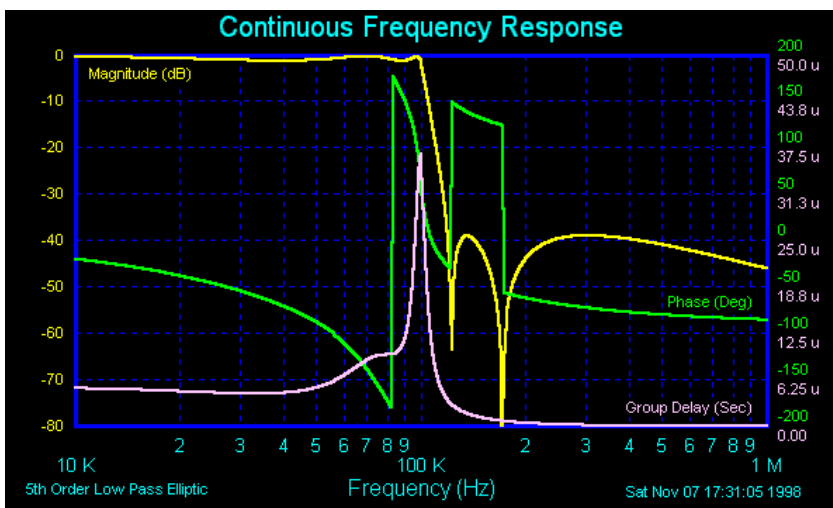
The Elliptic Filter contains a Chebyshev Type I style equiripple pass band, an equipped stop band, a sharp cut off, high group delay, and greatest stop band attenuation.

Like the Chebyshev Type I Filter, the Elliptic pass band attenuation is defined to be the same value as the pass band ripple amplitude. However, Filter Solutions allows the user the option of selecting any pass band attenuation in dB's that will define the filters cut off frequency.

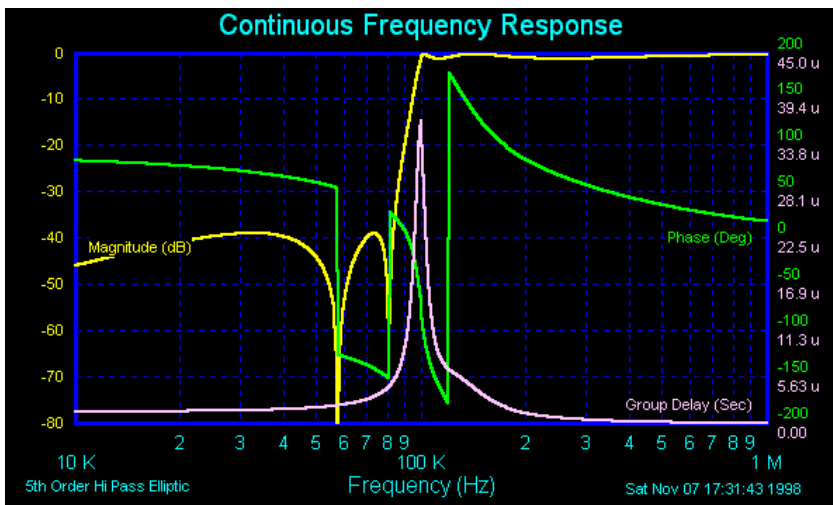
Below are examples of 5th order Elliptic low pass, high pass, band pass and band stop filters and low pass step response. The stop band ratio is 1.2 in all cases shown. Compare the stop band attenuation and the group delay to that of the Chebyshev II and Hourglass Filters.

Raised Cosine

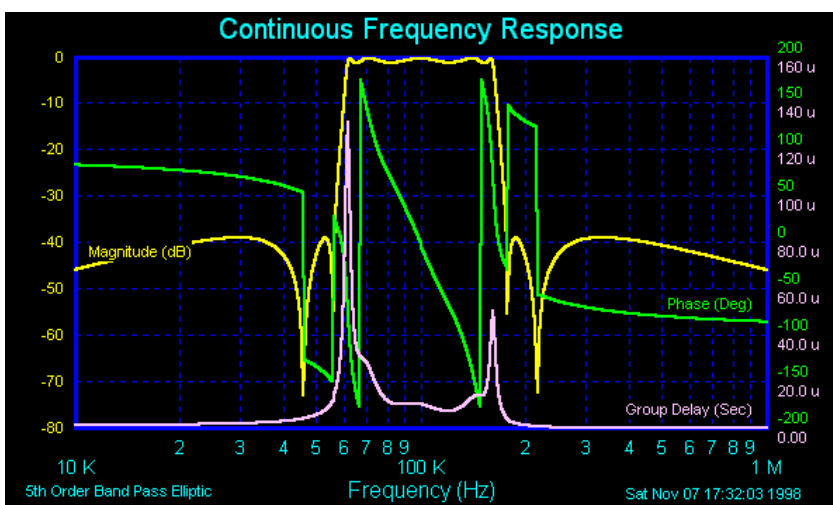
Elliptic Low Pass filter, 100KHz Cutoff Frequency



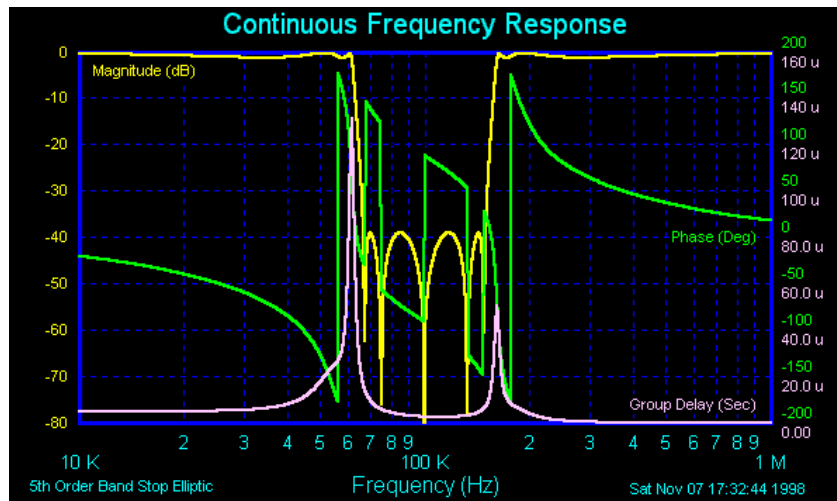
Elliptic High Pass filter, 100KHz Cutoff Frequency



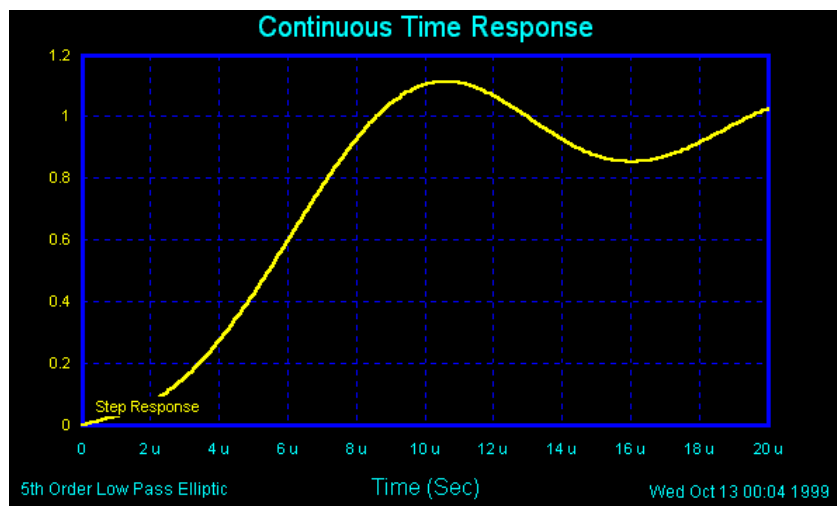
Elliptic Band Pass filter, 100KHz Cutoff Frequency, 100KHz Pass Band Width



Elliptic Band Stop filter, 100KHz Cutoff Frequency, 100KHz Pass Band Width



Elliptic Step Response



Matched Filters

The Matched Filter is for use in communications. The distinguishing characteristic of a Matched Filter is the step response approximating a ramp, and the impulse response approximates a pulse. The purpose of the Matched Filter is to maximize the signal to noise ratio and to minimize the probability of undetected errors received from a signal.

The function of a Matched filter is to optimize the signal to noise ratio at the sampling point of a bit stream. This happens if the filter applied to the bit stream has an impulse response that is the time inverse of the pulse shape that is being sampled. If the pulse is rectangular, the filter impulse response must therefore also be a rectangle, and the step response is a ramp.

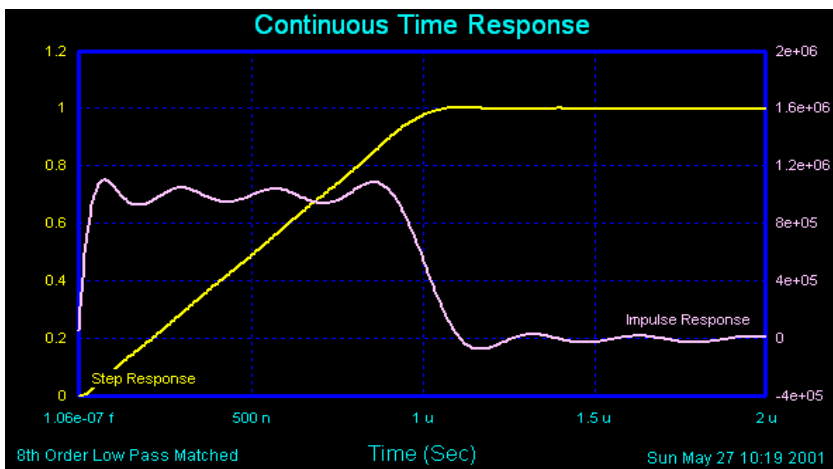
Filter Solutions and Filter Light allow you to define your Matched Filter by setting the rise time of the ramp. The proper use of the matched filter is to set the rise time to be equal to the pulse width of the pulses in a bit stream.

Since ideal continuous and IIR matched filter solutions are not realizable, they must be approximated. Filter Solutions uses an approximate solution that optimizes the time response of the

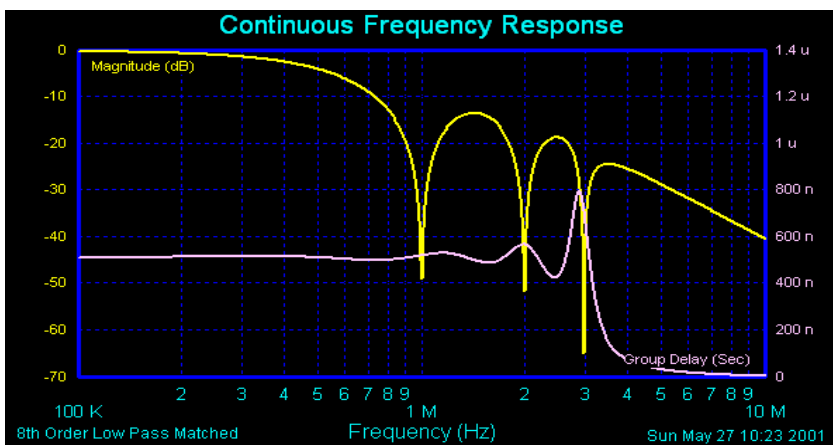
filter with the constraint that the transfer function zeros remain on the JW axis. Specifically, the integration of the square of the error between the filter impulse response and the ideal impulse response (a square pulse) is minimized under the mentioned restraint conditions. The purpose of the JW zeros constraint is to allow the filter to be realized with passive elements.

Below are examples of Matched filters step, impulse, and frequency responses. Below the frequency response is the Matched filter square wave response when the rise time of the filter is set to match the pulse width of the square wave.

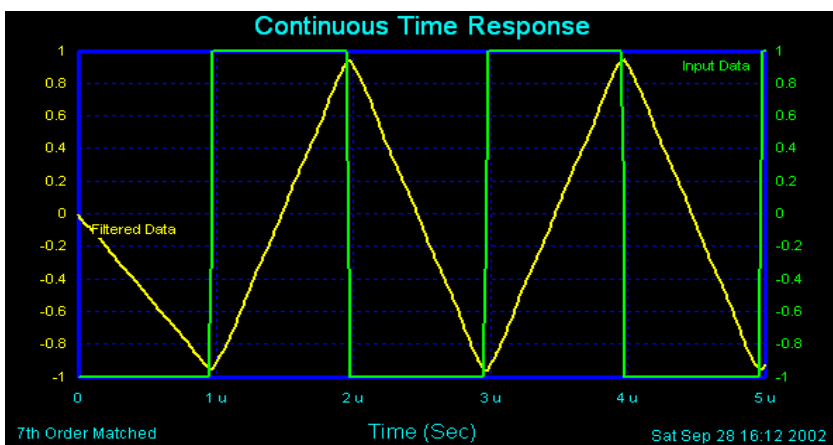
Matched Filter Step and Impulse Response



Matched Filter Frequency Response



Matched Filter Square Wave Response



Delay Filters

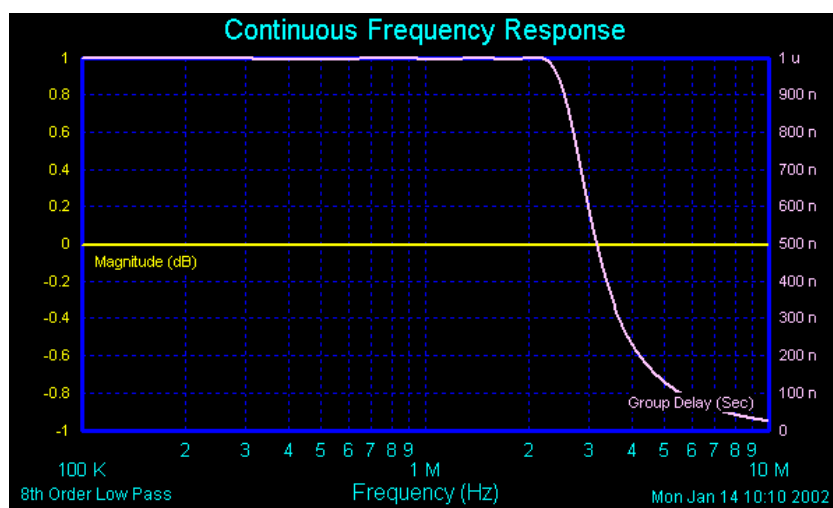
The Delay Filter simulates a transport delay frequency response. The frequency response magnitude of an ideal transport delay filter is unity for all frequencies, and the frequency response group delay is equal to the duration of the transport delay for all frequencies.

It is frequently necessary to account for transport delay in controls applications, and it is occasionally useful to delay a signal for timing purposes. Filter Solutions provides a Pade approximation of an ideal transport delay frequency response consisting of a series of all pass stages with a controlled group delay. With an equiripple period of 2.0, the group delay is designed to be accurate for frequencies up to $(N-1)/(T\pi)$ Hz where N is the order of the filter, and T is the design transport delay. This value may be adjusted slightly by adjusting the equiripple period. The same equiripple group delay response is available for modified Bessel Filters.

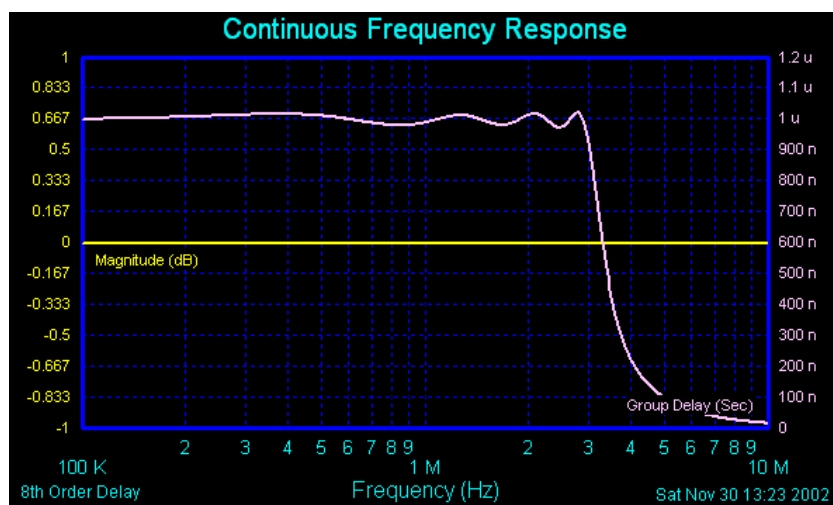
Filter Solutions allows you to define your Delay Filter by setting the delay time of the filter. The delay filter implemented by Filter Solutions optimizes the frequency response as opposed to the time response of the filter.

Below are examples of 8th order, 1 microsecond Delay filters frequency and step responses.

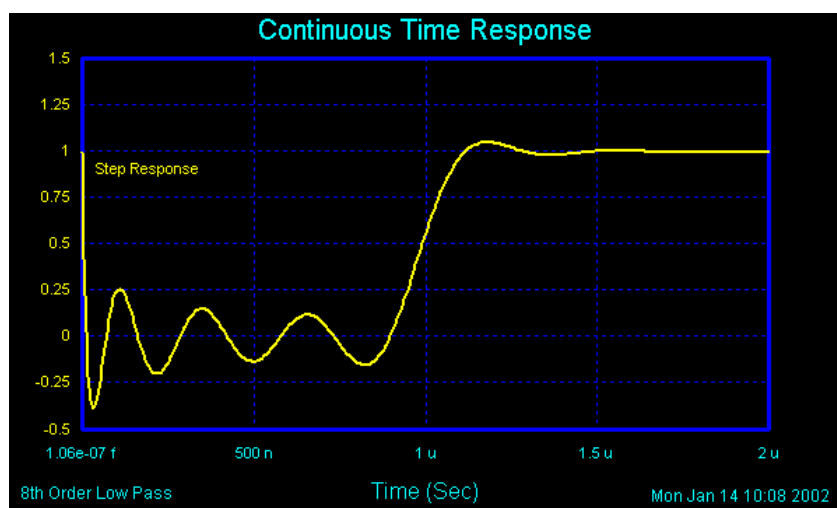
1 uSec Delay Filter Magnitude and Group Delay Response Ripple Period = 2.0

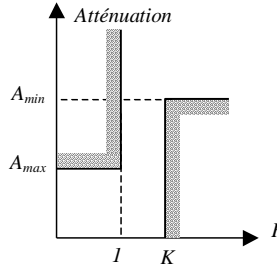
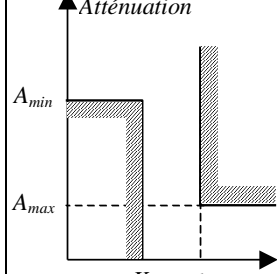
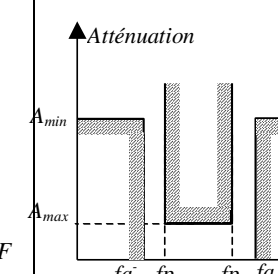
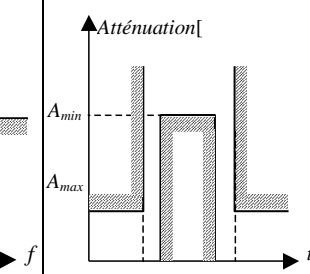
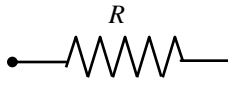
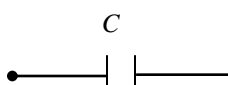
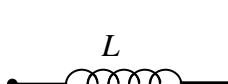
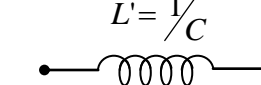
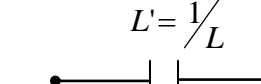
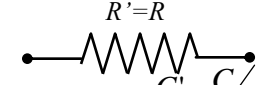
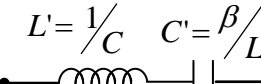
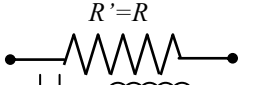
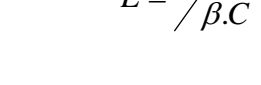
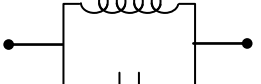
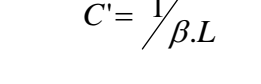


1 uSec Delay Filter Magnitude and Group Delay Response Ripple Period = 2.6

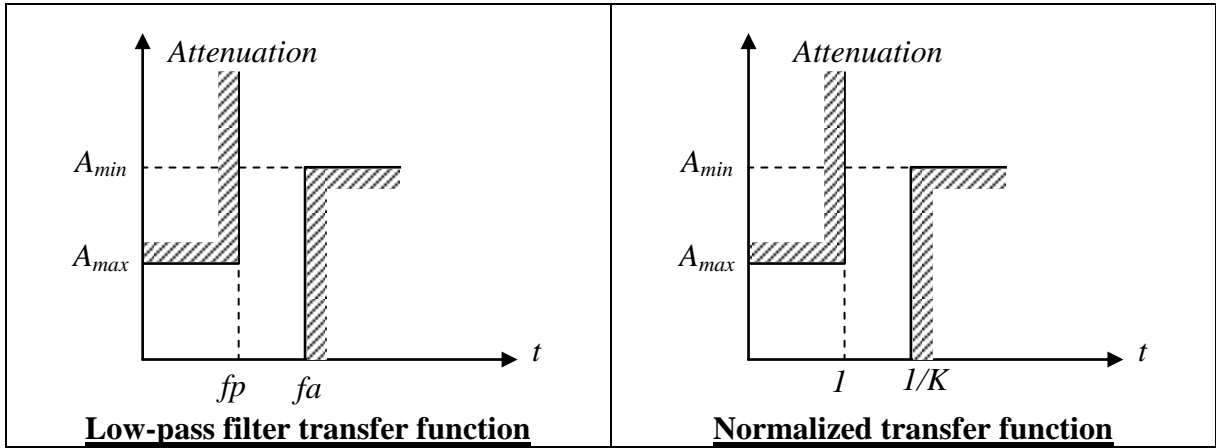


1 uSec Delay Filter Step Response



	<i>Low Pass</i>	<i>High Pass</i>	<i>Pass Band</i>	<i>Stop band</i>
T . F	$P = j\omega$	$P <----> \frac{1}{P}$	$P <---> \frac{1}{\beta} \left(\frac{P+1}{P} \right)$	$P <----> \left(\frac{\beta}{P+1} \right)$
ideal function.				
equivalent transformation.	  	  	   	   

Low pass filter (prototype)



$$K = \frac{fp}{fa} : \quad \text{Selectivity.}$$

A_{\max} : maximal Attenuation in the pass band.

A_{\min} : minimal Attenuation in the rejected band.

let n be the filter order; the poles are defined as

$$P_k = \alpha_k + j.B_k$$

$$P_k^* = \alpha_k - j.B_k$$

Chebycheff

We have

$$a_k = \sin\left[\frac{(2k-1)\pi}{2n}\right] \quad k = 1, 2, 3, \dots, n.$$

$$b_k = \gamma^2 + \sin^2\left[\frac{(k)\pi}{n}\right] \quad k = 1, 2, 3, \dots, n.$$

with

$$\gamma = \sin k\left(\frac{\beta_k}{2n}\right) \quad \beta = \ln\left[\coth\left(\frac{A_{\max}}{17.37}\right)\right]$$

therefore,

$$g_n = \frac{4a_k \cdot a_{k-1}}{b_{k-1} \cdot g_{k-1}} \quad g_a = \frac{2a_1}{\gamma}$$

P-configuration:

$$\begin{aligned} C_k &= g_k & k &= 1, 3, 5, \dots, n. \\ L_k &= g_k & k &= 2, 4, 6, \dots, n. \end{aligned}$$

T-configuration

$$\begin{aligned} C_k &= g_k & k &= 2, 4, 6, \dots, n. \\ L_k &= g_k & k &= 1, 3, 5, \dots, n. \end{aligned}$$

Butterworth

$$g_k = \sin\left[\frac{(2k-1)\pi}{2n}\right]$$

P-configuration

$$\begin{aligned} C_k &= g_n & k &= 1, 3, 5, \dots, n \\ L_k &= g_n & k &= 2, 4, 6, \dots, n \end{aligned}$$

T-configuration

$$\begin{aligned} C_k &= g_n & k &= 2, 4, 6, \dots, n \\ L_k &= g_n & k &= 1, 3, 5, \dots, n \end{aligned}$$

http://en.wikipedia.org/wiki/Distributed_element_filter

History

Development of distributed element filters began in the years before World War II. A major paper on the subject was published by Mason and Sykes in 1937.^[8] Mason had filed a patent^[9] much earlier, in 1927, and that patent may contain the first published design which moves away from a lumped element analysis.^[10] Mason and Sykes' work was focused on the formats of coaxial cable and balanced pairs of wires – the planar technologies were not yet in use. Much development was carried out during the war years driven by the filtering needs of radar and electronic counter-measures. A good deal of this was at the MIT Radiation Laboratory,^[11] but other laboratories in the US and the UK were also involved.^{[12][13]}

Some important advances in network theory were needed before filters could be advanced beyond wartime designs. One of these was the commensurate line theory of Paul Richards.^[14] Commensurate lines are networks in which all the elements are the same length (or in some cases multiples of the unit length), although they may differ in other dimensions to give different characteristic impedances. Richards' transformation allows a lumped element design to be taken "as is" and transformed directly into a distributed element design using a very simple transform equation.^[15]

The difficulty with Richards' transformation from the point of view of building practical filters was that the resulting distributed element design invariably included series connected elements. This was not possible to implement in planar technologies and was often inconvenient in other technologies. This problem was solved by K. Kuroda who used impedance transformers to eliminate the series elements. He published a set of transformations known as Kuroda's identities in 1955, but his work was written in Japanese and it was several years before his ideas were incorporated into the English-language literature.^[16]

Following the war, one important research avenue was trying to increase the design bandwidth of wide-band filters. The approach used at the time (and still in use today) was to start with a lumped element prototype filter and through various transformations arrive at the desired filter in a distributed element form. This approach appeared to be stuck at a minimum Q of five (see Band-pass filters below for an explanation of Q). In 1957, Leo Young at Stanford Research Institute published a method for designing filters which started with a distributed element prototype.^[17] This prototype was based on quarter wave impedance transformers and was able to produce designs with bandwidths up to an octave, corresponding to a Q of about 1.3. Some of Young's procedures in that paper were empirical, but later,^[18] exact solutions were published. Young's paper specifically addresses directly coupled cavity resonators, but the procedure can equally be applied to other directly coupled resonator types, such as those found in modern planar technologies and illustrated in this article. The capacitive gap filter (figure 8) and the parallel-coupled lines filter (figure 9) are examples of directly coupled resonators.^[15]

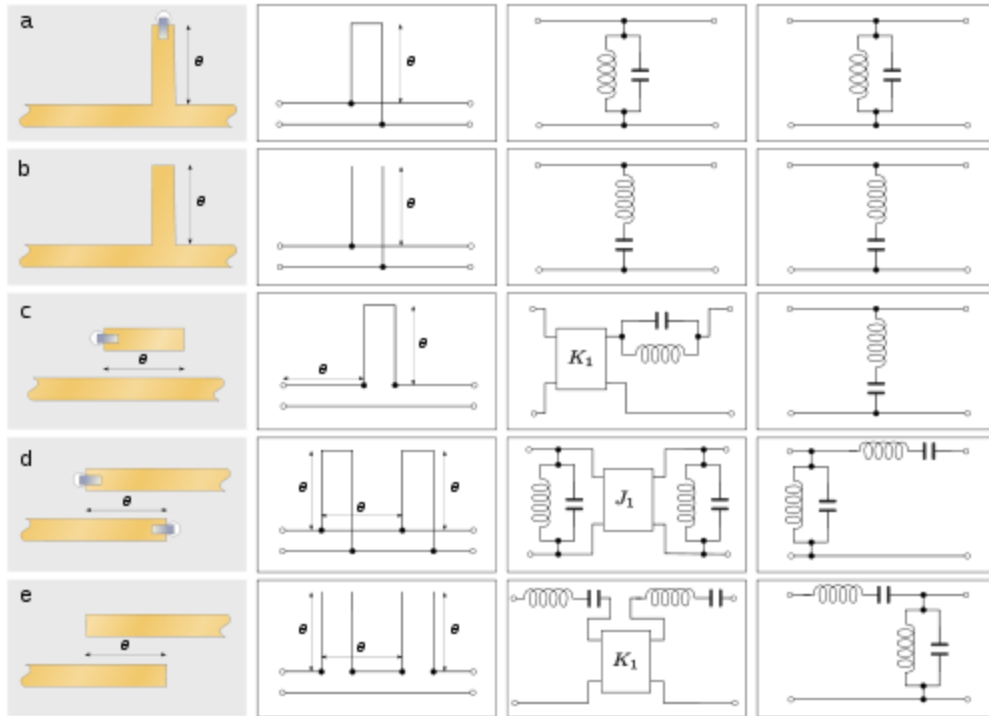


Figure 3. Some simple planar filter structures are shown in the first column. The second column shows the open-wire equivalent circuit for these structures. The third column is a semi-lumped element approximation where the elements marked K or J are impedance or admittance transformers respectively. The fourth column shows a lumped-element approximation making the further assumption that the impedance transformers are $\lambda/4$ transformers. **(a)** A short-circuit stub in parallel with the main line. **(b)** An open-circuit stub in parallel with the main line. **(c)** A short-circuit line coupled to the main line. **(d)** Coupled short-circuited lines. **(e)** Coupled open-circuited lines.



represents a strap through the board making connection with the ground plane underneath.

The introduction of printed planar technologies greatly simplified the manufacture of many microwave components including filters, and microwave integrated circuits then became possible. It is not known when planar transmission lines originated, but experiments using them were recorded as early as in 1936.^[19] The inventor of printed stripline, however, is known; this was Robert M. Barrett who published the idea in 1951.^[20] This caught on rapidly, and Barrett's *stripline* soon had fierce commercial competition from rival planar formats, especially *triplate* and *microstrip*. The generic term *stripline* in modern usage usually refers to the form then known as *triplate*.^[21]

Early stripline directly-coupled-resonator filters were end-coupled, but the length was reduced and the compactness successively increased with the introduction of parallel-coupled line filters,^[22] interdigital filters,^[23] and comb-line filters.^[24] Much of this work was published by the group at Stanford led by George Matthaei, and also including Leo Young mentioned above, in a landmark book which still today serves as a reference for circuit designers.^{[25][26]} The hairpin filter was first described in 1972.^{[27][28]} By the

1970s, most of the filter topologies in common use today had been described.^[29] More recent research has concentrated on new or variant mathematical classes of the filters, such as pseudo-elliptic, while still using the same basic topologies, or with alternative implementation technologies such as suspended stripline and finline.^[30]

The initial non-military application of distributed element filters was in the microwave links used by telecommunications companies to provide the backbone of their networks. These links were also used by other industries with large, fixed networks, notably television broadcasters.^[31] Such applications were part of large capital investment programs. However, mass-production manufacturing made the technology cheap enough to incorporate in domestic satellite television systems.^[32] An emerging application is in superconducting filters for use in the cellular base stations operated by mobile phone companies.^[33]

[edit] Basic components

The simplest structure that can be implemented is a step in the characteristic impedance of the line, which introduces a discontinuity in the transmission characteristics. This is done in planar technologies by a change in the width of the transmission line. Figure 4(a) shows a step up in impedance (narrower lines have higher impedance). A step down in impedance would be the mirror image of figure 4(a). The discontinuity can be represented approximately as a series inductor, or more exactly, as a low-pass T circuit as shown in figure 4(a).^[34] Multiple discontinuities are often coupled together with impedance transformers to produce a filter of higher order. These impedance transformers can be just a short (often $\lambda/4$) length of transmission line. These composite structures can implement any of the filter families (Butterworth, Chebyshev, etc.) by approximating the rational function of the corresponding lumped element filter. This correspondence is not exact since distributed element circuits cannot be rational and is the root reason for the divergence of lumped element and distributed element behaviour. Impedance transformers are also used in hybrid mixtures of lumped and distributed element filters (the so-called semi-lumped structures).^[35]

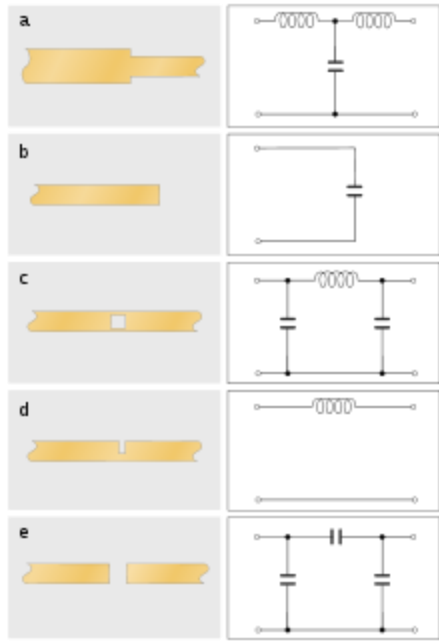


Figure 4. More stripline elements and their lumped-element counterparts. (a) An abrupt stepped impedance.^[34] (b) A line coming to an abrupt end.^[34] (c) A hole or slit in a line.^[36] (d) A transverse half-slit across the line.^[37] (e) A gap in the line.^[37]

Another very common component of distributed element filters is the stub. Over a narrow range of frequencies, a stub can be used as a capacitor or an inductor (its impedance is determined by its length) but over a wide band it behaves as a resonator. Short-circuit, nominally quarter-wavelength stubs (figure 3(a)) behave as shunt LC antiresonators, and an open-circuit nominally quarter-wavelength stub (figure 3(b)) behaves as a series LC resonator. Stubs can also be used in conjunction with impedance transformers to build more complex filters and, as would be expected from their resonant nature, are most useful in band-pass applications.^[38] While open-circuit stubs are easier to manufacture in planar technologies, they have the drawback that the termination deviates significantly from an ideal open circuit (see figure 4(b)), often leading to a preference for short-circuit stubs (one can always be used in place of the other by adding or subtracting $\lambda/4$ to or from the length).^[34]

A helical resonator is similar to a stub, in that it requires a distributed element model to represent it, but is actually built using lumped elements. They are built in a non-planar format and consist of a coil of wire, on a former and core, and connected only at one end. The device is usually in a shielded can with a hole in the top for adjusting the core. It will often look physically very similar to the lumped LC resonators used for a similar purpose. They are most useful in the upper VHF and lower UHF bands whereas stubs are more often applied in the higher UHF and SHF bands.^[39]

Coupled lines (figures 3(c-e)) can also be used as filter elements; like stubs, they can act as resonators and likewise be terminated short-circuit or open-circuit. Coupled lines tend to be preferred in planar technologies, where they are easy to implement, whereas stubs tend to be preferred elsewhere.

Implementing a true open circuit in planar technology is not feasible because of the dielectric effect of the substrate which will always ensure that the equivalent circuit contains a shunt capacitance. Despite this, open circuits are often used in planar formats in preference to short circuits because they are easier to implement. Numerous element types can be classified as coupled lines and a selection of the more common ones is shown in the figures.^[40]

Some common structures are shown in figures 3 and 4, along with their lumped-element counterparts. These lumped-element approximations are not to be taken as equivalent circuits but rather as a guide to the behaviour of the distributed elements over a certain frequency range. Figures 3(a) and 3(b) show a short-circuit and open-circuit stub, respectively. When the stub length is $\lambda/4$, these behave, respectively, as anti-resonators and resonators and are therefore useful, respectively, as elements in band-pass and band-stop filters. Figure 3(c) shows a short-circuited line coupled to the main line. This also behaves as a resonator, but is commonly used in low-pass filter applications with the resonant frequency well outside the band of interest. Figures 3(d) and 3(e) show coupled line structures which are both useful in band-pass filters. The structures of figures 3(c) and 3(e) have equivalent circuits involving stubs placed in series with the line. Such a topology is straightforward to implement in open-wire circuits but not with a planar technology. These two structures are therefore useful for implementing an equivalent series element.^[41]

edit Low-pass filters

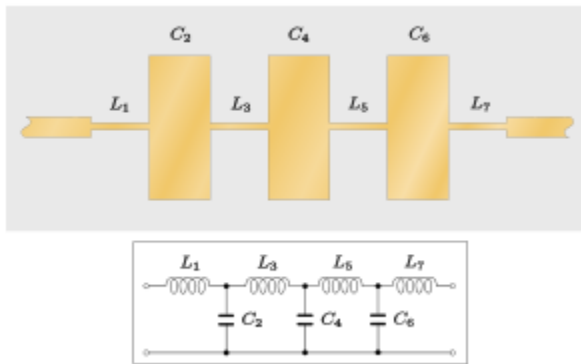


Figure 5. Stepped-impedance low-pass filter formed from alternate high and low impedance sections of line

A low-pass filter can be implemented quite directly from a ladder topology lumped-element prototype with the stepped impedance filter shown in figure 5. The filter consists of alternating sections of high-impedance and low-impedance lines which correspond to the series inductors and shunt capacitors in the lumped-element implementation. Low-pass filters are commonly used to feed direct current (DC) bias to active components. Filters intended for this application are sometimes referred to as *chokes*. In such cases, each element of the filter is $\lambda/4$ in length (where λ is the wavelength of the main-line signal to be blocked from transmission into the DC source) and the high-impedance sections of the line are

made as narrow as the manufacturing technology will allow in order to maximise the inductance.^[42] Additional sections may be added as required for the performance of the filter just as they would for the lumped-element counterpart. As well as the planar form shown, this structure is particularly well suited for coaxial implementations with alternating discs of metal and insulator being threaded on to the central conductor.^{[43][44][45]}

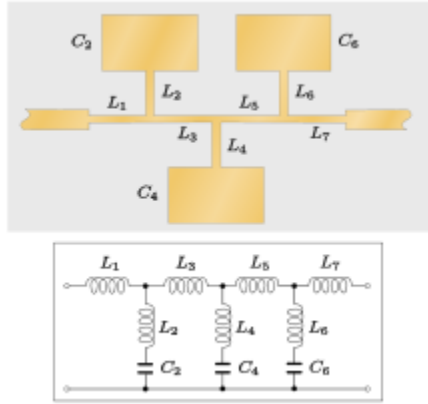


Figure 6. Another form of stepped-impedance low-pass filter incorporating shunt resonators

A more complex example of stepped impedance design is presented in figure 6. Again, narrow lines are used to implement inductors and wide lines correspond to capacitors, but in this case, the lumped-element counterpart has resonators connected in shunt across the main line. This topology can be used to design elliptical filters or Chebyshev filters with poles of attenuation in the stopband. However, calculating component values for these structures is an involved process and has led to designers often choosing to implement them as m-derived filters instead, which perform well and are much easier to calculate. The purpose of incorporating resonators is to improve the stopband rejection. However, beyond the resonant frequency of the highest frequency resonator, the stopband rejection starts to deteriorate as the resonators are moving towards open-circuit. For this reason, filters built to this design often have an additional single stepped-impedance capacitor as the final element of the filter.^[46] This also ensures good rejection at high frequency.^{[47][48][49]}

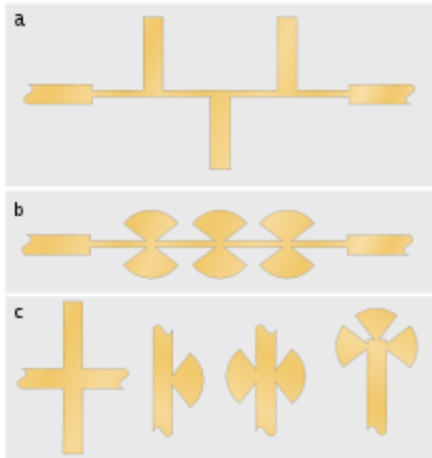


Figure 7. Low-pass filters constructed from stubs. (a) Standard stubs on alternating sides of main line $\lambda/4$ apart. (b) Similar construction using butterfly stubs. (c) Various forms of stubs, respectively, doubled stubs in parallel, radial stub, butterfly stub (paralleled radial stubs), clover-leaf stub (triple paralleled radial stubs).

Another common low-pass design technique is to implement the shunt capacitors as stubs with the resonant frequency set above the operating frequency so that the stub impedance is capacitive in the passband. This implementation has a lumped-element counterpart of a general form similar to the filter of figure 6. Where space allows, the stubs may be set on alternate sides of the main line as shown in figure 7(a). The purpose of this is to prevent coupling between adjacent stubs which detracts from the filter performance by altering the frequency response. However, a structure with all the stubs on the same side is still a valid design. If the stub is required to be a very low impedance line, the stub may be inconveniently wide. In these cases, a possible solution is to connect two narrower stubs in parallel. That is, each stub position has a stub on *both sides* of the line. A drawback of this topology is that additional transverse resonant modes are possible along the $\lambda/2$ length of line formed by the two stubs together. For a choke design, the requirement is simply to make the capacitance as large as possible, for which the maximum stub width of $\lambda/4$ may be used with stubs in parallel on both sides of the main line. The resulting filter looks rather similar to the stepped impedance filter of figure 5, but has been designed on completely different principles.^[42] A difficulty with using stubs this wide is that the point at which they are connected to the main line is ill defined. A stub that is narrow in comparison to λ can be taken as being connected on its centre-line and calculations based on that assumption will accurately predict filter response. For a wide stub, however, calculations that assume the side branch is connected at a definite point on the main line leads to inaccuracies as this is no longer a good model of the transmission pattern. One solution to this difficulty is to use radial stubs instead of linear stubs. A pair of radial stubs in parallel (one on either side of the main line) is called a butterfly stub (see figure 7(b)). A group of three radial stubs in parallel, which can be achieved at the end of a line, is called a clover-leaf stub.^{[50][51]}

[edit] Band-pass filters

A band-pass filter can be constructed using any elements that can resonate. Filters using stubs can clearly be made band-pass; numerous other structures are possible and some are presented below.

An important parameter when discussing band-pass filters is the fractional bandwidth. This is defined as the ratio of the bandwidth to the geometric centre frequency. The inverse of this quantity is called the Q-factor, Q . If ω_1 and ω_2 are the frequencies of the passband edges, then:^[52]

bandwidth $\Delta\omega = \omega_2 - \omega_1$,

geometric centre frequency $\omega_0 = \sqrt{\omega_1\omega_2}$ and

$$Q = \frac{\omega_0}{\Delta\omega}$$

[edit] Capacitive gap filter



Figure 8. Capacitive gap stripline filter

The capacitive gap structure consists of sections of line about $\lambda/2$ in length which act as resonators and are coupled "end-on" by gaps in the transmission line. It is particularly suitable for planar formats, is easily implemented with printed circuit technology and has the advantage of taking up no more space than a plain transmission line would. The limitation of this topology is that performance (particularly insertion loss) deteriorates with increasing fractional bandwidth, and acceptable results are not obtained with a Q less than about 5. A further difficulty with producing low- Q designs is that the gap width is required to be smaller for wider fractional bandwidths. The minimum width of gaps, like the minimum width of tracks, is limited by the resolution of the printing technology.^{[45][53]}

[edit] Parallel-coupled lines filter



Figure 9. Stripline parallel-coupled lines filter. This filter is commonly printed at an angle as shown to minimize the board space taken up, although this is not an essential feature of the design. It is also common for the end element or the overlapping halves of the two end elements to be a narrower width for matching purposes (not shown in this diagram, see Figure 1).

Parallel-coupled lines is another popular topology for printed boards, for which open-circuit lines are the simplest to implement since the manufacturing consists of nothing more than the printed track. The design consists of a row of parallel $\lambda/2$ resonators, but coupling over only $\lambda/4$ to each of the neighbouring resonators, so forming a staggered line as shown in figure 9. Wider fractional bandwidths are possible with this filter than with the capacitive gap filter, but a similar problem arises on printed boards as dielectric loss reduces the Q . Lower- Q lines require tighter coupling and smaller gaps between them which is limited by the accuracy of the printing process. One solution to this problem is to print the track on multiple layers with adjacent lines overlapping but not in contact because they are on different layers. In this way, the lines can be coupled across their width, which results in much stronger coupling than when they are edge-to-edge, and a larger gap becomes possible for the same performance.^[54] For other (non-printed) technologies, short-circuit lines may be preferred since the short-circuit provides a mechanical attachment point for the line and Q -reducing dielectric insulators are not required for mechanical support. Other than for mechanical and assembly reasons, there is little preference for open-circuit over short-circuit coupled lines. Both structures can realize the same range of filter implementations with the same electrical performance. Both types of parallel-coupled filters, in theory, do not have spurious passbands at twice the centre frequency as seen in many other filter topologies (e.g. stubs). However, suppression of this spurious passband requires perfect tuning of the coupled lines which is not realized in practice, so there is inevitably some residual spurious passband at this frequency.^{[45][55][56]}



Figure 10. Stripline hairpin filter

The hairpin filter is another structure that uses parallel-coupled lines. In this case, each pair of parallel-coupled lines is connected to the next pair by a short link. The "U" shapes so formed give rise to the name *hairpin filter*. In some designs the link can be longer, giving a wide hairpin with $\lambda/4$ impedance transformer action between sections.^{[57][58]} The angled bends seen in figure 10 are common to stripline designs and represent a compromise between a sharp right angle, which produces a large discontinuity, and a smooth bend, which takes up more board area which can be severely limited in some products. Such bends are often seen in long stubs where they could not otherwise be fitted into the space available. The lumped-element equivalent circuit of this kind of discontinuity is similar to a stepped-impedance discontinuity.^[37] Examples of such stubs can be seen on the bias inputs to several components in the photograph at the top of the article.^{[45][59]}

[edit] Interdigital filter



Figure 11. Stripline interdigital filter

Interdigital filters are another form of coupled-line filter. Each section of line is about $\lambda/4$ in length and is terminated in a short-circuit at one end only, the other end being left open-circuit. The end which is short-circuited alternates on each line section. This topology is straightforward to implement in planar technologies, but also particularly lends itself to a mechanical assembly of lines fixed inside a metal case. The lines can be either circular rods or rectangular bars, and interfacing to a coaxial format line is easy. As with the parallel-coupled line filter, the advantage of a mechanical arrangement that does not require insulators for support is that dielectric losses are eliminated. The spacing requirement between lines is not as stringent as in the parallel line structure; as such, higher fractional bandwidths can be achieved, and Q values as low as 1.4 are possible.^{[60][61]}

The comb-line filter is similar to the interdigital filter in that it lends itself to mechanical assembly in a metal case without dielectric support. In the case of the comb-line, all the lines are short-circuited at the same end rather than alternate ends. The other ends are terminated in capacitors to ground, and the design is consequently classified as semi-lumped. The chief advantage of this design is that the upper stopband can be made very wide, that is, free of spurious passbands at all frequencies of interest.^[62]

[edit] Stub band-pass filters

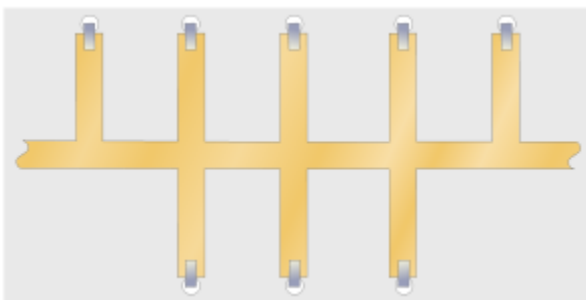


Figure 12. Stripline stub filter composed of $\lambda/4$ short-circuit stubs

As mentioned above, stubs lend themselves to band-pass designs. General forms of these are similar to stub low-pass filters except that the main line is no longer a narrow high impedance line. Designers have many different topologies of stub filters to choose from, some of which produce identical responses. An example stub filter is shown in figure 12; it consists of a row of $\lambda/4$ short-circuit stubs coupled together by $\lambda/4$ impedance transformers. The stubs in the body of the filter are double paralleled stubs while the stubs on the end sections are only singles, an arrangement that has impedance matching advantages. The impedance transformers have the effect of transforming the row of shunt anti-resonators into a ladder of series resonators and shunt anti-resonators. A filter with similar properties can be constructed with $\lambda/4$ open-circuit stubs placed in series with the line and coupled together with $\lambda/4$ impedance transformers, although this structure is not possible in planar technologies.^[63]



Figure 13. Konishi's 60° butterfly stub

Yet another structure available is $\lambda/2$ open-circuit stubs across the line coupled with $\lambda/4$ impedance transformers. This topology has both low-pass and band-pass characteristics. Because it will pass DC, it is possible to transmit biasing voltages to active components without the need for blocking capacitors. Also, since short-circuit links are not required, no assembly operations other than the board printing are required when implemented as stripline. The disadvantages are (i) the filter will take up more board real estate than the corresponding $\lambda/4$ stub filter, since the stubs are all twice as long; (ii) the first spurious passband is at $2\omega_0$, as opposed to $3\omega_0$ for the $\lambda/4$ stub filter.^[64]

Konishi describes a wideband 12 GHz band-pass filter, which uses 60° butterfly stubs and also has a low-pass response (short-circuit stubs are required to prevent such a response). As is often the case with distributed element filters, the bandform into which the filter is classified largely depends on which bands are desired and which are considered to be spurious.^[65]

[edit] High-pass filters

Genuine high-pass filters are difficult, if not impossible, to implement with distributed elements. The usual design approach is to start with a band-pass design, but make the upper stopband occur at a frequency that is so high as to be of no interest. Such filters are described as pseudo-high-pass and the upper stopband is described as a vestigial stopband. Even structures that seem to have an "obvious" high-pass topology, such as the capacitive gap filter of figure 8, turn out to be band-pass when their behaviour for very short wavelengths is considered.^[66]

A Comparative Study of Different Microstrip Planar Bandpass Filters Topologies in an Industrial Context

Pascal Moroni^{1#}, Cécile Debarge^{2#}, Chloé Schaffauser^{3#}, Jean-Louis Cazaux^{4#}, Cédric Quendo^{5*}, Éric Rius^{6*}

[#]ALCATEL ALENIA SPACE-FRANCE,
26, av. Champollion, 31037 Toulouse, France[#]
^{*}LEST, UMR CNRS n°165,
CS 83818, 29288 Brest, France

(1) pascal.moroni@alcatelaleniaspace.com, (2) cecile.debarge@alcatelaleniaspace.com,
(3) chloe.schaffauser@alcatelaleniaspace.com, (4) jean-louis.cazaux@alcatelaleniaspace.com,
(5) eric.rius@univ-brest.fr, (2) cedric.quendo@univ-brest.fr

Abstract— One of the most stringent specification in modern microwave equipment is the control of spurious levels. This is a daily concern for microwave engineers designing telecommunication or observation space-borne equipment. AAS-F has studied and developed planar bandpass filters in microstrip mode because they can be easily inserted into hybrids. The investigated filters topologies are Coupled Lines, Interdigitated, Hairpin, Pseudo-Elliptic Response and Dual Behaviour Resonator. Each of them has advantages and drawbacks, first in term of electrical response but also in term of industrial effective use. For each topology, a list of main characteristics has been identified to allow comparison and easier choice, depending of the targeted application. This includes the reachable bandwidth, the insertion losses or the synthesis easiness. Also, the filters sensitivity to mechanical environment or manufacturing process have been summarized in a handful way. Such a study can give precious inputs for designers in other microwave domains as well.

I. INTRODUCTION

AAS-F has studied and developed different bandpass planar filters topologies which can be easily inserted into space hybrids. This paper presents a study of their advantages and drawbacks to contribute to design of a microwave equipment.

II. ELECTRICAL SPECIFICATIONS AND INDUSTRIAL CRITERIA

In telecommunication or observation satellite equipment, one of the most stringent specification is the control of spurious levels. Indeed, mixing products or LO (local oscillator) harmonics at RF equipment output can be near the useful bandwidth with high levels. Some examples of specifications are given in Table 1.

In order to comply with these specifications, both mixers and filters play a big role. Regarding the latter, specific bandpass topologies have been studied, realized and compared: Coupled Lines, Interdigitated, Hairpin, Pseudo-Elliptic Response and Dual Behaviour Resonator filters. For each topology, a list of main characteristics has been identified to allow comparison and ease choice, depending of the targeted application. All studies have been made using Al₂O₃ substrate ($\epsilon_r=9.5$, h=0.254 mm).

In addition to electrical performance (frequency band, bandwidth, insertion loss, selectivity ...), other criteria were:

- synthesis easiness which is important to avoid long design phase,
- manufacturing aspects (etching sensitivity, post-fabrication tuning capability), which can increase or lower the final production cost,
- the final size impact,
- the sensitivity to cover effects (at a height of 2.5 mm) which can be a problem at further integration stage.

TABLE I
Spurious levels specification examples

	Out of band Spurious Levels	
	LO Harmonics Levels	nRF+mLO Spurious Levels
6/4 GHz Receiver	critical spurious 2LO < -45 dBm	critical spurious 2RF-4LO < -70 dBc
14/12 GHz Receiver	< -35 dBm	< -35 dBc
12/20 GHz Up-Converter	< -40 dBm	< -65 dBc
30/20 GHz Down-Converter	critical spurious 2LO < -5 dBm	critical spurious 2RF-4LO < -55 dBc
36/14 GHz Observation Receiver	< -40 dBm	< -60dBc

III. MAIN CHARACTERISTICS OF ALL INVESTIGATED FILTERS

A. Coupled Lines filters

Figures 1 and 2 present a Coupled Lines filter topology and its performances respectively.

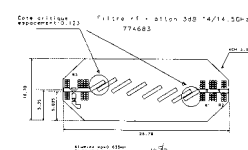


Fig. 1: Example of Coupled Lines filter in Ku-Band

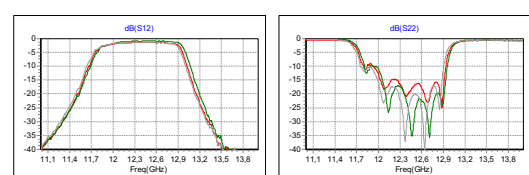


Fig. 2: Example of Coupled Lines filter performance

The different curves (S_{21}, S_{12} and S_{11}, S_{22}) correspond to measurement at -15°C , 25°C and 65°C .

Table II below summarizes the main electrical characteristics of this filter topology and its sensitivity to mechanical environment or manufacturing process.

TABLE II
Coupled Lines filters characteristics

Electrical characteristics	
Reachable bandwidth	15 %
Experienced frequency bands	All bands from L to Q
Insertion loss (typical)	1.5 dB in Ku-Band (6 poles)
Selectivity (20 dB attenuation)	At 4% from edge frequency
Out of band response	Spectrum not cleaned at every $2n f_0$
Synthesis and design	
Synthesis easiness	Models available on all microwave simulators
Manufacturing process	
Etching sensitivity	No
Tuning	Very difficult
Mechanical characteristics	
Size	Large
Cover effect	Yes

Selectivity is measured at the frequency at which rejection is 20dB and is given in percent of the edge frequency of the useful band.

Our conclusion is that this type of filter is handy and very easy to design but remains big and very sensitive to cover effect.

B. Interdigitated filters

Figures 3 and 4 and Table III present the topology and summarize the same data for the Interdigitated filters.

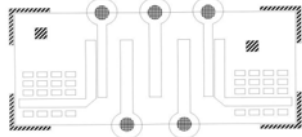


Fig. 3: Example of Interdigitated filter topology in Ku-Band

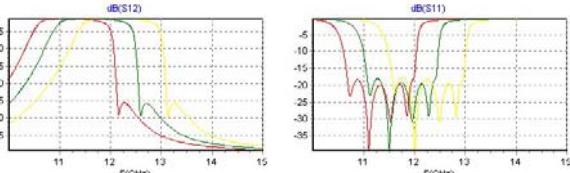


Fig. 4: Example of Interdigitated filter performance

TABLE III
Interdigitated filters characteristics

Electrical characteristics	
Reachable bandwidth	> 10 %
Experienced frequency bands	Ku
Typical insertion losses	1.5 dB in Ku band (5 poles)
Selectivity (20 dB attenuation)	At 4% from edge frequency
Out of band response	Dissymmetric – Spectrum not cleaned at every $(2n+1) f_0$

Synthesis and design	
Synthesis easiness	Via hole modelled separately. Models available on all microwave simulators
Manufacturing process	
Etching sensitivity	No
Via holes	Increase the manufacturing cost
Tuning	Impossible
Mechanical characteristics	
Size	Very small
Cover effect	Yes

This type of filter is very compact and presents very few out-of-band response but the necessary presence of via holes increase its manufacturing cost and delay.

C. Hairpin filters

Figures 5 and 6 and Table IV present the topology and summarize the same data for the Hairpin filter.

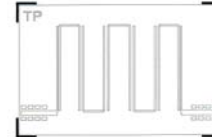


Fig. 5: Example of Hairpin filter topology in C-Band

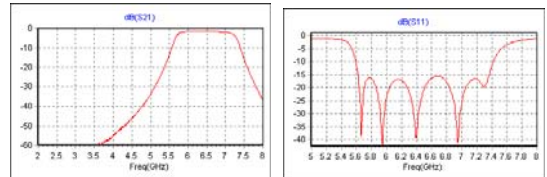


Fig. 6: Example of Hairpin filter performances in C-Band

TABLE IV
Hairpin filters characteristics

Electrical characteristics	
Reachable bandwidth	Between 5 and 15 %
Experienced frequency bands	C / Ku / K
Typical insertion losses	1 to 3 dB depending on poles number
Selectivity (20 dB attenuation)	7% to 10 % from edge frequency
Out of band response	Spectrum not cleaned at every $2n f_0$
Synthesis and design	
Synthesis easiness	Models available on all microwave simulators
Manufacturing process	
Etching sensitivity	Very low
Tuning	Impossible
Mechanical characteristics	
Size	Medium
Cover effect	Very weak

This type of filter presents a lot of advantages when filtering specification are stringent. It can easily replace Coupled Lines filter thanks to its smaller size and better electrical performances.

D. Pseudo-elliptic response filter

Figures 7 and 8 and Table V present the topology and summarize the same data for the Pseudo-elliptic response filter.

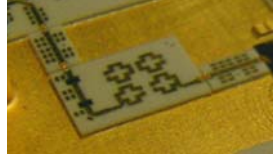


Fig. 7: Example of Pseudo-elliptic response filter topology in Ka band

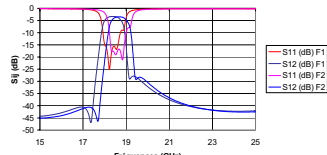


Fig. 8: Example of Pseudo-elliptic response filter performances in Ka band

TABLE V
Pseudo-elliptic response filters characteristics

Electrical characteristics	
Reachable bandwidth (4 poles)	2.5 %
Experienced frequency bands	C / Ku / Ka
Typical insertion losses	1.5 to 3 dB depending on bandwidth
Selectivity (20 dB attenuation)	1.5 % from edge frequency
Out of band response	Spectrum not cleaned at every $2n f_0$
Synthesis and design	
Synthesis easiness	Not easy. Models do not exist on microwave simulators. Need specific software for optimization [1]
Manufacturing process	
Etching sensitivity	Very high
Tuning	Impossible
Mechanical characteristics	
Size	Very small
Cover effect	Very weak

This filter has attracting electrical performance[2] but it is very sensitive to manufacturing process so its cost is high. This type of filter has to be used to clean spurious very close to the edge of the useful band.

E. Dual Behaviour Resonator filters

Figures 9 and 10 and Table VI present the topology and summarize the same data for the Dual Behaviour Resonator filter.

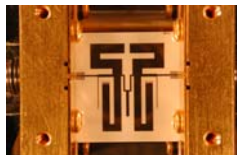


Fig. 9: Example of Dual Behaviour Resonator filter topology in C band

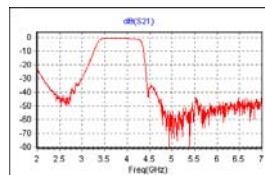


Fig. 10: Example of Dual Behaviour Resonator filter performances in C band

TABLE VI
Dual Behaviour Resonator filters characteristics

Electrical characteristics	
Reachable bandwidth	Between 15 and 20 %
Experienced frequency bands	C / Ku
Typical insertion losses	1 to 2 dB depending on poles number
Selectivity (20 dB attenuation)	5% to 10 % from edge frequency
Out of band response	Spectrum requires additional cleaning
Synthesis and design	
Synthesis easiness	Not easy, requests expertise
Manufacturing process	
Etching sensitivity	No
Tuning	Possible
Mechanical characteristics	
Size	Small
Cover effect	Very weak

This bandpass filter has been long promoted and studied by LEST-UBO team [3], [4]. 2% bandwidth is claimed but has not been experimented by AAS. It presents attracting performance and can meet stringent specifications. It can be tuned which is a strong advantage to compensate inaccuracies due to manufacturing process. Its drawback lies in spurious resonance which has to be dealt properly. All those filters have been selected by AAS-F for use into Flight Model Receivers.

IV. CONCLUSION

The choice guide for all microwave engineers can be the following: Hairpin filter is selected in most cases. Indeed, it is easily synthesized and its electrical performances are better than the Coupled Lines filter for an equivalent number of poles. If the aimed bandwidth is very low, Pseudo-elliptic response filter has to be considered. Contrarily, if the bandwidth has to be large with very stringent filtering specification, the Dual Behaviour Resonator filter has to be selected. If size is the strongest constraint, Interdigitated filter has to be adopted. In any cases, Coupled Lines filter topology will certainly be abandoned.

ACKNOWLEDGMENT

The authors want to acknowledge CNES and ESA technical staff for useful discussions. Also, the valuable help and experience of colleagues from AAS-F has been deeply appreciated. .

REFERENCES

- [1] D. Pacaud, "Applications of a coupling matrix identification software for the deisgn of filters and multiplexers", International Workshop on Microwave Filters, CNES Toulouse, France, September 2004.
- [2] F. Rouchaud, V. Madrangeas, M. Aubourg, « New classes of microstrip resonators for HTS microwave filters applications », IEEE MTT-S 1998.
- [3] C. Quendo, E. Rius, C. Person, "Narrow Bandpass Filters using Dual Behavior Resonators", Vol.51, N°3, March 2003, pp.734-743.
- [4] "Design of Microstrip Dual Behavior Resonator Filters: A Practical Guide", E.Rius et al., Microwave Journal, Vol.49,N°12, Dec.2006, pp.72-92.

Microstrip

Despite it's structural simplicity, the microstrip line is difficult to analyze rigorously. However extensive research has provided numerous approximate modelling techniques which are adequate for many design purposes. The following are a collection of some of the more useful formulae for microstrip circuit design.

1 EQUATIONS FOR MICROSTRIP LINES

The following variables are used in the formulae below:

ε_r	substrate dielectric constant
h	substrate thickness
w	microstrip physical line width
Z_0	characteristic impedance
ε_{eff}	microstrip effective permittivity
l_{eo}	effective open-end length extension
w_{eff}	microstrip effective width

In the following, f is in GHz and h is in millimeters.

1.1 Static Microstrip Synthesis

Find the required w/h ratio given desired characteristic impedance and substrate parameters (see [1]-[2]). Valid for low frequencies.

$$\frac{w}{h} = \begin{cases} \left[\frac{\exp H'}{8} - \frac{1}{4 \exp H'} \right]^{-1} & Z_0 > (44 - 2\varepsilon_r) \\ \frac{2}{\pi} [d_\varepsilon - \ln(2d_\varepsilon + 1)] & Z_0 < (44 - 2\varepsilon_r) \\ \frac{\varepsilon_r - 1}{\pi \varepsilon_r} (\ln d_\varepsilon + 0.293 - 0.517/\varepsilon_r) \end{cases} \quad (1)$$

$$\text{where } H' = \frac{Z_0 \sqrt{2(\varepsilon_r + 1)}}{119.9} + \frac{1}{2} \left(\frac{\varepsilon_r - 1}{\varepsilon_r + 1} \right) \left(\ln \frac{\pi}{2} + \frac{1}{\varepsilon_r} \ln \frac{4}{\pi} \right)$$

$$d_\varepsilon = \frac{59.95 \pi^2}{Z_0 \sqrt{\varepsilon_r}}$$

1.2 Static Microstrip Analysis

Find the low-frequency characteristic impedance given the physical dimensions of the line (see [1]-[2]):

$$Z_0(0) = \begin{cases} \frac{119.9}{\sqrt{2(\varepsilon_r + 1)}} \left[\ln \left(4h/w + \sqrt{16(h/w)^2 + 2} \right) \right] & w/h < 3.3 \\ -\frac{1}{2} \left(\frac{\varepsilon_r - 1}{\varepsilon_r + 1} \right) \left(\ln \frac{\pi}{2} + \frac{1}{\varepsilon_r} \ln \frac{4}{\pi} \right) \\ \frac{119.9\pi}{2\sqrt{\varepsilon}} \left\{ \frac{w}{2h} + \frac{\ln 4}{\pi} + \frac{\ln(e\pi^2/16)}{2\pi} \left(\frac{\varepsilon_r - 1}{\varepsilon_r^2} \right) \right. \\ \left. + \frac{\varepsilon_r + 1}{2\pi\varepsilon_r} \left[\ln \frac{\pi e}{2} + \ln \left(\frac{w}{2h} + 0.94 \right) \right] \right\}^{-1} & w/h > 3.3 \end{cases} \quad (2)$$

1.3 Static Effective Permittivity

Find the low-frequency effective permittivity given either electrical or physical characteristic of the microstrip (see [1]-[2]):

$$\varepsilon_{eff}(0) = \begin{cases} \frac{\varepsilon_r + 1}{2} \left[1 - \frac{1}{2H'} \left(\frac{\varepsilon_r - 1}{\varepsilon_r + 1} \right) \left(\ln \frac{\pi}{2} + \frac{1}{\varepsilon_r} \ln \frac{4}{\pi} \right) \right]^{-2} & w/h < 1.3 \\ \frac{\varepsilon_r + 1}{2} + \frac{\varepsilon_r - 1}{2} \left(1 + 10 \frac{h}{w} \right)^{-0.555} & w/h > 1.3 \end{cases} \quad (3)$$

where H' is defined as in (1), or equivalently as a function of w/h given by

$$H' = \ln \left(4h/w + \sqrt{16(h/w)^2 + 2} \right)$$

1.4 Effective Permittivity Dispersion

Gives frequency-dependent effective permittivity, obtained by curve-fitting to rigorous analytical results (see [7]):

$$\epsilon_{eff}(f) = \epsilon_r - \frac{\epsilon_r - \epsilon_{eff}(0)}{1 + P(f)} \quad (4)$$

$$\begin{aligned} \text{where } P(f) &= P_1 P_2 [(0.1844 + P_3 P_4) 10 f h]^{1.5763} \\ P_1 &= 0.27488 + [0.6315 + 0.525/(1 + 0.157 f h)^{20}] w/h \\ &\quad - 0.065683 \exp(-8.7513 w/h) \\ P_2 &= 0.33622 [1 - \exp(-0.03442 \epsilon_r)] \\ P_3 &= 0.0363 \exp(-4.6 w/h) \{1 - \exp[-(f h / 3.87)^{4.97}]\} \\ P_4 &= 1 + 2.751 \{1 - \exp[-(\epsilon_r / 15.916)^8]\} \end{aligned}$$

with a 0.6% accuracy over the ranges $0.1 \leq w/h \leq 100$, $1 \leq \epsilon_r \leq 20$, $0 \leq h/\lambda_0 \leq 0.13$, and $\epsilon_{eff}(0)$ is calculated from (3).

1.5 Impedance Dispersion

Gives frequency-dependent characteristic impedance, obtained by curve-fitting to rigorous analytical results, using the power-current definition for impedance (see [2]):

$$Z_0(f) = Z_0(0) (R_8/R_9)^{R_{12}} \quad (5)$$

where

$$\begin{aligned} R_1 &= 4.766 \exp[-3.228 (w/h)^{0.641}] \\ R_2 &= 0.016 + (0.0514 \epsilon_r)^{4.524} \\ R_3 &= 1.206 - 0.3144 \exp(-0.0389 \epsilon_r^{1.4}) [1 - \exp(-0.267 (w/h)^7)] \\ R_4 &= 1 + 1.275 [1 - \exp(-0.00463 R_1 \epsilon_r^{1.674} (hf/18.37)^{2.745})] \\ R_5 &= \frac{5.086 R_2 (hf/28.84)^{12}}{0.384 + 0.386 R_2} \frac{\exp[-22.2 (w/h)^{1.92}]}{1 + 1.3 (hf/28.84)^{12}} \frac{(\epsilon_r - 1)^6}{1 + 10(\epsilon_r - 1)^6} \\ R_6 &= [0.0962 + (19.47/hf)^6]^{-1} \\ R_7 &= [1 + 0.00245 (w/h)^2]^{-1} \\ R_8 &= 0.9408 \epsilon_{\text{eff}}^{R_4}(f) - 0.9603 \\ R_9 &= (0.9408 - R_5) \epsilon_{\text{eff}}^{R_4}(0) - 0.9603 \\ R_{10} &= 0.707 (0.00044 \epsilon_r^{2.136} + 0.0184) (hf/12.3)^{1.097} \\ R_{11} &= 1 + 0.0503 \epsilon_r^2 R_6 \{1 - \exp[-(w/15h)^6]\} \\ R_{12} &= R_3 \{1 - 1.1241 (R_7/R_{11}) \exp[-0.026(hf)^{1.1566} - R_{10}]\} \end{aligned}$$

The accuracy is specified to less than 1% for the ranges $0.1 \leq w/h \leq 10$, $1 \leq \epsilon_r \leq 18$, and $0 \leq h \cdot f \leq 30 \text{ GHz}\cdot\text{mm}$.

1.6 Microstrip Effective Width

The planar-waveguide model (see [3]) replaces a microstrip of width w by an ideal parallel-plane transmission line of width w_{eff} , where

$$w_{\text{eff}}(f) = \frac{h\eta_0}{Z(f)\sqrt{\epsilon_{\text{eff}}(f)}} \quad (6)$$

and where $Z(f)$ and $\epsilon_{\text{eff}}(f)$ are calculated using the models described in (4) and (5)

1.7 Open-End Length Correction

Gives the effective length extension due to fringing at microstrip open circuits (see [5]-[6]):

$$\frac{l_{eo}}{h} = \frac{1}{2\pi} \frac{w/h + 0.366}{w/h + 0.556} \left\{ 0.28 + \frac{\epsilon_r + 1}{\epsilon_r} [0.274 + \ln(w/h + 2.518)] \right\} \quad (7)$$

This is a static result from Hammerstad [5], and as noted by Leir [8] is valid for the extremely wide lines sometimes used for patch antennas, unlike a previous expression from Hammerstad [4].

If wide lines are not being used, the more accurate and frequency-dependent expression due to Jansen *et al.* [6] should be used, which is given by

$$\frac{l_{eo}}{h} = R_1 R_3 R_5 / R_4 \quad (8)$$

$$\begin{aligned} \text{where } R_1 &= 0.434907 \frac{\epsilon_{\text{eff}}^{0.81} + 0.26}{\epsilon_{\text{eff}}^{0.81} - 0.189} \frac{(w/h)^{0.8544} + 0.236}{(w/h)^{0.8544} + 0.87} \\ R_2 &= 1 + \frac{(w/h)^{0.371}}{2.358\epsilon_r + 1} \\ R_3 &= 1 + \frac{0.5274 \tan^{-1} [0.084(w/h)^{1.9413/R_2}]}{\epsilon_{\text{eff}}^{0.9236}} \\ R_4 &= 1 + 0.0377 \tan^{-1} [0.067(w/h)^{1.456}] \\ &\quad \times \{6 - 5 \exp [0.036(1 - \epsilon_r)]\} \\ R_5 &= 1 - 0.218 \exp(-7.5w/h) \end{aligned}$$

with a quoted accuracy of 2.5% over the range $0.01 \leq w/h \leq 100$ and $\epsilon_r < 50$. The effective dielectric constant $\epsilon_{\text{eff}}(f)$ should be calculated using the formula in (4).

1.8 Fringing Capacitance

The fringing capacitance of an open-circuited microstrip line is calculated from the open-end length extension as (see [1]-[2])

$$C_{\text{fringe}} \approx \frac{l_{eo} \sqrt{\epsilon_{\text{eff}}}}{c Z_0} \quad (9)$$

References

1. T. C. Edwards, *Foundations for Microstrip Circuit Design*, Wiley, Great Britian, 1981.
2. R. K. Hoffmann, *Handbook of Microwave Integrated Circuits*, Translation from the German of *Integrierte Mikrowellenschaltungen*, Artech House, 1987.
3. G. Kompa and R. Mehran, “Planar Waveguide Model for Calculating Microstrip Components”, *Electron. Lett.*, vol. 11, pp. 459-460, 1975.
4. E. Hammerstad and O. Jensen, “Accurate Models for Microstrip Computer Aided Design”, *1980 IEEE MTT-S International Microwave Symposium Digest*, (Washington), pp. 407-409, 1980.
5. E. Hammerstad, “Computer-Aided Design of Microstrip Couplers with Accurate Discontinuity Models”, *1981 IEEE MTT-S international microwave symposium digest*, Los Angeles, pp. 54-56.
6. M. Kirschning, R. H. Jansen, N. H. L. Koster, “Accurate Model for Open-End Effect of Microstrip Lines”, *Electron. Lett.*, vol. 17, pp. 123-125, 1981.
7. M. Kirschning and R. H. Jansen, “Accurate Model for Effective Dielectric Constant with Validity up to Millimeter-Wave Frequencies”, *Electron. Lett.*, vol. 18, pp. 272-273, Jan 1982.
8. E. Lier, “Improved Formulas for Input Impedance of Coax-fed Microstrip Patch Antennas”, *Proc. IEE*, vol. 129, Pt. H, pp. 161-164, Aug 1982.

A Method for Calculating the Frequency-Dependent Properties of Microstrip Discontinuities

WOLFGANG MENZEL AND INGO WOLFF

Abstract—A method is described for calculating the dynamical (frequency-dependent) properties of various microstrip discontinuities such as unsymmetrical crossings, T junctions, right-angle bends, impedance steps, and filter elements. The method is applied to an unsymmetrical T junction with three different linewidths. Using a waveguide model with frequency-dependent parameters, a field matching method proposed by Kühn is employed to compute the scattering matrix of the structures. The elements of the scattering matrix calculated in this way differ from those derived from static methods by a higher frequency dependence, especially for frequencies near the cutoff frequencies of the higher order modes on the microstrip lines. The theoretical results are compared with measurements, and theory and experiment are found to correspond closely.

I. INTRODUCTION

MICROSTRIP discontinuities such as crossings, T junctions, bends, and impedance steps are elements of many complex microstrip circuits like filters, power dividers, ring couplers, and impedance transformers. Therefore, knowledge of the exact reflection and transmission properties in dependence on the frequency is of great importance. Various approaches have been made to calculate equivalent circuits for those discontinuities. Oliner [1] used Babinet's principle to describe stripline discontinuities, Silvester and Benedek [2]–[4], and Stouten [5] calculated the capacitances of microstrip discontinuities, and Gopinath and Silvester [6], Gopinath and Easter [7], and Thomson and Gopinath [8] computed the inductive elements of the equivalent circuits. All the methods described in these papers are based on static approximations, and therefore are valid with sufficient accuracy only for low frequencies.

A method is presented in this paper for calculating the transmission properties of the discontinuities, taking into account the frequency-dependent energy stored in higher order cutoff modes of the microstrip line. A waveguide model for the microstrip line, described in [9], [10], and a field matching technique proposed by Kühn [11] are used. This method has the advantage that complex microstrip circuits containing discontinuities can be calculated in a way similar to that shown by Rozzi and Mecklenbräuker [12] for waveguide circuits recently. Earlier papers, which used the waveguide model, only described less complex structures, as for example symmetrical T junctions [17].

As comparisons of the theoretical results and the measure-

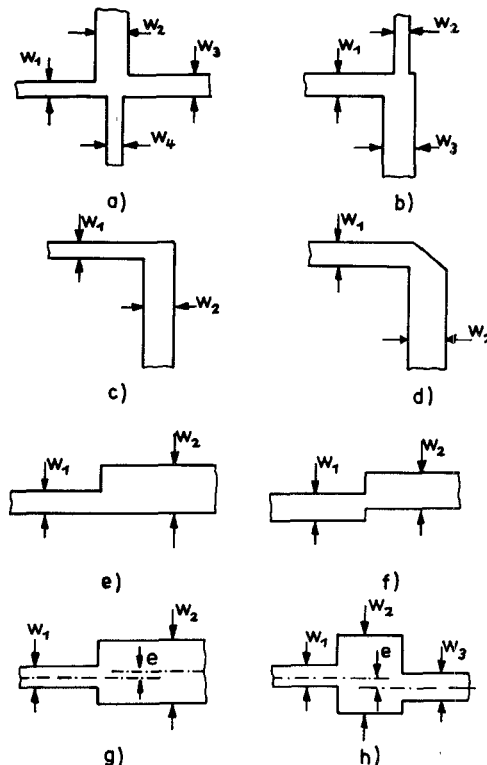


Fig. 1. Microstrip discontinuities which can be calculated by the theory described in this paper.

ments show, the dependence of the scattering matrix of microstrip discontinuities on the frequency is well approximated in a wide frequency range by the theory given in this paper.

II. THE FORMULATION OF THE FIELD PROBLEM

It is the aim of this paper, to develop a field theoretical method for calculating the transmission properties of microstrip discontinuities, some of which are shown in Fig. 1.

For all discontinuities it is allowed that lines of different widths are connected to each other. In contrast to most of the theories described in previous papers, the method can be applied to unsymmetrical discontinuities. It is to be explained by the example of an unsymmetrical microstrip T junction (Fig. 3).

The dynamical properties of the microstrip lines are described using a waveguide model (Fig. 2). It consists of a parallel plate waveguide of width w_{eff} and height h with

Manuscript received January 29, 1976; revised May 2, 1976.

The authors are with the Department of Electrical Engineering, University of Duisburg, Duisburg, Germany.

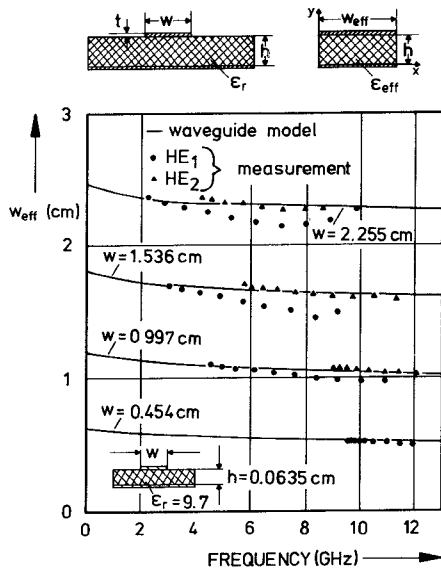


Fig. 2. Waveguide model of a microstrip line and effective width of the waveguide in dependence on the frequency. After [10].

plates of infinite conductivity at the top and bottom and with magnetic side walls. It is filled with a dielectric medium of the dielectric constant ϵ_{eff} . The effective width as well as the effective dielectric constant are frequency dependent. The height h of the waveguide model is equal to the height of the microstrip substrate material; ϵ_{eff} is the frequency-dependent effective dielectric constant as it can be computed for the microstrip line (e.g., [13]). The width of the waveguide model to a first approximation can be assumed to be equal to the frequency-independent effective width given by Wheeler [14]. As further investigations show [10], the effective width must also be frequency dependent. This is due to the physical fact that for higher frequencies the electromagnetic field is increasingly concentrated in the dielectric medium. The frequency-dependent effective width can be calculated from the characteristic impedance of the quasi-TEM mode (e.g., [15]), if the frequency-dependent effective dielectric constant is known. In Fig. 2 theoretical and experimental results for w_{eff} in dependence on the frequency are shown [10].

As in the case of the effective dielectric constant [16], a simple formula can be found to describe the frequency dependence of w_{eff} with sufficient accuracy in the relevant frequency range [17]

$$w_{\text{eff}}(f) = w + \frac{w_{\text{eff}}(0) - w}{1 + f/f_c} \quad (1)$$

where w is the width of the microstrip line, $w_{\text{eff}}(0)$ is the static value of the effective width according to Wheeler [14], and $f_c = c_0/(2w\epsilon_r^{1/2})$, where ϵ_r is the dielectric constant of the substrate material.

It is assumed that the height h of the microstrip line and the waveguide model is so small that the fields of the waveguide model are independent of the y coordinate (Fig. 2) in the relevant frequency range. At the top and bottom the tangential electric field strength must vanish. So only a

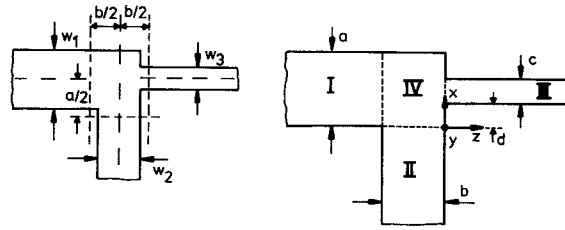


Fig. 3. Unsymmetrical microstrip T junction and introduced coordinate system.

TEM mode and TE_{n0} modes with E_y , H_x , and H_z components exist. The transversal electromagnetic field can be described using a scalar potential

$$\psi_{p0} = \sqrt{\frac{\epsilon_p}{w_{\text{eff}}h}} \frac{\sin\left(\frac{p\pi}{w_{\text{eff}}} x\right)}{\frac{p\pi}{w_{\text{eff}}}}, \quad \epsilon_p = \begin{cases} 1 & \text{for } p = 0 \\ 2 & \text{for } p \neq 0 \end{cases} \quad (2)$$

by the equations

$$\begin{aligned} E_t &= \sum_{p=0}^{\infty} (A_p e^{-\gamma z} + B_p e^{+\gamma z})(\mathbf{a}_z \times \nabla_t \psi_{p0}) \\ H_t &= - \sum_{p=0}^{\infty} Y_{p0} (A_p e^{-\gamma z} - B_p e^{+\gamma z}) \nabla_t \psi_{p0}. \end{aligned} \quad (3)$$

A_p and B_p are the amplitude coefficients, $\gamma = [(p\pi/w_{\text{eff}})^2 - \omega^2 \epsilon_{\text{eff}} \epsilon_0 \mu_0]^{1/2}$ is the propagation constant, \mathbf{a}_z is the unit vector of the z coordinate, ∇_t is the transversal Nabla operator, and $Y_{p0} = 1/Z_{p0} = \gamma/(j\omega\mu_0)$ is the complex characteristic wave admittance. Using normalized wave amplitudes and introducing the potential function, the transversal components of the electric and magnetic fields are given by

$$\begin{aligned} E_y &= \sum_{p=0}^{\infty} (a_p e^{-\gamma z} + b_p e^{+\gamma z}) \sqrt{Z_{p0}} \sqrt{\frac{\epsilon_p}{w_{\text{eff}}h}} \cos\left(\frac{p\pi}{w_{\text{eff}}} x\right) \\ H_x &= - \sum_{p=0}^{\infty} (a_p e^{-\gamma z} - b_p e^{+\gamma z}) \sqrt{Y_{p0}} \sqrt{\frac{\epsilon_p}{w_{\text{eff}}h}} \cos\left(\frac{p\pi}{w_{\text{eff}}} x\right) \end{aligned} \quad (4)$$

where $a_p = Z_{p0}^{1/2} \cdot A_p$ and $b_p = Z_{p0}^{1/2} \cdot B_p$.

In Fig. 3 an unsymmetrical microstrip T junction and the equivalent waveguide circuit is shown. a , b , and c are the effective widths of the three microstrip lines. The waveguide T junction is divided into four regions. The regions I, II, and III are filled with a dielectric medium of effective dielectric constants $\epsilon_{\text{eff}1}$, $\epsilon_{\text{eff}2}$, and $\epsilon_{\text{eff}3}$, corresponding to the three microstrip lines. In region IV an equivalent dielectric constant as defined in [18] for a microstrip disk capacitor is introduced, taking into account the electric stray field only at those sides of the region where no microstrip line is connected. The reference planes in the waveguide model are chosen to be the interfaces between region IV and the regions I, II, and III. Accordingly, the reference planes of the microstrip T junction are defined as shown in Fig. 3.

A complete solution for the electromagnetic field in the regions I, II, and III can be given by analogy with (4) taking into consideration the change of the coordinates:

$$\begin{aligned} E_y^I &= \sum_{p=0}^{\infty} \sqrt{Z_p^I} (a_p^I e^{-\gamma(z+b)} + b_p^I e^{+\gamma(z+b)}) \\ &\quad \cdot \sqrt{\frac{\epsilon_p}{ah}} \cos \left(\frac{p\pi}{a} x \right) \\ H_x^I &= - \sum_{p=0}^{\infty} \sqrt{Y_p^I} (a_p^I e^{-\gamma(z+b)} - b_p^I e^{+\gamma(z+b)}) \\ &\quad \cdot \sqrt{\frac{\epsilon_p}{ah}} \cos \left(\frac{p\pi}{a} x \right) \end{aligned} \quad (5a)$$

$$\begin{aligned} E_y^{II} &= \sum_{k=0}^{\infty} \sqrt{Z_k^{II}} (a_k^{II} e^{-\gamma x} - b_k^{II} e^{+\gamma x}) \sqrt{\frac{\epsilon_k}{bh}} \cos \left(\frac{k\pi}{b} z \right) \\ H_z^{II} &= \sum_{k=0}^{\infty} \sqrt{Y_k^{II}} (a_k^{II} e^{-\gamma x} - b_k^{II} e^{+\gamma x}) \sqrt{\frac{\epsilon_k}{bh}} \cos \left(\frac{k\pi}{b} z \right) \end{aligned} \quad (5b)$$

$$\begin{aligned} E_y^{III} &= \sum_{m=0}^{\infty} \sqrt{Z_m^{III}} (a_m^{III} e^{+\gamma z} + b_m^{III} e^{-\gamma z}) \\ &\quad \cdot \sqrt{\frac{\epsilon_m}{ch}} \cos \left(\frac{m\pi}{c} (x-d) \right) \\ H_x^{III} &= \sum_{m=0}^{\infty} \sqrt{Y_m^{III}} (a_m^{III} e^{+\gamma z} - b_m^{III} e^{-\gamma z}) \\ &\quad \cdot \sqrt{\frac{\epsilon_m}{ch}} \cos \left(\frac{m\pi}{c} (x-d) \right). \end{aligned} \quad (5c)$$

Following Kühn [11], the field in region IV is found by superimposing three standing wave solutions:

$$\begin{aligned} E_y^{IVa} &= \sum_{p=0}^{\infty} \sqrt{Z_p^I} c_p^{IVa} \cos(\beta^I z) \cos \left(\frac{p\pi}{a} x \right) \sqrt{\frac{\epsilon_p}{ah}} \\ H_x^{IVa} &= j \sum_{p=0}^{\infty} \sqrt{Y_p^I} c_p^{IVa} \sin(\beta^I z) \cos \left(\frac{p\pi}{a} x \right) \sqrt{\frac{\epsilon_p}{ah}} \end{aligned} \quad (6a)$$

$$\begin{aligned} E_y^{IVb} &= \sum_{k=0}^{\infty} \sqrt{Z_k^{II}} c_k^{IVb} \cos(\beta^{II}(x-a)) \cos \left(\frac{k\pi}{b} z \right) \sqrt{\frac{\epsilon_k}{bh}} \\ H_z^{IVb} &= -j \sum_{k=0}^{\infty} \sqrt{Y_k^{II}} c_k^{IVb} \sin(\beta^{II}(x-a)) \cos \left(\frac{k\pi}{b} z \right) \sqrt{\frac{\epsilon_k}{bh}} \end{aligned} \quad (6b)$$

$$\begin{aligned} E_y^{IVc} &= \sum_{m=0}^{\infty} \sqrt{Z_m^{III}} c_m^{IVc} \cos(\beta^I(z+b)) \cos \left(\frac{m\pi}{a} x \right) \sqrt{\frac{\epsilon_m}{ah}} \\ H_x^{IVc} &= j \sum_{m=0}^{\infty} \sqrt{Y_m^{III}} c_m^{IVc} \sin(\beta^I(z+b)) \cos \left(\frac{m\pi}{a} x \right) \sqrt{\frac{\epsilon_m}{ah}}. \end{aligned} \quad (6c)$$

β^v ($v = I, II$) are the phase constants of region I or II, respectively, calculated with the equivalent dielectric

constant of region IV instead of ϵ_{eff1} or ϵ_{eff2} . In the same way Z_v^{μ} is calculated from Z_v^{μ} .

Matching the magnetic field strength of regions I, II, and III to that of region IV, in each case only one term of the superimposed field after (6) must be taken into account, because of the boundary conditions of the magnetic walls. The connections between the field amplitudes of regions I and IV, and II and IV, can be found simply by comparison of the coefficients

$$c_p^{IVa} = -j \frac{a_p^I - b_p^I}{\sin(\beta_p^I b)} \sqrt{\frac{Z_p^I}{Z_p^I}} \quad (7)$$

and

$$c_k^{IVb} = -j \frac{a_k^{II} - b_k^{II}}{\sin(\beta_k^{II} a)} \sqrt{\frac{Z_k^{II}}{Z_k^{II}}} \quad (8)$$

whereas the coefficients of regions III and IV must be determined by a normal mode matching procedure at the interface III-IV:

$$c_M^{IVc} = -j \sum_{m=0}^{\infty} \sqrt{\frac{Z_M^I}{Z_m^{III}}} \frac{a_m^{III} - b_m^{III}}{\sin(\beta_M^I b)} \cdot K_{[m,M]}^{(1)} \quad (9)$$

with

$$K_{[m,M]}^{(1)} = \frac{\sqrt{\epsilon_m \epsilon_M}}{\sqrt{ac \cdot h}} \int_0^a \int_0^M \cos \left(\frac{m\pi}{c} x \right) \cos \left(\frac{M\pi}{a} x \right) dx dy.$$

If the electric field strength of regions I, II, and III is to be matched to the electric field of region IV, the tangential components of all three standing wave solutions [see (6)] have to be taken into account. This will be shown by the example of the field matching between regions I and IV. The tangential electric field of region IV in the plane $z = -b$ [Fig. 3(b)] is given by

$$E_y^{IV}|_{z=-b} = E_y^{IVa}|_{z=-b} + E_y^{IVb}|_{z=-b} + E_y^{IVc}|_{z=-b}. \quad (10)$$

Matching this field to that of region I leads to an equation which connects the amplitude coefficients of regions I and IV:

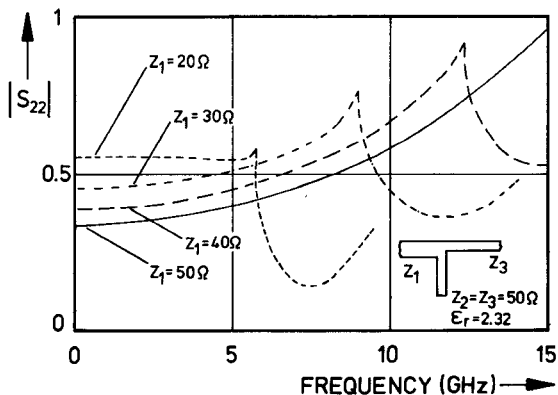
$$\begin{aligned} \sqrt{Z_p^I} (a_p^I + b_p^I) &= \sqrt{Z_p^I} c_p^{IVa} \cos(\beta_p^I b) + \sqrt{Z_p^I} c_p^{IVc} \\ &\quad + \sum_{k=0}^{\infty} \sqrt{Z_k^{II}} c_k^{IVb} K_{[k,p]}^{(2)} \end{aligned} \quad (11)$$

with

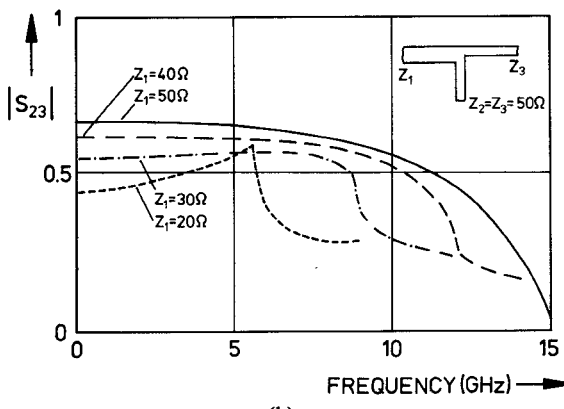
$$\begin{aligned} K_{[k,p]}^{(2)} &= (-1)^p \iint_{z=-b}^M \sqrt{\frac{\epsilon_k \epsilon_p}{ba}} \frac{1}{h} \\ &\quad \cdot \cos(\beta_k^{II}(x-a)) \cos \left(\frac{p\pi}{a} x \right) dx dy. \end{aligned}$$

In the same way the electric fields of regions II and III are matched to that of region IV.

From (7)-(9) the coefficients c_v^{IVa} , c_v^{IVb} , and c_v^{IVc} can be eliminated and introduced into the matching conditions of the electric field strength. In this way a set of $P + K + M + 3$ equations results, which connects the amplitudes a_v^I , a_v^{II} , a_v^{III} ($v, \mu, \eta = 0, 1, 2, \dots$) of the incident waves to the coefficients b_v^I , b_v^{II} , b_v^{III} of the reflected or transmitted waves.



(a)



(b)

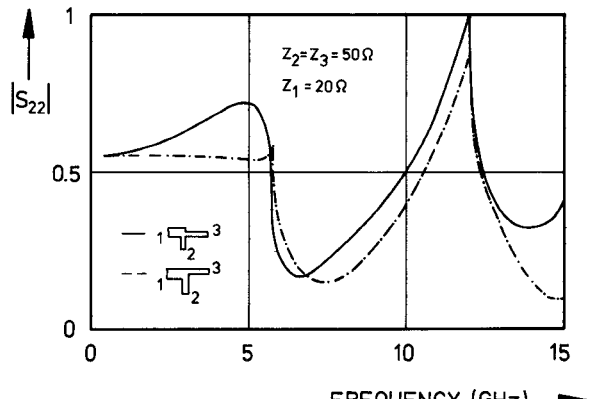
Fig. 4. Reflection coefficient $|S_{22}|$ (a) and transmission coefficient $|S_{23}|$ (b) of an unsymmetrical T junction with $Z_2 = Z_3 = 50 \Omega$ and different values of Z_1 . Substrate material Polyguide: $\epsilon_r = 2.32$, $h = 0.158$ cm.

P, K, M are the numbers of the highest order modes which are taken into account if the equations are evaluated numerically. If only an incident TEM mode at one port of the T junction is considered, the scattering parameters can easily be computed from the amplitudes of the incident and reflected or transmitted waves.

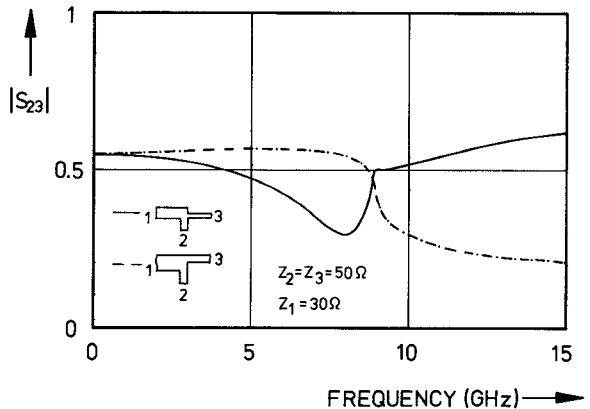
III. NUMERICAL RESULTS

The resulting equations have been evaluated numerically for different unsymmetrical microstrip T junctions on Polyguide substrate material. No relative convergence problems occur, and the results are of sufficient accuracy (error < 0.5 percent) even if only five higher order modes are taken into account in each line and the connecting field region.

The results shown in Figs. 4-6 have been computed with eight higher order modes. In this case a computing time (central processing time on a CD Cyber 72/76) of 50 ms is required for the calculation of the scattering matrix at one frequency. Fig. 4 shows the reflection coefficients $|S_{22}|$ and the transmission coefficients $|S_{23}|$ of T junctions with the characteristic impedances $Z_2 = Z_3 = 50 \Omega$ and different values of Z_1 on Polyguide material. At low frequencies ($f < 2$ GHz) the coefficients can be calculated from the static characteristic impedances. For higher frequencies the coefficients become frequency dependent. The reflection coefficients increase with increasing frequency, until they



(a)



(b)

Fig. 5. Reflection coefficient $|S_{22}|$ (a) and transmission coefficient $|S_{23}|$ (b) for two T junctions of equal characteristic impedances but different geometrical structure. Substrate material Polyguide: $\epsilon_r = 2.32$, $h = 0.158$ cm.

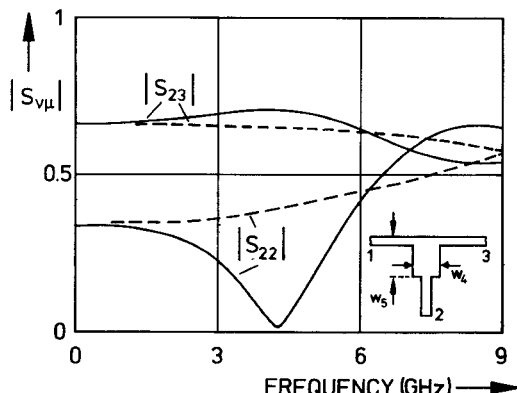


Fig. 6. Elements of the scattering matrix of a compensated microstrip T junction. — compensated T junction. - - uncompensated T junction. $Z_1 = Z_2 = Z_3 = 50 \Omega$. $w_4 = 1$ cm, $w_5 = 2$ cm. Substrate material Polyguide: $\epsilon_r = 2.32$, $h = 0.158$ cm.

reach a maximum at the cutoff frequency of the first higher order mode. The transmission coefficients decrease with increasing frequency. If $Z_1 = Z_3$, the maximum value of $|S_{22}|$ becomes 1, whereas $|S_{23}|$ decreases to zero. For different impedances of line 1 and line 2 the maximum value of $|S_{22}|$ decreases with increasing difference between the impedances. For frequencies higher than the cutoff frequency of the first higher order mode (normally this frequency range is not of great interest for practical use),

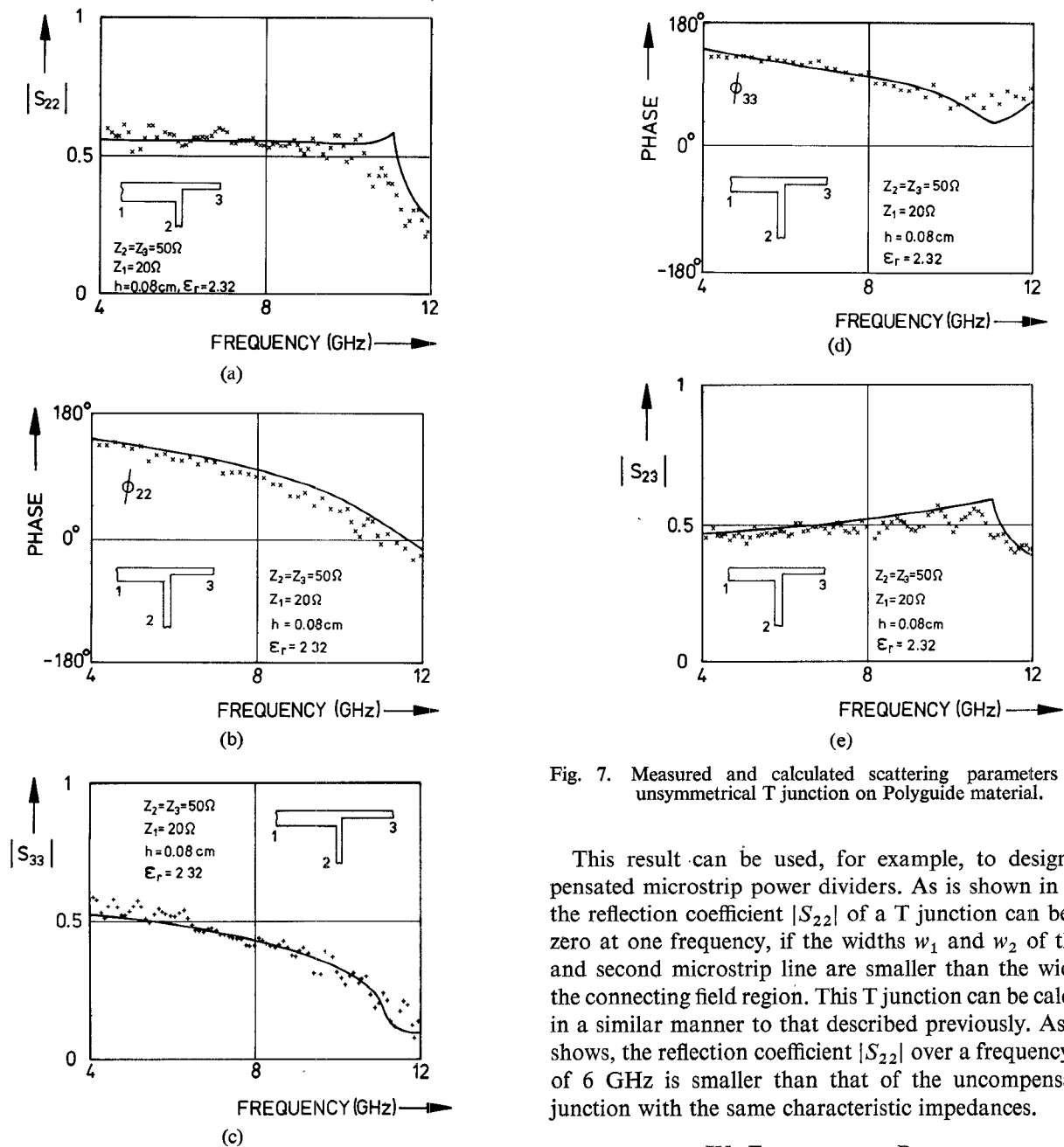


Fig. 7. Measured and calculated scattering parameters of an unsymmetrical T junction on Polyguide material.

This result can be used, for example, to design compensated microstrip power dividers. As is shown in Fig. 6, the reflection coefficient $|S_{22}|$ of a T junction can be made zero at one frequency, if the widths w_1 and w_2 of the first and second microstrip line are smaller than the widths of the connecting field region. This T junction can be calculated in a similar manner to that described previously. As Fig. 6 shows, the reflection coefficient $|S_{22}|$ over a frequency range of 6 GHz is smaller than that of the uncompensated T junction with the same characteristic impedances.

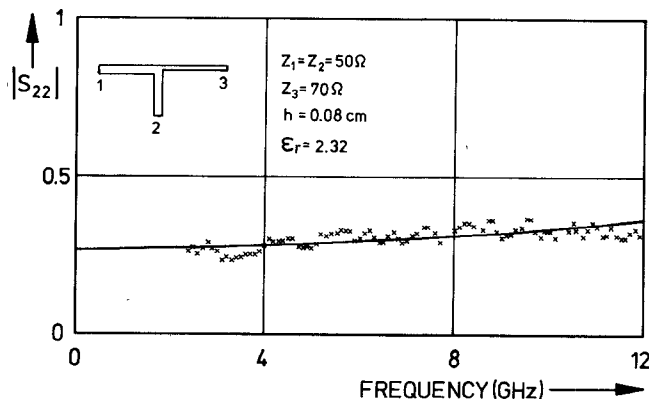
IV. EXPERIMENTAL RESULTS

Measurements have been performed with T junctions on Polyguide material ($\epsilon_r = 2.32$, $h = 0.0794$ cm) and have been compared to theoretical results. The measurements were carried out on an HP network analyzer connected to an automatic data acquisition system. An attempt was made to eliminate the influence of the microstrip-coax transitions on the measurements by determining the reflection and transmission coefficients of the transitions and correcting the measured scattering parameters. Because of difficulties with the terminations, deviations larger than the inaccuracies of the network analyzer occur. The influence of the line losses on the results have been taken into consideration, whereas radiation losses, which occur especially for substrate materials of small dielectric constant and large height, could not be taken into account.

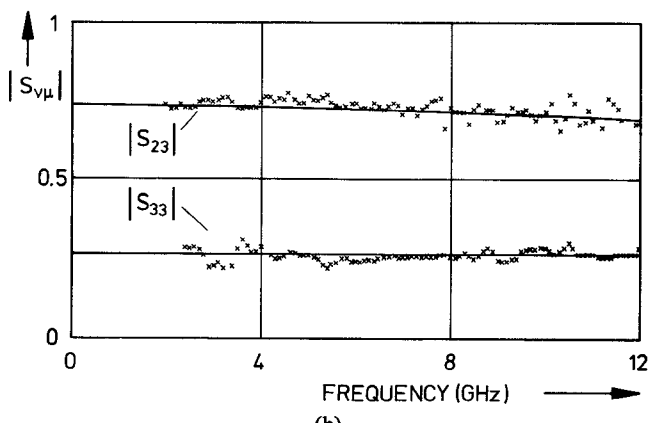
Figs. 7 and 8 show the measured and computed scattering parameters of two T junctions with 20–50–50 Ω and 50–

the reflection coefficients strongly decrease and again have a second maximum at the next cutoff frequency. For a 0.158-cm-thick Polyguide substrate material, which has a small dielectric constant, the variation of the reflection coefficient $|S_{22}|$ from 0 to 10 GHz is about 100 percent. The frequency dependence of the scattering matrix becomes smaller with decreasing values of height h and increasing dielectric constant ϵ_r , if the same frequency range is considered.

The calculation method described can also be used to study the influence of the geometrical structure on the transmission properties of discontinuities. By way of an example, Fig. 5 shows the reflection coefficients $|S_{22}|$ and the transmission coefficients $|S_{23}|$ for two unsymmetrical T junctions with equal characteristic impedances but different geometrical structures. It can clearly be recognized that a stronger frequency dependence arises if the discontinuity contains additional edges.



(a)



(b)

Fig. 8. Measured and calculated scattering parameters of an unsymmetrical T junction on Polyguide material.

50–70 Ω impedances as examples. All the measured absolute values and phases, in the light of the remarks made previously, correspond closely to theoretical results. Larger deviations between theory and experiment occur for thicker substrates, especially near the cutoff frequencies, for at these frequencies the radiated power becomes large. Additional difficulties occur with the measurements of those discontinuities, for the termination of lines of larger width is much more complicated. For example, Fig. 9 shows the calculated and measured results for a T junction on Polyguide material of height $h = 0.158$ cm. At low frequencies the termination of the 40- Ω line is very difficult, giving rise to the deviations between theory and experiment at 4 GHz. For frequencies near the cutoff frequency ($f \approx 12$ GHz) the measured reflection coefficient is smaller than the calculated one because of the radiated power.

V. CONCLUSIONS

A method is presented which can be used to calculate the dynamical properties of many microstrip discontinuities. As far as the authors know, this is the first method described in the literature for calculating the frequency-dependent properties of unsymmetrical microstrip discontinuities. In the case of normally used frequency ranges and microstrip lines, the method leads to results which are strongly supported by measurements. The computer

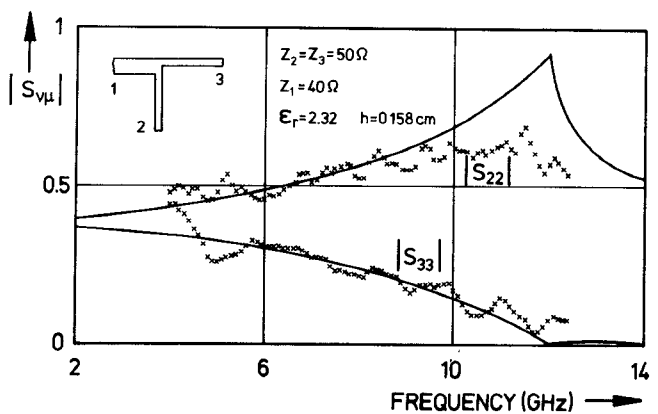


Fig. 9. Measured and calculated scattering parameters of an unsymmetrical T junction on thick Polyguide material.

programs do not need much computer storage and are relatively fast, so they can also be used in computer-aided design methods. Further developments of the existing programs may lead to the possibility of studying compensation methods for power dividers or similar circuits.

REFERENCES

- [1] A. A. Oliner, "Equivalent circuits for discontinuities in balanced strip transmission line," *IEEE Trans. Microwave Theory Tech. (Special Issue on Symp. on Microwave Strip Circuits)*, vol. MTT-3, pp. 134–143, Nov. 1955.
- [2] P. Silvester and P. Benedek, "Equivalent capacitances of microstrip open circuits," *IEEE Trans. Microwave Theory Tech.*, vol. MTT-20, pp. 511–516, Aug. 1972.
- [3] P. Benedek and P. Silvester, "Equivalent capacitances of microstrip gaps and steps," *IEEE Trans. Microwave Theory Tech.*, vol. MTT-20, pp. 729–733, Nov. 1972.
- [4] P. Silvester and P. Benedek, "Microstrip discontinuity capacitances for right-angle bends, T-junctions and crossings," *IEEE Trans. Microwave Theory Tech.*, vol. MTT-21, pp. 341–346, May 1973.
- [5] P. Stouten, "Equivalent capacitances of T-junctions," *Electron. Lett.*, vol. 9, pp. 552–553, Nov. 1973.
- [6] A. Gopinath and P. Silvester, "Calculation of inductance of finite-length strips and its variation with frequency," *IEEE Trans. Microwave Theory Tech.*, vol. MTT-21, pp. 380–386, June 1973.
- [7] A. Gopinath and B. Easter, "Moment method of calculating discontinuity inductance of microstrip right angled bends," *IEEE Trans. Microwave Theory Tech. (Short Papers)*, vol. MTT-22, pp. 880–883, Oct. 1974.
- [8] A. Thompson and A. Gopinath, "Calculation of microstrip discontinuity inductance," *IEEE Trans. Microwave Theory Tech.*, vol. MTT-23, pp. 648–655, Aug. 1975.
- [9] I. Wolff, G. Kompa, and R. Mehran, "Calculation method for microstrip discontinuities and T-junctions," *Electron. Lett.*, vol. 8, p. 177, Apr. 1972.
- [10] G. Kompa and R. Mehran, "Planar waveguide model for calculating microstrip components," *Electron. Lett.*, vol. 11, pp. 459–460, Sept. 1975.
- [11] E. Kühn, "A mode-matching method for solving field problems in waveguide and resonator circuits," *Arch. Elek. Übertragung*, vol. 27, pp. 511–513, Dec. 1973.
- [12] T. E. Rozzi and W. F. G. Mecklenbräuker, "Wide-band network modeling of interacting inductive irises and steps," *IEEE Trans. Microwave Theory Tech.*, vol. MTT-23, pp. 235–245, Feb. 1975.
- [13] R. Jansen, "A moment method for covered microstrip dispersion," *Arch. Elek. Übertragung*, vol. 29, pp. 17–20, 1975.
- [14] H. A. Wheeler, "Transmission-line properties of parallel wide strips by a conformal-mapping approximation," *IEEE Trans. Microwave Theory Tech.*, vol. MTT-12, pp. 280–289, 1964.
- [15] H. J. Schmitt and K. H. Sarges, "Wave propagation in microstrip," *Nachrichtentech. Z.*, vol. 24, pp. 260–264, 1971.
- [16] M. V. Schneider, "Microstrip dispersion," *Proc. Inst. Elect. Electron. Engrs.*, vol. 60, pp. 144–146, 1972.
- [17] R. Mehran, "The frequency-dependent scattering matrix of microstrip right-angle bends, T-junctions and crossings," *Arch. Elek. Übertragung*, vol. 29, pp. 454–460, Nov. 1975.
- [18] I. Wolff, "Statische Kapazitäten von rechteckigen und kreisförmigen Mikrostrip-Scheiben kondensatoren," *Arch. Elek. Übertragung*, vol. 27, pp. 44–47, Jan. 1973.

A Design Technique for Microstrip Filters.

Cornelis Jan Kikkert
 Electrical and Computer Engineering
 James Cook University
 Townsville, Queensland, Australia
 Keith.Kikkert@jcu.edu.au

Abstract— Most communication systems contain an RF front end, which performs analogue signal processing with RF filters. Microstrip filters are a low cost means of doing this. This paper describes a general design technique for microstrip or stripline filters. Four different microstrip filters are designed. The simulated and measured responses agree closely over a wide range of frequencies. This technique allows new filter topologies to be investigated.

I INTRODUCTION

Most communication systems require an RF front end, where RF filters and low noise amplifiers perform analogue signal processing. Microstrip RF filters are commonly used in receivers and transmitters operating in the 800 MHz to 30 GHz frequency range. The two most common types used are the parallel coupled line filter and the interdigital filter. A hairpin filter is a variation of the parallel coupled line filter, where the resonators are bent into a hairpin shape in order to achieve a more convenient aspect ratio. The design of these filters is well known [1-4] and generally involves the use of empirical relations. Microwave RF filters are designed using either low pass filter equations [1] with suitable transformations or using coupled resonators design procedures [2].

In this paper a novel technique is presented for determining the PCB layout required for the end resonator loading and coupling factors for any stripline or microstrip realisation. The design technique presented here is based on the adjustment procedure for helical filters, described in Zverev [2]. This book contains tables for normalised coupling (k) and normalised loaded Q (q) values and gives the following equations for these for Butterworth filters:

$$q_0 = q_n = 2 \sin \frac{(2-1)\pi}{2n} = 2 \sin \frac{\pi}{2n} \quad (1)$$

$$k_{ij} = \frac{1}{2\sqrt{\sin \frac{(2i-1)\pi}{2n} \sin \frac{(2j+1)\pi}{2n}}} \quad i=1,3,5,\dots \quad (2)$$

II DESIGN PROCEDURE

Four filters with a centre frequency of 1 GHz and a 75 MHz bandwidth are designed using this technique. Figure 1 shows the resulting interdigital filter.

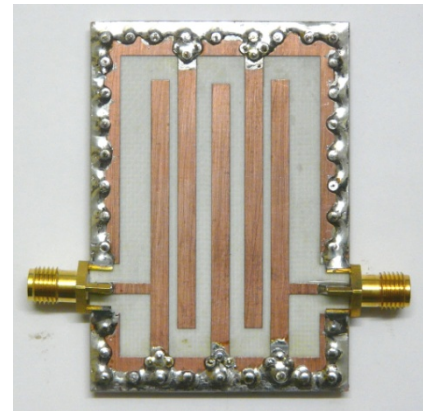


Figure 1. 1GHz interdigital filter.

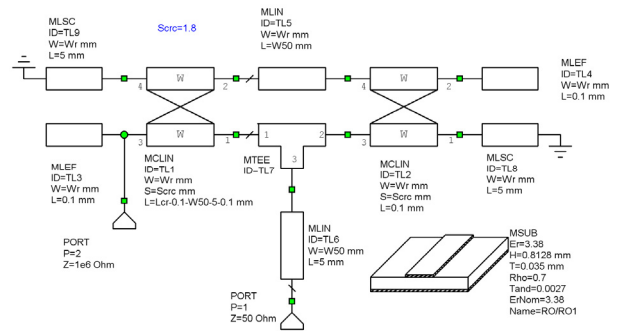


Figure 2. Test circuit for determining the required coupling gaps and resonator loading.

Figure 2 shows the Microwave Office [5] realisation of a coupled line structure, using two resonators. The structure corresponds to the first two resonators of the interdigital filter if figure 1.

The author has simulated many microstrip-line filters using Microwave Office [5] and ADS [6] with both circuit simulation and electromagnetic simulation. The author has found that all give accurate results, however the circuit simulation from Microwave Office gave the best agreement with the measurements on the actual filters produced and as a result that circuit simulation is used throughout this paper. Circuit simulation also has the advantage of being much faster.

The resonator of figure 2 is made up of different coupled line sections, the length Lct of one of these is made variable to enable the input tapping point, and thus the loaded Q of the first resonator, to be varied. An equation is used for the other coupled line length, to permit independent control of the input tapping point as well as the centre frequency by varying the total length of the resonator. To determine the resonator loaded Q and set the correct tapping point, the coupling distance between the coupled resonator sections (Scrc) is made large and the coupled resonator is split into two unconnected parts by disabling TL5 and TL9, to ensure that this coupled resonator does not effect the end resonator, as shown in figure 3. An end-effect, ground connection and T section is used to allow the model to be realised accurately. The resonator line width is a compromise between filter size, radiation losses and resistive losses. A resonator line width of 3 mm is chosen for these designs.

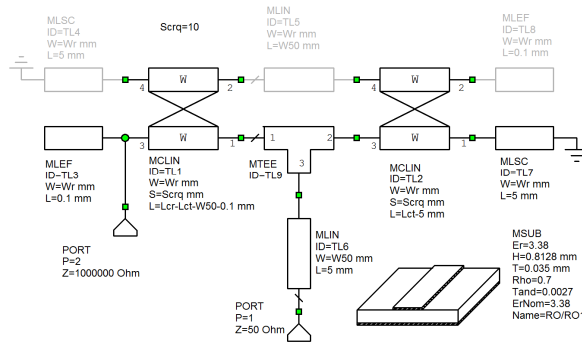


Figure 3. Test circuit for determining the resonator loading.

For helical filters, the adjustment of the loaded Q values for the end resonators involves the measurement of the 3 dB bandwidth of the field in the end resonator. During simulation of a microstrip filter, this loaded resonator bandwidth can be obtained by measured the voltage at the top of the resonator, (Port 2 of figure 1). Equation (3) shows the relationship between the 3dB bandwidth of this voltage and the loaded normalised q of the end resonators of the filter as:

$$\text{Resonator1 } \Delta_{3dB} = \frac{\text{Filter } BW_{3dB}}{q_1} \quad (3)$$

For a 5 resonator filter, equations (1) and (2) or filter tables give $q_0 = q_n = 0.6180$, $k_{12} = k_{45} = 1.0$ and $k_{23} = k_{34} = 0.5559$. From equation (3), the 3 dB resonator voltage bandwidth should thus be 121 MHz. The input tapping point and the line length are then tuned to achieve the correct bandwidth and centre frequency. When $Lct = 9.7$ mm and $Lcr = 45.3$ mm, the frequency response of figure 3 is obtained.

From Zverev [2], when observing the fields inside the end resonator of a helical filter, a double humped response as shown in the blue curve in figure 4 results,

with the distance between the peaks being related to the coupling coefficients as follows:

$$\Delta_{fp} = k_{12} BW_{3dB} \quad (4)$$

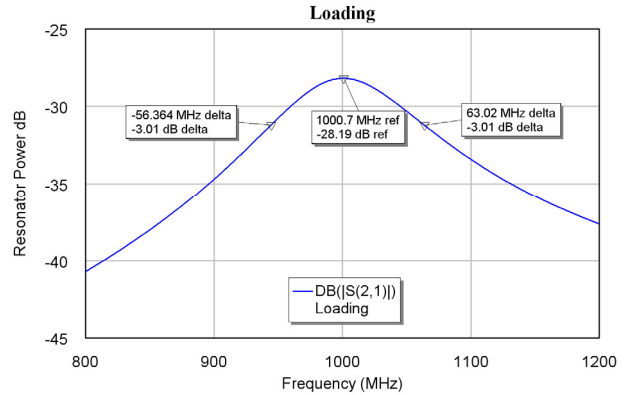


Figure 4. Frequency sweep of loaded end resonator of figure 2.

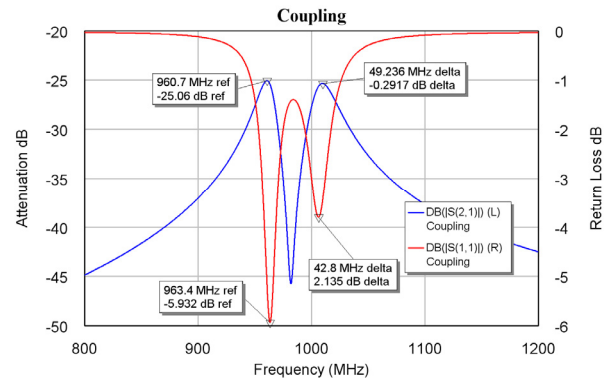


Figure 5. Frequency sweep of coupling test circuit.

This equation can also be used to determine the coupling gaps required. For the required filter $k_{12} = k_{45} = 1.0$, so that a distance between the peaks of 75 MHz is required. For the coupling between the inner resonators, $k_{23} = k_{34} = 0.5559$, corresponding to a 41.7 MHz distance between the peaks as shown in figure 5 is required.

In figure 2, elements TL5 and TL9 are enabled to determine the required coupling gaps (Scsc) by observing the voltage at port 2. Scsc is tuned to obtain the frequency response shown in figure 5. In order to make the peaks of the response as sharp as possible and thus allow an accurate determination of the peak values, the tapping point is made as small as possible. In addition, there will be minima in the S_{11} plot shown in red in figure 5. The S_{11} plot is sharper and provides a more precise but slightly different frequency spacing. As shown in figure 5, a 1.8 mm coupling gap results in a frequency spacing of 42.8 MHz when S_{11} is used and 49 MHz when the resonator voltage is used. The result from S_{11} is close enough to the required 41.7 MHz. The coupling for a 100 MHz frequency difference requires a

1.15mm coupling gap. Minor errors in the coupling gaps are not critical, as these values are used for the starting values for the filter optimization process, which then results in the final filter parameters.

The same design process can be applied for other filter types. The test circuits must be adapted for the different layouts. The combline filter layout is similar to that of the interdigital filter, however all the grounded connections are on the same side. The input tapping is the same as the interdigital filter, but the coupling gaps are 0.2 mm for the outer resonators and 1.8 mm for the inner resonators. The coupling gaps for the outer resonators are thus a lot smaller and that may limit the practicality of the filter. For the hairpin filter, the required tapping point is 3.7 mm from the start of the hairpin bend and coupling gaps of 0.45mm are required for the outer resonators and gaps of 0.95 mm are required for the inner resonators.

The test circuit for determining the tapping points for direct coupled filters is outlined in [7]. Using the procedure above, tapping points of 9.7 mm are required for the outer resonators and tapping points of 4 mm are required for the other resonators. For the direct coupled filter, the coupling lines are chosen to be 12.5% of a wavelength. This length has been found to give a reasonable stopband performance, whilst maintaining reasonable coupling tapping points.

III FILTER COMPARISON

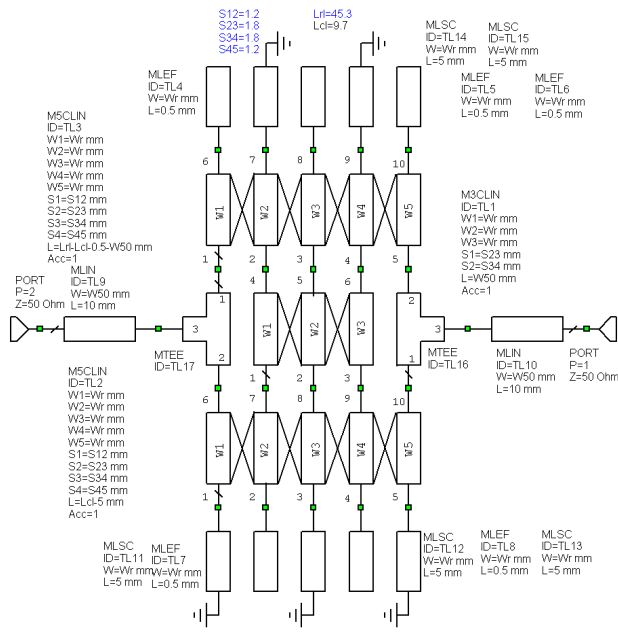
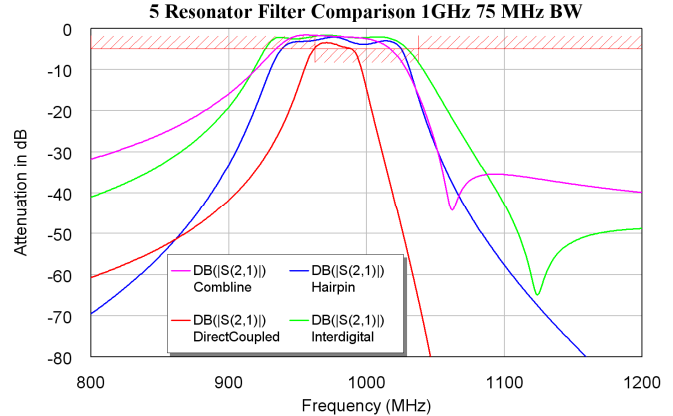


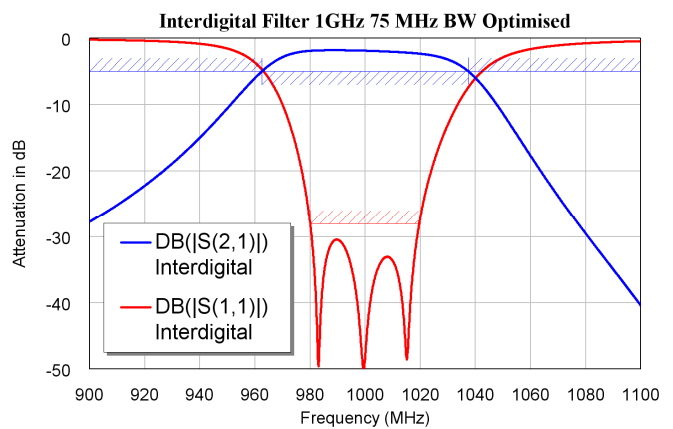
Figure 6. Circuit schematic for interdigital filter.

Once the coupling factors and tapping points have been determined, they are entered into the schematic circuit for each of the filter types. Figure 6 shows the schematic for the 5 resonator interdigital filter. Figure 7 shows the frequency response for the 4 different filter

types, with the tapping points and coupling gaps indicated above. It can be seen that the initial performance of the filters is close to specification. To complete the design procedure, the filters are optimised to provide the fine tuning required to fully meet the design specification. In addition some manufacturing constraints can be included. For instance for the filters designed here, the minimum coupling gap size was set at 0.5 mm, which is larger than the coupling gap of 0.2 mm calculated for the combline filter.



The optimization goals should be kept as simple as possible to maximize the speed of the optimisation. The corner frequencies of the filter are specified by setting three optimization goals as shown in figures 7 and 8.



The insertion loss of the filter is close to 1 dB, so that the filter is to have less than 4 dB attenuation from 962.5 MHz to 1037.5 MHz, and more attenuation elsewhere. In addition an optimization goal with S_{11} to be less than -25 dB from 980 MHz to 1020 MHz is added, to ensure that the filter has the lowest possible attenuation in the passband. For the interdigital filter, the frequency response after optimization is shown in figure 8.

The same optimization process is applied to the other 3 filters. Figure 9 shows the passband response of the 4

filters after optimization. Figure 10 shows the frequency response of these filters over a wide frequency range. The hairpin filter has a high stopband attenuation for frequencies less than the second harmonic, but has a harmonic response at that frequency. The direct coupled filter has a high stopband attenuation but has little attenuation at the third harmonic frequency. The combline and interdigital filters have smaller harmonic responses but have less stopband attenuation. The filter type to be used will thus depend on the stopband specifications. The direct coupled filter allow larger bandwidths to be realized [7] than the other filters.

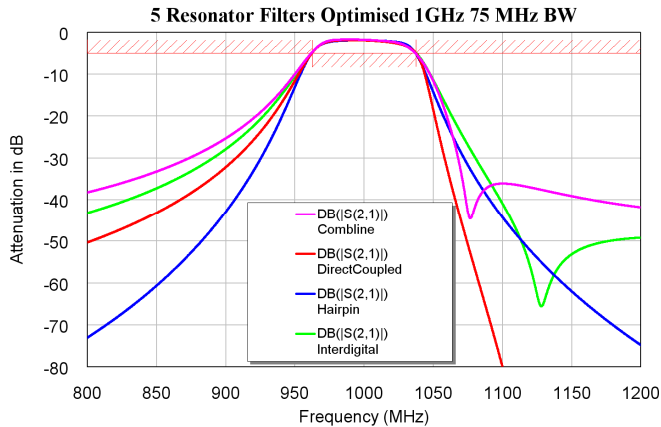


Figure 9. Comparison of filters, passband after optimisation.

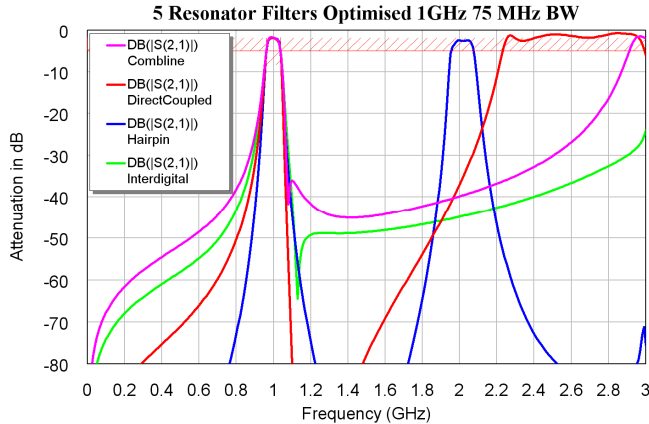


Figure 10. Comparison of filters, stopband after optimisation.

IV FILTER MEASUREMENTS

The 4 filters with the simulated performance shown in Figures 9 and 10 were built. Figure 1 shows the photograph of the interdigital. Figure 11 shows the combline filter, figure12 shows the hairpin filter and figure 13 shows the direct coupled filter. The interdigital filter is 42 x 60 mm in size, the combline filter is 41 x 60 mm, the direct coupled filter is 75 x 60 mm and the hairpin filter is 78 x 70 mm. The photographs are reproduced to approximately the same scale



Figure 11. 1GHz combline filter.

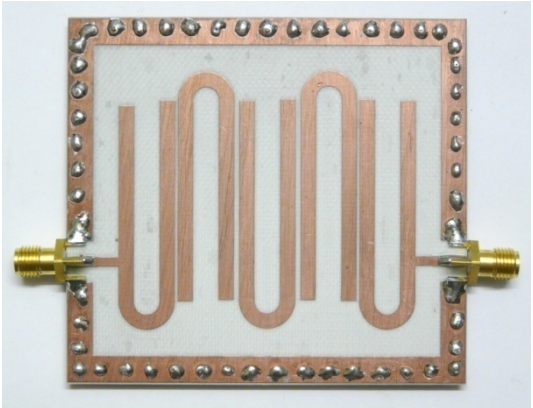


Figure 12. 1 GHz hairpin filter.

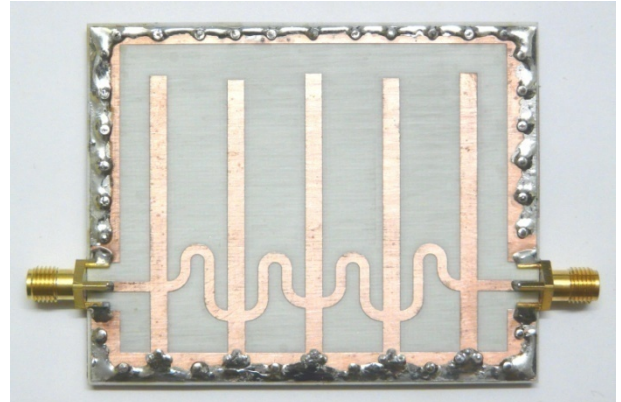


Figure 13. 1 GHz direct coupled filter.

Figures 14 to 15 show the measured frequency response of the filters. There is a remarkable agreement between the calculated and measured performance. The measured passband centre frequency of the combline, interdigital and direct coupled filters is 20 MHz or 2% lower than the design value. The resonators are thus 0.8 mm, or the substrate thickness, too long. This additional length is due to the via connecting the grounded end of the resonator to the bottom ground-plane. A second realization of those filters can take this effect into consideration to produce the correct centre frequency.

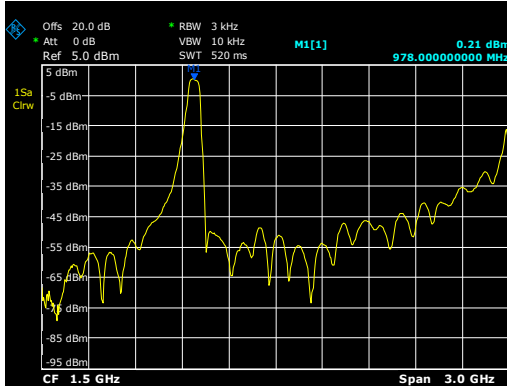


Figure 14. Interdigital filter frequency response.

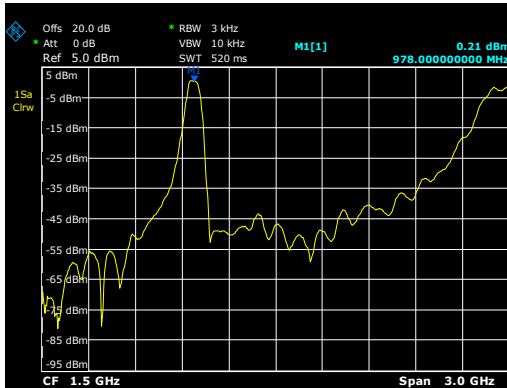


Figure 15. Combline filter frequency response.

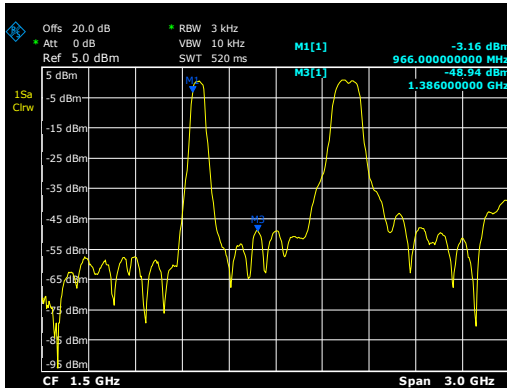


Figure 16. Hairpin filter frequency response.

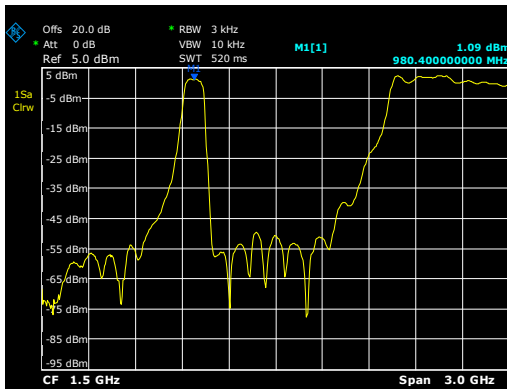


Figure 17. Direct coupled filter frequency response.

CONCLUSION

This paper describes a design procedure that can be used to design any coupled resonator filter, whose layout can be simulated. Four different filters are designed, each with a similar passband response, but a very different out of band response. This allows the appropriate RF filters to be selected, such that unwanted RF signals are filtered out effectively. This design technique can be used to design new filters topologies, which can provide cost effective analogue signal processing by the receiver front end. One example would be a filter with some hairpin resonators, to achieve a high stopband attenuation, coupled to interdigital resonators to remove the harmonic responses from the hairpin filter.

The measured filter performances closely match those obtained by computer simulation.

ACKNOWLEDGEMENT

The author acknowledges his employer James Cook University and in particular the staff of the School of Engineering for their support and encouragement. The author thanks Applied Wave Research (AWR) for making Microwave Office available to Universities at substantial discounted rates.

References

- [1] Matthaei, L. Young, and E. M. T. Jones, *Microwave Filters, Impedance-Matching Networks, and Coupling Structures*. Boston, MA: Artech House, 1980.
- [2] Zverev, A. I. *Handbook of filter Synthesis*, Book, Publisher John Wiley & sons, 1967 .
- [3] Pozar, D. *Microwave Engineering* , Third Edition, Wiley, 2005. pp. 416-438.
- [4] Toledo, N. G. "Practical Techniques For Designing Microstrip Tapped Hairpin Resonator Filters On Fr4 Laminates" Available: http://wireless.asti.dost.gov.ph/sitebody/techpapers/hairpin_pej.DOC.
- [5] Applied Wave Research, Inc. Microwave Office, http://web.awrcorp.com/Products/Microwave_Office/Overview.php [accessed 10 July 08]
- [6] Agilent Advanced Design System, http://eesof.tm.agilent.com/products/ads_main.html, [accessed 10 July 08]
- [7] Kikkert, C. J. "Designing Low Cost Wideband Microstrip Bandpass Filters", IEEE Tencon 2005, 21-24 November 2005, Melbourne, Australia.

The Design, Fabrication and Measurement of Microstrip Filter and Coupler Circuits

By Dana Brady
CAP Wireless, Inc.

These practical microstrip examples provide a valuable tutorial on the use of many different engineering resources: published references, comprehensive EDA tools, EM analysis and rapid prototyping equipment.

tools, combined with the lessons of their own experience. Their work is verified with the construction and testing of a finished circuit. This article describes two microstrip designs that were developed using different methods, fabricated quickly using a p.c. board milling machine, then measured to determine the accuracy of the design methods.

The example designs are a classic hairpin filter with a bandwidth of 3.7 to 4.2 GHz, and a 1 to 8 GHz directional coupler using the Schiffman sawtooth, or zig-zag, technique to reduce the size. The hairpin filter was designed and simulated using Agilent ADS 1.3 [1], with planar EM analysis using Sonnet Lite [2]. The coupler used a design-rule-based transformation, starting from an existing stepped-line coupler design. Both circuits were fabricated on a Protomat C100HF from LPKF Laser & Electronics [3], with measured results obtained using an HP (Agilent) 8753E network analyzer.

Design example #1: A 3.7 to 4.2 GHz hairpin filter

This filter was designed for a flat response over the 3.7 to 4.2 GHz band, with low insertion loss and return loss better than 16 dB across the band. The filter's application is

Today's microwave designers rely on many tools to help create effective circuits and systems. They use their libraries of published references, along with powerful EDA design tools and electromagnetic (EM) analysis

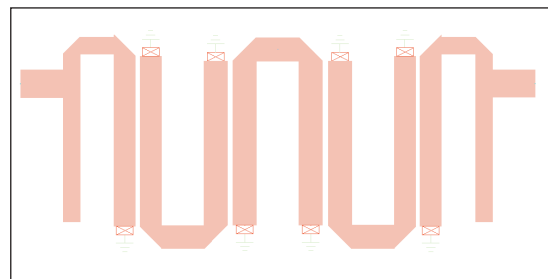


Figure 1 · Layout of the 3.7 to 4.2 GHz hairpin filter, designed with the help of ADS 1.3.

image rejection at the input of a synthesized block downconverter. A classic hairpin design was chosen, since experience has shown that it would meet the performance and size requirements for this design.

The filter was designed using ADS 1.3, with the resulting layout shown in Figure 1. This, of course, is the familiar hairpin configuration. The area occupied by the filter is approximately 500 by 1200 mils (0.5 x 1.2 in.), plus sufficient area beyond the hairpin loops to maintain consistent dielectric properties.

Figure 2 shows the design and optimization setup in ADS. Since this topology has symmetry around the center, it was designed as two sections, connected in a "back-to-back" configuration. With this reduction in the size of the mathematical problem, calculation time is significantly reduced.

The optimization was set up to obtain a minimum 16 dB return loss within a passband of 3.55 to 4.4 GHz, and a minimum stopband attenuation of 28 dB below 3.2 GHz and above 4.7 GHz. The optimization was set up for a frequency range of 3.0 to 5.0 GHz. A wider range is not required to obtain the desired results.

High Frequency Design

MICROSTRIP CIRCUITS

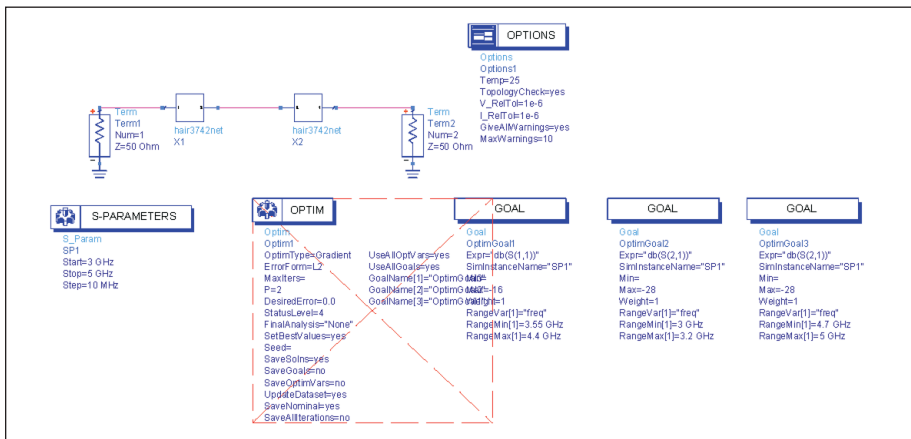


Figure 2 · Optimization setup in ADS. As noted in the text, the filter was simulated as two “mirror image” sections to exploit the filter’s symmetry.

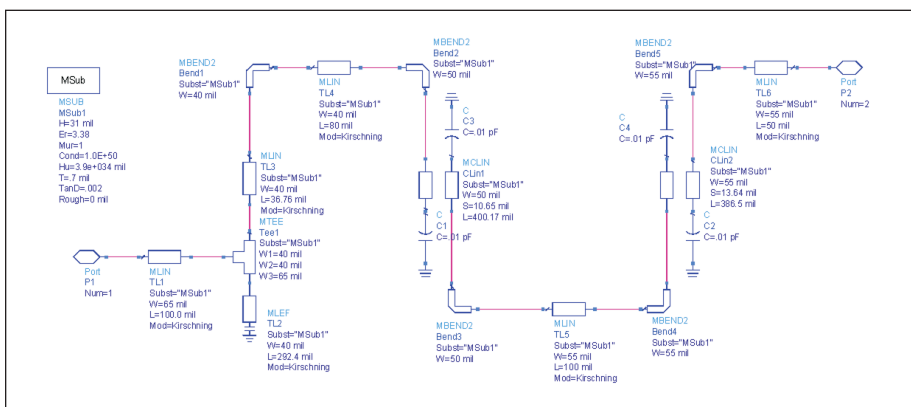


Figure 3 · The ADS simulation definition of the final design. Simulated performance data and filter layout are derived from this data.

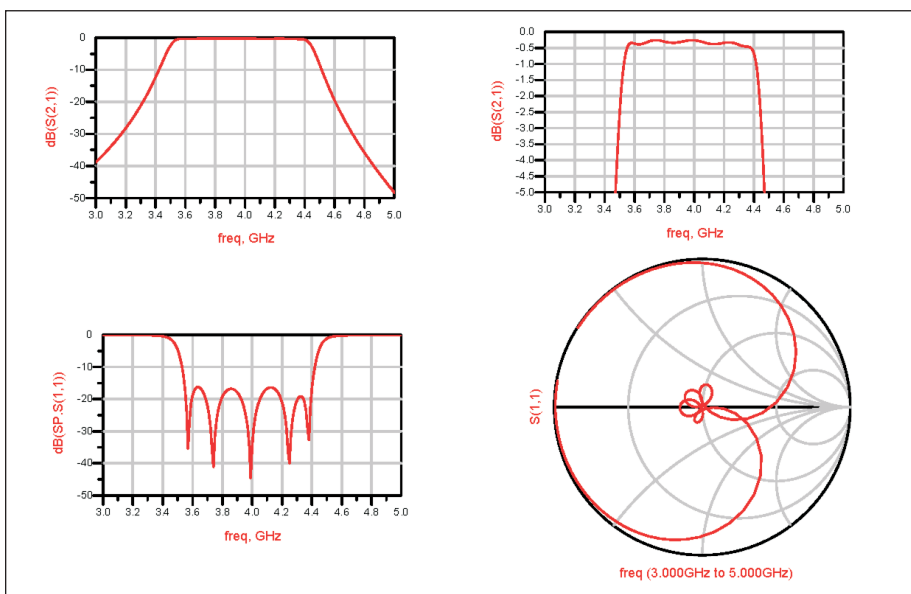


Figure 4 · Simulation results for the filter: (a) overall response, (b) passband response and insertion loss, (c) return loss, and (d) Smith chart impedance

The final ADS design for each “half filter” is shown in Figure 3, including the ports, microstrip lines, tees, bends and stubs. Note the 0.1 pF capacitances at the end of the stubs to account for end effect (fringing capacitance). These are also shown in the layout diagram of Figure 1.

Modeled performance is shown in Figure 4. These plots show the passband, stopband, return loss results of the ADS simulation, along with a Smith chart plot of input/output impedance. These plots show that the ADS model meets the filter’s design criteria.

EM analysis

A detailed diagram of the filter dimensions is shown in Figure 5. This layout data was used to set up an analysis of the circuit using the free Sonnet Lite planar electromagnetic field solver software from Sonnet Software, Inc.

Figure 6 shows the results of EM analysis. The passband response is slightly narrower than predicted by ADS, but will cover the desired 3.7 to 4.2 GHz band if the performance of the fabricated circuit matches this analysis. Passband flatness is very close to that modeled by ADS. Return loss response is less symmetrical across the passband than the ADS simulation, but it remains at 16 dB or better.

Fabricating a test filter

To compare the performance of the modeled hairpin filter design with its real-world counterpart, a test filter was fabricated on a typical microwave laminate, using a p.c. board milling machine (LPKF Protomat C100HF—see the sidebar on page 29).

Layout data from ADS (Figure 1) was used to create the necessary driver files for the milling machine. These dimensions were transferred directly from ADS into the LPKF setup software. Figure 7 is the layout for fabrication of the board.

High Frequency Design

MICROSTRIP CIRCUITS

Measured performance

After the board was milled to the desired pattern, connectors were attached and the filter was measured using an HP 8753E network analyzer. Figure 8 is the through performance (S_{21}) and return loss (S_{11}) of the prototype filter. The scale of this plot is 5 dB per division to show the overall passband/stopband performance down to -45 dB.

Figure 9 is the same as Figure 8, but with the passband plot scaled at 1 dB per division to show the passband flatness. The return loss plot remains at 5 dB per division.

The measurements show very good agreement with the models. The passband is slightly narrower than predicted by ADS, but by a smaller

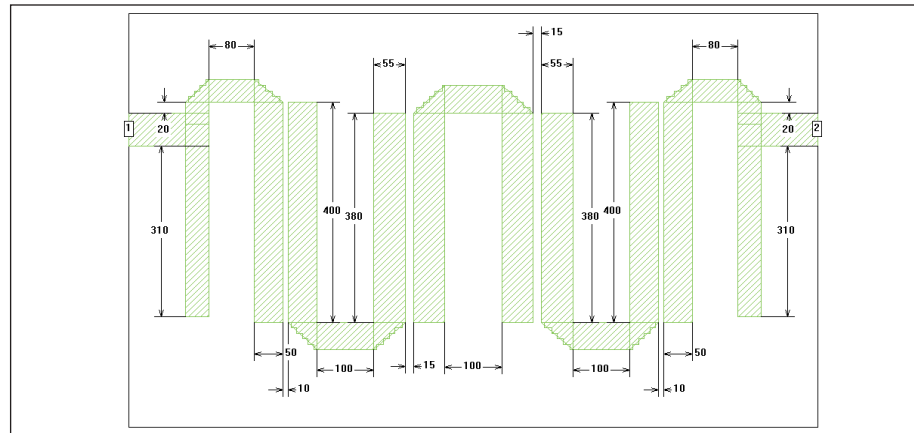


Figure 5 · Detailed dimensions of the hairpin filter.

amount than the Sonnet Lite analysis indicated. All three methods of modeling and measurement were in

agreement on the insertion loss and the flatness of the passband.

Although there are variations in

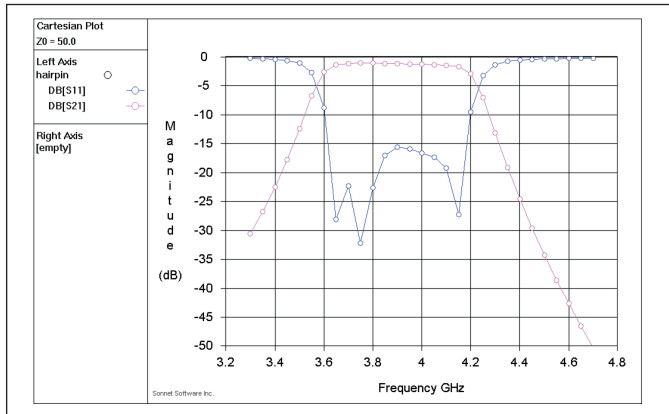


Figure 6 · EM analysis results from Sonnet Lite, which indicates that the response satisfies the design criteria.

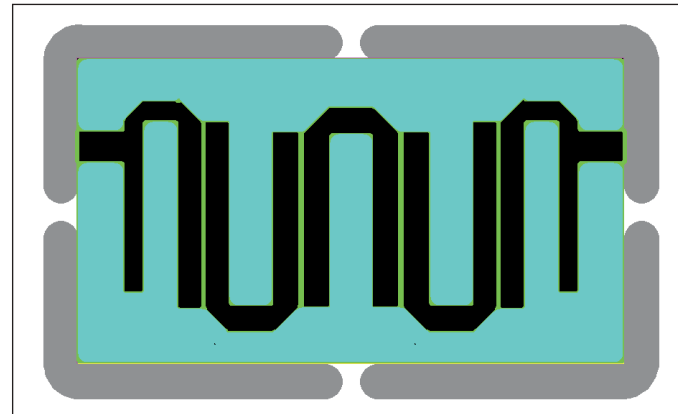


Figure 7 · Circuit board layout for milling with the LPKF machine.

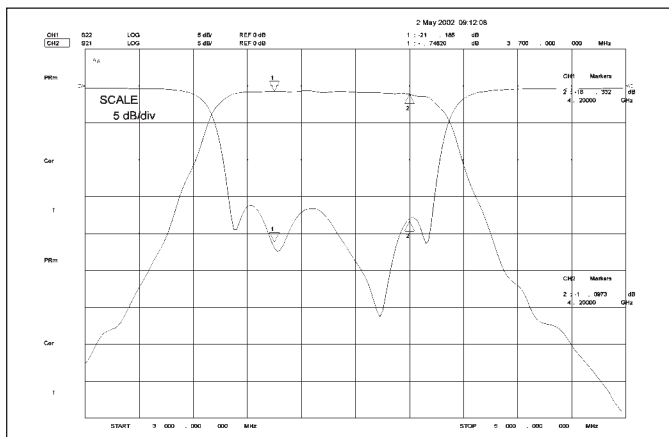


Figure 8 · Passband and return loss measurement of the prototype filter on a milled p.c. board.

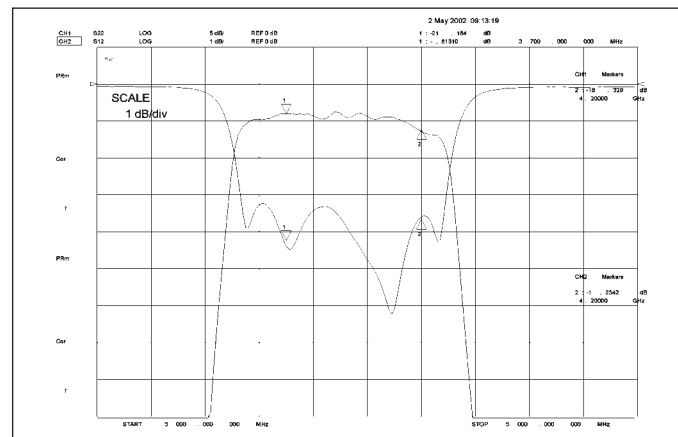


Figure 9 · Same as Figure 8, but 1 dB per division resolution to obtain a detailed passband measurement.

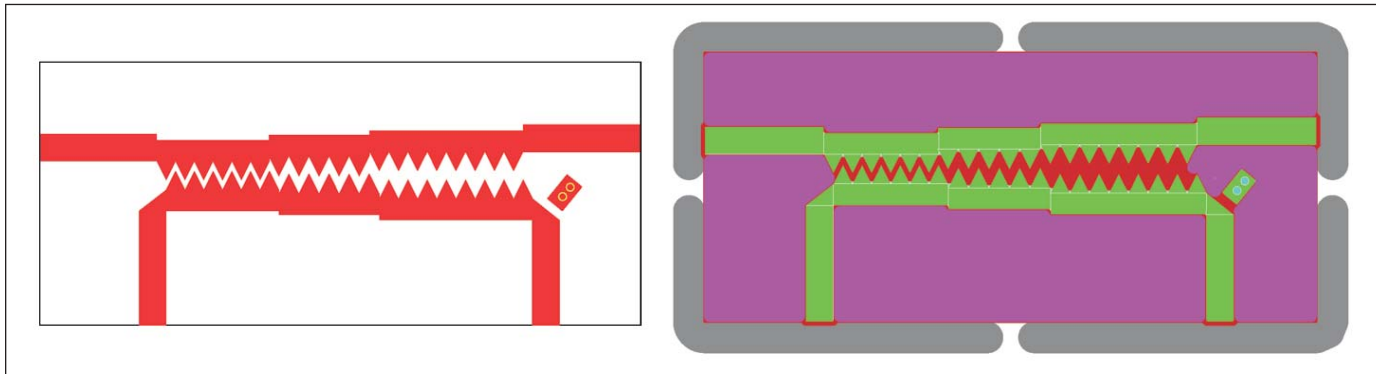


Figure 10 · This basic layout (left) and fabrication template (right) illustrate the technique used for the Schiffman reduced-size directional coupler.

the shape of the return loss plots among the modeled and measured data, each of them maintains the desired 16 dB specification, and clearly shows the expected “humps” of a multi-pole filter response.

Design example #2: A reduced-size stepped-line directional coupler

The next circuit we'll examine was developed using an empirical technique. We wanted to investigate a method of reducing the size of microstrip circuits developed by Schiffman, as described by Uysal [4]. This technique uses a sawtooth or zig-zag pattern to reduce the mechanical length required for a given electrical length.

An existing 1 to 8 GHz stepped line coupler, designed in ADS by CAP

Wireless colleague Paul Daughenbaugh, was used as the starting point. This design was translated into a layout for fabrication on the milling machine, similar to the one shown in Figure 10. This figure actually shows a different version of the coupler, but it clearly illustrates the technique.

An empirical method was used to obtain the new coupler layout from the straight-section coupler design, using the following rules:

- *Close-spaced coupler section*—The total length along the zig-zag path was made equal to the straight line length of this section. This reduced the length of this section by a factor of nearly half. The spacing between straight lines was maintained between the “interlocking” teeth, as measured across the gaps at right angles to their edges.

- *Wide-spaced coupler section*—The spacing between the lines of the third section was calculated at the mid-height of the teeth. At this wide spacing, it was assumed that the fields would couple according to this average spacing, rather than along the edge path of the first section. Also, the length reduction is less in this section. For simplicity, the same length as the original straight line section was used.

- *Center section*—The line spacing and the length reduction of the center section was calculated as the geometric mean of the first and third sections.

This “best guess” approach was necessary because it was not possible to analyze this structure using the available software tools. It is too complicated for analysis with Sonnet

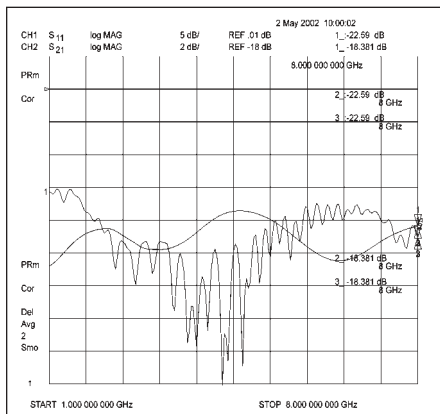


Figure 11 · Coupled port transmission and input port return loss.

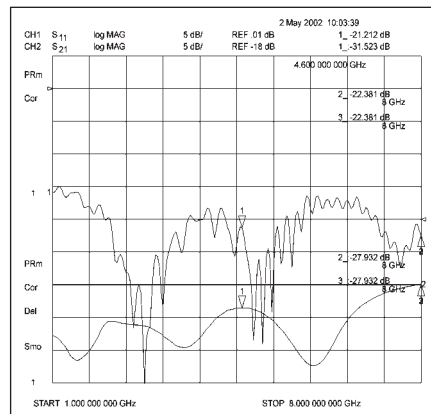


Figure 12 · Reverse coupling and output port return loss.

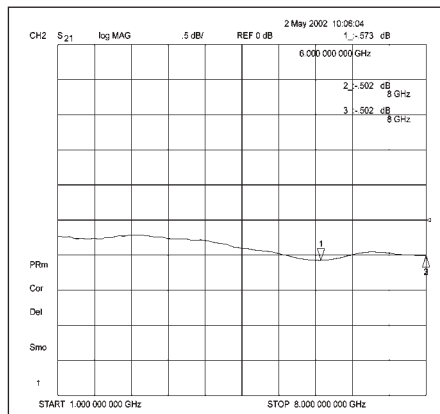


Figure 13 · Insertion loss (vertical scale is 0.5 dB per division).

Lite, and other analysis tools were not available.

Coupler performance

After fabrication with the LPKF milling machine, the coupler was evaluated for the degree of coupling, directivity across the 1 to 8 GHz band. In Figure 11, the coupled port transmission is the smooth line. The horizontal line at the center of plot is

-18 dB and the grid is 2 dB per division. Coupling is -19 dB \pm 1.5 dB over the measured frequency range. In the same figure, input return loss is plotted at 5 dB per division, referenced to 0 dB at the second line from the top. Worst case return loss is 16 dB at the lowest frequencies.

Reverse coupling is plotted in Figure 12, along with output port return loss. Both plots are 5 dB per

division. For reverse coupling, the center line is the reference, again at -18 dB, and coupling is -28 dB or better across the band, better than 31 dB at all but the high frequency end. The output port return loss is plotted using the same scale as input return loss in Figure 11, and also shows the same 16 dB worst case performance at 1 GHz.

Directivity (forward coupling

Using a Milling Machine for p.c. Board Prototyping



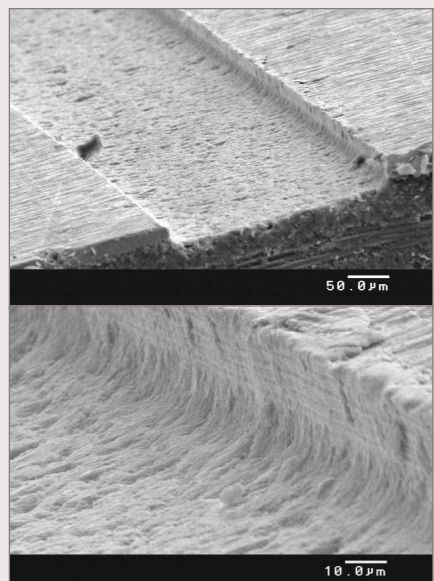
The positioning accuracy of the machine is very important, to maintain the necessary precision for both *x-y* axis dimensions and the depth of penetration. The machine must reliably cut the entire copper cladding layer, while removing a minimal amount of the underlying dielectric material.



The photo above is a closeup of the milling head. The C100HF uses dynamic *z*-axis positioning with a coaxial working depth limiter to maintain the milling depth. The penetration into the substrate is typically 0.2 mil (5 micron). The *z*-axis movement range is 14 mm (0.55 in.). An air bearing provides accurate, but non-contact surface sensing on soft or flexible boards, and on surface-sensitive materials.

The *x-y* positioning accuracy is less than 0.2 mil (5 micron) at a resolution of 0.3125 mil (7.9 micron). The following electron microscope photos show a milled path at two different magnifications—note the

50 micron and 10 micron scale references at the bottom of the photos.

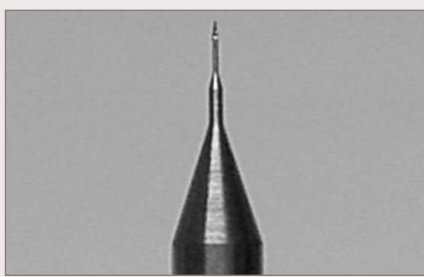


With a travel speed of 40 mm/sec (1.575 in.), both fine-pitch milling and runout of large areas is accomplished efficiently. If necessary, it is possible to build and test several iterations of a board design in a day. In some cases, the unit will be an acceptable alternative to conventional etched p.c. board fabrication for custom designs and small-quantity production.

Readers wishing to find out more about this unit may contact LPKF Laser & Electronics by telephone at 1-800-345-LPKF (1-800-345-5653), by e-mail at info@lpkfusa.com, or online at www.lpkfusa.com

The milling equipment used at CAP Wireless is the model Protomat C100HF from LPKF Laser & Electronics. This unit can accommodate a board up to 13.5 x 8 inches (340 x 200 mm). In addition to circuit boards, the unit can mill aluminum or brass mechanical parts or cut copper shielding foils.

The motor operates at variable speeds from 10,000 to 100,000 RPM, software controlled. The typical fine-pitch milling tool for boards like those described in this article is a 10 mil endmill, specified for a diameter variation of \pm 0.2 mils:



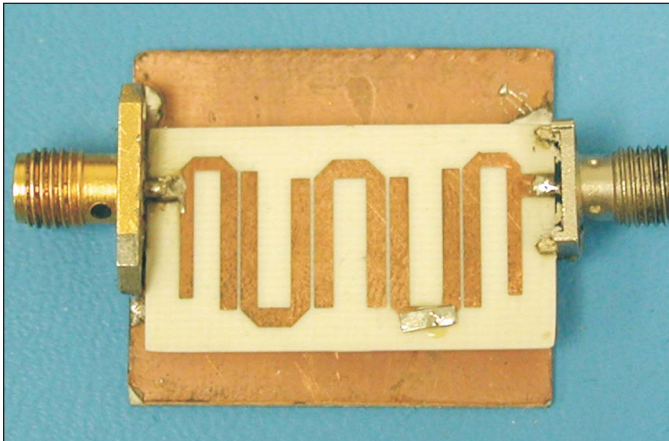


Figure 14 · Photo of the 3.7 to 4.2 GHz hairpin filter prototype board.

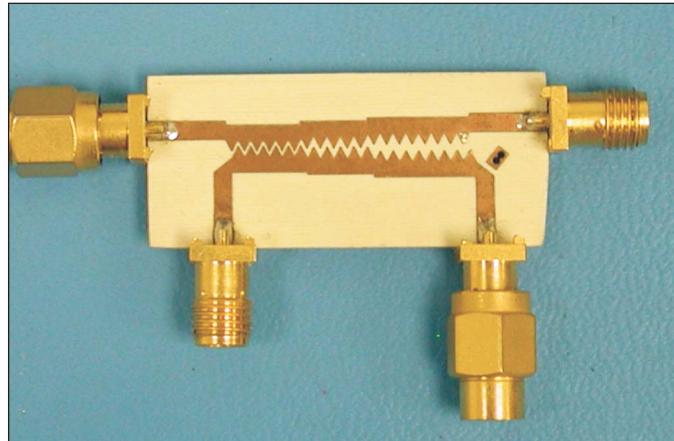


Figure 15 · Photo of the 1 to 8 GHz broadband coupler using the Schiffman, or zig-zag line, technique.

minus reverse coupling) is 10 dB over all but the extreme high end of the band. The design goal was >10 dB, with a target of 12 dB to allow extra margin. This margin was achieved over most of the band, which we consider to be an excellent result for a first iteration.

Figure 13 is insertion loss, which is 0.25 dB at 1 GHz, with a worst case of 0.57 dB at 6 GHz. The variation in insertion loss is just 0.33 dB across the entire 1 to 8 GHz band.

Notes on prototyping with a p.c. board milling machine

The ability to quickly fabricate a prototype p.c. board can change the engineering approach to certain designs. For the directional coupler, we were prepared for the possibility that several design iterations would be required to obtain a coupler with the desired performance. With some luck (and educated guesses based on experience), the first attempt resulted in a good coupler.

The photos in Figures 14 and 15 show the milled boards, with connectors attached for measurement. The hairpin filter board in Figure 14 even shows a patch soldered in place to cover a gap in one of the microstrip traces. This was caused by a small error in the layout file that became evident when the board was milled.

The coupler design may yet be modified to improve low-end return loss or flatten the coupling response. These small changes would probably not be considered with conventional fabrication using an outside board shop. Most companies no longer maintain in-house board etching labs, since environmental regulations, particularly in California, add significant cost and complexity to the chemical etching process.

Summary

It is hoped that these design examples show how we used many different design resources. To create these filter and coupler circuits, the experience of several engineers was combined with published data, advanced circuit theory simulation, EM analysis and, finally, fabrication and measurement. Each step in the process contributed to the overall design success.

References

1. Agilent Technologies, Inc.; information at www.agilent.com
2. Sonnet Software; information at www.sonnetusa.com

3. LPKF Laser & Electronics; information at: www.lpkfusa.com
4. Sener Uysal, *Nonuniform Line Microstrip Directional Couplers and Filters*, Artech House, 1993.

Additional Design References

5. G. Matthei, L. Young, E.M.T. Jones, *Microwave Filters, Impedance-Matching Networks, and Coupling Structures*, Artech House, ISBN 0-89006-099-1.
6. J.A.G. Mahlerbe, *Microwave Transmission Line Filters*, Artech House, ISBN 0-89006-063-0.

About the Author

Dana Brady is Senior Engineer at CAP Wireless, Camarillo, CA. Previously, he has held Senior Engineer positions at California Amplifier, Armatek and Amplica, and the Chief Scientist position at JCA Technology. He attended California Polytechnic State University and has experience in the design of many RF and microwave circuits and systems, including various microprocessor-controlled microwave subsystems. He can be reached by e-mail at: danab@capwireless.com

To submit a technical article for our consideration, simply e-mail a brief description to: editor@highfrequencyelectronics.com Author guidelines can be found on our web site: www.highfrequencyelectronics.com

Practical Aspects of Microwave Filter Design and Realization

IMS'05 Workshop-WMB



Microstrip Filter Design

Jia-Sheng Hong

Heriot-Watt University
Edinburgh, UK

J.Hong@hw.ac.uk



Dr. Jia-Sheng Hong
Department of Electrical, Electronic and Computer Engineering
Heriot-Watt University, UK
J.Hong@hw.ac.uk

Outline



Introduction



Design considerations



Design examples



Summary

Introduction- Driving forces

Recent development of microstrip filters has been driven by applications -

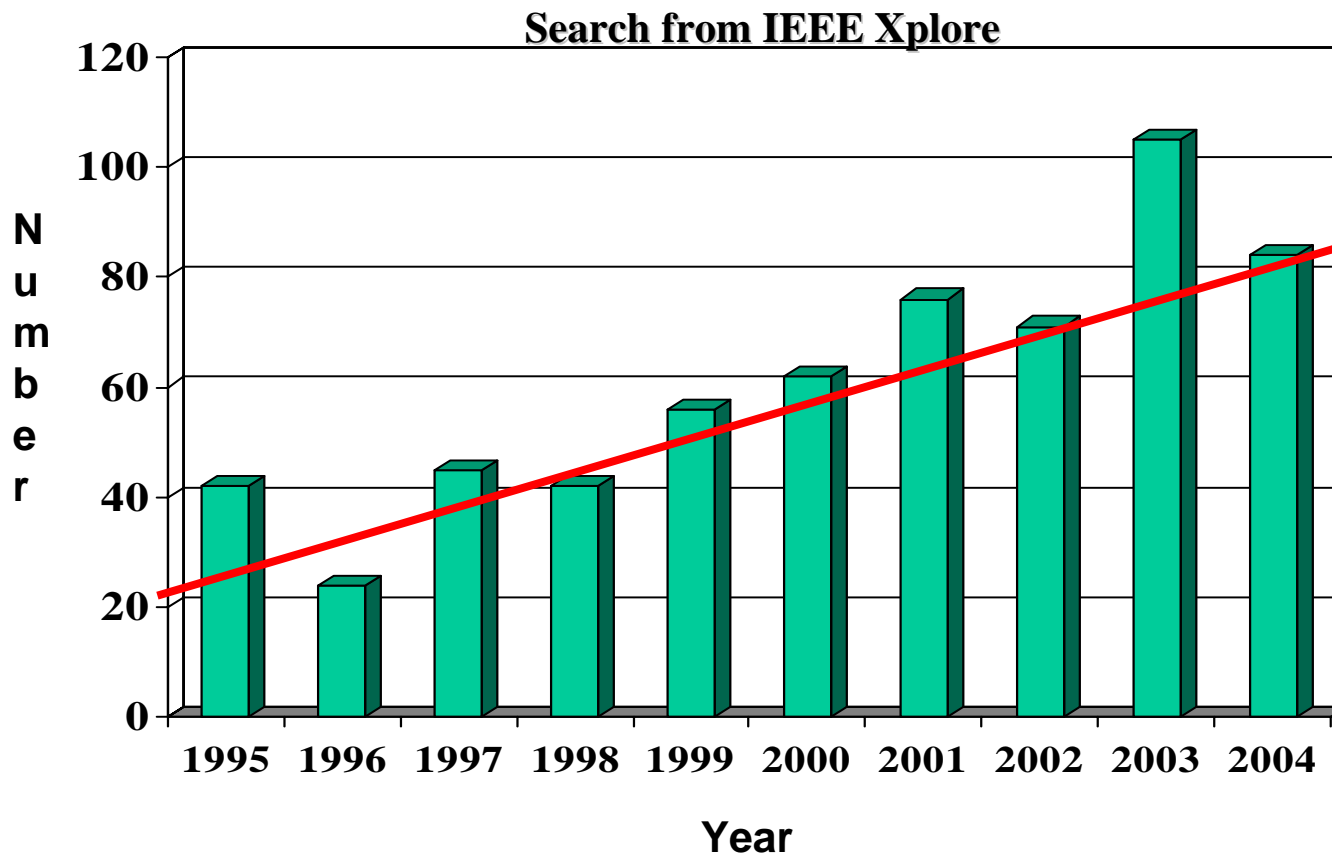
- Wireless communications**
- Wireless sensor/radar systems**
-

Driven by technologies -

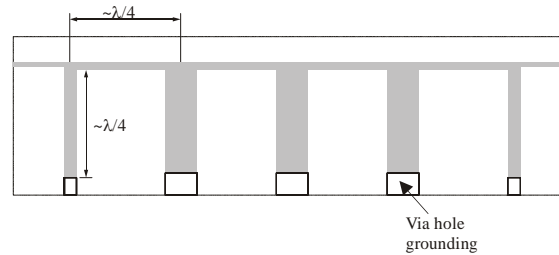
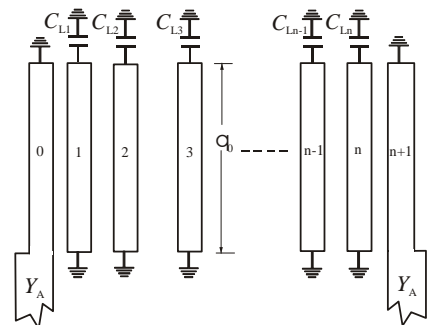
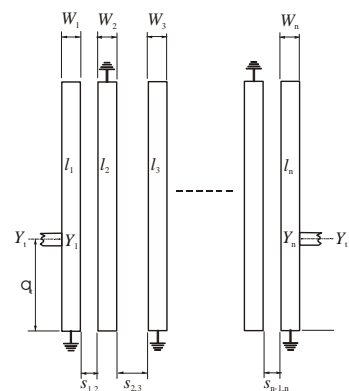
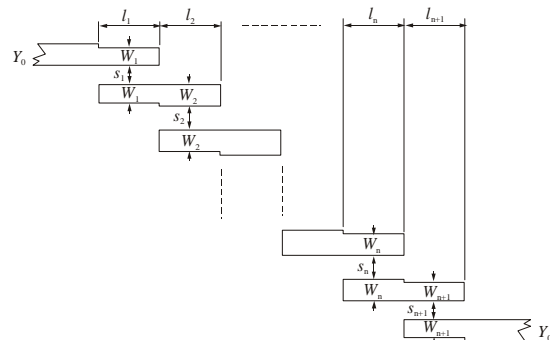
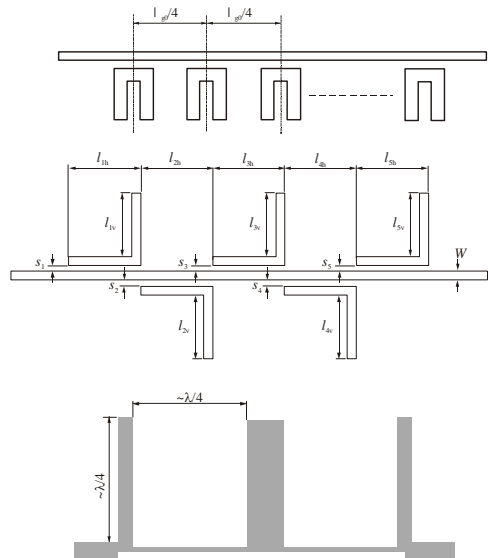
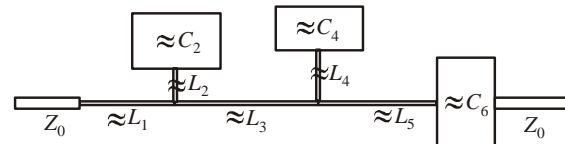
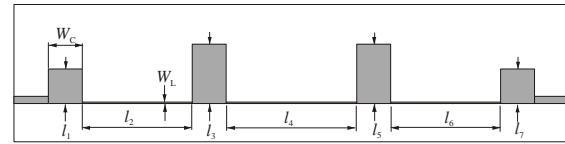
- High temperature superconducting**
- Micromachining**
- LTCC**
- Ferroelectric**
-

Introduction- Microstrip Filter Publications

Total 600+ in recent 10 years



Design Considerations- Topologies



Design Considerations- Topologies

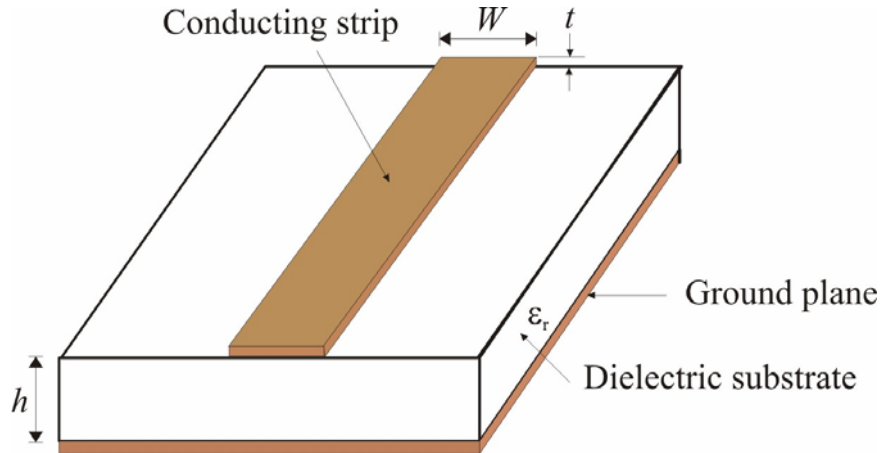
The choice of a topology depends on

- ✓ Characteristics of filters, such as chebyshev or elliptic
- ✓ Bandwidth
- ✓ Size
- ✓ Power handling

Design Considerations- Substrates

The choice of a substrate depends on

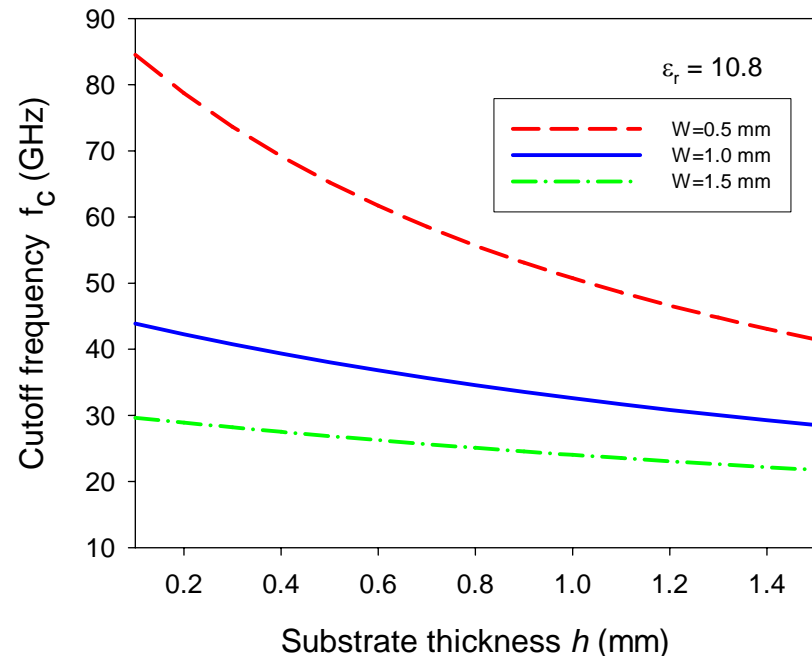
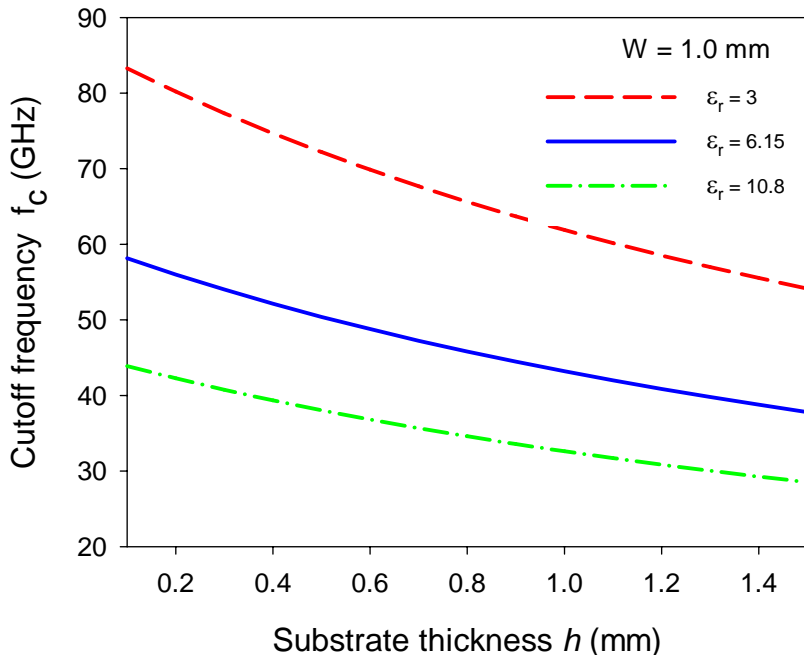
- ✓ Size
- ✓ Higher-order modes
- ✓ Surface wave effects
- ✓ Implementations – couplings, line/spacing tolerances, ...
- ✓ Dielectric loss
- ✓ Temperature stability
- ✓ Power handling – dielectric strength (breakdown), thermal conductivity



Design Considerations- Higher-order modes

- ✓ Keep operating frequencies below the cutoff frequency of the 1st higher-order mode,

$$f_c = \frac{c}{\sqrt{\epsilon_r}(2W + 0.8h)}$$

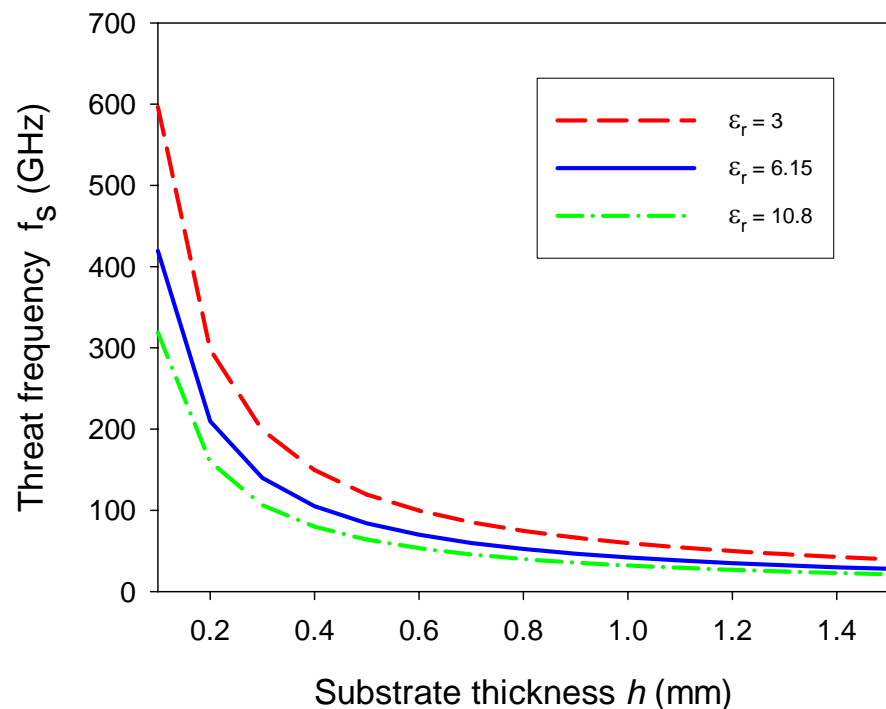


Design Considerations- Surface waves

- ✓ Keep operating frequencies below the threat frequency of the lowest surface wave mode,

$$f_s = \frac{c \tan^{-1} \epsilon_r}{\sqrt{2\pi h} \sqrt{\epsilon_r - 1}}$$

at which the surface mode couples strongly to the dominant mode of microstrip because the phase velocities of the two modes are close.



Design Considerations- Losses

There are three major losses in a microstrip resonator:

❑ Conductor loss

$$Q_c \propto \pi \left(\frac{h}{\lambda} \right) \cdot \left(\frac{377\Omega}{R_s} \right)$$

❑ Dielectric loss

$$Q_d \propto \frac{1}{\tan \delta}$$

❑ Radiation loss

$$\frac{1}{Q_u} = \frac{1}{Q_c} + \frac{1}{Q_d} + \frac{1}{Q_r}$$

Design Considerations- Power handling

- ❑ Peak power handling capability –
when the breakdown occurs in substrate

$$P_p \propto \frac{V_o^2}{2Z_c}$$

V_o is the maximum breakdown voltage of the substrate

Z_c is the characteristic impedance of the microstrip

**Narrower band filters result in higher electric field density,
leading to a lower peak power handling**

Design Considerations- Temperature effect

Temperature characteristic of a microstrip half-wavelength resonator on RT/Duroid substrate with $\epsilon_r = 10.2$, $h = 1.27$ mm

Copper CTE (coefficient of thermal expansion) = 17 ppm/ $^{\circ}\text{C}$

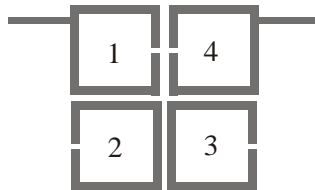
Substrate CTE = 24 ppm/ $^{\circ}\text{C}$

Substrate TCK (thermal coefficient of ϵ_r) = -425 ppm/ $^{\circ}\text{C}$

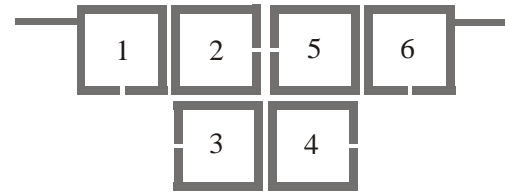
At 23 $^{\circ}\text{C}$	$f_0 = 1929.8$ MHz	$\Delta f = 0$
At 73 $^{\circ}\text{C}$ for copper CTE only	$f_0 = 1928.1$ MHz	$\Delta f = -1.7$ MHz
At 73 $^{\circ}\text{C}$ for substrate thickness CTE only	$f_0 = 1929.9$ MHz	$\Delta f = 0.1$ MHz
At 73 $^{\circ}\text{C}$ for substrate TCK only	$f_0 = 1949.4$ MHz	$\Delta f = 19.6$ MHz
At 73 $^{\circ}\text{C}$ (consider all)	$f_0 = 1947.8$ MHz	$\Delta f = 18.0$ MHz

- ✓ Frequency variation versus temperature is mainly due to dielectric constant change vs temperature

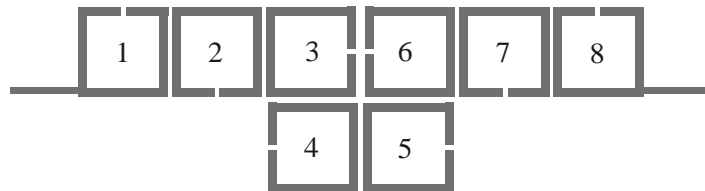
Design Examples- Open-loop filters



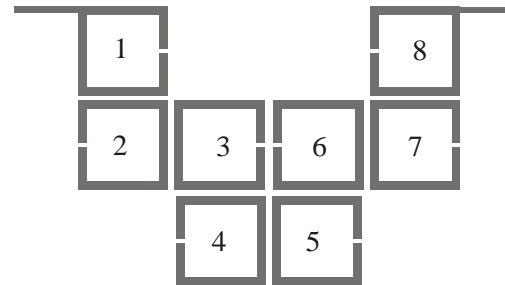
(a)



(b)



(c)



(d)

From: Jia-Sheng Hong and M.J.Lancaster, *Microstrip Filters for RF/Microwave Applications*,
John Wiley & Sons. Inc. New York, 2001

Design Examples- Open-loop filters

► Specifications:

Center frequency	985MHz
Fractional Bandwidth	10.359%
40dB-Rejection Bandwidth	125.5MHz
Passband Return loss	-20dB

► Design parameters for an 8-pole filter:

$$M_{1,2} = M_{7,8} = 0.08441$$

$$M_{3,4} = M_{5,6} = 0.05375$$

$$M_{3,6} = -0.01752$$

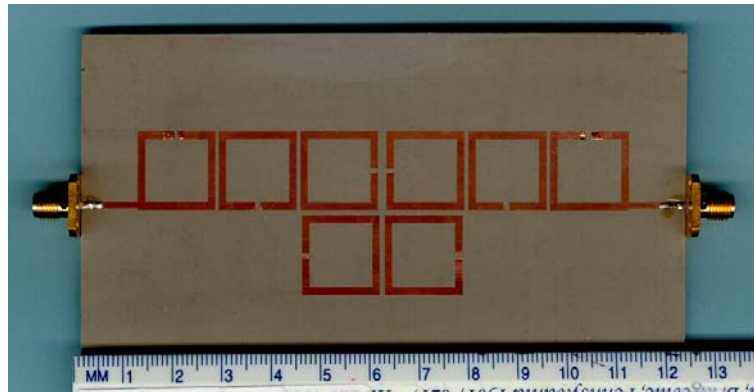
$$M_{2,3} = M_{6,7} = 0.06063$$

$$M_{4,5} = 0.0723$$

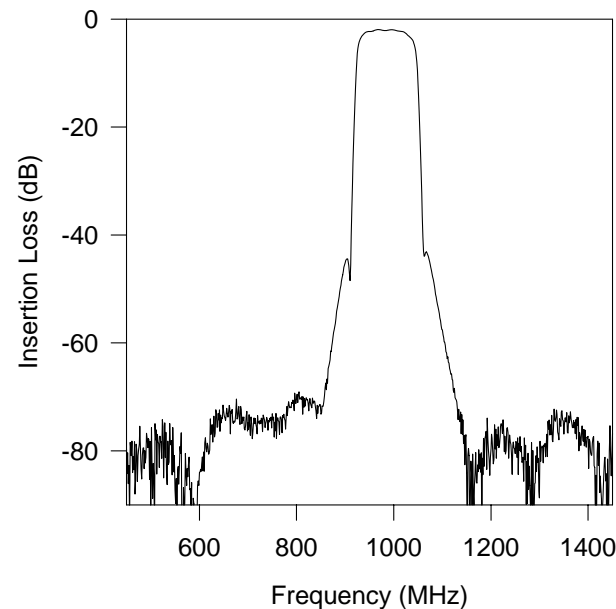
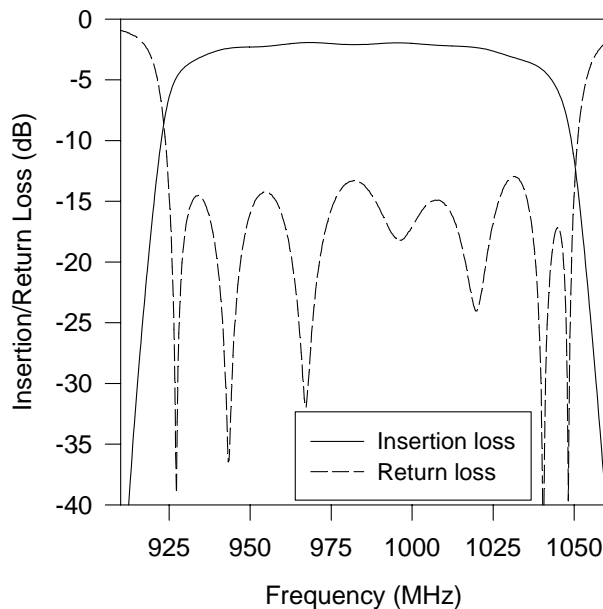
$$Q_{ei} = Q_{eo} = 9.92027$$

Design Examples- Open-loop filters

Realisation 1

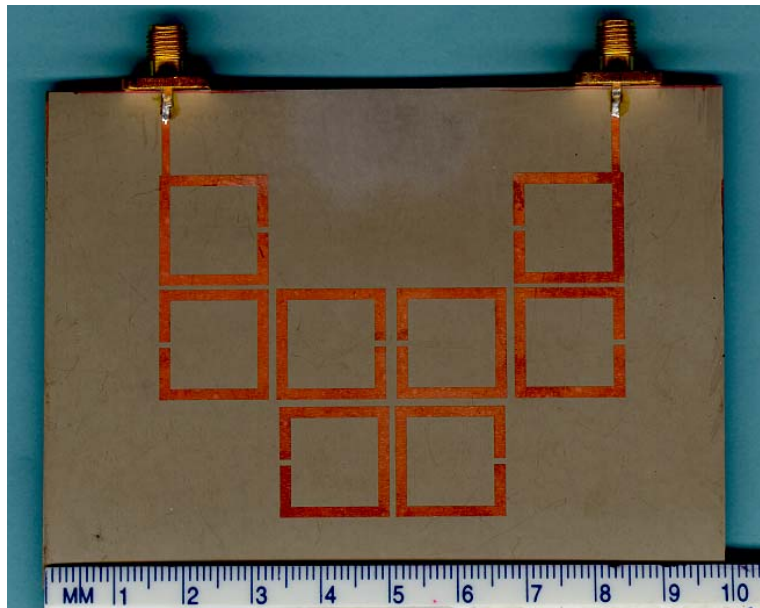


On RT/Duroid substrate with a relative dielectric constant of 10.8 and a thickness of 1.27mm. Each resonator has a size of 16 by 16 mm.

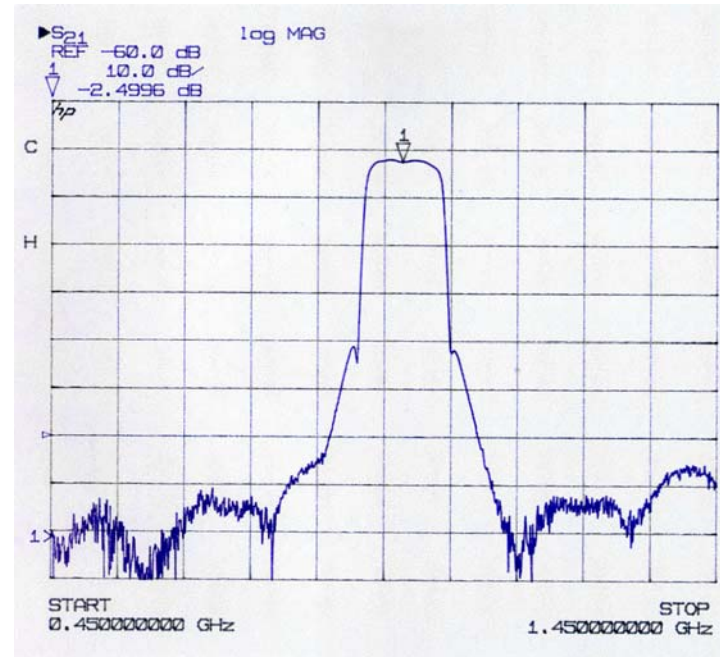


Design Examples- Open-loop filters

Realisation 2



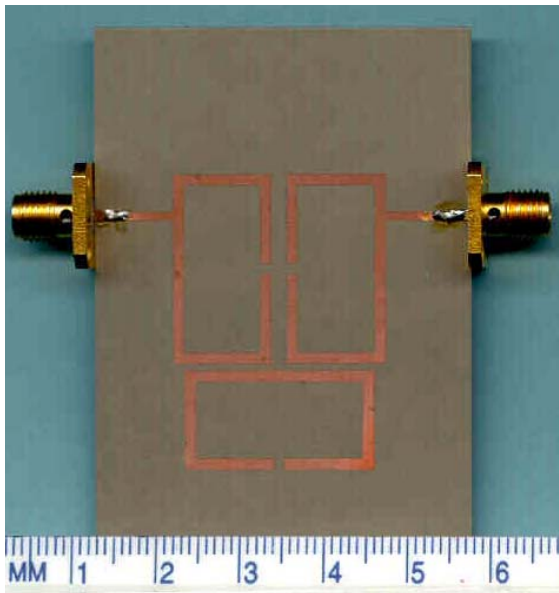
On RT/Duroid substrate with a relative dielectric constant of 10.8 and a thickness of 1.27mm



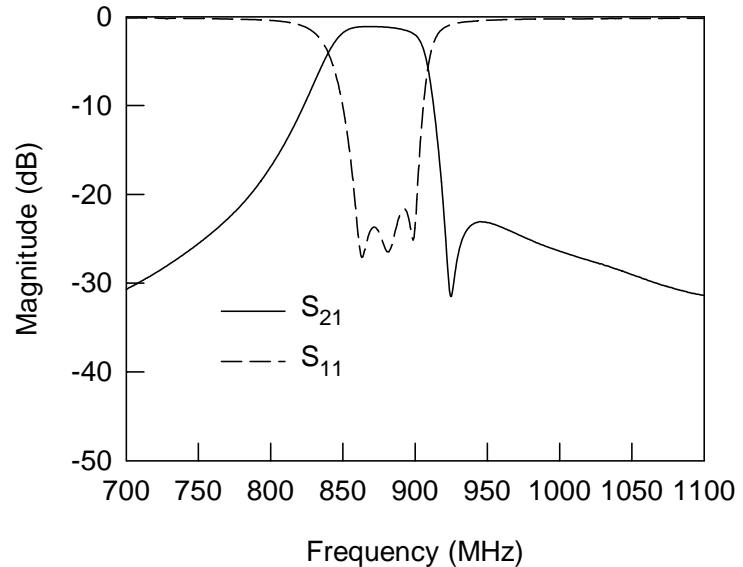
Design Examples- Trisection open-loop filters

Midband or centre frequency : 905MHz
Bandwidth of pass band : 40MHz
Return loss in the pass band : < -20dB
Rejection : > 20dB for frequencies \geq 950MHz

$$\begin{aligned}f_{01} &= f_{03} = 899.471 \text{ MHz} \\f_{02} &= 914.713 \text{ MHz} \\Q_{ei} &= Q_{eo} = 15.7203 \\M_{12} &= M_{23} = 0.04753 \\M_{13} &= -0.02907\end{aligned}$$



On RT/Duroid substrate with a relative dielectric constant of 10.8 and a thickness of 1.27mm

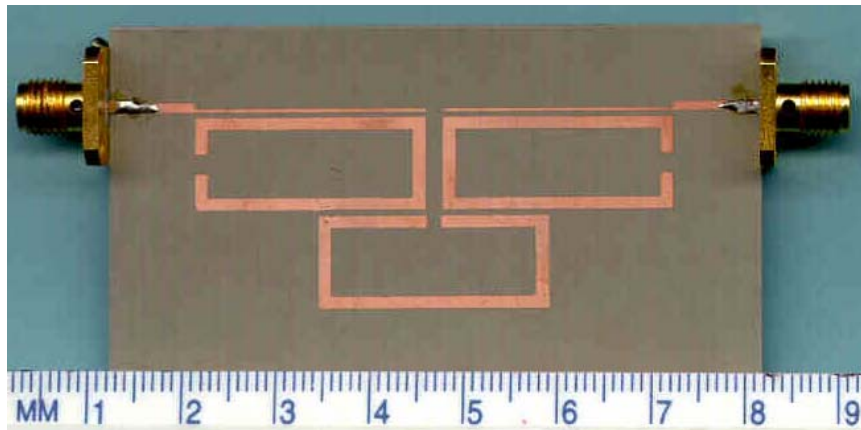


Measured response

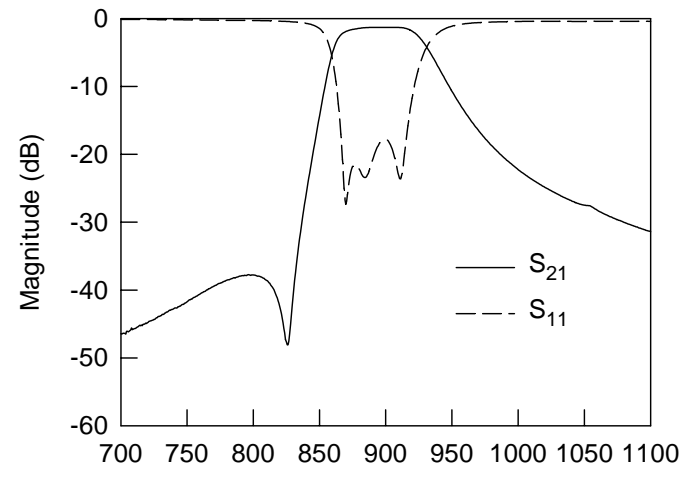
Design Examples- Trisection open-loop filters

Midband or centre frequency : 910MHz
Bandwidth of pass band : 40MHz
Return loss in the pass band : < -20dB
Rejection : > 35dB for frequencies \leq 843MHz

$$\begin{aligned}f_{01} &= f_{03} = 916.159 \text{ MHz} \\f_{02} &= 905.734 \text{ MHz} \\Q_{ei} &= Q_{eo} = 14.6698 \\M_{12} &= M_{23} = 0.05641 \\M_{13} &= 0.01915\end{aligned}$$

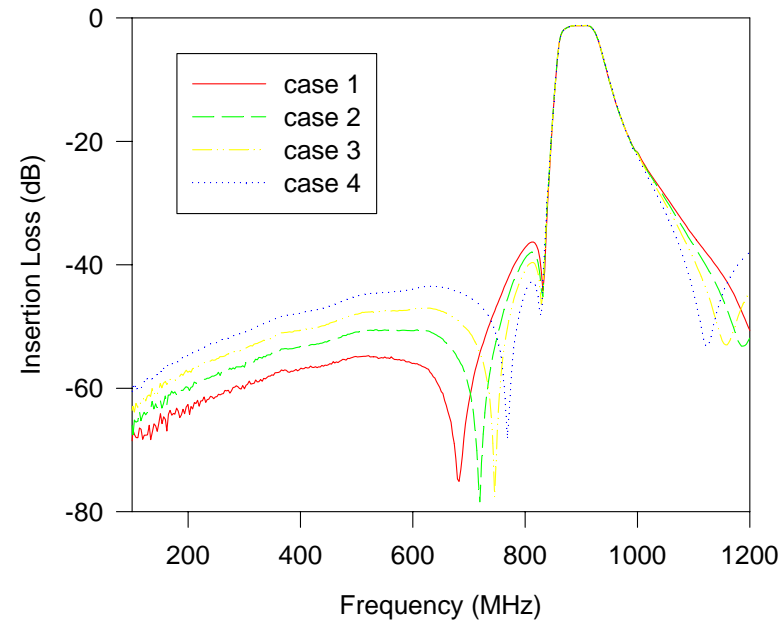
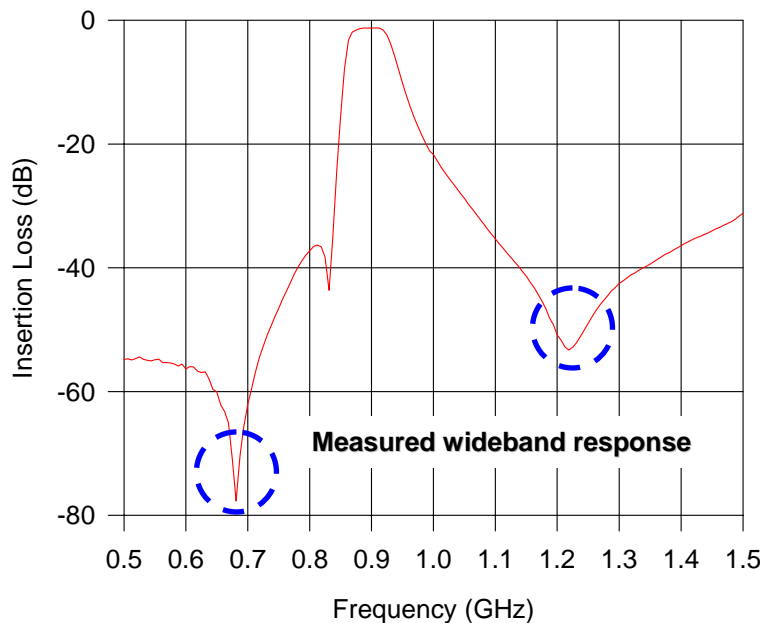
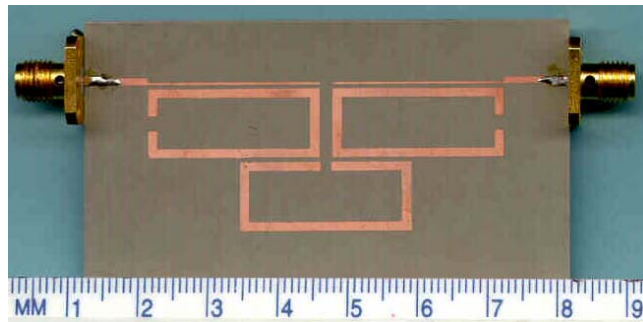


On RT/Duroid substrate with a relative dielectric constant of 10.8 and a thickness of 1.27mm



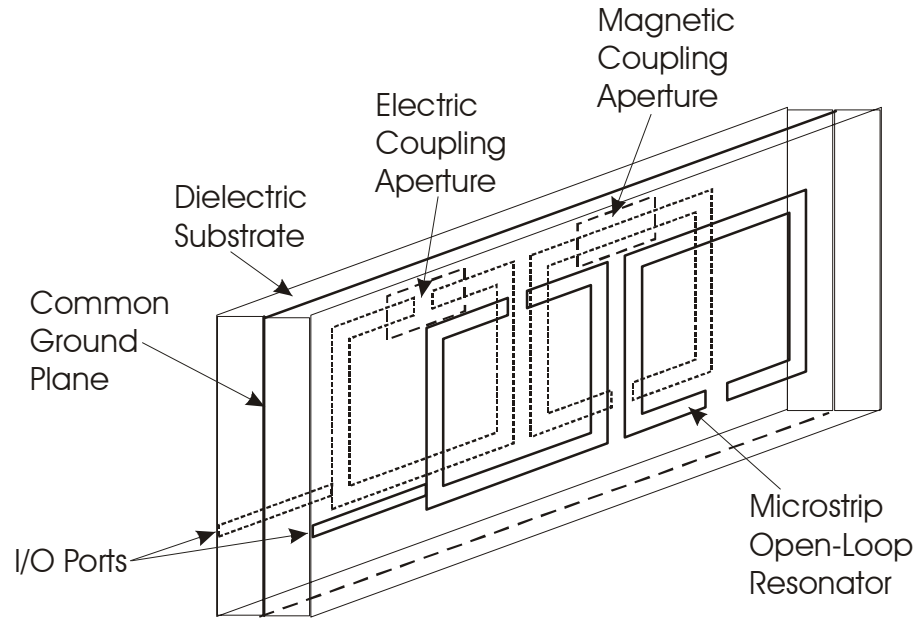
Measured response

Design Examples- Trisection open-loop filters

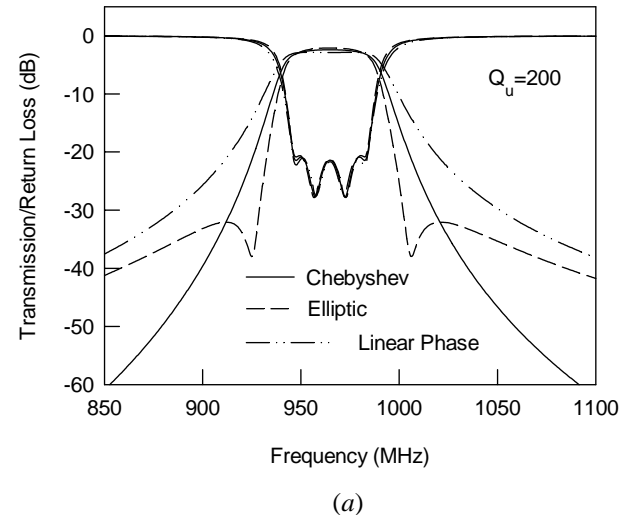
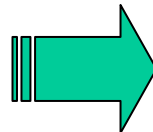
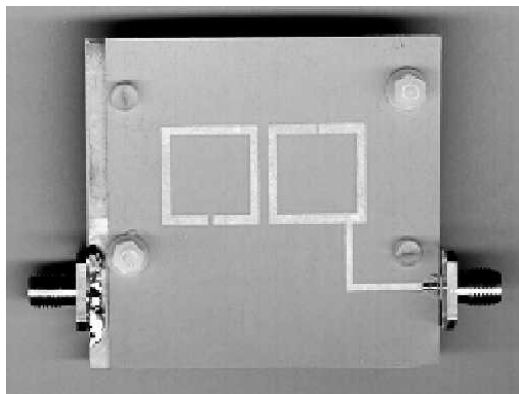


Experimental results on extra transmission zeros, where case 1 to 4 indicate the increase of direct coupling between the two feed lines.

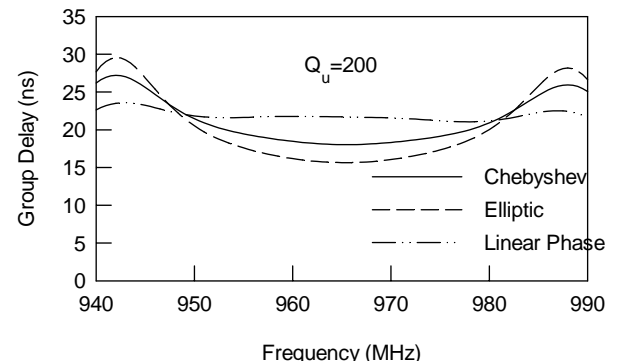
Design Examples- Multi-layer filters



Design Examples- Multi-layer filters



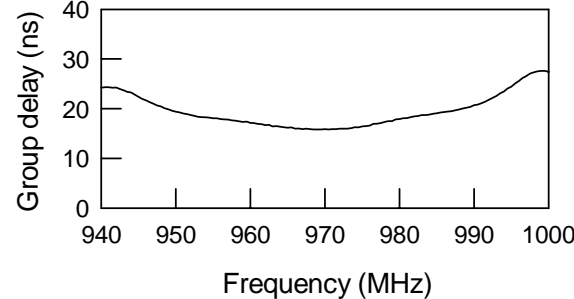
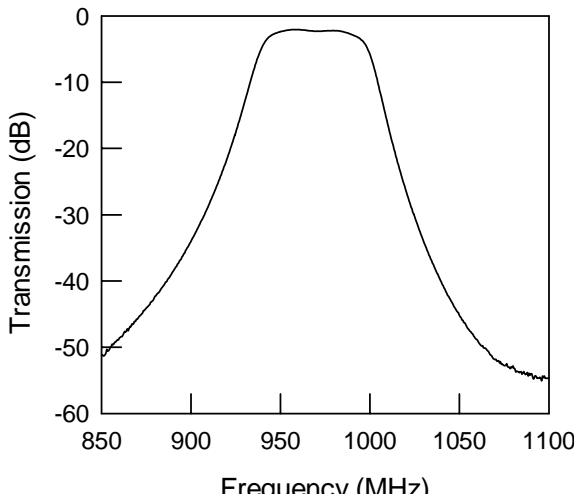
(a)



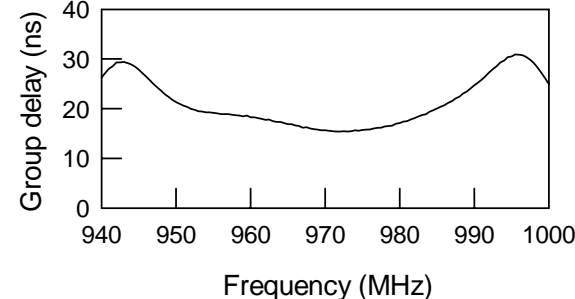
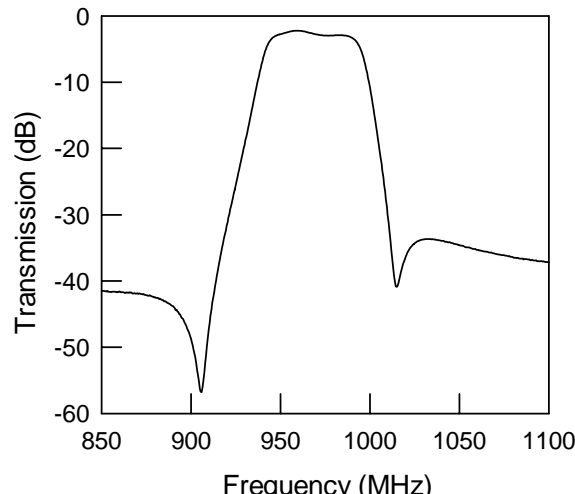
(b)

Design Examples- Multi-layer filters

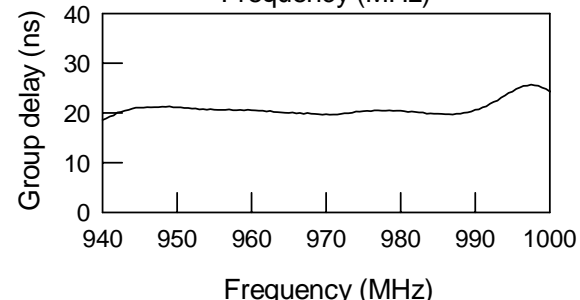
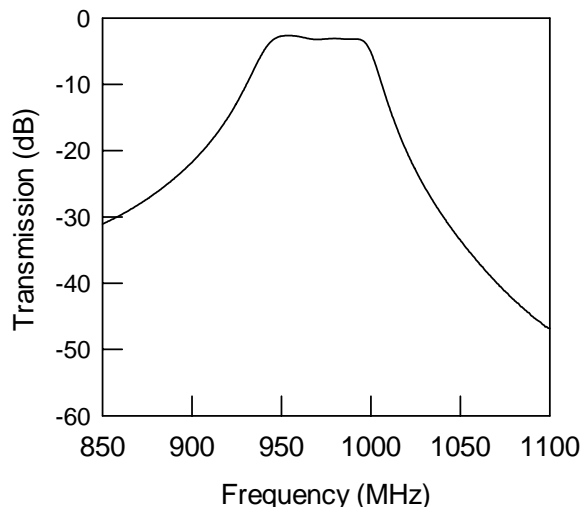
Experimental results



(a)



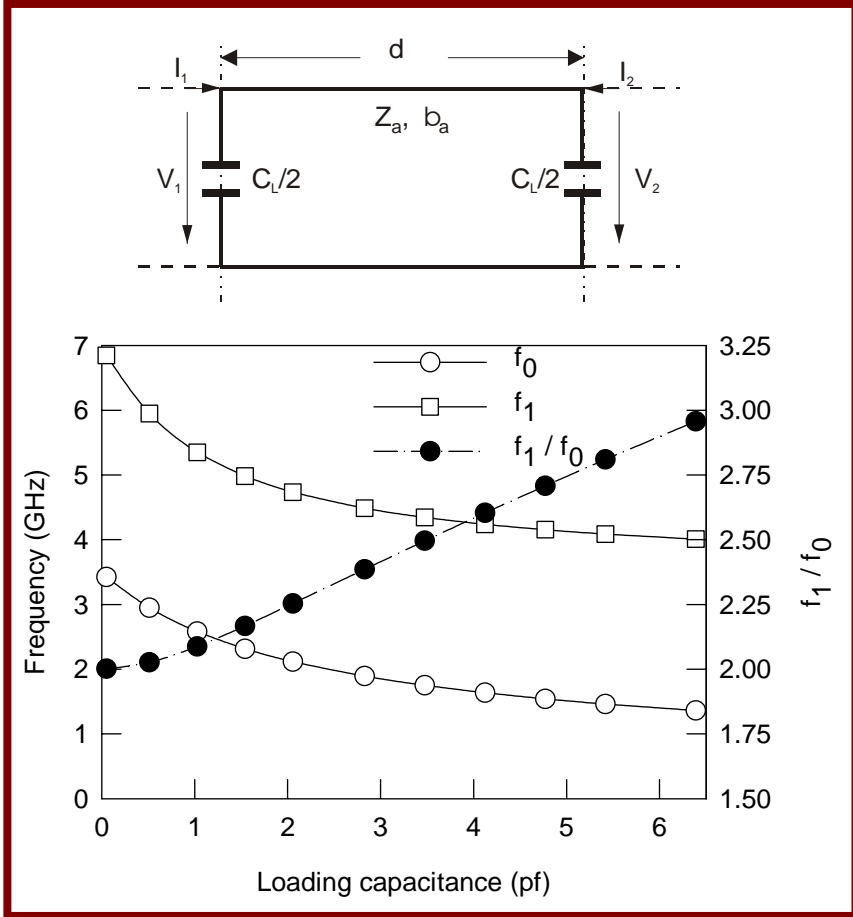
(b)



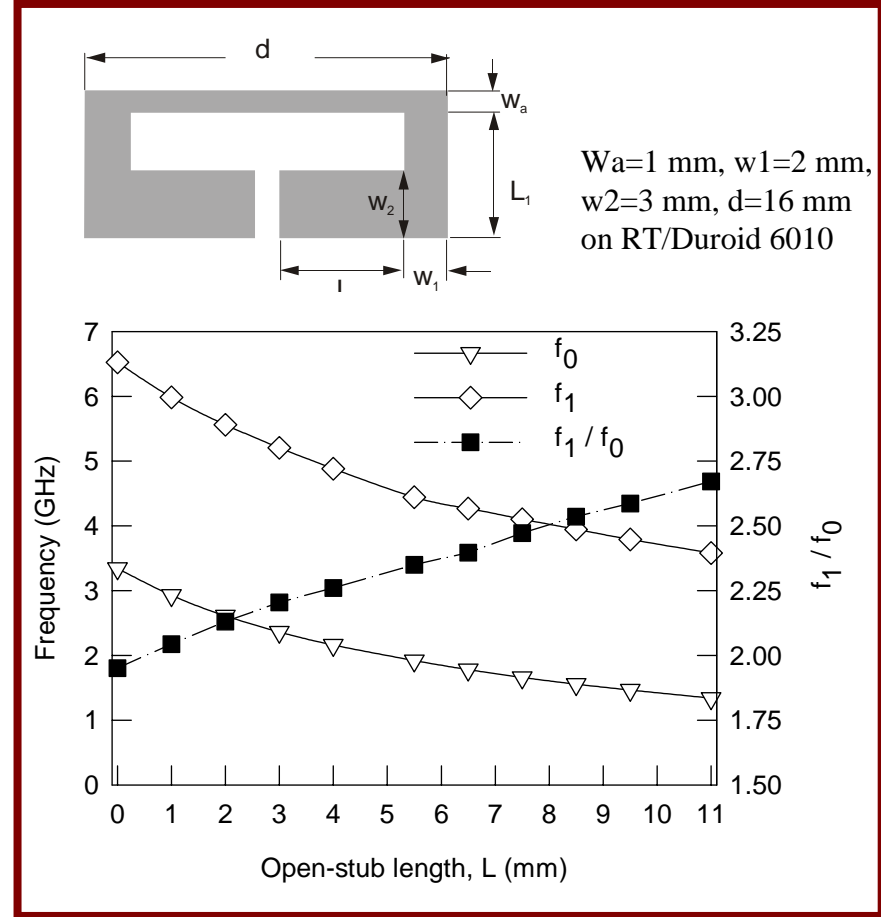
(c)

Design Examples- Slow-wave filters

Capacitively loaded line resonator



Microstrip slow wave resonator (I)



Design Examples- Slow-wave filters

Centre Frequency : 1335 MHz

3dB Bandwidth : 30 MHz

passband Loss : 3dB Max.

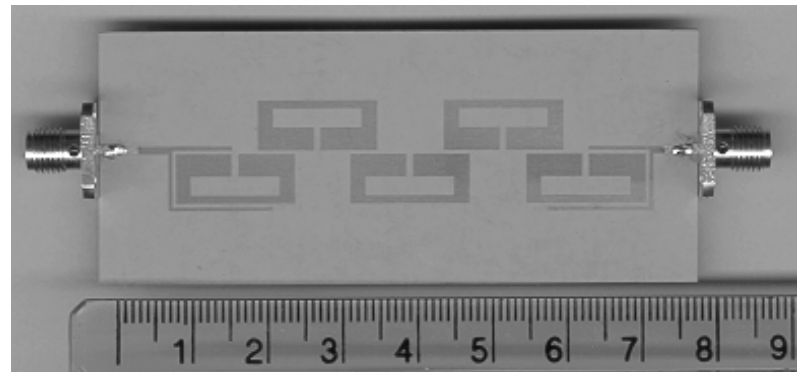
Min. stopband rejection :

D.C. to 1253 MHz 60dB

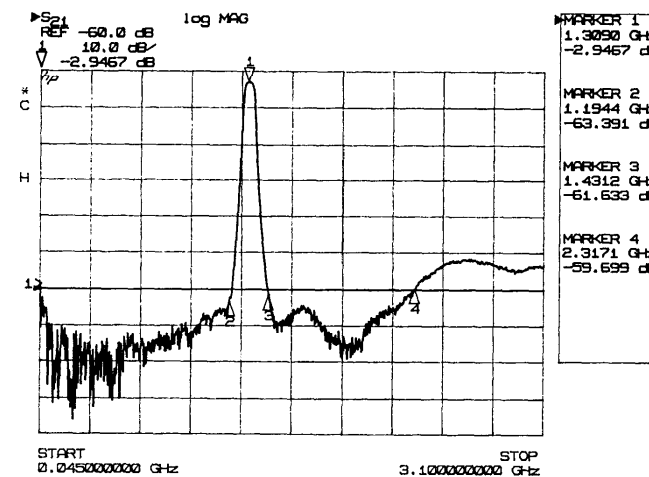
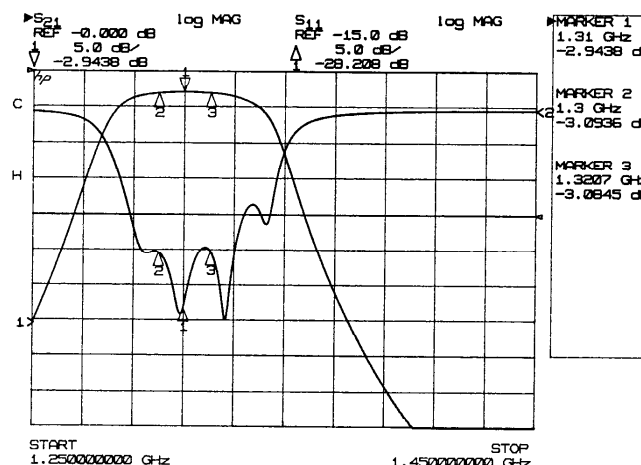
1457 to 2650 MHz 60dB

2650 to 3100 MHz 30dB

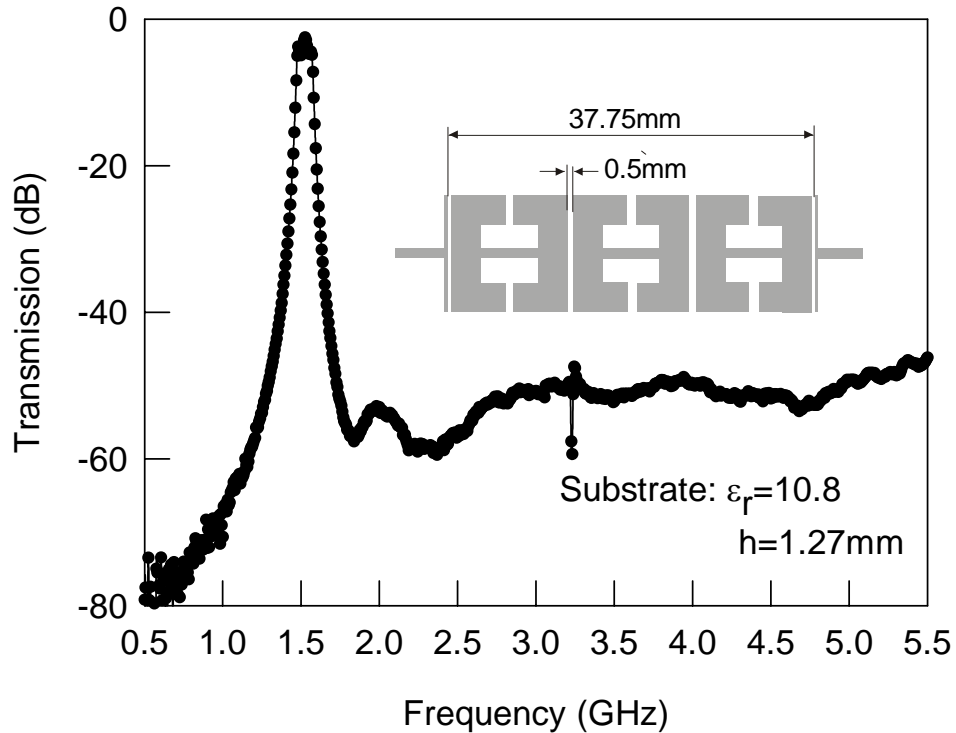
60dB Bandwidth : 200 MHz Max.



On RT/Duroid 6010 substrate

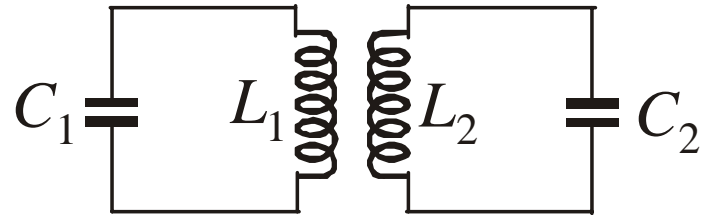
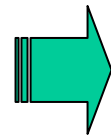
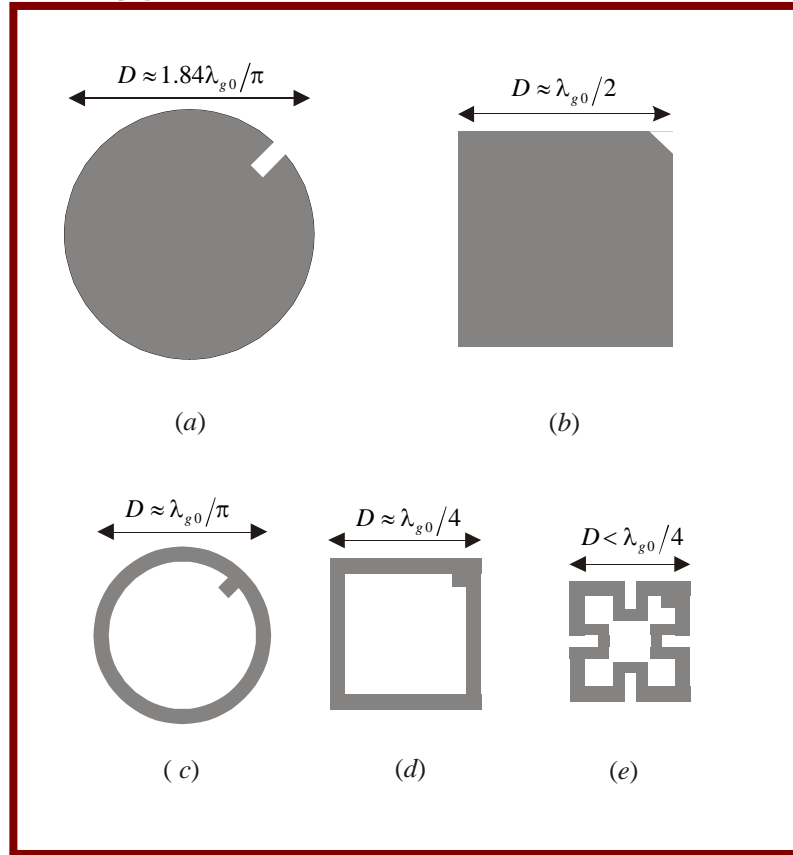


Design Examples- Slow-wave filters



Design Examples- Dual-mode filters

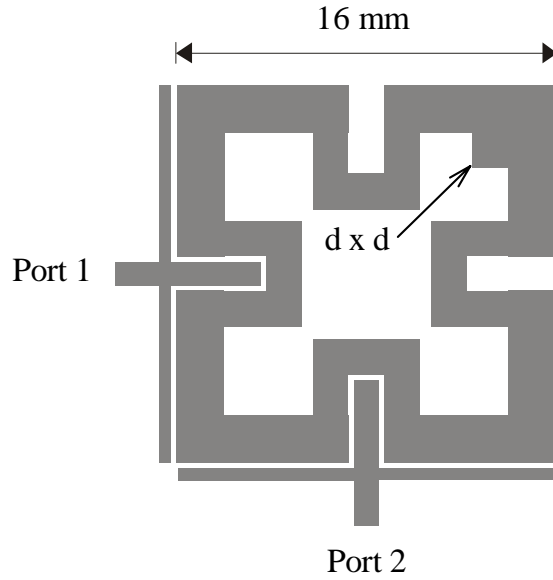
Type I dual-mode resonator



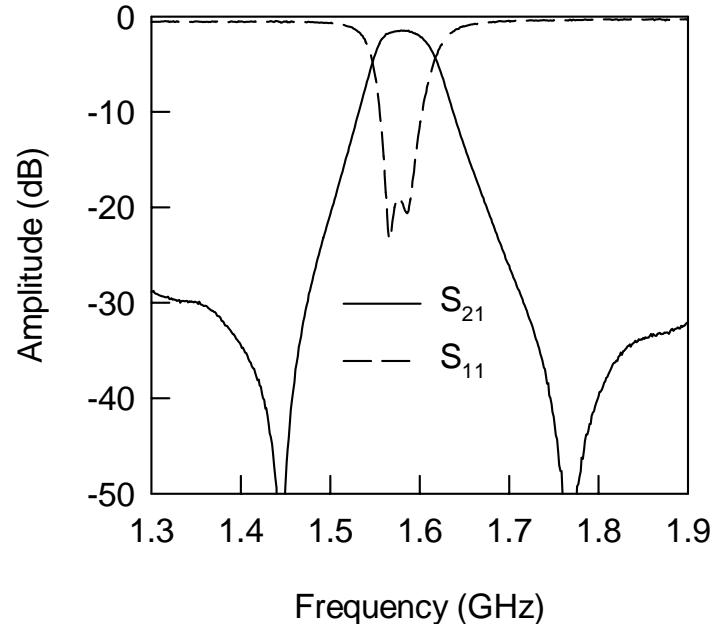
Mode 1

Mode 2

Design Examples- Dual-mode filters

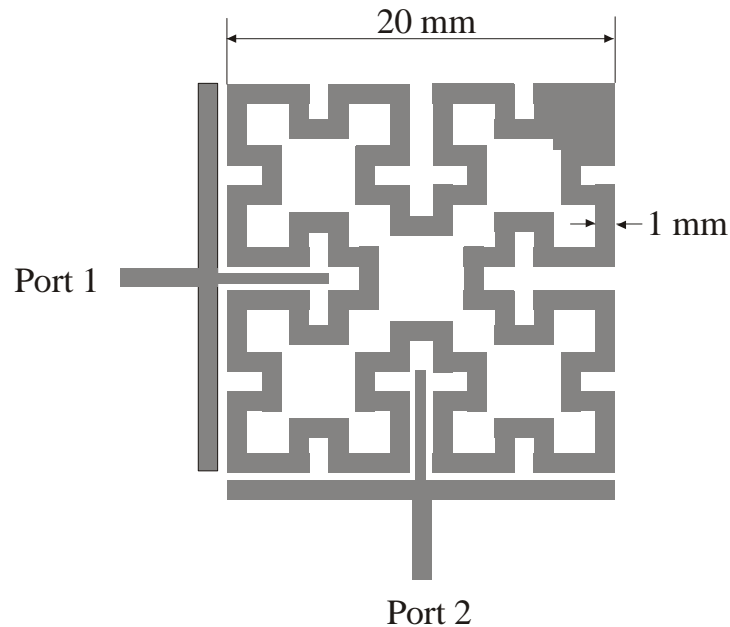


$d = 2 \text{ mm}$ on RT/Duroid
6010 substrate

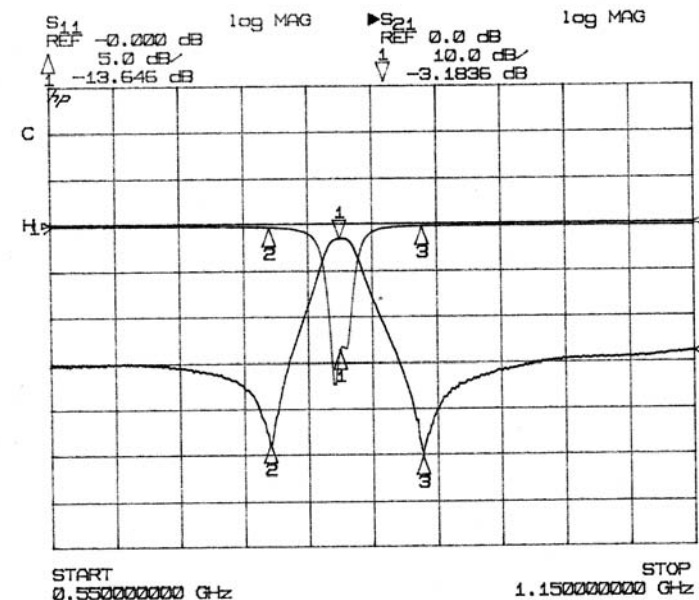


2.5% bandwidth at 1.58
GHz

Design Examples- Dual-mode filters



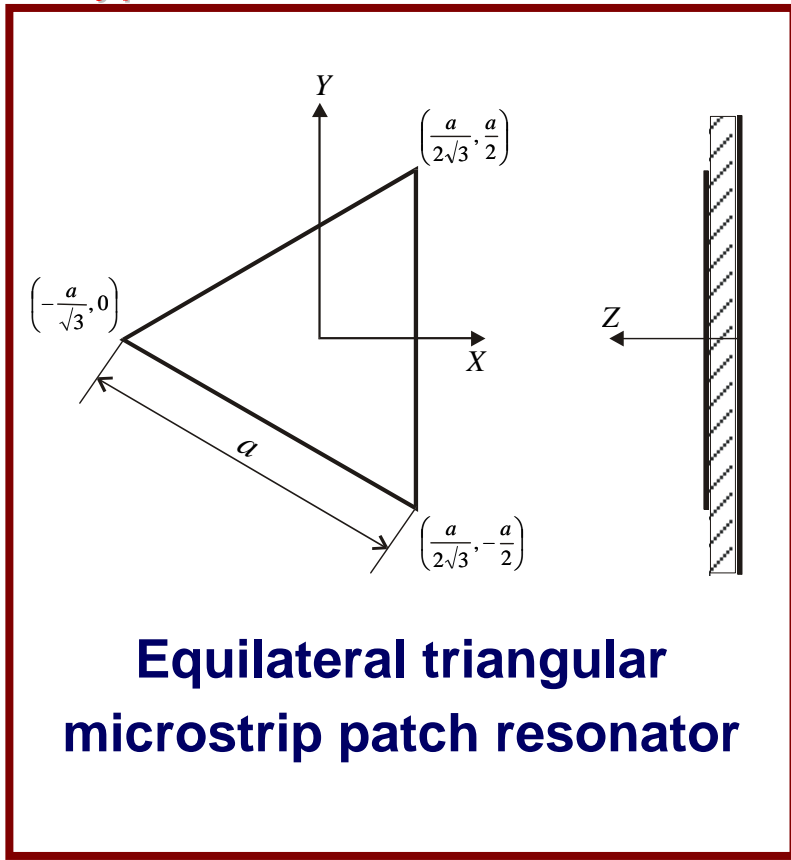
On RT/Duroid 6010 substrate



Centred at 820 MHz

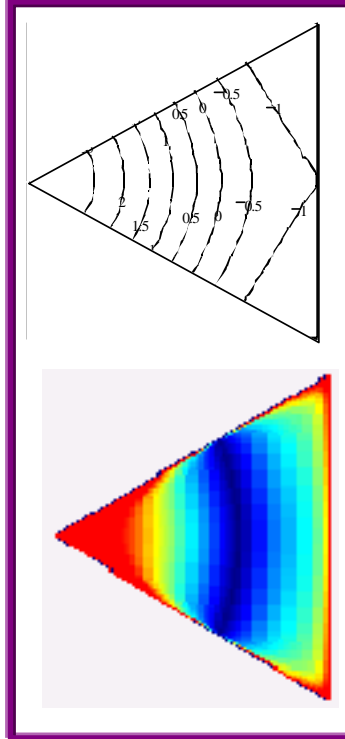
Design Examples- Dual-mode filters

Type II dual-mode resonator

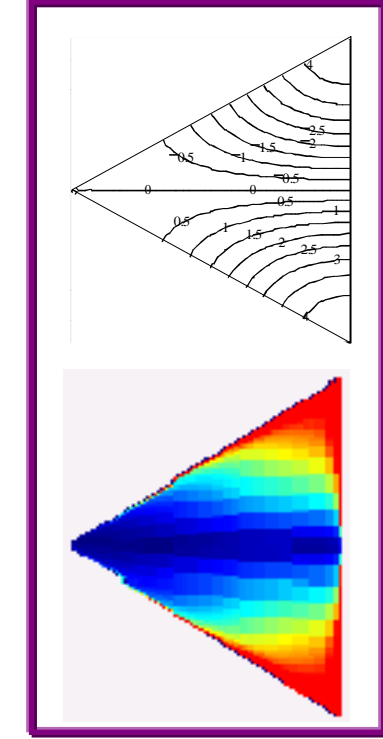


Electric Field Pattern

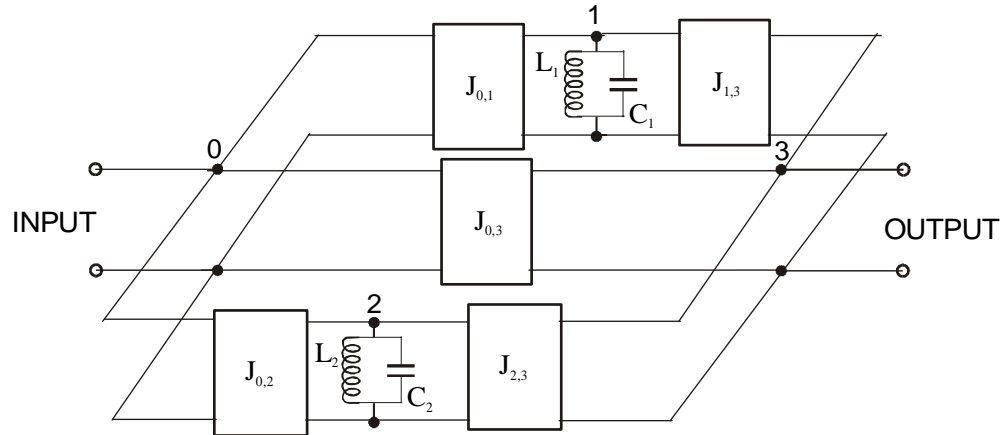
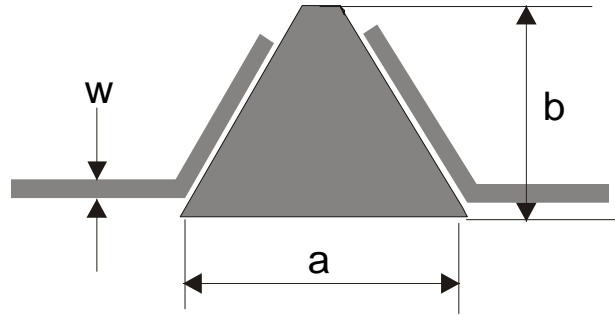
@ Mode 1



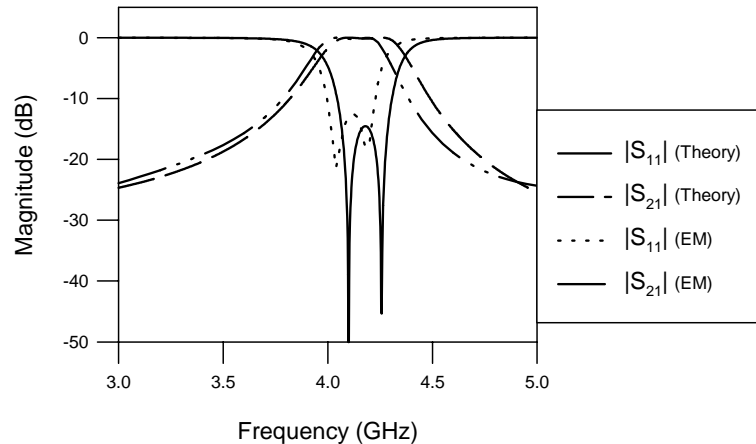
@ Mode 2



Design Examples- Dual-mode filters



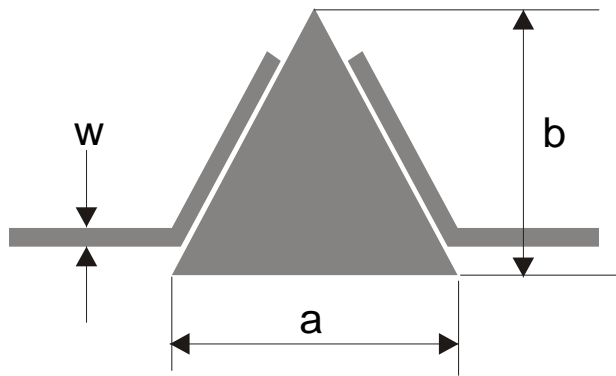
Circuit model (No coupling between the two modes)



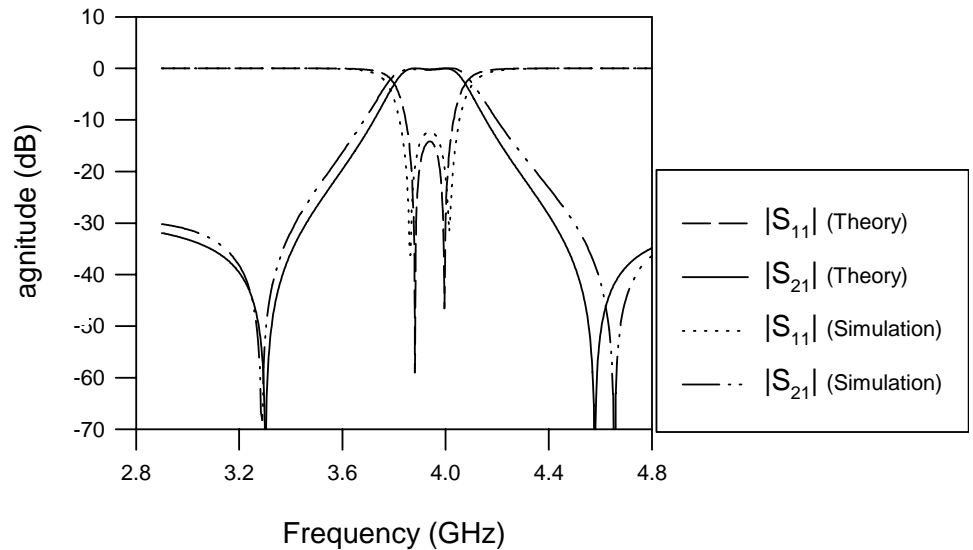
Frequency response

(a = 15 mm and b = 11.25 mm on a 1.27mm thick dielectric substrate with a relative dielectric constant of 10.8)

Design Examples- Dual-mode filters



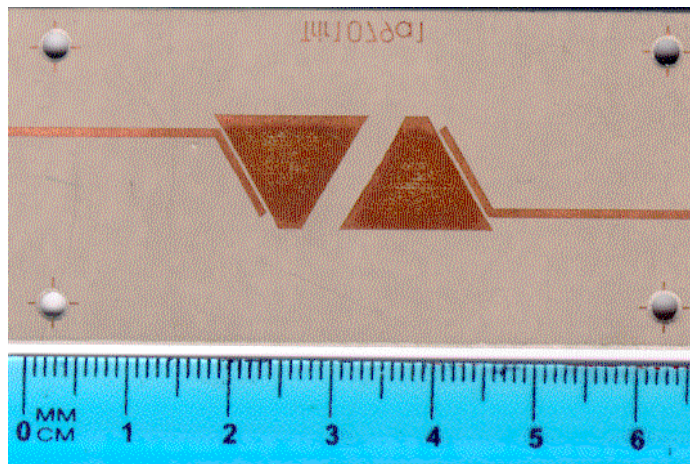
$a = 15 \text{ mm}$ and $b = 14 \text{ mm}$
on a 1.27mm thick dielectric
substrate with a relative
dielectric constant of 10.8



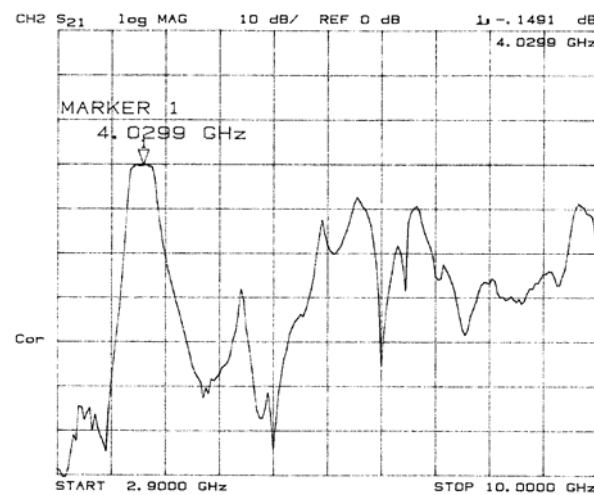
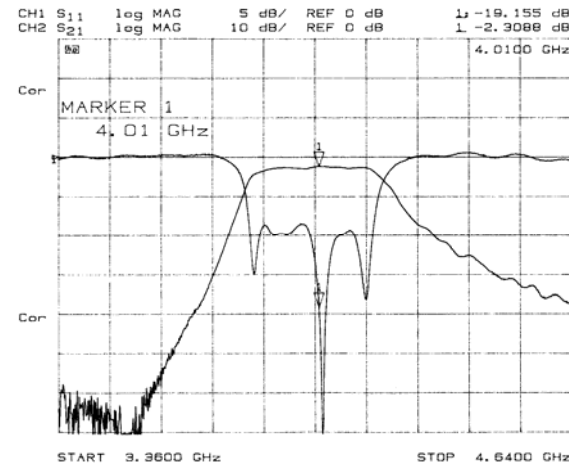
Frequency response

Design Examples- Dual-mode filters

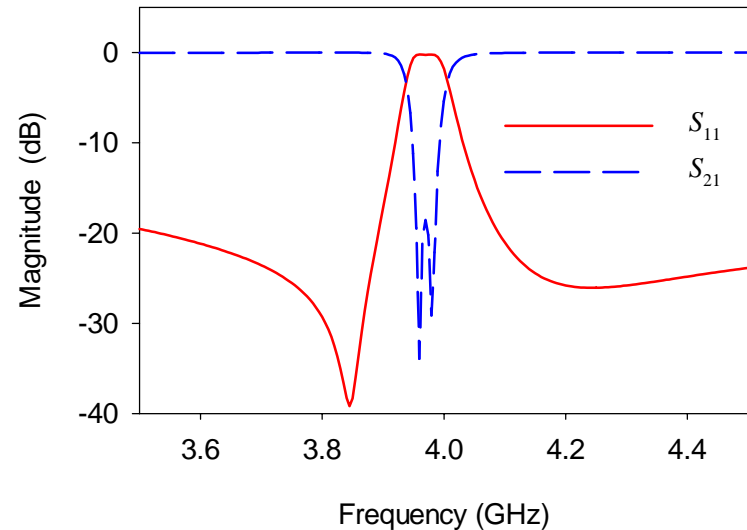
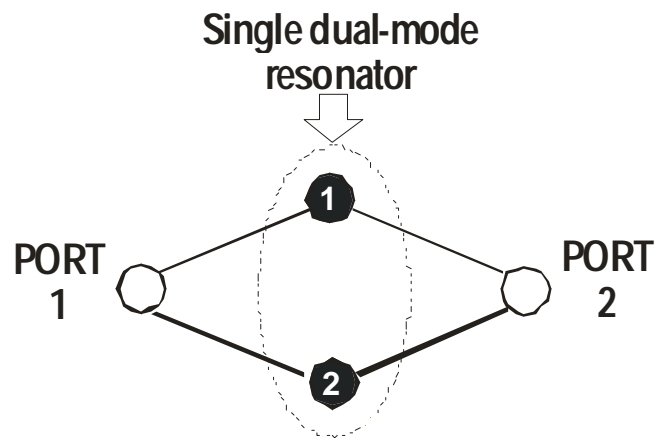
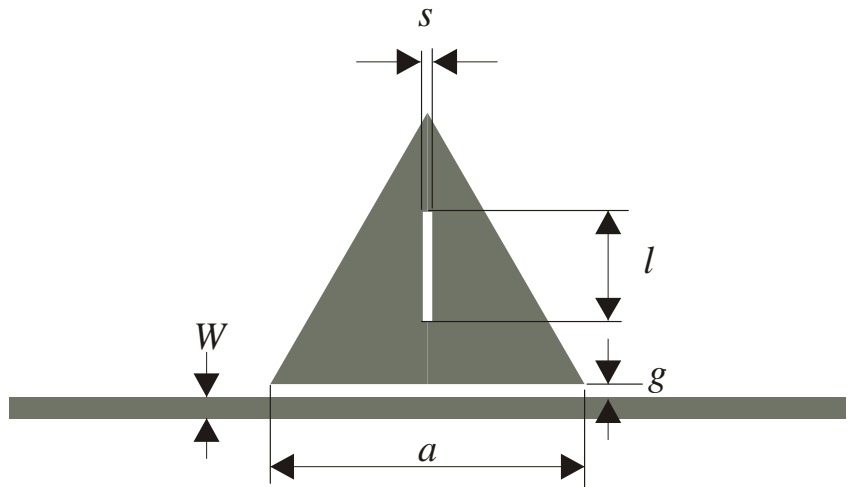
Four-pole dual-mode filters



On a substrate with a relative constant of 10.8 and a thickness of 1.27 mm

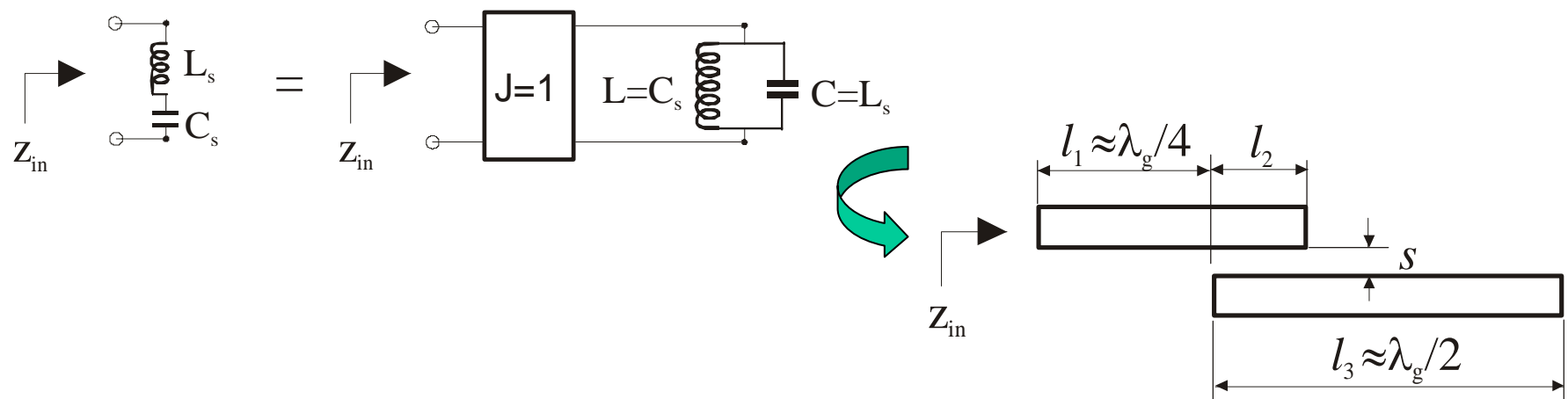
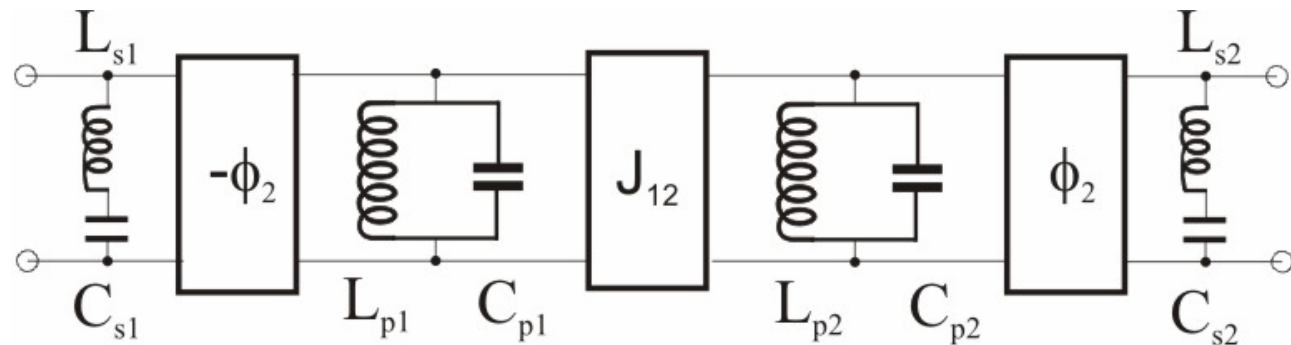


Design Examples- Dual-mode reject filters

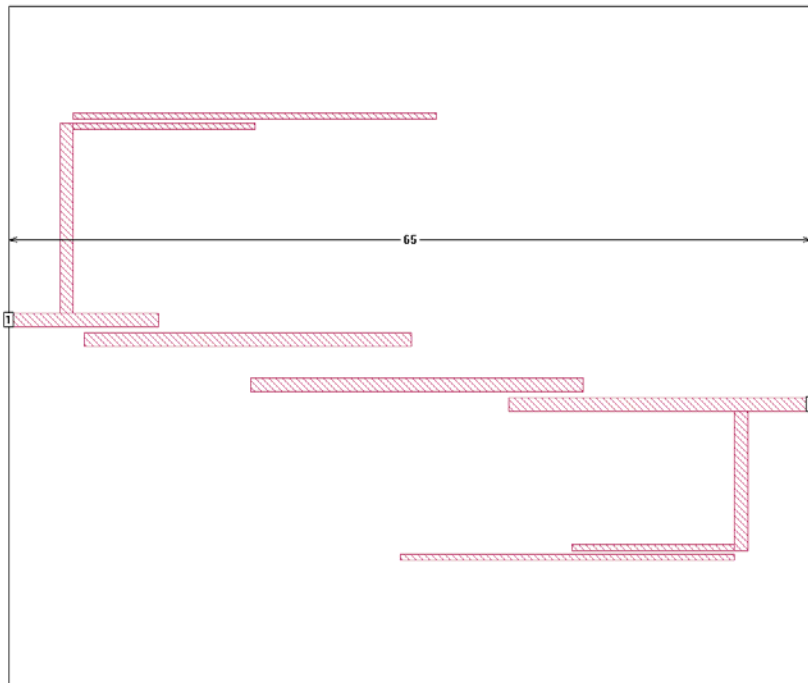


*The details to be presented in
another session (WE4C) at IMS2005*

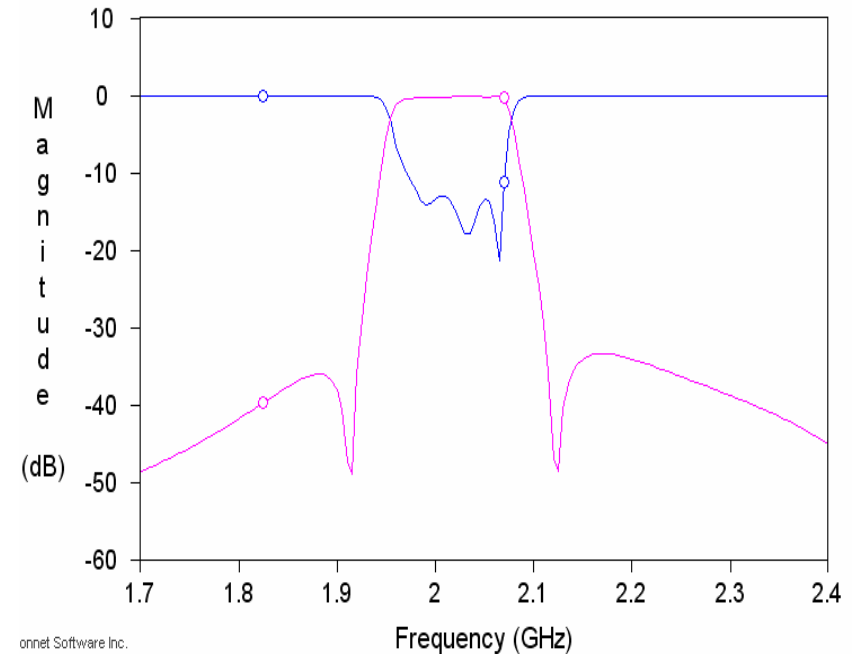
Design Examples- Extract-pole filters



Design Examples- Extract-pole filters

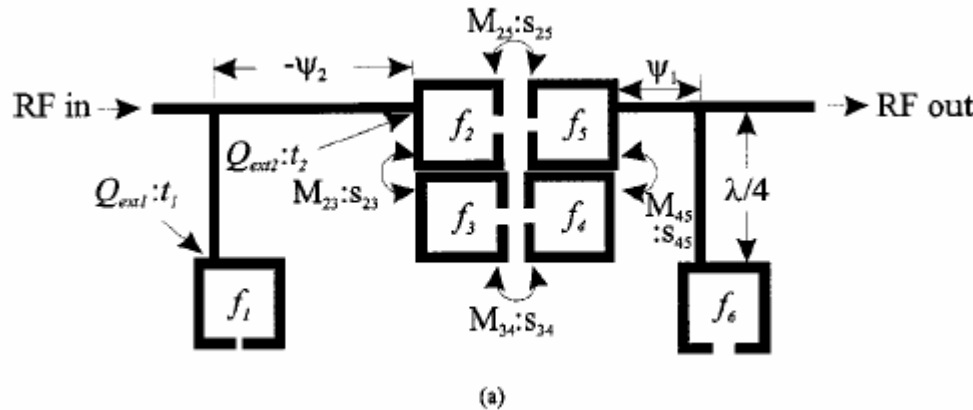


On RT/Duroid 6010 substrate

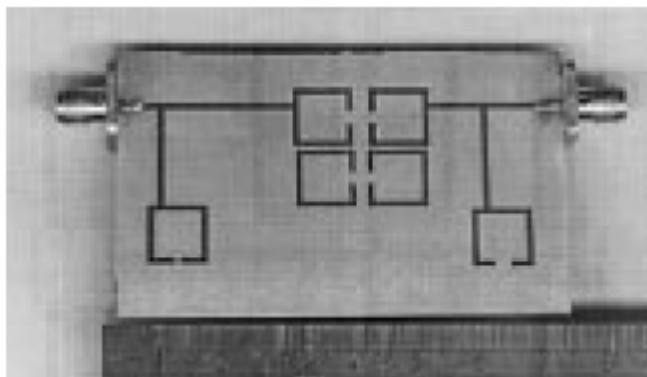


EM simulated performance

Design Examples- Extract-pole filters

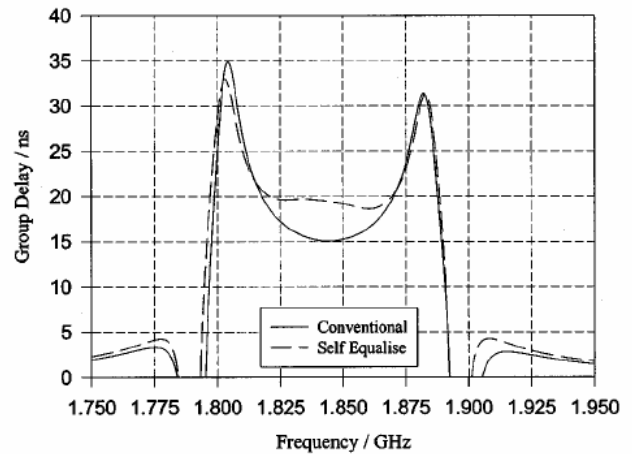
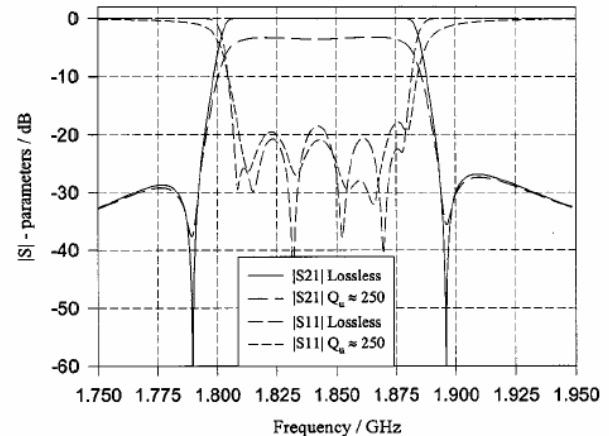


(a)

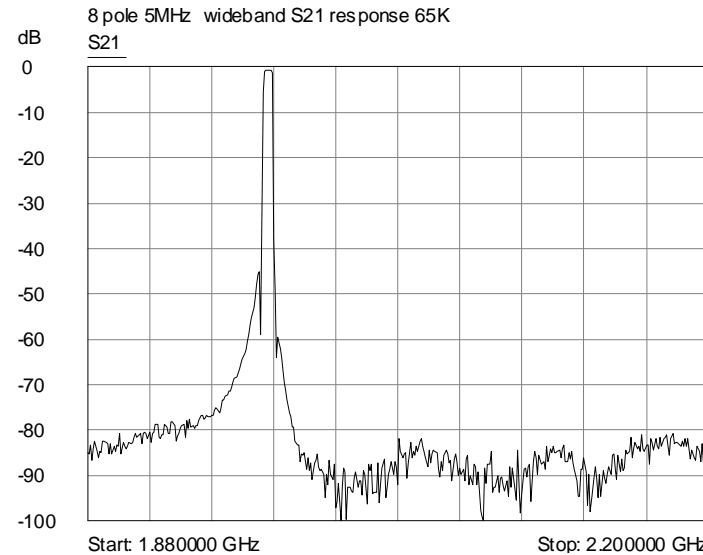
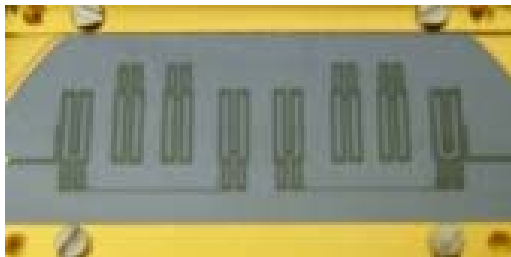
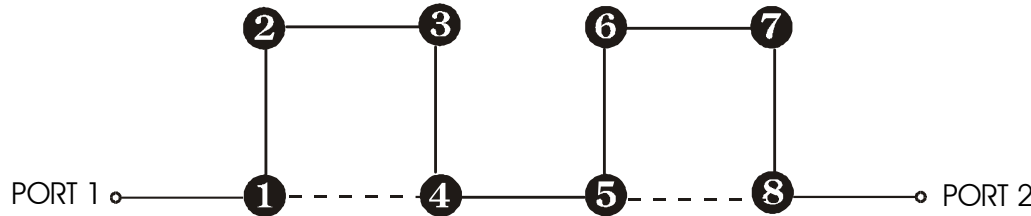


(b)

On RT/Duroid 6010 substrate

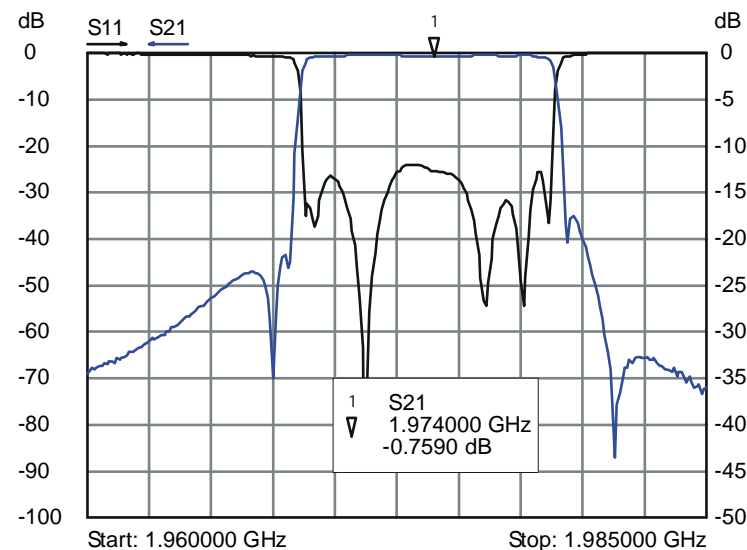
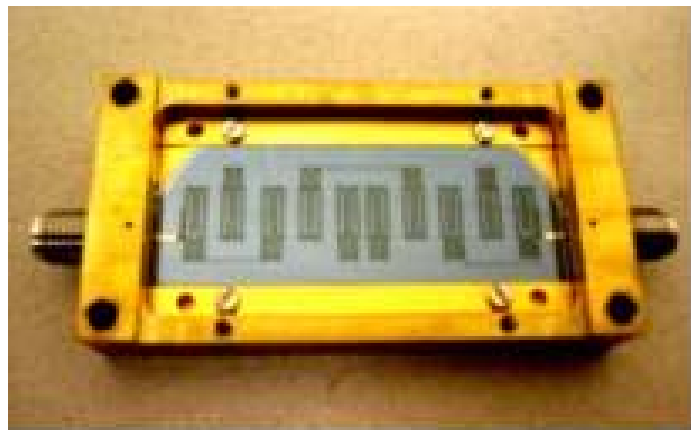
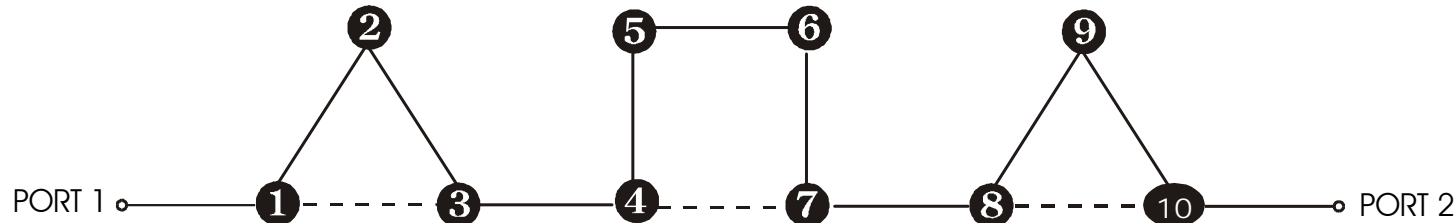


Design Examples- CQ filters



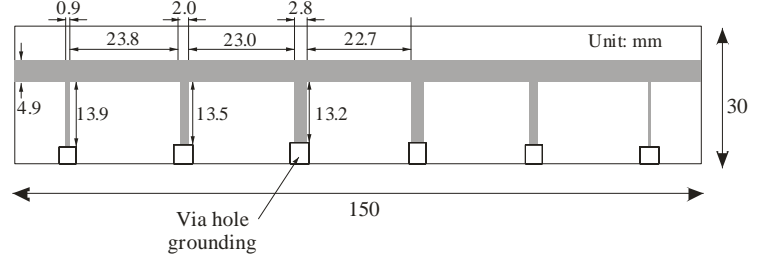
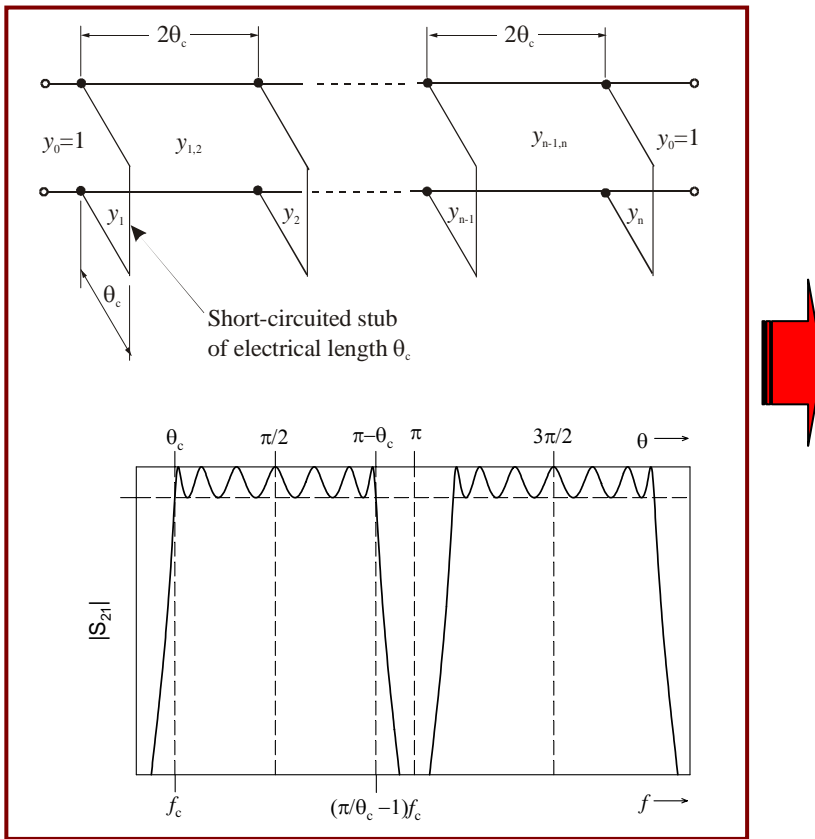
Another 18-pole filter of this type with group delay equalisation will be presented in TH1F session at IMS2005

Design Examples- CQT filters

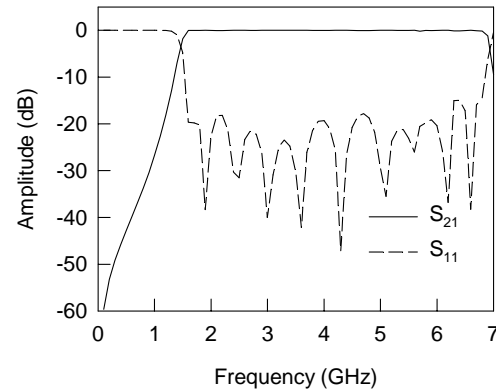


Design Examples- Wideband filters

Optimum stub bandpass or pseudo highpass



On substrate: $\epsilon_r = 2.2$, $h = 1.57$ mm



EM simulated performance

From: Jia-Sheng Hong and M.J.Lancaster, *Microstrip Filters for RF/Microwave Applications*,
John Wiley & Sons. Inc. New York, 2001

Summary

- ✓ Microstrip filter designs involve a number of considerations, including careful choice of topologies and substrates.
- ✓ Some design examples of new topologies with advanced filtering characteristics have been described, including –
 - Open-loop resonator filters
 - Multilayer filters
 - Slow-wave filters
 - Dual-mode filters
 - Extract pole, Trisection, CQ and CQT filters
 - Optimum wideband stub filters
- ✓ Driven by applications and emerging device technologies, many new and advanced microstrip filters have been developed and their designs are available in open literatures.

Design for Strip-Line Band-Pass Filters

J.K. Richardson

Mon, 2013-12-09 15:46

Strip widths and gap spacings are given in graphical form for band-pass filters using symmetrical strip lines.

June, 1968

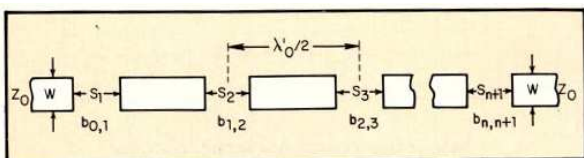
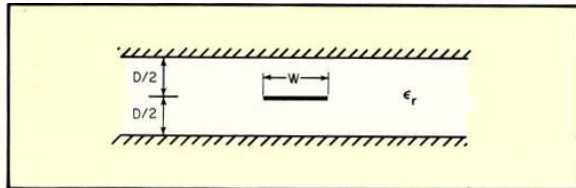


Fig. 1. Half wavelength end-coupled filter.



Strip-line band-pass filters can be

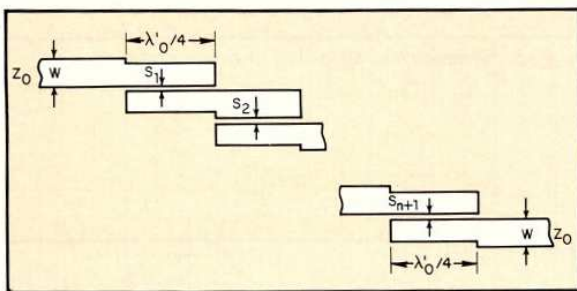


Fig. 2. Half wavelength side-coupled filter.

constructed either of half-wavelength strips capacitively coupled end-to-end as shown in Fig. 1, or using parallel coupling of the half-wavelength strips as shown in Fig. 2. The advantage of parallel or side coupling over end coupling is that the filter length is reduced by approximately half, and a symmetrical frequency-response curve is obtained. The advantage of end coupling over side coupling is that the width of the filter is much less and the widths of all resonator strips are the same. The gaps between adjacent strips may be greater for side coupling but not necessarily so. If the gaps

are greater, the gap tolerance for a given bandwidth is less; also, a broader bandwidth for a given tolerance can be achieved. Cohn has derived formulas which permit side-coupled filters to be accurately realized for bandwidths up to about 20% for a maximum flat response, and 30% for an equal ripple response. Other formulas are available to design end-coupled filters up to approximately the same bandwidths. The equations by Bradley and Cohn in the reference cited, are used here to construct graphs for determining band-pass filter dimensions as a function of normalized bandwidth. These graphs are for symmetrical strip line in the form shown in Fig. 3.

Design procedure

In designing these filters, first decide upon the required frequency response and the rate of attenuation beyond cut-off; then calculate the number of resonators required and the values of the equivalent low-pass prototype elements.

For the end-coupled filter, Fig. 1, it is necessary to determine the susceptance of the capacitative gaps between resonant elements; 1. as a function of strip-line geometry and permittivity of the dielectric between ground planes, and 2. as a function of the required frequency response and normalized bandwidth. Next, by eliminating the susceptance values from the two sets of equations, it is possible to obtain expressions which explicitly relate the ratios S/D and W/D (See Figs. 1-3) in terms of bandwidth and frequency response. The spacings between strips will differ from one resonator to another, being least for the first and last sections.

For the side-coupled filter, Fig. 2, a similar procedure is adopted, except that instead of susceptances it is

necessary to evaluate even- and odd-mode characteristic impedance of the coupled resonator strips. By eliminating the impedance values from two further sets of equations, the ratios S/D and W/D are obtained as a function of bandwidth and frequency response. As with end-coupled filters, the spacings between resonator strips will be smallest for the end sections, but the strip widths differ from one section to another. However, for bandwidths less than 1%, the value of W/D does not significantly differ from that obtained for the terminal strips.

A difference exists between the electrical length of the resonator strips, $\lambda'_0/2$, and the physical length for both filter types. Due to fringe fields, the electrical length is greater than the physical one, and a reduction in the latter is essential if the filter is to have an accurately positioned center frequency. Unfortunately, the formulas available to determine the necessary reduction in physical length are only approximate and have not been given in this article.

Design formulas for end-coupled filters

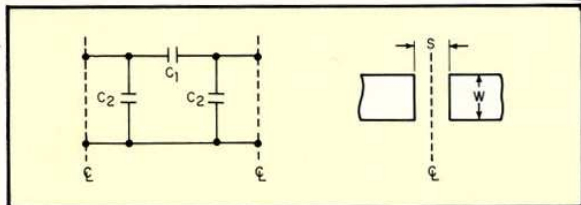


Fig. 4. Equivalent circuit of series gap in strip line (center line representation).

The equivalent circuit of a series gap in an end-coupled filter (center line representation) comprises a series capacitance, C_1 , and two shunt capacitances, C_2 (Fig. 4). Following are approximate analytical relations, which relate the normalized susceptances, b_1 and b_2 , associated with C_1 and

C_2 , to S , D and $\lambda'_0 (= \lambda_0 / \sqrt{\epsilon_r})$, the wavelength in the

dielectric medium:

$$(1) b_1 = \frac{D}{\lambda'_0} \ln \left\{ \cosh \left(\frac{\pi S}{2D} \right) \right\}$$

and

$$(2) b_2 = \frac{-2D}{\lambda'_0} \ln \left\{ \cosh \left(\frac{\pi S}{2D} \right) \right\}$$

Equations (1) and (2) are accurate for $W/D > 1.2$. For $S/D < 0.2$, $|b_1| > 10 |b_2|$, and for $S/D < 0.1$, $|b_1| > 75 |b_2|$. For the preliminary analysis of the end-coupled filter, S/D is assumed small enough that $|b_2|$ may be neglected.

The normalized susceptance of the $(i+1)$ -th gap of an end-coupled filter with n stages, $b_{i,i+1}$, may be expressed as follows:

$$(3) b_{i,i+1} = X_{i,i+1} / (1 - X_{i,i+1}^2)$$

where

$$(4) X_{0,1} = \sqrt{\frac{\pi W}{2g_0 g_1}} = X_{n,n+1}$$

and

$$(5) X_{i,i+1} = \frac{\pi W}{2\sqrt{g_i g_{i+1}}} [for (n-1) \geq i \geq 1]$$

where

$$(6) \frac{W}{2} = \frac{f_2 - f_1}{f_2 + f_1}$$

f_1 and f_2 are the lower and upper cut-off frequencies, respectively, and

$$(7) \frac{2}{f_0} = \frac{1}{f_1} + \frac{1}{f_2}$$

where f_0 is the center frequency of the filter and g is the normalized value of a low-pass prototype element.

Equation 1 can be rearranged into a form in which S/D is expressed as an explicit function of the series susceptance, b_1 . From (1),

$$(8) \frac{\pi S}{2D} = ar \coth \left\{ \exp \left(\frac{b_1 \lambda'_0}{D} \right) \right\}$$

and utilizing the identity

$$(9) ar \coth \theta = 1/2 \ln \left(\frac{\theta + I}{\theta - I} \right)$$

substituting for b_1 from Eq. 3, and omitting the i subscripts, Eq. 8 becomes

$$(10) \frac{S}{D} = \frac{I}{\pi} \ln \left\{ \coth \left(\frac{\lambda'_0}{2D} \cdot \frac{X}{I-X^2} \right) \right\}$$

The value of W/D can be found from the equation given by Cohn for the characteristic impedance, Z_o , of a symmetrical strip line (Fig. 3):

$$(11) Z_0 = \frac{94.15/\sqrt{\epsilon_r}}{\frac{W}{D} + \frac{\ln 4}{\pi}}$$

from which it follows:

$$(12) \frac{W}{D} = \frac{94.15}{\sqrt{\epsilon_r} Z_0} - 0.441$$

Design formulas for end-coupled filters (continued)

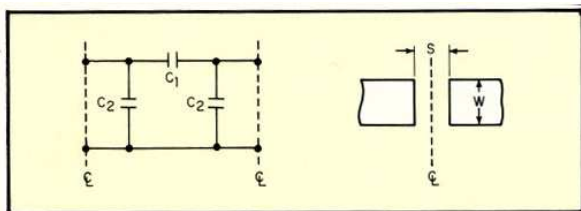


Fig. 4. Equivalent circuit of series gap in strip line (center line representation).

better than 1% providing $\lambda'_0/D \geq 6$.

Referring to the equivalent circuit of the series gap (Fig. 4), parameter X may be expressed as a function of both b_1 and b_2 :

$$(13) X = |\tan(\phi/2 + ar \tan b_2)|$$

where

$$(14) \phi = -ar \tan(2b_1 + b_2) - ar \tan b_2$$

Therefore,

$$(15) X = |\tan(\psi/2)|$$

where

$$(16) \psi = -ar \tan(2b_1 + b_2) + ar \tan b_2$$

From Eq. 3, $b = X/(1-X^2)$.

Substituting from Eq. 15 and providing

However, it has been assumed that b_2 is negligibly small in comparison with b_1 ; yet for $S/D \approx 0.46$, $|b_1| = |b_2|$, and for larger values of S/D , $|b_2|$ becomes increasingly greater than $|b_1|$.

The following analysis, which accounts for b_1 and b_2 , shows that Eq. 10 may be used for S/D as large as 0.6 accuracy of

$$(17) \quad +\pi/2 > \psi > -\pi/2, \\ b = |1/2 \tan \psi|$$

Substituting for b_1 and b_2 from Eqs. 1 and 2 into Eq. 16, and simplifying, ψ may be expressed directly in terms of S/D :

$$(18) \quad \begin{aligned} \psi &= \arctan \left[\frac{2D}{\lambda'_0} \ln \left\{ \sinh \left(\frac{\pi S}{2D} \right) \right\} \right] \\ &- \arctan \left[\frac{2D}{\lambda'_0} \ln \left\{ \cosh \left(\frac{\pi S}{2D} \right) \right\} \right] \end{aligned}$$

Utilizing equations 17 and 18, b can be obtained as a function of S/D and λ'_0/D and compared with b_1 obtained from Eq. 1 as a function of the same parameters. Graphs have been prepared with the ratios b/b_1 and b_1/b plotted in Figs. 5 and 6 as functions of λ'_0/D for $1.0 \geq S/D \geq 0.1$. Note that for $S/D < 0.5$, $b > b_1$ and for $S/D > 0.6$, $b_1 < b$.

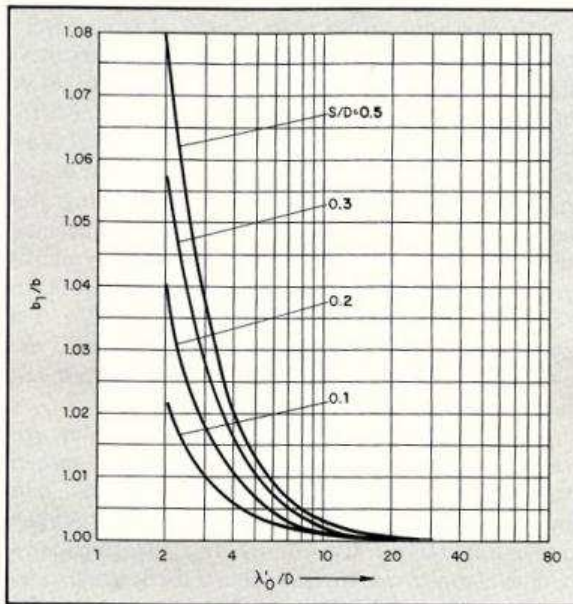


Fig. 5. Effective series susceptance ratio vs resonant wavelength/ground-plane spacing ratio.

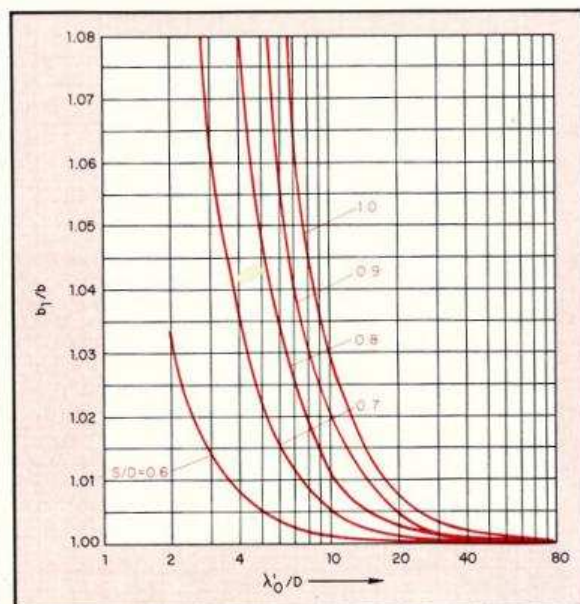


Fig. 6. Effective series susceptance ratio vs resonant wavelength/ground-plane spacing ratio.

The effect of the difference between b and b_1 on the value of strip spacing can be determined for relatively small differences by differentiating S with respect to b_1 in Eq. 10. Upon simplification, the following result is obtained:

$$(19) \quad \Delta S \approx \frac{D}{\pi} \cdot \frac{\Delta b}{b_1}$$

where $\Delta b = b - b_1$. For $b_1 \lambda'_0/D \leq 0.5$, Eq. 19 has a maximum error of approximately 4%. By considering Figs. 5

and 6, in conjunction with Eq. 19, the error in gap spacing obtained by using Eq. 10 (which does not account for the shunt susceptances, b_2) may be determined.

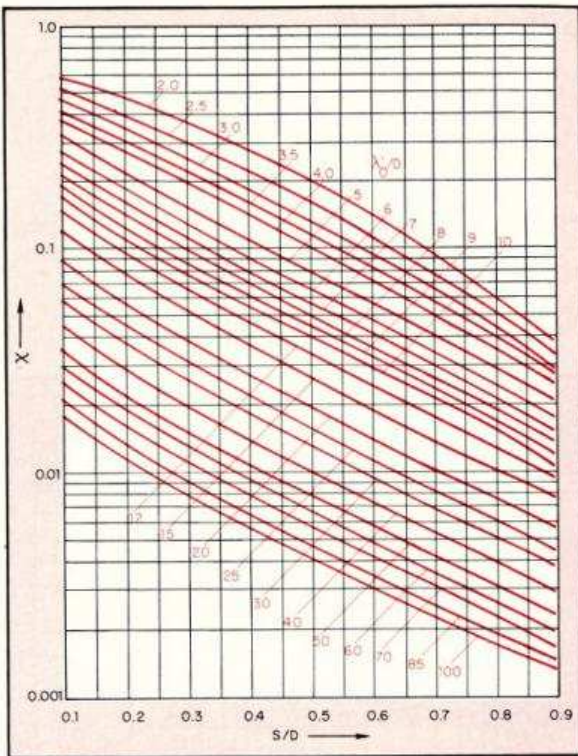


Fig. 7. Normalized bandwidth parameter vs strip spacing ratio for end-coupled filters.

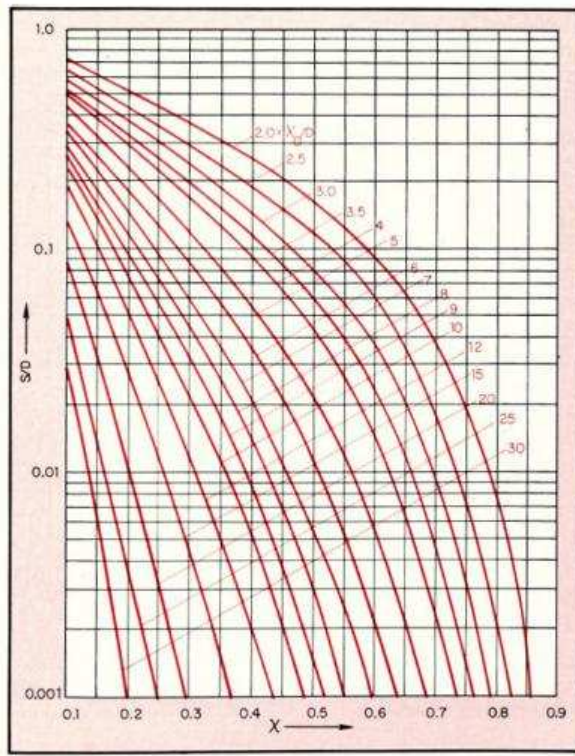


Fig. 8. Strip spacing ratio vs normalized bandwidth parameter for end-coupled filters.

Unfortunately, it is not possible to obtain an explicit expression for S/D in terms of X , accounting for b_1 and b_2 , because of the transcendental nature of Eq. 18. Nevertheless, utilizing Eqs. 12, 15 and 18, a set of graphs has been prepared giving X as a function of S/D for $100 \geq \lambda'_0/D \geq 2$ and $1 > X > 0$ (Figs. 7 and 8) and W/D as a function of ϵ_r for $Z_o = 50 \Omega$ (Fig. 9).

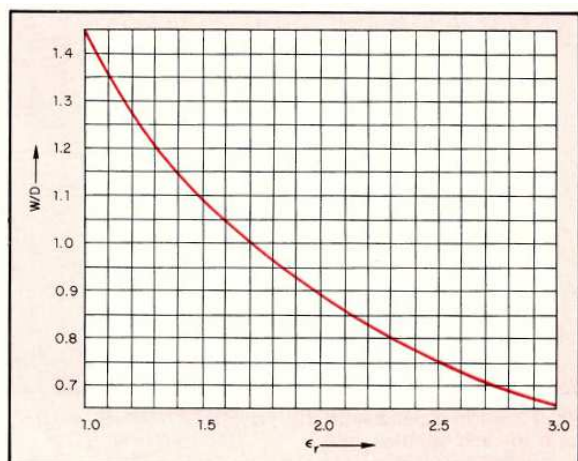


Fig. 9. Strip width ratio vs relative permittivity for end-coupled filters.

A lower limit of two for λ'_0/D is selected; because, if $\lambda'_0/2$ is less than D , higher modes will be generated, and loss by lateral radiation takes place. And from Eq. 1, b_1 is always positive if $S/D > 0$; while from Eq. 3, b is positive only if $X < 1$. Consequently, for Eqs. 1 and 3 to be consistent, $1 > X > 0$.

Design formulas for side-coupled filters

Design formulas for side-coupled filters

The equations which related the even and odd mode impedance, Z_{oe} and Z_{oo} , respectively, to W/D , S/D and ϵ_r

have been given by Cohn (Ref. 4) and may be expressed as follows:

$$(20) \quad Z_{oe} = \frac{94.15/\sqrt{\epsilon_r}}{\frac{W}{D} + \frac{\ln 2}{\pi} + \frac{I}{\pi} \ln \left\{ I + \tanh \left(\frac{\pi S}{2D} \right) \right\}}$$

and

$$(21) \quad Z_{oo} = \frac{94.15/\sqrt{\epsilon_r}}{\frac{W}{D} + \frac{\ln 2}{\pi} + \frac{I}{\pi} \ln \left\{ I + \coth \left(\frac{\pi S}{2D} \right) \right\}}$$

Equations 20 and 21 are accurate to approximately 1% for $W/D = 0.35$, and become increasingly accurate for $W/D > 0.35$, and become increasingly accurate for $W/D > 0.35$.

Rearranging (20) and (21), and subtracting from the other, the ratio W/D can be eliminated and the following expression obtained:

$$(22) \quad \frac{I}{\pi} \ln \left\{ \coth \left(\frac{\pi S}{2D} \right) \right\} = \frac{94.15}{\sqrt{\epsilon_r}} \left(\frac{I}{Z_{oo}} - \frac{I}{Z_{oe}} \right)$$

Solving for S/D using a similar procedure to that used to obtain Eq. 10 from Eq. 1, S/D can be expressed explicitly as a function of ϵ_r , Z_{oo} and Z_{oe} :

$$(23) \quad \frac{S}{D} = \frac{I}{\pi} \ln \left[\coth \left\{ \frac{94.15}{2\sqrt{\epsilon_r}} \left(\frac{I}{Z_{oo}} - \frac{I}{Z_{oe}} \right) \right\} \right]$$

A further set of equations relating Z_{oe} and Z_{oo} to the bandwidth parameter, X , have also been given by Cohn (Ref. 2), and may be expressed as follows:

$$(24) \quad \begin{aligned} (Z_{oe})_{i,i+1} &= Z_o [1 + X_{i,i+1} + X_{i,i+1}^2] \\ &= Z_o \cdot (1 + X_{i,i+1}^3) / (1 + X_{i,i+1}) \end{aligned}$$

and

$$(25) \quad \begin{aligned} (Z_{oo})_{i,i+1} &= Z_o [1 - X_{i,i+1} + X_{i,i+1}^2] \\ &= Z_o \cdot (1 + X_{i,i+1}^3) / (1 + X_{i,i+1}) \end{aligned}$$

where $n > i > o$ X is defined in Eqs. 4 and 5 with

$$(26) W = \frac{f_2 - f_1}{f_o}$$

$$(27) 2f_o = f_1 + f_2$$

Substituting for Z_{oe} and Z_{oo} from Eqs. 24 and 25 into Eq. 23, and eliminating the i subscripts and simplifying,

$$(28) \frac{S}{D} = \frac{I}{\pi} \ln \left[\coth \left\{ \frac{94.15}{\sqrt{\epsilon_r} Z_o} \cdot \frac{X(1-X^2)}{(1-X^6)} \right\} \right]$$

As the maximum permissible value of X is 0.5 (Ref. 3), the term X^6 can usually be neglected.

Substituting for S/D from Eq. 28 into Eq. 20, and for Z_{oe} from Eq. 24, an explicit expression for W/D is obtained:

$$(29) \frac{W}{D} = \frac{94.15}{\sqrt{\epsilon_r} Z_o} / (1+X+X^2) \\ - \frac{I}{\pi} \ln \{ 2(I+I/\psi) \}$$

where

$$(30) \ln \psi = \frac{94.15}{\sqrt{\epsilon_r} Z_o} \cdot \frac{2(1-X^2)}{(1-X^6)}$$

For very narrow bandwidths, corresponding to $X < 0.01$, W/D can be taken as equal to that of the terminating strips, as given by Eq. 15 or graphically in Fig. 9. Moreover, both the X^2 and X^6 terms can be neglected in Eq. 28 for narrow bandwidths.

Hence, ratios S/D and W/D can be found for side-coupled filters as a function of the parameters X , ϵ_r , and Z_o . Additional graphs have been prepared (Figs. 10-12) in which S/D and W/D are plotted as functions of X for values of ϵ_r and for $Z_o = 50\Omega$.

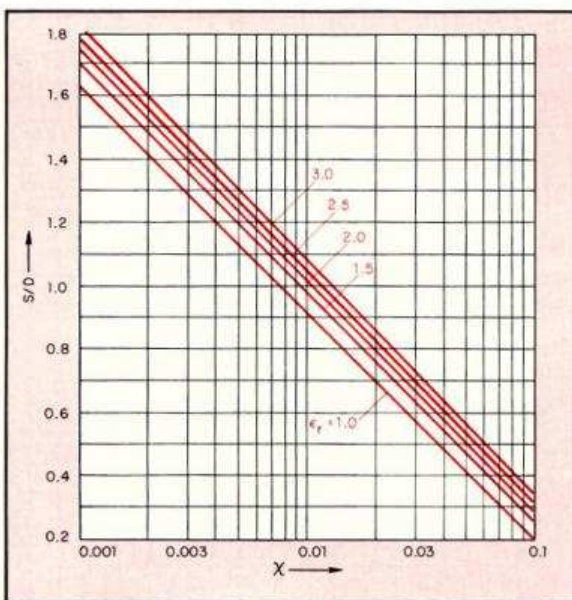


Fig. 10. Strip spacing ratio vs normalized bandwidth for side-coupled filters.

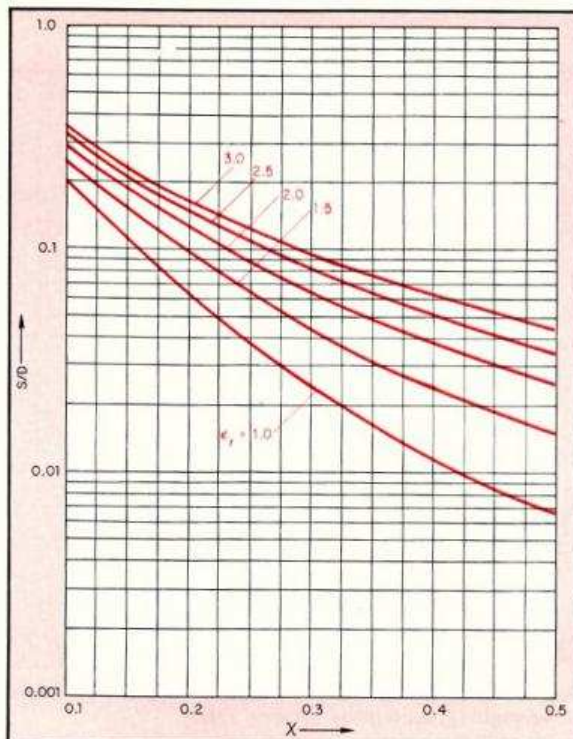


Fig. 11. Strip spacing ratio vs normalized bandwidth parameter for side-coupled filters.

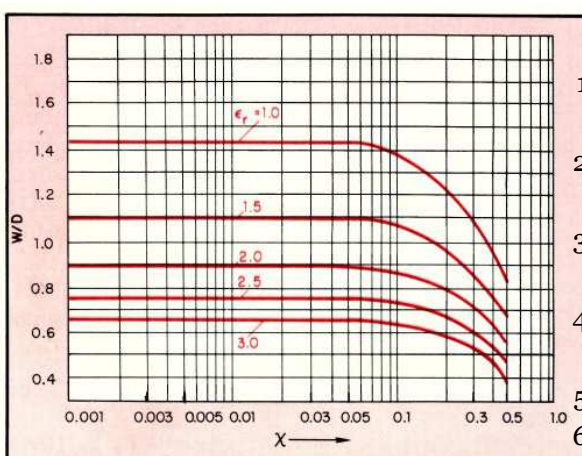


Fig. 12. Strip width ratio vs normalized bandwidth parameter for side-coupled filters.

References

1. E.G. Bradley, "Design and Development of Strip Line Filters," *IRE Trans. MTT*, (April, 1956).
2. S.B. Cohn, "Parallel Coupled Strip Line Resonator Filters," *L'Onde* [France], (October, 1957).
3. J.K. Richardson, "Gap Spacing for End Coupled and Side Coupled Band Bass Filters," *IEEE Trans. MTT*. (June, 1967).
4. S.B. Cohn, "Shielded Coupled Strip Transmission Line," *IRE Trans. MTT*, (October, 1957).
5. E.G. Bradley, *op.cit.*
6. S.B. Cohn, "Direct Coupled Resonator Filters," *Proc. IRE*, (February, 1957).
7. H.M. Altschuler and A.A. Oliner, "Discontinuities in the Centre Conductor of Symmetric Strip Transmission Line," *IRE Trans. MTT*, (May, 1960).
8. G.L. Matthew, L. Young and E.M.I. Jones, *Microwave Filters, Impedance-Matching Networks, and Coupling Structures*, (McGraw-Hill Book Co., 1964).
9. E. Rubins, W. Fromm and H. Keen, "New Techniques for High Q Microwave Components," *IRE Convention Record, Part 8*, (1954).

A New Filter Synthesis Technique— The Hourglass

BYRON J. BENNETT, MEMBER, IEEE

Abstract — This new synthesis procedure produces in its own right filters which have better passband and stopband characteristics than conventional maximally-flat filters. In addition its use throughout filter design unifies, simplifies, and systematizes synthesis procedures. This carries through even to the design of equiripple constant time-delay networks with equiripple amplitude characteristics.

I. INTRODUCTION

FIG. 2 shows the response of an $n = 5$ maximally-flat filter with specified transmission zeros at $\omega = 1.1, 1.4$, and ∞ . Fig. 3 shows the response of the hourglass filter for the same set of specifications. The improvement in the passband achieved by the hourglass over the maximally-flat filter is due to the distribution of reflection coefficient zeros throughout the passband. The improvement in the stopband is because the natural modes of the hourglass are nearer the passband and further from the stopband than the corresponding maximally-flat natural modes.

The conditions just described are the result of reciprocal location of the reflection coefficient zeros with respect to the transmission zeros. This technique yields filters comparable to the classical constant- k filters with m -derived end sections. As opposed to the classical filters, the specified magnitude at the band edge may be realized exactly.

The hourglass allows for the design of an entirely new set of filters. At certain points the designs converge to known designs. For instance the Butterworth filter is the special case of the hourglass with all specified transmission zeros at infinite frequency. At least one constant- k m -derived combination may be realized by the hourglass algorithm [5]. Also the inverse Chebyshev filter based on the hourglass has an equiripple character over a part of the passband and thus is itself an elliptic filter.

Although the hourglass technique leads to very important designs in its own right, it also provides a direct and easy design access to traditional equiripple designs. Simple transformation of the zeros of hourglass designs leads directly to standard Chebyshev, Chebyshev rational fraction, and elliptic (Cauer) designs. In particular the standard Chebyshev filter with all transmission zeros at infinite frequency may be obtained without a complicated root-finding technique. The method is less complicated than

Manuscript received March 16, 1987; revised December 8, 1987. This paper was recommended by Associate Editor E. Sanchez-Sinencio.

The author is with the Department of Electrical Engineering, Montana State University, Bozeman, MT 59717-0007.

IEEE Log Number 8823903.

that proposed by Guillemin [8]. The hourglass route to Chebyshev rational fraction filters offers an alternative to that proposed by Guillemin [8] and Bennett [9].

The methods of phase equalization or constant time-delay are seldom discussed in the textbooks. When they are, discussion is generally restricted to phase equalization using all-pass networks after a given design for prescribed amplitude. Use of the hourglass makes it possible to obtain a polynomial with a prescribed equiripple time-delay tolerance. This involves an iterative procedure as usual but it is very different and more direct than that previously proposed [6]. Finally, with this polynomial as a denominator, a numerator polynomial can be found such that the resulting transfer function has an equiripple passband characteristic. Equiripple time-delay and equiripple amplitude may be obtained in different frequency ranges.

The rationale for placing reflection coefficient zeros in positions reciprocal to specified transmission zeros follows. The substantive discussion will relate initially to low-pass filters with later extension to other frequency ranges.

II. THE HOURGLASS

The z -plane will be reserved for the low-pass hourglass.

Approximation in filter design is often begun with the assumption of a rational fraction $K(z)$ whose zeros are the zeros of the reflection coefficient at the load under the best possible conditions of match and whose poles are the transmission zeros of the transfer function $G(z)$, where $z = x + jy$. Filter networks have traditionally been designed with a rational fraction $K(z)$ as a starting point [1]:

$$K(z) = (\epsilon_z)[F(z)/P(z)]. \quad (1)$$

The functions $F(z)$ and $P(z)$ are polynomials with real coefficients.

In standard fashion this $K(z)$ is related to $H(z)$ and $G(z)$ as follows:

$$\begin{aligned} H(z)H(-z) &= K(z)K(-z) + 1 \\ &= D(z)D(-z)/P(z)P(-z) \end{aligned} \quad (2)$$

and

$$\begin{aligned} G(z)G(-z) &= 1/H(z)H(-z) \\ &= P(z)P(-z)/D(z)D(-z) \\ &= N(z)N(-z)/D(z)D(-z). \end{aligned} \quad (3)$$

When $F(z)$ and $P(z)$ are related by the process to be described and when $\epsilon_z = 1$, the absolute values of the

coefficients of $D(z)D(-z)$ are always symmetrical about the center of the polynomial and are often larger at each end. Hence the name—hourglass.

The zeros of transmission determine $P(z)$:

$$P(z) = a_n \prod_{i=1}^n (z - z_i) = \sum_{i=0}^n a_i z^i. \quad (4)$$

For the hourglass approximation, $\epsilon_z = 1$ and

$$F(z) = z^n P(1/z) = \sum_{i=0}^n a_{n-i} z^i. \quad (5)$$

Note that $F(z)$ may be obtained from the reciprocals of the zeros of $P(z)$ or by reversing the order of coefficients of $P(z)$.

With $P(z)$ and $F(z)$ thus related, the zeros of $H(z)$ determined from (2) are on the unit circle provided $|z_i| > 1$. Proof of this is contained in [2] and [5]. Another proof follows:

Consider the following for r real zeros and q pairs of complex zeros of $P(z)$:

$$\begin{aligned} H(z)H(-z) &= [F(z)F(-z)/P(z)P(-z)] + 1 \\ &= \frac{(-1)^r \prod_{i=1}^{q+r} (\alpha_i z^2 + 1) \prod_{i=1}^q (\bar{\alpha}_i z^2 + 1)}{\prod_{i=1}^{q+r} (z^2 + \alpha_i) \prod_{i=1}^q (z^2 + \bar{\alpha}_i)} + 1. \end{aligned} \quad (6)$$

For this formulation the constant α_i may be real, complex, or infinite. If $|\alpha_i| > 1$ and the following transformation is implemented

$$z^2 = (s+1)/(s-1) \quad (7)$$

then

$$H(s)H(-s) = \frac{(-1)^r \prod_{i=1}^{q+r} [(\alpha_i + 1)s + (\alpha_i - 1)] \prod_{i=1}^q [(\bar{\alpha}_i + 1)s + (\bar{\alpha}_i - 1)]}{\prod_{i=1}^{q+r} [(\alpha_i + 1)s - (\alpha_i - 1)] \prod_{i=1}^q [(\bar{\alpha}_i + 1)s - (\bar{\alpha}_i - 1)]} + 1 \quad (8)$$

and the real part of $[(\alpha_i - 1)/(\alpha_i + 1)]$ is greater than zero. Thus for this condition the zeros of the numerator of $H(-s)H(-s)$ are always on the s -plane j -axis. Since (7) transforms the s -plane j -axis to the z -plane unit circle, the zeros of $H(z)H(-z)$ are on the unit circle. The transmission zeros determine the location of the $H(z)$ zeros on the unit circle.

If $F(z)$ is of higher order than $P(z)$, $|K(jy)|$ approximates zero over a large percentage of the range of frequencies $-1 < y < 1$. At $x = 0$ and $y = 1$, $|K(jy)| = \epsilon_z$. If $F(z)$ is of the same order as $P(z)$, $|K(jy)|$ approximates the nonzero value $\epsilon_z a_n / a_0$ and again $|K(jy)|$ is equal to ϵ_z when $y = 1$.

The low-pass hourglass approximation will be defined only for $|z_i| > 1$. Thus $|\alpha_i| > 1$. However this condition is not a strict requirement for all possible low-pass z -plane designs. If zeros of transmission occur outside the passband but inside the unit circle, the resulting zeros of $H(z)$

may not lie on the unit circle although good filters may still be obtained. However if transformation is to be used to obtain Chebyshev characteristics, then the condition $|z_i| > 1$ should be observed.

The location of the hourglass zeros of $F(z)$ may be modified so that the common geometric mean of reflection coefficient zeros and transmission zeros, appropriately paired, is other than 1. The zero locations may be multiplied by k such that

$$0 \leq k < y_0$$

where y_0 is the lowest transmission zero frequency. With k chosen in this range, no reflection coefficient zeros will be outside the passband. If k is chosen to be just under y_0 , the stopband rejection will be extremely high but the passband ripple will also be extremely high. If $k = 1$, this is, of course the basic hourglass condition. If $k = 0$, this is the maximally-flat condition. After k is chosen then $|F(z)/P(z)|$ must be multiplied by a constant so that its value for $z = j1$ is 1. The band edge is thus maintained at $\omega = 1$ and ϵ_z may be chosen for the prescribed band edge amplitude. In example 1 the effect of using $k > 1$ is demonstrated.

If any one reflection coefficient zero is moved from its basic hourglass position to a higher passband frequency, the stopband rejection will be improved at the expense of a less flat passband characteristic.

The discussions to follow may be aided by reference to Fig. 1. The horizontal arrows in the diagram indicate transformation of p -plane zeros to z -plane zeros and z -plane zeros to p -plane zeros. In the text a move from $N(p)$ to $N(z)$ means that the zeros of $N(p)$ are trans-

formed to zeros of $N(z)$ using (15) and $N(z)$ is obtained from them. A move from $D(z)$ to $D(p)$ means that the zeros of $D(z)$ are transformed to zeros of $D(p)$ using (13) and $D(p)$ is obtained from them. The vertical arrow marked hourglass indicates use of the hourglass algorithm to obtain $D(z)$ from $N(z)$. The dotted vertical arrow indicates two different operations which will be described in the text.

For the basic hourglass design the movement is only from $N(z)$ to $D(z)$. An hourglass design is described in Example 1 and compared to the maximally-flat design for the same transmission zeros.

III. OTHER FILTER DESIGNS—USE OF THE HOURGLASS

A. Chebyshev Rational Fraction Filters

The p -plane ($p = \sigma + j\omega$) will be reserved for filters other than the hourglass.

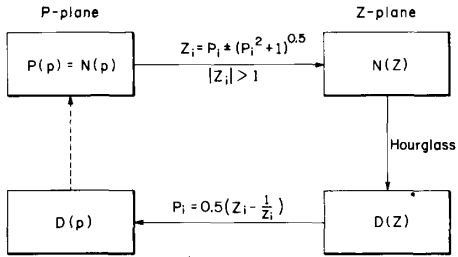


Fig. 1. Diagram of hourglass operation.

In this paper the Chebyshev rational fraction filter will be defined as one which has arbitrarily specified transmission zeros. As such it includes the Chebyshev filter ($N(p) = 1$) but does not include the elliptic (or Cauer) filter.

One purpose of this paper is to present a design alternative to that proposed by Guillemin [8] and Bennett [9] for this type of filter.

In Fig. 1 the movement is from $N(p)$ to $N(z)$ to $D(z)$ to $D(p)$. In the move from $N(z)$ to $D(z)$ an ϵ_z corresponding to the decibel (dB) tolerance required is used. For a given decibel tolerance:

$$\begin{aligned}\epsilon_p &= (10^{0.1dB} - 1)^{0.5} \\ \epsilon_z &= -(1/\epsilon_p) + [(1/\epsilon_p)^2 + 1]^{0.5}.\end{aligned}\quad (9)$$

Proof of the validity of this method follows:

In the useful range

$$0 \leq \omega \leq 1 \quad (10)$$

the absolute value of the following function is unity:

$$Q(p) = \frac{(-1)^q [p + (p^2 + 1)^{0.5}]^q \prod_{i=1}^n [m_i p + (p^2 + 1)^{0.5}] [\bar{m}_i p + (p^2 + 1)^{0.5}]}{[-p + (p^2 + 1)^{0.5}]^q \prod_{i=1}^n [-m_i p + (p^2 + 1)^{0.5}] [\bar{m}_i p + (p^2 + 1)^{0.5}]} \quad (11)$$

For consistency in this formulation, m_i must be finite, may not be equal to 1, but may be complex.

$$R(p) = Q(p) + 1. \quad (12)$$

$|R(p)|$ is equiripple and bounded by 0 and 2 in the same frequency range. Also $R(p)R(-p)$ is rational, has equiripple characteristics in range (10), and has poles $p_i = 1/(m_i^2 - 1)^{0.5}$ for $\operatorname{Re} m_i > 0$. Substituting

$$p = 0.5(z - 1/z) \quad (13)$$

into (12) results in

$$Q(z) + 1 = \frac{(-1)^q z^{2q} \prod_{i=1}^n [(1 + m_i)z^2 + (1 - m_i)][(1 + \bar{m}_i)z^2 + (1 - \bar{m}_i)]}{\prod_{i=1}^n [(1 - m_i)z^2 + (1 + m_i)][(1 - \bar{m}_i)z^2 + (1 + \bar{m}_i)]} + 1. \quad (14)$$

This result is consistent with (6) provided $\alpha_i = (1 + m_i)/(1 - m_i)$. Thus (14) is the hourglass formulation ($\epsilon_z = 1$) for $H(z)H(-z)$. The denominator of (14) may also be obtained by transformation of the poles of (11) $p_i = 1/(1 - m_i^2)^{0.5}$ using

$$z_i = p_i \pm (p_i^2 + 1)^{0.5} \quad (15)$$

obtained by solving (13) for z_i and choosing $|z_i| > 1$. The numerator of $Q(z)$ may be obtained by reversing the coefficients of the denominator. The poles and zeros of (14) become the poles and zeros of $R(p)R(-p)$ when transformed to the p -plane using $p_i = 0.5(z_i - 1/z_i)$. Thus it is established that hourglass formulation in the z -plane leads to p -plane Chebyshev rational fraction (equiripple) passband characteristics.

If the specified zeros of $G(p)$ are all at infinite frequency, the result is the standard Chebyshev Filter. For this case, since the zeros of the Butterworth $D(z)$ are known, no rootfinding operation is required. Use of ϵ_z according to (9) merely changes the radius of the circle in the z -plane.

Transformation (13) relating variable z to variable p is the same as that used by Darlington [3] to convert a power series in z into an expansion in Chebyshev polynomials in p . Substitution of the hourglass for the power series in z results in p -plane passband equiripple characteristics.

B. The Hourglass Inverse Chebyshev — Relation to the Elliptic Filter

A Convergence Property:

It has been established that for any set of transmission zeros external to the passband, a set of reflection coefficient zeros may be found in the bounded and closed region $-1 \leq \omega \leq 1$ such that the magnitude of the rational fraction $F(p)/P(p)$ has an equiripple characteristic in that region. If there exists an analytic relationship which deter-

mines the locations of transmission zeros from the locations of reflection coefficient zeros and if, for any possible distribution of reflection coefficient zeros in the defined bounded and closed region, no transmission zeros may be located in the passband, then the Bolzano-Weierstrass theorem may be invoked insuring convergence to the sets which accomplish both conditions.

A process using this convergence property was first proposed by this author [4] and later discussed by

Guillemin [8]. The hourglass implementation simplifies the process and also produces a new filter design known as the hourglass inverted Chebyshev filter.

Use of the Convergence Property:

For either the p -plane elliptic filter or the z -plane hourglass inverted Chebyshev filter, a transition region must

exist. The range will be defined as

$$1 \leq y \leq y_2 \quad (16)$$

for the z -plane and

$$1 \leq \omega \leq \omega_2 \quad (17)$$

for the p -plane. The relationship between ω_2 and y_2 is from (13):

$$\omega_2 = 0.5(y_2 + 1/y_2). \quad (18)$$

Both filter designs may be obtained simultaneously beginning with assumption of transmission zeros at any location outside the pass band in the p -plane or outside the unit circle in the z -plane (they may even be complex).

With assumed p -plane zeros, with $\epsilon_z = 1$, and with the dotted arrow operation in Fig. 1 defined as *division of ω_2 by the zeros of $D(p)$* (this is the analytic connection which locates the transmission zeros for a given set of reflection coefficient zeros), the movement is from $N(p)$ clockwise and back to $N(p)$. This continuing process converges. Finally the function $G(z) = N(z)/D(z)$ is an hourglass inverted Chebyshev function with 3 dB point at $y=1$ and the upper transition frequency at y_2 . This function also has an equiripple passband characteristic in the range

$$-1/y_2 \leq y \leq 1/y_2. \quad (19)$$

If the elliptic filter design is required, a final move should be made from $D(z)$ to $D(p)$ using ϵ_z from (9). Then $G(p) = N(p)/D(p)$ is the appropriate filter function with ω_2 the upper transition frequency.

IV. HIGH-PASS AND BAND-PASS RANGES

Straightforward low-pass to high-pass and low-pass to band-pass transformations may be used to convert any low-pass designs to high-pass and band-pass ranges. Most band-pass transformations produce symmetrical transfer functions only. The following transformations may be used in the case of both symmetrical and unsymmetrical band-pass designs.

A. The Band-Pass Hourglass

The s -plane ($s = \sigma + j\omega$) will be reserved for the band-pass hourglass. The transformation to use is

$$[2s_i^2 + (\omega_i^2 + 1)]/(\omega_i^2 - 1) = z_i^2. \quad (20)$$

Specified s -plane transmission zeros are transformed to the z -plane using (20), with $|z_i| > 1$. The hourglass condition should be met in the z -plane and the resulting zeros of $D(z)$ transformed to the s -plane using (20) to obtain $D(s)$. In this instance the band-pass hourglass is obtained in the s -plane. The order n must be even.

B. The Band-Pass Chebyshev with Arbitrary Transmission Zeros

The transformation to use is

$$[p_i^2 + 1]/(\omega_i^2 - 1) = 0.25(z_i - 1/z_i)^2. \quad (21)$$

Again specified p -plane transmission zeros are transformed to the z -plane using (21) and choosing $|z_i| > 1$. The

hourglass condition is met and after using ϵ_z from (9), the zeros of $D(z)$ are transformed to the p -plane using (21) to obtain $D(p)$. The result is a standard band-pass Chebyshev rational fraction filter characteristic. The order n must be even.

V. CONSTANT TIME-DELAY DESIGN

A. Low-Pass

The Hourglass algorithm and the convergence property previously discussed make it possible to begin with *any p-plane Hurwitz polynomial* and to modify it to obtain a natural mode polynomial $D(p)$ which has an equiripple time-delay characteristic in a prescribed frequency range. This iterative process follows the same pattern as the elliptic filter development. In this case the analytic connection which determines the time-delay zeros from the reflection coefficient zeros is more complicated. The time-delay zeros are the zeros of the polynomial obtained by differentiation of the rational fraction formed by the even and odd parts of $D(p)$, and $D(p)$ in turn is directly related to the p -plane reflection coefficient zeros, all of which are in the passband, the closed and bounded region $-1 \leq \omega \leq 1$. The convergence property is thus intact.

It is often convenient but not necessary to start with a Bessel polynomial in the z -plane. The only restriction for the z -plane polynomial is that its zeros must lie outside the unit circle. This restriction is in general easy to meet.

The time-delay tolerance is governed by ϵ_z but since the final natural mode polynomial is squared

$$\epsilon_p = [(10^{db/20}) - 1]^{0.5}$$

The relationship between ϵ_z and ϵ_p remains the same. See (9).

The assumed Bessel polynomial $Be(z)$ is first divided by its constant term and then it is scaled so that its highest order term is ϵ_z . The zeros of the resulting polynomial must all be located outside the z -plane unit circle. If this is not the case, the choice of ϵ_z is too high. With a proper choice of ϵ_z , the movement in Fig. 1 is now from $D(z)$ clockwise and back to $D(z)$ using the same ϵ_z each time. This time the dotted arrow in Fig. 1 indicates *determination of $N(p) = P(p)$ from $D(p)$ using (22)*.

The time-delay for $D(p)$ is

$$\begin{aligned} G_1(p) &= P_1(p)P_1(-p)/D_1(p)D_1(-p) \\ P_1(p)P_1(-p) &= X(p)[dY(p)/dp] - Y(p)[dX(p)/dp] \end{aligned} \quad (22)$$

where

$$X(p) = Ev[D_1(p)] \quad \text{and} \quad Y(p) = Od[D_1(p)].$$

After convergence and moving (Fig. 1) finally from $D(z)$ to $D(p)$

$$G(p) = N(p)N(-p)/[D(p)]^2$$

has equiripple characteristics for both time-delay and magnitude.

Note that this final $G(p)$ is obtained by moving the zeros of $D(-p)$ to the LHP. The percent tolerance is the same for both amplitude and time delay. Indeed the normalized time-delay and normalized amplitude are identical over the entire real frequency spectrum.

With $D(p)$ arranged so that its constant term is unity, the value of its first-order coefficient is the value of time-delay at zero frequency.

In order to obtain equiripple time-delay over a different range

$$0 \leq \omega \leq \omega_2 \quad (23)$$

the last transfer from z to p may be done using

$$p_i = (\omega_2/2)(z_i - 1/z_i). \quad (24)$$

After this, if equiripple amplitude is required in range (10), the movement in Fig. 1 for the first time should be counterclockwise from $D(p)$ directly to $D(z)$ to $N(z)$ to $N(p)$. The reverse hourglass should be used to determine $N(z) = P(z)$ from $D(z)$. Movement from $D(p)$ to $D(z)$ requires (15) and movement from $N(z)$ to $N(p)$ requires (13). For determination of $N(z)$ using the reverse hourglass:

$$\begin{aligned} N(z)N(-z) &= P(z)P(-z) \\ &= D(z)D(-z) - F(z)F(-z)\epsilon_z^2. \end{aligned} \quad (25)$$

The constant term of $D(z)$ and also of $P(z)$ should be unity for this equality. Because of the hourglass relationship between $F(z)$ and $P(z)$, the coefficients of $P(z)P(-z)$ are found by solving a series of equation sets. Each set consists of two equations in two unknowns. A solution is always possible unless $\epsilon_z = 1$. For any p -plane Hurwitz polynomial ϵ_z is never equal to 1. It follows that any Hurwitz polynomial with even order zeros, when it is used as a natural mode polynomial, may be equalized with transmission zeros such that it has an equiripple characteristic over any given bandwidth with a passband tolerance unique to that bandwidth.

If a wider range is chosen for the time delay approximation, the percent ripple is smaller for amplitude than for time-delay and the stopband rejection is worse. In many cases the stopband characteristic may not be acceptable. The procedure to be described will improve it. The passband amplitude characteristic will not be exactly equiripple but its tolerance will be limited. The time-delay tolerance will retain its original value and will be equiripple in character.

This final step requires approximation of $P(z)P(-z)$ by a polynomial $P^*(z)P^*(-z)$ whose zeros are double. Thus

$$P^*(z)P^*(-z) = \left[\sum_{j=0}^k b_j^* z^j \right]^2. \quad (26)$$

The zeros of $P^*(z)$ are symmetrical with respect to the jy -axis. Approximation is accomplished by a simple Taylor series match. For instance if a fourth-order $P^*(z)$ is chosen, then

$$b_0^* = 1, \quad b_2^* = b_2/2, \quad \text{and} \quad b_4^* = [b_4 - (b_2^*)^2]/2. \quad (27)$$

A better stopband characteristic is obtained by increasing the number of transmission zeros at infinite frequency. Movement of $P^*(z)$ to $P^*(p) = N^*(p)$ results in $G(p) = N^*(p)/D(p)$ which has equiripple time-delay in the range chosen and approximately equiripple amplitude in range (10).

Arbitrary transmission zeros may be specified. Such specification requires modification of $P^*(z)$. In all cases specified transmission zeros must appear as double poles in $K(z)K(-z)$ and as double zeros in

$$P_1(z)P_1(-z) = \sum_{j=0}^m c_j z^j \quad (28)$$

with $c_0 = 1$, and $c_j = 0$ for $j = 1, 3, 5, \dots, (2n-1)$.

Thus with arbitrary transmission zeros specified, $P(z)P(-z)$ is in this case approximated by

$$P^*(z)P^*(-z)P_1(z)P_1(-z) = \left[\sum_{j=0}^k b_j^* z^j \right]^2 \left(\sum_{j=0}^m c_j z^j \right). \quad (29)$$

For example, if $k = 4$:

$$b_0^* = 1, \quad b_2^* = (b_2 - c_2)/2, \quad \text{and}$$

$$b_4^* = [b_4 - 2b_2^*c_2 - c_4 - (b_2^*)^2]/2. \quad (30)$$

An example illustrating this utilization of arbitrary transmission zeros is described in [5].

Finally a technique similar to that proposed by Reméz [7] may be used to modify $N^*(p)$ to obtain absolutely equiripple passband amplitude with somewhat less passband tolerance and better stopband characteristics. The process is relatively simple. A squared polynomial $N(p)N(-p)$ of order $2m$ can produce $m+1$ extrema in the range $0 \leq \omega \leq 1$ (considering the band edges). Since $G(p)G(-p)$ has only m degrees of freedom in the coefficients of $N(p)N(-p)$ and $m+1$ degrees of freedom are required, the tolerance must be unique. An iterative procedure establishes the tolerance for the given arrangement. For those who would require the ultimate in design, this technique should be considered. A result of this procedure is presented in Example 3.

Simultaneous equiripple stopband and passband characteristics may be obtained using the Reméz algorithm. For this case, the minimum stopband amplitude must also be unique. Passband ripple will be higher in this case.

B. Band-Pass

The ability to obtain equiripple time-delay characteristics over a different frequency range than for constant amplitude makes constant time-delay band-pass design possible. Design for arbitrary zeros using this method yields near equiripple amplitude characteristics.

For band-pass constant time-delay design, the p -plane zeros of $D(p)$ obtained for equiripple time-delay in the range $0 \leq \omega \leq \omega_2$ are transferred to the z -plane using (21).

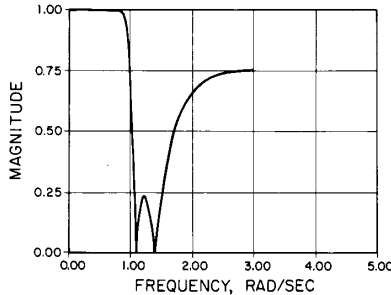


Fig. 2. Maximally-flat filter characteristic: transmission zeros at $\omega = 1.1, 1.4, \infty$.

Then $P(z)P(-z)$ is determined from $D(z)D(-z)$ using the reverse hourglass as in the low-pass case. Arbitrary transmission zeros may be treated as before. Again double natural modes may be avoided by the methods just described. The transfer of $N(z)$ to $N(p)$ using (21) results in the appropriate band-pass function $G(p) = N^*(p)/D(p)$.

Example 1

For an $n = 5$ hourglass filter the transmission zeros are specified at $\omega = 1.1, 1.4$, and ∞ .

Then

$$\begin{aligned} N(z) &= P(z) = [(1/1.1^2)z^2 + 1][(1/1.4^2)z^2 + 1] \\ &= 0.4216562658z^4 + 1.336650363z^2 + 1 \\ F(z) &= [z^4 + 1.336650363z^2 + 0.4216562658]z. \end{aligned}$$

For $\epsilon_z = 1$ (3 dB at $\omega = 1$):

$$D(z)D(-z) = F(z)F(-z) + P(z)P(-z).$$

The RHP zeros of $D(z)D(-z)$ are

$$\begin{aligned} -0.06073471319 &\pm j0.9981539433 \\ -0.34990658030 &\pm 0.9367845991 \\ -1 + j0. & \end{aligned}$$

These zeros are all on the unit circle. From these zeros

$$\begin{aligned} D(z) &= z^5 + 1.8212825872z^4 + 2.90628849z^3 \\ &\quad + 2.90628849z^2 + 1.821282587z + 1 \\ G(z) &= N(z)/D(z). \end{aligned}$$

This response function is plotted in Fig. 3 and may be compared to the corresponding standard maximally-flat filter function shown in Fig. 2. The scales are identical for ready comparison.

The effect of multiplying the reflection coefficient zeros by a fixed factor (1.045 in this case leading to a geometric mean frequency of $1.045^{0.5}$) is shown in Fig. 4. The result is increased rejection in the stopband but increased ripple in the passband. After this modification, the hourglass compares favorably with the Chebyshev rational fraction filter characteristic (shown in Fig. 5), which has the same passband tolerance and which is normalized to the same 3-dB bandwidth (an iterative process is required to design this Chebyshev rational fraction filter in order to keep the transmission zeros at the same locations).

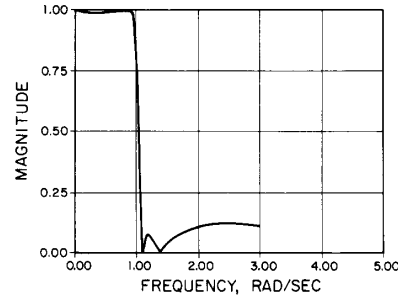


Fig. 3. Hourglass filter characteristic: transmission zeros at $\omega = 1.1, 1.4, \infty$.

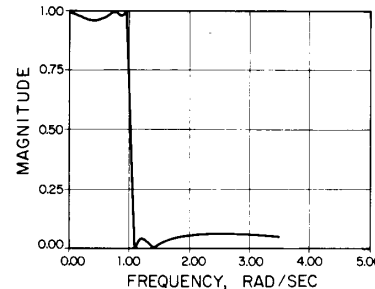


Fig. 4. Hourglass filter characteristic: reflection coefficient zero locations multiplied by 1.045.

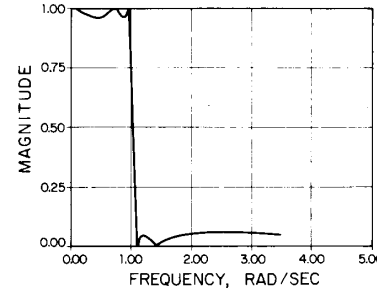


Fig. 5. Chebyshev rational fraction filter: same passband tolerance as hourglass of fig. 4.

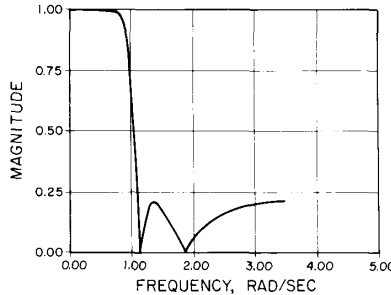
Example 2

For an $n = 5$ hourglass inverted Chebyshev filter the lower limit of the stopband is specified as $y_2 = 1.1$. Development of this response function requires an iterative process. For this example five transmission zeros are located initially at infinite frequency in the z -plane. The hourglass formulation yields the first $D_1(z)$ and it is the fifth-order Butterworth.

Transfer of the zeros of this polynomial to the p -plane results in passband real frequency zeros whose values are the same as the imaginary components of the z -plane zeros of $D_1(z)$:

$$\omega_{D1} = 0, 0.5877852523, 0.9510565163.$$

These zeros are divided into $\omega_2 = 1.004545455$. (The p -plane transformation of $y_2 = 1.1$) to determine p -plane

Fig. 6. Maximally-flat inverse Chebyshev characteristic: $n = 5$.

transmission zeros at this iteration:

$$\omega_{N1} = \infty, 1.709034806, 1.056241598.$$

These zeros are then transformed to the z -plane:

$$y_{N1} = \infty, 3.09464085, 1.396309699.$$

From these zeros

$$N_2(z) = P_2(z) = 0.0535457817z^4 + 0.617301659z^2 + 1.$$

Then according to the hourglass algorithm:

$$F(z) = (z^4 + 0.617302659z^2 + 0.0535457817)z$$

and with $\epsilon_z = 1$

$$D_2(z)D_2(-z) = F_2(z)F_2(-z) + P_2(z)P_2(-z)$$

The zeros of $D_2(z) = P_2(-z)$ are again transferred to the p -plane:

$$\omega_{D2} = 0, 0.7659725073, 0.9855050278.$$

Dividing ω_{D2} into ω_2 :

$$\omega_{N2} = \infty, 2.159955785, 1.216840688.$$

After a number of iterations, this process converges to

$$y_{N+} = \infty, 1.586502763, 1.131185434.$$

Finally, the Hourglass algorithm yields

$$N(z) = 0.3104922229z^4 + 1.178805924z^2 + 1$$

$$D(z) = z^5 + 2.001082499z^4 + 3.132768798z^3 + 3.132768798z^2 + 2.001082499z + 1.$$

The response of $G(z) = N(z)/D(z)$ is shown in Fig. 7 and may be compared to the response of the standard maximally-flat inverted Chebyshev filter response shown in Fig. 6.

Example 3

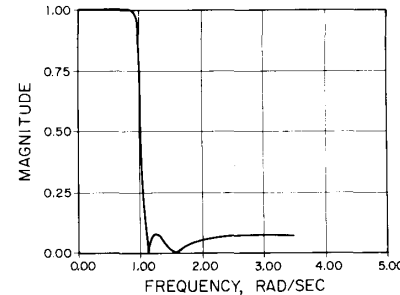
a) Determine the transfer function of a ninth-order filter which has 0.0555897412 dB time-delay ripple in the frequency range

$$0 \leq \omega \leq 1.2.$$

b) Determine the amplitude tolerance in the range

$$0 \leq \omega \leq 1.$$

c) Modify the numerator $N(p)$ of $G(p)$ to obtain improved stopband characteristics.

Fig. 7. Hourglass inverse Chebyshev characteristic: $n = 5$.

Results are given to a large number of places so the reader may verify each step. Using the method outlined one may begin with the ninth-order Bessel polynomial

$$B_9 = z^9 + 45z^8 + 990z^7 + 13860z^6 + 135135z^5 + 945945z^4 + 4729725z^3 + 16216200z^2 + 34459425z + 34459425.$$

For 0.0555897412 dB time-delay, $\epsilon_p = [(10 \text{ dB}/20) - 1]^{0.5} = 0.08012820519$, and from (9) $\epsilon_z = 0.04$. Thus B_9 should be scaled and rearranged so that its constant term is 1 and the ninth-order coefficient is 0.04. The resulting polynomial is

$$B_9^* = 0.04z^9 + 0.3742144067z^8 + 1.711556271z^7 + 4.981581222z^6 + 10.09763875z^5 + 14.69487403z^4 + 15.27509324z^3 + 10.88792372z^2 + 4.810076705z + 1.$$

The zeros of B_9^* are now transferred to the p -plane using (13) and $D(p)$ is constructed from them:

$$D(p) = 75.82899647p^9 + 172.3321418p^8 + 335.1040791p^7 + 394.9669793p^6 + 373.492478p^5 + 250.2580456p^4 + 126.9079842p^3 + 43.86831133p^2 + 9.677144613p + 1.$$

Now $P_1(p)P_1(-p)$ is obtained from $D(p)$ by using (22). See dotted arrow in Fig. 1.

$$P_1(p)P_1(-p) = 13067.77337p^{16} + 32100.64536p^{14} + 34144.85213p^{12} + 18004.08646p^{10} + 5607.038017p^8 + 628.6744875p^6 + 169.3514569p^4 - 43.79604003p^2 + 9.667144613.$$

The move in Fig. 1 is now from $N(p) = P(p)$ to $N(z)$ to $D(z)$. The polynomial $F_1(z)F_1(-z)$ should have two zeros at zero frequency.

After one iteration

$$D_2(z) = 0.04z^9 + 0.3761402923z^8 + 1.722400505z^7 + 5.01075512z^6 + 10.14612374z^5 + 14.74838733z^4 + 15.31407713z^3 + 10.9051595z^2 + 4.813619371z + 1.$$

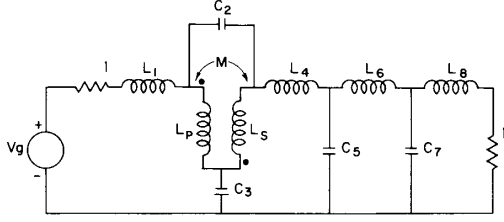


Fig. 8. Passive network realization for Example 3.

This process is continued until finally $D(z)$ converges to

$$\begin{aligned} D(z) = & 0.04z^9 + 0.3765207701z^8 + 1.725692366z^7 \\ & + 5.023364928z^6 + 10.17425639z^5 \\ & + 14.78816922z^4 + 15.34985438z^3 \\ & + 10.92412232z^2 + 4.81818549z + 1. \end{aligned}$$

When the zeros of this polynomial are transformed to the p -plane the natural mode polynomial which results has an equiripple time-delay characteristic in range (10).

For equiripple time-delay in range (23) with $\omega_2 = 1.2$, either transformation (24) may be used on the zeros of $D(z)$ or $D(p)$ may simply be properly scaled. Then the zeros of this new $D(p)$ are transferred back to the z -plane using (15). The resulting new $D(z)$, which produces the proper $D(p)$ for equiripple time-delay in range (23), may be used as a basis for amplitude equiripple design for $G(p)$ in range (10).

This new $D(z)$ is

$$\begin{aligned} D(z) = & 0.01201972635z^9 + 0.1145365694z^8 \\ & + 0.5667775036z^7 + 1.852976546z^6 + 4.318566654z^5 \\ & + 7.336282758z^4 + 8.993477666z^3 \\ & + 7.613937045z^2 + 4.015249149z + 1. \end{aligned}$$

The tolerance for amplitude may now be calculated from the high-order coefficient of $D(z)$. Thus $\epsilon_z = 0.01201972635$. Therefore $\epsilon_p = 0.02404292627$ and the decibel ripple $= 20\log(1 + \epsilon_p^2) = 0.005019534712$. This is considerably less ripple than for the time-delay.

Now the reverse hourglass is implemented. The polynomial $P(z)P(-z)$ is determined from $D(z)D(-z)$ using (22).

Solutions of sets of two equations in two unknowns yields

$$\begin{aligned} P(z)P(-z) = & -0.0006356056851z^{16} \\ & - 0.0005245244759z^{14} + 0.0025159006z^{12} \\ & - 0.009070313002z^{10} + 0.03763877906z^8 \\ & - 0.1409391105z^6 + 0.422495689z^4 \\ & - 0.8943517257z^2 + 1. \end{aligned}$$

When the zeros of $P(z)$ are transformed to the p -plane and $P(p)P(-p)$ is formed then

$$\begin{aligned} G(p) = & [P(p)P(-p)]/[D(p)]^2 \\ = & [N(p)N(-p)]/[D(p)]^2 \end{aligned}$$

is an equiripple amplitude function in range (10) and is an

equiripple time delay function in range (23) with $\omega_2 = 1.2$.

The numerator and denominator of $G(p)$ are

$$\begin{aligned} N(p)N(-p) = & -239.4014349p^{16} - 953.469118p^{14} \\ & - 1477.683619p^{12} - 1172.35736p^{10} \\ & - 487.359168p^8 - 115.7517777p^6 \\ & - 5.706752196p^4 - 3.691509496p^2 + 1 \end{aligned}$$

$$\begin{aligned} [D(p)]^2 = & [14.75559793p^9 + 40.67971173p^8 \\ & + 94.0904444p^7 + 133.7170162p^6 \\ & + 150.7862475p^5 + 121.5474106p^4 \\ & + 73.59010872p^3 + 30.57076442p^2 \\ & + 8.056027652p + 1]^2. \end{aligned}$$

The time-delay at zero frequency may be identified as the coefficient of the first-order term of $[D(p)]^2$. Its value is 16.112055304.

Better stopband characteristics are obtained by approximation of the numerator of $G(p)$ by a squared function of lower order. The reason for using the squared function is to avoid use of double natural modes. To accomplish this the zeros of $N(p)$ are transferred to the z -plane and there the resulting $N(z)$ is approximated in a Taylor sense by an eighth-order function which is the square of a fourth-order even function. The zeros of the resulting $N(z)$ are then transferred to the p -plane to form the new $N(p)$ which is a squared function. The square root of the entire $G(p)$ may be taken resulting in

$$\begin{aligned} N(p) = & 4.036686956p^4 - 0.4704783515p^2 + 1 \\ D(p) = & 14.75559793p^9 + 40.67971173p^8 + 94.0904444p^7 \\ & + 133.7170162p^6 + 150.7862475p^5 \\ & + 121.5474106p^4 + 73.59010872p^3 \\ & + 30.57076442p^2 + 8.056027652p + 1 \end{aligned}$$

and

$$G(p) = N(p)/D(p).$$

The final $G(p)$ has just over 0.9-dB amplitude variation in the passband but it is not exactly equiripple. The percent tolerance group delay remains the same.

The network which realizes this function may be obtained by standard cascade synthesis and is presented in Fig. 8 to complete the example. The values of the circuit elements are

$$\begin{aligned} L_1 &= 0.1404807003 & L_6 &= 2.348526865 \\ C_2 &= 0.5269170231 & C_7 &= 0.9857533977 \\ C_3 &= 4.366689701 & L_8 &= 2.150147751 \\ L_4 &= 0.9713956648 & L_p &= 1.484452548 \\ C_5 &= 1.025159034 & L_s &= 1.428715776 \\ & & M &= 0.6053598464. \end{aligned}$$

The normalized amplitude response of this network, its time-delay, and phase characteristics are shown in Fig. 9.

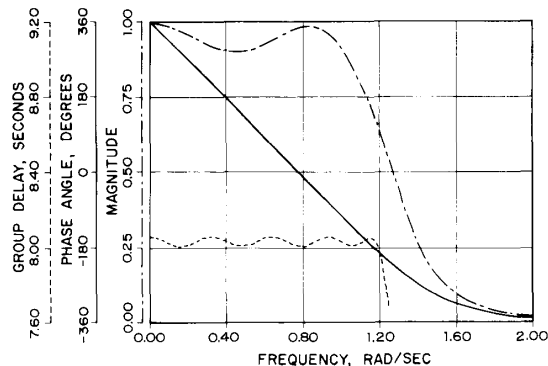


Fig. 9. Amplitude, time-delay, and phase characteristics—circuit of Fig. 8.

Finally, as promised, the application of the Reméz algorithm yields

$$N(p) = 3.879688534p^4 - 0.6741027151p^2 + 1.$$

The new $G(p)$ has the same equiripple time-delay as before and has exactly equiripple passband amplitude response with a tolerance of 0.688 dB.

It is also possible to find an $N(p)$ such that $G(p)$ has equiripple passband and equiripple stopband characteristics. The ripple is unique for a given distribution of transmission zeros. The $G(p)$ associated with the following $N(p)$ has a 4.064 dB passband ripple and a minimum stopband attenuation of 22 dB in the range $1.2 \leq \omega \leq \infty$:

$$N(p) = 4.431261523p^8 + 19.7978974p^6 + 22.36594185p^4 + 4.234234833p^2 + 1.$$

In this case, four transmission zeros are used for passband amplitude equalization and five are left for the stopband. The passband tolerance can be reduced by using six transmission zeros for passband equalization and three transmission zeros in the stopband.

V. CONCLUSION

Hourglass filters with finite transmission zeros have better passband and stopband characteristics than maximally-flat filters with the same transmission zeros. The hourglass algorithm may be used to obtain transfer functions possessing equiripple time-delay and equiripple am-

plitude characteristics simultaneously. It may be used to equalize in an equiripple sense the amplitude of any Hurwitz polynomial whose zeros are of even order. Finally it may be used as a general design base for Chebyshev, Chebyshev rational fraction, hourglass inverse Chebyshev, and elliptic (Cauer) filters.

REFERENCES

- [1] A. Sedra and P. Brackett, *Filter Theory and Design: Active and Passive*. Beaverton, OR: Matrix, 1978.
- [2] G. Polya and G. Szegö, *Problems and Theorems in Analysis*, vol. 1, New York, Heidelberg, Berlin: Springer-Verlag, pp. 108, 302, 1972.
- [3] S. Darlington, "Network Synthesis Using Tchebycheff Polynomial series," *Bell Syst. Tech. J.*, vol. XXXI, pp. 613-665, July 1952.
- [4] B. J. Bennett, "A note on filter synthesis," *IRE Trans. Circuit Theory*, vol. CT-1, pp. 61-64, Sept. 1954.
- [5] —, "The hourglass and constant time delay," in *Conf. Proc. 28th Midwest Symp. on Circuits and Systems*, pp. 364-368, Aug. 1985.
- [6] H. Pilotty and V. Ulbrich, "Über den Entwurf von Allpassen, Tiefpassen, und Bandpassen mit einer im Tschebyscheffschen approximierten konstanten Gruppenlaufzeit," *Arch. Elek. Übertragung.*, vol. 14, pp. 452-67, Oct. 1960.
- [7] E. Reméz, "Sur le calcul effectif des polynomes de Tschebyscheff," *Comptes Rendus, Academie des Sciences, Paris, France*, vol. 199, pp. 199-220, 1962.
- [8] A. E. Guillemin, *Synthesis of Passive Networks*. New York: Wiley, 1957, pp. 645-654.
- [9] B. J. Bennett, "Synthesis of electric filters with arbitrary phase characteristics," *1953 IRE Convention Rec.*, part 5, Circuit Theory, pp. 19-26.



Byron J. Bennett received the B.S. degree in electrical engineering from Texas Technological University, and the M.S. and Ph.D. degrees in electrical engineering from Stanford University, Stanford, CA.

His professional experience includes employment with General Electric, Philco, IBM, and Stanford Research Institute. At Stanford Research Institute he led the group which developed magnetic character sensing and the first computers to be used by the banking industry. His university experience includes faculty appointments at Texas Technological University, Temple University, San Jose State College, Stanford University, and Montana State University. From 1963 to 1983 he was Dean of the College of Engineering at Montana State University. He is a recipient of the Texas Technological University Distinguished Engineer Award and the IEEE Centennial Medal. At present he is Professor of Electrical Engineering at Montana State University.



LINEAR PHASE ANALOG FILTER DESIGN WITH ARBITRARY STOPBAND ZEROS

Douglas R. Huard¹, Jonny Andersen², Robert G. Hove³

¹ Tektronix, Inc., Beaverton, OR.

² University of Washington, Dept. of Electrical Engineering, Seattle, WA.

³ Boeing Commercial Airplane Group, Seattle WA.

Abstract

Many types of signal transmission systems require such accurate recovery of information that distortion of any kind is a problem. Circuit design engineers are increasingly being asked to reduce distortion in systems as performance demands escalate. One important problem area is time distortion, or varying group delay, where the different frequency components of a signal experience unequal transit times. This paper describes current progress on a computer design method for filters that simultaneously approximates passband flat delay as well as equiripple amplitude response and stopband attenuation requirements. The delay variation has been found to be less than that of comparable designs of the same order using the standard method of separately deriving the transfer functions for the desired amplitude response and the all-pass delay equalizer. Total delay, or transit time, of the signal is also significantly less in the new approach.

Design Algorithm

An approach is presented for solving the approximation problem as required for the design of analog filters that simultaneously produce equiripple passband amplitude characteristics and equiripple group delay. The resulting transfer function is non-minimum phase. The focus here is primarily on the algorithm and computation method (which will hereafter be referred to as the hourglass algorithm) which, when implemented on a personal computer, produces the transfer function by means of the iterative process illustrated in figure 1. There is also an option of placing arbitrary zeros on the $j\omega$ axis for high attenuation of specific undesired frequency components. If no specifications exist for phase or its derivative, group delay, the computation of the algorithm reduces to an especially simple form useful in approximating a specified filter amplitude characteristic with arbitrary zeros.

The hourglass transfer function derivation, while computationally intensive, is a straightfor-

ward sequence of program loops that are easy to visualize, as described in [1], and can offer advantages in PC software development as compared to that required for the complex optimization routines used in many all-pass equalization algorithms.

The hourglass filter algorithm was originally developed by Bennett[2] as a new method of finding a filter transfer function which simultaneously approximates both group delay and amplitude requirements in a single transfer function and network structure. It is referred to as the hourglass filter because of the symmetry in the coefficients of the denominator polynomial derived during the computation cycle. Further research on the hourglass filter problem, in order to clarify the computations and design options and to explore its limitations, revealed several additional properties.

Specifically, there does not appear to be a theoretical limit in the maximum order of the hourglass designs which progressively evolve into higher orders when demands are made for increasingly higher stopband attenuation or less passband delay ripple. For example, computation of the 9th order filter design shown in figure 3, having a moderate stopband beginning an octave above the passband where attenuation is required to exceed 40dB, proceeded in a straightforward manner. The 8th order numerator has one set of 4 zeros in the passband with quadrant symmetry, i.e., mirror images about the $j\omega$ axis, and one pair on the positive and negative real axis. It was found, however, that attempts to obtain a transfer function for higher levels of stopband attenuation, e.g., 60 dB an octave above the passband, becomes extremely difficult unless a method such as Remez' second algorithm is introduced into the computation process.

The procedure to derive transfer functions using the hourglass algorithm makes use of Feldtkeller's equation, along with a relationship between the transmission zeros and the reflection zeros, as shown in equations (1) and (2):

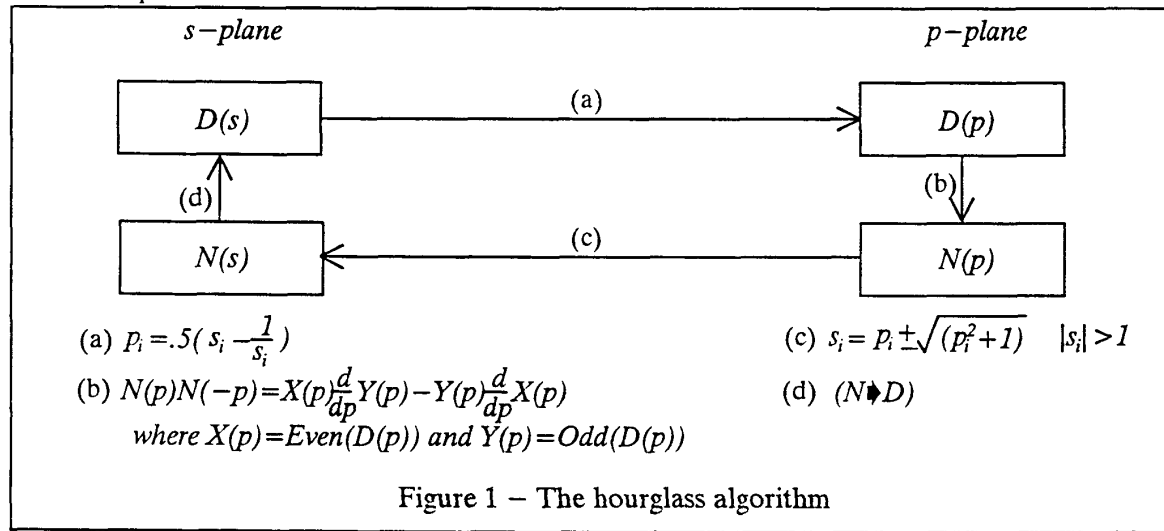
$$D(s)D(-s)=N(s)N(-s)+\epsilon_s^2 F(s)F(-s) \quad (1)$$

$$F(s)=s^n N(1/s) \quad (2)$$

Here, $D(s)$ represents the denominator of the transfer function, $N(s)$ represents the numerator, and $F(s)$ represents the reflection zero polynomial[3]. Note that given a value for epsilon (ϵ_s) and either a numerator polynomial or a denominator polynomial, the system of equations above reduces to two equations with two unknowns. Thus, a numerator polynomial may be found from a denominator polynomial ($D \nparallel N$), or a denominator polynomial may be found given a numerator polynomial ($N \nparallel D$).

Development of a transfer function is accom-

plished with the iterative loop shown in figure 1. This loop exists in two planes, the s -plane and the p -plane. The p -plane is a simple frequency transformation in which the final transfer function is found. Equations (a) and (c) in figure 1 below are frequency transformations between the s -plane and the p -plane. Equation (b) represents the time delay of $D(p)$. Finally, equation (d) denotes use of Feldtkeller's equation along with the relationship between the transmission zeros and reflection zeros to find $D(s)$ from $N(s)$ as described above.



As mentioned earlier, if no specification of group delay exists, the approximation of a minimum phase transfer function satisfying amplitude requirements becomes computationally simple by first forming a numerator from the arbitrarily specified transmission zeros in the s -plane. These zeros may be imaginary, complex, or infinite, but must have magnitudes that are greater than unity. The hourglass algorithm is then used ($N \nparallel D$) to find a corresponding denominator polynomial. Epsilon (ϵ_s) is defined as one in this case. An example is shown in figure 2 of a 7th order filter.

If equiripple group delay is required, the computation process is more involved and begins with a denominator in the s -plane. It is often convenient but not necessary to begin with a Bessel polynomial. The only restriction on this polynomial is that its zeros lie outside the unit circle [2]. The polynomial must first be frequency and magnitude scaled[1] such that the coefficient of the highest order term equals ϵ_s and the constant term equals 1. Epsilon (ϵ_s) may be found from the desired group delay ripple in dB using equations (3) and (4). Group delay ripple in dB is defined as: $20\log(\max. \text{delay}/\min. \text{delay})$.

$$\epsilon_p = \sqrt{10^{0.05(\text{dB})} - 1} \quad (3)$$

$$\epsilon_s = -\frac{1}{\epsilon_p} + \sqrt{\frac{1}{\epsilon_p^2} + 1} \quad (4)$$

The iterations then proceed clockwise from $D(s)$ to $D(p)$ to $N(p)$ to $N(s)$ and back to $D(s)$. Once this iteration process converges on $D(s)$ (i.e., when the polynomial coefficients change by less than some pre-determined amount), $N(s)$ is found from $D(s)$ through the use of the hourglass algorithm ($D \nparallel N$), and both $N(s)$ and $D(s)$ are transferred to the p -plane. The resulting transfer function, formed by $N(p)N(-p)$ as a numerator and $D^2(p)$ as a denominator, has equiripple amplitude and equiripple group delay.

While this design certainly accomplishes the major objectives of equiripple amplitude and equiripple group delay within a single transfer function, it will frequently be desired to push the stopband attenuation to more than 40 or 50 dB. This is accomplished by matching the coefficients of the numerator with a squared even numerator of lower order, which must be done in a way that doesn't destroy the

equiripple group delay characteristic of the transfer function. Once this has been accomplished, the transfer function possesses both double order zeros and double order poles at all locations. This allows the square root of the entire transfer function to be taken, which reduces the order by a factor of two without destroying the equiripple group delay.

This approximation process, while preserving the equiripple group delay, does unfortunately destroy the equiripple amplitude characteristics of the transfer function. Therefore, the last step in the approximation process is optimizing the transmission zero locations to once again produce equiripple amplitude characteristics. This is straightforward if there is only one set of quadrantly symmetric zeros, however, for numerators of higher order (>6) this requires a computerized optimization routine, such as a modified version of Remez' second algorithm. It should be noted that quadrantal transmission zeros do not affect the delay of the transfer function, only the amplitude.

Present work is concerned with developing a robust optimization routine and evolving the computational methods to allow the designer a wide range of flexibility in choosing the important filter parameters: group delay ripple, amplitude ripple, and stopband attenuation.

Design Examples

The 7th order filter shown in figure 2 is an example of an hourglass filter without an explicit group delay specification. Transmission zeros were arbitrarily specified at 1.4, 1.7, and 2.9 radians/second, and the hourglass algorithm was used to find a denominator polynomial given the numerator polynomial ($N \cdot D$).

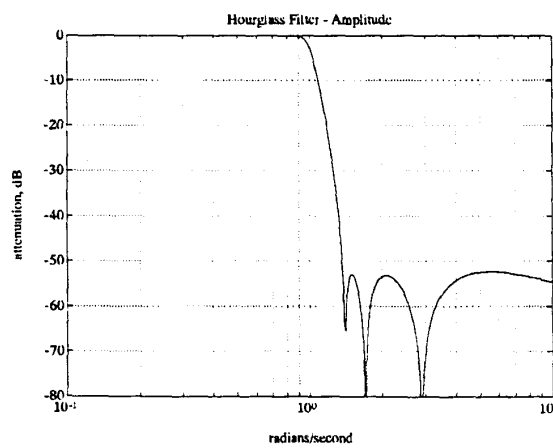


Figure 2 – A 7th order hourglass filter

The 9th order filter amplitude and group delay responses shown in figures 3 and 4 are a result of approximating the numerator of an 18th order filter by an eighth order numerator, taking the square root of the denominator, and optimizing the zero locations to produce equiripple passband and stopband attenuation. The filter still has equiripple group delay, but has vastly improved stopband characteristics as compared to the 18th order transfer function.

This 9th order filter was designed to have 0.4 dB of amplitude ripple in the passband extending to 1.0 radian/second with .08686 dB of group delay ripple. The stopband begins at 2.0 radians/second and is required to have no less than 40 dB of attenuation. The group delay ripple was approximately 0.0896 seconds peak to peak. A comparison was made between this hourglass filter design and a nearly equivalent combination of a lowpass filter with an all-pass equalizer as is typically used for realizing a specified amplitude and group delay requirement.

For this comparison, a 4th order lowpass filter transfer function was derived having the same 0.4 dB passband ripple extending to 1.0 radian/second. The stopband was also required to begin at 2.0 radians/second and have at least 40 dB of attenuation; it actually was 45 dB (figure 5). A 5th order all-pass equalizing function was then derived, producing a total of 9 poles for both networks (the same order as the hourglass filter transfer function). This combination produced approximately 0.2368 seconds peak to peak of group delay variation over the passband or about 2.5 times more than the 9th order hourglass filter. In addition, the hourglass filter's equiripple group delay range extends to 1.1 radian/second, whereas the combination filter designed for comparison has approximately flat group delay only to 1.0 radian/second.

Another important feature is apparent from the two comparative group delay plots. The hourglass filter delay can be seen from figure 4 to have approximately 9.0 seconds of total delay. The comparison filter and all-pass combination group delay shown in figure 6 has approximately 14.5 seconds total delay, or 60% more. The choice of a smaller transit time for a signal through a filter is usually preferred.

Conclusion

The paper presents details on solving the approximation problem relative to a new linear phase filter design approach. The hourglass transfer function has the qualities of approximating passband flat delay and flat amplitude in an equiripple manner. There is also the option of shaping the stopband by placing the transmission zeros arbitrarily where needed. A comparison demonstrated that the new

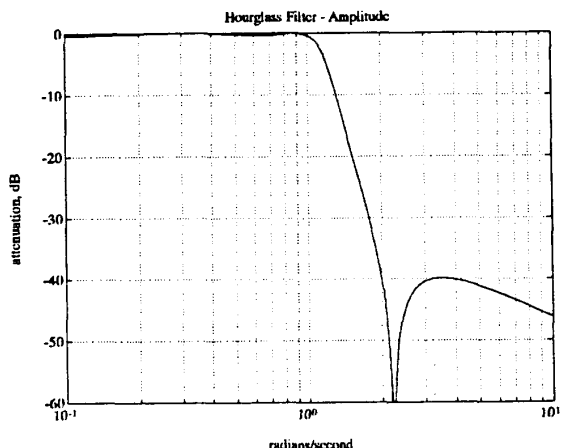


Figure 3 -- 9th order hourglass amplitude

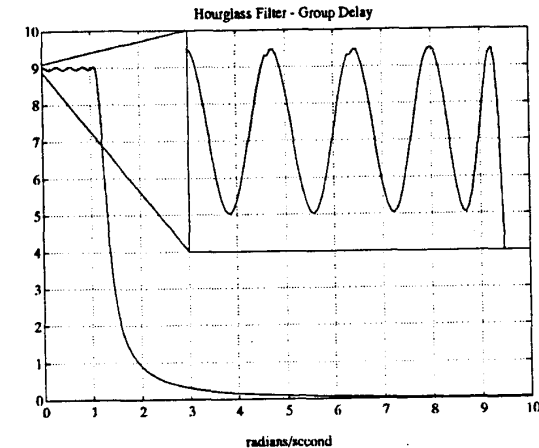


Figure 4 -- 9th order hourglass delay

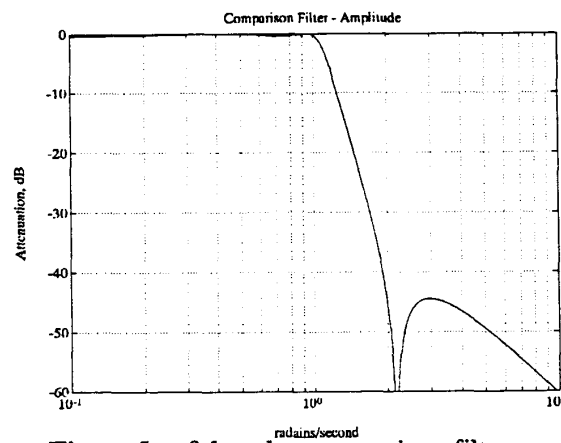


Figure 5 -- 9th order comparison filter amplitude

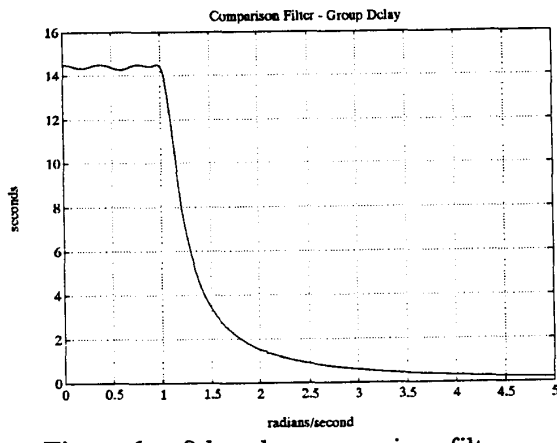


Figure 6 -- 9th order comparison filter delay

hourglass designs could produce a filter having less delay ripple and less total delay than an equivalent lowpass/all-pass filter combination of the same order. Continuing work is being directed toward implementing the hourglass algorithms into a flexible PC design methodology which permits a designer to quickly find the desired transfer function that meets requirements for passband group delay and amplitude ripple as well as stopband attenuation.

[1] Huard, Douglas R. "Linear Phase Filtering Using the Hourglass Algorithm." *Master's Thesis*,

Dept. of Electrical Engineering, University of Washington. March 1991.

- [2] Bennett, Byron J. "A New Filter Synthesis Technique – The Hourglass." *IEEE Transactions on Circuits and Systems*, vol 35, pp 1469–1477. December 1988.
- [3] Sedra, A. L. and Brackett, P. O. *Filter Theory and Design: Active and Passive*. Beaverton, OR. Matrix. 1978.